VOLUME 124 NUMBER 1

THE ASTROPHYSICAL JOURNAL

AN INTERNATIONAL REVIEW OF SPECTROSCOPY AND ASTRONOMICAL PHYSICS

JULY 1956

PRELIMINARY RESULTS WITH A VACUUM SOLAR SPECTROGRAPH *Robert R. McMath, Orren C. Mohler, A. Keith Pierce, and Leo Goldberg* 1
THE WIDTH OF THE INFRARED HELIUM LINE IN THE SOLAR SPECTRUM *Orren C. Mohler and Leo Goldberg* 13
ON A POSSIBLE INTERSTELLAR GALACTIC CORONA *Lyman Spitzer, Jr.* 20
A MODEL FOR NONTHERMAL RADIO-SOURCE SPECTRA *N. G. Roman and F. T. Haddock* 35
INTERSTELLAR POLARIZATION IN THE SOUTHERN MILKY WAY *Elske van P. Smith* 43
DISTANCES FOR SOUTHERN EARLY-TYPE STARS, ESPECIALLY IN CARINA AND OTHER H II REGIONS *Dorrit Hoffleit* 61
THE GALACTIC CLUSTER M11 *H. L. Johnson, A. R. Sandage, and H. D. Wahlquist* 81
SYMMETRIC GALACTIC NEBULAE. II *Hugh M. Johnson* 90
SPECTROPHOTOMETRY OF PLANETARY NEBULAE *R. Minkowski and L. H. Aller* 93
THE INTERPRETATION OF THE SPECTRUM OF NGC 7027 *L. H. Aller and R. Minkowski* 110
THE CHEMICAL COMPOSITIONS OF FIVE STARS WHICH SHOW SOME OF THE CHARACTERISTICS OF POPULATION II *E. Margaret Burbidge and G. R. Burbidge* 116
ANOMALOUS ABUNDANCES OF MANGANESE, STRONTIUM, AND EUROPIUM IN HD 151199 *G. R. Burbidge and E. Margaret Burbidge* 130
A SPECTROPHOTOMETRIC ANALYSIS OF TWO METALLIC-LINE STARS *G. R. Miczaika, F. A. Franklin, A. J. Deutsch, and J. L. Greenstein* 134
COMPARATIVE STUDY OF FIVE CARBON STARS IN THE VISUAL AND INFRARED SPECTRAL REGIONS *Yoshio Fujita* 155
THE RADIAL VELOCITY VARIATION OF THETA OPHIUCHI *A. Van Hoof, F. Bertiau, S.J., and R. Deurinck* 168
LINE BROADENING IN THE SPECTRA OF O- AND EARLY B-TYPE STARS *Arne Slettebak* 173
REDISCUSSION OF ECLIPSING BINARIES. I. Z. HERCULIS *Daniel M. Popper* 196
REDISCUSSION OF ECLIPSING BINARIES. II. S. ANTLIAE *Daniel M. Popper* 208
DIFFUSION AND SEVERING OF MAGNETIC LINES OF FORCE *E. N. Parker and M. Krook* 214
AXISYMMETRIC MAGNETIC FIELDS AND FLUID MOTIONS *S. Chandrasekhar* 232
EFFECT OF INTERNAL MOTIONS ON THE DECAY OF A MAGNETIC FIELD IN A FLUID CONDUCTOR *S. Chandrasekhar* 244
ON THE EFFECT OF FLUID MOTION ON THE INITIAL DECAY OF A MAGNETIC FIELD IN A SPHERE *Siciy C. Pao* 266
RADIATIVE EQUILIBRIUM OF A LINE-ABSORBING ATMOSPHERE. II *Jean I. F. King* 272
THE EXTINCTION OF THE LIGHT OF THE NIGHT SKY. I. *G. Costantine and A. Hammad* 298
THE EXTINCTION OF THE LIGHT OF THE NIGHT SKY. II. *G. Costantine and A. Hammad* 302
CHEMICAL HEATING FOR METEORITES *Harold C. Urey and Bertram Donn* 307
METEOR IONIZATION AND ITS DEPENDENCE ON VELOCITY *Gerald S. Hawkins* 311
ANNOUNCEMENT 314

THE UNIVERSITY OF CHICAGO PRESS
CHICAGO, ILLINOIS, U.S.A.

July 1956 Vol. 124, No. 1

THE ASTROPHYSICAL JOURNAL

AN INTERNATIONAL REVIEW OF SPECTROSCOPY AND ASTRONOMICAL PHYSICS

Founded in 1895 by George E. Hale and James E. Keeler

Published in Collaboration with the American Astronomical Society

S. CHANDRASEKHAR, *Managing Editor*
A. BLAAUW, *Associate Editor*
Yerkes Observatory of the University of Chicago

EDITORIAL BOARD

HAROLD F. WEAVER (1956-60)
Berkeley Astronomical Department
University of California

MARTIN SCHWARZSCHILD (1954-58)
Princeton University Observatory

LEO GOLDBERG (1955-59)
The Observatory of the University of Michigan

HORACE W. BABCOCK (1953-57)
Mount Wilson Observatory of the Carnegie Institution of Washington

G. HERZBERG (1952-56)
National Research Council, Ottawa

The Astrophysical Journal is published bimonthly by the University of Chicago at the University of Chicago Press, 5750 Ellis Avenue, Chicago 37, Illinois, during January, March, May, July, September, and November. ¶Two volumes are published per year, one beginning with the January issue and the other beginning with the July issue. On all orders from the United States and its possessions the subscription price is $7.50 per volume or $15.00 per year; the price of single copies is $3.50. ¶On all orders from Canada the subscription price is $8.00 per volume or $16.00 per year; the price of single copies is $3.65. On all orders from all other countries the subscription price is $8.25 per volume or $16.50 per year; the price of single copies is $3.75. (Orders for service of less than a volume will be charged at the single-copy rate.) ¶Subscriptions are payable in advance. Please make all remittances payable to The University of Chicago Press, in United States currency or its equivalent by postal or express money orders or bank drafts. (Exception: members of The American Astronomical Society must send their subscriptions and remittances to the Treasurer of the Society.)

The following is an authorized agent:

For the British Commonwealth, except North America and Australasia: The Cambridge University Press, Bentley House, 200 Euston Road, London, N.W. 1, England. Prices of yearly subscriptions and of single copies may be had on application.

Claims for missing numbers should be made within the month following the regular month of publication. The publishers expect to supply missing numbers free only when losses have been sustained in transit, and when the reserve stock will permit.

Business correspondence should be addressed to The University of Chicago Press, Chicago 37, Illinois.

Communications for the editors and manuscripts should be addressed to: S. Chandrasekhar, Editor of THE ASTROPHYSICAL JOURNAL, Yerkes Observatory, Williams Bay, Wisconsin.

Line drawings and photographs should be made by the author, and all marginal notes such as co-ordinates, wave lengths, etc., should be included in the cuts. It will not be possible to set up such material in type.

One copy of the corrected galley proof should be returned as soon as possible to the editor, Yerkes Observatory, Williams Bay, Wisconsin. Authors should take notice that the manuscript will not be sent to them with the proof.

The cable address is "Observatory, Williamsbay, Wisconsin."

The articles in this journal are indexed in the *International Index to Periodicals*, New York, N.Y.

Applications for permission to quote from this journal should be addressed to The University of Chicago Press, and will be freely granted.

Microfilms of complete journal volumes are available to regular subscribers only and may be obtained at the end of the year. Orders and inquiries should be addressed to University Microfilms, 313 North First Street, Ann Arbor, Michigan.

Notice to subscribers: If you change your address, please notify us and your local postmaster immediately.

Entered as second-class matter, July 31, 1940, at the Post-Office at Chicago, Ill., under the Act of March 3, 1879.
Acceptance for mailing at special rate of postage provided for in United States Postal Act of October 3, 1917, Section 1103, amended February 28, 1925.
Copyright 1956 by the University of Chicago.

[PRINTED IN U.S.A.]

THE ASTROPHYSICAL JOURNAL

AN INTERNATIONAL REVIEW OF SPECTROSCOPY AND ASTRONOMICAL PHYSICS

VOLUME 124 JULY 1956 NUMBER 1

PRELIMINARY RESULTS WITH A VACUUM SOLAR SPECTROGRAPH*

ROBERT R. MCMATH, ORREN C. MOHLER, A. KEITH PIERCE, AND LEO GOLDBERG
McMath-Hulbert Observatory, University of Michigan, Pontiac, Michigan

Received February 7, 1956

ABSTRACT

New observations of the solar spectrum with a high-resolution vacuum spectrograph reveal a wealth of detail in the cores of all Fraunhofer lines observed both in the normal disk and in areas exhibiting various kinds of solar activity. The lines show fluctuations in width, intensity, and position over intervals as small as 2 seconds of arc. A representative collection of photographs is presented, together with tentative conclusions derived from inspection and preliminary measurement.

Measurements of Doppler shifts have been carried out in considerable detail for the two lines Cr λ 4626 and Ba+ λ 5853. The random turbulent velocity at the center of the disk is 0.70 km/sec for the chromium line and 0.44 km/sec for the ionized barium line. For both lines the random turbulent velocity appears to increase toward the limb. The velocity shifts observed for the Hα and sodium D lines are of the same order of magnitude as those of the weaker metallic lines.

The disk observations of the Fraunhofer lines of hydrogen and ionized calcium seem to be consistent with a qualitative model of the low chromosphere, consisting of relatively hot clouds of gas and with cooler regions both above and between the hot regions. Both the K_2 emission in ionized calcium and the wide absorption features in Hα seem to originate in the hot regions; from the appearance of these line features near the limb, it seems that the hot regions contribute a substantial fraction of the hydrogen and ionized calcium emission in the very low chromosphere. The profiles of Hα at the extreme limb and of the K line and other strong metallic lines on the disk favor the conclusion of Adams and Burwell that central self-reversal is a general characteristic of most strong chromospheric profiles. The similarity between the intensity and velocity fluctuations in the core of the strong magnesium line λ 5167 and in those of neighboring weaker lines implies either a chromospheric origin for the centers of these weaker lines or the extension of the photospheric granules into the low chromosphere. The preliminary nature of the foregoing results is emphasized.

INTRODUCTION

The existence of local fluctuations in temperature and velocity in the solar atmosphere has been recognized for a long time from the granular structure of the photosphere and from the mottled appearance of spectroheliograms. Because of observational limitations, however, it has usually not been possible to take account of these inhomogeneities in the derivation of empirical models of the photosphere and chromosphere. Thus it has been customary to attempt the representation of observations by models with spherical symmetry, on the assumption that small-scale fluctuations will introduce only second-order effects, which can be averaged out. Evidence is accumulating from a variety of

* This work was supported in part by Contract N6onr-232-V with the Office of Naval Research.

sources (cf. Böhm 1954; de Jager 1954; Athay and Menzel 1956), however, that spherically symmetric models fail to agree with the observations in a number of important respects and that some of the most interesting properties of the atmosphere are connected with its small-scale structure.

Investigation of the fine details of the solar atmosphere is hampered by seeing disturbances in the earth's atmosphere, which limit the image resolution to $\frac{1}{2}$ second of arc under the very best conditions, and more commonly to about 1–2 seconds of arc. The limitation set by the earth's atmosphere has been more generally recognized than has the equally serious limitation imposed by insufficient resolution and scattered light in the spectrograph, which are caused both by imperfections in spectroscopic gratings and by bad seeing inside the spectrograph.

Recently, a very great advance in the art of ruling gratings, by Dr. H. W. Babcock of the Mount Wilson and Palomar Observatories, made both feasible and desirable the construction at the McMath-Hulbert Observatory of a very large vacuum spectrograph designed especially for high-resolution spectroscopy of fine details of the solar surface. Photographs of the solar spectrum made with this instrument have revealed a wealth of detail in the cores of the Fraunhofer lines which seems to make possible the direct investigation of inhomogeneities in the solar atmosphere. We present in this article a more or less representative collection of these photographs together with certain tentative conclusions that may be drawn from them on the basis of inspection and a few preliminary measurements. It is hoped that this preliminary presentation will stimulate the interest of solar physicists in the many problems that now seem to have been brought into the realm of possible solution by the vacuum spectrograph and by other instruments of similar power that may be constructed.

A detailed description of the vacuum spectrograph has been given elsewhere (McMath 1956), and therefore only a few of the more relevant features will be described here. The main instrument consists of an all-mirror, completely achromatic, grating spectroscope, which is entirely inclosed in a horizontal vacuum tank 4 feet in diameter and 52 feet in length. The grating was especially ruled for the vacuum spectrograph by Dr. Babcock on the ruling engine of the Mount Wilson and Palomar Observatories. Its grooves are 133 mm long and are spaced 600 to the millimeter, the ruled area being 203 by 133 mm.

An investigation of the instrumental profile by both photographic and photoelectric means (Pierce 1956) shows that the instrumental correction to the profiles of solar lines is small. A determination of grating resolution, made from observations of the hyperfine structure of Hg λ 5461 in the fifth order, yields a half-width of 0.010 A. By comparison, the theoretical resolving power is 0.0089 A; hence the grating develops 90 per cent of its theoretical resolving power in this order. Photographs made in the sixth order clearly resolve the central components of the line λ 5461, which is partly resolved in the fifth order. The implied resolving power in the sixth order is therefore 660000, as compared with the theoretical value of 730000. The departures from the theoretical values are due in part to errors in the figures of the spherical mirrors and to the aberrations attendant upon their use off-axis. In practice, the solar observations reported here have been made with slit-widths of two to four times the van Cittert (1930) value, in order to shorten the exposure times. When the wider slits are used, the instrumental profile approximates a truncated triangle.

Scattered light has been evaluated from observations of the central intensities of absorption lines which are known to be saturated. Measurements have been made on the profiles of the sodium D lines that resulted from the passage of sunlight through a 50-cm-long absorption tube containing sodium vapor. The profiles were obtained with flat bottoms of variable width, up to several angstroms, by heating the tube to appropriate temperatures. The observed central intensities of the saturated lines in the fifth order were about 3 per cent. In the same order the white scattered light is about 0.7 per cent (Pierce 1956). The Rowland ghost pattern consists of three lines spaced at inter-

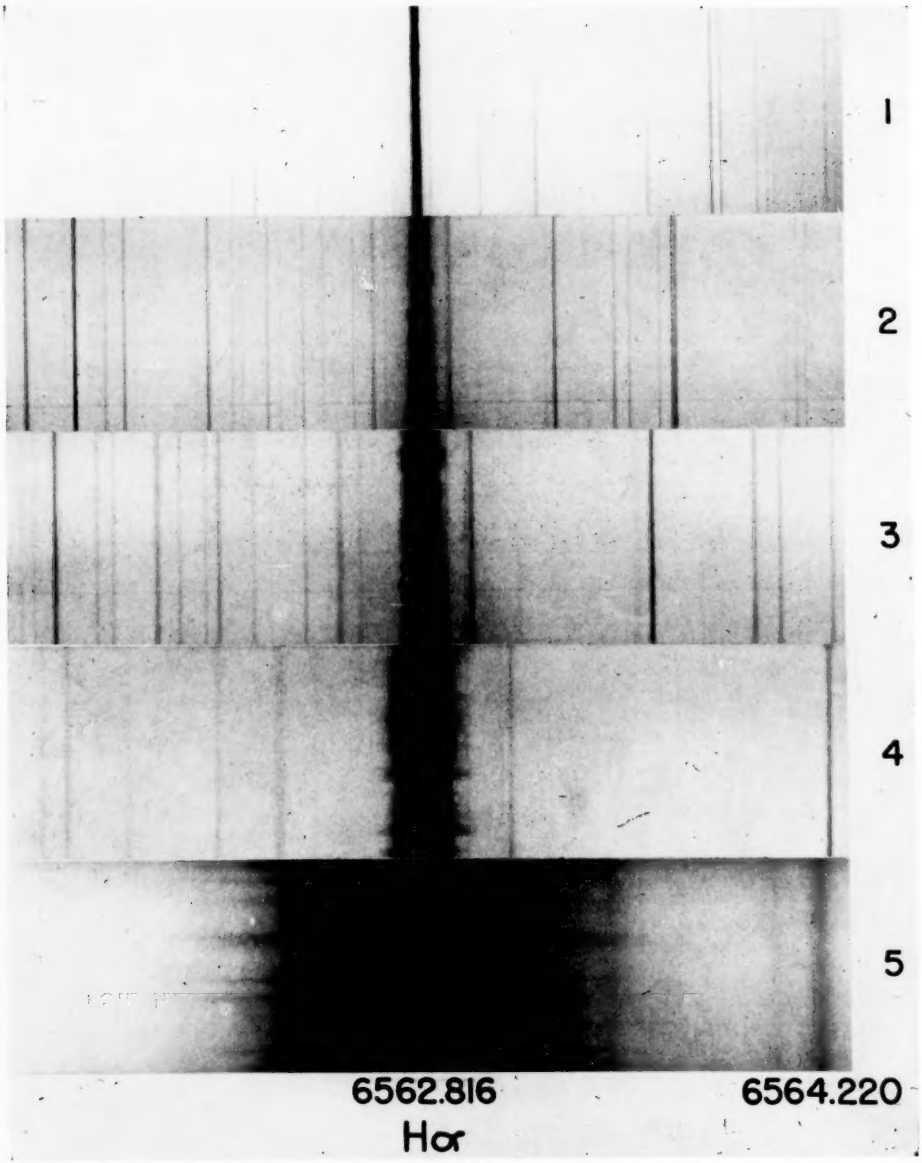

FIG. 1.—The Hα line in the solar spectrum

Order	Exposure (Seconds)	Slit (μ)	Plate Dispersion (mm/A)	Order	Exposure (Seconds)	Slit (μ)	Plate Dispersion (mm/A)
I	2	175	1.20	IV	6	175	6.0
II	4	175	2.00	V	180	175	28.3
III	5	175	3.43				

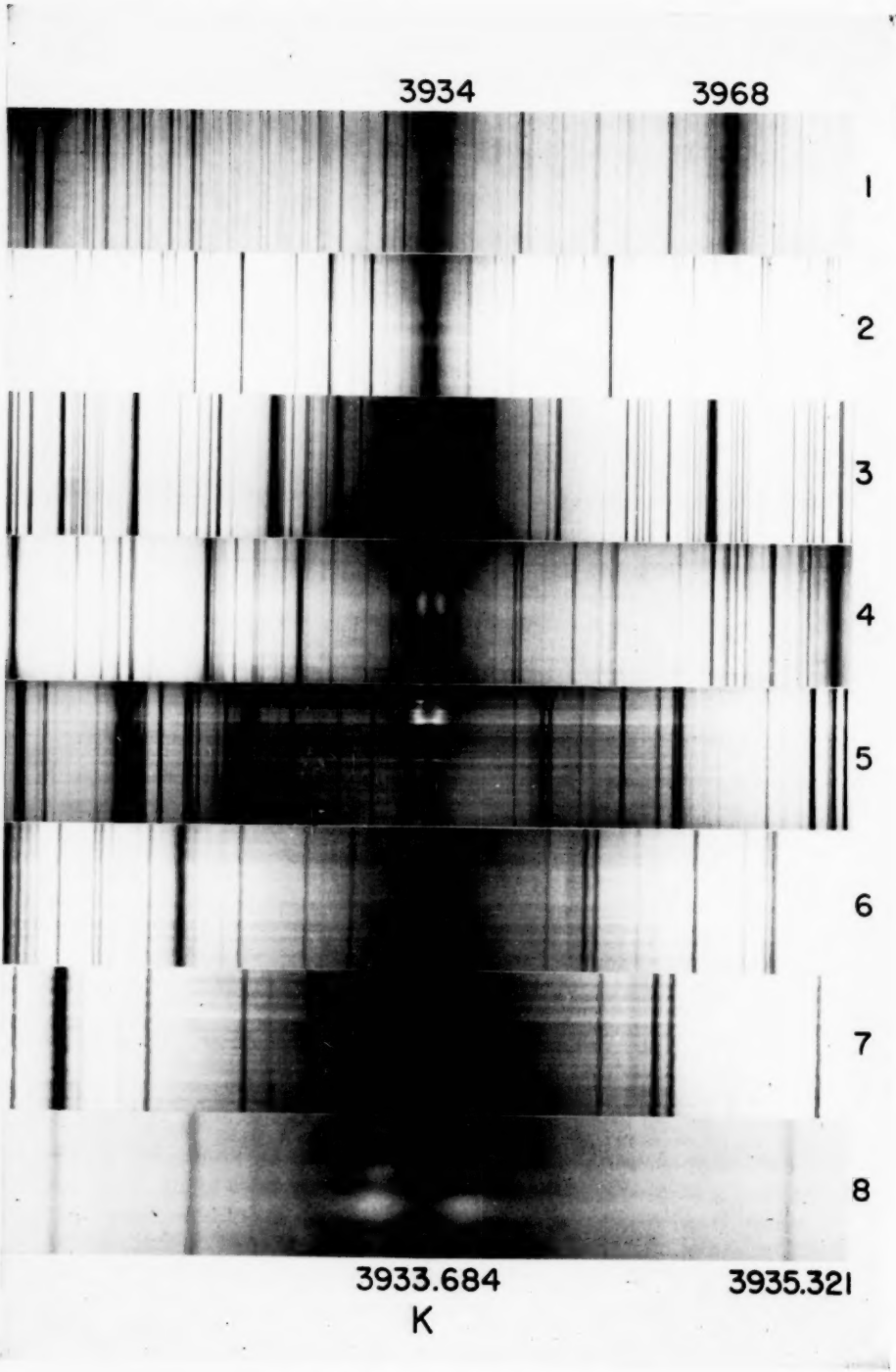

FIG. 2.—*Continued on opposite page*

vals of 1.2 A on either side of the principal line. The total ghost intensity is about 1.8 per cent in the fifth order; the remainder of the scattered light comes from the tails of the instrumental profile.

Since the grating is normally employed in the fourth and higher orders, more than ordinary precautions must be taken to eliminate contamination of the spectrum by overlapping orders. The band width and central wave length of the radiation admitted to the spectrograph are controlled by a small prism monochromator which precedes the main instrument. The dispersing element of the monochromator is a 30° prism of calcium fluoride, which, together with imaging mirrors of 24 inches in focal length, forms a spectrum about 8 mm long from Hα to K on the entrance slit of the grating spectrograph. Since the dispersion at λ 5000 is about 380 A/mm and the entrance slit is normally about 0.1 mm in width, the band width at this wave length is about 38 A. The grating is employed at relatively large angles of incidence, and hence the dispersion varies with wave length as well as with order. As the spectrograph is normally employed, the dispersion is in the range between 5 and 25 mm/A.

Figures 1 and 2 illustrate the variation of dispersion with order for the Hα and K lines. Irregularities in the structures of these lines are apparent in even the first and second orders. However, as the dispersion is increased to about 5 mm/A and greater, the cores of both lines are seen to be composed of large numbers of relatively small elements, varying in width and intensity. At about the same dispersion (5 mm/A), the metallic lines of intermediate to weak intensity also begin to reveal structure. In Figure 1, the iron line at λ 6569.22 (near the extreme right edge of the fourth-order strip) shows pronounced irregularities in the fourth-order spectrum, which are much less evident in the third order. Similarly, in Figure 2, the jagged nature of the iron line λ 3937.34 (near the right-hand edge of the seventh-order strip) is easily visible in the higher orders but is difficult to see in the fourth or lower orders, where the dispersion is much smaller.

THE HYDROGEN LINES

The lines of hydrogen and ionized calcium possess particularly interesting structures, which appear to result from inhomogeneities in temperature and density within the chromosphere. A typical photograph of the Hα line, taken under average seeing conditions, is shown in Figure 3. The photograph was made with the spectrograph slit placed radially to the sun's disk near the north point, with the edge of the sun forming the bottom limit of the spectrum. The fainter lines on either side of Hα are all caused by telluric water vapor. One has the impression that the line core of Hα is composed entirely of separate elements. The average thickness of the smallest line elements is about 5 seconds of arc. The width of the line at half-intensity varies from a minimum of $1\frac{1}{2}$ to a maximum of $1\frac{3}{4}$ A. The shifts of the line center range within ±0.2 A, the average being about 0.01 A, or 0.6 km/sec. Preliminary measurements of the intensity fluctuations in the line center indicate that the range is from 3 to 6 per cent in units of the central-disk continuous spectrum. At the edges of the line core, the intensity fluctuations are much greater and are sometimes as high as 15 per cent. On the average, the central intensities

FIG. 2.—The region of the K line in the solar spectrum

Order	Exposure (Seconds)	Slit (μ)	Plate Dispersion (mm/A)	Order	Exposure (Seconds)	Slit (μ)	Plate Dispersion (mm/A)
I	15	125	0.92	V	30	175	5.7
II	30	125	1.89	VI	30	175	7.9
III	30	125	2.95	VII	20	175	11.6
IV	30	175	4.18	VIII	360	225	23.2

of the wide elements are greater than those of the narrow ones. Near the edge of the sun, the elements widen markedly and merge smoothly into the chromospheric emission bulge. The streaked pattern of the line persists to within about 5 seconds of arc from the sun's edge.

Microdensitometer tracings of the streaks show the large variations in the width of the Hα line very clearly, and frequently the line profiles are noticeably asymmetrical. None of the tracings, either from photographic plates or from direct photoelectric recording, has confirmed the small structure near the center of the Hα line reported previously (Pierce 1954). It is probable that the feature actually results from imperfect elimination of overlapping grating spectra.

The dark detail in the center of the spectrum in Figure 3 marks the position of a small dark filament of the type observed on spectroheliograms. The redward extensions of the Hα line in the filament show that it was moving toward the sun's surface, into a bright point that appears as a light streak in the line center. The line-of-sight velocity of the dark filament is approximately 15 km/sec. The observed motions in dark filaments are sometimes very large. Figure 4 shows the Hα line shift of a small filament, apparently a high-speed dark flocculus, moving with an average velocity of approach of 260 km/sec. The internal motions within this filament are also large and complicated. Velocities of this size are not common on the sun, being found only in the more active prominences or filaments.

Photographs have also been made of the second, third, and fourth members of the Balmer series. The structure of the Hβ line is essentially identical with that of Hα, but the Hδ line (see Fig. 5) differs significantly in appearance. The general line structure is similar to that in Hα and Hβ, but the elements are fewer in number, and a relatively homogeneous, diffuse line core can also be seen.

THE K LINE

The structure in the K line of Ca II (Fig. 6) is similar to that in Hα, although, unlike Hα, the K line exhibits the well-known double reversal at its center, which is apparent even on spectrograms of relatively low resolving power. The smallest line elements or striations in the K line are 3–5 seconds of arc in thickness, as they are for hydrogen. Both the central absorption and the emission flanks of the line core show pronounced variations in intensity. In general, the violet side of the K_2 emission is brighter than the redward component. It is interesting to note that when a quiescent prominence is seen in projection on the disk, it appears to absorb radiation only from the central K_3 component of the line, as shown in Figure 6, about 2–3 minutes of arc from the limb. The absorption from the prominences is confined to such a narrow wave-length band in the K line that a resolving power of 100000 or more must be used to show them clearly as filaments in K-line disk spectroheliograms.

A solar flare makes a striking picture when its spectrum is photographed at the K line of calcium. Figure 7 refers to the postmaximum spectrum of a small flare of July 1, 1955, 15^h45^m U.T. The edge of the sun is at the bottom. The flare emission, which is located about 2 minutes of arc from the limb, is clearly asymmetrical. It is noteworthy that the bright plage region, about 4.5 minutes of arc from the limb, shows strong continuous emission that extends all the way across the photograph, whereas the flare, which is much brighter than the plage near the line center, has much less intense continuous emission. Just below the plage, a dark streak indicates the position of a filament on the disk. The streaks near the top of the spectrum, close to the edge of the sun, tend to assume the curvature of the emission bump caused by the solar chromosphere. The same effect is shown in the Hα photographs and appears to be due to the decrease with height of the tangential optical depth.

Figure 8 shows the complicated spectrum of an eruptive prominence of simple spike-shaped form. The prominence evidently consists of a number of smaller clouds moving

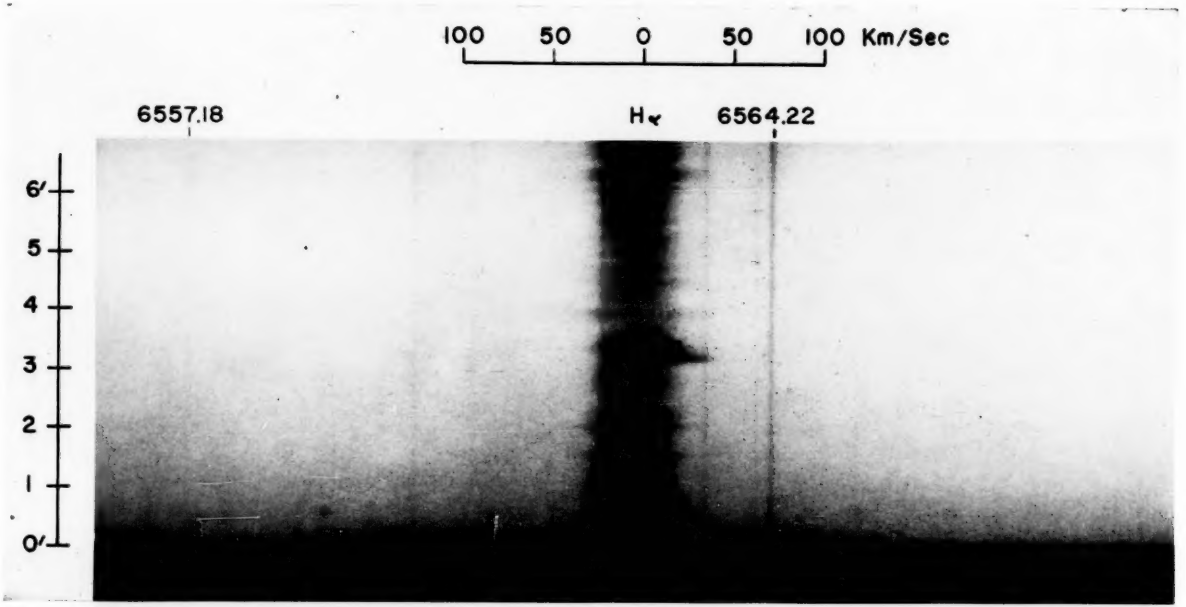

FIG. 3.—Hα line in solar spectrum. August 3, 1955. II-F plate. Exposure 40 seconds; slit 125 μ; fourth order. Near north limb. Limb at bottom

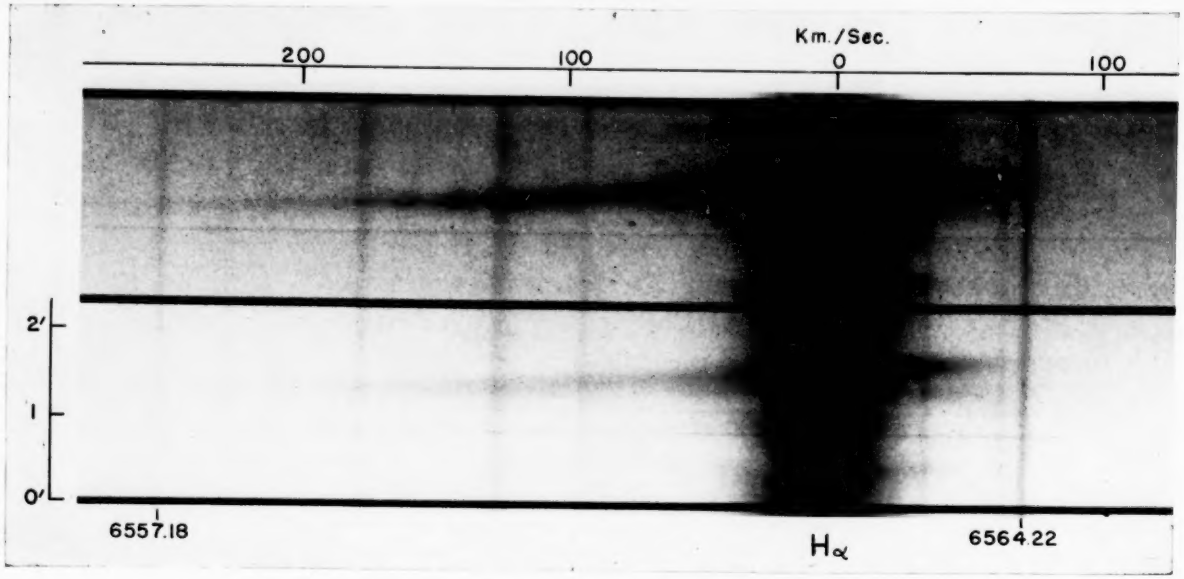

FIG. 4.—High-speed dark flocculus in Hα, July 11, 1955, 16:50 U.T. I-F (3) plate, 10-second exposure

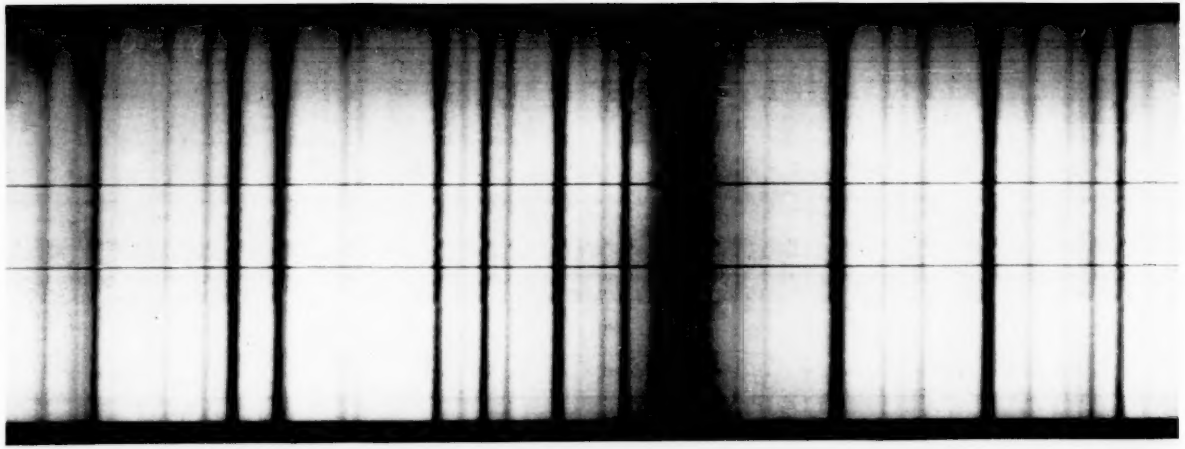

FIG. 5.—The Hδ line in the solar spectrum, October, 1955, $09^{d}15^{h}40^{m}$, center of disk. The separation of the two wires running parallel to the dispersion near the center of the spectrum is about 135 seconds of arc.

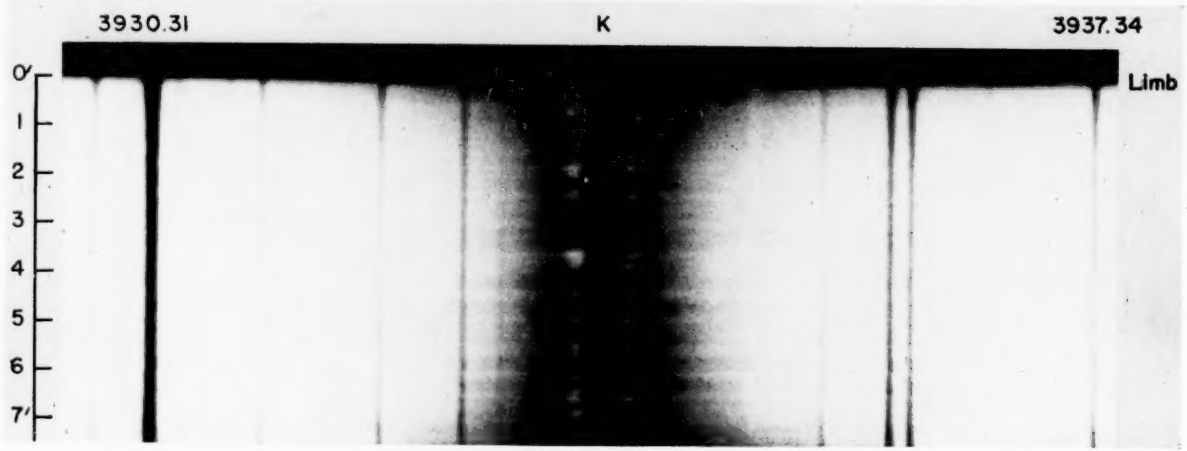

FIG. 6.—Dark filament in K line of calcium. July 26, 1955, 14:15 U.T. II-F plate. Exposure 8 minutes; slit 125 μ; seventh order. Limb at top of plate.

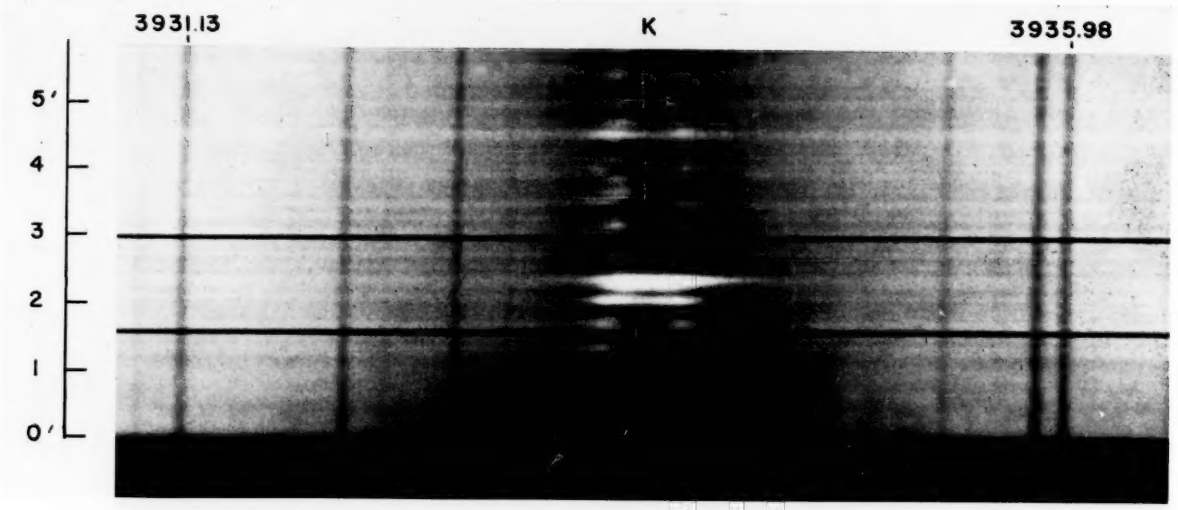

FIG. 7.—Postmaximum of a small flare—K line of calcium. July 1, 1955, 15:45 U.T. Limb at bottom

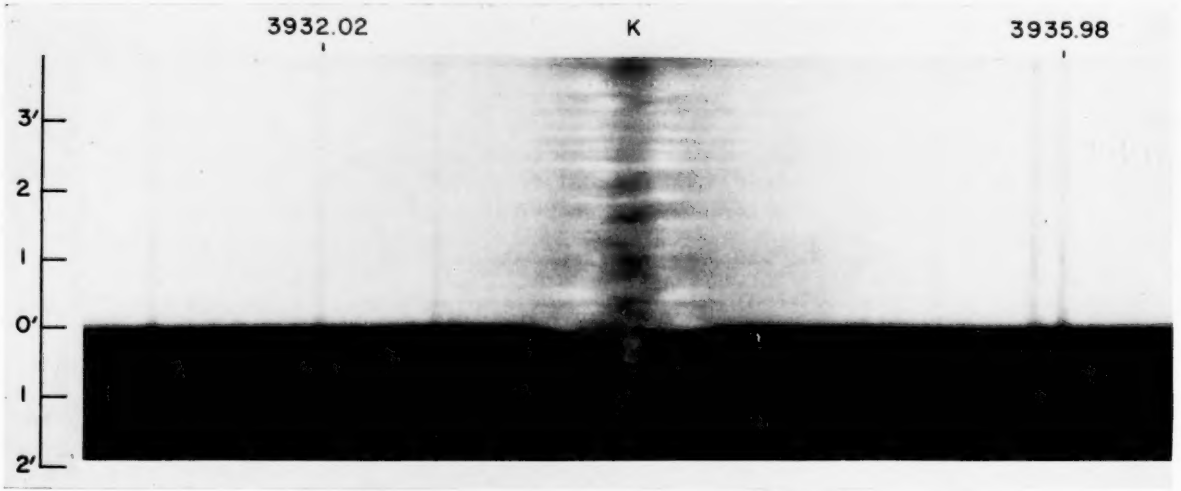

FIG. 8.—Eruptive prominence. K line of calcium. August 3, 1955, 14:05 U.T. Southeast limb at bottom. Royal Pan film, 5-minute exposure, slit 175 μ.

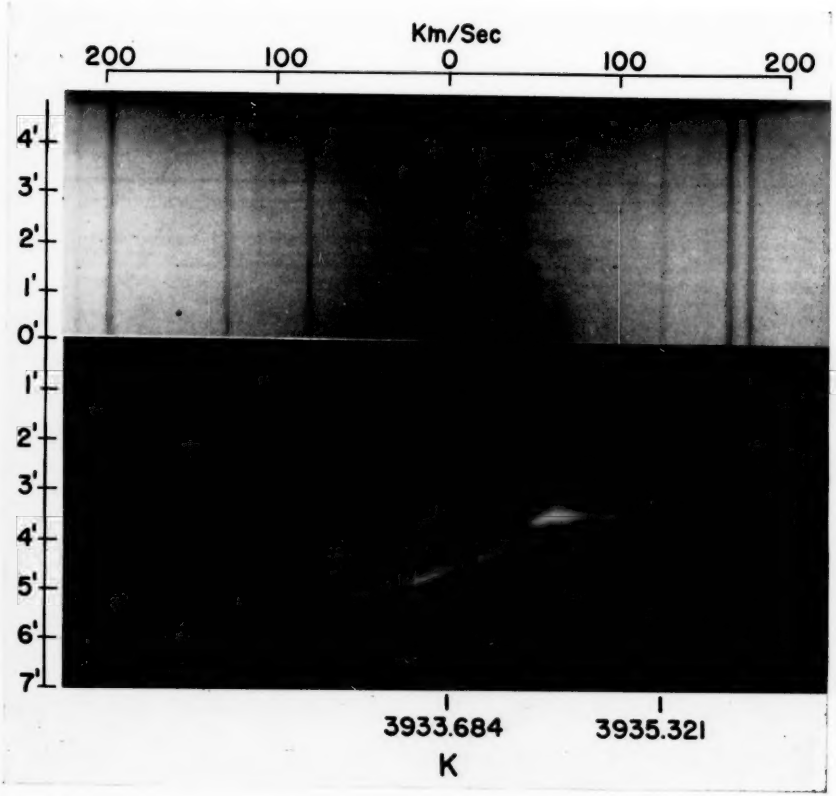

FIG. 9.—Eruptive prominence in K line of Ca^+. August 2, 1955, 14:00 U.T. Southeast limb. Royal Pan film, exposure 5 minutes; slit 175 μ. Limb spectrum of K line at top.

in different directions and with complicated internal velocity patterns. The upper portion of the prominence evidently has larger internal motions than the lower. Another eruptive prominence (see Fig. 9), much more complicated in form and much larger in size than the spike-shaped object of Figure 8, displays an almost unrecognizably distorted K line. The total spread in velocity is from −92 to +140 km/sec, which is comparable to that in two other eruptive prominences observed so far with the vacuum spectrograph.

METALLIC LINES

The lines of elements other than hydrogen, helium, and ionized calcium also exhibit interesting structures. Even on days when the seeing is less than average, the velocity fluctuations impart a characteristic zigzag appearance to all lines, both strong and weak. In addition, when the seeing is better than average, all the lines show intensity fluctuations that give the lines the appearance of being broken up into a series of elements with more or less random Doppler displacements. The sizes of the smallest elements are about 2 seconds of arc and would presumably be even smaller under better seeing conditions. The intensity and velocity fluctuations are well shown by the sodium D lines. The shorter-wave-length line, D_2, at λ 5889, is badly blended with water vapor, but D_1 at λ 5896 is almost completely free from blends. The appearance of the latter line is illustrated in Figure 10. In many respects the structure is similar to that of the hydrogen and calcium lines. The line elements have roughly the same thickness as those in hydrogen and calcium, and their velocity displacements are nearly all less than 1 km/sec. The sodium lines show, more clearly than the stronger hydrogen and calcium lines, a tendency for some of the streaks to appear inclined to the direction of dispersion. If the inclination is real and not caused by the blurring together of adjacent horizontal elements by imperfect seeing, it would imply the existence of rotating gas masses in the atmosphere. The intensity variations at the line center are generally less than 3 per cent of the continuous background, but, since the average central intensity is only 6 per cent (Shane 1941), the variations in residual intensity are relatively large and must be taken into account in theoretical discussions of the central intensity. In strip *A*, Figure 10, the center is divided by a bright band separating an exposure of 30 seconds (*top*) from one of 15 seconds (*bottom*). The dark streaks are from dust and bubbles in the quartz field lens, which acts also as an entrance window.

If the intensity fluctuations in the metallic lines are caused by temperature fluctuations in the photosphere, it might be expected that lines of neutral and ionized elements would behave differently. Figure 11 shows the spectrum of four lines of neutral iron, magnesium, and nickel, together with one line of ionized iron near λ 5168. In general, the velocity shifts and intensity fluctuations in the various lines are closely correlated, but over the normal disk the intensity variations in the ionized iron line are appreciably less than those in the neutral lines. Near the edge of the sun (*top of spectrum*, Fig. 11) a small, bright facula appears as a bright streak in the continuous spectrum. In the facular region the higher temperature apparently causes the neutral lines to fade, while the ionized iron line enhances conspicuously.

The appearance of the same group of lines over an active plage region associated with a group of newly formed sunspots near the center of the disk is shown in Figure 12. It can be seen that the behavior of all five lines in this region is quite similar, apart from very small differences between the ionized iron line and the neutral lines. All the lines show a large-scale violet shift of 1.0 km/sec in the spot region in the center of the spectrum. Shifts of this kind have been observed in other spot groups and indicate a general upwelling of material in these areas.

Sunspot regions are the seats of two additional kinds of line shifts which are well shown at high dispersion, namely, those caused by the Evershed and Zeeman effects. Figure 13 shows a group of chromium lines near λ 5298, photographed with the slit of

the spectrograph crossing a large sunspot. The image of the spot umbra appears in the plate as a thick, dark line running parallel to the direction of dispersion. The gray strips that border the umbra are caused by the spot penumbra, and just on the edges of the penumbra are thin bright streaks, which are formed where the image of a bright ring surrounding the penumbra intersected the spectrograph slit. At the time of observation, the spot was 63° east of the central meridian of the sun, at 26° north latitude. The slit of the spectrograph was nearly radial to the edge of the sun's image. The Evershed shifts of the spectrum lines in the spot are indicated schematically in the drawing above the photograph. The shifts increase to a maximum of 4 km sec at the edge of the penumbra, but there the increase stops abruptly, and immediately outside the penumbra the line quickly returns to its normal position.

DOPPLER SHIFTS IN METALLIC LINES

Measurements of Doppler shifts in metallic lines were first made by Richardson and Schwarzschild (1950) on a group of three neutral iron lines at λ 6300 photographed with lower resolution and dispersion than that of the vacuum spectrograph. From these measurements, a root-mean-square velocity of 0.37 km sec was obtained, which was interpreted as the velocity appropriate to relatively large photospheric granules 2 seconds of arc in diameter. Richardson and Schwarzschild also suggested that the larger values of 2–3 km sec obtained from the curve of growth and from line profiles could be attributed to much smaller turbulent elements of diameter, smaller than the thickness of the layer in which the lines are formed. Plaskett's (1954) measurements on five lines of iron and one of nickel at λ 5900 are in good agreement with those of Richardson and Schwarzschild. Plaskett interprets the velocity shifts as originating in large-scale, organized motions in a roughly isothermal region that lies above the granulation and in which the absorption lines are formed. Thiessen (1955) argues that the Doppler shifts do refer directly to motions in the granules and that when the observations of Richardson and Schwarzschild are corrected for scattered light, the root-mean-square velocity is increased to 1.85 km sec.

The improved resolution of the vacuum spectrograph should permit the measurement of Doppler shifts with greater accuracy than has been possible heretofore. Preliminary measurements of the displacements have been made on two excellent spectrograms, one containing the ionized barium line λ 5853 and the other the chromium line λ 4626. The measurements were made with a "dot" reticle on a two-co-ordinate measuring engine under rather low power. The vertical travel along the line was made in steps of $\frac{1}{20}$ mm (0.70 second of arc) for the full 50-mm line length. Settings were made by centering the small dot appearing in the field of view on the core of the line, which, in the case of the two lines measured, appeared very sinuous but well defined in most positions. Histograms have been prepared from the observed velocity displacements for the intervals 0–2, 2–4, 4–6, and 6–8 minutes of arc from the limb. A second exposure on the same plate covers 4 minutes of arc on either side of the center of the sun's disk.

The histograms approximate a normal distribution for which a random turbulent velocity can be found for each of the 2 minutes of arc intervals from the limb and for the 4 minutes of arc interval on either side of center of the disk. Values of $\xi = (\sqrt{2})\sigma_v$ for the two lines are plotted as a function of position on the disk in Figure 14. The apparent increase in dispersion of the velocities to the limbward, visible to the eye on the plate, is confirmed by the measures, but the results are as yet too rough to establish any law for this variation.

The ξ's obtained for Cr λ 4626 are 60 per cent larger than those of Ba^+ λ 5853. This difference is as yet unexplained. Both lines appear to the same height in the flash spectrum. The chromium line arises from a 0.96–3.63-volt transition and the ionized barium line from a 0.60–2.71-volt transition. The increase in dispersion to limbward suggests either an increasing velocity dispersion with height in the sun's atmosphere or possibly

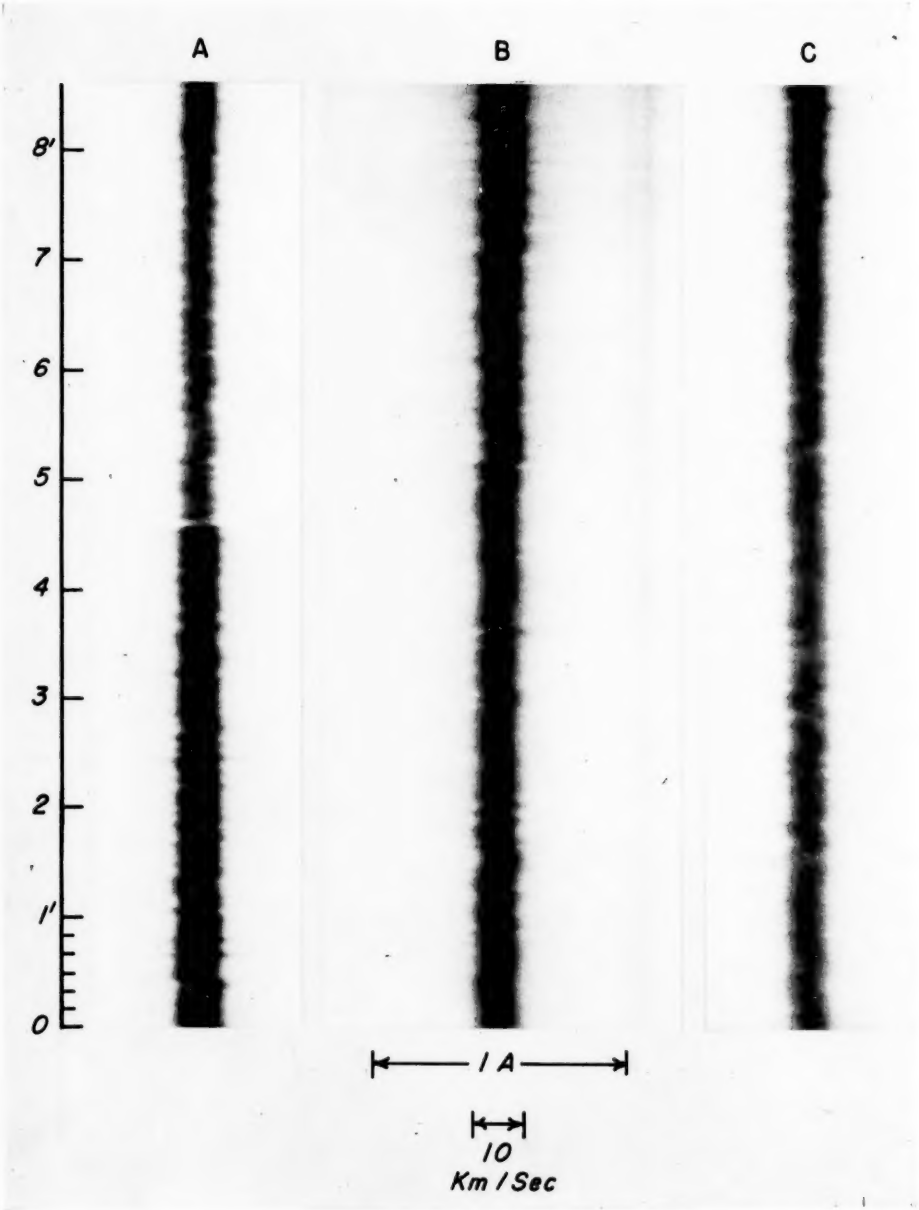

FIG. 10.—D_1 line of sodium at the center of the sun's disk. Royal Pan film. Slit 125 μ; fifth order. *A*: July 30, 1955, 14:15; exposure 15 and 30 seconds; seeing 2–3. *B*: September 28, 1955, 12:55; exposure 45 seconds; seeing 3. *C*: October 4, 1955, 14:40; exposure 7 minutes; seeing 2.

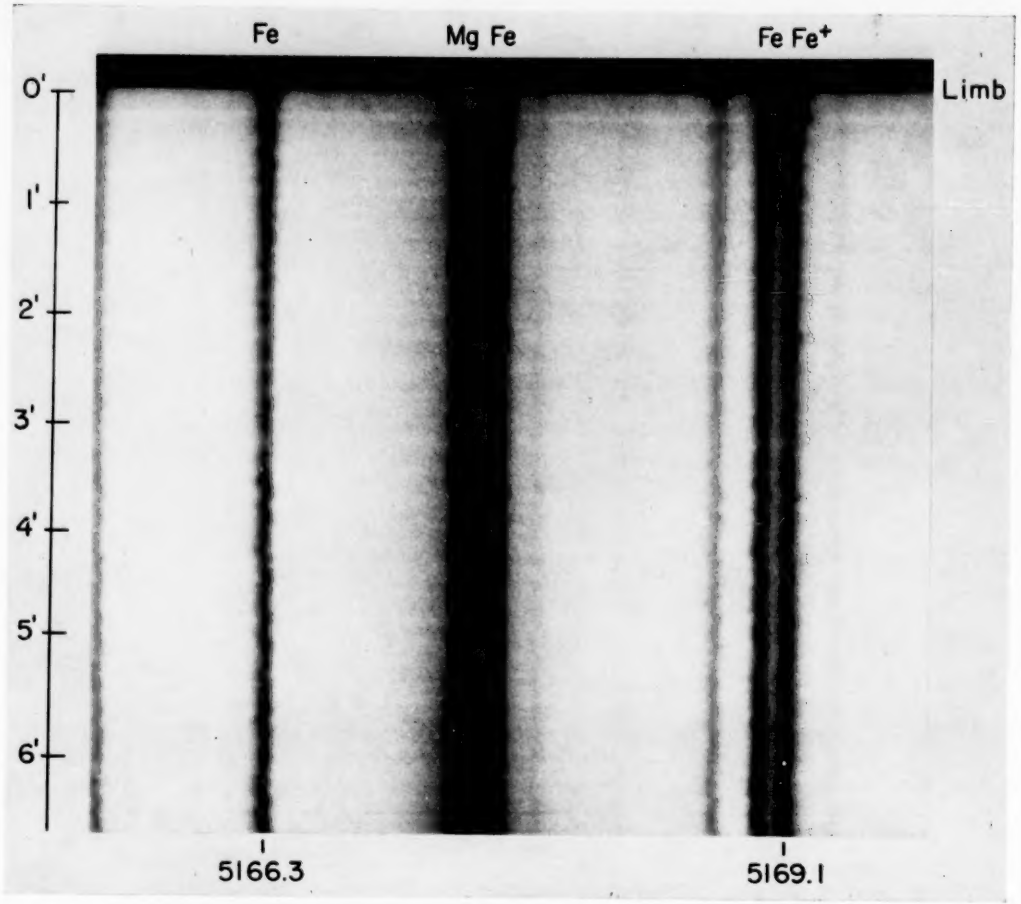

FIG. 11.—Spectrum of a facular area on the northwest limb of the sun. July 22, 1955. Royal Pan film, exposure 30 seconds; seeing 3–4; fifth order. Developed D19, 5 minutes. Note the great enhancement of the Fe^{+} line λ 5169 in the facula.

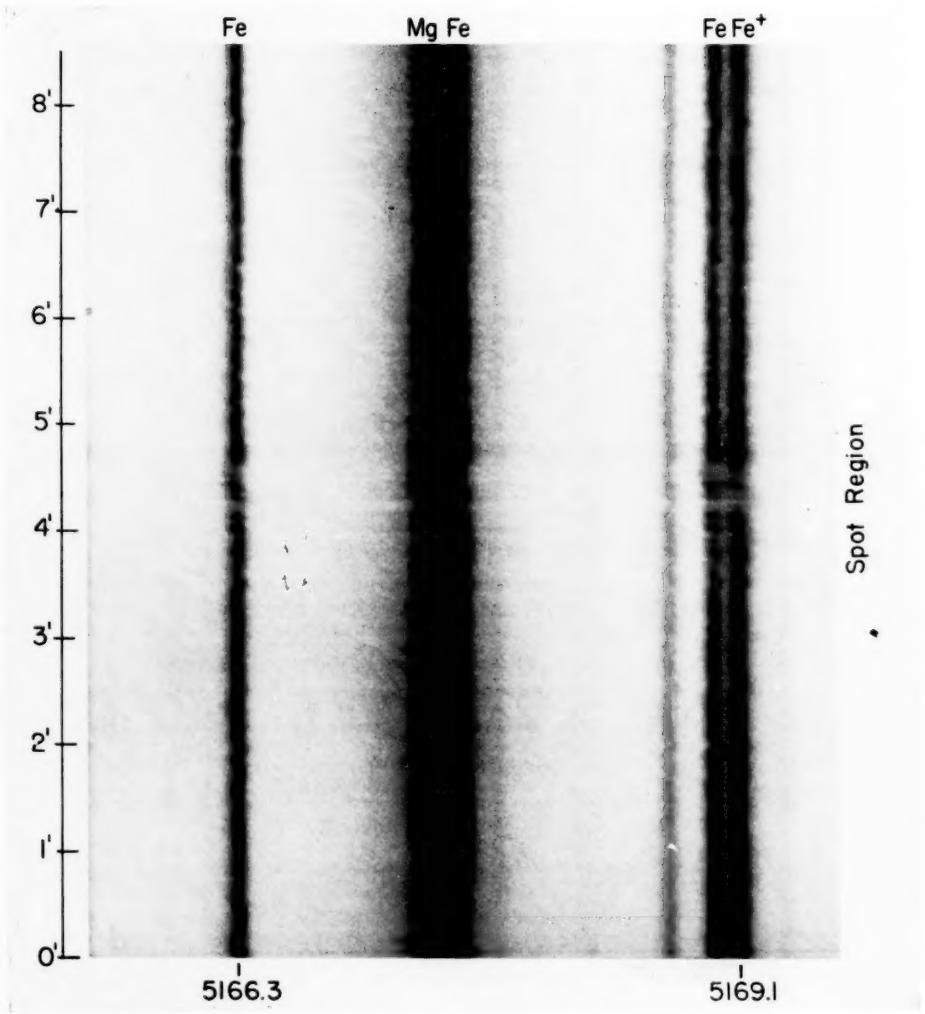

FIG. 12.—Spectrum in the region of magnesium b_2, taken between a group of very small spots which later developed into a larger, bipolar group. August 24, 1955, 12:59 U.T. Seeing 1–2. Royal Pan film, exposure 20 seconds; slit 125 μ; fifth order. Note the general displacement to the violet in the spot region, indicating an upwelling of gases here.

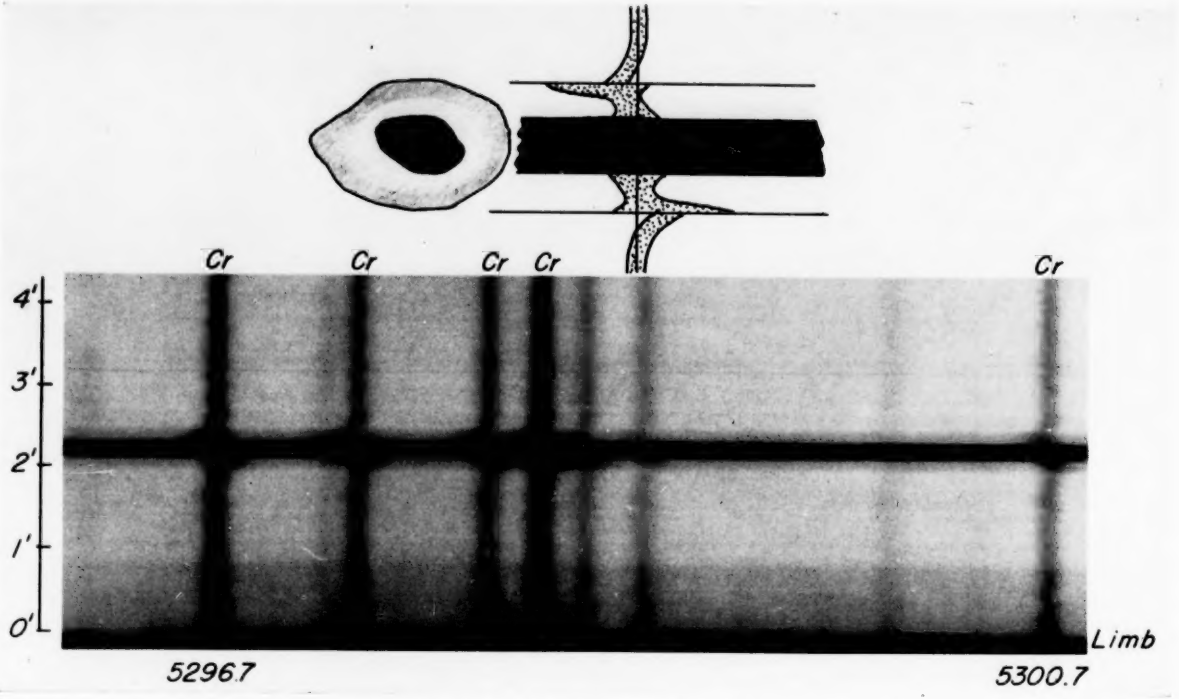

FIG. 13.—Spot spectra showing Evershed effect, September 2, 1955, 1210 U.T. Royal Pan Film, 20-second exposure; slits 125 μ; fifth order; seeing 3–4.

a nonisotropic velocity field, in which the tangential velocities are greater than those in the radial direction (Allen 1949). A more critical test will be obtained from detailed measurements on lines with different excitation potentials of the same element.

THE STRUCTURE OF THE CHROMOSPHERE

The appearance of the lines of hydrogen and ionized calcium near the limb furnishes convincing evidence that the structures in the cores of these lines are of chromospheric origin. Figures 3 and 6 illustrate the appearance of the Hα and K lines, respectively, when the slit of the spectrograph is placed radially to the limb. As the limb is approached, the line cores widen and merge smoothly with the chromospheric emission bulge. This behavior, coupled with the similarity in intensity between the line on the disk and that in the chromospheric bulge, makes it seem certain that the line structure seen on the disk arises entirely from the chromosphere.

If we accept the chromospheric origin of the cores of the hydrogen and calcium lines, their study can contribute answers to many important questions of chromospheric

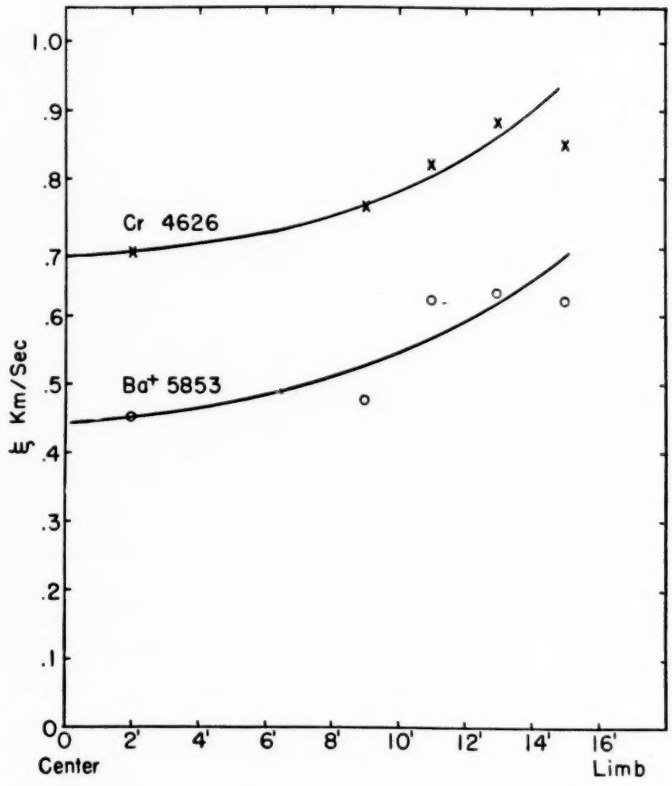

FIG. 14.—The root-mean-square space velocity, ζ, in kilometers per second measured for the lines Cr λ 4626 and Ba^+ λ 5853 at different points on the solar disk.

structure, which in the recent past have been approached almost entirely through observation and analysis of the limb spectrum both in and out of eclipse. In particular, the observation of the chromosphere against the disk eliminates the troublesome integration along the tangential line of sight which is unavoidable in limb observations and which can mask many important features of the chromospheric structure. Even in advance of the detailed measurement and analysis of the hydrogen and calcium line profiles, it is possible to draw from the photographs certain qualitative conclusions bearing on the question of temperature and density fluctuations in the chromosphere.

One of the most puzzling anomalies of the chromospheric flash spectrum is the presence side by side of low-excitation metallic lines and very high-excitation lines of neutral and ionized helium. As pointed out by Menzel (1931), the ionization temperature required by the metallic lines is in the neighborhood of 5000°, but that demanded by the helium lines is closer to 20000°. Other lines of evidence leading to conflicting temperature values have been summarized by van de Hulst (1953). A possible path out of the difficulty was indicated by Giovanelli (1949) in a suggestion that the chromosphere might consist of alternate hot and cool gas columns, and this idea received further support in the interpretation by Hagen (1954) of his center-limb observations of the radio-frequency emission at wave length 1 cm.

Recently nonuniform models identifying the hot and cool zones with the so-called spicules and the regions in between have been proposed by Woltjer (1954) and by Athay and Menzel (1956). The Woltjer and Athay-Menzel models differ in important respects. In the former model, which was derived from a photometric investigation of Hα filter photographs, the spicules are identified as regions of relatively high temperature and high density, in which most of the Balmer emission and presumably all the helium emission originates. In the latter model, which is based upon the analysis of continuum and helium line intensities in the flash spectrum, the spicules are regions of relatively low temperature and high density. The hydrogen emission comes entirely from the cool spicules; on the other hand, the helium emission comes from the "interspicular" regions at heights below 4000 km and from the spicules themselves at greater heights.

Before commenting upon the relationship between the structures of the Fraunhofer line cores and the chromosphere, we wish to point out that the use of the term "spicule" to denote the general filamentary structure of the chromosphere may be somewhat misleading. The term was introduced by Roberts (1945) to describe specifically the small spikelike structures that could be seen protruding radially from the lower 4000–5000-km layer of the chromosphere near the poles and which were frequently observed in rapid motion outward from the sun. A review of solar literature shows that for many decades the term "jet" has been used to describe both the fundamental, fringelike structure of the chromosphere and the larger spikelike members that extend beyond the average level. It appears premature, however, to employ either "spicule" or "jet" to designate features of the chromosphere observed on the disk. Instead, we shall simply refer to "hot" and "cool" regions and defer to the future the question of their possible identification with either jets or spicules.

Clues to the possible origin of the various features of the hydrogen and calcium line structures can be derived from an intercomparison of the detailed structures in the disk lines Hα, K, and 10830 of He I. Only very few of these comparisons have been made as yet, and therefore the conclusions we draw from them are very tentative and subject to modification after further observations are secured during the next observing season. Photographs of the helium line with the vacuum spectrograph confirm the intensity fluctuations previously demonstrated by spectroheliograms by L. and M. d'Azambuja (1938) and from observations with a PbS cell by Mohler (1952). According to Mohler and Goldberg (1956), the half-width of the line is nearly 1 A, which is in accord with its origin in high-temperature zones. Inasmuch as both the K_2 emission and the absorption in the 10830 lines are enhanced over the plages (Mohler 1952), we conclude tentatively

that the emission wings of the K-line core are formed in the hot regions of the chromosphere, although probably at lower levels than the helium line. This conclusion, which is based on the assumption that the correlation between K_2 emission and 10830 absorption holds over undisturbed regions of the chromosphere as well as in plages, seems reasonable but must be checked by observation. As a corollary, we suppose that the central absorption reversal in the K line (K_3) results from the passage of radiation from the hot regions through the cooler regions. The exact geometry of the hot and cool regions is not clear as yet, but the patchy character of the K_2 and helium emissions appears to require that the hot regions be discrete rather than continuous in form, and the invariable presence of the K_3 absorption requires that the cool regions lie both between and above the hot regions.

An interesting feature of the K_2 emission is its asymmetry, in the sense that the violet component is almost always brighter than the red component. This asymmetry was noted by Jewell (1896) but appears to have been overlooked in recent years. St. John's (1910) wave-length measurements on the K_3 absorption and K_2 emission led him to conclude that the former were consistent with descending motion at a mean velocity of about 1 km/sec, whereas the latter implied a mean upward velocity of about 2 km/sec. St. John's results suggest that the asymmetry of the K_2 profile may be due to differential radial motion between hot and cool regions, the hot regions rising and the cool regions falling. Unfortunately, although the measured displacements at the center of the disk are of about the right order of magnitude to account for the intensity asymmetry, St. John's explanation in terms of radial motion is ruled out by the persistence of the asymmetry right up to the limb. It is tempting to speculate instead that the asymmetry results from the expansion of hot clouds, optically thick in the K line, as they move up from the photosphere into a cooler surrounding medium. This question can probably be settled by precise wave-length measurements referred to an absolute standard instead of to the neighboring weaker Fraunhofer lines employed by St. John.

Photographs of the Hα and K lines have been made a few minutes apart and with special precautions taken to maintain the spectrograph slit over the same region of the disk, for the purpose of correlating the structures in the two lines. Microphotometer tracings made parallel to the lengths of the two lines and away from the line center show an inverse correlation between the intensities in the two lines. Hence the wide, dark features in Hα coincide with the bright K_2 features, from which we conclude that at least the extremities of the broad absorption features in Hα originate in the hot regions of the chromosphere. The correspondence between Hα and K_2 is in excellent agreement with the spectroheliographic results of d'Azambuja (1930), who, in agreement with many early workers, found that the bright features observed in K_{232} spectroheliograms matched almost exactly the dark features in Hα spectroheliograms obtained with the second slit displaced about 0.5 A from the line center. It is interesting to note that essentially the same regions of the chromosphere produce emission in the K line but absorption in Hα. The explanation seems to be that, as long as the optical depth anywhere in a chromospheric line is greater than zero, it will appear in emission if its source function is greater than the residual intensity in the underlying photospheric line and in absorption if the converse is true. The residual intensity near the center of the photospheric K line is apparently smaller than the K_2 emission source function, but at least for distances greater than 0.3 A from the center of Hα the situation appears to be reversed.

The question now arises as to whether the apparent absence of a double reversal in the centers of the first members of the Balmer series implies the absence of cool-region emission in these lines. We remark, first of all, that even if the profiles of all intense chromospheric emission lines exhibited central self-reversals, it does not necessarily follow that all strong Fraunhofer lines should appear doubly reversed, as does the K line. The effect would be most conspicuous when the intensity of the emission profile is

large compared with the residual intensity in the photospheric absorption line and when the width of the chromospheric line is small compared with that of the photospheric line. These conditions are realized in the K line, for which the photospheric profile is enormously wide and essentially flat-bottomed. The situation in Hα is quite the opposite, however, since the low atomic weight of hydrogen produces a much broader chromospheric emission profile, comparable in width with that of the photospheric absorption line. Further, as pointed out in the preceding paragraph, the effect of the chromosphere is not to fill in the edges of the photospheric line core with emission but rather to increase the absorption. Hence the double reversal could not appear, except near the limb, where darkening would enhance the intensity of the chromospheric line relative to the residual intensity of the photospheric line.

We conclude that the absence of obvious double reversals in the center of Hα does not preclude the presence of significant emission contributions from the cool regions, and we consider next the positive evidence favoring the existence of such emission. First, microdensitometer tracings taken across the chromospheric bulge in Hα show centrally reversed profiles, the separation between the emission maxima amounting to about 1.6 A. A double reversal begins to become apparent about 2 seconds of arc inside the limb, and the central dip in the emission profile disappears about 4 seconds of arc outside the limb. The apparent doubling of Hα in the low chromosphere has been well known to solar observers for many years. In their classic paper, "The Flash Spectrum without an Eclipse," Adams and Burwell (1915) observe that not only Hα and Hβ but essentially all the stronger lines in the low chromosphere are "double reversals," and they conclude that "double reversal is a universal characteristic of all lines in the chromospheric spectrum at a low level." It has been argued (de Jager 1952) that the effect is due to the influence of scattered light, which is undoubtedly true in part, but the explanation of the entire effect on the basis of scattered light is unconvincing, especially since the double reversal in the K line cannot be so explained. Additional evidence favoring the double reversal of strong lines in the low chromosphere is suggested by the appearance of the profiles of strong Fraunhofer lines, as seen, for example, in the Utrecht *Atlas*. It is characteristic of virtually all very strong lines, e.g., λ 4383 of Fe I and λ 5173 of Mg I, that they possess relatively sharp central cores, 0.3–0.4 A in width, which are connected to the outer parts of the profiles by rather sharply defined shoulders. It is tempting to suggest that the cores of these strong Fraunhofer lines result from the superposition on the photospheric lines of a centrally reversed chromospheric profile similar to that exhibited by the K line. The shoulders in the observed line cores would then arise from the filling-in of the photospheric line with emission from the hot chromosphere.

If the cores of the strong Fraunhofer lines are formed in the chromosphere, one might expect that the pattern of intensity and velocity fluctuations in these lines would be different from those of neighboring weaker lines that are presumed to originate in the photosphere. That this is not the case is shown in Figures 11 and 12, where it is seen that, apart from the small facular area near the limb in Figure 11, the velocity shifts and intensity fluctuations in the magnesium line are rather closely synchronized with those in the neighboring weaker lines of iron, ionized iron, and nickel. The weakest of these lines, for which the velocity and intensity fluctuations are plainly apparent, is Ni λ 5168.7, with a Rowland intensity of 1. If the cores of the medium-strong lines are formed in the photosphere and if their velocity and intensity fluctuations arise in the granules, it is evident that the granule columns extend into the low chromosphere. Further, the excitation and velocity characteristics of the layers in which the cores of lines of Rowland intensity 1 are formed are similar to those in the low chromoshpere. It is still not clear, on this picture, why the neutral and ionized iron lines at λ 5169 (Figs. 11 and 12) apparently strengthen in the same local regions of the normal photosphere and why they also weaken together in the plage region at the center of Figure 12. There also appears to be no obvious correlation between the intensity and velocity fluctuations in

the lines, as might be expected if the hot and cold granules were systematically rising and falling, respectively.

Alternatively, it might be conjectured that the cores of the medium-strong lines originate in the chromosphere. It is interesting to note that Plaskett (1954) found only a very small correlation between granule brightness and velocity shift and suggested that the absorption lines are formed in a roughly isothermal region above the granulation. Whether this region is to be identified with the top of the photosphere or the bottom of the chromosphere can be decided only on the basis of additional observations in which the structures of the hydrogen and ionized calcium lines, on the one hand, are intercompared with those of the weaker metallic lines.

We wish to comment, finally, on the question of the optical depths at the centers of the hydrogen lines, a subject on which there has been a certain amount of controversy which the disk observations may help to resolve. For example, de Jager (1952) calculates that the radial optical depth at the center of Hα reaches unity only at the very bottom of the chromosphere. Thomas (1950) argues that the central Hα optical depth is much higher, and Athay and Thomas (1955) obtain a value in the neighborhood of 100, from analysis of the Balmer emission gradients in flash spectra. The chromospheric model of Böhm-Vitense (1955) also derives a high value, about 40, for the optical depth.

It should be possible, from analysis of photometric line profiles, to determine the optical depths of the hot and cool regions at the centers of the hydrogen and calcium lines. Such a study is under way, but even in advance of its completion it seems possible to state that de Jager's conclusion is probably incorrect. For, if the optical depth at the center of Hα is as small as unity, we should expect the line structure to disappear in the later members of the Balmer series. Referring to the photograph of Hδ in Figure 5, we observe that the structure is still present, although the chromospheric elements are much fewer in number. Since the optical depth at the line center is proportional to the product of the f-value and the wave length, the ratio of the values for Hα and Hδ is about 46. We conclude that the central optical depth in Hα is much greater than unity and may be as high as 50.

In summary, the observations of the Fraunhofer lines of hydrogen and ionized calcium seem to be consistent with a qualitative model of the low chromosphere consisting of relatively hot clouds of gas and with cooler regions both above and between the hot regions. Both the K_2 emission in ionized calcium and the wide absorption features in Hα apparently originate in the hot regions; and, from the appearance of these line features near the limb, it seems that the hot regions contribute a substantial fraction of the hydrogen and ionized calcium emission in the very low chromosphere. This result is in disagreement with the Athay-Menzel (1956) model, in which nearly all the hydrogen emission in the lower 500 km of the chromosphere is assigned to the cold spicules. The fact that the hot regions occupy a substantial fraction of the volume of the very low chromosphere may explain why in the flash spectrum both the emission at the head of the Balmer series and in the H^- and electron-scattering continuum at λ 4700 appear to reach a maximum at about $h = 500$ km (Athay, Menzel, Pecker, and Thomas 1955). The profiles of Hα at the extreme limb and of the K line and other strong metallic lines on the disk favor the conclusion of Adams and Burwell (1915) that central self-reversal is a general characteristic of most strong chromospheric profiles. The similarity between the intensity and velocity fluctuations in the core of the strong magnesium line at λ 5167 and in those of neighboring weaker lines implies either a chromospheric origin for the centers of all medium-strong Fraunhofer lines or the extension of the photospheric granules into the low chromosphere. Finally, we emphasize again the preliminary and tentative nature of the foregoing results.

We are highly indebted to our colleague, Dr. Helen W. Dodson, for numerous valuable discussions of chromospheric problems relevant to this paper, and to Drs. Athay and

Menzel for sending us a copy of their paper in advance of publication. We are also grateful to McGregor Fund of Detroit, to the James Foundation of New York City, and to the Detroit Edison Company for the funds that made possible the construction of the vacuum spectrograph.

REFERENCES

Adams, W. S., and Burwell, C. G. 1915, *Ap. J.*, **41**, 116.
Allen, C. W. 1949, *M.N.*, **109**, 343.
Athay, R. G., and Menzel, D. H. 1956, *Ap. J.*, **123**, 285.
Athay, R. G., Menzel, D. H., Pecker, J. C., and Thomas, R. N. 1955, *Ap. J., Suppl.*, **1**, No. 12, 505.
Athay, R. G., and Thomas, R. N. 1955, *Ap. J., Suppl.*, Vol. **1**, No. 12.
Azambuja, L. d'. 1930, *Ann. Obs. Paris, Meudon*, Vol. **8**, Fasc. II.
Azambuja, L. and M. d'. 1938, *Bull. Astr.*, **11**, 349.
Böhm, K.-H. 1954, *Zs. f. Ap.*, **35**, 179.
Böhm-Vitense, E. 1955, *Zs. f. Ap.*, **36**, 145.
Cittert, P. H. van. 1930, *Zs. f. Phys.*, **65**, 547.
———. 1931, *ibid.*, **69**, 298.
Giovanelli, R. G. 1949, *M.N.*, **109**, 298.
Hagen, J. P. 1954, *J. Geophys. Res.*, **59**, 158.
Hale, G. E., and Ellerman, F. 1903, *Pub. Yerkes Obs.*, **3**, 3.
Hulst, H. C. van de. 1953, *Handbook of the Solar System*, ed. G. P. Kuiper, Vol. **1**, chap. 5.
Jager, C. de. 1952, *Rech. Astr. Obs. Utrecht*, Vol. **13**, Part 1.
———. 1954, *Nature*, **173**, 680.
Jewell, L. E. 1896, *Ap. J.*, **3**, 89.
McMath, R. R. 1956, *Ap. J.*, **123**, 1.
Menzel, D. H. 1931, *Pub. Lick Obs.*, **17**, 283.
Mohler, O. C. 1952, *Ap. J.*, **115**, 323.
Mohler, O. C., and Goldberg, L. 1956, *Ap. J.*, **124**, 13.
Pierce, A. K. 1954, *Ap. J.*, **120**, 233.
———. 1956, to be published.
Plaskett, H. H. 1954, *M.N.*, **114**, 251.
Richardson, R. S., and Schwarzschild, M. 1950, *Ap. J.*, **111**, 351.
Roberts, W. O. 1945, *Ap. J.*, **101**, 136.
St. John, C. E. 1910, *Ap. J.*, **32**, 36.
Shane, C. D. 1941, *Lick Obs. Bull.*, **19**, 119.
Thiessen, G. 1955, *Zs. f. Ap.*, **35**, 237.
Thomas, R. N. 1950, *Ap. J.*, **111**, 165.
Woltjer, L. 1954, *B.A.N.*, **12**, 165.

THE WIDTH OF THE INFRARED HELIUM LINE IN THE SOLAR SPECTRUM*

ORREN C. MOHLER AND LEO GOLDBERG
McMath-Hulbert Observatory, University of Michigan, Pontiac, Michigan
Received February 9, 1956

ABSTRACT

Measurements of intensity and half-width are reported for the Fraunhofer line He I λ 10830. After correction for instrumental broadening and blending, the width at half-intensity, averaged over the center of the disk and the four limbs, is 0.91 A. Within the error of measurement, the line widths show no center-to-limb variation. The line appears to be broadened entirely by the Doppler effect, with $\Delta\lambda_D = 0.55$ A, corresponding to an r.m.s. velocity of about 15 km/sec. If the broadening is entirely thermal, the kinetic temperature is about 50000° K. Although the line is probably formed in localized hot regions of the chromosphere, it is not yet clear whether or not the derived velocity contains a turbulent, as well as a thermal, component.

INTRODUCTION

The Fraunhofer line He I λ 10830, $2^3S-2^3P^0$, is for several reasons a unique feature of the solar spectrum. First, it is the only identified absorption line in the spectrum of the normal disk that appears to originate entirely in the chromosphere. Second, its extremely high excitation potential (19.7 ev) and its origin from a highly metastable energy level make the line an extremely sensitive indicator of local physical conditions. In particular, its variation in intensity from point to point across the solar disk, even in otherwise undisturbed regions, can give information on the temperature fluctuations in the chromosphere, which are not so directly observable in eclipse flash spectra.

Early observations of the 10830 line, following its discovery in the solar spectrum by H. D. and H. W. Babcock (1934), were handicapped by the poor quality of photographic emulsions in the 1 μ region. Even so, a remarkable spectroheliogram by L. and M. d'Azambuja (1938) revealed the fluctuating character of the line intensity over the disk and its enhancement at the limb, in filaments, and in plage regions. More systematic, as well as quantitative, measurements became possible following the perfection of the lead sulphide cell as an energy detector. As a result of observations made in 1951, Mohler (1952) confirmed the qualitative results of the d'Azambujas and also summarized the results of over one hundred preliminary measures of equivalent widths referring to the center and limbs of the undisturbed disk, to plage regions, to filaments, and to flares. The most striking results of this preliminary study were (1) that, while the average equivalent width at the equatorial limbs was greater by a factor of 3 than the average value at the center of the disk, the mean polar limb intensity was only about 50 per cent larger than that at the disk center and (2) that the equivalent width in a large high-speed flocculus associated with the bright flare of May 19, 1951, attained the relatively enormous value of 2420 mA as compared with normal average values of 45 mA at the center of the undisturbed disk and 306 mA in plages.

In view of the possibility that the behavior of the 10830 line may vary with the sunspot cycle, it was considered important to make continuing systematic intensity observations, which now extend over a period of four years, 1951–1954, inclusive. The observations have been made with lead sulphide detectors in conjunction with both the McGregor spectrometer at the McMath-Hulbert Observatory and a similar instrument attached to the Snow telescope at the Mount Wilson Observatory.

* This work was supported in part by Contract N6onr-232-5 with the Office of Naval Research.

Even on early tracings of the infrared solar spectrum, for example, those contained in the McMath-Hulbert *Atlas* (Mohler, Pierce, McMath, and Goldberg 1950), the 10830 line appears much wider than would be expected on the basis of thermal Doppler broadening at a temperature of 6000° K. But limitations in resolving power made it impossible to measure the line width with assurance. Recently, however, the loan of a very good Babcock grating to the Snow telescope project by the Mount Wilson and Palomar Observatories has led to the beginning of measurements of the half-width of the 10830 line. This paper accordingly reports the results of the first series of line-width measurements as well as the outcome of continued intensity measurements since 1951.

OBSERVATIONS

Figure 1 is a photograph of the spectrum of the sun's east limb made with the 75-foot McGregor tower telescope and the 50-foot vacuum spectrograph (McMath 1956) of the McMath-Hulbert Observatory. The slit of the spectrograph was directed along the radius of the solar disk that passed through the east point of the sun's equator. The helium line appears both as an emission spike, extending eight seconds of arc beyond the edge of the disk, and as an absorption line on the disk itself. The line is a blend of two lines whose laboratory wave lengths are 10830.249 and 10830.340 A. The blend can be separated only under unusually favorable conditions. The third component of the triplet, λ 10829.040, is ordinarily perceptible in disk spectra just inside the solar limb as a very feeble dark line and can also be photographed as a faint emission line in the chromosphere. The water-vapor lines at λ 10832.12, and 10834.02 provide convenient wavelength standards for the measurement of the helium line.

The graininess of the I-Z emulsion and the faintness of the line make it difficult to see, except near the limb and over active regions and filaments. Nevertheless, the patchy nature of the intensity distribution over the disk is plainly apparent and is roughly similar in character to that shown by the Balmer lines of hydrogen and the H and K lines of ionized calcium. It has not yet been determined whether there is a detailed correspondence between the features shown by the helium line and those revealed by the hydrogen and calcium lines, but it is probable that the patterns are related. The irregular structure of the helium line appears to be superposed on a much narrower line of uniform intensity, which is not solar in origin and presumably arises from atmospheric water vapor.

The combined equivalent widths of the three helium lines that make up the triplet at λ 10830 have been measured on direct-intensity tracings, made with the lead sulphide cell, at five positions on the solar disk for the last three and one-half years. A typical limb tracing of the spectral region is shown in Figure 2. The annual average values of the equivalent widths for the center of the disk, the north and south polar limbs, and the east and west ends of the solar equator are presented in Table 1. The units are milliangstroms. The mean square error for the annual average values is less than 1 mA, and hence the differences from year to year may be real, but they do not, as yet, show a change with sunspot numbers. It will be necessary to investigate observations obtained during a maximum of sunspots for possible correlation of spot numbers and helium equivalent widths.

The introduction of a Babcock grating into the Snow telescope installation has made possible the measurement of the half-widths of the 10830.25 and 10830.34 blend on recent tracings of high resolving power. The dimensions of the grating are 6×8 inches and the number of rulings approximately 120000. Since the grating is normally used in the second order, its theoretical resolving power is 240000. The observed half-widths, measured directly from tracings made on several dates at the center of the disk and at the north, east, south, and west limbs, are collected in Table 2. The measured half-widths must be corrected both for the blending of the two components of the 10830 line and for the finite resolving power of the spectrograph.

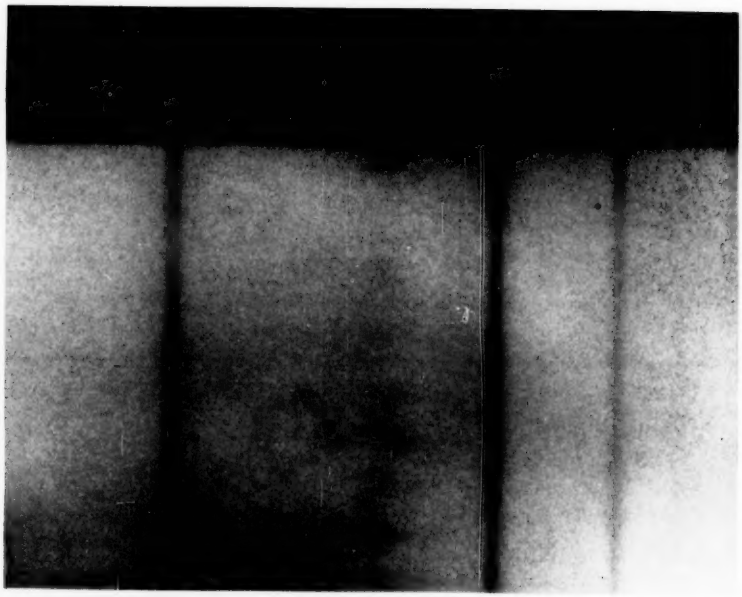

FIG. 1.—Spectrum of the sun's east limb. From left to right the lines are: 10827.14 Si I; 10829.04 He I (weak, visible at limb only); 10830.25, 10830.34 He I; 10832.12 HOH; 10833.47 calcium; 10834.02 HOH; 10836.64 HOH?

The correction for blending is almost negligible, since the separation of the components is small compared with the half-width and the blending increases both the depth and the width of the profile in nearly the same proportion. We investigated the effect of blending upon the half-width by constructing a theoretical blended profile on the assumption that the true profiles of the components could be represented by error functions, with areas in the same ratio as the theoretical intensities, namely, 5:3:1. In Figure 3 the computed profile is compared with an observed individual profile. The agreement is within the experimental error of a single profile, and measurement of the computed

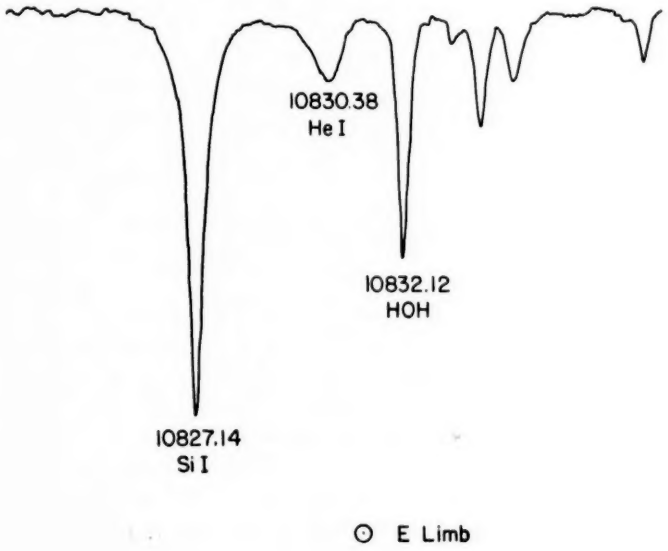

FIG. 2.—A typical limb tracing of the sun's east limb in the 10830 region

profile shows that, if the Doppler width $2\Delta\lambda_D$ is taken as 1.2 A, the blending increases the true half-width by about 25 mA, or about 2.5 per cent.

The finite resolving power was investigated in two ways: first, by the separation of closely spaced spectral lines (see, for example, the *Q*-branch of the 1.27 μ band of atmospheric 0_2 in Fig. 4) and by observation of the emission profile of the λ 13570 line of the isotope Hg^{198} made with the same slit-width as that used for the 10830 observations. From the observed line separations in the oxygen band, the resolving power at 1.3 μ with narrow slit was found to be in excess of 200000. The profile of the Hg^{198} line is shown in Figure 5. Its half-width is very nearly 71 mA, corresponding to a resolving power of about 90000. The instrumental profile is unsymmetrical, but the deviations from sym-

metry probably cannot affect appreciably the 10830 half-widths, which are about fifteen times as great as the instrumental half-width. Inasmuch as the error of measurement appears to be roughly twice the instrumental half-width, it seems hardly necessary at this time to employ the method of Voigt profiles (van de Hulst and Reesinck 1947) in applying the instrumental correction. We have therefore merely subtracted the instrumental half-width from the observed line widths. The total correction to be subtracted, including that due to blending, is 96 mA.

The mean value of the corrected half-width, averaged over the center of the disk and the four limbs, is 914 mA. Within the root-mean-square error of measurement, which is 110 mA, the half-widths, unlike the equivalent widths, do not show a center-to-limb variation.

DISCUSSION

Considering the extremely low pressures in the chromosphere, it is most unlikely that a very weak helium line, especially one arising from an s–p transition, is broadened by anything but random motions. This expectation is confirmed by the Gaussian form of

TABLE 1

ANNUAL AVERAGE VALUES OF EQUIVALENT WIDTHS OF λ 10830, IN MILLIANGSTROMS

	1951	1952	1953	1954
Center	64	71	74	60
North	72	98	96	77
East	140	120	139	119
South	76	91	105	70
West	132	113	162	136

TABLE 2

MEASURED HALF-WIDTHS OF THE λ 10830 LINE OF He I, IN ANGSTROMS

Date	Half-width
Center of disk:	
1953 June 25	1.04
December 12	1.14
	1.33
	0.95
	0.79
Average	1.05
West limb:	
1953 December 12	0.95
	1.04
	1.14
Average	1.04
South limb:	
1953 December 12	0.79
	0.95
	1.10
Average	0.95
East limb:	
1953 December 12	1.24
	0.79
1954 January 27	1.14
	0.90
	0.95
Average	1.00
North limb:	
1953 November 25	1.10
	0.95
December 12	1.01
	0.97
	1.04
Average	1.01

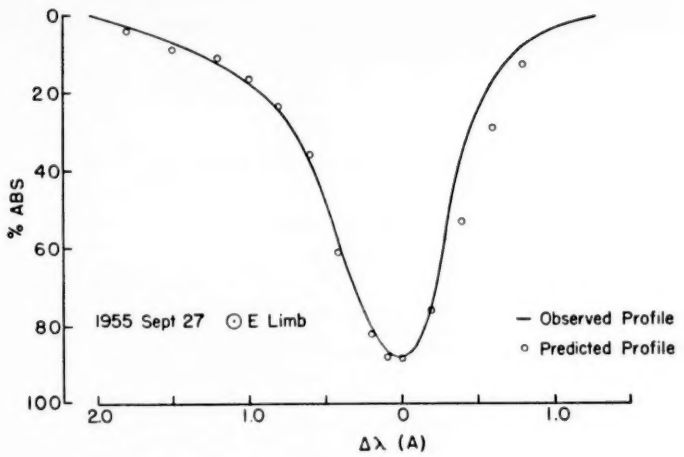

FIG. 3.—Comparison of computed and observed profiles for 10830

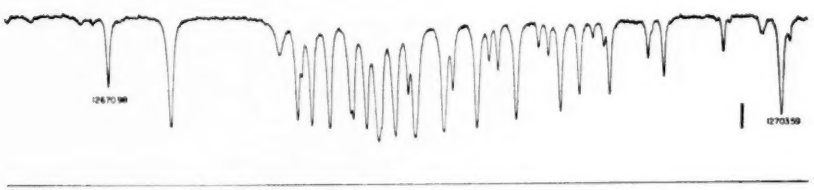

FIG. 4.—Tracing of the Q-branch of the 1.27 μ band of atmospheric oxygen

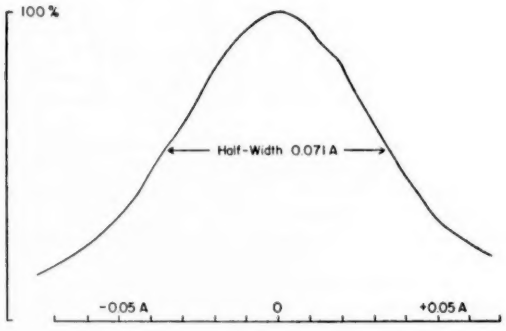

FIG. 5.—Observed emission profile Hg^{198}, λ 13570

the observed profiles, as shown in Figure 3. If δ is the observed line width at half the percentage central absorption, the corresponding Doppler width, $2\Delta\lambda_D$, is given by

$$2\Delta\lambda_D = \left(\frac{0.4343}{\log 2}\right)^{1/2} \delta . \tag{1}$$

In turn, $\Delta\lambda_D$ is related to the most probable space velocity ξ_0 by

$$\xi_0 = \frac{c}{\lambda} \Delta\lambda_D . \tag{2}$$

If δ is taken as 0.91 A, then $\Delta\lambda_D = 0.55$ A, and $\xi_0 = 15$ km/sec. It is interesting to compare this value with those obtained from other helium lines observed in emission in the flash spectrum. From measurements on the widths of the emission lines λ 5876, λ 4026, and λ 3819, which are, respectively, the first, third, and fourth members of the series $2^3P^0 - n^3D$, Redman and Suemoto (1954) conclude that ξ_0 increases regularly with height from the value 11 km/sec at height 600 km to about 16 km/sec at height 2600 km. Both emission and absorption measurements refer to an integration over a wide range of heights in the chromosphere; the former include all heights along the line of sight tangential to the moon's limb, whereas the latter represent a radial integration over all heights.

It is not at present possible to derive the distribution of 2^3S atoms with height. According to Athay and Menzel (1956), the emission per unit volume from atoms in higher states shows a maximum at $h = 1150$ km. But the absorption intensity from the metastable 2^3S level may be distributed differently. It does, however, seem safe to conclude that ξ_0 has a value not far from 15 km/sec in those regions of the chromosphere where the helium lines are formed. The question now arises whether this velocity is primarily thermal or turbulent in origin. Redman and Suemoto (1954) believe that the evidence from both hydrogen and helium lines favors the idea that the increase of ξ_0 with height is chiefly a turbulent, rather than a temperature, phenomenon, as advocated by Unsöld (1952). They point out, however, that their analysis neglects variations in chromospheric properties along the line of sight and that serious complications arise when the chromosphere is treated as a field of filaments or jets. On the other hand, it is becoming increasingly difficult to escape the conclusion that temperature and density fluctuations in the chromosphere play a leading role in determining the character of its spectrum. The center-limb variation in the intensity of 1-cm radio radiation (Hagen 1954) and the analysis of flash spectra (Athay and Menzel 1956) both lead to consistent models only if, as proposed by Giovanelli (1949), the chromosphere is assumed to consist of alternate "hot" and "cold" columns. According to Athay and Menzel (1956), the temperatures in the height range 1500–3500 km are nearly constant at about 6000° K in the cold regions and at about 20000° K in the hot ones. They suggest that the helium emission occurs only in the hot regions.

Rather more direct evidence for the temperature fluctuations, which at present is only qualitative, is given by recent new observations of the Fraunhofer lines of hydrogen, helium, and ionized calcium (McMath, Mohler, Pierce, and Goldberg 1956) made with the vacuum spectrograph of the McMath-Hulbert Observatory. The patchy appearance of the He I λ 10830 absorption has already been referred to (see Fig. 1). Further, the cores of the lines of hydrogen and ionized calcium also show pronounced fluctuations in width and intensity, which are exceedingly difficult to interpret on any basis other than that of temperature fluctuations. For example, it appears probable that the wide absorption features in the hydrogen lines are formed in the hot chromospheric regions, the increased width being a consequence of the higher temperatures of these regions as compared with the bordering cool zones.

The evidence for temperature fluctuations in the chromosphere, together with the irregular intensity distribution of the 10830 line on the disk, strongly suggests that the line is formed only in local regions of relatively high temperature. Whether or not the line width results entirely from thermal broadening still remains to be determined. The value $\xi_0 = 15$ km/sec implies a temperature of about 50000° K, which seems rather large, even for the hot regions of the chromosphere. Further evidence on this question may come from the analysis of the hydrogen and calcium lines now in progress.

REFERENCES

Athay, R. G., and Menzel, D. H. 1956, *Ap. J.*, in press.
Azambuja, L. and M. d'. 1938, *Bull. Astr.*, **11**, 349.
Babcock, H. D. and H. W. 1934, *Pub. A.S.P.*, **46**, 132.
McMath, R. R., Mohler, O. C., Pierce, A. K., and Goldberg, L. 1956, *Ap. J.*, **124**, 1.
Mohler, O. C. 1952, *Ap. J.*, **115**, 323.
Mohler, O. C., Pierce, A. K., McMath, R. R., and Goldberg, L. 1950, *Photometric Atlas of the Near Infrared Solar Spectrum λ 8465–25,242* (Ann Arbor: University of Michigan Press).
Redman, R. O., and Suemoto, Z. 1954, *M.N.*, **114**, 238.
Unsöld, A. 1952, *Zs. f. Naturforsch.*, **7a**, 121.

ON A POSSIBLE INTERSTELLAR GALACTIC CORONA*

LYMAN SPITZER, JR.
Princeton University Observatory
Received March 24, 1956

ABSTRACT

The physical conditions in a possible interstellar galactic corona are analyzed. Pressure equilibrium between such a rarefied, high-temperature gas and normal interstellar clouds would account for the existence of such clouds far from the galactic plane and would facilitate the equilibrium of spiral arms in the presence of strong magnetic fields. Observations of radio noise also suggest such a corona.

At a temperature of 10^6 degrees K, the electron density in the corona would be 5×10^{-4}/cm^3; the extension perpendicular to the galactic plane, 8000 pc; the total number of electrons in a column perpendicular to the galactic plane, about 2×10^{19}/cm^2; the total mass, about $10^8 M_\odot$. The mean free path would be 4 pc, but the radius of gyration even in a field of 10^{-5} gauss would be a small fraction of this. Such a corona is apparently not observable optically except by absorption measures shortward of 2000 A.

Radiative cooling at 10^6 degrees would dissipate the assumed thermal energy in about 10^9 years. Cooling by conduction can apparently be ignored, especially since a chaotic magnetic field of only 10^{-5} gauss will sharply reduce the thermal conductivity. At 3×10^6 degrees, near the maximum value consistent with confinement by the Galaxy's gravitational field, radiative cooling is unimportant, and a corona at this temperature might be primeval. The energy source needed at the lower temperatures may be provided by material ejected at high speed from stars or possibly by compressional waves produced by the observed moving clouds. Condensation of cool matter from the corona may perhaps account for the formation of new spiral arms as the old ones dissipate.

Within recent years it has become well established that interstellar gas clouds are found within the "spiral" arms of our Galaxy. Interstellar absorption lines, H II regions around early-type stars, and the 21-cm line of neutral hydrogen all give concordant evidence. The mean density of hydrogen atoms within a spiral arm appears to be about 1/cm^3. However, the density distribution is nonuniform. According to the present picture—summarized by Spitzer (1954)—within a typical cloud of neutral hydrogen, where the temperature is about 100° K, the density is about 10 atoms/cm^3, as shown by Strömgren (1948). Between the clouds the density is less by a factor of perhaps 100, and the temperature is presumably greater by the same factor. The interstellar gas may be assumed to be at a nearly uniform pressure within the galactic plane, this pressure amounting to 10^{-13} dynes/cm^2.

The possible presence of gas elsewhere in the Galaxy—between the spiral arms and at a great distance from the galactic plane—has not been discussed in detail, largely because of a virtually complete lack of observational information. However, there are a number of observations which suggest that gas may actually be present far from the galactic plane. The present paper provides a brief theoretical discussion of such an "interstellar galactic corona," the reasons for suspecting its presence, its density and kinetic temperature, and its possible importance in the origin of spiral arms and in other contexts as well. At the present time, only a preliminary and tentative analysis is appropriate in so new a field. Hence no great precision is needed, and no firm conclusions can be drawn.

I. OBSERVATIONAL EVIDENCE

The evidence indicating the possible presence of an interstellar galactic corona is of two types. First, the analysis of normal interstellar clouds indicates that regions outside the arms may be permeated by a medium at a pressure about the same as that in the

* The essential conclusions of the paper were presented to a meeting of Commission 34 (Interstellar Matter) of the International Astronomical Union at Dublin, Ireland, on August 31, 1955.

clouds. Second, observations of radio noise suggest that some of the noise originates from a corona surrounding our Galaxy.

a) Clouds at High Latitude

In some ways the simplest indication of an interstellar galactic corona is obtained from an examination of normal clouds at great distances from the galactic plane. Münch (1956) has found a number of such clouds in a systematic investigation of all accessible B and O stars brighter than 8.0 mag. with a galactic latitude of 30° or more. For example, HD 215733, some 1500 pc from the galactic plane, shows four K components, with a velocity spread of 46 km/sec. In thirteen stars at distances of 500 pc or more from the galactic plane, thirty-five components were observed. While the distances of these clouds cannot be determined directly, the number of components appears to be greater than would be anticipated if the clouds were all within about 200 pc of the galactic plane. Moreover, stars at about 500 pc from the plane tend to show less complex lines than do the more distant stars. Hence it seems probable that an appreciable fraction of these clouds is more than 500 pc from the plane. If the root-mean-square velocity of the interstellar atoms, in the direction perpendicular to the galactic plane, is assumed to equal 10 km/sec, corresponding to a kinetic temperature of about 10000° K for H atoms, the density of the gas at 500 pc should be only 5 per cent of the density in the galactic plane.

If a normal galactic cloud, with a density of 10 H atoms/cm^3, were placed in such a medium, in which the pressure was only 5 per cent of the internal pressure within the cloud, the cloud would expand at the speed of sound, about 1 km/sec for a temperature of 100° K. Hence a cloud 5 pc in radius would double its radius in about 5×10^6 years, and its pressure would drop to that in the surrounding medium in about 10^7 years. For comparison, the half-period of oscillation back and forth across the galactic plane (i.e., the time between one passage across the galactic plane and the subsequent passage, in the opposite direction) is about 4×10^7 years, for amplitudes of 200 pc or less; for clouds rising higher above the galactic plane the corresponding half-period is greater. Thus any cloud at large z is very likely to be in pressure equilibrium with the medium surrounding it.

However, if the density at 500 pc above the plane is only 5 per cent of its value in the plane, any cloud will be so rarefied that its absorbing power should be slight. In addition to the reduced number of calcium atoms in the line of sight, with reduced cloud density the electron density will also be reduced, and the fraction of calcium atoms that are singly, instead of doubly, ionized will be diminished accordingly. It is doubtful whether any perceptible absorption line would be produced by a cloud in which the pressure had fallen by a factor of 20 or more. Thus we may conclude that the measures by Münch suggest strongly that the clouds at large z are moving through a medium in which the gas pressure is comparable with that in the galactic plane. A tenuous gas at a high kinetic temperature, in the range of 10^5 to 3×10^6 degrees, provides a simple explanation for the continued existence of absorbing clouds far from the galactic plane.

b) Equilibrium of Spiral Arms

The presence of high-temperature gas between the spiral arms is suggested by the equilibrium of the gas in a spiral arm. This subject has been considered by Chandrasekhar and Fermi (1953), who determined the magnetic field strength from the condition that the gravitational pressure equals the sum of the material and magnetic pressures. However, the root-mean-square velocity of 5 km/sec adopted in their work seems low. The exponential distribution of radial velocities, proportional to $\exp(-v/5)$, found by Blaauw (1952), yields a root-mean-square velocity of $5(2)^{1/2}$ km/sec in one dimension only. If an isotropic velocity distribution is assumed, the three-dimensional root-mean-

square velocity, which occurs in the equations of Chandrasekhar and Fermi (1953), becomes $5(6)^{1/2}$, or about 12 km/sec.

With this increased velocity, the kinetic pressure is increased by a factor of 6 and becomes nearly equal to the gravitational pressure. If the difference is attributed to the magnetic pressure, the magnetic field becomes about 3×10^{-6} gauss. This determination is quite uncertain, since it depends on the difference between two uncertain and nearly equal quantities. However, if a substantially greater magnetic field is assumed, it is difficult to account for equilibrium. For example, if the magnetic field, B, is found from the amplitude of oscillation of the lines of force, following the analysis given in the earlier part of the Chandrasekhar-Fermi paper but utilizing the more realistic value of v found above, B is found to be 3×10^{-5} gauss, yielding a magnetic pressure an order of magnitude greater than the gravitational. In this computation α, the root-mean-square angular deviation of the lines of force from the direction of the spiral arm, was taken to be 0.13 radian, in accordance with the analysis by Stranahan (1954).

Evidently, the gravitational pressure cannot by itself counterbalance large magnetic pressures. If a magnetic field as great as 10^{-5} gauss is assumed, either B must have about the same value both inside and outside the spiral arm, or the gas in the spiral arm must be held in by the pressure of an external gas.

Clearly, the situation will be greatly eased if a spiral arm is assumed to be imbedded in a rarefied gas with a pressure equal to the gas pressure in spiral arms. In such a case there is no difficulty in confining the gas in a spiral arm, especially in view of the possible existence of magnetic fields in the rarefied gas surrounding the spiral arm. Since the magnetic field may actually be less than 10^{-6} gauss (see Spitzer 1954), this evidence is certainly not strong, but it is at least suggestive.

c) Radio Noise

It was suggested by Shklovsky (1952) that much of the cosmic radio noise received on earth might originate in an extended spherical corona surrounding the Galaxy. Support for this suggestion has been obtained by Baldwin (1954) from measures on M31 at a wave length of 3.7 meters. The angular size of the emitting region accompanying this galaxy appears to indicate a spherical corona some 10 kpc in radius, responsible for about two-thirds the total energy radiated by M31 at these wave lengths. Confirming evidence in the case of our own Galaxy has also been obtained by Baldwin (1956). The background of 3.7-meter radiation received at high galactic latitudes has been explained on the assumption of a spherical galactic corona some 10–20 kpc in radius. At most longitudes the observations agree rather well with a theoretical curve computed on this basis. However, the very large deviations observed at about 0° galactic longitude raise some question as to whether lesser irregularities at other longitudes may affect the observed noise levels. Further measurement and analysis are required for conclusive results, but an extended rarefied corona is at least suggested by these data.

Since the radio emission is presumably nonthermal in origin, the radio observations cannot in any case yield values of the density. The interpretation of these radio waves in terms of relativistic electrons moving in a coronal magnetic field, as suggested by Shklovsky (1952), has been discussed by Burbidge (1956). However, the extension of the corona perpendicular to the galactic plane is directly related to the kinetic temperature, and, as we shall see later, a radius between 10 and 20 kpc corresponds to a kinetic temperature of about 10^6 degrees for ionized H atoms.

d) Related Suggestion by Pickelner

The possibility of an extended corona of gas has also been discussed by Pickelner (1953, 1955). However, he considers a homogeneous substratum of relatively cool gas, with a density of 0.1 H atoms/cm^3 and with turbulent motions of some 70 km/sec, an

essentially different picture from the high-temperature corona analyzed here. The chief observational evidence cited by Pickelner is the presence of wide H and K absorption lines, which Spitzer, Epstein, and Li Hen (1950) observed in supergiant B stars and which they attributed to stellar absorption. A re-examination of these data confirms that these wide, shallow absorption features are unquestionably stellar in at least some cases. Of the twelve stars listed by Spitzer, Epstein, and Li Hen as showing this "stellar" absorption, three are known spectroscopic binaries. For two of these, χ Aur and μ Sgr, comparison of two plates taken on different dates shows a shift of the sharp interstellar component relative to the wide absorption feature. On the third, ι Ori, only one plate was available. Furthermore, this wide absorption shows a definite correlation with spectral type, with the strongest absorption in χ Aur (cB3), 67 Oph (cB7), μ Sgr (cB8), α Cyg (cA2), and HD 199478 (cB8), and relatively weak absorption for the other eight stars, of types ranging from cB2 to O8. While some of this wide absorption might perhaps be interstellar in origin, rather than truly stellar or possibly circumstellar, the available evidence does not seem to support this possibility.

From a theoretical standpoint, the Pickelner corona seems difficult to maintain. The dissipation of turbulent energy at such a high Mach number would be very rapid, requiring a large source of energy to maintain the motion. While this proposal cannot be excluded, it will not be discussed further in the present paper.

II. EQUILIBRIUM DENSITY

a) Pressure Equilibrium

In the interstellar medium generally, approximate pressure equilibrium is believed to obtain. The same situation presumably applies to a very hot interstellar corona. Any deviations from hydrostatic equilibrium will produce pressure disturbances traveling at the local sound velocity. At a temperature of 10^6 degrees, a sound wave moves at 170 km/sec and travels 10000 pc in about 6×10^7 years. Unless unsuspected additional influences are operative, hydrostatic equilibrium within a corona should be a realistic assumption. We shall assume that pressure equilibrium also exists between such a corona and the normal interstellar medium.

On this assumption the density in the corona is a known function of the temperature. In the normal obscuring H I cloud, the density and temperature are generally assumed to be 10 H atoms/cm^3 and 100° K, respectively. Hence, from the familiar gas law and equality of pressure, we obtain for n_e and n_p, the density of electrons and protons in the corona,

$$n_e = n_p = \frac{5 \times 10^2}{T}. \tag{1}$$

At the high temperature envisaged, hydrogen will be nearly completely ionized. At a coronal temperature of 10^6 degrees, n_e is 5×10^{-4} atoms/cm^3.

b) Extension Perpendicular to Galactic Plane

The extension of the corona perpendicular to the galactic plane may also be determined from the temperature, if isothermal conditions are assumed. We compute the "coronal height," z_c, defined as the value of z at which the density is $1/e$ times its value in the galactic plane, at z equal to zero. In hydrostatic equilibrium we have

$$\frac{d \log n(z)}{dz} = -\frac{mK(z)}{kT}, \tag{2}$$

where m is the mean mass per particle, here equal to half the mass of an H atom, and $K(z)$ is the gravitational acceleration in the z direction, perpendicular to the galactic

plane, as a function of z, the distance from the galactic plane. We use c.g.s. units in these equations. Equation (2) may be integrated to yield

$$\log \frac{n(z)}{n(0)} = -\frac{\psi(z)}{T}, \tag{3}$$

where

$$\psi(z) \equiv \frac{m}{k} \int_0^z K(z)\, dz . \tag{4}$$

Evidently z_c is the solution of the transcendental equation

$$\psi(z_c) = T . \tag{5}$$

Values of $K(z)$ for z up to 500 pc have been determined by Oort (1932). For values of z greater than 4000 pc, Oort computes $K(z)$ from the attraction of a central galactic nucleus containing 1.7×10^{11} solar masses and 10000 pc away. With Oort's values of $K(z)$, the values of $\psi(z)$ in Table 1 have been obtained; although the unit of distance in

TABLE 1

VALUES OF $\psi(z)$

z(pc)	100	150	200	400	600
$\psi(z)$	2.18×10^{3}	4.70×10^{3}	7.84×10^{3}	2.18×10^{4}	3.66×10^{4}
z(pc)	1000	1500	2000	4000	6000
$\psi(z)$	6.85×10^{4}	1.13×10^{5}	1.62×10^{5}	4.06×10^{5}	7.22×10^{5}
z(pc)	10000	15000	20000	40000	60000
$\psi(z)$	1.40×10^{6}	2.08×10^{6}	2.56×10^{6}	3.48×10^{6}	3.83×10^{6}
z(pc)	100000	200000	400000	1000000	∞
$\psi(z)$	4.12×10^{6}	4.30×10^{6}	4.46×10^{6}	4.53×10^{6}	4.58×10^{6}

TABLE 2

EXTENSION OF CORONA PERPENDICULAR TO GALACTIC PLANE

T(° K)	3×10^{4}	10^{5}	3×10^{5}	10^{6}	3×10^{6}	4.6×10^{6}
z_c(pc)	520	1400	3200	7500	27000	∞
$n_e z_c$(cm^{-2})	2.7×10^{19}	2.2×10^{19}	1.6×10^{19}	1.2×10^{19}	1.4×10^{19}	∞

equation (4) is taken to be the centimeter, for convenience in the following tables z is given in parsecs. The values of z_c obtained from equation (5) are given in Table 2, together with values of the product $n_e z_c$, where the value of n_e is taken at z equal to zero. For T less than 10^6 degrees K, the corona is restricted to z values of less than 1700 pc. In this range, $K(z)$ is produced by the local material in the galactic plane and is nearly constant for z between 400 and 2000 pc. As a result, z_c varies almost linearly with T, and $n_e z_c$ is nearly constant. For greater z, the attraction of the central bulge becomes important. For z greater than 10000 pc, $K(z)$ falls off about as $1/z^2$, and $\psi(z)$ approaches a finite value as z approaches infinity. As a result, z_c becomes infinite at a temperature of 4.6×10^6 degrees K.

For T much greater than 10^6 degrees, the corona cannot, in fact, be held in by the gravitational attraction of the Galaxy. Analysis of isothermal conditions is somewhat

idealized, unless we make the rather drastic assumption that this hypothetical high-temperature gas pervades all intergalactic space. While an intergalactic medium can certainly not be excluded at the present time, there seems little to be gained by considering such a possibility in the complete lack of any observational evidence bearing on the subject. We shall assume, then, that the density of the galactic corona approaches zero for sufficiently large z. In the equilibrium configuration, evaporation of coronal protons and electrons into intergalactic space occurs from some limiting surface, and this evaporation keeps the outer surface cool. The gravitational attraction of the Galaxy on this cool layer then provides the pressure needed to confine the inner isothermal regions. If the inner isothermal region of the corona were to be at a temperature of 4×10^6 degrees, the mass of the cool outer region would have to be comparable with that of the inner region; in fact, it may be shown that the mean temperature of all the coronal atoms cannot much exceed 10^6 degrees. We shall take 3×10^6 degrees as a generous upper limit on the coronal temperature.

The total mass of such a corona can be determined from the data in Table 2. For T no greater than 3×10^6 degrees, the values of $n_e z_c$ do not change rapidly with T, and average about 2×10^{19}/cm^2, corresponding to a mass of about 3×10^{-5} gm/cm^2, or 6×10^{-5} gm in a column 1 cm square in cross-section extending all the way through the Galaxy. For comparison, the total gravitating mass in a column through the galactic plane, as determined by Oort, is about 10^{-2} gm/cm^2, roughly half of which may be attributed to the interstellar material near the galactic plane. When account is taken of the concentration of this cool gas in spiral arms, we find that a few per cent of the total mass of the interstellar material in the Galaxy may be in the corona. If the possibility of much higher coronal densities near the galactic nucleus is ignored, the total mass of the corona is about $10^8 M_\odot$.

c) Mean Free Path and Radius of Gyration

Another quantity which is a simple function of temperature is the mean free path, l. This quantity, about the same for electrons as for protons, may be set equal to the root-mean-square velocity, multiplied by the self-collision time, t_c, discussed by Spitzer (1956), following the analysis by Chandrasekhar (1942). For the densities and temperatures of interest, the logarithmic term occurring in these expressions is about 30, and we have, approximately,

$$l = \frac{2.0 \times 10^{-15} T^2}{n_e} \text{ pc} . \tag{6}$$

Combining equations (1) and (6), we obtain

$$l = 4.0 \times 10^{-18} T^3 \text{ pc} . \tag{7}$$

We see that the mean free path rises very rapidly with T. Even at the maximum temperature of 3×10^6 degrees K, l is only 108 pc, a small fraction of the coronal extension.

The radius of gyration, a, is likely to be much less than the mean free path. For protons at 10^6 degrees, moving in a magnetic field of 10^{-5} gauss, the root-mean-square radius of gyration, a, is about 1.3×10^8 cm, or about 4×10^{-11} pc. Even with a vastly smaller magnetic field, the particles would gyrate about the magnetic lines of force many times between collisions. At 10^{-15} gauss, for example, a is 0.4 pc for protons and 10^{-5} pc for electrons, both at 10^6 degrees.

d) Optical Observability

Finally, we discuss how material at this density might be detected by direct optical means. We have already seen that N, the number of coronal electrons, or protons, in the line of sight per square centimeter, is about 2×10^{19}, a rough average of the values of

$n_e z_c$ given in Table 2. This value of N is about the number of atoms in the line of sight through 1 cm of air or through the inner corona of the sun, viewed tangentially to the solar limb. The total optical thickness for electron scattering is only 1.3×10^{-5}, probably much too small to be observed.

While an interstellar corona should emit the same type of radiation as the solar corona, the rate of emission per atom is reduced in about the same ratio as the density, or by a factor in the general neighborhood of 10^{-11}. It is evident that the intensity of the coronal emission, when reduced by so large a factor, is entirely unobservable.

It may be noted that the Balmer lines would be unobservable even if the recombination coefficient were independent of the temperature. The emission measure of the interstellar corona, defined as $n_e^2 z_c$, where n_e is in cm^{-3} and z_c is in parsecs, is at most 0.1. For H II regions in the Galaxy an emission measure of about 100 is the least that can be detected. Similarly, the thermal radio emission, generated by free-free transitions, is entirely unobservable.

While the interstellar corona can apparently not be observed by its emission spectrum, the number of atoms is sufficient to produce a measurable absorption line. A column of interstellar gas containing 10^{12} sodium atoms/cm^2 produces measurable D lines. The difficulty with this technique in the case of the solar corona is that at a high kinetic temperature the atoms will mostly be highly ionized, and the ultimate lines will all be in the far ultraviolet. If the state of ionization is like that in the solar corona, the ultimate resonance doublet of Mg X, at 609 and 625 A, should be extremely strong, since the number of magnesium ions in the line of sight in all stages of ionization would be about $10^{16}/cm^2$; if 1 per cent of these atoms were in the ionized state Mg X, this doublet would be heavily absorbed. However, it is uncertain whether much radiation shortward of the Lyman limit can reach the earth, in view of probable heavy absorption by neighboring H I clouds. The ion O VI, which is isoelectronic to Mg X, has a corresponding doublet at 1038 and 1032 A and might be sufficiently abundant to produce measurable absorption, especially since the ionization potential of O VII has the relatively high value of 739 volts. Similarly, the ultimate lines of N V and C IV, at about 1240 and 1550 A, respectively, might be observable. It would appear that, in principle, an interstellar corona could be detected and analyzed by means of spectroscopic measures from a satellite.

III. RATE OF COOLING

We now consider the rate at which the kinetic temperature of a hypothetical interstellar corona would change with time, in the absence of any heating. Two mechanisms will be considered—radiation and conduction.

a) Radiative Cooling

Radiative cooling is very slow at temperatures above 10^6 degrees. Cooling by free-free transitions in a gas at high temperatures has been analyzed by Cillié (1932) and Spitzer (1942). The rate of radiation, ϵ_{ff}, is given by

$$\epsilon_{ff} = \frac{2^5 \pi e^6 Z^2 n_e n_i}{3h m_e c^3} \left(\frac{2\pi kT}{3 m_e} \right)^{1/2} = 1.42 \times 10^{-27} Z^2 n_e n_i T^{1/2} \text{ erg/cm}^3 \text{ sec}, \tag{8}$$

where the various symbols have their usual meanings. A time of cooling, t_d, may be defined as the time required to dissipate all the internal kinetic energy if the cooling rate remains constant. Evidently, for a proton-electron gas,

$$t_d = \frac{3 n_e kT}{\epsilon_{ff}}. \tag{9}$$

Values of t_d for free-free radiation, with the electron density, n_e, taken from equation (1), are given in the upper row of Table 3. Evidently for a temperature in excess of 10^6 degrees, the cooling time for free-free transitions is considerably greater than the present value of 5×10^9 years for the age of the universe.

Cooling by inelastic collisions is likely to be somewhat more important. The effect of this process in the solar corona has been considered by Woolley and Allen (1948). They find that excitation of the Mg X doublet is responsible for half the energy radiated in inelastic impacts. The total energy radiated in this way is found to be thirteen times that radiated in free-free transitions. However, this ratio may be expected to vary somewhat as T changes from the 10^6 degrees considered by Woolley and Allen. The rate of radiation by free-free emissions varies as $T^{1/2}$. On the other hand if we assume that the

TABLE 3

COOLING TIME, t_d, IN YEARS

	T(° K)				
	3×10^4	10^5	3×10^5	10^6	3×10^6
t_d(f-f only)	1.1×10^8	5.8×10^8	3.5×10^9	1.8×10^{10}	9.5×10^{10}
t_d	2.6×10^5	4.4×10^6	7.9×10^7	1.3×10^9	1.8×10^{10}

energy of the important excited levels varies as T, then the cross-section for inelastic impact varies as $1/T^2$, and the rate of emission produced by inelastic impact varies as $1/T^{1/2}$. This same result is obtained if excitation of some particular level is considered, whose energy of excitation is small compared to kT (as is the case for Mg X at 10^6 degrees) and whose relative abundance does not change with T. Hence the ratio of radiation rates for inelastic impacts and for free-free transitions may, on the average, vary about as $1/T$. For ϵ_{in}, the rate of energy radiation in inelastic impacts, we shall therefore write

$$\epsilon_{in} = \frac{13 \times 10^6 \epsilon_{ff}}{T} = 1.85 \times 10^{-20} n_e^2 T^{-1/2} \text{ erg/cm}^3 \text{ sec}. \tag{10}$$

Equation (10), while it may be approximately valid over a large range in T, is certainly not accurate in detail. Detailed cross-sections for particular levels and the relevant ionic abundances must both be considered in an accurate result. It should be noted that, if equation (10) were rigorously correct and if the energy input were independent of T, the gas would be thermally unstable at the equilibrium point and T would either rise or fall until a new equilibrium was reached. We shall use equation (10) for very rough results, with the understanding that the detailed behavior of ϵ_{in} with T is doubtless considerably more complicated.

If we now use equations (8) and (10) to compute the final cooling times, including both processes, we obtain the values in the lower row in Table 3. At the lower temperatures the cooling time is evidently very short.

b) Conductive Cooling

Next we consider the conduction of heat by the coronal electrons. We first assume that no magnetic field is present. The coefficient of thermal conductivity, denoted by $\mathfrak{K}$,

may be taken from the monograph by Spitzer (1956); we obtain, for an electron-proton gas,

$$\mathfrak{K} = 0.0943 \times 20 \left(\frac{2}{\pi}\right)^{3/2} \frac{k^{7/2} T^{5/2}}{m_e^{1/2} e^4 \ln \Lambda}, \tag{11}$$

$$\mathfrak{K} = 6.1 \times 10^{-7} T^{5/2} \text{ erg/cm sec deg}.$$

Equation (11) takes into account the reduction of conductivity both by electron-electron collisions and by the thermoelectric effect; in computing the numerical value, $\ln \Lambda$ (Spitzer 1956, Table 5.1) has been set equal to 30, an appropriate value for the conditions of interest here. Evidently $\mathfrak{K}$ varies rapidly with T.

We are interested primarily in the time required for heat conduction to cool the corona. This problem is usually analyzed in terms of normal modes, with the cooling times of the various modes determined as eigen-values of the problem. In the present instance, however, the differential equations of the problem are too complicated to permit a simple solution in these terms. As an alternative method of approach, we shall evaluate the conductive heat flux in a hypothetical steady state, in which the corona is assumed to be maintained at a constant temperature. Between the corona and the cool gas in the galactic plane there is assumed to be a transition region of thickness z_t. The cooling time is then equal to the total internal energy of the corona, in a column 1 cm^2 in cross-section, divided by the conductive heat flux per square centimeter per second. To simplify the problem further, a one-dimensional corona will be assumed. This method of approach should yield the correct order of magnitude for the cooling time.

In a steady state the familiar basic equation of heat conduction in one dimension is

$$\frac{d}{dz}\left(\mathfrak{K} \frac{dT}{dz}\right) = \epsilon, \tag{12}$$

where ϵ is the rate of radiation of energy per cubic centimeter per second. We shall neglect free-free emissions, since they are small compared to line radiation at the temperatures of interest; accordingly, ϵ may be set equal to ϵ_{in}. If we substitute from equations (10) and (11), with n eliminated by use of equation (1), we obtain

$$T^{5/2} \frac{d}{dz}\left(T^{5/2} \frac{dT}{dz}\right) = M \equiv 7.6 \times 10^{-9}. \tag{13}$$

Equation (13) may be solved at once with the change of variable

$$T^{5/2} du = dz, \tag{14}$$

and T found as a function of u. One of the constants of integration can be eliminated by adjusting the point at which u vanishes. The final solution becomes

$$T = Lu + \tfrac{1}{2} M u^2, \tag{15}$$

where L is a constant of integration. Substitution of equation (15) in equation (14) gives a relation that may be integrated, in principle, to yield u as a function of z. The energy flux, F, is given by

$$F = 6.1 \times 10^{-7} \frac{dT}{du}. \tag{16}$$

We investigate the solution in two special cases: (*a*) L very large and (*b*) L very small. In the former case, T equals Lu, and dT/du in equation (16) is simply L. Equation (14) may be integrated directly, and we obtain

$$T = (3.5 L z)^{2/7}. \tag{17}$$

Thus, if z and T vanish together, while T equals the coronal temperature, T_c, when z equals z_t, equation (16) yields, for F,

$$F = \frac{1.74 \times 10^{-7} T_c^{7/2}}{z_t} \text{ erg/cm}^2 \text{ sec}. \tag{18}$$

Next we consider case b, in which L is negligible and T equals $\frac{1}{2}Mu^2$. In this situation equation (14) gives

$$T = \left(\frac{M}{2}\right)^{1/6} (6z)^{1/3}, \tag{19}$$

and the flux becomes

$$F = 8.6 \times 10^{-7} M^{1/2} T^{1/2} \text{ erg/cm}^2 \text{ sec}. \tag{20}$$

Evidently, the variation of T with z is closely similar in these two cases.

We are now in a position to discuss the physical significance of these results. In solution a, M is neglected, and all radiative cooling is therefore ignored. In this situation the heat flux is uniform throughout the transition region under discussion, but its magnitude varies inversely with z_t, the thickness of this region. As z_t increases, however, the emission of radiation from the enlarged transition region can no longer be ignored. In fact, the flux now increases with increasing height.

Case b arises when the radiation of energy just uses up all the flux entering the transition region at the upper boundary, so that at the lower boundary, where T is practically zero, F also vanishes. Evidently, case b corresponds to the thickest possible transition region; a thicker region would radiate more energy than it would receive across the upper boundary. Also, case b corresponds to the least value of F across this boundary.

In an actual case let us suppose that the transition region is initially very thin so that case a is valid. In this situation the transition region will grow in thickness until either z_t is comparable with z_c, the value of z at which the coronal density has dropped to $1/e$ of its value near the galactic plane, or until the thickness of the transition region reaches the upper limit set in case b. This upper limit is approximately reached when equations (18) and (20) yield about the same value for F, i.e., when

$$z_t = \frac{1}{7}\left(\frac{2}{M}\right)^{1/2} T_c^3 = 7.5 \times 10^{-16} T_c^3 \text{ pc}. \tag{21}$$

At 3×10^6 degrees, the upper limit on z_t is about 20000 pc, which is close to the value of 25000 pc given for z_c at this temperature in Table 2. At all lesser temperatures the upper limit on z_t is substantially less than z_c. We may consider, therefore, that the thickness of the transition region will grow to the limit set by equation (21) and that the conductive heat flow out of the corona is correctly given by equation (20).

The cooling time for conduction, t_F, is now obtained from the condition that in the time t_F the total flow of heat out of the corona would equal the thermal energy stored in the corona. This condition yields the equation

$$t_F = \frac{3 n_e k T_c z_c}{F}. \tag{22}$$

Substitution from equations (1) and (20) yields

$$t_F = \frac{2.7 \times 10^8}{T_c^{1/2}} \left(\frac{z_c}{3.08 \times 10^{18}}\right) \text{years}. \tag{23}$$

The values of t_F listed in Table 4 have been computed from equation (23), with values of z_c obtained from Table 1.

The term "conductive cooling" is perhaps somewhat misleading, as the process is really the rate of radiation from the transition region between the corona and a cool galactic gas. This radiation loss is then assumed to be equal to the loss of energy by conduction from the corona to the transition layer.

It may seem surprising that the times in Table 4, which include the effects both of radiation and of conduction, are in most cases substantially greater than those in Table 3, which include the effects of radiation alone. The reason for this is that the radiation considered in Table 4 originates in a very thin surface layer, of a thickness equal to the upper limit in equation (21), and this radiation loss is assumed to be offset by the thermal energy in the corona. For T equal to 3×10^4, for example, the thickness z_t is only 0.02 pc, as compared with a value of 550 pc for z_c at this temperature. Evidently, for a temperature such that t_d is less than t_F, an initially isothermal corona will cool primarily by uniform radiative losses rather than by conduction into a radiating transition layer.

TABLE 4

TIME OF CONDUCTIVE COOLING, IN YEARS

T_c	3×10^4	10^6	3×10^6	10^8	3×10^8
t_F	8.2×10^6	1.2×10^9	1.6×10^9	2.0×10^9	4.2×10^9

The rate of cooling by conduction will be reduced even further if, as seems likely, a magnetic field is present, with the lines of force tangled by some sort of turbulent motion. Transverse to a magnetic field $\mathfrak{H}$ is reduced by about the factor $(a/l)^2$, where a is the radius of gyration and l is the mean free path. We have already seen that this factor may reasonably be as small as 10^{-20}. Even with a magnetic field as low as 10^{-15} gauss, no heat conduction transverse to the lines of force need be considered, and conduction will occur only along the lines of force. If these lines are sufficiently tangled, a point in the corona at a height z from the galactic plane can be reached only along a line of force many times z in length. These considerations simply reinforce the result that conductive cooling of a galactic corona may be ignored.

The chief conclusion to be drawn from this section is that for any temperature appreciably less than 3×10^6 degrees the effective time for the corona to cool by radiation in the coronal lines is likely to be less than 5×10^9 years, and the corona cannot be primeval, a by-product of the original creation of the Galaxy. Instead, some continual heating process must operate if a high-temperature corona is to exist. The required heating rate is, however, low.

IV. PROBLEMS OF DYNAMICS AND COSMOLOGY

The possible existence of an interstellar corona in the Galaxy poses a number of additional problems, besides those discussed in the preceding sections. The more important of these are the following: the possible origin of such a corona, the possible methods of heating, the types of motion possible in such a medium, and the role of such a medium in the formation of spiral arms. These problems cannot be explored with the same definiteness as has been possible for the density distribution and rate of cooling. A brief preliminary exploration of those topics is presented here.

a) Heating

The problem of origin of such a corona reduces primarily to the problem of heating. Considerable amounts of gas would presumably have been left originally at great dis-

tances from the galactic plane when the stars were formed. Also, evaporation of gas from the relatively cool clouds near the plane would provide a steady source of material for such a corona. Hence the central problem in explaining for the existence of such a corona is to account for its high temperature.

As we have already seen, the simplest hypothesis is that the corona is itself entirely primeval and was formed at a high temperature some 5×10^9 years ago. This explanation is possible only if the coronal temperature is substantially in excess of 10^6 degrees, and perhaps too great to be consistent with confinement of the corona by the gravitational field of the Galaxy. Since the values in Table 3 are somewhat uncertain, however, the hypothesis of a primeval hot corona which has persisted to the present time cannot be excluded.

If the corona is not assumed to be primeval and its temperature is taken to be not appreciably greater than 10^6 degrees, then the coronal gases must be in thermal equilibrium, with the energy gains balancing the losses. We may readily compute L_{cor}, the total luminosity of the corona, which must then be balanced by some energy source. If the coronal temperature is taken to be 10^6 degrees, the cooling time, according to Table 3, is 1.3×10^9 years. We neglect cooling by conduction, which would reduce slightly the cooling time at this temperature if a magnetic field were entirely absent. Since we have already seen that the mass of the corona may be set equal to $10^8 M_\odot$, we obtain

$$L_{cor} = 1.2 \times 10^{39} \text{ ergs/sec} = 3.2 \times 10^5 L_\odot . \tag{24}$$

This value is a small fraction of the total luminosity of the Galaxy.

We compare L_{cor} with the energy radiated by the cooler interstellar matter in the galactic plane. The H II regions radiate much of the energy emanating from O stars beyond the Lyman limit, which, for the Galaxy as a whole, probably amounts to about 1 per cent of the total galactic luminosity, or about $10^8 L_\odot$ in order of magnitude. As a check, we compute the energy radiated if 1 per cent of the volume of the Galaxy, with an assumed thickness of 200 pc and a radius of 10000 pc, is assumed to contain ionized hydrogen at a temperature of 10000° K and a density of 1 proton/cm^3. On capture by a proton, an electron radiates about 15 ev, or 2.4×10^{-11} erg. The number of such captures per second at 10000° K is $4.3 \times 10^{-13} n_e^2$ (Spitzer 1956). The total energy radiated is 2×10^{41} ergs/cm^3, or $5 \times 10^7 L_\odot$. Evidently, the energy radiated by an interstellar corona at 10^6 degrees is some two orders of magnitude less than that radiated by the familiar H II regions of the Galaxy.

On the other hand, the energy dissipated by the motions of the interstellar gas is much less. According to Kahn (1955) and Seaton (1955), this energy goes into the H I regions and is mostly responsible for the energy radiated from these regions. The rate of energy dissipation in this process is obtained from the density of kinetic energy and the dissipation time, which in this case is the time between collisions. In the normal interstellar gas, moving with a root-mean-square velocity of 12 km/sec (see Sec. I) and with a mean density of 1 H atom/cm^3, averaged over the clouds and the intercloud regions, the density of kinetic energy is 3.6×10^{43} ergs/pc^3. If collisions between clouds are assumed to dissipate this energy in 10^7 years and the interstellar material is assumed to fill one-third of a volume 200 pc thick and 10^4 pc in radius, the rate of dissipation of kinetic energy is 2.4×10^{39} ergs/sec, or $6 \times 10^5 L_\odot$. Evidently, the radiation of energy from the corona appears to be of the same order of magnitude as the dissipation of kinetic energy by the low-temperature clouds.

Several mechanisms might provide this required energy for heating a galactic corona. One possibility is that compressional waves, produced by moving clouds in the galactic plane, become converted to shock waves in the rarefied gas above and convert their energy into heat. This mechanism has been suggested by Biermann (1946) and Schwarzschild (1948) as a possible means for heating the solar corona. In the interstellar case the

ratio of cloud velocity to sound velocity is much greater than in the solar atmosphere, and a greater efficiency of transfer from directed kinetic energy to heat energy may be expected. More information is needed to indicate whether or not this mechanism can actually provide the necessary energy.

Direct heating by stellar radiation seems improbable. Visible light cannot directly produce high temperatures. More energetic photons, with several hundred electron volts of energy, could readily heat a gas to 10^6 degrees. However, the total flux of radiant energy required would be rather great, since at these frequencies the optical thickness of the corona would not exceed 10^{-3} and the required galactic luminosity at wave lengths below 100 A would exceed $10^8 L_\odot$. There is no known indication of so great an X-ray flux from the Galaxy.

A mechanism that seems considerably more promising is the high-speed ejection of material from stars. Replenishment of the interstellar medium by stellar ejection has been discussed by Thackeray (1948) and Biermann (1955). According to these authors, the bulk of the emission comes from the early-type stars, which presumably lose matter both by outward motion of the atmosphere at velocities of about 10–100 km/sec and by corpuscular emission at about 1000 km/sec. Much of the emitted gas will presumably strike normal cool clouds in the galactic plane and lose its kinetic energy by increasing slightly the temperature of these clouds. However, early-type stars near the edge of a spiral arm or at considerable distances above the galactic plane may be expected to emit some material which will leave the galactic plane without first striking any substantial amounts of cool gas. This material, moving through the galactic corona, will transfer its kinetic energy to the random thermal energy of the corona.

In addition to the O and B stars, which are primarily confined to the spiral arms, some emission occurs from type II stars, which may already be at considerable distances from the galactic plane. Supernovae, which account for perhaps 1 per cent of the total matter ejected from stars, are believed to occur among stars of both population types.

The energy flow of $3 \times 10^5 L_\odot$ required by equation (24) would be produced by a mass of $0.01 M_\odot$ per year ejected into the corona at a velocity of 600 km/sec. This rate of mass ejection is about that attributed to supernovae and, according to Biermann (1955), is two orders of magnitude less than the probable rate of corpuscular emission from early-type stars. While again no definite conclusions can be drawn at present, this mechanism appears to be a very promising means of keeping a corona hot.

A related source of heating is by means of cosmic-ray particles, with energies of several billion volts per nucleon. However, the results obtained by Spitzer (1948) on heating by cosmic rays may be used to show that this mechanism cannot lead to high temperatures if the flux and spectrum of the energetic particle are the same as observed on earth. We infer that cosmic rays are probably not responsible for heating the corona.

b) Motions

While the motions of a possible corona are even more hypothetical than the existence of such a system, certain properties of these motions can be explored theoretically. In the unlikely case that the magnetic field is everywhere much less than 10^{-18} gauss, electrons and protons move in nearly straight lines over distances comparable with a parsec (see eq. [7]). Any turbulence in this case must have a scale much greater than 1 pc. The motion of a cool cloud through such a medium is difficult to analyze, since the cloud radius may be comparable with the mean free path. The one simplication is that the motions are probably subsonic, since the observed cool clouds are mostly moving less rapidly than the probable sound velocity, which in ionized hydrogen at 10^6 degrees amounts to 170 km/sec. Heat conduction from the corona to the cloud will form a transition layer surrounding the cloud, and the motions of this layer will complicate the dynamics.

It seems likely that the magnetic field will exceed 10^{-15} gauss, in which case the radii of gyration of both electrons and protons will be less than 1 pc. In this situation the effective mean free path transverse to the magnetic field is now the radius of gyration, and the gas behaves like a conventional fluid, except that inhomogeneities along the line of force tend to be eliminated rapidly. In this case the gas will flow smoothly around a cool cloud moving through it, with possible generation of turbulent motion in its wake. Conduction of heat to the cool cloud will presumably be negligible. A detailed solution of this hydromagnetic problem will depend, of course, on the geometry of the lines of force, especially if the magnetic field, B, is assumed to be so large that the magnetic energy density, $B^2/8\pi$, becomes comparable with the kinetic energy density, $\frac{1}{2}\rho v^2$.

c) Condensation of Spiral Arms

One interesting feature of a possible galactic corona is that it may provide a mechanism for the formation of new spiral arms. Such a mechanism may be needed to explain why the observed clouds of gas and dust have a spiral structure rather than a circular one. For example, a cloud of gas in the solar neighborhood becomes so distorted by the nonuniformity of galactic rotation that in 5×10^9 years it becomes a lane with an inclination of only 0.3° to a circular path; i.e., its distance from the galactic center increases by only 5 pc in 1000 pc of distance along the lane. While the 21-cm data obtained by van de Hulst, Oort, and Muller (1954) do, in fact, indicate a nearly circular lane of neutral hydrogen stretching almost a quarter of the way around the Galaxy, the measures suggest an inclination of at least 1°. The outer arms in M31 are also nearly circular, but the data are not sufficiently precise to reveal an inclination of 1° or less.

While the evidence is still insufficient for definite conclusions, the present configuration of spiral arms in our Galaxy and in M31 appears consistent with the hypothesis that from time to time enormous complexes of relatively cool gas are formed in the galactic plane and become sheared by differential galactic rotation into the familiar spiral arms. The gas then condenses both into grains and into new stars, many of which are of early type. In time, as some of the gas condenses into stars, the remainder is swept away in some way, and the arm disappears, its place being taken by a newly formed arm.

The corona may perhaps be tentatively identified as the source of material from which the new arms condense and into which the remnants of old arms evaporate. How can the corona be expected to condense into a cool mass of gas? We have already seen that under some conditions the rate of radiation might be expected to rise with decreasing temperature, with resulting thermal instability. Under such conditions some of the corona would presumably cool and contract, with the remaining coronal gases expanding to take the place of the gas that had contracted. A more detailed study of the ions and their radiating energy levels would be required to indicate whether or not such a mechanism could occur and whether most of the corona would be thermally stable most of the time.

One difficulty with this hypothesis is that the total mass of the corona is at least an order of magnitude less than the total mass of cooler gas. Thus condensation of the entire corona would scarcely provide the material for one spiral arm. However, the condensation will presumably be a gradual process, and, if new material streams into the corona as the condensation proceeds, a spiral arm may be formed with much more material than is in the corona at any one time. Another difficulty is that, if much material is to return to the corona from old spiral arms, the rate of heating must probably be increased by at least an order of magnitude over the estimates given previously. In view of these difficulties and the many uncertainties in this field, the role of an interstellar corona in the evolution of a galaxy is somewhat hypothetical but seems of potentially great importance.

REFERENCES

Baldwin, J. E. 1954, *Nature*, **174**, 320.
———. 1956, *M.N.*, in press.
Biermann, L. 1946, *Naturwiss.*, **33**, 118.
———. 1955, *Gas Dynamics of Cosmic Clouds: Proceedings of the Cambridge Symposium in July, 1953*, chap. 39, p. 212.
Blaauw, A. 1952, *B.A.N.*, **11**, p. 459 (No. 436).
Burbidge, G. R. 1956, *Ap. J.*, **123**, 178.
Chandrasekhar, S. 1942, *Principles of Stellar Dynamics* (Chicago: University of Chicago Press), chap. ii.
Chandrasekhar, S., and Fermi, E. 1953, *Ap. J.*, **118**, 113.
Cillié, G. 1932, *M.N.*, **92**, 820.
Hulst, H. C. van de, Muller, C. A., and Oort, J. H. 1954, *B.A.N.*, **12**, 117 (No. 452).
Kahn, F. D. 1955, *Gas Dynamics of Cosmic Clouds: Proceedings of the Cambridge Symposium in July, 1953*, chap. 12, p. 60.
Münch, G. 1956, in preparation.
Oort, J. 1932, *B.A.N.*, **6**, 249 (No. 238).
Pickelner, S. B. 1953, *C.R. Acad. Sci. URSS*, **88**, 229; *Pub. Crimean Ap. Obs.*, **10**, 74.
———. 1955, *Mém. Soc. R. Sci. Liége*, **4-15**, 595.
Schwarzschild, M. 1948, *Ap. J.*, **107**, 1.
Seaton, M. J. 1955, *Ann. d'ap.*, **18**, 206.
Shklovsky, I. S., 1952, *Astr. J., U.S.S.R.*, **29**, 418.
Spitzer, L. 1942, *Ap. J.*, **95**, 329.
———. 1948, *ibid.*, **107**, 6.
———. 1954, *ibid.*, **120**, 1.
———. 1956, *Physics of Fully Ionized Gases* (New York: Interscience Publishers).
Stranahan, G. 1954, *Ap. J.*, **119**, 465.
Thackeray, A. D. 1948, *Observatory*, **68**, 22.
Woolley, R.v.d.R., and Allen, C. W. 1948, *M.N.*, **108**, 292.

A MODEL FOR NONTHERMAL RADIO-SOURCE SPECTRA

N. G. Roman and F. T. Haddock
Naval Research Laboratory, Washington, D.C.
Received January 25, 1956; revised March 2, 1956

ABSTRACT

A model is presented to explain the observed radio spectrum of Cassiopeia A on the assumption that the underlying nonthermal emission process has an intrinsic spectrum which follows the law, $S(\nu) \propto \nu^{-\alpha}$. With only minor adjustments, the same model can explain several rather different source spectra.

I. INTRODUCTION

Of the few spectra observed for radio "stars," most seem to consist of two regions in which the flux is proportional to $\nu^{-\alpha}$, separated by a plateau where the flux changes slowly with frequency. The exponent, α, is approximately constant for these sources, but the width of the plateau varies from source to source. In addition, the few observations at low frequencies indicate that the flux may decrease rapidly with decreasing frequency in this region. While the physical mechanism producing the emission from nonthermal sources is not definitely known, it is very possible that the emission is synchrotron radiation from relativistic electrons moving in a magnetic field. If the energy spectrum of the electrons is proportional to E^{-n}, the radiated power will be proportional to $\nu^{-\alpha}$, where $\alpha = (n - 1)/2$ (Hoyle 1954; Twiss 1954). Hence, it is worthwhile to investigate the ways in which a $\nu^{-\alpha}$ spectrum can be modified to produce the observed spectra.

II. THEORETICAL MODEL FOR CASSIOPEIA A

Greenstein and Minkowski (1953) investigated the effect of imbedding nonthermal sources in an amorphous H II region in an attempt to explain partially the radio spectrum of the Crab Nebula. Their model C4 (four equally intense sources at optical depths 0, 1, 2, and 3, respectively, at 100 Mc/s) resembles the observed curves except for the position of the plateau. However, if the area subtended by the H II region were more than an order of magnitude larger than the area subtended by the nonthermal source, the thermal emission from the amorphous region should be detectable at centimeter wave lengths as an addition to the nonthermal flux. Moreover, it might become difficult to account for the high densities required to produce the necessary optical depths in so large a volume of space.

Instead of imbedding the nonthermal sources in an amorphous H II region, let us assume that H II regions lie between us and the source and cover only a fraction, β, of its total angular extent. Let us assume, further, that, in addition to the dense H II regions of temperature T and optical depth $\tau_1 = s_1/\nu^2$ at frequency ν, a tenuous H II region of optical depth $\tau_2 = s_2/\nu^2$ covers the entire source. The flux received at the earth will be modified from $S(\nu) \propto \nu^{-\alpha}$ to

$$\frac{S(\nu)}{\zeta} = \beta\nu^2 (1 - e^{-s_1/\nu^2}) + \beta\gamma\nu^{-\alpha} e^{-s_1/\nu^2} + (1 - \beta)\gamma\nu^{-\alpha} e^{-s_2/\nu^2}, \tag{1}$$

where $\zeta = 2kT\Omega/c^2$; $\gamma = (T_N/T_T)\nu^{2+\alpha}$; k is Boltzmann's constant; Ω is the solid angle subtended by the nonthermal source; c is the velocity of light; T_N is the equivalent temperature of the nonthermal source at frequency ν; and $T_T \equiv T$ is the temperature of the H II region. The tenuous medium in front of the dense medium has been ignored; it could be included by redefining the optical depth of the dense medium as $(s_1 - s_2)/\nu^2$,

but in practical cases the correction is trivial. Finally, the thermal emission from the tenuous medium not in front of the dense material would still be ignored. It can become important only if $\beta \ll 1$ and $\nu^2 \ll s_2$. Most measurements have been made in the low-frequency region, in which $\gamma\nu^{-\alpha} \gg s_1$. Under these conditions, equation (1) reduces to

$$\frac{S(\nu)}{\zeta\gamma} = \beta\nu^{-\alpha}e^{-s_1/\nu^2} + (1-\beta)\,\nu^{-\alpha}e^{-s_2/\nu^2}. \tag{2}$$

If $\beta \geq 0.5$, the spectrum will be appreciably flattened near $\nu = (s_1)^{1/2}$, while beyond $\nu = (s_2)^{1/2}$ the flux will drop rapidly with decreasing frequency because of the factor e^{-s_2/ν^2}.

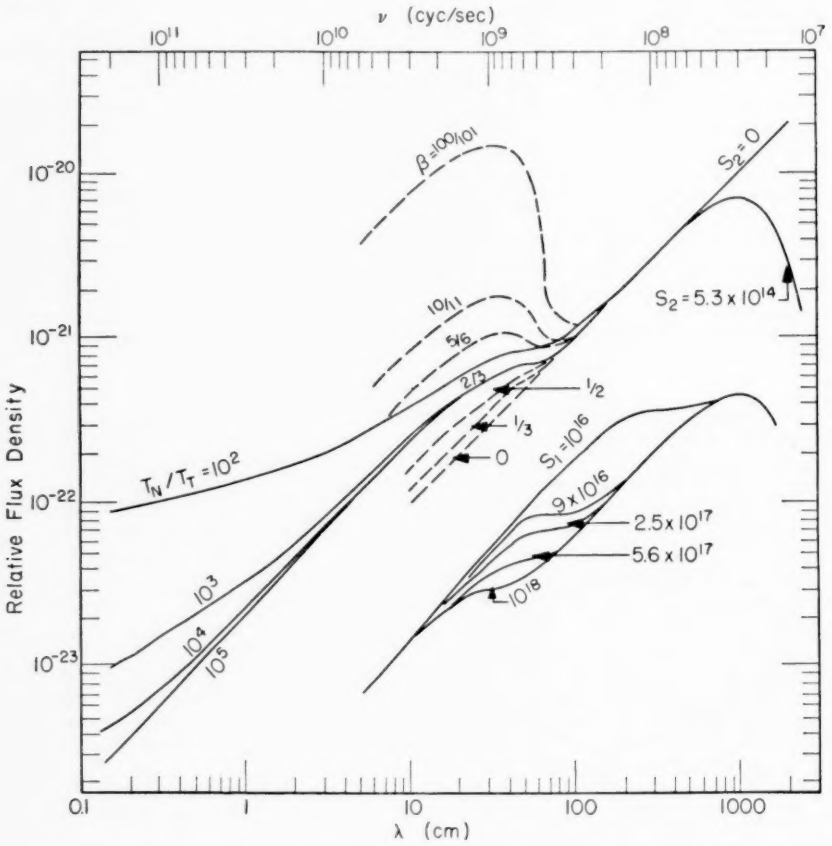

FIG. 1.—Spectra derived from the equation

$$S(\nu)/\zeta = \beta\nu^2\,(1 - e^{-s_1/\nu^2}) + \beta\gamma\nu^{-\alpha}e^{-s_1/\nu^2} + (1-\beta)\,\gamma\nu^{-\alpha}e^{-s_2/\nu^2},$$

showing the effect of changing the parameters γ, β, and s_2. The inset, which is shifted vertically, shows the effect of changing s_1 at a constant $\beta = \frac{2}{3}$. $s_1 = 5.6 \times 10^{17}$ for the main set of curves. The values of T_N/T_T are for $\nu = 10^8$ cyc sec^{-1}.

Equation (1) has seven parameters: T, Ω, γ, β, α, s_1, and s_2. Hence, it can be used to fit a large variety of observed spectral distributions, and, conversely, the fact that a given spectrum can be fitted by this equation has little significance without some independent restrictions on the parameters. The equation is useful because, as we shall see later, the model on which it is based and the values of the parameters derived for Cassiopeia A are physically reasonable. In addition, other, rather different, source spectra can also be fitted within the observational uncertainty, by changing only β, Ω, and, for Virgo A which is near the galactic pole, s_2 also.

The quantities T and Ω enter equation (1) as a product and cannot be derived separately; in equation (2) the same product also contains γ. If Ω can be determined from other measurements, γ can be determined from the amount of flux received from the source at intermediate and low frequencies, and T from the value of γ and the shape

TABLE 1

DATA PRESENTED AT DUBLIN* FOR CASSIOPEIA A

Frequency	Observer	Flux×10²⁴	
9400	Razin and Plechkov	4.6	±25%
1420	Westerhout and Muller	26	20
500	Adgie	56	25
400	Seeger	31.6	15
300	Razin and Plechkov	16	30
210	Adgie	121	20
207	Grebenkemper, Hagen, and McClain	67	25
38	Adgie	435	10
30	Lovell	450	20
22.6	Lovell	460	20
22.6	Hey and Hughes	940	25
19	Lovell	272	20
16	Lovell	<110	....
15.5	Wells	220	....
12.5	Wells	120	....

* Meeting of Commission 40 of the International Astronomical Union, Dublin, Ireland, September, 1955.

of the curve at very high frequencies. In general, however, the product $T\Omega\gamma$ can be treated as a single parameter which depends on the brightness of the source. If the spectrum is plotted on a log-log scale and the best parallel straight lines drawn through the linear parts of the spectrum, the slope of these lines is α, and their separation (i.e., the ratio of the intensities) is $\beta/(1-\beta)$. Finally, s_2 can be determined from the formula $s_2 = \frac{1}{2}\alpha\nu_m^2$, where ν_m is the maximum of the spectral curve. There is no simple way to determined s_1 exactly, but an estimate can be made from the fact that $s_1/\nu^2 = 1$ near the middle of the plateau. Figure 1 illustrates the effects of changing γ, β, s_1, and s_2.

The most thoroughly observed spectrum of a radio "star" is probably that for Cassiopeia A (see Fig. 2 and Table 1). Using this spectrum to determine the constants in equation (2), we find: $\alpha = 1.1$, $\beta = \frac{2}{3}$, $s_1 = 5.6 \times 10^{17}$, $s_2 = 5.3 \times 10^{14}$, and $\zeta\gamma = 3.8 \times 10^{-10}$ in c.g.s. units. The values of s_1 and s_2 correspond to $\tau_1 = 1$ at $\nu = 7.5 \times 10^8$ sec^{-1} and $\tau_2 = 1$ at $\nu = 2.3 \times 10^7$ sec^{-1} or to emission measures 1.7×10^6 and 1200 for the clouds and the regions between the clouds, respectively, if $T = 10^4$ degrees. (Emission measure $= N_i N_e l$ pc cm$^{-6} = 1.85 \times 10^{-17} \times T^{3/2}\tau\nu^2/g$, where l is the path length, N_i and N_e are the ionic and electronic densities, T and ν are in c.g.s. units, and g is the Gaunt factor, which varies slowly with frequency (Burkhardt, Elwert, and Unsöld 1948;

Strömgren 1948). Figure 2 shows the observed points and the curve obtained by substituting the foregoing constants in equation (2).

The emission measures can be checked against the densities which can be expected in interstellar space. For the tenuous region, we derive the reasonable value of about 1 free electron/cm^3 if the absorption is uniformly distributed between us and the source. Moreover, if Cassiopeia A is 3 or 4 kpc distant, the low-frequency absorption agrees with the value derived by Shain (1954) from studies of the continuous galactic radiation at low frequencies.

There are several possible explanations for the denser absorption. The intensity of the H I absorption between us and radio sources indicates cloud densities of about 200 atoms/cm^3 (Hagen, Lilley, and McClain 1955). If a cloud immediately in front of the

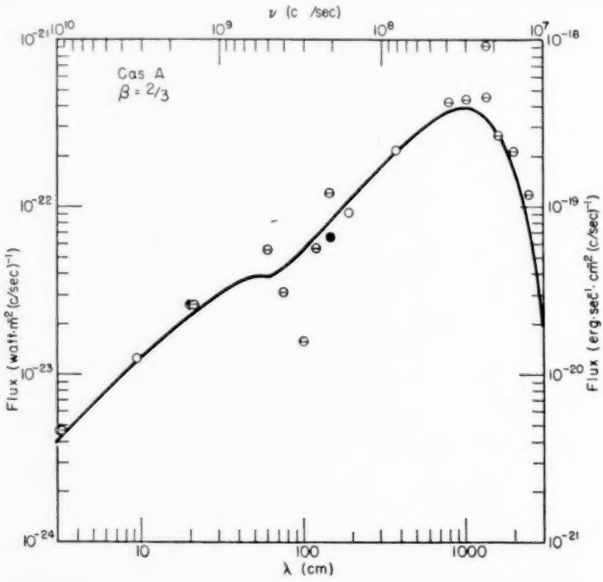

FIG. 2.—Observed fluxes and theoretical spectrum for Cassiopeia A. The symbols used in Figs. 2-7 indicate observed fluxes from the following references: *open circle:* Pawsey (1955); *filled circle:* Kraus *et al.* (1954); *circled cross:* Hagen *et al.* (1954); *circled horizontal bar:* data presented at the meeting of Commission 40 of the International Astronomical Union, Dublin, Ireland, September, 1955 (see Table 1); *circled vertical bar:* Haddock and McCullough (unpublished).

nonthermal source were as dense as 300 atoms/cm^3, an ionizing radiation from the source equivalent to that of thirty early O stars would ionize it to a depth of 10 pc and thus produce the emission measures required for the dense clouds. However, the problems mentioned in connection with the work of Greenstein and Minkowski might still arise; the thermal emission is reduced by only one order of magnitude. The thermal region must still be nearly as large as the nonthermal source, although the total optical depth is several times smaller than on their model. Moreover, clouds of such high density probably occur in the line of sight only about once per kiloparsec and hence are unlikely to be very near the nonthermal source. At a distance of 100 pc from the nonthermal source, ten thousand times as much ionizing radiation as that from an O5 star would be necessary to produce the observed emission measures, even in the absence of intervening clouds of lower density!

In view of these difficulties, it seems more likely that the dense nonthermal emitting regions are surrounded by regions of comparable density. In fact, it may well be these regions rather than the radio sources themselves which produce the spectra studied by Minkowski and Aller (1954). These could be ionized by either radiation or high-velocity ions and electrons from the nonthermal source. The electron density derived from the optical spectra of Cassiopeia A is 10^3–10^4 electrons/cm^3; in such a medium, path lengths of 1–0.01 pc would provide the required emission measures for the dense absorption. Moreover, for the same nonthermal emission, the volume of gas ionized would be inversely correlated with its density. The fact that some low-frequency radiation escapes may be explained in two ways. The source is highly turbulent, and hence the surround-

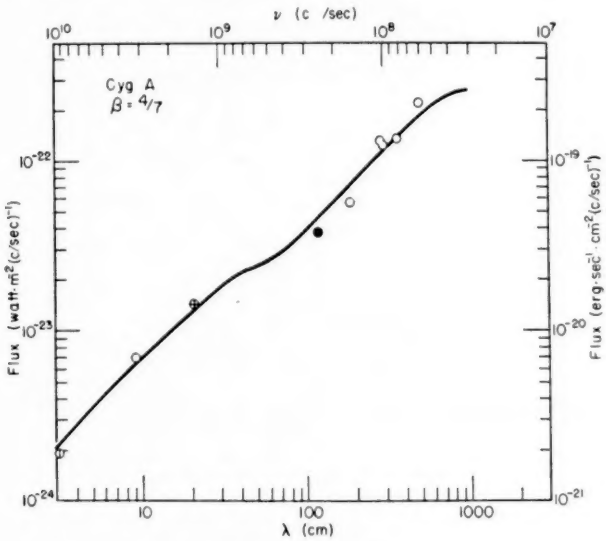

FIG. 3.—Observed fluxes and theoretical spectrum for Cygnus A

ing material will be irregularly distributed and may contain regions of such low density that the absorption is negligible. Alternatively, the nonthermal source may occur in small patches of different intensity and hence different ionizing power. The optical studies have indicated two types of filaments in Cassiopeia A: sharp, red bits with low-velocity dispersion and diffuse bits with very high-velocity dispersion (Minkowski 1954). Minkowski (1954) has remarked about the apparent correlation of radio emission from nonthermal sources and the optically measured velocity dispersion in these sources. If the same correlation exists between velocity dispersion and ionizing power, as would be expected, the sharp bits and the material surrounding them should have much lower emission measures than the diffuse bits, and hence the absorption of their radiation should be much smaller. On this picture the fraction of the radio intensity at moderate frequencies due to the sharp and the diffuse bits would be $(1 - \beta)$ and β, respectively.

III. APPLICATION OF THE THEORY TO OTHER SOURCES

Because of the flexibility of equation (2), it is important to test its applicability to the spectra of other sources. Figures 3–7 illustrate the observations for Cygnus A, Virgo A, Centaurus A, IC 443, and Taurus A and the curves obtained from $\beta = \frac{4}{7}, \frac{3}{4}, \frac{4}{5}, \frac{9}{10}$, and

0.95, respectively. The constant $\zeta\gamma$ has also been adjusted to give the correct magnitudes for the flux. A priori, there is no reason to keep s_1 constant for various sources. On the contrary, it would be expected to vary appreciably. However, since the observations are neither numerous nor precise enough to determine s_1 accurately, the value derived for Cassiopeia A is used for the other sources also. Cygnus A could be represented equally well by a curve with $\beta = 0$ and a slightly smaller value of α. Again the observational data

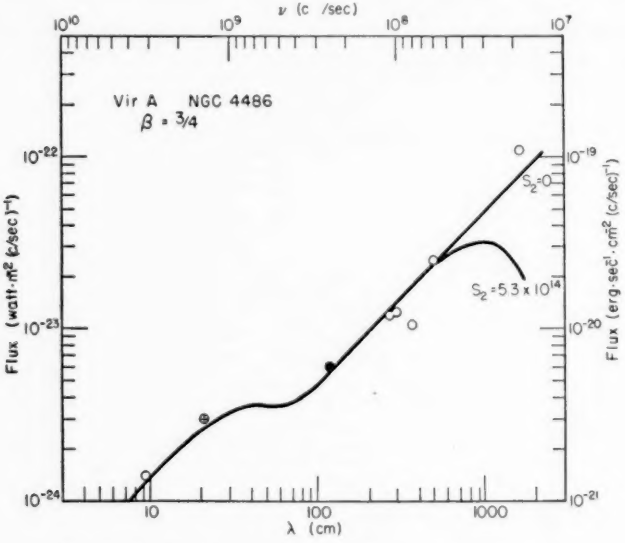

FIG. 4.—Observed fluxes and theoretical spectrum for Virgo A

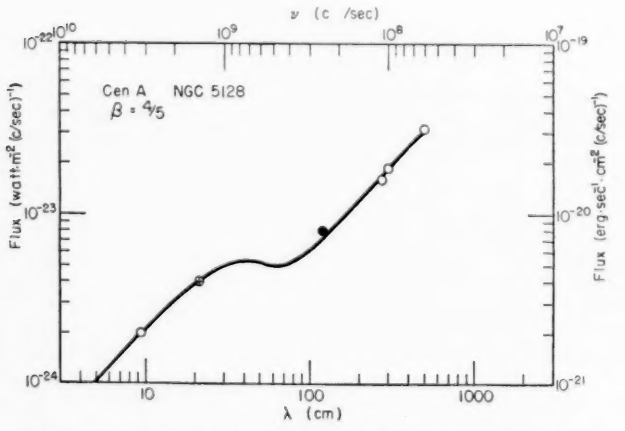

FIG. 5.—Observed fluxes and theoretical spectrum for Centaurus A

do not suffice to determine the parameters more precisely. Finally, s_2 is determined only for Cassiopeia A and for Virgo A (for which $s_2 = 0$). There is some indication that $s_2 > 0$ for IC 443. Since Virgo A is near the Galactic pole, the apparent lack of over-all tenuous absorption may indicate that most of this is unassociated with the sources. The value of α could vary for different types of sources, but the observations provide no evidence of this; if a value of α is assumed, the observations determine the parameter $\zeta^{\alpha}\gamma$ for each curve within about 10 per cent.

Thus we see that the observed plateaus in the spectra of nonthermal radio sources can be reasonably expected and that the variations between different spectra can be

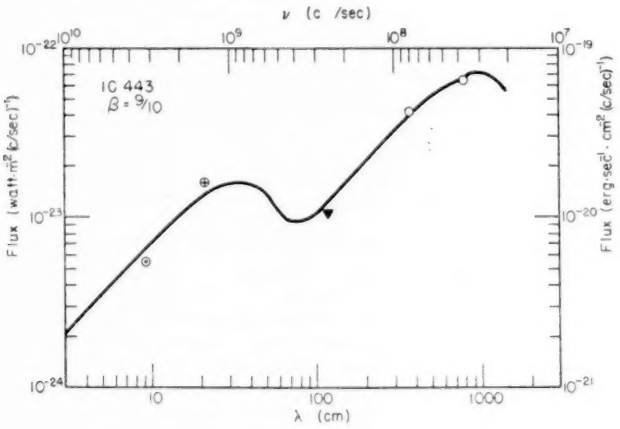

FIG. 6.—Observed fluxes and theoretical spectrum for IC 443

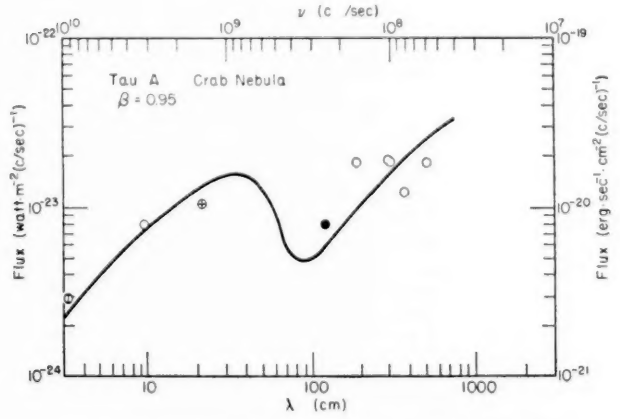

FIG. 7.—Observed fluxes and theoretical spectrum for Taurus A

explained, within observational uncertainties, by varying only the fraction of the source covered by dense absorbing regions. This, rather than the actual numerical parameters derived, is the important feature of the theory. More accurate and complete observations are needed to test the model as well as to provide better values for the constants. Accurate observations of the slopes of spectra at the highest available frequencies should provide useful information on the role of H II regions in the spectra of nonthermal sources. The positions of the drop in flux at the low-frequency end of the spectra may eventually provide a gauge of distance for galactic radio sources similar to interstellar-line intensity for stars, but this remains to be checked from much greater evidence.

REFERENCES

Burkhardt, G., Elwert, G., and Unsöld, A. 1948, *Zs. f. Ap.*, **25**, 310.
Greenstein, J. L., and Minkowski, R. 1953, *Ap. J.*, **118**, 1.
Haddock, F. T., Mayer, C. H., and Sloanaker, R. M. 1954, *Nature*, **174**, 176.
Hagen, J. P., Lilley, A. E., and McClain, E. F. 1955, *Ap. J.*, **122**, 361.
Hagen, J. P., McClain, E. F., and Hepburn, N. 1954, *Proc. I.R.E.*, **42**, 1811.
Hoyle, F. 1954, *J. Geophys. Res.*, **59**, 180.
Kraus, J. D., Ko, H. C., and Matt, S. 1954, *A.J.*, **59**, 439.
Minkowski, R. 1954, *J. Geophys. Res.*, **59**, 177.
Minkowski, R., and Aller, L. H. 1954, *Ap. J.*, **119**, 232.
Pawsey, J. L. 1955, *Ap. J.*, **121**, 1.
Shain, C. A. 1954, *Australian J. Phys.*, **7**, 150.
Strömgren, B. 1948, *Ap. J.*, **108**, 242.
Twiss, R. Q. 1954, *Phil. Mag.*, **45**, 249.

INTERSTELLAR POLARIZATION IN THE SOUTHERN MILKY WAY

ELSKE VAN P. SMITH*
Harvard College Observatory
Received February 3, 1956; revised March 18, 1956

ABSTRACT

Polarization observations are reported for over two hundred stars in the southern Milky Way between longitudes 200° and 350°. Analysis of these and other data for the north seems to confirm the model of a polarizing medium where the elongated particles are aligned perpendicular to the spiral-arm axis. Light from stars in the Sagittarius or Perseus arms appears to acquire most of its polarization from dust clouds lying in the Orion arm. The amount of polarization per unit extinction is lower in the southern Milky Way than in the northern. Although the possibility of a difference in the optical properties of the grains is not ruled out, an alternative hypothesis seems preferable. We suggest that the particles are more rigidly aligned in the center of the spiral arm, through which the line of sight passes when we look northward, than at the periphery of the arm. Finally, we discuss in some detail individual regions in the southern Milky Way, including Vela, Carina, the Coal Sack in Crux, and Scorpius. The Scorpius region, in particular, shows that local structure may considerably distort the general effect.

I. INTRODUCTION: INSTRUMENTATION AND THE POLARIZATION SYSTEM

All previous observations of interstellar polarization have been carried out in the Northern Hemisphere, so that a large segment of our Galaxy has remained unexplored. The southern Milky Way is of particular interest, since here the field of view covers the inner edge of the Orion arm and the whole of the Sagittarius arm; one can also penetrate to the second inner spiral arm. In an attempt to fill this gap, more than two hundred stars between 200° and 350° longitude were observed for polarization at the Boyden Station of Harvard Observatory in South Africa.

The greater part of the data was obtained with the 60-inch Rockefeller reflector. A calcite crystal[1] served as the polarizing analyzer and was mounted in a photoelectric polarimeter used in conjunction with the amplifier of the Linnell-King photometer. Initial plans included a seeing-compensation scheme which utilized both rays emerging from the calcite, but these plans had to be abandoned because of instrumental difficulties. Hence the observations discussed here were made by the use of only the ordinary ray.

The technique of observation and reduction resembles that described by Hiltner (1951), with some modifications. To measure the amount of polarization, the amplifier gain was increased by a factor of approximately 10 over that required for the total intensity of the star. Since the dark current was far below the zero reading of the recorder tape, it was possible only to read differences in intensity at complementary positions of the calcite crystal. This procedure necessitated separate readings to obtain the total intensity; these were made at the beginning and end of each set of observations. As in Hiltner's procedure, master sine-curves were used in the reductions.

Since the mirror of the 60-inch telescope has no central hole, the polarimeter was attached at the Newtonian focus. A combination of a second flat mirror, mounted normal to the Newtonian, and a set of tilted glass disks partially compensated for elliptical polarization introduced by the Newtonian flat. Although this device considerably reduced the instrumental polarization, nevertheless some remained, as was shown by observations of nearby stars that could be assumed to be unpolarized. To correct for this instrumental polarization, it became necessary to establish an error-free system of polarization, which we obtained from measurements made with the 13-inch Boyden

* Now at Sacramento Peak Station of Harvard Observatory, Sunspot, New Mexico.

[1] Generously donated by the Polaroid Corporation, Cambridge, Mass.

refractor. The 13-inch polarimeter consisted simply of a rotating piece of polaroid mounted in place of the filter holder of a photometer, kindly loaned by the Washburn Observatory South African Expedition. A depolarizer in front of the 1P21 photomultiplier eliminated the problem of sensitivity changing with the plane of vibration. Careful observations of unpolarized, nearby stars confirmed the absence of any instrumental polarization. However, the position angles of the plane of vibration on the 13-inch, or Smith, polarization system differ by $-2°$ from those of Hall (Hall and Mikesell 1950; Hall, unpublished) and of Hiltner (1951, 1954), as determined from data on stars measured in common with one or another of the northern observers. The zero point of the 13-inch system was carefully checked, and no cause of the difference could be found. No such systematic difference appears when amounts of polarization are compared. The 60-inch observations were reduced to the Smith system by means of calibration-curves derived from a comparison of 60-inch data with 13-inch data for the same stars.

TABLE 1

DISPERSIONS IN COMPARISONS BETWEEN DATA OF SMITH (EPS), HALL (JSH), AND HILTNER (WAH)

	σ_θ			σ_P		
	JSH	WAH	EPS	JSH	WAH	EPS
EPS ($P<0^m050$)	12°3	4°2	...	0^m0083	0^m0034	...
EPS ($P>0^m050$)	5.3	3.5	...	.0125	.0046	...
JSH	...	3.3	4°5	...	.0093	0^m0082
13-in ($P<0^m050$)	7.1	2.6	4.0	.0101	0.0048	.0055
13-in ($P>0^m050$)	5.5		2.5	0.0132		0.0044

In view of the method of calibration, a calculation of probable errors in the observations would have little meaning, but we may estimate that they are, in general, less than ± 0.004 mag. for individual values of the amount of polarization, $P_{\Delta m}$, and less than $\pm 4°$ in position angle, θ. An additional measure of the accuracy of the final values of the derived polarizations lies in the dispersions found from comparisons with other systems. A correction of $-2°$ was applied to the residuals in position angle used in computing the dispersions which compare the Smith observations with those of Hall or Hiltner. Hall's position angles required a conversion from the plane of polarization to the plane of vibration by the addition of 90°. Similarly, his percentage polarization had to be changed into magnitude increments by the relation

$$P_{\Delta m} = 46.05 P_{\%} ,$$

to bring his values into the same units as those used by Smith and Hiltner. Table 1 lists the dispersions in the comparisons among the three sets of observations. The Smith observations represent the finally adopted values of the polarization. Generally, these consist of the 60-inch data, but weighted means were used when 13-inch observations were also available. The first and second rows give the simple comparisons of Smith's data with those of Hall or Hiltner, separated into small and large amounts of polarization. The third row compares Hall's data with those of Hiltner and Smith for stars observed in common by all three. The Hall-Smith comparisons are clearly similar to the Hall-Hiltner dispersions for the same stars. Since the 13-inch data actually define the Smith system, separate comparisons with the observations of Hall and Hiltner are of interest. Too few stars were observed in common with Hiltner to permit a breakdown

into small and large polarizations. The 13-inch Smith figures actually refer to comparison between 13-inch and reduced 60-inch observations and are therefore an indication of the success of the calibrations. Table 1 shows that the dispersion in the comparisons of Smith's data with those of Hiltner is considerably less than with those of Hall. In all probability we may attribute this to the quality of the skies under which the respective observations were obtained.

II. THE CATALOGUE

Table 2 presents the spectral, photometric, and polarimetric data for all the stars observed.

Column 1 gives the *HD* or *HDE* number of the star.

Columns 2 and 3 list the galactic co-ordinates of the star, as referred to the Lund pole (Ohlson 1932).

Column 4 notes the spectral type on the MK system (Johnson and Morgan 1953) when it is available (Sharpless 1952; Hiltner 1954; Morgan, Code, and Whitford 1955; Hoffleit, unpublished; Houck, unpublished); otherwise *HD* spectral types are given.

Columns 5 and 6 give, respectively, the magnitude to a tenth on the *V* system of Johnson and Morgan (1951) and the color on the C_1 system of Stebbins, Huffer, and Whitford (1940). When more than one photoelectric magnitude or color (Oosterhoff 1951; Bok and van Wijk 1952; Sharpless 1952; Hiltner 1954; Morgan, Code, and Whitford 1955; Hoffleit, unpublished; Houck, unpublished) was available for a given star, the mean is listed. Colors from the Cape Zone photographic catalogue (Jackson and Stoy 1954, 1955) were also included in the mean, as the accuracy seems to be comparable to that obtained from photoelectric equipment. If no photoelectric magnitude was known, the magnitude given is that converted to the *V* system from the Cape or *HD* catalogues.

Column 7 gives the color excess, E_1, determined on the basis of the Morgan, Harris, and Johnson list (1953) of normal colors.

Column 8 lists the approximate distance modulus, where the absolute magnitude is generally taken from the published table of Morgan and Keenan (1951), and the visual absorption is given by the relation $A_v = 6.1\ E_1$ (Morgan, Harris, and Johnson 1953).

Columns 9–12 give the polarimetric data. The percentage polarization, $P_{\%}$, derives from the observed magnitude increment, $P_{\Delta m}$, by $P_{\%} = 46.05\ P_{\Delta m}$. The position angle of the plane of vibration is referred to both the equatorial and the galactic co-ordinate system, which are denoted by θ_E and θ_G, respectively. Values which are less certain than the majority, as discussed in the first section, are indicated by the following code: a period (.) denotes an uncertainty of 0^m005–0^m010 in $P_{\Delta m}$ and 5°–10° in θ; a colon (:) signifies an uncertainty of 0^m010–0^m020 in $P_{\Delta m}$ and 10°–20° in θ; quantities followed by a double colon (::) are uncertain by more than 0^m020 or 20°.

Column 13 gives the number of observations of each star. Figures in parentheses indicate observations with the 13-inch; others refer to the 60-inch observations.

III. RELATION OF POLARIZATION TO SPIRAL STRUCTURE

Figure 1 illustrates the projected space distribution, in galactic co-ordinates, of the maximum of the electric vector of polarized starlight between longitudes 210° and 360°. One notes that the maximum of the electric vector has a preferential direction parallel to the galactic equator, as was already found in the north by Hall and Mikesell (1950) and by Hiltner (1951). Superimposed on this general phenomenon are important regional variations, which appear to be correlated with the orientation of the axes of spiral arms to the line of sight. This correlation is such that when we are looking transverse to a spiral arm, i.e., the axis of the arm crosses the line of sight, the maximum of the electric vector is far more uniformly aligned than it is when we are looking along a spiral arm. The region between $l = 265°$ and $l = 310°$ corresponds to the segment of the Milky Way

TABLE 2

POLARIZATION AND RELATED DATA OF SOUTHERN STARS

HD	ℓ	b	Sp	m_v	C_1	E_1	m_o-M	P_ℓ	$P_{\Delta m}$	θ_E	θ_G	No.
35149	166°.7	-16°.4	B1 V	4.9	-.20	+.04	7.9	0.4	.008	70°	10°	2
36629	175.6	-18.0	B2 V	7.6	-.13	+.10	9.6	1.8	.040	98	36	2
36958	175.9	-16.1	B3	7.4	-.18	+.04	8.4	1.3·	.028·	39:	156:	3
37041	176.7	-17.9	09.5 Vp	5.1	-.16	+.11	8.6	0.5	.011	71	9	2
37061	176.7	-17.8	B1 V	6.9	0.00	+.24	8.6	1.3	.028	60·	178	2
42051	181°.5	-11°.4	B3	8.9	+.01	+.23		1.7	.038	106°	43°	2
259597	171.2	+ 1.3	B0.5:V:nne	8.5	-.16	+.09	11.4	1.1:	.023:	70	8	2
46769	178.0	- 1.8	B3e	5.6	-.12	+.10		1.2·	.025·	122	60	2
47129	173.6	+ 1.2	08	6.0	-.12	+.16	9.7:	1.0	.022	155	93	2
47398	175.1	+ 0.8	B2	8.3	-.13	+.10		1.3	.029	160	98	2
51354	165°.3	+10°.9	B3ne	7.0	-.22	0.00		0.9·	.020·	139°	75°	2
52559	176.9	+ 6.3	B2e	6.4	-.12	+.11		1.1·	.023·	63	1	2
54662	191.9	+ 0.6	06	6.1	-.15	+.14	10.3:	0.8·	.017·	142	81	2
61709	213.6	- 3.5	B1	8.2	-.04	+.20		1.7·	.038·	126·	67·	3
61827	214.7	- 4.0	08:	7.7	+.13	+.41	9.9:	1.9	.041	2	125	4(2)
62150	214°.9	- 3°.9	B3 Ia	7.7	+.10	+.32	12.7	2.4	.053	143°	84°	4(1)
-32°4348	213.2	- 2.0	B	9.0	+.37	+.63		2.8	.061	123	65	3
62844	215.0	- 3.0	B0	8.1	+.21	+.47		1.7·	.038·	4	125	2
63804	216.4	- 2.7	B	7.6	+.51	+.77		2.5	.055	23	145	2
68450	222.1	- 1.2	B0 II	6.5	-.14	+.12	11.8	-	-	-	-	2
68761	222°.0	- 0°.9	B0.5 III	6.6	-.17	+.08	10.5	<0.4	<.008	-	-	3
69106	222.1	- 0.5	B0.5 II	7.2	-.17	+.08	11.9	-	-	-	-	4
71304	229.4	- 3.1	09 III?	8.2	+.12	+.39	11.5	1.3	.028	36°	163°	2
73882	227.9	+ 1.3	08(V)	7.3	+.06	+.34	9.9:	1.8	.040	163	112	5(3)
75860	231.9	+ 0.9	B1.5 Iab	7.7	+.23	+.47	11.3	1.7	.037	138·	89·	3
76968	237°.9	- 2°.9	B0 II	7.1	-.09	+.17	11.3	1.2·	.026·	178°	130°	4
77581	230.9	+ 4.6	B0.5 Ib	6.9	+.10	+.35	10.8	3.5	.077	80	33	5(3)
77718	235.4	+ 0.6	B2	8.7	+.19	+.42		2.7	.059	20	154	3
78785	235.8	+ 1.5	B2	8.7	+.14	+.37		4.5	.097	5	140	2
78958	233.8	+ 3.3	B0.5 II	9.1	+.20	+.45	11.6	3.1	.068	91	46	3
79573	239°.1	- 0°.6	WC6	10.8				5.5·	.119·	156°	112°	3
80077•	239.3	- 0.1	B2 Iape	7.7	+.53	+.76:	10.1:	3.8	.082	147	103	3
298298	240.3	- 2.9	B1 Vpe	9.1	+.03	+.27	10.7	1.9·	.042·	164·	119·	2
298310•	240.2	- 1.1	B0					2.5	.055	164·	120·	2
298369	240.8	- 0.4	B1 Vp	9.5	+.05	+.29	10.9	1.5·	.032·	162·	119·	3
298387	241°.6	- 1°.8	B2 V	10.3	-.07	+.16	11.9	1.7	.036	139°	96°	2
298383	241.8	- 1.3	A0 Ib	9.7	+.29	+.41	12.2	5.1	.111	148	105	3
81370	242.0	- 1.4	B0 IV:	8.8	-.09	+.17	12.0	2.5	.054	128·	85·	2
298377	241.6	- 0.8	B1 IV:	10.4	+.01	+.25	12.7	2.3	.050	140·	98·	3
83043	243.9	- 1.0	B1 V:pe	8.5	-.12	+.12	11.0	1.7	.036	160·	120·	2

TABLE 2 (Continued)

HD	ℓ	b	Sp	m_v	C_1	E_1	m_o-M	F$_\lambda$	P_{obs}	θ_E	θ_G	No.
83597	244°3	- 1°0	B1 Vpe	9.3	-.08	+.16	11.5	1.3	.029	157°	117°	2
300167	244.9	- 0.8	B2	8.7	+.40	+.63		1.1	.024	112	73	3
300214	244.6	- 0.4	B	8.6	+.41	+.67		5.2	.112	146	108	2(2)
84567	230.0	+18.1	B2	6.4	-.20	+.03		0.8	.020	71	30	4(3)
84881	245.6	- 0.2	B2	8.7	+.14	+.37		3.4	.074	154	116	2
90615	252°0	+ 0°4	B0 II	8.2	-.01	+.25	11.9	1.1·	.024·	133°	103°	2
90706	252.2	+ 0.3	B3 I:	7.2	+.09	+.31	11.6	2.7	.059	151	121	6(3)
90831	252.2	+ 0.4	B2 III	9.4	+.07	+.30	11.7	1.3·	.028·	150·	120·	3
90832	252.2	+ 0.3	B1 III	9.1	+.04	+.28	11.7	1.2·	.027·	150·	120·	4
300774	252.2	+ 0.6	B3	9.7	+.21	+.43		2.5	.054	165·	136·	2
91824	253°4	+ 0°3	07	7.9	-.16	+.13	12.1:	1.8·	.038·	107°	79°	3
91850	253.4	+ 0.3	B1 IV:	9.2	-.04	+.20	11.8	2.8	.060	108	80	3
91943	253.5	+ 0.2	B0.5 Ib	6.8	-.10	+.15	11.9	1.2	.025	110	82	6(3)
91969	253.6	+ 0.2	B0 Ib	6.6	-.13	+.13	11.8	1.8	.038	111	83	5(3)
91983	253.6	+ 0.1	B1 III	8.6	-.11	+.13	12.1	1.9·	.042·	127	99	2
92007	253°6	+ 0°2	B0 II	8.1	-.09	+.17	12.3	1.2·	.025·	123°	95°	2
92044	253.6	+ 0.1	B0.5 II	8.3	-.06	+.19	12.3	1.3·	.028·	142	114	3
92060	253.5	+ 0.4	B2	8.7	+.06	+.29		3.2	.070	122	94	5
92206•	253.9	- 0.1	07	7.7	-.07	+.22	11.4	2.9	.062	87	59	6
92207•	253.8	- 0.2	A0 Ia	5.5			11.2:	3.2	.070	112	84	6(3)
92420	253°7	+ 0°7	B2	9.0	+.01	+.24		2.8	.060	96°	69°	6
92740	254.8	- 0.7	WN7	6.4	-.10			2.2	.048	100	73	2
93131	255.3	- 1.0	WN7	6.5	-.16			2.9	.064	100	74	2
93206	255.4	- 0.9	B0 Ib:	6.5	-.07	+.19	11.3	2.9·	.064·	112·	86·	2
93342	255.2	- 0.3	B0 III:	9.0	+.19	+.45	10.7:	1.4·	.031·	70°	44·	2
93403	255°2	- 0°3	05 (f)	7.3	-.02	+.27:		2.2	.047	100°	74°	5
93795	255.6	- 0.2	A0 Ia	9.0	+.28	+.40	13.6	2.2·	.048·	95·	70·	3
93890	255.4	+ 0.4	B	9.1	+.27	+.53		<0.5	<.010	-	-	2
94369	255.5	+ 1.1	B1 I	7.4	+.01	+.25	12.4	1.2	.025	142	118	3(3)
94909	255.7	+ 2.0	B0 Ib	7.3	+.10	+.36	11.1	4.7	.103	117	93	5
96248	257°6	+ 0°3	B1 Iab	6.6	-.03	+.21	11.8	0.9	.020	132°	110°	5(3)
96261	257.6	+ 0.4	B1 Ib	7.6	-.04	+.20	12.4	1.7	.037	112	90	2
96670	257.9	+ 0.4	08	7.4	-.06	+.22	10.7:	1.7	.036	177	156	7
96880	257.9	+ 1.0	B1 Ib	7.6	+.10	+.34	11.5	2.3	.049	60	39	4(3)
97222	258.4	+ 0.3	B0 II:	8.7	-.03	+.23	12.5:	1.3	.028	118	98	3
97253	258°5	+ 0°1	06	7.0	-.06	+.23:		1.0·	.022·	143°	123°	5
97848	258.5	+ 1.5	09 IV	8.7	-.14	+.13	12.7	0.7·	.016·	86:	66:	2
97950•	259.5	- 0.6	WN5 + O	9.0	+.32			1.2	.026	130	110	2
97966	258.7	+ 1.1	07.5	8.9	-.12	+.17	12.7:	0.5·	.011·	94:	73:	2
98733	259.6	+ 0.7	B1 Ib	8.0	-.05	+.19	12.8	1.0·	.022	70·	52·	2
99546	260°1	+ 1°6	08	8.3	-.15	+.13	12.2	1.5	.032	120°	103°	2
99953	261.6	- 2.2	B2 Ia	6.5	+.01	+.24	12.0	2.0	.044	103	86	5(3)
100099	261.7	- 2.5	09.5 V?	8.1	-.09	+.18	11.1	1.1	.023	108:	92:	3
100199	261.6	- 1.6	B1 Ibp	8.1	-.11	+.13	13.3	<0.5	<.010	-	-	3
102997	263.6	0.0	B5 Ia	6.1	+.01	+.20	12.4	1.2·	.026·	74·	62·	5

TABLE 2 (Continued)

HD	ℓ	b	Sp	m_v	C_1	E_1	m_o-M	F_β	$F_{\Delta m}$	θ_E	θ_G	No.
103779	264°.5	- 1°.2	B0.5 Ib	7.2	-.15	+.10	12.6	0.7	.015	80°	69°	4(3)
104631	265.0	0.0	B1 II	6.8	-.09	+.15	11.0	0.4:	.008:	69	59	3
104705	265.1	- 0.5	B0.5 III	7.8	-.14	+.11	11.5	<0.4	<.008	-	-	3
110360	269.6	+ 1.9	O7	9.4	-.07	+.22	13.1:	1.4:	.030:	90	89	2
110432:	269.6	- 0.5	B2nne	5.4	-.04	+.19:	7.0:	2.0	.044	76	75	5(3)
110639	269°.8	+ 1°.2	B1 Ib - II	8.4	+.19	+.43	11.3	3.5	.075	89°	89°	2
110660	269.8	- 1.5	B1 V	10.0	+.12	+.36	11.0	2.9	.063	72	72	1
110863	270.0	+ 2.0	B1 Vp	9.0	+.04	+.28	10.5	2.9:	.062:	93	93	3
110984	270.1	+ 1.4	B0 IV	9.0	+.11	+.37	10.9	5.3	.115	88	88	3(3)
111124	270.2	- 0.4	B0	9.1	+.20	+.46		1.2	.025	22	23	2
111193	270°.2	+ 2°.3	B0	8.0	-.03	+.23		3.4	.073	80°	80°	4(3)
311999:	270.5	+ 1.0	O9.5 IV	10.9	+.12	+.44	12.7	2.9	.062	94	95	2
111579	270.6	+ 1.3	B2	9.2	+.19	+.42		5.5	.120	103:	104:	3
312052	270.6	- 0.7	B	11.5	+.12	+.38		2.6	.056	57	58	2
312051	270.7	- 0.6	B	11.3	+.22	+.48		3.0:	.065:	53	54	2
112027	271°.0	+ 1°.5	B2	9.2	+.16	+.39		2.4	.052	53°	55°	2
312155	271.3	0.0	B0					1.6	.035	43	45	2
112272	271.2	- 1.8	B0.5 Ia	7.4	+.25	+.50	11.4	1.1	.023	55	57	4(3)
312259	271.6	+ 0.9	B	10.6	+.43	+.69		5.5	.119	90	93	3
312258	271.7	+ 0.9	B	10.4	+.47	+.73		6.4:	.140:	88	91	3
112784	271°.7	+ 1°.9	O9.5 III	8.3	-.11	+.17	12.3	1.8:	.040:	84°	87°	3
112953	271.9	+ 1.5	B2	9.1	+.24	+.47		4.6	.099	81	84	2
113034	271.8	+ 0.6	B1 I:	9.3	+.37	+.61	12.1:	4.6	.099	80	83	4(3)
113163	272 .1	+ 1.7	B5 IV	7.8	0.00	+.19	8.8	2.4	.052	88	92	6(3)
113422	272.2	+ 0.7	B1 Ia	8.3	+.26	+.50	12.3	5.7	.125	82	86	5(3)
312256	272°.3	+ 0°.8	B	9.8	+.24	+.50		4.0	.088	100:	104:	2
113511	272.1	- 1.6	B0 III:	9.1	+.08	+.34	11.5	1.9::	.041::	70:	74:	2
113754	272.4	- 0.7	B0	9.5	+.19	+.45		4.6	.100	71	76	2
114011	272.8	+ 1.3	B1.5 Ia(+)	9.3	+.24	+.51	13.2+	<1.1:	<.025:	-	-	3
114122	272.7	- 0.4	B0	8.7	+.14	+.40		2.7	.059	84	89	2
114340	273°.2	+ 2°.6	B1 Ia+	8.2	+.12	+.36	13.0+	5.0	.108	74°	80°	3
114341	273.2	+ 2.2	B0 III:nn	8.6	+.05	+.31	11.2:	2.3	.050	78	84	2
114478	273.0	- 0.5	B1 II	8.8	+.10	+.34	11.8	1.6	.035	71	77	2
115363	273.6	- 1.4	B1 Ia+	7.8	+.15	+.39	12.4+	3.1	.067	58	65	2
115704	274.1	+ 0.2	B0	8.2	+.08	+.34		3.5	.075	71	79	3
115746	273°.8	- 1°.2	B2	9.4	+.03	+.26		2.3	.050	60°	68°	2
116119	274.4	+ 0.2	B9 I	8.1	+.21	+.35	12.2	2.9	.064	76	84	3
117111	274.5	- 3.4	B1 Vpe	7.6	-.09	+.15	9.9	1.4	.030	70	80	3(3)
117707	275.0	- 3.2	B0.5 I	9.5	+.13	+.38	13.7	2.4	.052	58	68	2
122324	280.7	+ 4.9	B0	9.1	+.08	+.34		4.5:	.097:	81	98	2
122450	279°.8	+ 1°.5	B0	9.3	+.08	+.34		1.2:	.027:	70°	87°	2
122879	280.0	+ 1.2	B0 Iab	6.4	-.08	+.18	11.8	1.6	.035	70	87	5(3)
123056	279.9	+ 0.5	O9.5 V	8.2	-.08	+.18	11.2	1.6	.035	66	84	5
124909	281.0	- 0.4	B2	9.2	-.01	+.22		1.3	.029	55	75	2
125206	281.2	- 0.6	B2	8.0	-.02	+.21		2.2	.047	58	78	3(3)

TABLE 2 (Continued)

HL	ℓ	b	Sp	m_v	C_1	E_1	m_o-M	P_{ℓ}	P_{Am}	θ_E	θ_G	No.
125241	281°3	- 0°4	09 I	8.4	+.04	+.31	13.0	2.0	.044	67°	87°	2
126940	282.6	- 0.5	B2	9.5	+.09	+.32		4.7	.102	80	103	2
134959•	288.2	- 2.0	B0	8.1	+.33	+.59		6.0	.130	66	98	6
135591	287.8	- 3.4	09 Ib	5.3	-.20	+.07	10.9	0.7•	.016•	43	76	2
136003	290.3	+ 0.1	B1	6.8	-.05	+.19		2.9	.063	66	99	5(3)
136239	288°8	- 2°6	B2 Ia+	8.0	+.34	+.57	12.5+	4.6	.100	67°	100°	6(3)
136488	287.1	- 5.5	WC8	9.4	0.00			2.9	.064	66	100	2
138764	324.2	+35.0	B8s	5.1	-.14	+.01		0.6	.014	72	118	5(3)
142468	295.6	- 1.6	B0	8.0	+.13	+.39		2.3	.050	45	86	5
142565	295.7	- 1.8	B0 Ib	9.0	+.08	+.34	12.9	1.9•	.042•	40	81	2
142634	295°7	- 1°8	B0(II)p	9.0	+.18	+.44	11.5:	2.6	.057	55°	96°	3
142775	295.7	- 1.8	B2	9.3	+.20	+.43		1.9	.041	35	76	2
142983	324.4	+27.3	B3n	4.9	-.13	+.09		0.9	.020	122	170	2
144969	301.0	+ 1.0	B0.5 Ia	8.4	+.37	+.62	11.6	3.0•	.065•	27	70	1
144970	300.8	+ 0.8	B0	9.9	+.27	+.53		2.3•	.051•	45	88	1
145664	298°8	- 2°0	B2	8.4	+.03	+.26		3.7	.081	52°	96°	5
145794	298.5	- 2.5	B2	8.8	-.02	+.21		1.6•	.035•	34	78	2
145846	299.0	- 2.1	B2 Vpe	9.0	+.04	+.27	10.0	3.6	.079	52	96	2
146919	299.1	- 3.2	B1.5 Ia	8.7	+.14	+.38	13.4	3.4	.073	32	77	5
147049	299.4	- 3.0	B2	7.7	+.01	+.24		2.3	.050	43	89	3(3)
147331	299°8	- 3°0	B0 Ia	8.8	-.01	+.25	14.3	2.0•	.043•	39°	85°	2
147421	299.2	- 3.8	B2	9.0	-.11	+.12		2.5•	.054•	59•	105•	3
147888	321.5	+16.4	B3	6.5	+.01	+.23		2.8	.061	52	101	6(4)
147889	320.8	+15.7	B3	7.9	+.27	+.49		3.2	.069	175	44	7(3)
147932	321.6	+16.4	A	7.0				2.5	.055	58	107	5(3)
147933	321°6	+16°3	B5n	4.6	-.03	+.16		2.3	.051	47°	96°	3(3)
148184	325.8	+19.3	B3e	4.5	-.01	+.21		1.8	.039	113	164	1
148546	311.1	+ 5.9	09.5I	7.8	-.02	+.25	12.8	2.0	.043	6	53	2
150475	312.9	+ 4.2	08.5	8.8	0.00	+.28	11.6	0.7:	.016:	71:	120:	5
151397	312.1	+ 2.0	B2	9.9	-.02	+.21		1.8	.038	5	55	3
151932	310°9	+ 0°2	WN8	6.5	0.00			1.2	.025	43°:	94°::	1
151985	314.0	+ 2.6	B2	3.4	-.22	+.01		0.5	.010	25	76	(2)
152408	311.9	+ 0.3	08 fp	5.8	-.06	+.22	9.2	0.7	.016	39	90	3(2)
152667	312.2	+ 0.2	B0 Ia?p	6.2	-.01	+.27	11.6:	-	-	-	-	2
152723	312.5	+ 0.2	06	7.0	-.06	+.23:	10.6:	1.2•	.025•	43::	94::	1
153426	314°9	+ 1°0	B2	7.5	-.06	+.17		2.3	.050	0°	52°	3
154040	314.4	- 0.1	B2e	10.0	+.03	+.26		0.8:	.017:	70•	123•	3
154090	318.6	+ 3.0	B1 Iab	4.9	-.01	+.23	10.0	-	-	-	-	2
154445	347.0	+21.4	B1 V	5.5	-.11	+.13	7.9	3.5	.077	88	147	4(3)
154450	317.5	+ 1.6	B0.5 IVp	8.7	+.04	+.29	10.9	0.6	.012	71	124	2
154911	315°5	- 0°4	B0e	9.2	+.04	+.30		1.6•	.035•	138°	11°	2
156134	318.9	0.0	B0 I	8.2	+.16	+.42	12.0	2.5	.054	117	172	2
156154	319.0	+ 0.1	07	8.3	+.13	+.41	10.8	2.0	.044	123	178	2
156201	319.2	+ 0.1	B0	8.0	+.20	+.46		1.5	.033	124	179	2
158705	323.9	- 0.3	B0	8.1	+.24	+.50		1.8	.039	122•	179•	3

TABLE 2 (Continued)

HD	ℓ	b	Sp	m_v	C_1	E_1	m_0-M	P%	P_{am}	θ_E	θ_G	No.
159176•	323°3	- 1°3	07	5.7	-.11	+.18	9.6	1.6	.034	163°	40°	4(3)
159975	344.8	+10.9	B8	4.6				0.8:	.018:	101:	160:	1
160529	323.4	- 3.1	A2 Ia+	6.7	+.48	+.56	10.3+	7.2	.156	18	76	5(3)
316197	328.5	- 0.5	B3 V	9.6	+.13	+.35	9.5	5.5	.120	174	52	2
161056	346.4	+10.1	B5n	9.2	+.05	+.24	9.0:	3.5	.077	66	126	3
161103	329°0	+ 0°4	B2:pe(III-IV)	8.5	+.07	+.30	10.4:	4.9	.106	170°	48°	5
316204	328.1	- 1.1	B2 III	9.2	+.02	+.25	11.8	4.0	.088	166	44	2
161291	329.2	- 0.6	B1 Iab	8.9	+.24	+.49	12.4	6.5	.142	1	59	3
161306	344.1	+ 8.5	B(0)ne	8.2	+.13	+.39		3.5	.075	64	124	3
316332•	327.3	- 2.1	B3 Ia	9.5	+.55	+.77	11.7	1.8	.040	15	74	2
316285	329°8	- 1°4	Beq					3.1	.068	162°	41°	2
161961	351.3	+11.4	B0.5 III	7.8	-.04	+.21	10.9	2.3	.050	74	135	2
162168	324.8	- 4.5	B0	8.5	+.15	+.41		2.5	.054	169	48	2
316415	328.0	- 2.6	B3	10.0	+.24	+.46		2.5·	.054·	3	63	1
162717	332.6	- 0.5	B3	9.2	+.17	+.39		3.0	.065	176	55	3
162718	332°0	- 0°8	B0ne	8.9	+.17	+.43		3.5	.076	0°	59°	2
162742	328.5	- 3.0	B3	8.4	+.06	+.28		2.7:	.058:	159·	38·	2
316569	327.9	- 3.5	B3 II	9.4	+.02	+.24	12.4	1.3	.028	11	71	2
316568	326.0	- 3.5	B2pe(IV-V)	9.7	+.01	+.24	11.2:	1.7	.038	8	68	2
162978	332.2	- 1.1	B2	6.2	-.14	+.09		1.2	.026	179	58	4(4)
163065	327°4	- 4°1	B1 Iab	8.6	+.05	+.29	13.3:	1.7·	.038·	38°	98°	1
163453	329.6	- 3.3	B0.5:pe(V)	9.3	+.18	+.43	10.3	2.0	.043	16	76	2
316730	328.3	- 4.2	B3	9.6	+.02	+.24		1.4:	.031:	169	49	1
164018	334.4	- 1.3	B3	9.3	+.18	+.40		1.4:	.031:	119:	179:	1
164019	329.6	- 4.0	B0 Ia:	9.3	-.03	+.23	14.9:	2.4	.052	177	57	1
164438	338°1	+ 0°3	09 IV	7.2	+.02	+.29	10.2	1.0	.021	70°	130°	3
164536	333.7	- 2.4	B3	6.8	-.16	+.06		0.8	.018	153	33	4(3)
164906	333.7	- 2.8	B1 IV:pe	7.5	-.06	+.18	10.2	<0.5	<.010	-	-	2
164947	333.8	- 2.8	B5	8.4	-.11	+.08		0.8	.018	71·	131	1
165052	333.8	- 2.9	07	6.9	-.10	+.17	10.9	-	-	-	-	2
165517	333°4	- 3°7	Be	8.6	+.11	+.37		1.4:	.030:	44°:	105°:	3
165793	323.3	- 9.5	B0	6.6	-.17	+.09		1.0·	.021·	155·	37·	2
165998	336.5	- 2.4	B3	8.7	+.23	+.45		2.4·	.052·	81	142	2
166418	341.2	- 0.5	B0 II	8.1	+.07	+.33	11.3	3.0	.065	86	147	3(3)
166540	341.1	- 0.7	B0.5 IV	7.9	-.04	+.21	10.6	0.7·	.016·	70	131	3
168552	342°0	- 2°7	B3 Ib	8.2	+.04	+.26	12.3	0.4	.008	98°	160°	2
168571	341.8	- 2.9	B1 Ib - II	7.9	+.13	+.37	11.1	1.1	.024	94	156	2
169454	345.2	- 2.2	B 1 Ia+	6.7	+.29	+.53	10.5+	2.1	.045	16	78	3(3)
169827	342.5	- 4.1	B5	8.1	+.03	+.21		2.3	.050	115	177	1
170938	344.5	- 4.5	B1 Ia	7.9	+.28	+.52	11.7	3.8	.082	117	6	4(3)
171432	342°3	- 6°5	B1 Ia	7.0	-.03	+.21	12.7	1.8	.040	120°	2°	2
171589	346.4	- 4.6	O7 f	8.2	-.03	+.26	11.6:	0.8·	.017·	177·	59:	3
172252	348.7	- 4.3	B0 V:e	9.5	+.21	+.47	11.8	4.7	.102	148	30	2
172510	346.3	- 5.9	B1 V	8.7	-.02	+.22	10.6	2.6·	.056·	166	49	3
179406	356.0	- 9.8	B3n	5.3	-.04	+.18		1.6:	.035:	172	55	2

TABLE 2 (Continued)

HD	ℓ	b	Sp	m_v	C_1	E_1	m_o-M	P_λ	$P_{\Delta m}$	θ_E	θ_G	No.
181615	349°.6	-15°.3	B8p + F2p	4.5				1.5:	.033:	166°	51°	2
183143	20.9	- 0.5	B7 Ia	6.8	+.38	+.54	10.5	6.8	.147	0	60	2
184915	359.6	-14.7	B0.5 III	5.0	-.14	+.11	8.8	1.4:	.031:	165°	48°	4

TABLE 2. REMARKS

HD 298310	Classified as G in HDE; new classification on basis of ADH prism plates.
80077	Spectrum peculiar, consequently E_1 may be in error.
92206 92207	In H II region, No. 31 of Hoffleit's catalogue (1953) HD 92206 must be exciting star.
97950	Peculiar star, possibly very high luminosity excites H II region. Hoffleit No. 57.
110432	Emission star, surrounded by cluster of faint stars. Assumed to be of luminosity class V for purposes of determining distance modulus.
311999	Exciting star of emission nebula lying beyond Coal Sack (Lindsay 1941; Houck unpublished).
134959	Surrounded by group of faint stars, some of which may have affected polarization measures.
159176	In galactic cluster NGC 6383, and excites H II region.
316332	Highly reddened star yet relatively small polarization. Hiltner (1954) has laready drawn attention to this star.

where the line of sight traverses the Orion spiral arm, and here the alignment is most uniform and closely parallel to the galactic equator. This roughly confirms the hypothesis that the elongated polarizing particles are aligned perpendicular to the spiral-arm axis (Davis and Greenstein 1951; Hoag 1953). Such a model assumes that, in the ideal situation, the aligning force, presumably a magnetic field, orients the particles so that the maximum of the electric vector lies parallel to the spiral-arm axis. This hypothesis may be tested more definitively by mathematically relating interstellar polarization with spiral structure. The possibility that the magnetic field lies in a plane different from that of the galactic equatorial plane in some regions of the Milky Way cannot be entirely excluded on the basis of present data. The following discussion attempts to show that there is good evidence that the two planes are coincident over the greater part of the Milky Way and that the magnetic field is closely related to spiral structure.

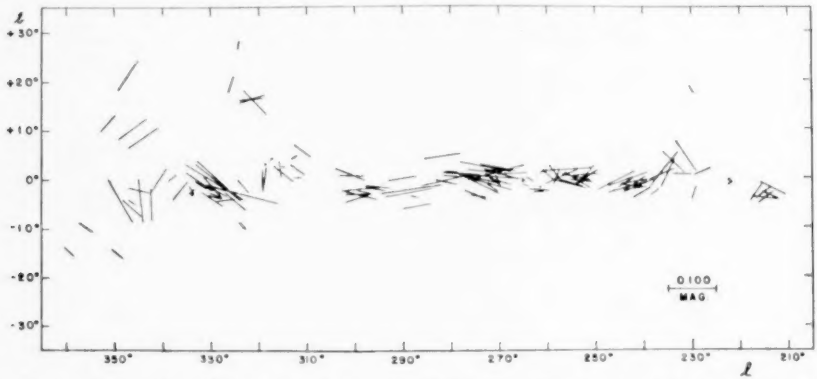

FIG. 1.—Interstellar polarization in the southern Milky Way. The direction is determined by the position angle of the plane of vibration, whereas the length of the line is proportional to the amount of polarization as indicated by the scale. Solid circles imply that the starlight suffers no or negligible polarization.

We shall follow a procedure similar to Hoag's (1953; unpublished).[2] First let us define the parameter

$$P^* = P_{\Delta m} (\sin \theta_G - \cos \theta_G) , \tag{1}$$

where $P_{\Delta m}$ is the observed amount of polarization in magnitudes and θ_G is the position angle of the plane of vibration referred to the galactic co-ordinate system. We may further define $E_{\max}$ as the maximum of the electric vector, described jointly by P and θ_G. The difference between the orthogonal components of $P_{\Delta m}$ serves as a measure of the collimation of $E_{\max}$ in the galactic plane and strongly favors those $E_{\max}$ which lie closely parallel to the galactic equator. For individual stars the value of P^* has relatively little significance; only when averaged over several stars is it meaningful. Thus the dispersion in position angle is inversely incorporated into P^*. Actually, P^*/A, the amount of polarization per unit absorption, represents the physically significant parameter, for it takes into account the dependence of polarization on the amount of extinction.

Supposing that the particles are aligned normal to the spiral-arm axis, we may predict that

$$\frac{P^*}{A} = k (1 - \cos \alpha) , \tag{2}$$

[2] The following analysis resulted largely from private correspondence with Dr. A. A. Hoag, to whom I am much indebted.

where k is a constant of proportionality to be determined from the observations and a is the angle between the axis of the arm and the line of sight. Obviously, for the Orion arm we may use the approximation

$$\cos a = \sin |l - l_0| . \tag{3}$$

The galactic longitude of the region under consideration is given by l, whereas l_0 denotes the longitude at which the arm lies perpendicular to the line of sight. Although l_0 could be determined from our knowledge of spiral structure in the Galaxy, an independent method consists in plotting P^*/A as a function of longitude, as shown in Figure 2. The function P^*/A reaches a maximum at $l_0 = 290°$ in the south and 125° in the north. Similarly, the constant k derives from the slope of P^*/A plotted against $(1 - \sin |l - l_0|)$. Such graphs for both the southern and the northern hemisphere are given in

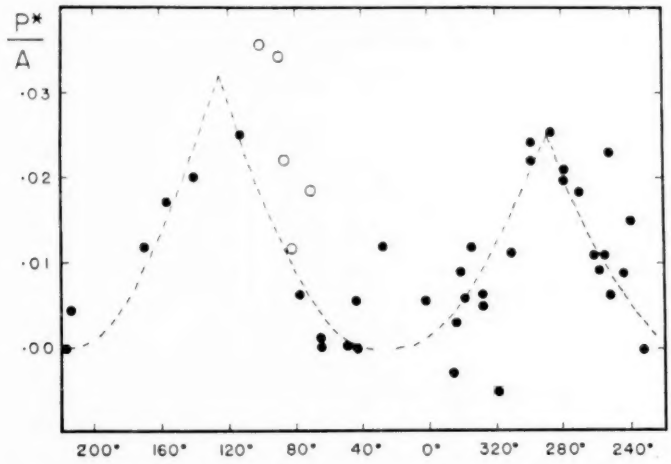

FIG. 2.—Variation of the parameter P^*/A with galactic longitude. This parameter is defined in the text. Equations (4) describe the dotted curves. The solid circles are derived from data on associations probably lying in the Orion arm in the north and in the Sagittarius arm in the south. Open circles refer to data obtained for the Perseus arm aggregates.

Figure 3, from which we find $k = 0.025$ and 0.032, respectively. Therefore, equation (2) may now be written

$$\text{(South)} \qquad \frac{P^*}{A} = 0.025\,(1 - \sin |l - 290°|) , \tag{4a}$$

$$\text{(North)} \qquad \frac{P^*}{A} = 0.032\,(1 - \sin |l - 125°|) . \tag{4b}$$

The observational data used for this part of the analysis are those reported in the earlier portion of this paper for the Southern Hemisphere and those published by Hall and Mikesell (1950) and by Hiltner (1951) for the Northern Hemisphere. Each point in Figures 2 and 3 represents an aggregate or perhaps only a group of stars within a given region of space. Only stars in the Orion and Sagittarius arms were used for the southern data, while only Orion arm aggregates (Morgan, Whitford, and Code 1953)

entered into the analysis leading to equation (4*b*). Although the southern stars lie for the most part in the Sagittarius arm, much of the obscuring and polarizing matter is near the sun and constitutes part of the Orion arm. The Coal Sack and the Vela dark nebula, for instance, are at distances of approximately 150 and 500 pc from the sun, as determined from star-count analyses (Greenstein 1937; Lindsay 1941). In spite of considerable scatter, the observational data do satisfy equations (4).

Hence the model of a polarizing medium lying in the solar vicinity, with the particles aligned in planes normal to a given axis, seems to be roughly confirmed. We have assumed this axis to correspond to the axis of the Orion arm. The form of the curve in Figure 2 excludes the possibility that the axis is that of the Sagittarius arm. Since the Orion arm passes through the sun from approximately longitude 210° to 30°, one would expect l_0 to occur at 300° and 120°, whereas actually the observations indicate l_0 at 290° and 125°. The agreement is fair within the deviations due to local effects and uncertainties in the exact location of our spiral arm.

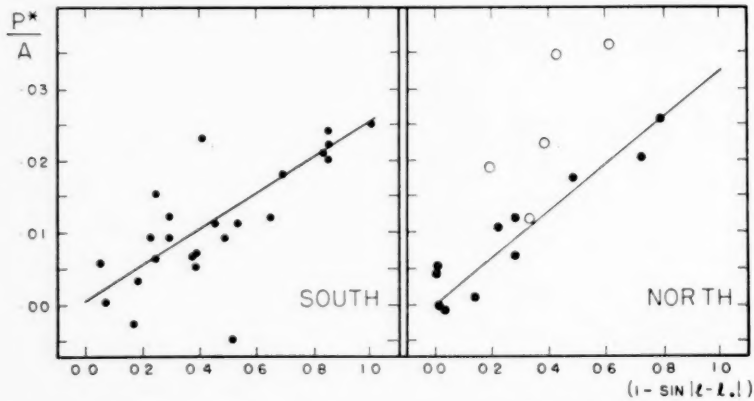

FIG. 3.—The parameter P^*/A plotted against $(1 - \sin |l - l_0|)$. The slopes of the lines are 0.025 and 0.032 for the south and north, respectively. See Fig. 2 for an explanation of the symbols used.

Whereas l_0 depends solely on spiral structure in the vicinity of the sun, the constant k depends on the optical properties of the polarizing particles and on their degree of alignment. We must now consider how the difference in k between the northern and southern hemispheres may be explained. The discrepancy is even greater when Perseus arm associations are considered. These appear as open circles in Figures 2 and 3 and clearly have an even greater value of k, near 0.06, than the northern Orion arm aggregates, with $k = 0.032$. One might attribute the discrepancy to a difference in the optical properties of the grains. This seems hardly likely, as the extinction properties could then also be expected to differ appreciably. Although there is some evidence for slight differences in the interstellar reddening law (Johnson and Morgan 1955), they are small, and considerable evidence points to a generally homogeneous medium if peculiarities due to excited nebulae are ignored (Stebbins and Whitford 1945; Divan 1955; Houck 1955).

The factor P/A is perhaps a more convincing parameter, as it does not include the cosine factor involved in P^*/A and therefore does not depend on the model of the polarizing medium. An examination of the data for the southern and northern observations indicates that P/A varies with longitude in the same general manner as P^*/A, though the scatter is greater. The difference between the northern and southern data exists for P/A as well as for P^*/A and therefore appears to be real.

The second contributing factor is the degree of alignment. We tentatively suggest that the difference is due to a concentration of the aligning force, probably a magnetic field, toward the central axis of a spiral arm. Such a concentration would result in the elongated particles' being less rigidly aligned at the periphery of an arm than at its center. Consequently, the value of k should be lower at the edge of an arm. Studies of spiral structure in the solar neighborhood (Morgan, Whitford, and Code 1953; van de Hulst, Muller, and Oort 1954) indicate that the sun is located near the edge of the Orion arm nearest the galactic center. If we look southward, therefore, the line of sight passes through only an outer section of the arm, whereas northward it crosses the center. The difference in the values of k thus conforms to our hypothesis.

The Perseus arm data may represent an aspect of the same phenomenon. Not too great weight can be given to distance determinations by star counts, but such analyses do indicate that the obscuring clouds in this field lie within our own arm (Wernberg

TABLE 3

DATA ON INDIVIDUAL REGIONS

Region	l	b	$\overline{\theta_G}$	σ_θ	$\overline{P/A}$	$\overline{P^2/A}$	$\overline{m_0-M}$	No. Stars
Vela	241°	−1°1	106°	14.4	0.020	+0.015	11.6	10
Carina (1)	252	+0.4	120	11.7	.015	+ .006	11.7	5
NGC 3293	253	+0.2	90	13.0	.028	+ .023	11.9	7
η Carinae	255	−0.8	70	14.0	.018	.....	.....	6
Carina (2)	257	+0.5	101	32.7	.020	+ .011	11.8	8
Carina (3)	259	+1.4	74	21.5	.016	+ .009	12.6	4
Centaurus (1)	263	−1.1	74	15.0	.015	+ .011	12.1	6
Coal Sack	272	0	81	10.8	.021	+ .018	11.7	14
Coal Sack	272	>0	87	10.2	.026	.....	.....	20
Coal Sack	272	<0	67	15.8	.017	.....	.....	14
Centaurus (2)	281	−0.5	86	9.4	.024	+ .020	.....	8
Circinus	288	−2.6	91	13.0	.030	+ .025	10.9::	3
Norma	299	−3.0	89	7.6	.026	+ .024	11?	5
NGC 6231	311	+0.2	88	8.2	.009	+ .008	10.6	4
Scorpius	319	+1	.....	.....	.010	− .007	.....	5
Sagittarius	328	−2.1	59	14.9	0.022	+0.006	.....	18

1941; Heeschen 1951). None of the Orion arm associations considered previously lie in the same field as the Perseus aggregates, so a direct comparison is not possible. The spread in position angle for Perseus aggregates is lower than in most other parts of the Milky Way. Perhaps we are dealing with a cloud or complex whose particles are better aligned than in the general case because it happens to lie near the center of the arm, where the aligning force reaches its greatest strength. In most regions such an ideal situation does not exist because several clouds are involved, some of which may be at some distance from the central axis. Unfortunately, knowledge of distances of dark nebulae are too scant and uncertain for us to test this hypothesis very critically.

Observations of stars whose light might be polarized by interstellar clouds lying in either the Sagittarius or the Perseus arm are too few to enable us to study the polarizing medium in these spiral arms. Clouds in the Orion arm would also influence the polarization and complicate the analysis.

IV. INDIVIDUAL REGIONS OF SPECIAL INTEREST IN SOUTHERN MILKY WAY

Table 3 summarizes the important characteristics of the various regions. For convenience, numbers are given in parentheses after the constellation name when more than one group of stars lies in a given region. Some of these groups may form associations or

be members of associations, since the stars are grouped according to distance modulus as well as field. An extension of the Morgan, Whitford, and Code paper (1953) assigning Roman numerals to aggregates in the southern Milky Way will probably result from the work of the Washburn South African Expedition. Arabic rather than Roman numerals are used here, to avoid confusion at a later time.

The dispersion in position angle, σ_θ, serves as a rough indication of the degree of parallelism for the planes of vibration of the polarized light from the several stars in a given group. Since the sample of data leading to each σ_θ is small, the tabulated quantities carry small weight. A more reliable parameter is P^*/A, discussed previously, which may be defined as the amount of polarization per unit absorption parallel to the galactic equator.

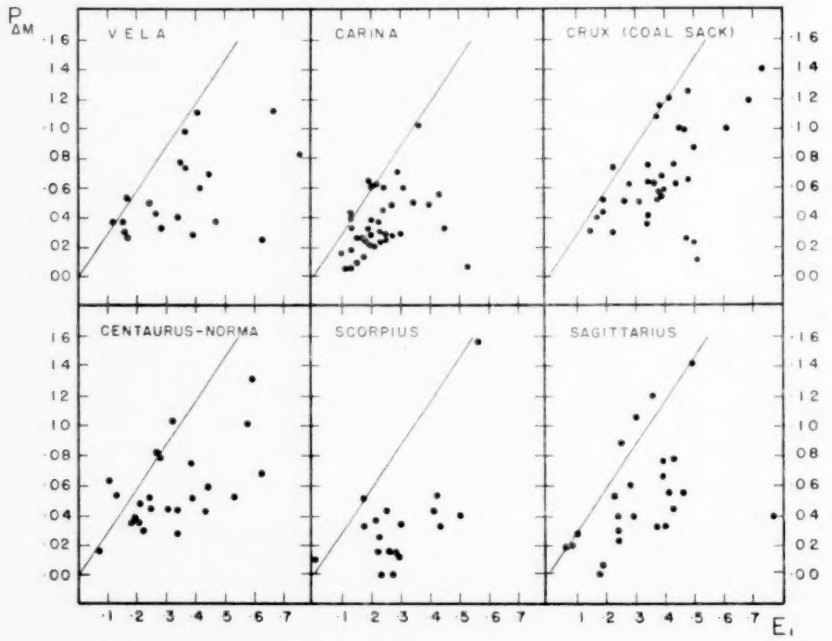

FIG. 4.—Relation between polarization and color excess. The line is defined by relation (5) in the text.

The relation between polarization and color excess for the several regions is shown in Figure 4. The relation

$$P_{\Delta m} = 0.34E_1 \tag{5}$$

represents the maximum ratio of polarization to color excess and defines the line drawn in each diagram. A few points lie above this line, since the relation is actually derived from the several highest ratios observed. The scatter is considerable in all cases but varies from one region to the next, as does the percentage of stars lying near the maximum slope.

Vela

Present data on spiral structure, though still meager, suggest that the direction of longitude 240° points between the Orion and Sagittarius arms. A streamer may possibly exist connecting the two arms at a distance of about 1.5–2 kpc from the sun and extending from 220° to 240°. Several members of an OB association at $l = 240°$ and at 2 kpc (Houck, unpublished) were observed for polarization. The Vela dark nebula (Greenstein 1937), lying at approximately 500 pc and therefore part of the sun's spiral arm, probably contributes most of the reddening and polarization. The patchy distribution of the amounts of polarization and absorption may be seen in Figure 5, wherein the radii of the circles are proportional to the absorption.

Carina

The Carina region is highly complex; here the stars observed probably lie in that part of the Sagittarius arm where it curves away from us along the line of sight. For the most

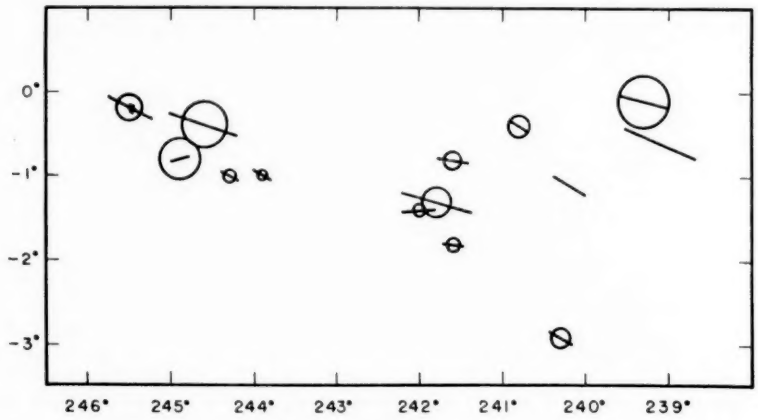

FIG. 5.—Polarization in Vela. The figure portrays the projected space distribution of the maximum of the electric vector in the Vela region. The radii of the circles are proportional to the color excesses.

part, the absorption does not exceed 2 mag. This is one of the few regions where the obscuring clouds may be in the Sagittarius and not in the Orion arm (Bok 1937). Perhaps the scatter of the points in the plot of P^*/A against longitude (Fig. 2) at $l \sim 255°$ may result from the fact that some of the absorption occurs in the Orion arm and some in the Sagittarius arm. Figure 6 illustrates the polarization in the Carina region projected on the star field. The group at $l = 252°$, Carina (1), which may form an aggregate at 2.2 kpc, has rather low polarization in comparison with the color excess, but the dispersion in position angle, 12°, is quite low.

The galactic cluster, NGC 3293 at $l = 253°$, $b = +0°.2$, and at a distance of about 2.3 kpc, may be associated with the afore-mentioned aggregate. An H II region, No. 26 in Hoffleit's catalogue (1953), lies near the cluster, but it is difficult to relate the observed polarization with direction of the wisps or streamers of the nebulosity. Several stars in or superposed on the η Carinae nebula were also observed for polarization, as shown in Figure 6.

The stars near $l = 258°$ are separated into two distinct groups, Carina (2) and (3), on the basis of their respective distances. The more distant group is the less reddened, per-

haps because of the irregularity of the absorbing medium. Possibly the general disorder of the polarization in the region as a whole may be ascribed to the inhomogeneity of the interstellar clouds. Bok and van Wijk (1952) have already commented on the patchiness of the obscuration in this locality.

The Coal Sack

The Coal Sack in Crux gives the appearance of a fairly uniform, compact dust cloud. Star counts indicate that it is at a distance of about 150 pc (Unsöld 1929; Lindsay 1941), which places it in the sun's spiral arm. Absorptions ranging from 1 to 3 mag. are similarly derived from star counts. Analysis of reddening data correlated with distances gives a somewhat complex picture. The highest obscuration occurs in the neighborhood of $l = 271°.5$, $b = +1°.0$, and diminishes irregularly outward from this center. In the southern part of the nebula the absorption is not quite so high as in the northern section, but direct photographs suggest that it is also less uniform. An OB aggregate happens to lie well behind the Coal Sack ($m_0 - M = 11.7$, $r = 2.2$ kpc) but in the same line of sight (Houck, unpublished). Magnitudes and colors are known for nearly all the stars I observed, and MK spectral types for a great many (Houck, unpublished); so many available data make possible a fairly detailed study of the region. Nevertheless, we still lack a quantitative picture of the distribution of the absorbing medium.

Unfortunately, even the brightest of the stars observed lie well beyond the Coal Sack, so we can make no comparison between stars in front of and behind the dust cloud. The stars at distances of less than 2 kpc are not highly reddened, but fortuitously they are all situated at the periphery of the cloud, where the absorption is less. The polarization characteristics for these stars are quite comparable to those for the members of the aggregate. The uniformity of the polarization characteristics suggests that, even for the more distant stars, the Coal Sack is the predominant dust cloud.

In regard to distance effects, then, we may consider the Coal Sack as a unified region. A glance at Figure 7, however, shows that both polarization and absorption differ between the northern and southern portions. Let us take $b = 0°$ as the dividing line and find the quantitative polarization characteristics for the two fields. The results are incorporated in Table 3, in addition to those for the Coal Sack aggregate proper. Not only is the deviation of the position angle in the southern half higher than in the northern, but the means of the angles differ by 20°, with the planes of vibration in the north being more closely parallel to the galactic equator than in the south. We note further that the ratio of polarization to absorption for the north considerably exceeds that in the south. Local structure within the nebula must surely cause this disparity; perhaps there are several small clouds rather than one uniform one. The peculiar motions of these clouds may either directly align the particles differently or distort the magnetic field, which in turn causes the grains to become preferentially oriented in divergent directions. The irregular structure in the south suggests that here the cloud is broken up into smaller units than in the north.

Centaurus to Sagittarius

The Milky Way from $l = 280°$ to $l = 310°$ is heavily obscured by complex dark nebulae (Bok 1937; Code and Houck 1955). Not many early-type stars are known in this region, probably because of the overlying absorption. Table 3 summarizes the results of polarization measurements in this longitude interval. Stars used in compiling these data were selected on the basis of probable membership in the Sagittarius arm. This selection necessitated some guesswork relative to distance moduli for those stars whose spectral type on the MK system was unknown. The observational data satisfy fairly well the polarization model already discussed.

At $l = 311°$ in Scorpius we have the cluster NGC 6231 and the associated aggregate (Morgan, González, and González 1953). Although the absorption is not exceptionally

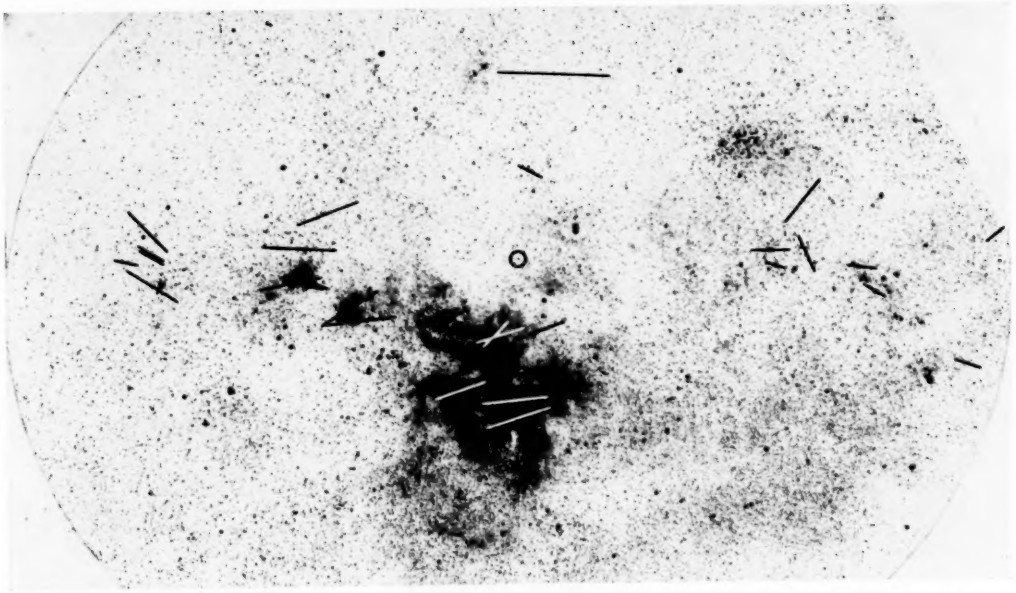

FIG. 6.—Polarization in Carina projected on the star field. The η Carinae nebula appears near the center of the plate; NGC 3293 lies to the west, namely, on the left. The lower edge of the plate lies parallel to the galactic equator.

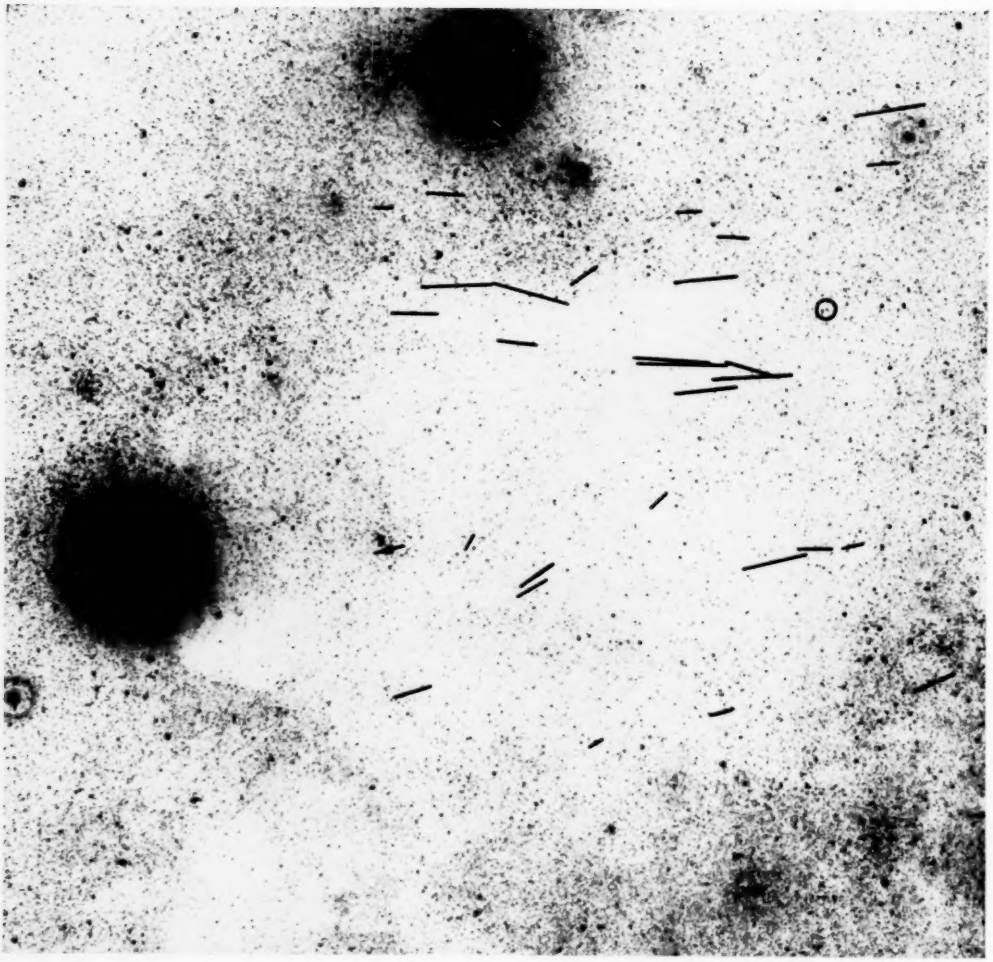

FIG. 7.—Polarization in the Coal Sack. The lower edge of the plate lies parallel to the galactic equator, which runs closely through the middle. East is on the right.

high, it is not negligible; yet the polarization for all stars observed is very low. The resulting P^*/A for the region lies far below the predicted value. This state of affairs continues as we proceed to greater longitudes, as illustrated in Figure 8. The obscuration here also is exceedingly complex and patchy, giving the appearance, in fact, of turbulence. Photographs taken in Hα light indicate that the hydrogen emission also has a very turbulent appearance (Bok 1955), which suggests that both gas and dust are irregularly distributed. The situation may be comparable to that suggested for the southern section of the Coal Sack: several small clouds making up a big complex, whose motion is directly or indirectly responsible for the disorder in the alignment of the particles.

In Sagittarius the obscuration increases still further but remains very irregular. Many cases of high polarization exist, but the planes of vibration lie at considerable angles relative to the galactic equator, making P^*/A close to zero in spite of the fact that P/A is high. Many of the stars observed have also been studied by Hall and Mikesell (1950) and by Hiltner (1951, 1954).

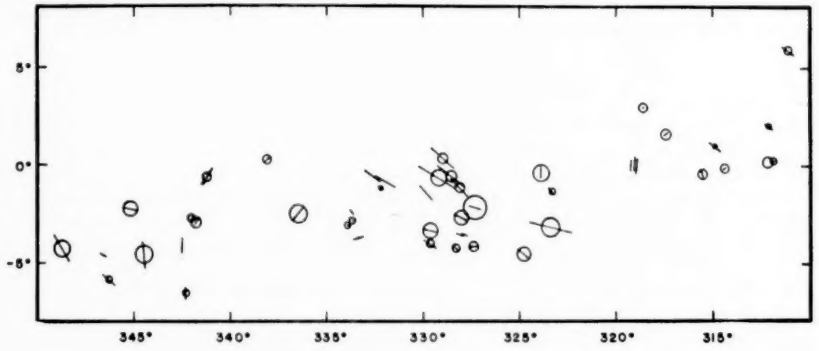

FIG. 8.—Polarization and color excess in Scorpius-Sagittarius

Disorder is the predominant characteristic of the polarization at greater longitudes, which is to be expected from the polarization model. From South Africa I observed only a few stars in this region, which had already been covered from the north. Figure 8 includes these observations, to illustrate the general trend.

V. CONCLUSION

We have seen that polarization measurements relate well to spiral structure if we envisage the polarization as caused by grains which are preferentially aligned perpendicular to the spiral-arm axis. Nevertheless, aberrations due to local structure may be quite severe, as in the Scorpius region. The data available at present allow us to study the polarizing medium within our own spiral arm, the Orion arm. Future observations should concentrate on aggregates in the more distant spiral arms, such as the one beyond Perseus and the second inner arm. A few scattered observations of this type already exist but are insufficient to provide a clear general picture.

Finally, I should like to express my appreciation to the many persons who have aided me in the course of this work. In particular, I am grateful to the Harvard Observatory Council for the opportunity to observe at the Boyden Station. I am indebted to R. B. Dunn, who contributed generously to the design and construction of the polarimeter used on the 60-inch telescope. T. E. Houck and the Washburn Observatory were most

generous in allowing me the use of some of their equipment and in supplying me with data prior to publication. My special thanks go to Drs. B. J. Bok and J. S. Hall, who gave me much of their time, advice, and encouragement.

REFERENCES

Bok, B. J. 1937, *The Distribution of the Stars in Space* (Chicago: University of Chicago Press), pp. 82 ff.
———. 1955, *A.J.*, **60**, 146.
Bok, B. J., and van Wijk, U. 1952, *A.J.*, **57**, 213.
Code, A. D., and Houck, T. E. 1955, *Ap. J.*, **121**, 553.
Davis, L., and Greenstein, J. L. 1951, *Ap. J.*, **114**, 206.
Divan, L. 1954, *Ann. d'ap.*, **17**, 456.
Greenstein, J. L. 1937, *Harvard Ann.*, **105**, 359.
Hall, J. S., and Mikesell, A. H. 1950, *Pub. U.S. Naval Obs.*, Vol. **17**, Part I.
Heeschen, D. S. 1951, *Ap. J.*, **114**, 132.
Hiltner, W. A. 1951, *Ap. J.*, **114**, 241.
———. 1954, *ibid.*, **120**, 41.
Hoag, A. A. 1953, *A.J.*, **58**, 42.
Hoffleit, D. 1953, *Harvard Ann.*, Vol. **119**, No. 2.
Houck, T. E. 1955, private communication.
Hulst, H. C. van de, Muller, C. A., and Oort, J. H. 1954, *B.A.N.*, **12**, 117.
Jackson, J., and Stoy, R. H. 1954, *Ann. Cape Obs.*, Vol. **17**.
———. 1955, *ibid.*, Vol. **18**.
Johnson, H. L., and Morgan, W. W. 1951, *Ap. J.*, **114**, 522.
———. 1953, *ibid.*, **117**, 313.
———. 1955, *ibid.*, **122**, 142.
Lindsay, E. M. 1941, *Proc. Roy. Irish Acad., A*, Vol. **46**, No. 11.
Morgan, W. W., Code, A. D., and Whitford, A. E. 1955, *Ap. J. Suppl.*, **2**, 41 (No. 14).
Morgan, W. W., González, G., and González, G. 1953, *Ap. J.*, **118**, 323.
Morgan, W. W., Harris, D. L., and Johnson, H. L., 1953, *Ap. J.*, **118**, 92.
Morgan, W. W., and Keenan, P. C. 1951, *Astrophysics*, ed. Hynek (New York: McGraw-Hill Book Co.), chap. i.
Morgan, W. W., Whitford, A. E., and Code, A. D. 1953, *Ap. J.*, **118**, 318.
Ohlson, J. 1932, *Ann. Obs. Lund*, No. 3.
Oosterhoff, P. T. 1951, *B.A.N.*, **11**, 299.
Sharpless, S. 1952, *Ap. J.*, **116**, 251.
Stebbins, J., Huffer, C. M., and Whitford, A. E. 1940, *Ap. J.*, **91**, 20.
Stebbins, J., and Whitford, A. E. 1945, *Ap. J.*, **102**, 318.
Unsöld, A. 1929, *Harvard Bull.*, No. 870.
Wernberg, G. 1941, *Uppsala Ann.*, Vol. **1**, No. 4.

DISTANCES FOR SOUTHERN EARLY-TYPE STARS, ESPECIALLY IN CARINA AND OTHER H II REGIONS

DORRIT HOFFLEIT
Harvard College Observatory
Received December 7, 1955; revised February 9, 1956

ABSTRACT

Spectral and luminosity classes, as well as apparent magnitudes and colors, have been obtained for some hundred and fifty southern stars, mainly in the η Carinae region, with some thirty in other southern H II regions and about twenty in the general direction of the galactic center. The distribution of these stars in the galactic plane is discussed. The distribution of color excesses with respect to observed bright and dark nebulosities confirms the over-all association of gas and dust in the Milky Way. Color excesses are highest in areas where H II emission is strong. K-line intensities tend to be strong in areas of H II emission but relatively weak in other regions.

I. INTRODUCTION

Continuing our investigations of the structure of the Milky Way in the general vicinity of Carina, Dr. Bart J. Bok and I, two years ago, initiated a program for determining accurate spectral classes, magnitudes, and colors of approximately one hundred early-type stars (Bok 1952; Bok and van Wijk 1952; Hoffleit 1953; Bok 1955; Hoffleit 1955). The observational part of the program, which has been carried out at the Boyden Station of Harvard Observatory, also included a number of early-type stars near the direction of the galactic center and, for comparison of our material with the Yerkes system, a selected group of stars in Orion. In addition, Campbell M. Wade made out a similar list of stars that appear to be the exciting agents of H II regions catalogued by Bok, Bester, and Wade (1953, 1955) in a survey of the Milky Way between galactic longitudes 260° and 355°.

The distribution of the selected B-type stars in Carina (11 per cent of the total known) is compared in Figure 1 with the distribution of all the known O6–B5 stars in the area in which previous investigations on the apparent association of B stars and nebulosity had been carried out (Hoffleit 1953). In selecting the stars for the present study, I attempted to get a representative distribution of stars both in and out of conspicuous nebulosity and, in so far as could be judged from earlier material, of a wide range in luminosity class. Only a few of the selected stars are conspicuously grouped; five are members of the cluster NGC 3293.

Slit spectra with a dispersion of approximately 100 A/mm were taken at the 60-inch Rockefeller reflector, mainly by M. J. Bester, T. E. Houck, Henry J. Smith, and Mrs. Elske von P. Smith. Photoelectric photometer records for the determination of blue and yellow magnitudes and colors were likewise obtained at the 60-inch, primarily by Mrs. Smith and Mr. Houck. All reductions and analyses of this material were carried out at Harvard, chiefly by myself, although Mr. Wade and Miss M. Rimbach took part in some of the photoelectric reductions.

Combining the new material with the earlier data published by Bok and van Wijk (1952) and by Oosterhoff (1951), we now have either revised spectral classes on the Yerkes system (Morgan, Keenan, and Kellman 1943) or magnitudes and colors on the Bok–van Wijk system (1952) for 156 southern stars listed in Table 2. Distances could be estimated for 123 of these.

II. THE ORION STARS

Before embarking on the reductions of the southern stars, we felt it advisable to test our systems of spectral classification, magnitude, and color against the Yerkes Observa-

tory systems, in order that distance determinations should ultimately be reasonably consistent. From the list published by Sharpless (1952) on the Orion aggregate of early-type stars, I selected sixteen stars representing all luminosity classes among spectral classes O9–B9, in order to check the accuracy of my spectral and luminosity classifications.

For these stars the average difference in the assignment of spectral class amounts to ±0.03 spectral division. In the assignment of the luminosity classes there was exact agreement in all but three cases. Two of the stars for which the Harvard spectra are of only moderate quality, I assigned to classes B2 IV: and B1 IV, whereas the Yerkes classes are B2 III and B2 V, respectively. In the third case I called a Yerkes B2 III star B2 V. While the latter discrepancy corresponds to an absolute-magnitude difference of 1.5, it represents but little difference in the appearance of the spectrum as such.

Photoelectric measurements on twenty-one Orion stars, all of luminosity class V, were carried out on the same system as that of Bok and van Wijk. All were observed

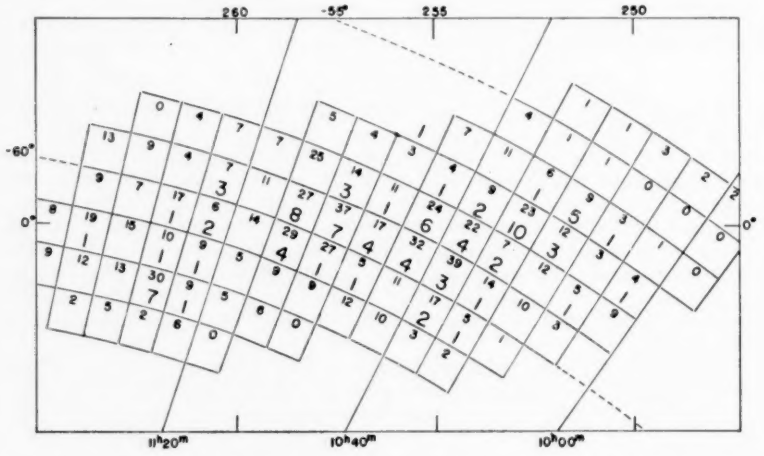

FIG. 1.—The distribution of B stars in Carina. Areas marked are 8m R.A. by 1° Decl. *Small numbers:* the total numbers of *HD* and *HDE* stars of classes O6–B5 in each small area. *Large numbers:* the numbers for which more accurate new data are presented in Table 2.

against HD 35912 as standard. Sharpless' determinations of the spectral class, yellow magnitude, color, and color excess (based on filters having effective wave-length transmission at 5540 and 4420 A) are repeated in the first five columns of Table 1. The Harvard magnitudes and colors relative to HD 35912 are given in the sixth and seventh columns. Corning 5551 and 3385 filters were used; the blue filter transmits considerable light at wave lengths shorter than 3900 A. There is excellent agreement in the yellow magnitudes. The probable error of a single difference from Sharpless' determinations amounts to ±0.04 mag. Repeat measurements on different nights yielded a probable error for the Harvard values of ±0.012 mag. and of ±0.008 mag. for the colors.

The colors, determined on the Bok–van Wijk system, are on a somewhat more open scale than those determined by Sharpless. For establishing the zero point of this correlation, however, only indirect comparisons are possible; but they indicate a linear relationship between the two systems for all colors between −0.20 and +1.60 of the Sharpless scale and between −0.36 and +1.52 on the Bok–van Wijk scale (Fig. 2).

Sharpless has shown (1952) that his colors, $B - V$, are on the same system as John-

son's (1953) for stars with color indices greater than about −0.1. In this range, Johnson and Morgan have eight stars in common with Oosterhoff (1951). The conversion from Oosterhoff's to the Bok–van Wijk colors is

$$C_{b-y} = 1.14 + 1.11C_1 ,$$

where C_1 refers to the Oosterhoff colors and C_{b-y} to the Bok–van Wijk colors in Table VIII (not Table IV) of their paper (1952). The open circles in Figure 2 represent the Oosterhoff colors thus reduced to the Bok–van Wijk system. These all represent stars of spectral classes A0 and later. The dots in the figure represent the Orion stars listed in Table 1. For these stars the colors had been measured relative to HD 35912, whose color

TABLE 1

INTERCOMPARISON OF SHARPLESS' AND HARVARD SYSTEMS OF MAGNITUDE, COLOR, AND COLOR EXCESS

HD	SHARPLESS DATA*				HARVARD RESULTS				
	Sp.	m_y	$B-V$	E_y	m_y	ΔC	C_{b-y}	Normal Color	E
35912	B2	6.35	−0.18	+0.05	6.35	0	−0.34	−0.34	0.00
34179†	B8 V	8.02	− .03	+ .07	8.03	+0.24	− .10	− .22	+ .12
34317	A0 V	6.41	− .02	− .02	6.43	+ .28	− .06	− .18:	+ .12
34511†	B5 V	7.39	− .10	+ .06	7.39	+ .06	− .28	− .28	.00
34959	B5p	6.50	− .11	+ .05	6.61	+ .14	− .20	.....	.....
35203†	B6 V	7.97	− .09	+ .06	8.06	+ .12	− .22	− .26	+ .04
35298†	B9 V	7.88	− .14	− .07	7.89	+ .12	− .22	− .20	− .02
35407	B5 V	6.31	− .16	.00	6.27	+ .07	− .27	− .28	+ .01
35501	B8 V	7.42	− .06	+ .04	7.42	+ .18	− .16	− .22	+ .06
35588	B3 V	6.15	− .18	+ .02	6.09	+ .04	− .30	− .32	+ .02
35673	B9 V	6.50	.00	+ .07	6.50	+ .24	− .10	− .20	+ .10
35730	B5p	7.20	− .15	+ .01	7.18	+ .04	− .30	.....	.....
35834†	B8 V	7.67	− .05	+ .05	7.72	+ .20	− .14	− .22	+ .08
35881	B8 V	7.77	− .09	+ .01	7.77	+ .12	− .22	− .22	.00
35910	B6 V	7.58	− .10	+ .05	7.55	+ .11	− .23	− .26	+ .03
36012†	.....	7.24	− .10	.....	7.36	+ .05	− .29	.....	.....
36013†	B1.5 V	6.88	− .13	+ .12	6.87	+ .08	− .26	− .35	+ .09
36133	B2 V	6.94	− .09	+ .14	7.08	+ .03	− .31	− .34	+ .03
36392†	B3 V	7.56	− .14	+ .06	7.52	+ .06	− .28	− .32	+ .04
36429	B5 V	7.56	− .13	+ .03	7.52	+ .08	− .26	− .28	+ .02
36627	B6 V	7.56	− .11	+ .04	7.56	+ .10	− .24	− .26	+ .02
36741	B2 V	6.58	−0.20	+0.03	6.55	−0.02	−0.36	−0.34	−0.02

* *Ap. J.*, **116**, 251, 1952.
† Half-weight.

on the Bok–van Wijk system was not known. A plot of the $B - V$ of Sharpless against ΔC_{b-y} = Color of star *minus* color of HD 35912 was simply adjusted to give the best agreement with the open circles at $B - V = 0$. This then implies a color index of −0.34 for the comparison star HD 35912 on the Bok–van Wijk system.

Normal color indices (ninth col., Table 1) have been adopted in accordance with the scale determined by Bok and van Wijk (1952) as given in the accompanying tabulation.

Spectral class	B0	B1	B2	B3	B4	B5
Normal color	−0.38	−0.36	−0.34	−0.32	−0.30	−0.28

The color excesses given in the tenth column correspond to these values. The systematic difference between these and the Sharpless blue-yellow colors (fifth col.) is negligible, while the probable error of a single difference amounts to ± 0.04 mag., corresponding to an uncertainty of 10 per cent in the distance.

These results indicate that our subsequent determinations for the southern stars should be effectively on the same scale as the Yerkes distance determinations for the northern stars. Unfortunately, however, the Orion stars studied here provide but a small range in color excess in comparison with the absorptions found in the Carina region.

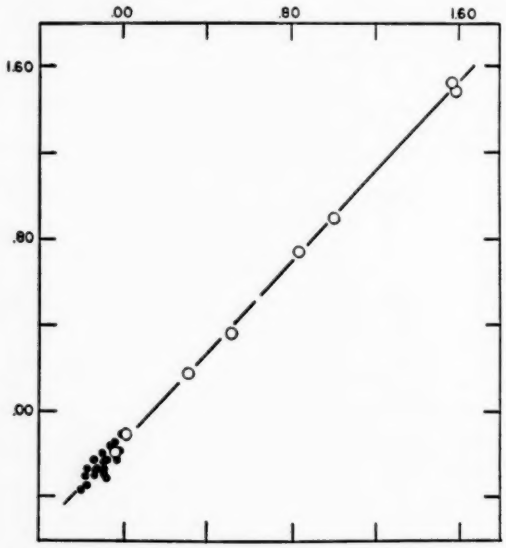

FIG. 2.—Relation between the Harvard system of colors (*ordinates*) and Sharpless' system (1952). *Open circles:* Oosterhoff colors reduced to the Bok–van Wijk (Harvard) system; *dots:* observed relative colors adjusted in ordinate to give best fit at Sharpless' color 0.00.

III. THE CATALOGUE OF SOUTHERN STARS

Table 2 is a catalogue of all the southern stars (other than the Wolf-Rayet types) for which either new spectra or new photoelectric measurements have been obtained. The spectra, reclassified on the Morgan-Keenan-Kellman system (1943), show satisfactory agreement with accurate classifications for some of the same stars obtained elsewhere (Morgan, Whitford, and Code 1953; Bidelman 1954; Hiltner 1954; Morgan, Code, and Whitford 1955).

Bok–van Wijk and Oosterhoff yellow magnitudes and colors, all reduced to the Bok–van Wijk system, are included for numerous stars. Oosterhoff's magnitudes have been corrected by -0.15 mag. to reduce them to the m_y of the Bok–van Wijk system. Similarly, recent determinations by Morgan, Code, and Whitford (1955) for twenty-three of the stars are included, their magnitudes having been reduced by 0.1. The relation between their colors and those in Table 2 is shown in Figure 3. Most of the magnitudes (m_y) and colors (C_{b-y}) in Table 2 are based on two measurements each, whence the average probable errors are found to be ± 0.014 in magnitude and ± 0.010 in color.

Three stars listed by Bok and van Wijk, namely, HD 93403, 90615, and 97222, were selected as comparison stars relative to which the magnitudes and colors of neighboring stars were measured. The following stars from Oosterhoff's list were also used as comparison stars: HD 90706, 91943, 101205, 136003, 145664, 149729, 153426, 156134, and 159176. Of these, Oosterhoff has noted two as double: HD 101205 (I 422, 7.7–7.7) and HD 159176 (h 4962, 5.7–10.5, in the galactic cluster NGC 6383). The latter was used for only one star, HD 158186, for which two estimates are in satisfactory accord; the faint component of the double comparison star is too faint to have introduced any appreciable error. HD 101205, however, appears to have varied. It was used as a standard of comparison for six stars, each observed on three nights. Their apparent synchronous

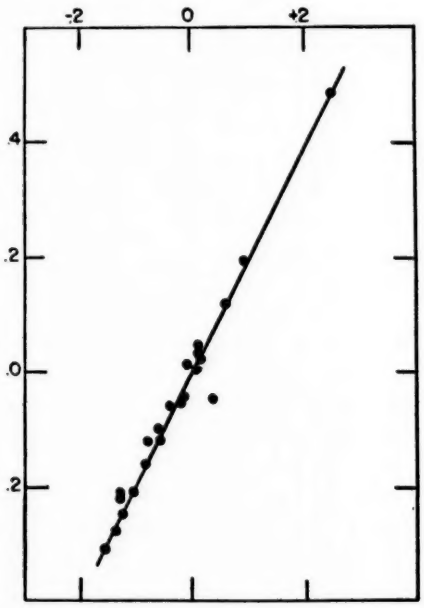

FIG. 3.—Relation between the Harvard colors (*ordinates*) and those of Morgan, Code, and Whitford (1955).

variations indicate that HD 101205 varies by 0.15 or 0.20 mag. I have attempted to allow for this apparent variation, in the deduced magnitudes of HD 101008, 101084, 101131, 101190, 101191, and 101332. Unfortunately, none of these had been measured relative to any other comparison stars; hence the results for them must be of somewhat lower weight than those for the majority of the stars in Table 2.

Three other stars—HD 97484, 152667, and 152723—also appeared to vary by 0.1–0.3 mag. HD 97484 is the eclipsing binary, EM Carinae, for which S. Gaposchkin (1946) found a period of 3.41 days and a photographic amplitude of 0.20 mag. The one spectrum plate obtained at the 60-inch shows double hydrogen lines and a single strong K line. I believe this is the first observation of the star as a spectroscopic binary.

HD 152667 and 152723 were measured relative to HD 153426. Either they or the standard comparison star may therefore vary. All three are too bright (6 or 7 mag.) for

TABLE 2

STARS IN CARINA, SOUTHERN H II REGIONS, AND SCORPIO-SAGITTARIUS

HD	Sp.*	m_v	C_{b-v}	Source†	Normal Color	M_{V0}	E	d	Long.	Neb.‡	K:4026
88661	B0ne	5 51	−0.40	O, H	−0 38	−3 9:	−0 02	800	251		
89201	B1 I	7 84	+ .43	H	− .36	−6 5	+ 79	1200	251	2 blue	−3
90187	B1nne	8 88	− .04	B	− .36	−3 2:	+ 32	1300	252	Near 12	+2
90273	O7	9 02	− .13	B, O	− 44:	−5 7:	+ 31	4300:	252	11 Ha	0:
90578	B1 5 III	9 27	− .14	B	− .35	−4 2	+ 21	3000	252	11 Ha	−4
90615	B0 II	8 17	− .02	B, O, Std	− 38	−5 2	+ 36	2000	253	Dark between 11 and 13 Ha	−4
90706	B4 I	7 04	+ .23	O, Std	− 30	−6 0	+ 53	1200	252	Outskirt 11	−1
90801	B2 V	9 43	.00	B	− 34	−2 6	+ 34	1200	253	Thin	−5
90831	B2 III	9 36	+ .12	B	− 34	−4 1	+ 46	1700	253	13 red	−3
90832	B1 III	9 11	+ .08	B	− 36	−4 3	+ 44	1700	253	Between 11 and 13 Ha	−4:
91421	WN 5	8 89	− .13	H						20 Ha	−2:
91572	O7	8 16	− .22	O, H	− 44:	−5 7:	+ .22	3550:	253	24 Ha	0
91597	(B3)	9 87	− .21	H					255	17 Ha	
91824	O7	7 82	− .29	O	− 44:	−5 7:	+ .15	3600	253	26 Ha	−1
91850	B1 IV:	9 15	− .03	O	− 36	−3 8	+ 33	1800	253	26 Ha	−4
91943	B0 5 I	6 64	− .21	O, Std, M	− 37	−6 5	+ 16	2900	253	26 Ha	−4
91969	B0 Ia	6 05	− .25	M	− 38	−6 7	+ 13	3200	253	26 Ha	−3
91983	B1 III	8 52	− .17	H	− 36	−4 3	+ 19	2300	253	26 Ha	−3
92007	B0 II	7 78	− .12	H	− 38	−5 2	+ 26	2200	253	26 Ha	−2
92044	B0 5 II	8 22	− .09	H	− 37	−5 1	+ 28	2400	253	26 Ha	−2
92061	(B5)	8 90	− .18	H					253	29 blue	
92206	O7	7 68	− .10	H	− 44:	−5 7:	+ 34	2200	254	31 Ha	+1:
92207	A0 Ia								254	31 Ha	
92383	B0 V	9 34	− .13	H	− 38	−3 9	+ 25	2500	253	30 Ha	−6
92505	B3 IV:	6 88	− .30	H	− 32	−2 8:	+ 02	900	255	22 Ha	−5
92554	O9 5 II:	8 60	+ .05	O	− 39:	−5 3:	+ 44	2200	255	22 Ha	+4
93030	B0 V				− 38	−3 9			256	Outskirts η	−9
93190	B2e	8 51	− .04	B, M					255	η Ha	−3
93206	B0 I	6 32	− .12	O, M	− 38	−6 5	+ 26	2000	255	η Ha	−1:
93321	B5 V	9 61	− .21	B	− 28	−1 3	+ 07	1300	255	η Lane Ha	−8
93342	B0 III:	9 04	+ .34	B	− 38	−4 5	+ 72	1000	255	η Ha	+1
93403	O6	7 21	− .05	B, O, Std, M	− 46:	−6 0	+ 41	1700	255	η Ha	+4
93723	B3 IV	8 46	− .15	B	− 32	−2 8	+ 17	1200	255	η Lane Ha	−5
93795	A0 Ia	8 51	+ .51	B	− 18	−7 0	+ 69	2600	255	η Ha	
93843	O6	7 30	− .29	B, O	− 46:	−6 0	+ 17	3100	255	η Ha	+3
93890	(B)	9 14	+ .49	H					256	36 Ha	
94201	(B5)	9 34	− .15	H					256	36 Ha	
94369	B1 I	7 34	+ .03	O	− 36	−6 5	+ 39	2400	256	Outskirts η	−2:
94493	B0 5 I	7 19	− .24	O	− 37	−6 5	+ 13	4100	257	Thin Ha	−4
94909	(B5)	9 18	− .03	H					257	40 Ha	
94909	B0 I	7 28	+ .20	O, M	− 38	−6 0	+ 58	1200	256	Outskirts η	+3
94935	(B5)	8 59	− .04	H					257	40 Ha:	
94988	(B3)	9 26	− .11	H					257	40 Ha:	
95095	(B3)	9 55	+ .07	H					257	40 Ha:	
95461	B0 I	8 88	+ .12	O, M	− 38	−6 5	+ 50	3800	257	47 Ha	+4
95731	B0 II	9 00	− .06	O, M	− 38	−5 2	+ 32	3300	257	47 Ha	+1
96042	O9 5 Ve	8 32	− .11	H	− 39	−4 5	+ 28:	1900	257	47 Ha	+3:
96139	(Oe)	8 69	+ .11	H					257	Thin?	
96248	B1 I	6 51	− .05	O, M	− 36	−6 5	+ 31	1950	258	Thin	−3
96446	B2 V	6 59	− .34	B	− 34	−2 6	.00	700	258	Thin	−9
96587	A2 V	9 68	+ .06	H	− 09	+1 2	+ 15	350	258	49 Ha	
96622	O9 5 IV	8 86	− .08	B	− 39	−4 4	+ 31	2200	258	Thin dark	+2
96638	O8	8 52	.00	B, O	− 42	−5 3	+ 42	2200	258	Thin dark	−3
96670	O8	7 34	− .10	B, O, M	− 42	−5 3	+ 32	1600	258	Thin	+1:
96810	B4 II:	8 63	+ .04	B	− 30	−4 5	+ 34	1950	258	Thin dark?	−3
97151	B1e	7 63	− .31	B	− 36:	−3 2	+ 05	1300	258	51 Ha	
97166	O8	7 84	− .17	B, O	− 42	−5 3	+ 25	2400	258	Edge 51 Ha	0:
97222	B0 II:	8 75	− .05	B, Std	− 38	−5 2	+ 33	2900	258	51 Ha	−5:
97253	O6	7 04	− .10	B	− 46	−6 0	+ 36	1800	259	Thin	+1:
97381	B1 III	8 23	− .14	B, O	− 36	−4 3	+ 22	1950	259	Thin	−2
97434	O8:	8 07	− .10	O, H	− 42	−5 3	+ 32	2250	259	Thin	−2:
97484	O5:	8 38	+ .09	H	− 48:	−6 0:	+ 57	2000	259	55 Ha	+4
		8 53	+ .06				+ 54:				
97499	B2 5 V	9 15	− .17	H	− 33	−2 3	+ 16	1350	259	56 red?	−2
97557	B3 III	7 15	− .20	B	− 32	−3 7	+ 12	1100	258	Thin+dark	−4
97629	(B5)	9 53	− .13	H					259	55 Ha	
99416	B0 5 V	8 81	− .15	B	− 37	−3 5	+ 22	2500	260	Rel. clear	−1
99897	O7	8 33	− .12	H	− 44	−5 7	+ 32	3100	261	63 Ha	+2
99953	B1 I	6 43	+ .03	O, M	− 35	−6 0	+ 38	1300	262	Weak Ha	−3
100242	B0 IV:	8 30	− .12	B, O	− 38	−4 2:	+ 26	1700	261	Rel. clear	0:
100276	B0 5 II	7 13	− .21	B, O, M	− 36	−5 1	+ 15	2000	261	Rel. clear	−1
100335	B6 III:	7 75	− .20	B	− 26	−3 1	+ 06	1300	261	Rel. clear	−3
100381	B2 V	8 67	− .21	B	− 34	−2 6	+ 13	1300	261	Rel. clear	−4
100943	B5 Ia	7 05	− .12	O, M	− 28	−6 0	+ 16	2800	261	Rel. clear	
101008	O9 V	9 14	− .27	H	− 40	−4 7	+ 13	4350	262	68 Ha	−2
101084	B1 V	9 23	− .14	H	− 36	−3 2	+ 22	1900	262	68 Ha	−3
101131	O8	7 07	− .24	H	− 42	−5 3	+ 18	2000	262	68 Ha	+3
101190	O7	7 21	− .18	H	− 44	−5 7	+ 26	2100	262	68 Ha	0
101191	O8	8 45	−0.17	H	−0.42	−5.3	+0.25	3200	262	68 Ha	−3

TABLE 2—*Continued*

HD	Sp.*	m_v	C_{b-v}	Source†	Normal Color	M_{V_0}	E	d	Long.	Neb.‡	K:4026
101205	O8	6.40	−0.22	O, Std	−0.42	−5.3	+0.20	1400	262	68 Hα	+1
101332	B0.5 II	7.54	− .15	H	− .37	−5.2	+ .22	2100	262	68 Hα	−4
101545	O9.5 Ib	6.26	− .24	O	− .39	−6.0	+ .15	2000	263	Thin Hα out skirts 63	−3
102997	B4 Ia	6.47	+ .04	O, M	− .29	−7.0	+ .33	2300	264	Rel. clear	+5
106068	B9 I	5.82	+ .05	O, M	− .20	−6.5	+ .25	1620	266		Stellar
106343	B2 Ia+	6.14	− .17	O	− .34	−7.0	+ .17	2900	267		
106362	B1 I	7.30	− .27	O	− .36	−6.5	+ .09	4700	267		−4
112272	B0.5 Ia	7.44	+ .49	O, M	− .37	−6.5	+ .86	850	271		−6
112364	B1 I	7.31	− .06	O	− .36	−6.5	+ .30	2900	271		−4
115842	B0.5 I	5.96	+ .01	O, M	− .37	−6.5	+ .38	1300	275		−4
117111	B2 Ve	7.51	− .16	O, M	− .34	−2.6	+ .18	700	275		−6
117460	B2 III	7.08	− .20	O	− .34	−4.1	+ .14	1250	275		−4
117707	B0.5 I	9.45	+ .27	O	− .37	−6.5	+ .64	3600	275		+3
117797	O6	9.20	+ .18	O	− .46:	−6.0	+ .64	2500	275		+3
135240	O8.5				− .41	−5.2			287		−4
135591	O9 I	5.32	− .36	H	− .40	−6.2	+ .04	1800	287	H II 28802	−6
136003	(B1)	6.68	− .08	O, Std					290		
137603	(Oe)	10.04	+ .94	H					288	H II 28802	
144695	O9 V	9.80	+ .29	H	− .40	−5.0	+ .69	1900	299	H II	+1
144900	O9 III	9.71	+ .45	H	− .40	−4.7	+ .85	1100	300	H II 30000	−3
144918	(B0)	10.02	+ .49	H					300	H II 30000	
144969	B0.5 I(a)	8.40	+ .66	H	− .37	−6.5	+1.03	900	300	H II 30000	−3
144970	(B0)	9.89	+ .49	H					300	H II 30000	
145664	(B2)	8.32	+ .08	O, Std					299	H II 29902	
145846	B2 Ve	8.88	+ .10	O	− .34	−2.6:	+ .44	700	299	H II 29902	−2
146919	B0.5 Ia	8.60	+ .30	O	− .36	−6.8	+ .66	2600	299	H II 29902	+1
147331	O9.5 Ia	8.74	.00	O	− .39	−6.8	+ .38	5300	300	H II 29902	+4
149729	(B2)	8.96	− .24	O, Std					301		
150135	O6				− .46:	−6.0			304	H II 30402	0
150136	O7:				− .44:	−5.7			304	H II 30402	−2
150197	B0 I	9.47	+ .14	H	− .38	−6.5	+ .52	4700	305	H II 30402	+3
150958	O6				− .46:	−6.0			306	H II 30402	+4
151300	O6	9.24	+ .21	H	− .46:	−6.0	+ .67	2400	306	H II 30402	+2
151932	(OC)	6.44	+ .01	H					310	H II 31100	
152408	(Oep)	5.72	− .10	H					311	H II 31100	
152667	O9.5 I	6.14	+ .02	H	− .39	−6.5	+ .40	1300	312	H II 31100	+1:
152723	O6.5	7.03	− .11	H	− .45	−6.0	+ .34	1900	312	H II 31100	+3
153426	(B2)	7.38	− .14	O					314	H II 31500	
153919	(Od)	6.48	− .03	H					315	H II 31500	+1:
156134	B0 I	8.16	+ .37	O, Std	− .38	−6.5	+ .75	1500	319	H II 31800	−3
156154	O7	8.20	+ .33	O	− .44	−5.7	+ .77	1000	319	H II 31800	+1
158186	B0 V	6.92	− .23	H	− .38	−3.9	+ .15	1000	323	H II 32300	−5
158926	B2 V				− .34	−2.6			319	Clear?	−7
159176	O7**	5.61	− .21	O, Std, M	− .44	−5.7	+ .23	1100	323	H II 32301	
161291	B0.5 Ib	8.88	+ .47	B	− .37	−6.0	+ .84	1400	329	Dark	−4
161756	B3 V(e?)	6.20	− .05	B	− .32	−2.0:	+ .27	230	330	Dark	−6
163453	B0.5?pe V††	9.27	+ .33	B	− .28	−5.7:	+ .61	2400:	329	Dark?	
163613	B1 I–II	8.48	+ .10	B	− .36	−6.0	+ .46	2750	330	Dark?	−4
163685	B3 IV	5.90	− .23	B	− .32	−2.8	+ .09	450	330	Rel. clear (irregular)	−7
163984	B3 IV	8.28	− .12	B	− .32	−2.8	+ .20	1050	329	Rel. clear (irregular)	−6
164019	B0 II:	9.21	− .02	B, O	− .38	−5.2	+ .36	3300	330	Rel. clear	0:
164106	B5 III	8.94	− .02	B	− .28	−1.3	+ .26	620	330	Rel. clear	−1
164402	B0 II	5.73:	− .28	O, M	− .38	−5.2	+ .10	1200	335	H II 33402	−5
164637	B0 II	6.57:	− .31	O, M	− .38	−5.2	+ .07	1900	335	H II 33402	−7
165207	B2 IV	8.19	− .32	B	− .34	−3.3:	+ .02	1900	329	Dark	−8
167264	B0 I	5.25	− .22	O, M	− .38	−6.5	+ .16	1550	338	Dark	−4
172910	B3.5 V	4.71	− .38	O	− .31	−1.8	− .07	200	327	Clear	−8
175191	B4 V				− .30	−1.6			338	Clear?	−9
175362	B7.5 V	5.22	− .36	O	− .23	−0.7	− .13	120:	327	Clear?	−6
180885	B6 V	5.45	− .32	O	− .26	−1.1	− .06	180	330		−9
300777	B2:	9.20	+ .11	B	− .34	−2.6:				Near neb. 13 red	−2
300814	B3 III	9.30	+ .17	B	− .32	−3.7	+ .49	1300	252	Rel. clear	−6
302686	B3 V	9.96	− .22	H	− .32	−2.0	+ .10	1950	252	6 blue	−3
		8.89	− .16				+ .16	1050			
303004	B1 III	10.02	+ .45	H	− .36	−4.3	+ .81	1100	252	25 blue	−3
303056	B5 V:	9.63	− .17	H	− .28	−1.3	+ .45	550	252	27 blue	
303202	B2 V:	9.72	− .10	B	− .34	−2.6	+ .24	1700	255	η Hα	−3
303299	B0 Ve	9.30	− .01	B	− .38	−3.9	+ .37	1900	254	η Hα	−1:
305298	(B)	10.80	− .02	H					253	21 Hα	
305452	B2 III	9.41	− .16	B	− .34	−4.1	+ .18	3300	255	η Hα	−5
305556	B0 II	8.74	− .16	B	− .38	−5.2	+ .22	3700	255	η Hα	−1:
305560	O9.5 I:	8.76	+ .08	B	− .39	−6.5:	+ .47	3800	255	η Lane Hα	+2
305619	O9.5 Ia	9.49	+ .18	B	− .39	−6.5:	+ .57	4300	255	η Hα	+2
306041	B1.5 III	9.64	− .16	B	− .35	−4.2	+ .17	4000	257	Near 51, Hα	−5
306059	B3.5 V	9.42	− .14	B	− .31	−1.8	+ .17	1200	258	Thin	−3
306141	B1 V	9.87	+ .24	B	− .36	−3.2	+ .60	1000	258	Thin+dark	−4
316197	B3 V	9.56	+ .24	B	− .32	−2.0	+ .58	540	328		−6
316341	B4 V	9.65	+ .16	B	− .30	−1.6	+ .46	620	327		−6
319699	O7	9.81	+0.50	H	−0.44	−5.7	+ .94	1400	317	H II 31800 b	

* Spectra in parentheses are taken from the *Henry Draper Catalogue*.

† Source for magnitudes and colors in third and fourth columns are as follows: "B," Bok and van Wijk (1952); "O," Oosterhoff (1951); "M," Morgan, Code, and Whitford (1955); "H," Hoffleit new results. "Std." signifies a standard of comparison taken from the Bok–van Wijk or Oosterhoff lists.

§ Estimates of spectral class from objective-prism plates, dispersion at Hγ 45 A/mm.

** Spectral class from Morgan, Code, and Whitford (1955).

Spectral class from Bidelman (1954).

‖ HD 101205, possibly variable, used as comparison star.

†† Spectral class from Hiltner (1954).

‡ Numbers refer to the number of the nebulosity in *Harvard Ann.*, Vol. **119,** No. 2, 1953, for Carina, and to the Bok, Bester, and Wade Catalogue of H II regions, *Harvard Reprint,* No. 416, 1955.

reliable estimates on the Harvard patrol plates. Four photoelectric measurements each of HD 152667 and 153426 were obtained. In each case one of the four estimates is appreciably fainter than the other three. If these stars are also binaries, the available spectra give no confirmation.

Another possible variable is HD302686. Two measurements indicate its magnitude as 9.7, while a third gives 8.7, the latter value relative to each of two comparison stars. This star is at the center of a small blue nebula, No. 6 in the list of nebulosities in Carina (Hoffleit 1953). On an objective-prism plate taken with the ADH telescope, Hβ is suspected to be in emission, although no emission is seen on the adequately exposed B3 V-

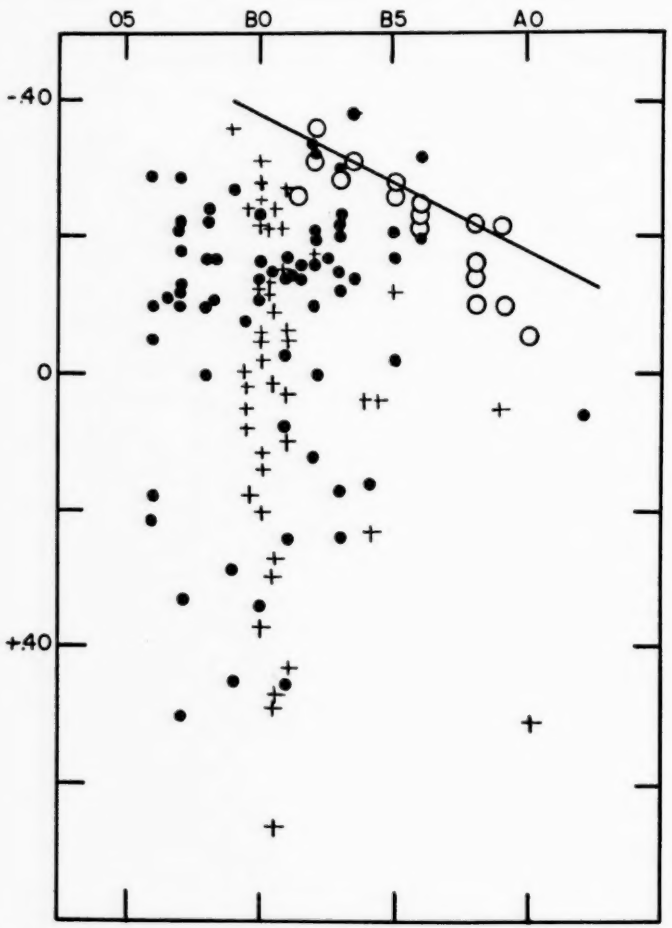

FIG. 4.—Color indices as a function of spectral class. *Open circles:* stars in Orion, all of luminosity class V; *crosses:* stars of luminosity classes I and II; *dots:* all others in Table 2 except stars with emission lines.

type spectrum obtained with the 60-inch. Examination of about a hundred and fifty patrol plates (AM series, 1.5-inch Cooke lens) suggests a possible variation of about 0.4 mag., in contrast to the 1 mag. indicated photoelectrically. It is not impossible, however, that the discordant observation may represent a misidentification at the telescope.

In Figure 4 the observed color indices listed in Table 2 are plotted against the spectral classes. Unlike those of the selected Orion stars of Table 1 (*open circles* in Fig. 4), the colors show a large dispersion, indicating that many of the stars are highly reddened. The minimum limiting values in such a diagram, however, should represent the normal color indices unaffected by absorption, provided that not all the stars are in regions of obscuration. The slant line in the figure represents the adopted normal colors of Bok and van Wijk. They vary linearly from -0.38 at B0 to -0.28 at B5. The few points lying above this line could represent uncertainties in either color or spectral class. Systematic errors as great as 0.04 mag. in the normal colors are unlikely in view of the previous comparisons with Sharpless' results in Orion.

The color excesses for stars in different longitude intervals have been examined for possible correlations with bright nebulosity. The material was sorted into three groups: Hα emission, reflection nebulosity, and no apparent nebulosity in the line of sight of the stars. The figure shows no clear differentiation in color excess between the three groups nor any pronounced dependence of color excess on longitude for the stars as a whole.

Distances in parsecs have been estimated from the relation

$$5 \log d = m_v - M + 5 - 5E .$$

The factor 5 used to convert from color excess to total absorption was found by Bok and van Wijk to be consistent with the factor 4 generally employed for deriving total photographic absorptions from excesses on the International System. The probable errors of the apparent magnitudes and color excesses could account for errors of not more than 10 or 15 per cent in the distances. The uncertainties arising from errors in M are less readily evaluated. For the present, the absolute magnitudes corresponding to the spectral and luminosity classes must be taken from the Yerkes calibrations (Keenan and Morgan 1951; Struve 1953). Relatively little material has been available on accurate parallaxes and luminosities of high-luminosity early-type stars. Hence considerable uncertainty must exist in the assignment of discrete values of mean absolute magnitudes to the individual stars in Table 2, especially those of luminosity classes I and II, of whose absolute-magnitude dispersion we have little knowledge. An uncertainty in M, conservatively estimated at only $\frac{1}{2}$ mag., would introduce an uncertainty of nearly 30 per cent in the distances of the individual stars. The tabulated values of the distances of the supergiants are subject to errors of this order, which may be either random or systematic.

The distances listed in the ninth column of Table 2 are plotted in Figure 5 in a polar diagram as a function of galactic longitude. The larger symbols represent the O types and B0–B2 stars of luminosity classes I and II. The others are less likely to define spiral structure. It is to be stressed that no attempt has been made to attain uniform percentage distribution in the numbers of stars in various longitude intervals. The heavy concentration of points between longitudes 250° and 262° is accentuated by the concentration of the observational program in this area. The general character of Figure 5 would not be altered if we were to restrict it to the stars that are specifically involved in Hα nebulosity (indicated in the eleventh col.).

The relative intensities of the interstellar K line, listed in the final column of Table 2, are discussed in a later section.

IV. ON THE SPIRAL STRUCTURE IN CARINA

The B-type stars in Carina appear to be most numerous at about 1.2 and 2 kpc (Fig. 5). Whether or not the deficiencies of points in this direction at 1.5 and 2.7 kpc are real must be tested with data from neighboring fields, which are still lacking. The two straight

lines in the upper right corner of Figure 5 represent schematically the two spiral arms in the Northern Hemisphere first mapped by Morgan, Sharpless, and Osterbrock (1952). The other three straight lines in the figure have been drawn through the concentrations of B stars in Carina and approximately parallel to the northern arms. The right-hand segment of the first line between the sun and the galactic center represents the third spiral arm indicated by Morgan and his co-workers (1953). The new observations presented here might be looked upon as indicating the extension of this arm toward Carina. But, in view of the suspected uncertainty in the adopted absolute magnitudes and the

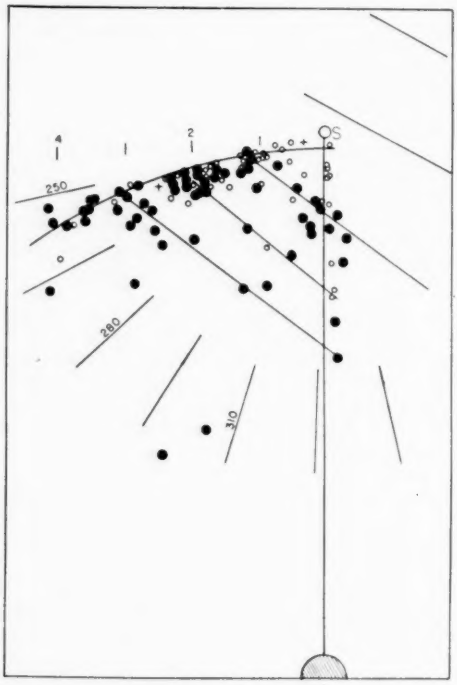

FIG. 5.—The distribution in the galactic plane of the stars in Table 2. *Solid circles:* stars of spectral classes O6–O8 and O9–B2 stars of luminosity classes I and II. *Open circles:* later spectral or lower luminosity classes; *crosses:* two A-type supergiants. Galactic center (indicated at lower edge of graph) at 8 kpc from the sun in longitude 327°. *Curved line:* arc of a circle 7.7 kpc from the galactic center; intervals of 1 kpc indicated. *Upper three diagonal lines:* spiral arms determined by Morgan *et al.*, the others drawn parallel thereto and through the concentrations in Carina (longitudes 250°–265°).

fragmentary nature of the material for the greater longitudes, it is still unwise to present conclusions on the structure of the spiral arms in this quadrant as definitive. In the general direction of η Carinae, however, the evidence seems fairly conclusive that the stars are spread out over a wide range in distance. Figure 5 by itself is not sufficient to decide conclusively between the two old divergent hypotheses, whether the spiral arm through the η Carinae nebula is directed across or essentially along the line of sight.

The indicated dispersion in the distances might conceivably be diminished if we could group into means data for stars definitely belonging to the same cluster or other spatial

association in which all the stars may be considered as effectively at the same distance. Examination of direct photographs of the Carina region indicates three such possible physical groups (Table 3), each including four or five of the stars in Table 2.

NGC 3293 is a tight cluster, and there is little doubt that the five stars listed are, in fact, members. Their individual indicated distances range from 2.2 to 3.2 kpc, with a mean of 2.6 ± 0.2 kpc. This corresponds to a probable error of about 0.3 kpc for a single star. The other two groups are more loosely structured. The four stars in the cluster associated with the nebula IC 2944 have more poorly determined individual distances (1.4–3.2; mean 2.1 ± 0.5) because their common photometric comparison star proved to be variable. The third group, at a mean distance of 1.7 ± 0.3 kpc, is more widely scattered in the sky and is unnamed. None of these groups includes stars at the largest distances shown in Figure 5. The two loose groups include dwarfs; but only one of the dwarfs appears exceptionally nearby for group membership (HD 96446).

In the H II regions between longitudes 260° and 355°, Mr. Wade selected two or more stars as the possible exciting agents in each of six nebulae. In four of these cases the distances derived for two stars in the same nebula differed by 0.2–0.7 kpc. In region H II 29902, three stars yield the discordant results 0.7, 2.6, and 5.3 kpc. The first is presumably a foreground dwarf star. The color excesses of the other two differ appreciably, being +0.66 and +0.38, respectively. In H II 30402, the two determinations, 2.4 and 4.7 kpc, differ by a factor of 2.

TABLE 3

CLUSTERING AMONG THE CARINA STARS

Close Cluster NGC 3293				Loose Associations							
				IC 2944				Unnamed			
HD	m_y	Sp.	kpc	HD	m_y	Sp.	kpc	HD	m_y	Sp.	kpc
91943	6.64	B0.5 I	2.9	101084	9.23	B1 V	2.0	96248	6.51	B1 I	2.0
91969	6.05	B0 Ia	3.2	101131	7.07	O8	1.9	96446	6.59	B2 V	0.7
91983	8.52	B1 III	2.3	101191	8.45	O8	3.2	96662	8.86	O9.5 IV	2.2
92007	7.78	B0 II	2.4	101205	6.40	O8	1.4	96638	8.52	O8	2.2
92044?	8.22	B0.5 II	2.4					96670	7.34	O8	1.6

The stars within the bounds of the strong η Carinae nebula itself have indicated distances ranging from 1.3 to 4.3 kpc. If the spiral arm in this direction were indeed more or less tangential to the line of sight, this spread would not be surprising. On the other hand, averaging data might only conceal any existing evidence for this.

The curved line passing near the sun in Figure 5 is an arc of a circle concentric with the galactic nucleus, 8 kpc from the sun in longitude 327°. If we ignore the gaps at 1.5 and 2.7 kpc in the distributions of the B stars in Carina and note that the numbers of B stars in the *Henry Draper Catalogue* are known to fall off toward smaller galactic longitudes, Figure 5 could be interpreted as exhibiting a spiral arm which is about 7.7 kpc from the galactic center. This would agree with Elske von P. Smith's interpretation (1955) of her polarization measurements in the southern Milky Way. She considers the line-of-sight distribution of material in Carina beyond about 2 kpc as the extension of Morgan's spiral arm in Sagittarius. Her conclusions are based on the apparent alignment of the interstellar dust particles. In general, observations made perpendicular to a spiral arm indicate high polarization and systematic orientation of position angles for the direction of polarization. In a direction along a spiral arm, on the other hand, the polarization is gen-

erally low and the angles heterogeneous. The structure of the nebulosities in Carina, however, indicates that it is a highly turbulent region. And in a highly turbulent region the nonalignment of the dust particles might not necessarily indicate that we are looking along a spiral arm rather than across it. In any case, observations at longitudes less than 250° are necessary to resolve the patterns portrayed in Figure 5.

V. COLOR EXCESSES IN THE SUPERGIANTS AND DWARFS

Having noted that color excesses of B-type supergiants average somewhat higher than those for dwarfs, I previously suggested (Hoffleit 1953, 1955) that the relatively young supergiants might still be surrounded by a residual shell of the primordial globule out of which they are believed to have originated. The present observations are used to test this hypothesis; but observational selection effects still vitiate its confirmation.

In Figure 6 the color excesses in Table 2 are plotted as a function of the indicated distance, the different symbols representing various luminosity groups. Beyond 2 kpc, all

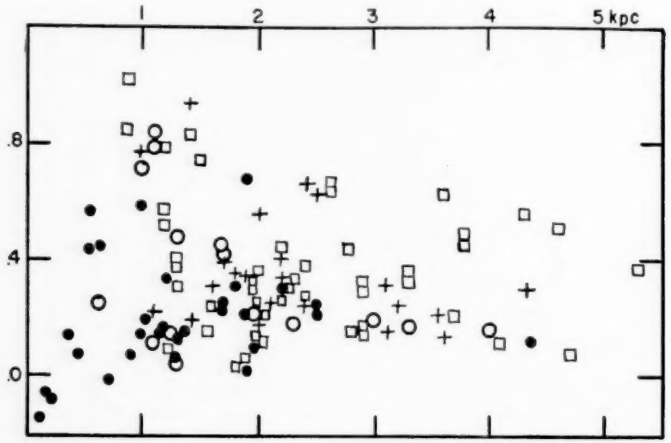

FIG. 6.—Color excess as a function of distance from the sun. *Crosses:* classes O6–O8; *squares:* O9 and B stars of luminosity classes I and II; *open circles:* luminosity class III; *dots:* luminosity classes IV–V.

the stars show excesses of 0.1 mag. or greater, indicating that nearly all the stars beyond this limit in the fields represented are obscured by $\frac{1}{2}$ mag. or more. Among all the luminosity groups the dispersion in color excess is high. The largest excesses, on the whole, appear to correspond to the relatively nearby stars. That this should be wholly the effect of uncertainties in the corrections for total absorption or in the absolute magnitudes of the supergiants seems improbable. Stars more highly reddened than about $E = 0.6$ at great distances would, in general, be fainter than the apparent magnitude limit of the present survey.

With the exception of one low-weight O9 V star, no dwarfs are represented at distances beyond 2.5 kpc. An intercomparison of the characteristics of supergiants and dwarfs should therefore be limited to stars within this approximate distance. For these, the color excesses tend to average slightly larger for the supergiants than for the dwarfs (Table 4, upper half), although the dispersions in all the groups are large. An average difference of 0.2 mag. between the high (I and II) and the low (IV and V) luminosity groups, if real, could not be attributed to the normal intrinsic difference in color index

between supergiants and dwarfs, especially as a few dwarfs are found to be highly reddened, while many supergiants are not. Hence these results again suggest that within 2 kpc heavy absorption occurs in relatively discrete clouds.

The selection of stars in the upper half of Table 4, however, favors the discovery of high color excesses among the supergiants relative to the dwarfs. To 9.5 mag. and 2.5 kpc, dwarfs with an absolute magnitude of −3 have a limiting observable color excess of 0.7 mag. Supergiants with an absolute magnitude of −6 and a color excess not over 0.7 mag. at 2.5 kpc would, however, be 6.5 mag. or brighter. Limiting our comparisons of mean color excesses, then, to stars with apparent magnitude limits of 6.55 for supergiants and 9.55 for dwarfs, we find the values in the second half of Table 4. While the supergiants still show a greater average color excess than the dwarfs, the differences are not adequately greater than their probable errors. Data on much fainter dwarf stars are desirable. Among the stars nearer than 2.5 kpc in Table 2, ten have color excesses greater than 0.7 mag., all of luminosity classes I–III.

TABLE 4

AVERAGE COLOR EXCESSES

CLASS	ALL STARS TO 2.5 kpc			CARINA STARS 1–2 kpc		
	m_y Average	No.	Average $E \pm$ p.e.	No.	Average $E \pm$ p.e.	Distance (kpc)
B I–II	6.9	27	+0.39±0.03	9	+0.49±0.05	1.3
B III	8.7	12	.39± .02	8	.42± .06	1.4
B IV–V	8.2	28	0.21±0.03	11	0.24±0.03	1.4
High−low			+0.18±0.04		+0.25±0.06	
	Brighter than					
B I–II	6.55	10	+0.24±0.03	5	+0.27±0.03	1.8
B IV–V	9.55	18	0.15± .03	8	0.22±0.02	1.5
High−low			+0.09±0.04		+0.05±0.03	

All the stars with high color excess within 2 kpc, represented here, are apparently situated within areas of either Hα or dark nebulosity. The reddened nearby dwarfs are all apparently imbedded in dark material. The one very reddened dwarf at 1.9 kpc is an O9 star in an H II region. At least one of the high-luminosity stars is surrounded by a small blue reflection nebula. Are most of these examples of reddening to be attributed to normal statistical sampling of stars accidentally observed behind very dense independent obscuring patches, or is the obscuring material specifically associated with the individual stars? If the reddened stars and the discrete obscuring clouds were aligned purely by chance, the average color excess should not be higher for the supergiants than for the dwarfs at the same average distance, unless supergiants simply show a stronger preference for the dusty regions than do the dwarfs.

Supergiants are considered younger than dwarfs of the same spectral class. If high-luminosity stars do originate from dark globules, the supergiants might be more likely than the dwarfs to be surrounded by local dust shells—the remnants of the primordial globules. If the high reddening does represent such residual dust shells, they would presumably be short-lived, and not many supergiants would still reveal them to any appreciable extent. The material available on stars at any one given distance is small, however,

and the analysis of the spottiness of the obscuring material is still too sketchy for us to ascertain how much of the reddening is due to irregular dust clouds between us and the star and how much might safely be attributed to material directly associated with the star itself.

VI. INTERRELATIONS BETWEEN GAS AND DUST

The color excesses discussed in the previous paragraphs have disclosed the presence of dust relative to selected O- and B-type stars, while an intercomparison of direct photo-

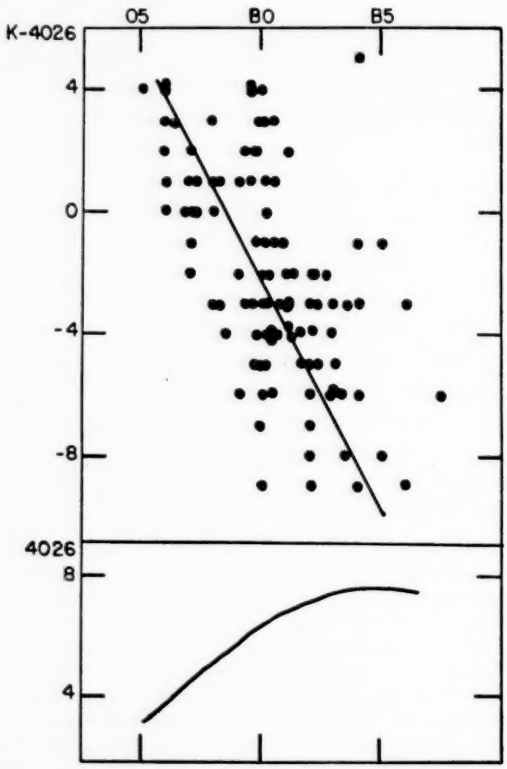

FIG. 7.—Estimates of the variation of K:4026 (arbitrary scale) with spectral class. *Lower curve:* average variation of the comparison line, 4026.

graphs in red and blue light has revealed (Hoffleit 1953) the distribution of hydrogen gas in the regions studied. In addition, the spectra obtained with the 60-inch may give some indication of the presence of interstellar ionized calcium between us and the selected B-type stars. This is of interest for a study of the interrelations between interstellar gas and dust.

The spectra from which the two-dimensional spectral classifications in the second column of Table 2 were determined have been used for estimating the intensity of the interstellar K line relative to He II 4026 as a comparison line. The values of the intensity

ratio K:4026, given in the final column of Table 2 and in Figure 7 as a function of spectral class, are on an arbitrary scale, 10 representing a strong and 1 a barely perceptible line. Likewise, the unidentified interstellar band at 4430 was examined; but it was adequately exposed for simple eye-estimates on only sixteen plates. These few indicated no correlations with color excess, K-line intensity, or distance.

From spectral classes O6–B5 the stellar K line, though increasing in intensity, is negligibly weak or invisible. The helium line, 4026, reaches maximum intensity at B2. However, it varies by only about three units on the adopted intensity scale. Its estimated variation on this scale is shown in the lower half of Figure 7. In Figure 8 the K-line intensities, now corrected for the average variation of 4026, are plotted against distance. In the Carina region there is only little evident correlation. In the H II regions and in Sagittarius the more distant stars do show appreciably stronger interstellar K lines.

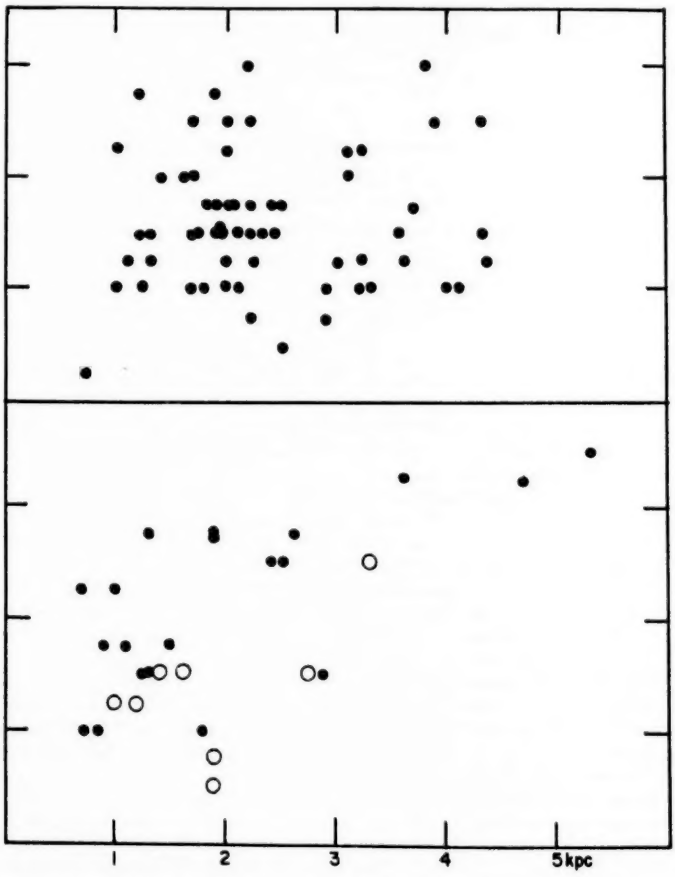

FIG. 8.—Variation of K line with distance from the sun. *Upper diagram:* the Carina region; *lower diagram:* dots for H II regions; open circles for Scorpio-Sagittarius.

In Table 5, I have separated most of the material of Table 2 into three longitude groups: the Carina region, embracing the stars from longitudes 250° to 265°; the H II regions between 285° and 325° (practically all the stars on our program in this interval had been chosen because of their apparent involvement in H II regions); and the Sagittarius stars between 325° and 340°. These three groups represent a wide variety in the appearance of the general star field. The Carina region has about as complicated an assortment of gaseous and dark nebulosity as it is possible to find. The Sagittarius fields represented have little emission nebulosity but a wide range in the transparency of the interstellar dust clouds. In each of the three groups the stars are subdivided by distance, the divisions in each group corresponding more or less to the natural groupings noted in Figure 5. Table 5 shows the variation with distance of color excess and the interstellar K line in each of these groups.

TABLE 5

VARIATION OF COLOR EXCESS AND K-LINE INTENSITY WITH DISTANCE

Region	d (kpc)	No.	E	K Line
Carina (250°–265°)	1.5	21	0.35	3.8
	1.5–3	40	.30	4.4
	3	16	.27	4.8
H II (285°–325°)	1.5	6	.61	4.0
	1.5–2	4	.46	4.2
	2–4	2	.66	6.5
	4	2	.45	9.5
Sgr (325°–340°)	0.7	8	.19	0.9
	1–2	6	.23	0.7
	2	2	0.41	4.0

Only in the Sagittarius region does there seem to be any semblance of correlation between distance and color excess, and there the average value of the absorption is smaller than in the other groups, which are rich in emission. In the H II regions the color excesses are found to range from 0.04 to 1.03 mag., but they average higher than in either of the other two groups. The K line, on the other hand, does show some increase in intensity with distance in all three groups, although the relation is not the same in all three.

In Table 6 I have re-sorted the material in the three longitude groups according to the prevailing character of the nebulosity in the area immediately surrounding each star. In Carina the emission areas show a relatively low general absorption in comparison with the obviously dark areas. On the other hand, the stronger K-line intensity in the Hα areas suggests that more ionized calcium atoms are present in the Hα clouds than in the dark obscuring clouds in Carina. In the Sagittarius regions there is a marked dependence of color excess on the apparent prevalence of dust clouds but no corresponding correlation with K-line intensity; in fact, there is a strong deficiency of interstellar calcium except for the two most distant objects.

Summarizing the results from these two tables, we find that Hα emission tends to occur in or near regions of high color excess, confirming the over-all association of gas and dust in the Milky Way. On the other hand, the specific spots where Hα appears strongest in Carina do not generally coincide with the spots having the highest color excess. In Sagittarius, where we have no emission nebulae represented, the average color excess is smaller than in the H II regions. Here the dependence of color excess on apparent

obscuration is clearly marked. The interstellar calcium gas seems to be statistically well correlated with the presence of interstellar hydrogen, being relatively weak or absent where no hydrogen emission is observed.

VII. THE SMALL ROUND NEBULAE

In previous publications (Hoffleit 1953; Bok 1955) I have discussed several small bright nebulae whose central stars—if, indeed, they are the activating source of the nebular light—are of too late a type to permit the classification of the nebulae as planetaries. Improved spectral classes and color excesses are now available for two of the red and three of the blue small nebulae (Table 7). The central star of blue nebula

TABLE 6

COLOR EXCESS AND K-LINE INTENSITY AS FUNCTIONS OF APPARENT NEBULOSITY

Region	Character	No.	E	K Line
Carina	Conspicuous Hα	36	+0.28	4.7
	Relatively clear	7	+ .24	5.1
	Blue reflection nebulosity	3	+ .57	3.3
	Dark nebulosity	2	+ .48	2.0
H II Regions		14	+ .55	5.2
Sagittarius	Clear	2	− .03:	0.0
	Intermediate absorption	4	+ .23	3.2
	Conspicuous dark	5	+0.35	1.2

TABLE 7

CENTRAL STARS OF SMALL ROUND NEBULAE

Neb. No.*	HD	Sp.	E	K Line	d (pc)
Red:					
30	92383	B0 V	0.25	0	2500
49	96587	A2 V	.15	Stellar	350
Blue:					
6	302686	B3 V	.13:	+4	1950:
25	303004	B1 III	.81	+3	1100
27	303056	B5 V:	0.45	.....	550

* Harvard Ann., **119**, 53.

No. 6 appears to be variable, and its spectrum may have emission lines. Hence the color excess recorded for it may not have the same meaning as for the others. For the two red nebulae, the color excesses of the central stars are considerably smaller than for the other two blue nebulae, in accordance with the differences noted between H II and dusty regions in the Carina field as a whole. The three values of the interstellar K-line intensity do not happen to confirm the indications from the field stars, but they are too few in number to be conclusive.

VIII. COMPARISONS WITH EARLIER HARVARD ESTIMATES OF DISTANCE

The Bok–van Wijk paper (1952) dealt separately with four discrete fields in what I have designated as the Carina region, namely, SA 193, the GL Carinae, η Carinae, and

Vela fields. The distance moduli that Bok and van Wijk determined in these fields depended upon the spectral classes of the *Henry Draper Catalogue* and mean absolute magnitudes corresponding to luminosity class about III–IV. It is of interest to see to what extent the present revisions in spectral class have altered the distances.

For the stars we have in common, the average distances in both systems are given in Table 8, as well as the distributions among the various luminosity groups and the number of stars reclassified O6–O8. Of the latter, Miss Cannon had classified only two as Oe5, the others as B types. About 54 per cent of the stars in Table 2 have been reclassified earlier than by Miss Cannon, 27 per cent later. This would increase somewhat the inferred average distances. The major contribution to the large increases noted in Table 8,

TABLE 8

COMPARISON WITH BOK AND VAN WIJK DETERMINATIONS OF DISTANCE

Field	Distances		No.	O6–O8	I–II	III	IV–V
	B-vW	New					
SA 193	1060	1760	5	0	1	1	3
GL Car	1030	1870	14	4	2	3	5
η Car	1250	2470	12	2	4	2	4
Vela	1190	2170	7	1	1	3	2
Sgr	950	1390	11	0	3	1	7
All			49	7	11	10	21

however, comes from the appreciable percentage of high-luminosity stars. Among all the B stars in Table 2, between longitudes 250° and 265°, the following numbers and percentages apply:

Luminosity class	I–II	III	IV–V
Number	26	12	21
Percentage	44	20	36

In the H II regions two-thirds of the B stars are supergiants, but in the Sagittarius fields only one-third. Among the northern blue giant stars classified by Morgan, Code, and Whitford (1955), the corresponding relative numbers and percentages are similar:

Luminosity class	I–II	III	IV–V
Number	381	177	410
Percentage	39	18	43

In SA 193 Bok and van Wijk had found that the absorption increased steadily with their estimated distances. The present limited results (seven stars) do not clearly support this contention, as indicated in the accompanying table.

HD	99953	100335	100381	100242	100276	99416	99897
Distance	1300	1300	1300	1700	2000	2500	3100
Color excess	0.38	0.06	0.13	0.26	0.15	0.22	0.32

Perhaps the most spectacular single difference between the Bok–van Wijk and the present results is for HD 93795. On the basis of Miss Cannon's estimate of B3 on a small-

dispersion spectrum (400 A/mm), they derived a color excess of +0.83 mag. and a distance of 320 parsecs. Three spectra obtained with the 60-inch indicate a spectral class of A0 Ia, showing sharp lines, a strong K line, and 4481 stronger than 4471. This revision decreases the apparent absorption and puts the star eight times farther away, at 2600 parsecs.

The distances I had estimated (Hoffleit 1953) depended on average values of the total absorption taken from the Bok–van Wijk paper and representing a wide area in the neighborhood of each star. Moreover, the absolute magnitudes I adopted for the *HD* spectra corresponded to main-sequence luminosities. Hence it should be expected that the estimates of distance for individual stars will depart strikingly from the present results. The average difference for all stars common to my earlier measurements (1953) and Table 2 is 900 parsecs, the new values being some 60 per cent larger than the old.

IX. SUMMARY

1. The distributions of selected early-type stars in Carina, southern H II regions between Carina and Sagittarius, and regions near the galactic center are shown in Figure 5. The data are still insufficient to define the orientation of the spiral arms in Carina with certainty. Possible concentrations at 1.2 and 2 kpc are indicated. The diagram emphasizes the need for extensive observations at longitudes less than 250°.

2. Intercomparisons between the new and previous Harvard estimates of the distances of the Carina nebulosities illustrate the danger of assuming mean absolute magnitudes when luminosity classes are not available. Even when they are, the absolute magnitudes still tend to be the greatest source of uncertainty in the distances, especially for stars of luminosity class I.

3. The newly determined distances average 0.5–1 kpc larger than previous estimates, primarily because of the high percentage of stars found to be supergiants. In Carina, 44 per cent of the B-type stars studied belong to luminosity classes I and II; in the H II regions, 67 per cent; and in the Scorpio-Sagittarius fields 33 per cent.

4. The hypothesis has been offered that some high-luminosity stars may still be surrounded by a residual of the primordial dust cloud out of which they originated. A test of this hypothesis on the basis of relative color excesses of supergiant and dwarf stars is vitiated by observational selection effects; data on fainter dwarf stars are needed.

5. Intercomparisons between color excess, intensity of the interstellar K line, and distance reveal significant differences between the complex Carina region, the H II regions, and the Sagittarius fields.

6. The average values of both color excess and interstellar K-line intensity are greater in extended areas where there is diffuse Hα emission than where such emission is absent, indicating an over-all association of gas and dust in the spiral arms. However, where both absorption and emission nebulosities are intermingled, as in Carina, the absorption is stronger in the dark than in the emission patches. Thus in the H II regions the average color excess is +0.55 mag.; in Carina the average varies from +0.24 in relatively clear spots to +0.28 where Hα is conspicuous, to +0.48 in the dark areas. In Sagittarius, where none of the stars considered here is in the line of sight of an emission nebulosity, the color excess is negligible in clear spots and averages +0.35 where the obscuration is most obvious.

7. In Sagittarius both the color excess and the intensity of the K line are found to increase with distance. In Carina and the H II regions no correlation between distance and color excess is indicated. All three types of regions show some correlation between distance and the K-line intensity, but the relation is not the same in all three.

8. In general, interstellar ionized calcium is strong where clouds of hydrogen emission are strongest and weak where hydrogen emission is absent. In regions of dark nebulosity the K line is of intermediate intensity.

REFERENCES

Bidelman, W. P. 1954, *Pub. A.S.P.*, **66**, 250.
Bok, B. J. 1952, *Proc. Am. Phil. Soc.*, **96**, 540; *Harvard Reprint*, Ser. II, No. 42.
———. 1955, *Gas Dynamics of Cosmic Clouds*, ed. H. C. van de Hulst and J. M. Burgers (Amsterdam: North Holland Publishing Co.), p. 27; *Harvard Reprint*, No. 409.
Bok, B. J., Bester, M. J., and Wade, Campbell M. 1953, *Phys. Blätter*, **9**, 245.
———. 1955, *Daedalus*, **86**, 9; *Harvard Reprint*, No. 416.
Bok, B. J., and van Wijk, U. 1952, *A.J.*, **57**, 213; *Harvard Reprint*, Ser. II, No. 45.
Gaposchkin, S. 1946, *Harvard Ann.*, Vol. **115**, No. 5.
Hiltner, W. A. 1954, *Ap. J.*, **120**, 41.
Hoffleit, D. 1953, *Harvard Ann.*, Vol. **119**, No. 2.
———. 1955, *Gas Dynamics of Cosmic Clouds*, ed. H. C. van de Hulst and J. M. Burgers (Amsterdam: North Holland Publishing Co.), p. 29; *Harvard Reprint*, No. 409.
Johnson, H. L., and Morgan, W. W. 1953, *Ap. J.*, **117**, 313.
Keenan, P. C., and Morgan, W. W. 1951, *Astrophysics*, ed. J. A. Hynek (New York: McGraw-Hill Book Co.), p. 23.
Morgan, W. W., Code, A. D., and Whitford, A. E. 1955, *Ap. J. Suppl.*, **2**, 41.
Morgan, W. W., Keenan, P., and Kellman, E. 1943, *Atlas of Stellar Spectra* (Chicago: University of Chicago Press).
Morgan, W. W., Sharpless, S., and Osterbrock, D. E. 1952, *Sky and Telescope*, **11**, 138; *A.J.*, **57**, 3.
Morgan, W. W., Whitford, A. E., and Code, A. D. 1953, *Ap. J.*, **118**, 318.
Oosterhoff, P. T. 1951, *B.A.N.*, **11**, 299.
Sharpless, S. 1952, *Ap. J.*, **116**, 251.
Smith, E. von P. 1955, Ph.D. dissertation, Radcliffe College, unpublished; abstract, *A.J.*, **60**, 179.
Struve, O. 1953, *Sky and Telescope*, **12**, 186.

THE GALACTIC CLUSTER M11*

H. L. JOHNSON, A. R. SANDAGE, AND H. D. WAHLQUIST
Lowell Observatory; Mount Wilson and Palomar Observatories
Carnegie Institution of Washington, California Institute of Technology
Received March 2, 1956

ABSTRACT

The results of three-color photographic-photoelectric photometry on about 400 stars in the galactic cluster M11 are given. The cluster reddening is found to be $E_{(B-V)} = 0.42$ mag.; the apparent distance modulus, 12.3 mag.; and the true distance, 1660 parsecs. The ratio of the two color excesses, $E_{(U-B)}/E_{(B-V)}$, has been found to be 0.72. The color-magnitude diagram for M11 appears to be consistent with present-day ideas on stellar evolution. The age of M11 is intermediate between the Pleiades and Praesepe.

I. INTRODUCTION

Three-color photometric observations, made by the process of photographic interpolation between photoelectrically measured standards, are here reported for about 400 stars in and near the galactic cluster M11. This cluster is very rich in stars and contains many more yellow giant stars than do most galactic clusters; in these respects, it is similar to the galactic cluster, M67 (Johnson and Sandage 1955). The cluster M11 appears in the sky in the direction of the Scutum cloud. It is probably closer to the sun than is the Scutum cloud and is therefore seen in projection against the very rich background.

II. THE OBSERVATIONS

The photoelectric observations were made with the McDonald 82-inch telescope in the manner described for Praesepe (Johnson 1952), and the probable errors listed there for the cluster stars also apply to M11. The tie-in with the U, B, V system depends upon special observations on five different nights. The photoelectrically obtained values for the cluster standard sequence stars are listed in Table 1.

The photographic observations were made with the 100-inch telescope on Mount Wilson in the manner described for M67 (Johnson and Sandage 1955). The plate and filter combinations were the same as those previously described. Four plates in each of the three wave-length bands were measured to yield U, B, and V magnitudes. Table 2 gives the results for 399 selected stars in M11. To check the photographic system, magnitudes for the standards of Table 1 were read back through the calibration-curves. The adopted values for these stars are also listed in Table 2. Intercomparison of Tables 1 and 2 shows the lack of magnitude and color equations in the final data. The photographic data are therefore on the U, B, V system. The probable error of a single measurement for a U, B, or V magnitude is ± 0.031 mag. The probable error of the tabulated means in Table 2 is ± 0.015 mag.

With the exception of the yellow giants, the stars in the field of M11 were chosen at random for measurement. Every yellow giant was measured which was within the correction-free field of 10 minutes of arc radius from the center of M11. This biased procedure of selection gives approximately two times more yellow giants in the color-magnitude diagram than would be the case if the stars had been chosen strictly at random. This statistical bias was introduced to define better the yellow giant sequence. The luminosity function is not under discussion here.

* Contributions from the McDonald Observatory, No. 264.

All stars in Table 2 are labeled by their Küstner numbers (1923), by their Wallenquist numbers (1936), or by supplementary letters. The photoelectric standards and the faint supplementary stars are identified in Figure 1.

III. THE COLOR-MAGNITUDE DIAGRAM

The observed color-magnitude diagram, V versus $B - V$, for M11 is shown in Figure 2. All the stars listed in Table 2 are plotted. A well-populated cluster main sequence is evident, as well as many yellow giant stars. The color-magnitude diagram for this cluster is of the usual galactic-cluster type, similar to the Praesepe cluster or the Hyades, rather than of the globular-cluster type. The diagram is markedly different from that for M67, even though the two clusters are quite similar in physical appearance.

TABLE 1

PHOTOELECTRIC STANDARDS IN M11

Star	V	$B-V$	$U-B$	N	Star	V	$B-V$	$U-B$	N
Küstner nos.:					*Küstner nos.:*				
20	14.06	+0.82	+0.44	1	615	9.34	+0.50	+0.20	Std.
38	12.64	+0.41	+0.17	1	616	11.71	+0.45	+0.25	2
47	15.11	+0.50	+0.29	1	620	9.21	+1.25	+1.10	1
56	11.58	+1.49	+1.39	1	668	14.38	+0.55	+0.33	1
66	13.43	+1.33	+1.02	1	669	14.58	+0.59	+0.41	1
68	11.59	+1.69	+1.90	1	671	14.18	+0.76	+0.43	1
71	14.04	+0.46	+0.32	1	672	14.75	+0.45	+0.41	1
72	14.36	+1.65	. . .	1	*Wallenquist nos.:*				
82	13.43	+1.40	+1.36	1					
91	11.93	+0.33	+0.18	2	81	15.18	+0.44	+0.35	1
94	13.11	+0.28	+0.08	1	265	14.96	+1.59	+1.81	1
132	11.64	+0.38	+0.23	3	*Supplementary stars:*				
149	14.58	+0.52	+0.32	1					
224	11.81	+1.40	+1.15	2	A	15.81	+0.83	+0.24	2
287	14.25	+0.42	+0.32	1	B	15.21	+1.60	+1.70	1
317	12.36	+0.42	+0.25	2	C	15.06	+0.64	+0.43	2
427	11.72	+1.52	+1.43	2	D	15.90	+2.00	. . .	1
530	10.81	+0.61	+0.12	1	E	15.76	+1.59	+1.79	1
562	11.92	+0.34	+0.16	2	F	16.01	+1.65	+1.84	1
584	12.87	+0.40	+0.19	2	H	15.45	+0.75	+0.33	1
593	11.97	+0.34	+0.04	2	J	14.75	+2.43	+1.96	2
601	12.04	+0.42	+0.12	1	K	14.54	+0.58	+0.41	1

The color-magnitude diagram appears to be nearly free from field stars brighter than $V = 13$. At about this magnitude numerous stars which are off the M11 sequences begin to appear. Most of these are quite red and are undoubtedly the brightest stars of the background Scutum cloud. The solid slanting line in Figure 2 gives the approximate plate limit of the present data and shows that we have reached only a few magnitudes into the membership of the Scutum cloud.

In order to make more convenient a detailed analysis of the properties of M11, a mean main sequence has been derived from the values for all observed quantities for all the stars in given magnitude intervals. These intervals were $\frac{1}{2}$ mag. for $V < 14$ and $\frac{1}{4}$ mag. for $V > 14$. The yellow giants and all other stars that obviously are not cluster main-sequence stars were omitted from this computation. The results are listed in Table 3.

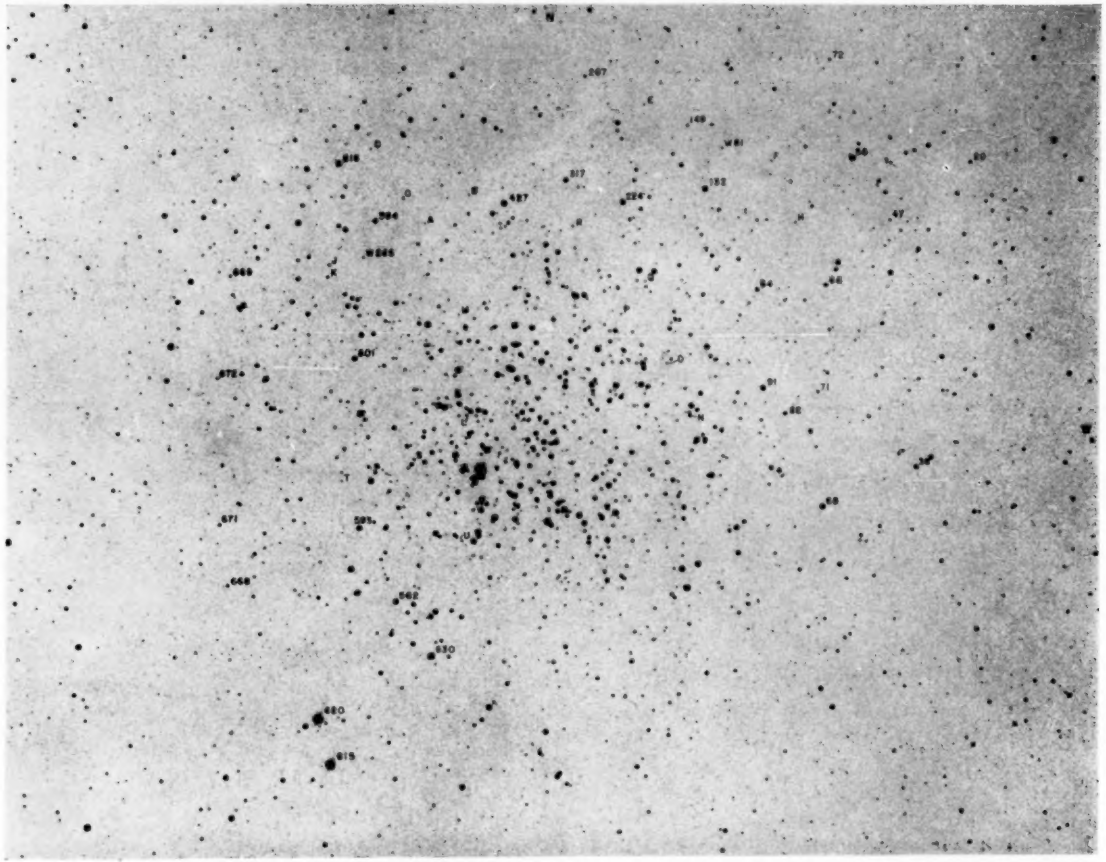

FIG. 1.—Identification chart for the photoelectric standards of Table 1 and for the supplementary stars of Tables 1 and 2. Unprefixed numbers are due to Küstner. Numbers prefixed by W are due to Wallenquist.

TABLE 2. COLORS AND MAGNITUDES OF 399 STARS IN M 11.

Star Kustner Nos.	V	B-V	U-B
20	14.10	+.78	+.48
35	12.71	.38	.11
38	12.70	.38	.20
46	12.39	.27	.15
47	14.96	.53	.33
56	11.58	1.44	1.40
60	12.35	.30	.10
61	12.35	.36	.12
66	13.47	1.35	1.07
67	12.59	.37	.18
68	11.63	1.71	1.89
71	14.00	.47	.32
82	13.39	1.49	1.33
87	12.72	.34	.16
91	11.95	.36	.18
92	14.09	.44	.39
94	13.07	.29	.11
98	14.63	.54	.28
99	13.23	.36	.19
101	14.33	.45	.39
102	12.48	.39	.16
103	14.56	.51	.34
106	13.97	.39	.38
108	14.05	.38	.29
116	12.85	.27	.11
120	13.50	.33	.27
123	11.41	.41	.15
124	13.43	.36	.25
127	14.75	.52	.42
128	11.63	.31	.11
129	12.53	2.06	-
130	14.37	.76	.51
132	11.69	.39	.26
133	12.72	.27	.02
134	11.33	.38	.09
136	11.59	1.60	1.35
138	13.11	.31	.16
139	14.10	.39	+.31
141	11.75	.38	-.06
143	11.04	1.98	+2.26
144	13.84	.39	.32
145	12.55	.43	.21
148	11.38	1.60	1.74
151	14.38	.60	.36
152	13.88	.43	.36
153	14.80	.58	.30
154	13.69	.30	.31
156	14.59	.46	.32
157	13.47	.36	.21
158	14.11	.54	.35
159	14.50	.56	.38
160	14.78	.55	.37
161	13.23	.37	.22
162	13.47	.36	.21
163	12.88	.34	.18
164	14.25	.56	.33
166	14.73	.52	.32
168	13.41	1.50	1.48
169	13.31	.32	.13
170	12.58	.33	.08
173	14.76	.70	.28
174	6.17	.48	.26
179	11.80	1.19	.84
180	13.87	.44	.41
183	12.54	.38	.21
185	12.32	.39	.10
188	14.81	.57	.43
190	12.67	.36	.11
191	11.72	.42	.02
193	11.77	.38	.09
194	13.69	.35	.32
195	13.62	.37	.32
197	11.74	.35	.09
199	14.49	.49	.34
200	14.68	.65	.20
202	13.89	.46	.39
205	14.82	.66	.26
207	12.66	.39	.14
208	14.66	.49	.33
211	14.73	.63	.31
213	14.00	.49	.32
215	14.03	.51	.43
216	14.03	.43	.38
217	13.08	.39	.19
218	14.63	.59	.37

Star Kustner Nos.	V	B-V	U-B
219	14.51	+.68	+.37
222	13.76	.30	.10
223	12.71	.42	.14
224	11.79	1.40	1.13
227	11.34	.52	.15
228	14.20	.63	.48
233	11.37	.39	.15
234	13.06	.38	.01
235	14.16	.49	.41
238	11.90	.42	.19
239	11.55	1.72	1.94
240	13.60	.61	.38
241	12.62	.61	.26
243	11.46	.49	.26
247	14.32	.49	.31
250	13.36	.39	.32
251	14.32	.53	.48
252	14.74	.59	.31
254	11.98	.38	.12
255	14.22	.43	.41
256	14.50	.49	.42
258	13.57	.38	.33
260	13.40	.38	.25
262	13.81	.36	.31
263	11.39	1.25	.77
272	11.59	.49	.06
275	13.81	.46	.32
276	13.22	.86	.56
280	11.76	.55	.38
282	14.89	.52	.42
283	12.20	.33	.07
284	14.49	.44	.30
286	11.24	1.51	1.71
287	14.24	.47	.38
288	14.26	.53	.44
289	14.36	.49	.34
290	12.83	.40	.10
292	13.14	.38	.20
296	14.76	.53	.37
297	13.45	.41	.21
298	14.91	.52	.32
301	15.00	.59	.50
302	12.59	.35	.12
303	13.19	.38	+.26
305	12.88	.32	-.03
306	14.72	.57	+.35
308	10.82	.54	.02
309	12.55	.38	.10
311	14.38	.51	.39
313	11.91	1.48	1.29
314	13.71	.51	.37
317	12.38	.39	.30
320	14.70	.59	.39
321	14.56	.55	.35
322	13.21	.36	+.20
323	12.66	.40	-.29
326	11.65	1.51	+1.36
327	12.29	.36	.15
328	12.11	.39	.15
329	11.86	1.40	1.33
332	12.01	.45	.19
333	12.97	.39	.24
334	12.05	1.44	+1.19
335	12.62	.41	-.03
336	10.30	.37	-.59
339	11.82	1.55	1.54
340	13.74	.50	.36
345	14.21	.57	.39
346	12.39	.38	.07
348	13.79	.41	.41
349	13.50	.60	+.28
350	12.79	.25	-.21
355	11.81	.46	+.10
356	12.18	.31	.18
357	14.61	.60	.36
358	11.50	.52	.24
362	14.40	.54	.33
364	12.64	.44	.25
365	12.86	.38	.19
366	12.25	.39	.07
369	13.66	.39	.27
370	14.65	.60	.41
373	14.42	.61	.38
378	12.11	.39	.19
380	12.45	.45	.29

Star Kustner Nos.	V	B-V	U-B
382	14.36	+.46	+.44
384	12.67	.35	.06
388	13.67	.39	.33
389	13.07	.37	.24
391	13.84	.52	.46
392	13.98	.56	.41
393	12.32	.44	.07
394	11.77	.38	.09
395	14.58	.50	.42
397	12.63	.40	.08
398	12.46	.39	.10
403	13.62	.41	.32
404	11.81	.45	.09
406	15.12	.63	.48
408	14.53	.67	.34
409	14.18	.45	.37
413	12.87	.38	.25
414	11.26	.46	.16
415	13.83	.50	.35
416	14.21	.50	.38
420	12.97	.41	.32
421	14.24	.51	.37
422	14.60	.53	.36
423	13.91	.41	.39
425	11.38	.40	.00
426	13.09	.34	.25
427	11.71	1.46	1.44
433	14.93	.54	.52
434	11.59	.45	.13
436	11.19	.41	.14
438	13.04	.49	+.16
440	11.37	.38	-.29
443	13.26	.38	+.22
445	12.67	.32	-.02
446	14.02	.39	+.30
448	11.12	1.09	.49
451	13.98	.49	.36
453	14.21	.51	.37
454	14.95	.53	.30
455	12.12	.40	.13
456	11.44	1.50	1.36
457	14.71	.58	.36
459	14.06	.45	+.38
461	11.39	.42	-.01
462	12.79	.33	+.31
464	11.33	.48	.04
465	12.37	.33	+.12
467	12.13	.39	-.04
468	13.52	.42	+.34
470	14.56	.45	.39
471	13.46	.42	.27
472	12.62	1.52	1.18
473	11.55	1.80	1.90
474	14.79	.76	.25
475	14.19	.38	.36
479	14.26	.49	.29
480	12.45	.38	.10
482	13.03	.41	.24
483	14.85	.45	.34
486	13.49	.43	.22
488	14.19	.45	.33
489	12.81	.37	.17
491	11.94	.40	.11
495	12.87	.43	.20
496	12.50	.31	.12
501	13.69	.32	.37
504	14.37	.53	.41
506	11.08	.48	.24
507	14.14	.47	.33
510	13.66	.42	.33
512	12.09	.31	.10
513	14.92	.53	.54
514	14.68	.63	.31
515	14.81	.44	.43
516	11.13	1.79	1.40
521	13.60	.42	.36
522	12.74	.44	.19
524	14.00	.51	.43
525	11.25	1.73	1.49
526	11.88	.51	.22
527	14.92	.36	.60
528	11.81	.43	.19
529	14.01	.40	.37
530	10.84	.64	.07
531	13.84	.41	.29

Star Kustner Nos.	V	B-V	U-B
532	14.49	+.70	+.42
533	12.16	.39	.22
534	12.88	.32	.04
537	13.46	.42	.27
538	14.24	.46	.39
539	11.37	1.74	1.93
540	14.50	.58	.36
543	14.55	.67	.33
545	13.56	.47	.54
548	13.30	.79	.50
549	12.80	.37	.19
550	12.82	.44	.24
556	12.52	.39	.32
560	13.29	.49	.22
562	11.88	.38	.17
566	12.88	.35	.19
568	14.57	.50	.42
569	14.58	.53	.33
575	14.55	.58	.43
576	13.91	.46	.41
577	14.66	.59	.46
579	13.11	.46	.33
580	11.98	.44	.24
581	14.31	.51	.48
582	14.42	.53	.31
584	12.86	.39	.20
585	13.13	.39	.19
586	11.85	1.46	1.33
588	13.63	.69	.33
589	14.17	.41	.35
590	13.93	.49	.37
592	13.97	.67	.44
593	11.97	.38	.02
595	12.23	.47	.26
597	11.88	1.59	1.50
598	14.47	.57	.46
599	13.53	.50	.31
600	13.23	.43	.29
601	12.03	.39	.14
602	11.75	1.51	1.42
603	12.51	.34	.21
604	13.22	.43	.24
607	14.76	.61	.46
608	12.79	.89	.43
609	14.50	.55	.45
610	12.73	.36	.13
612	14.74	.63	.33
615	9.32	.52	.19
616	11.60	.46	.29
617	14.42	.97	.43
618	14.59	.51	.44
620	9.18	1.22	1.11
624	11.95	1.00	.51
625	13.00	.38	.22
627	12.48	.32	.13
630	11.92	.44	.31
631	14.53	.84	.33
632	13.91	.51	.43
635	14.28	.47	.35
639	14.36	.49	.41
658	11.90	1.45	1.41
667	12.65	.16	.37
668	14.42	.51	.38
669	14.64	.48	.50
671	14.15	.79	.41
672	14.54	.49	.36
675	12.14	.44	.21
682	11.51	1.62	1.67
684	12.44	.49	.25

Wallenquist Nos.

68	15.02	.56	.33
81	15.10	.54	.29
89	14.17	1.53	-
90	13.56	1.78	-
99	14.92	.67	.18
100	15.17	.58	.14
102	15.14	.59	.45
103	15.13	.65	.33
105	14.85	.59	.54
109	13.59	1.96	-

Star Wallenquist Nos.	V	B-V	U-B
111	15.11	+.54	+.35
119	15.06	.70	.14
126	15.06	.51	.41
129	14.70	1.51	-
137	14.78	.79	.29
141	14.58	.79	.44
144	15.16	.78	.06
145	15.07	1.03	.11
150	14.08	1.36	.86
155	15.20	.58	.55
157	14.88	.55	.29
160	14.77	.51	.53
166	13.59	1.63	1.19
171	14.78	.63	.37
174	15.05	.67	.30
177	14.84	1.01	.29
184	14.93	.54	.44
191	15.03	1.01	.22
194	14.77	.52	.50
197	14.21	.50	.38
198	14.97	.59	.28
199	15.07	.68	.38
200	15.25	.66	.31
205	15.17	.68	.36
206	15.13	.63	.39
209	15.03	.86	.10
210	14.95	.76	.18
212	15.11	.67	.21
213	14.68	.67	.18
214	15.23	.60	.21
216	14.92	.58	.35
217	14.40	1.56	-
225	14.78	.55	.33
226	15.13	.69	.29
228	14.69	1.51	-
231	14.94	.59	.44
235	14.85	.91	.15
237	14.97	.66	.31
240	15.26	.59	.47
243	14.96	.66	.20
245	13.84	1.38	.74
249	14.94	.59	.36
250	15.03	.62	.27
251	15.10	.68	.56
252	15.25	.81	.42
265	14.93	1.61	-
268	13.88	1.86	-
270	15.18	.59	.33
272	15.24	.68	.41
283	14.37	1.73	-
349	11.62	1.47	1.32

SUPPLEMENTARY STARS

A	15.82	+.84	-
C	15.15	.59	+.41
H	15.50	.68	.18
K	14.57	.54	.52
L	14.91	.56	.28
M	15.61	.72	-
N	13.86	1.93	-
O	15.37	.66	.21
P	15.41	.51	+.27
Q	15.45	.77	-.04
R	14.95	.65	+.32
S	14.83	.54	.61
T	15.67	.63	.28
U	15.03	+.61	+.44

Since very narrow main sequences have been found in other galactic clusters, such as Praesepe (Johnson 1952), the Pleiades (Johnson and Morgan 1951, 1953), NGC 2362 (Johnson 1950; Johnson and Morgan 1953), and the Coma Berenices star cluster (Weaver 1952; Johnson and Knuckles 1955), it seems safe to assume that these mean values actually represent the true positions of the individual main-sequence cluster stars in the color-magnitude diagram. Haffner and Heckmann (1937, 1940) have shown, however, that some 20 per cent of the Praesepe stars probably are doubles. If we assume that this proportion holds in M11, we can estimate that the values in Table 3 may be about 0.1 mag. too bright to represent main-sequence single stars.

We shall not plot here the mean color-magnitude diagram, V versus $B - V$, from Table 3, but we shall, instead, plot the other color-magnitude diagram that this table permits—V versus $U - B$. This diagram is shown in Figure 3, and its interpretation leads us into the next section.

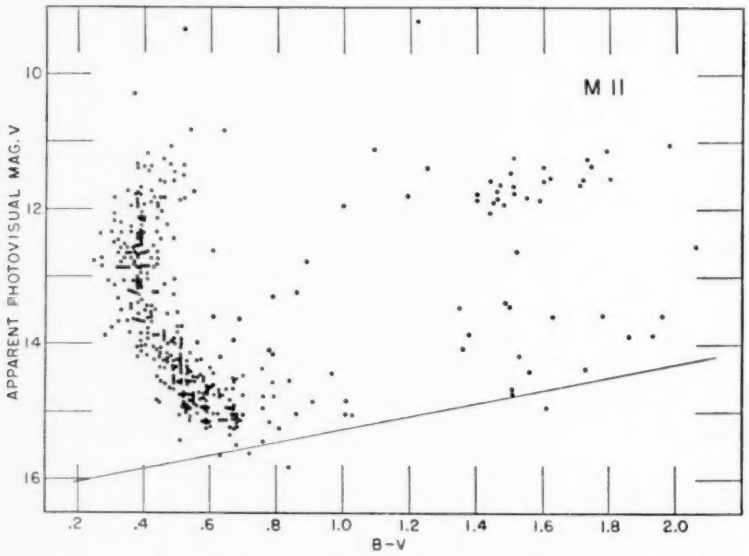

FIG. 2.—The color-magnitude diagram for M11 from Table 2

TABLE 3

THE MEAN MAIN SEQUENCE FOR M11

V	$B-V$	$U-B$	No. of Stars	V	$B-V$	$U-B$	No. of Stars
11.32	+0.44	+0.12	11	14.12	+0.46	+0.36	26
11.80	+ .42	+ .15	24	14.36	+ .51	+ .38	22
12.29	+ .38	+ .15	29 ½-mag. intervals	14.61	+ .56	+ .37	33 ½-mag. intervals
12.73	+ .37	+ .15	38	14.86	+ .57	+ .36	35
13.24	+ .39	+ .22	30	15.13	+0.64	+0.35	25
13.76	+0.42	+0.35	35				

IV. THE REDDENING OF THE CLUSTER

Figure 3 should be compared with Figure 6 of Johnson and Morgan (1953). The similarity of the two figures in the region of the hydrogen dip (A stars) is evident. Johnson and Morgan's Table 14 shows that $U - B$ goes through a maximum, at about A5 V, of $+0.09$ mag. On the assumption that this value of $+0.09$ mag. also corresponds to the *unreddened* color of the M11 stars at the $U - B$ maximum in Figure 3, we compute the reddening in $U - B$ to be $E_{(U-B)} = +0.29$ mag.

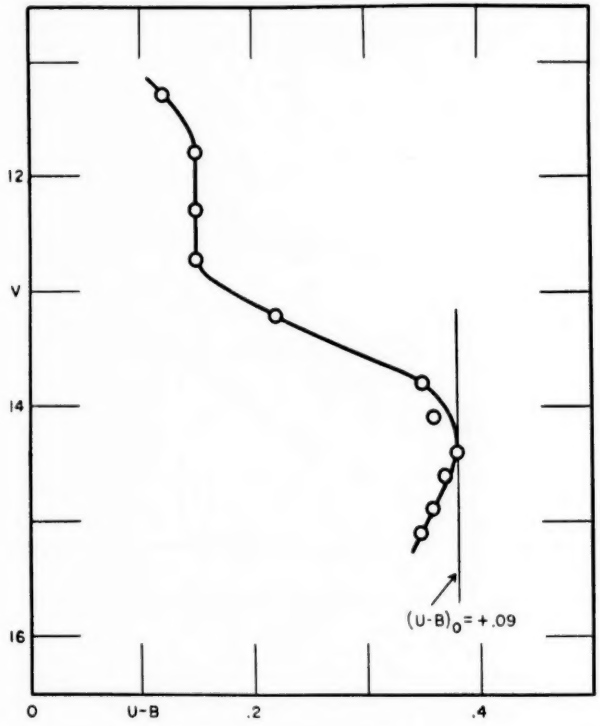

FIG. 3.—The color-magnitude diagram in the arguments V and $U - B$. The data are from Table 3

The two-color index diagram, $U - B$ versus $B - V$, plotted from Table 3, is shown in Figure 4. The smooth line, drawn by hand, proceeds through the points in the same order as does the one in Figure 3. As in Figure 3, the line $(U - B)_0 = +0.09$ is tangent at the maximum in $U - B$.

We now make use of the fact that, by definition (Johnson and Morgan 1953, p. 322), $(U - B)_0 = 0$ at A0 V. This means that the $(U - B)_0 = 0$ line intersects the cluster-curve at the same point as does the $(B - V)_0 = 0$ line and that, further, $E_{(B-V)}$ equals the observed $B - V$ at this point. We find that $E_{(B-V)} = +0.405$ mag. The ratio of these two color excesses, $E_{(U-B)}/E_{(B-V)} = 0.72$, confirms exactly the value found by Johnson and Morgan (1953). A second way of estimating the reddening of M11 is by the "Q" method developed by Johnson and Morgan (1953) for individual main-sequence

stars. This method cannot be applied to the brighter M11 stars because, as Figures 3 and 4 demonstrate, these stars exhibit, in their colors, effects of their higher luminosity. However, if the Q method is applied to the two bluest points on the *normal* main-sequence line of Figure 4 (not those on the hooked portion), we find $E_{(B-V)} = +0.42$ mag.

Armin Deutsch has estimated spectral types for several M11 stars, and he has permitted us to use them in our discussion. Table 4 lists these types, the intrinsic colors

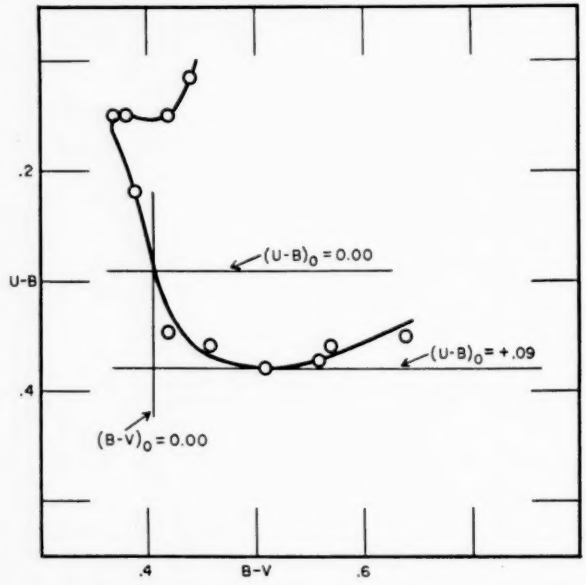

FIG. 4.—The two-color index diagram for the B- and A-type stars in M11. The data are from Table 3

TABLE 4

THE CLUSTER REDDENING FROM SPECTRAL TYPES

Star*	Sp.	$(B-V)_0$	$B-V$	$E_{(B-V)}$
141	B9 V	−0.05	+0.38	+0.43
193	B9 V	− .05	+ .38	+ .43
308	B8 V	− .09	+ .54	+ .63
336	B3p	− .20	+ .37	Nonmember
358	A0 V	.00	+ .52	+ .52
434	A0 III:	.00	+ .45	+ .45
436	B9 V	− .05	+ .41	+ .46
455	A5 V:	+ .15	+ .40	+ .25
461	A0 V	.00	+ .42	+ .42
506	B9 V	−0.05	+0.48	+0.53
Mean				+0.46±0.02(p.e.)

* Küstner numbers.

taken from Johnson and Morgan, the observed $B - V$ from Table 2, and the color excesses. We now have three values of $E_{(B-V)}$: +0.405, +0.42, +0.46. Since the scatter of the individual excesses of Table 4 is large, we give the spectroscopic determination lower weight and adopt $E_{(B-V)} = +0.42$ and $E_{(U-B)} = +0.30$.

V. THE DISTANCE OF THE CLUSTER

The distance modulus for M11 is obtained by fitting the cluster main sequence to the "age zero" main sequence computed by Johnson and Hiltner (1956) after shifting Figure 2 by $E_{(B-V)} = 0.42$ along the color axis. The procedure is illustrated by Figure 5. The apparent modulus is 12.3 ± 0.2 (p.e.) mag. The true modulus, after correction for interstellar absorption [$A_v = 3.0E_{(B-V)}$] is 11.1 mag., corresponding to a distance of 1660 parsecs.

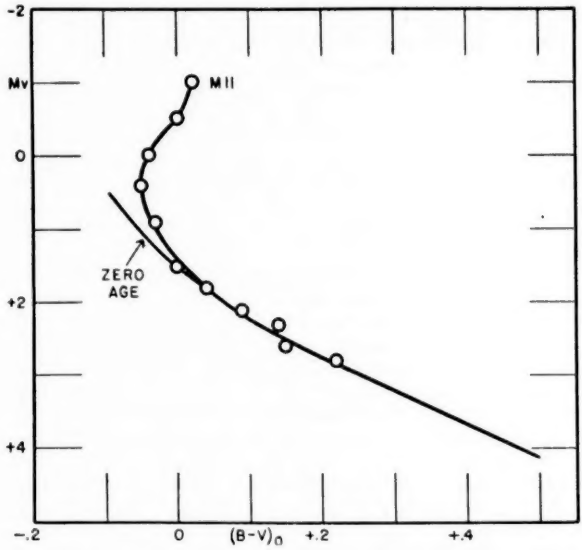

FIG. 5.—The fit of the M11 main sequence to the sequence of zero age computed by Johnson and Hiltner (1956).

The use of this age-zero main sequence, which leads to a significantly smaller distance for M11 than would a fit directly to nearby stars of large parallax but unknown age, seems justified observationally by the work of Johnson and Hiltner (1956), Johnson and Knuckles (1955), and Blaauw, Hiltner, and Johnson (1956). The point here is this: the nearby stars of large parallax probably are a mixture of stars of various and unknown ages and evolutionary motion away from the main sequence toward the higher luminosities. The positions of the brighter M11 stars illustrate the effect of this evolutionary motion for a number of stars, all of about the same age but with slightly different masses. On the other hand, it seems likely that the faintest M11 main-sequence stars are very little evolved and should not be compared directly with the evolved nearby stars without making some correction for the probable evolution. The age-zero main sequence is supposed to make this correction. In view of the errors possible in the foregoing procedure and in the determination of the cluster reddening and absorption, we estimate that

the probable error of our derived modulus may be about ± 0.2 mag. We should point out that, in obtaining the distance modulus from a fit on the main sequence, it is assumed that if there are chemical-composition differences between M11 and the stars used in determining the age-zero main sequence, they have little or no effect upon the initial position of the main sequence. It should further be mentioned that our apparent modulus of 12.3 is only as good as the zero point of absolute magnitude for the age-zero main sequence. If this be changed, our modulus will change.

VI. THE EVOLUTIONARY SIGNIFICANCE OF M11

The upward bend of the observed main sequence in M11 shown in Figure 5 is consistent with current ideas of evolution. The departure shown in this figure is in very good agreement with the theoretical diagrams of R. J. Tayler (1954, Fig. 3) and of Sandage (1954, Fig. 4). The main-sequence termination point in M11 occurs near $M_v = -1.0$ and falls between that of the Pleiades and that of Praesepe, suggesting that the age of M11 is intermediate between these two clusters.

The yellow giants in M11 are almost unique among galactic clusters, since they average 1 mag. brighter than the usual giants of luminosity class III at $M_v = 0.0$. However, this situation is entirely expected in populous clusters younger than the Hyades and Praesepe (i.e., with main-sequence terminations brighter than $M_v = 0$), since most current evolutionary theories predict that the entire giant and supergiant region of the M_{bol}, log T_e plane, with the exception of the wedge-shaped Hertzsprung gap, will contain stars if clusters of *all* ages from 10^6 to 5×10^9 years can be found and plotted in a composite diagram. The absolute magnitude of $M_v = -1$ for the M11 giants is therefore not surprising.

One might ask why younger clusters, such as the Pleiades and NGC 2362, do not contain yellow or red intermediate giants at $M_v \approx -3$ to $M_v \approx -4$. The number of giants in a cluster at any given time is determined by the number of main-sequence stars which are immediate candidates for evolution. A convenient index for comparison of clusters is the ratio of the number of giants to the number of main-sequence stars within, say, 2 mag. of the termination point. This ratio in M11 is about 15/100 (obtained by counting in Fig. 1 and dividing the number of giants by the statistical bias of 2). For the Pleiades, Hertzsprung (1928) lists only 4 stars on the main sequence within 2 mag. of the termination point. If the M11 giant to main-sequence ratio applies, we would predict that the Pleiades should contain 0.6 giant. This agrees with the fact that no giants are known in the Pleiades. If the same ratio of 15/100 applies to the Hyades, we expect about 6 Hyades giants. Four are known. The extreme sparseness of 2362 likewise explains the absence of giants in this cluster. Hence the absolute mganitude and the number of giants in M11 do not appear to be anomalous by comparison with other known aggregates.

M11 is not the only cluster known to contain intermediate giants. NGC 2287 studied by A. N. Cox (1954) has 5 intermediate giants at $M_v = -2$. The positions of the main and giant sequences in M11 and NGC 2287 fit well into the scheme of systematics shown in the composite diagram in the previous paper on M67 (Johnson and Sandage 1955, Fig. 6).

VII. SUMMARY

Three-color photometric observations on many stars in M11 permit the determination of a color-magnitude diagram. These observations, together with Deutsch's spectral types for a few stars, give the reddening and distance to the cluster. M11 is a populous galactic cluster with a well-defined main sequence, which terminates at the bright end between that of the Pleiades and that of Praesepe. Its age is intermediate between these two clusters. M11 has many yellow giants, including several of later type than K0. These yellow giants are brighter than those of the Hyades and Praesepe. This is expected

from current evolutionary hypotheses, since the main sequence in M11 terminates at about $M_v = -1.0$. The large number of giants in M11 is not anomalous when the abnormally large population of the cluster itself is considered. M11 is therefore another observational example of the scheme of evolution which has been discussed by many authors over the last fifteen years (Schönberg and Chandrasekhar 1942; Harrison 1944; Ledoux 1949; Sandage and Schwarzschild 1952; Roy 1954; Sandage 1954; Tayler 1954; Johnson and Sandage 1955; etc.).

REFERENCES

Blaauw, A., Hiltner, W. A., and Johnson, H. L. 1956, in preparation.
Cox, A. N. 1954, *Ap. J.*, **119**, 188.
Haffner, H., and Heckmann, O. 1937, *Göttingen Veröff.*, No. 55.
———. 1940, *ibid.*, Nos. 66 and 67.
Harrison, M. H. 1947, *Ap. J.*, **105**, 322.
Hertzsprung, E. 1928, *M.N.*, **89**, 660.
Johnson, H. L. 1950, *Ap. J.*, **112**, 240.
———. 1952, *ibid.*, **116**, 640.
Johnson, H. L., and Hiltner, W. A. 1956, *Ap. J.*, **123**, 267.
Johnson, H. L., and Knuckles, C. F. 1955, *Ap. J.*, **122**, 209.
Johnson, H. L., and Morgan, W. W. 1951, *Ap. J.*, **114**, 522.
———. 1953, *ibid.*, **117**, 313.
Johnson, H. L., and Sandage, A. R. 1955, *Ap. J.*, **121**, 616.
Küstner, F. 1923, *Veröff. Sternwarte Bonn*, No. 18.
Ledoux, P. 1949, *Mém. Inst. d'Ap. Liége*, No. 309.
Roy, A. E. 1952, *M.N.*, **112**, 484.
Sandage, A. R. 1954, *Mém. Soc. R. Sci. Liége*, **14**, 254 (*Communications du Colloque d'Astrophysique de Liége*, **1953**).
Sandage, A. R., and Schwarzschild, M. 1952, *Ap. J.*, **116**, 463.
Schönberg, M., and Chandrasekhar, S. 1942, *Ap. J.*, **96**, 161.
Tayler, R. J. 1954, *Ap. J.*, **120**, 332.
Wallenquist, A. 1936, *Meddel. Uppsala*, No. 65.
Weaver, H. F. 1952, *Ap. J.*, **116**, 612.

SYMMETRIC GALACTIC NEBULAE. II*

HUGH M. JOHNSON†
Yerkes and McDonald Observatories
Received February 20, 1956

ABSTRACT

An earlier catalogue of symmetric galactic nebulae is extended, and a map of all is given. Eleven new nebulae are listed.

This paper extends a previous catalogue of symmetric galactic nebulae (Johnson 1955) with new plates obtained in the same way by H. Abt at the McDonald Observatory in 1954–1955. Dr. Abt kindly placed the new plates at the writer's disposal so that the extension might be homogeneous with the earlier material.

Table 1 of this paper contains errata and addenda to the catalogue (Table 1) of the

TABLE 1

ERRATA AND ADDENDA TO THE FIRST CATALOGUE

No.	Remarks
54.....	Exclude NGC 6760 from the catalogue
78.....	E 106 = IC 1470; central star Sp. O7; a planetary nebula, according to Woronzow-Weljaminow (1953), but it appears to have dust lanes (cf. Pease 1920)
86.....	BD+63°2093; Sp. G8 V from a McDonald plate by H. Abt; BD+63°2093p = N 5647, Sp. B3 (Brodskaya (1955), must refer to a star 2′ preceding BD+63°2093, both near the center of S 105
94....	BD+53°708, Sp. B6 V from a McDonald plate by H. Abt
119....	S 37 = Min II 4 (cf. Hase and Shajn (1954)
132....	YM 28 = II 9 in the planetary-nebula catalogue of Abell (1955)

first paper, with an identical numbering in each first column. Table 2 continues the catalogue of the first paper in the same style, so that no further explanation of it is needed. Reference was made to the catalogues of Minkowski (1948), Hoffleit (1953), Shajn and Hase (1953), Hase (1954), Hase and Shajn (1954), Bok, Bester, and Wade (1955), and Gum (1956), in addition to those formerly listed. The number of the apparently new (YM) nebulae is continued from the earlier catalogue.

Figure 1 maps most of the area covered by Hα plates and the distribution of the symmetric nebulae in Ohlsson's (1932) galactic co-ordinates. The 18°-wide belt runs along 85 per cent of the length of the Milky Way and widens to include the south half of Gould's Belt. The size of the filled circles is approximately to scale for the largest nebulae but is about ten times too large for the smallest. The figure shows the concentration of the nebulae to a plane with the pole $l = 348°$, $b = +89°.0$, or $\alpha = 191°.1$, $\delta = +27°.8$; their gross clustering tendency; and their abrupt excursion into the Orion-Lepus region of Gould's Belt. The overlapping of some filled circles on the scale of the diagram leaves fine-scale clustering and multiple nebulae unpictured. But, although not every nebula in the catalogues is resolved in Figure 1, only YM 29 falls outside the given area. Longi-

* *Contributions from the McDonald Observatory, University of Texas*, No. 265.

† Now at the State University of Iowa.

tudinal gaps of symmetric nebulae near $l = 15°$, 70°, 110°, 215°, and 245° confirm similar gaps in survey catalogues of general emission nebulae such as those of Sharpless (1953) and Gum (1956), wherever these catalogues cover the relevant longitudes. This suggests that the symmetric nebulae which the writer has catalogued are related to amorphous galactic nebulae rather than to the planetary nebulae, which are more smoothly distributed and more dispersed in latitude within 10° of the equator (Minkowski 1951). The problem of classification is not settled; see, for example, the remarks of Bok and Minkowski (1955).

The relation of symmetric nebulae to young or peculiar stars is still not clear. Some Be stars are centered in symmetric nebulae, but the large-scale clustering of symmetric nebulae is not quite compatible with that of the Be stars (Minkowski 1951). While there are gaps of Be stars near $l = 15°$ and $l = 245°$ like those of symmetric nebulae, there is

TABLE 2

THE CATALOGUE OF SYMMETRIC NEBULAE

No.	Nebula	l	b	a	b	i	Br.	Star	Sp.	Assoc.	r (kpc)	Notes
1	NGC 1169	113°3	− 9°8	2'5			1					1
2	YM 37	121.7	−15.6	3.5	2'1	56°	1					2
3	IC 359?	136.2	−15.7	1.9			1					1
4	Hub I 4	136.9	−14.6	11	6	77	1					2, 4
5	YM 38	141.8	−14.6	0.9			1					1
6	YM 39	141.9	−14.6	1.8			1					1
7	YM 40	174.9	−11.7	41			1	39732	Ma	I Ori	0.5	
8	YM 41	180.5	−10.5	9			1	42050	B5			
9	Ced 65	181.2	−11.0	9			1	42004	B9			
10	NGC 2149	183.9	−13.6	4.9			1					1
11	NGC 1954/ 1957?	184.7	−22.3	4.4	1.8	0	1					2
12	YM 42	184.8	− 9.2	3.5	1.2	73	1					2
13	YM 43	187.3	−18.5	2.7			1					2
14	NGC 2076	188.8	−20.3	3.4			1					1
15	IC 438	190.5	−19.3	2.8			1					2
16	YM 44	195.4	−14.2	3.5	2.1	5	1					1
17	NGC 2207	196.2	−15.7	4.9	2.7	61	1					1
18	NGC 2196	196.2	−16.8	3.5	2.7	74	1					1
19	IC 2154	196.9	−19.9	2.5			1					1
20	NGC 2217	202.3	−16.9	4.4			1	−27°2916				
21	NGC 2295	204.2	−11.4	3.2			1					1
22	Gum 14	227.9	+ 1.4	132			1	73882	O8(V)		0.8	3, 5
23	Ced 106n	229.2	+ 1.7	25			2	74804	B5			3
24	Gum 17	230.5	+ 1.9	124			1	75759	B2			3
25	NGC 2736	234.6	+ 0.7	14	0.9	78	2	−45°4764		I Vel?		
26	YM 45	235.6	− 0.3	6			2	77271	K0	I Vel		
27	Gum 24	236.8	− 0.6	2.7			2			I Vel.		2
28	Gum 25	236.9	− 0.9	9	7	11	3	−48°4352		I Vel		
29	YM 46	238.0	+ 1.4	6			2			I Vel?		1
30	NGC 3199	251.3	− 0.8	18	11	28	2	89358	Oa			
31	YM 47	251.9	− 0.4	9	7	74	3	−57°3073		II Car?	1.8?	
32	NGC 3324	253.9	− 0.1	12			2	92206	B	II Car or I Car?	1.8	3

NOTES TO TABLE 2

1. Star not identified.
2. No star visible.
3. Cluster associated.
4. Continuous spectrum according to Hubble (1922).
5. MK spectral type.

a concentation of Be stars near $l = 215°$, where there is a gap of symmetric nebulae. The two mutual gaps probably arise from obscuring clouds, since open clusters also are scarce there. Late-type stars are found in "comet-like" or "fan-shaped" emission nebulae. When they are conical and viewed within the vertex angle, these objects as well as "elephant's-trunk" nebulae might be classed as symmetric nebulae in the present sense.

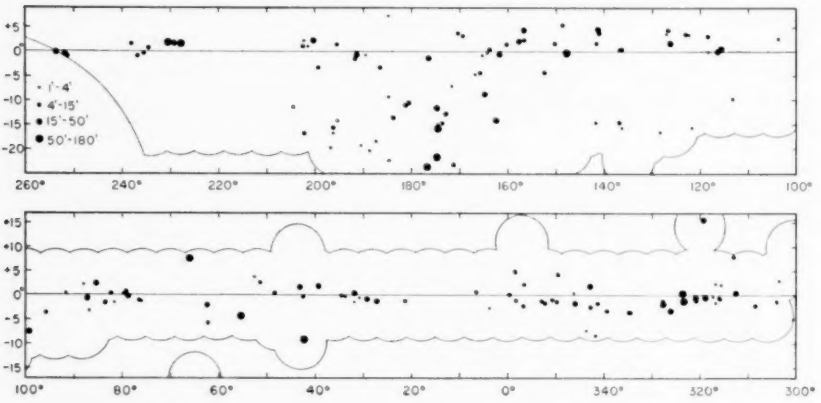

FIG. 1.—The distribution of symmetric galactic nebulae in galactic co-ordinates

This paper is part of work done on a National Science Foundation grant to Professors W. W. Morgan and B. Strömgren in 1953. The writer wishes to thank Professors Strömgren and Morgan for the opportunity to prepare this report with their valuable advice, Dr. H. Abt for the use of his plates, and Dr. C. S. Gum for his catalogue in advance of publication.

REFERENCES

Abell, G. O. 1955, *Pub. A.S.P.*, **67**, 258.
Bok, B. J., Bester, M. J., and Wade, C. M. 1955, *Proc. Amer. Acad. Arts and Sci.*, **86**, 9.
Bok, B. J., and Minkowski, R. 1955, *I.A.U. Symposium No. 2* (Amsterdam: North-Holland Publishing Co.), p. 36.
Brodskaya, E. S. 1955, *Pub. Crimean Ap. Obs.*, **14**, 136.
Gum, C. S. 1956, *Mem. R.A.S.*, **67**, Part IV.
Hase, V. T. 1954, *Pub. Crimean Ap. Obs.*, **11**, 42.
Hase, V. T., and Shajn, G. A. 1954, *Pub. Crimean Ap. Obs.*, **11**, 39.
Hoffleit, D. 1953, *Harvard Ann.*, Vol. **119**, No. 2.
Hubble, E. 1922, *Ap. J.*, **56**, 162.
Johnson, H. M. 1955, *Ap. J.*, **121**, 604.
Minkowski, R. 1948, *Pub. A.S.P.*, **60**, 386.
———. 1951, *Pub. Obs. U. Michigan*, **10**, 25.
Ohlsson, J. 1932, *Lund Ann.*, No. 3.
Pease, F. G. 1920, *Ap. J.*, **51**, 276.
Shajn, G. A., and Hase, V. T. 1953, *Pub. Crimean Ap. Obs.*, **10**, 210.
Sharpless, S. 1953, *Ap. J.*, **118**, 362.
Woronzow-Weljaminow, B. A. 1953, *Gasnebel und neue Sterne* (Berlin: Verlag Kultur und Fortschritt, p. 701.

SPECTROPHOTOMETRY OF PLANETARY NEBULAE

R. MINKOWSKI AND L. H. ALLER
Mount Wilson and Palomar Observatories
Carnegie Institution of Washington, California Institute of Technology
and
University of Michigan Observatory
Received February 13, 1956

ABSTRACT

Measurements of the line and continuous spectra of several bright planetary nebulae by methods of photographic spectrophotometry have been carried out with the Cassegrain spectrographs at the 60- and 100-inch reflectors of the Mount Wilson Observatory. The results of extensive observations are reported for NGC 40, NGC 1535, NGC 2022, NGC 2392, and NGC 7662. Additional material has been obtained for IC 351, IC 1747, J 320, NGC 2165, and NGC 2440. In each object the slit was placed on a selected position in the nebula and the exposures carefully guided. The line intensities, expressed on the scale $I(\mathrm{H}\beta) = 100$, are given for lines from the Balmer limit to λ 9000.

I. INTRODUCTION

For a number of astrophysical problems it is desirable to have reliable measurements of emission-line intensities in typical gaseous nebulae. On the one hand, for theoretical studies, it is necessary to know the emission per typical unit volume in the radiation of hydrogen and other permanent gases. On the other hand, nebulae in which line intensities have been accurately measured may serve as photometric standards to which other, and often much fainter, objects can be compared.

Recent investigations (Liller and Aller 1954; MacRae and Stock 1954; Code 1956) have demonstrated the value of photoelectric techniques for the measurement of the intensities of the stronger lines. For the present, at least, the weaker lines must be measured by photographic photometry. It also is possible to select smaller regions in the nebula for detailed analysis. Previous photographic spectrophotometric studies (Berman 1930; Plaskett 1931; Page 1936, 1942; Aller 1941, 1951) have been confined to the stronger lines. Wyse (1942) attempted to measure the weaker lines with the aid of eye-estimates on scale plates. The most interesting planetary nebula from the standpoint of the richness of spectrum and range in excitation is NGC 7027 (Bowen, Minkowski, and Aller 1955). Similar spectrophotometric techniques have been applied to other nebulae.

We selected a number of nebulae ranging from low to high excitation which were well placed for the long exposures required to record moderately faint lines and continua. For obvious reasons, most of them were rather bright. We included the ring objects NGC 1535, NGC 2022, NGC 2392, and NGC 7662 and the somewhat irregular structure, NGC 40. A few additional observations were secured of IC 351, IC 1747, J 320, NGC 2165, and NGC 2440. The faintest object on our list, NGC 2022, was chosen because of its high excitation.

II. THE OBSERVATIONAL TECHNIQUE

The observations discussed in this paper were all secured with Cassegrain spectrographs at the 60- and 100-inch reflectors at the Mount Wilson Observatory. At the 60-inch reflector we used a two-prism spectrograph with the 3-inch Schmidt camera, which gives a dispersion of about 170 A/mm at Hγ. At the 100-inch telescope we used the two-prism spectrograph with the Schmidt camera of 6-inch focal length, which gives a dispersion of 110 A/mm at Hγ. This optical arrangement permitted us to obtain plates in

good definition from the near infrared to the Balmer limit. Since both spectrographs were equipped with auxiliary guiding eyepieces, it was possible to keep the slit placed accurately upon a selected portion of the nebula for the entire exposure. In this way, differences of excitation in different parts of the nebula may be compared. No attempt has been made to obtain integrated intensities of the nebular images. Since the lines have an intensity range of over a thousand fold, it is necessary to secure observations ranging in exposure time from a few seconds to many hours.

Table 1 gives the nebulae and comparison stars observed and the spectrographs employed. The JS plate series refers to the 60-inch Cassegrain spectrograph; the E series to the 100-inch Cassegrain spectrograph. For the photographic and visual regions, the 103*a*-F emulsion was used; for the infrared, hypersensitized I-N plates were employed. The sixth and eighth columns give the range of exposure times on nebula and comparison stars for each plate secured.

III. PHOTOMETRIC CALIBRATION

To measure the intensities of the nebular lines and continua, it is necessary to establish the relation between photographic blackening and intensity as well as the effects of plate sensitivity, atmospheric transparency, and telescope reflectivity plus spectrograph transmission. The first step is accomplished by a suitable photometric standardization; the second is carried out most expeditiously by photographic suitable comparison stars.

Because of the small size of the plates used in the spectrographs, it was necessary to impress the photometric standards on a larger piece cut from the same plate and then to develop nebular and calibration plate together. We photographed the calibration standards with the 32-inch camera and the coudé spectrograph, adjusting the exposure times to be comparable with those at the telescope. Thus calibration exposures ranging from a minute to many hours had to be secured. The change in slope of the calibration-curve with exposure time is very small. In a single calibration exposure it is difficult to obtain the proper densities for *all* relevant wave lengths. Fortunately, the development procedures were kept the same for all plates.

To compare the standard stars, of known energy distribution, with the nebulae, which are several magnitudes fainter, we adopted the following device. A small piece of ground quartz was placed over the slit of the spectrograph. We then ran the image of the comparison star out of focus by a prearranged amount and placed a portion of the luminous ring of the out-of-focus image on the slit. Thus we provided a diffuse illumination of the slit with a source of known energy distribution.

The transmission of the quartz diffuser as a function of wave length was calibrated photoelectrically in the laboratory by Edison Pettit, under conditions closely simulating those obtained at the telescope. In addition, the calibration was checked photographically at the telescope. For this purpose, stellar spectra obtained with the diffuser were compared with spectra of the same stars obtained without the diffuser and widened by a rapid trailing back and forth of the focal stellar image on the slit with a frequency adequate to avoid the intermittency effect.

The standard energy-distribution stars which served for comparison stars include α Lyrae, which was observed by Williams (1938), Williams and Hall (1941), Kienle, Strassl, and Wempe (1938), and Barbier and Chalonge (1940), as well as ϵ Persei, β Cephei, and η Ursae Majoris, which have been observed by Kienle, Strassl, and Wempe, by Barbier and Chalonge, or by both groups.

The energy distribution in Vega was measured by photographic photometry by R. Williams for $\lambda\lambda$ 3700–9000 and by photoelectric photometry for the near infrared by Williams and Hall. The most frequently used comparison star, ϵ Persei, has been measured by Kienle's group and by Barbier and Chalonge, whose results are in good agreement with one another. Redward of λ 3700 the energy distribution corresponds to a color temperature of 26000° K; shortward of λ 3700 the color temperature is 23000° K. The

TABLE 1

SPECTROPHOTOMETRIC OBSERVATIONS OF PLANETARY NEBULAE

	α	δ	Plate	Emul.	Exposures	Comparison Star	Exposures
NGC 40	$0^h10^m.2$	$+72°11'$	JS 753	I-N	420^m	β Cephei	60^m
			JS 754	103*a*-F	420^m	β Cephei	60^m
			JS 755	103*a*-F	420^m	β Cephei	60^m
			JS 756	103*a*-F	150^m		
			JS 757	103*a*-F	64^m, 64^m*	β Cephei	15^m
			JS 758	103*a*-F	100^m		
			JS 759	103*a*-F	480^m	β Cephei	60^m, 15^m
			JS 761	103*a*-F	60^m, 60^m*	β Cephei	60^m
			JS 762	103*a*-F	70^m	ϵ Persei	60^m
			JS 763	103*a*-F	180^m	β Cephei	60^m, 15^m
			JS 766	103*a*-F	90^m	β Cephei	60^m
						ϵ Persei	60^m
IC 351	3 44.3	+34 55	JS 775	103*a*-F	91^m		
NGC 1535	4 11.9	−12 52	JS 769	103*a*-F	225^m	ϵ Persei	60^m
			JS 771	103*a*-F	322^m	ϵ Persei	60^m
			JS 774	103*a*-F	60^m, 20^m, 7^m	ϵ Persei	60^m
J 320	5 2.8	+10 39	JS 775	103*a*-F	60^m		
NGC 2022	5 39.3	+ 9 02	E 2283	103*a*-F	435^m	η Ursa Major	60^m
			JS 769	103*a*-F	110^m	ϵ Persei	60^m
			JS 770	103*a*-F	510^m	ϵ Persei	60^m
			JS 772	103*a*-F	145^m		
IC 2165	6 19.4	−12 57	JS 774	103*a*-F	180^m		
NGC 2392	7 26.3	+21 02	E 2236	103*a*-F	120^m	ϵ Persei	60^m
					8^m, 2^m	ϵ Persei	10^m
			E 2237	103*a*-F	60^m, 30^m, 15^m, 4^m	ϵ Persei	60^m
			E 2238	103*a*-F	180^m, 90^m		
			E 2268	103*a*-F	480^m	ϵ Persei	60^m
			E 2270	103*a*-F	360^m	ϵ Persei	60^m
			E 2269	I-N	520^m	ϵ Persei	60^m
			E 2282	I-N	430^m	ϵ Persei	60^m
			E 2284	I-N	120^m	ϵ Persei	60^m
			JS 762	103*a*-F	120^m	ϵ Persei	60^m
			JS 764	103*a*-F	194^m	ϵ Persei	15^m, 60^m
			JS 765	103*a*-F	60^m, 60^m†	ϵ Persei	60^m
			JS 766	103*a*-F	336^m	ϵ Persei	60^m
			JS 768	103*a*-F	60^m	β Cephei	60^m
			JS 776	103*a*-F	410^m	ϵ Persei	60^m
NGC 2440	7 39.7	−18 05	JS 771	103*a*-F	116^m	ϵ Persei	60^m
NGC 7027	21 05.2	+42 01	E 1729	I-N	360^m	ϵ Persei	60^m
			E 1730	I-N	390^m	α Lyrae	60^m
			E 1731	I-N	330^m	α Lyrae	60^m
						α Lyrae	60^m
			E 1746	I-N	67^m, 25^m	ϵ Persei	60^m
			E 1747	I-N	10^m, 150^m	α Lyrae	60^m
NGC 7027	21 05.2	+42 01	E 1748	I-N	360^m	ϵ Persei	60^m
						α Lyrae	60^m
			E 1751	103*a*-F	120^m	ϵ Persei	60^m
					4^m	α Lyrae	60^m
			E 1752	103*a*-F	80^s, 25^s, 10^s, 40^m	α Lyrae	10^m, 1^m
			E 1753	103*a*-F	13^m		
			E 1754	103*a*-F	13^m	ϵ Persei	60^m, 10^m
					4^m	α Lyrae	10^m
			E 1755	103*a*-F	80^s, 25^s, 10^s, 5^s	α Lyrae	2^m, 20^s
			E 1757	103*a*-F		ϵ Persei	10^m, 3^m

* A 2-mag. diaphragm was placed in the optical system for this exposure.

† A 1-mag. diaphragm was placed in the optical system for this exposure.

TABLE 1—*Continued*

	α	δ	Plate	Emul.	Exposures	Comparison Star	Exposures
NGC 7662 . .	23^h23^m5	+42°16′	E 2203	I-N	480^m	ϵ Persei	60^m
			E 2205	I-N	480^m	ϵ Persei	60^m
			E 2220	I-N	120^m, 40^m	ϵ Persei	60^m
			E 2202	I-N	420^m	ϵ Persei	60^m
			E 2204	I-N	450^m	ϵ Persei	60^m
			E 2222	I-N	120^m	ϵ Persei	60^m
			E 2224	I-N	60^m, 2^m, 4^m, 8^m, 15^m	. . . . .	. . . . .
			E 2225	I-N	60^m, 30^m, 30^s, 1^m, 2^m	. . . . .	. . . . .
			E 2226	I-N	6^m	ϵ Persei	10^m
					15^m, 30^m	ϵ Persei	60^m
			JS 760	103*a*-F	425^m	. . . . .	. . . . .
			JS 765	103*a*-F	360^m	ϵ Persei	15^m
NGC 7662 . .	23 23.5	+42 16	JS 767	103*a*-F	15^m, 15^m†, 15^m*, 61^m	ϵ Persei	15^m
			JS 773	103*a*-F	15^m, 15^m†, 15^m*, 30^m	ϵ Persei	15^m

Balmer discontinuity, D, is 0.06. For β Cephei (which served as a comparison star for NGC 40), only the Barbier and Chalonge data are available. The Kienle data for η Ursae Majoris give a less steep slope than do the Barbier and Chalonge data. If the two curves are forced to fit at λ 5000, the deviation is about $\Delta \log I = 0.04$ at λ 3900. In the region $\lambda\lambda$ 5000–6000 both sets of curves are in good agreement. We have adopted the Barbier and Chalonge results.

In the comparison of the nebular-line intensities with the stellar energy distribution, the confluence of the stellar lines at the Balmer limit provides some difficulty. One may draw the energy-distribution envelope over the stellar lines and, using the data of Barbier and Chalonge, make some allowance for this effect. Nevertheless, the intensities of the higher members of the Balmer series may be given only imperfectly.

The observational procedure consisted in observing the nebula and comparison star at as nearly as possible the same mean zenith distance. Exposures on the nebula ranged from a few minutes to about 8 hours, whereas those on the comparison star varied from a few minutes to about 1 hour. It was manifestly impossibly to give the star and the nebula the same exposure for the observations intended to reach the fainter lines and the nebular continuum.

The ultraviolet spectrum of NGC 7027 was observed at McDonald in 1946, but for the other objects it was possible to secure observations only from the limit of the Balmer series to the infrared. All our spectrograms have been traced parallel to dispersion with the Mount Wilson photographically recording microphotometer.

Great care had to be taken to avoid even a tiny error in alignment of these small-scale plates, which can result in considerable difficulties. If the alignment is not perfect, the intensity of Hβ, for example, is measured at a different point in the nebula than is that of Hα or the high numbers of the Balmer series. The only nebula in which difficulties were encountered was NGC 7662. Here the Balmer decrement measured at the center of the bright ring did not agree with those measured at two different points of the outer fainter ring. The discrepancies were systematic and corresponded to a slight systematic error in the alignment of the spectrograms in the microphotometer, amounting to about 40 μ between Hα and λ 3727. Once the alignment error has been estimated, for each wave length it is possible to find the point on the nebular image where the intensity was actually measured. If a plot of intensity versus distance along the slit is now made for each line and a smooth curve drawn connecting the points, one may determine the small correction needed to reduce all intensities to the same selected points in the nebula. The

maximum correction for any line at any point in NGC 7662 was about 20 per cent. For the brightest central strip the corrections are negligible. In NGC 40 and particularly in NGC 2392 condensations appear so conspicuous as easily to permit an accurate alignment of the spectra upon the microphotometer. The measurements of NGC 7027, NGC 1535, and NGC 2022 do not indicate any evidence of alignment troubles.

The reduction of the microphometric tracings gives the fundamental observational datum, the ratio $I_\lambda(\text{neb.})/J_\lambda(*)$, where

$$J_\lambda(*) = A I_\lambda(*) \frac{d\lambda}{d\chi} T_\lambda \exp\left[-k_\lambda(\sec z_s - \sec z_n)\right] . \quad (1)$$

Here I_λ(neb.) is the intensity of the nebular line, A is a constant independent of wave length for each plate, $I_\lambda(*)$ is the intensity in the continuum of the comparison star at the wave length λ, and $d\lambda/d\chi$ is the dispersion on the tracing; T_λ is the transmission of the quartz diffuser (determined by Pettit); k_λ is the atmospheric extinction coefficient; and z denotes the zenith distance of the star or nebula.

We must now discuss the correction for atmospheric extinction. We attempted to observe the comparison star at the same zenith distance as the nebula; and, for the Mount Wilson observations of NGC 7027, the atmospheric extinction corrections are so small that they have been neglected. The maximum error in comparing lines in the λ 6400 region with lines in the λ 3700 region is about 0.01 in the logarithm.

For the subsequent observations of NGC 40, NGC 2392, NGC 2022, and NGC 7662 the effects of differential atmospheric extinction are small. They are relatively large for the few miscellaneous observations we have secured of NGC 1535 and other objects.

During a long nebular exposure, say about 8 hours, z varies. We have calculated the effects of atmospheric extinction and have found that it is sufficiently accurate to use in equation (1) the mean value of z during an exposure for all the observations that have been secured.

The determination of the appropriate absorption coefficient, k_λ, is a somewhat more difficult matter. For the reduction of the observations of NGC 7027 obtained at the McDonald Observatory in 1946, Popper's (1937) values for Mount Hamilton, corrected for the altitude of Mount Locke in accordance with the procedures suggested by Fowle (1933), have been used. Unfortunately, no direct measures of the extinction were then available.

The atmospheric extinction at Mount Wilson has been studied by a number of observers since the solar investigations of C. G. Abbot (1908). On a number of nights on which we secured observations, photoelectric measures were carried out by Edison Pettit or by Harold Johnson. These measures indicate a sizable fluctuation in the atmospheric extinction from night to night, so we have deemed it best to use for the entire series of our observations a set of mean coefficients adopted from the six-color photometry of Stebbins and Whitford (1945). Since (except for NGC 1535 and a few other objects) the zenith distances of the star and nebula are about the same, the correction for atmospheric extinction is not serious. On the nights devoted to the long exposures the transparency of the sky seemed constant throughout.

Each exposure yields a series of relative intensities of emission lines, the shorter exposures giving the stronger lines; the longer exposures being necessary to get the weaker lines. The derived intensities are to be put on a common system by combining the results from the various plates. To combine results from exposures of two different lengths, lines common to the two plates have to be used. To be determined is the shift of zero point between the two intensity systems. It now appears that more plates of intermediate exposure would have been desirable.

The selection of the proper slit-width for these objects is a serious problem. The slit-width should be sufficiently wide that the top of the line on the trace represents the

actual intensity of the line integrated over its width. The photometric accuracy increases as the slit is widened beyond this minimum width; but at the same time the resolution decreases, and faint lines can no longer be separated from the continuous spectrum. The slit-width used at the 100-inch was $0''.68$, corresponding to 25 μ on the plate for NGC 7027 with its very rich spectrum. For the other objects the slit-width was $1''.3$, corresponding to 49 μ on the plate for the 100-inch, and $3''.7$, corresponding to 42 μ on the plate for the 60-inch. From the agreement obtained between various plates, the internal probable error is about 15 per cent for the weaker lines measured on several plates and about 5 per cent for lines of intermediate intensity measured on stronger plates. For individual lines the actual errors may be substantially greater, particularly for the weakest lines, where errors of the order of 30–50 per cent are possible. Smaller errors might have been secured for the stronger lines by widening the spectrograph slit, but the loss of resolution would have obliterated many of the weaker lines.

IV. RESULTS FOR INDIVIDUAL NEBULAE

The results for NGC 7027 have been described elsewhere (Bowen, Minkowski, and Aller 1955). These intensities refer to the brightest condensation in the north-preceding part of the nebula. Our plates also permitted the determination of the intensities in the fainter north-following part of the nebula. The intensities measured in this fainter part are less certain but show no definite signs of stratification effects in the nebula.

The Ring Nebula in Andromeda NGC 7662 has been more intensively studied than almost any other planetary. It is a bright object, favorably placed for long exposures during the best observing season. Olin Wilson has studied the internal motions with the multislit; isophotic contours have been traced from his slitless spectrograms and from direct photographs secured at Palomar by one of us (Aller 1956). The integrated magnitude has been measured photoelectrically by Liller (1955), while Code has measured the stronger lines with his photoelectric scanner.

The slit of the spectrograph was placed north of the central star, across the brightest portion of the bright ring. We traced the 100-inch spectrograms at five points—the center of the bright ring, the inner portions of the outer ring, and the outer portions of the outer ring. The much smaller scale of the 60-inch plates precluded such a detailed study, and we have measured only the brightest part of the bright ring.

Table 2 gives the intensities measured on the 100-inch spectrograms. The measurements in the outer ring showed some scatter, much of which must certainly be attributed to the extremely mottled structure of the outer parts of the nebula.

Table 3 gives the intensities derived from the 60-inch plates. With the spectrograph employed there, it was possible to introduce diaphragms into the optical path in such a way as to cut down the beam by 1 or 2 mag. Thus, keeping the exposure time at the telescope fixed at some convenient interval (15 minutes was actually used), it was possible to measure the intensities of the stronger lines with respect to those of moderate intensity, without resort to the method of combining intensities otherwise employed. Fewer lines were measured on the 60-inch spectrograms. Nevertheless, a comparison of the results for the 100-inch and 60-inch spectrograms shows a reasonably good over-all agreement.

The intensity measurements in the bright ring should be reasonably reliable—at least, probably as good as can be attained with a narrow slit and photographic photometry without a much more extended program. The scatter of the values in the outer ring renders these measures less reliable. The probable errors are larger, not only because the accidental errors are presumed to be greater, but also because the irregularities in the nebular structure are much more marked. It is impossible to set the analyzing beam in the microphotometer always upon the same point in the nebula—and, since the alignment is not perfect and the nebular knots are small, different parts of the knots will be

TABLE 2

LINE INTENSITIES IN NGC 7662 MEASURED AT THE 100-INCH REFLECTOR

Wave Length	Ident.	−10″8	−5″4	Center of Ring	+5″4	+10″8
8862.8	H			6.2		
8750.5	H			2.8		
8665.0	H			2.0		
8196.6+8236.4	He II			1.5		
8045.6	[Cl IV]		1.0	2.6	2.0	
7751.0	[Ar III]		2.7	3.7	1.4	
7592.8	He II			0.8		
7530.5	[Cl IV]			1.5		
7319.9+7330.2	[O II]		1.2	2.4	1.5	
7135.8	[Ar III]	4.6	5.9	13.8	5.0	1.3
7065.3	He I		3.2	4.9	1.7	
6716+6730	[S II]		2.1	1.9	1.5	
6678.2	He I	2.3	5.4	5.9	3.9	1.6
6562.9	Hα	30	155	390	161	85
6363.8	[O I]				0.7	
6300.3+6312.1	[O I]+[S III]		1.6	2.6	1.8	
6086.9	[Fe VII] [Ca V]			0.68	1.1	
5875.6	He I	3.3	10.2	16	7.0	5.8
5801.4	C IV			pr		
5537.8	[Cl III]			0.9	0.7	
5517.7	[Cl III]			0.6		
5426.6	[Fe VI]			0.33		
5411.5	He II		1.8	6.0	4.8	
5006.9	[O III]	98	710	1700		340
4959.0	[O III]	36	236	550	260	110
4922.0	He I			1.3		
4861.3	Hβ	10.8	36	100	48.7	26.5
4740.2	[Ar IV]	1.3	3.3	8.0	5.4	2.0
4724.2+4725.6	[Ne IV]			0.8		
4711.3	[Ar IV]		3.6	7.7	5.9	2.4
4685.7	He II		6.0	51	36	4.9
4658.4	C IV			0.3		
4647.5+4649.1	C III+O II		0.8	1.8		
4640.6	N III		2.1	5.3	2.6	
4634.2	N III			2.2		
4541.6	He II		0.7	2.4	1.8	
4471.5	He I	0.75	2.9	4.3	1.7	1.6
4388.0	He I			0.6		
4379.1	N III			0.4		
4363.2	[O III]	2.2	7.1	18.7	9.8	4.8
4340.4	Hγ	3.5	14.9	44	22.5	11.0
4267.1	C II		0.45	1.15	0.8	
4237				0.14		
4227.4				0.20		
4219				0.21		
4199.9	He II		0.3	1.4	1.1	
4187.0	C III		0.3	1.0	0.4	
4180.9	[Fe V]			0.16		
4143.8	He I			0.33		
4120.8	He I			0.31		
4101.7	Hδ	2.05	8.8	23.2	13.3	6.3
4068.6+4076.3	[S II]		0.75	1.8	1.2	
4026.1	He I		1.6	2.8	1.4	
3967.4+3970.1	[Ne III]+H I	3.0	11.6	33	18.1	9.2
3888.9	H I	2.1	6.8	17	8.4	5.1
3868.7	[Ne III]	6.1	30	89	42	21.9
3858.0	He II			0.62		

TABLE 2—*Continued*

Wave Length	Ident.	−10″8	−5″4	Center of Ring	+5″4	+10″8
3835.4	H I	0.8	3.0	7.7	5.0	2.1
3819.7	He I	...	0.83	1.6	1.0	...
3797.9	H I	0.66	2.2	5.7	3.8	1.4
3791.3	O III	...	...	0.8	...	...
3770.7	H I	0.55	1.8	4.6	2.9	1.3
3759.9	O III	...	1.3	5.8	4.5	1.4
3757.2	O III	...	...	2.2	1.7	...
3750.2	H I	0.7	1.4	3.8	2.6	1.2
3734.3	H I	0.5	1.2	3.4	2.3	1.0
3728.8	[O II]	2.1	2.9	3.1	2.0	1.0
3726.0	[O II]		4.5	5.6	2.9	1.6
3721.8	H I	...	1.5	3.6	1.8	...
3712.0	H I	...	1.1	2.2	1.7	...
3703.8	H I+He I	...	1.2	2.3	1.6	...
3697.2	H I	...	0.7	1.5	...	...
3691.5	H	...	0.6	1.3	...	...
3686.9	H	...	...	0.9	...	...
3683	H	...	...	0.73	...	...

traced at different wave lengths. These difficulties seemed to be particularly great for NGC 7662.

NGC 2392

As in our observations of NGC 7662, the slit of the spectrograph was placed on the brightest portion of the brighter ring south of the nucleus but also included portions of the fainter outer ring at either side. The orientation difficulties, which turned out to be so troublesome in NGC 7662, were minimized for this object because a bright knot in

TABLE 3

LINE INTENSITIES IN NGC 7662 MEASURED AT THE 60-INCH REFLECTOR

λ	*I*	λ	*I*
6716+30	2.28	4143.8	0.6
6678.2	4.05	4101.7	28
6563	404	4068+76	1.6
6300.3+6312.1	3.4	4026.1	2.7
5875.6	20	3967+3970	39
5411.5	8.7	3924	0.4
4959.0	370	3888.9	19.6
4861.3	100:	3868.7	87
4740.2	9.5	3835.4	9.7
4711.3	9.6	3819.7	1.1
4685.7	49	3797.9	6.8
4640.6	5.1	3770.7	5.0
4541.6	2.9	3759.9	4.9
4471.5	4.3	3756	1.9
4388.0	0.4	3750.2	3.6
4363.2	19.7	3734.3	3.0
4340.4	46.5	3726+29	10.7
4267.1	0.7	3721.8	3.1
4200	1.2		

the nebulosity fell on the slit on one side so that the plate could be aligned in the microphotometer with its aid.

We give the intensities measured on the E plates at several positions listed in Table 4 near the center of the bright ring and at points chosen on either side, all expressed on the scale Hβ = 100 in the center of the bright ring. Also the intensities derived from the 60-inch plate are listed for comparison in Table 5.

TABLE 4

LINE INTENSITIES IN NGC 2392 E SPECTROGRAPH
100-INCH REFLECTOR*

Wave Length	−15″	−10″	Center of Bright Ring	+10″	+15″
7751.0	.....	.....	4.3	.....	.....
7592.8	.....	.....	.....	.....	.....
7319.9+7330.2	.....	.....	13.5	.....	.....
7135.8	.....	.....	17.3	.....	.....
6716+30	.....	5.8	21.2	3.8	.....
6678.2	.....	.....	3.3	.....	.....
6650	.....	.....	.....	.....	.....
6562.9	75	72	380	54	56
6300.3+6312.1	.....	.....	8.7	.....	.....
5875.6	.....	.....	9.9	.....	.....
5411.5	.....	.....	5.4	.....	.....
5006.9	212	227	1100	185	194
4959.0	64	70	326	49	53
4861.3	21	23	100.0	19.6	18
4740.2	.....	4.1	9.2	4.4	.....
4724.2	.....	.....	2.0	.....	.....
4711.3	.....	5.0	10.0	4.2	.....
4685.7	13.2	15.5	57	15.6	13.4
4658.4	.....	.....	2.4	.....	.....
4640.6	.....	.....	1.1	.....	.....
4634.2	.....	.....	pr	.....	.....
4541.6	.....	.....	2.7	.....	.....
4471.5	.....	.....	2.7	.....	.....
4363.2	6.0	8.2	26.4	7.0	6.0
4340.4	10.9	11.7	44.1	9.7	9.1
4227.4	.....	.....	3.6	.....	.....
4200.0	.....	.....	1.5	.....	.....
4143.8	.....	.....	1.0	.....	.....
4101.7	7.0	7.7	28	6.8	5.8
4076.3+4068	.....	.....	1.2	.....	.....
4069	.....	.....	4.5	.....	.....
4026.1	.....	.....	1.7	.....	.....
3968.7	6.9	8.9	30.5	6.6	6.0
3888.9	5.0	5.8	17.4	4.0	3.0
3868.7	17.4	17.3	78	12.6	14.6
3835.4	.....	2.9	7.7	2.6	.....
3797.9	.....	.....	5.6	.....	.....
3770.7	.....	.....	4.8	.....	.....
3760.0	.....	.....	1.7	.....	.....
3750.2	.....	.....	2.9	.....	.....
3734.3	.....	.....	2.1	.....	.....
3727	16.7	13.0	71	5.7	.....
3712.0	.....	.....	1.5	.....	.....
3703.8	.....	.....	1.4	.....	.....

* The sign on the settings +15″, +10″, etc., is arranged so as to agree with the convention for NGC 7662 in the sky. λ 3770 may be blended. [N II] is strengthened at −0″15 with respect to Hα. Notice the peculiar distribution of λ 4686 with respect to Hβ! The 4227 line is certainly real; no identification has been found.

The remarkable features of this nebula are many. It certainly is not a simple shell structure—and, indeed, may not be shell-like at all. The outer "ring" consists of a number of knots and condensations. The inner ring is broken and irregular. The excitation level is likewise unusual, in that strong [Ne v] lines are observed simultaneously with a strong λ 3727 [O II]. The spectrum of the central star has been studied in some detail. It seems to correspond to a spectral class of about O9.5 and an excitation temperature in the neighborhood of 30000° K (Wilson and Aller 1954).

At first glance, it seems that the outer portion of the nebulosity may be regarded as an amorphous mass whose intensity gradually falls off with distance from the central

TABLE 5

INTENSITIES OF LINES OF INTERMEDIATE STRENGTH IN NGC 2392 AS MEASURED WITH THE 60-INCH REFLECTOR (BRIGHT RING)

λ	I	λ	I	λ	I
6716+30	19.2	4712	9.2	4101.7	19.8
6678.2	4.4	4658.4	3.5	4069+76	4.1
6300+6312	9.4	4640.6	1.6	4026.1	2.8
5875.6	9.5	4541.6	2.7	3888.9	17.0
5411.5	6.7	4471.5	2.5	3835.4	6.7
4861.3	(100.0)	4363.2	18.3	3797.9	6.3
4740.2	6.9	4227.4	3.9	3770.7	5.4
4724	3.0	4200.0	1.7	3727	55.2

TABLE 6

COMPARISON OF INTENSITIES IN NGC 2392 AS MEASURED WITH THE CROSSLEY REFLECTOR AND AT MOUNT WILSON

λ	Ident.	I (Mt. W.)	I(L)	λ	Ident.	I (Mt. W.)	I(L)
3203	He II		26	3970	[Ne III]	30	30
3341	[Ne V]		36	4101	Hδ	28	23
3428	[Ne V]		84	4340	Hγ	44	53
3727	[O II]	71	76	4686	He II	57	60
3868	[Ne III]	78	78	4861	Hβ	100	88

star. Upon this amorphous mass are superposed numerous knots and condensations, some of which attain a fair size. The knots show a lower level of excitation than does the main body of the nebula. In 1944 and 1945 a number of slitless spectrograms were obtained with the quartz spectrograph at the Crossley reflector of the Lick Observatory. The photometric procedures and reduction methods are described elsewhere (Aller 1951). Measurements of line intensities in the brightest portion of the bright ring are compared in Table 6. Note the great strength of the [Ne v] lines. In addition, the intensities of the lines in some of the bright knots have been measured. We give in Table 7 the values for one of these knots on the scale Hγ = 50. Hβ was not measurable on the slitless plate used. The [Ne v] lines are missing, and λ 3727 is relatively much stronger than in the main body of the nebula. In a weaker knot the relative intensities of λλ 3727, 3868, 4101, and 4340 were found to be 3.0, 3.4, 1.2, and 1.8, respectively. Here the intensity of the amorphous background has been subtracted so that the values refer to the knots them-

selves. The intensities derived from the slit spectra include both the contribution of the knot and that of the amorphous background.

Since much superior slitless spectrograms are now available, it does not seem worth while to discuss the older material further. Isophotic contours of the nebula provide more definitive data on the knots and condensations (Aller 1956).

Fewer lines have been observed than in NGC 7662 or NGC 7027. The nebula is intrinsically fainter, and for a given exposure a smaller number of lines is recorded.

TABLE 7

INTENSITIES IN AN OUTER KNOT OF NGC 2392

λ	Ion	*I*	λ	Ion	*I*
3727	[O II]	168	4101	Hδ	26
3868	[Ne III]	73	4340	Hγ	50
3970	[Ne III] +H	26	4686	He II	30

TABLE 8

INTENSITIES IN NGC 40

λ	Ident.	Weak Knot	Center	Strong Knot
6716+30	[S II]	43.7	54.6	97.0
6562.9	Hα+[N II]	541.0	800.0	1500.0
6300	[O I]	7.8	20.0	18.0
5876	He I	19.8	15.3	21.0
5755	N II+Sky	4.9	29.5	9.8
5007	[O III]	33.3	26.6	32.0
4959	[O III]	15.0	13.1	13.0
4861	Hβ	93.1	100.0	166.0
4340	Hγ	34.6	43.0	73.0
4101	Hδ	18.4	22.5	40.0
3969	H	11.2	11.9	25.0
3889	H	12.5	11.6	24.7
3835				10.5
3797				18.7
3770				13.5
3750				7.9
3727	[O II]	172.0	206.0	341.0

NGC 40

This low-excitation nebula is intrinsically rather faint, and only the strongest lines of the usual prominent elements have been measured. The results obtained are disappointing in view of the effort expended. Because of the far northern declination (+70°), it was possible to observe this nebula only with the 60-inch reflector. The slit was set 4″ north of the central star; tracings were made at three different points in the nebula.

Table 8 gives the measured intensities at the three points, the intensity of Hβ being take as 100. Some of the strongest and some of the weakest lines were measured on one plate only; these are indicated by an asterisk. The lines of [O II], [N II], [S II], and He I are strong. The higher numbers of the Balmer series were measured on only one plate and gave somewhat discordant values; λ 3869 is blended with [Ne III], λ 3889 is confused

with He I, while Hα is strongly blended with [N II]. M. L. White (1952) estimated the average 6584 [N II] Hα ratio to be 0.76 in this nebula; hence about half the radiation in the red line is to be attributed to [N II].

The N_1 and N_2 lines seem to be concentrated toward the center of the nebula. Furthermore, the positions of the condensations observed in [O III] do not always agree with the positions of the [O II] knots. Hence conditions of excitation vary from point to point in the extremely complex nebula NGC 40. Direct photographs indicate that this nebula does not have a spherically symmetric structure, although there are some vague hints of a basic cylindrical symmetry.

Even after allowing for these blends, the Balmer decrement seems to be too steep, as though the nebula was affected by interstellar absorption. Observations obtained by one of us in 1938 with a slitless spectrograph (Aller 1941) showed also a steep decrement, although the individual intensity values are not in good agreement. The λ 3727 [O II] line is almost twice as bright as Hβ, according to our present measures. Relative to other

TABLE 9

LINE INTENSITIES IN NGC 2022

λ	Ident.	I(Mt. W.)	I(L)	λ	Ident.	I(Mt. W.)	I(L)
6562.9	H I	306.0	.....	4101.7	Hδ	19.4	15.8
5875.6	He I	6.6	.....	3967.4	[Ne III]+H	21.4	20.6
5411.5	He II	16.7	.....	3888.9	H I	8.3	8.7
5006.9	O III	.....	550.0	3868.7	[Ne III]	36.7	35.6
4959.0	O III	189.0	197.0	3727	[O II]	.....	15.4
4861.3	Hβ	100.0	100.0	3444.0	O III	.....	10.9
4740.2	[A IV]	9.5	.....	3428.7	[Ne V]	.....	53.2
4711	[A IV]	13.2	.....	3345.8	[Ne V]	.....	26.2
4685.7	He II	101.0	86.0	3312.3	O III	.....	8.0
4541.6	He II	3.4	.....	3203.1	He II	.....	44.0
4363.2	[O III]	10.5	11.2	3132.8	O III	.....	45.0
4340.4	Hγ	41.7	39.1				

lines, it is stronger than in other planetaries, although the λ 3727/Hβ ratio is only slightly larger than in certain of the knots in NGC 2392 or in the ansae of NGC 7009. The [O III] lines are very weak in this nebula.

Further long exposures on this nebula would appear unprofitable. If an intensive study of a low-excitation nebula is planned, it would be better to observe some object such as BD+30°3639, or Anon 18^h15^m, whose surface brightnesses are very much greater. These objects are small, a circumstance that provides no particular difficulty when they are observed with a large telescope. BD+30°3639 has a complex nuclear spectrum; the central star of Anon 18^h15^m seems to have a perfectly continuous spectrum.

NGC 2022

Although it is an intrinsically somewhat faint object, NGC 2022 was selected for study because of its high excitation. It is a rather regular ring nebula, characterized by a particularly strong λ 4686. Earlier work (Aller 1951) had suggested that it was perhaps the highest-excitation regular-shaped nebula.

Our adopted intensities, I(Mt. W.) (see Table 9), are based on plates secured with both the 60-inch and the 100-inch reflectors. For comparison we give the intensities, I(L), measured on a spectrogram secured with the Crossley quartz slitless spectrograph at the Lick Observatory in 1944. The two sets of intensities are in good agreement. Although the Lick plate did not register the fainter lines, it does show that the ultraviolet

[Ne V], [O III], and He II lines are strong. The [O II] λ 3727 radiation is present, and the image in this line is large. Tentative intensities previously published by one of us (Aller 1941) were based on a plate of questionable photometric calibration taken in 1934 by Stoy. The present set of intensities should be much more reliable, even though the intensities of some of the lines in the far ultraviolet may be overestimated.

NGC 1535

This beautiful double-ring planetary has a more nearly regular structure than most other representatives of its class. Even so, large-scale slitless spectrograms reveal irregularities in both rings. In spite of its unfavorable declination, the object was included in our program, and exposures ranging from 7 minutes to 5 hours and 22 minutes were secured with the JS spectrograph at the 60-inch telescope.

TABLE 10

LINE INTENSITIES IN NGC 1535 AS MEASURED WITH THE 60-INCH REFLECTOR

λ	Ident.	Bright Ring	Outer Ring	Previous Values* Bright Ring
6562.9	Hα	361.0	48.0	.....
5875.6	He I	20.0	8.6	.....
4959.0	[O III]	363.0	.....	.....
4861.3	Hβ	100.0	27.6	100.0
4740.2	[Ar IV]	5.2	.....	.....
4712.0	[Ar IV]	6.7	.....	.....
4685.7	He II	19.8	.....	24.0
4640.2	N III	4.1	.....	.....
4541.6	He II	4.3	.....	.....
4471.5	He I	7.2	.....	6.0
4363.2	[O III]	16.4	4.3	19.0
4340.4	Hγ	51.6	13.9	49.0
4101.7	Hδ	28.8	7.6	21.0
3969	[Ne III], Hε	40.0	11.0	30.0
3888.9	Hζ	21.8	6.9	21.0
3868.7	Ne III	89.0	22.0	74.0
3835.4	Hη	7.7	.....	.....

* *Ap. J.*, **113**, 134, Table 3, 1951.

In spite of the small scale of the resulting spectrograms, we measured the intensities both in the bright inner ring and in the outer fainter ring. They are given in Table 10, with the intensity of Hβ in the brighter ring chosen as 100. The high-excitation lines are missing from the outer ring.

Comparison of the measures for the bright ring with values previously published by one of us shows reasonably good agreement. Ultraviolet spectra show that the lines of O III, λ 3444, λ 3346, and He II λ 3203 are present, although much weaker than in other high-excitation objects considered—in accordance with our expectations. Further exposures on this object seem unprofitable unless much faster optics can be employed.

We have also secured observations of the low-excitation objects IC 1747 and J 320 and the higher-excitation objects NGC 2165, NGC 2440, and IC 351. In NGC 2165 and NGC 2440 only lines of intermediate strength have been measured. Wyse (1942) has given eye-estimates of the intensities of all the lines he could observe, and one of us has published intensities for the stronger lines (Aller 1951). Table 11 contains the results for IC 351 and J 320. They are based on one plate per nebula.

In Table 12 we compare the results for NGC 2165 and NGC 2440 with those obtained some years ago by one of us. The Mount Wilson plates cover only lines of intermediate intensity. Exposures were not obtained for the stronger lines; for the weaker lines a higher dispersion would have been appropriate, in order to minimize the effects of the continuum.

NGC 2165 appears as a small, nonuniform disk, whereas NGC 2440 resembles NGC 7027 in a number of features. In particular, NGC 2440 seems to show a combination of low- and high-excitation features. For example, the low-ionization lines of [O I] λ 5755; [O II] λ 3727, and also λ 5200 are stronger in NGC 2440 than in NGC 1535. On the other hand, He II, λ 5411, and λ 4686, as well as λ 4640 N III, and 4740 [A IV] are stronger

TABLE 11

LINE INTENSITIES IN IC 351 AND J 320

λ	IC 351	J 320	λ	IC 351	J 320	λ	IC 351	J 320
6563	350	280	4686	52	...	4101	24	27
4959	300:	310	4363	15	20	3969	31	46
4861	100	100	4340	49	44	3868	78	93

TABLE 12

INTENSITIES FOR NGC 2165 AND NGC 2440

λ	NGC 2165		NGC 2440	
	I Mt. W.	*I* Lick	*I* Mt. W.	*I* Lick
3797	0.50	0.48	...	...
3835	0.55	0.53	1.01	...
3889	1.41	1.80	2.04	...
3967	...	4.30	4.60	3.70
4026	0.22	0.18	...	...
4076	0.21	0.20	0.30	...
4101	1.95	2.60	...	2.60
4200	0.10	0.12	...	...
4340	...	4.60	...	5.20
4363	1.58	2.10	...	2.90
4471	0.44	0.34	0.42	0.27
4541	0.21	0.18	0.22	0.30
4640	0.35	0.47	0.87	1.00
4712	0.66	0.72	1.60	1.60
4740	0.56	0.65	1.45	...
4861	...	10.00	...	10.00
5192–99	...	...	1.95	...
5411	0.72	...	1.1	...
5755	...	...	2.8	...
5875	1.74	...	2.1	...
6085	0.18	...	...	...
6300	0.74	...	4.8	...
6364	0.30	...	1.6	...
6678	0.64	...	1.2	...
6713+6730	0.93	...	4.27	...

than in NGC 1535. The λ 4640 line may arise from a nuclear star, since it is shorter than any of the other lines on the plate. There is little evidence for any stratification effects; the low- and high-excitation radiations appear to arise in contiguous or well-mixed regions.

V. THE CONTINUOUS SPECTRA OF THE PLANETARIES

In addition to their characteristic bright emission-line spectra, the planetaries also show an underlying continuum. Some of it must originate from the recombination of protons and electrons; some of it may come from double photon emission, a mechanism suggested by Breit and Teller (1940) and favored by Greenstein and Spitzer (1951).

In principle, the determination of the energy distribution in the continuum should be a simple process; one compares the nebula with the standard star. In practice, it is difficult primarily because of the *extreme* faintness of the continuum in all objects investigated except NGC 7027. With practicable exposure times, the measured intensities in the blue region are derived from very low photographic densities where slight errors in the calibration-curves lead to appreciable errors in the intensities. If a wide slit is used, this trouble can be partly overcome, but at the price of a spectrum of lower purity, in which the contributions of weak lines are added to the true continuum. Even at best, the presence of the weaker lines makes it difficult to estimate the position of the continuum in much the same way as the presence of stellar absorption lines makes it hard to find the continuum in an absorption-line star. Because of the very small dispersion in the infrared, it is also difficult to take into account the effects of the atmospheric-absorption bands which may be allowed for only approximately.

If the central star is bright, the scattering and diffraction effects produced by the web supporting the secondary mirror may cause trouble. The measured nebular emission, therefore, may be partly affected by diffracted light from the central star. In NGC 2392, which has low surface brightness and a very bright central star, the results obtained suggest strongly that the measured energy distribution in the continuum is affected by stellar light; the measured intensity increases by a factor of more than 6 from λ 8000 to λ 4000. In the light of present knowledge, this result appears impossible, and it seems better to disregard it until the possible effect of scattered light in this case has been investigated. On the other hand, in NGC 7027 the central star is too faint to be observed, and this difficulty disappears, of course.

The energy distribution in the continuum of the nebula, $I_c(n)$, follows from a direct measure of the ratio $I_c(n)/I_\lambda(s)T$, where $I_\lambda(s)$ denotes the energy distribution in the stellar continuum and T the transmission of the quartz diffuser.

NGC 7027 is the only object for which results of some value could be obtained. This nebula has a relatively strong continuum which is prominent at the red end of even moderately exposed plates. The line spectrum, however, is exceedingly rich, so that the location of the continuum is difficult. Observations covering the visual and infrared regions (λλ 4000–8500) were obtained on 103*a*-F and I-N emulsions at the Mount Wilson Observatory, whereas the McDonald plate covers the interval λλ 3200–5000. In the λλ 4000–4700 region the Texas plate shows a steeper gradient than do the Mount Wilson plates, although the fit is not much poorer than one might expect. Using the best average fit on a $1/\lambda$ plot, the deviations in log I are within ± 0.075. When we consider the difficulty in drawing in the continuum, about a 10 per cent discrepancy over the common range is not surprising.

The measured energy distribution is given in Table 13. Both Vega and α Persei were used as comparison stars. The Balmer continuum is much stronger than the general continuum, and the influence of numerous weak and moderately strong emission lines, which operates so disadvantageously in other parts of the spectrum, should play no role. On the assumption that the Balmer continuum is a pure recombination spectrum and

that there is no self-reversal, the electron temperature T_e may be obtained from the emission intensity E_λ at two points λ_1 and λ_2 from

$$\log E_1 - \log E_2 = \frac{0.4343hc}{kT_e}\left(\frac{1}{\lambda_1} - \frac{1}{\lambda_2}\right). \quad (2)$$

The observed intensities are, of course, to be corrected for interstellar reddening. With the differential correction of 1.43 mag. between λ 3750 and λ 8750 found from the ratio of the Paschen and Balmer lines in the following paper (Aller and Minkowski 1956), the measured intensities in the Balmer continuum vary reasonably well as $1/\lambda$ and lead to $T_e = 12300 \pm 3600$, in satisfactory agreement with the value 14300 derived from line intensities.

The intensities immediately to the red of the Balmer limit are low and could therefore not be determined with great accuracy. They contradict, however, the result by Page

TABLE 13

ENERGY DISTRIBUTION MEASURED IN THE SPECTRUM OF NGC 7027

λ	log I		λ	log I
	McDonald *Qff* 2 8270	Mt. Wilson		Mt. Wilson
3300	1.85	.....	4800	1.74
3400	1.91	.....	5000	1.77
3500	1.97	.....	5200	1.85
3600	2.02	.....	5400	1.89
3700	1.16	.....	5600	1.92
3800	1.19	.....	5800	1.95
3900	1.25	.....	6000	1.98
4000	1.34	1.39	6200	2.00
4100	1.40	1.44	6400	2.03
4200	1.45	1.49	6600	2.05
4300	1.53	1.53	6800	2.07
4400	1.59	1.58	7000	2.07
4500	1.65	1.62	7500	2.04
4600	1.70	1.67	8000	1.98
4700	1.74	1.70		

(1942), who found constant intensity in this region. The McDonald results lead to a value of $\Delta \log I$ of about 0.9 for the Balmer discontinuity; the Mount Wilson results above λ 4000 carry some suggestion that the McDonald intensities below λ 4300 are too low and that $\Delta \log I$ may be slightly smaller. The observed value would lead to an electron temperature of only 6600° if the two-quantum emission contributed in the amount computed by Spitzer and Greenstein (1951). An electron temperature as low as this is contradicted by the gradient of the continuous spectrum and by the values of around 14000° found from line intensities. It seems necessary to assume that the two-quantum emission is weak in NGC 7027. Actually, the two-quantum emission may be squelched at high densities. Seaton (1954) has made quantitative estimates of the degree of suppression of two-quantum emission as a function of density. Its weakness in NGC 7027 agrees with the suggestion by Seaton and with the result of Aller (1954), who found for the average electron density the value of 1.7×10^4 cm^{-3} and concluded that the local densities in condensations must be much higher, to explain the [S II] transauroral- and

nebular-line intensities. It is impossible to find out exactly how much of the two-quantum emission is present. If this emission were entirely absent, the observed discontinuity would lead to an electron temperature of 20000°. This is to be considered as an upper limit.

Redward from the Balmer discontinuity the intensity increases, as would be expected. This contradicts the result of Page, who found nearly constant intensity. But the shape of the intensity distribution between the Balmer limit and λ 8000 defies any theoretical interpretation. This discordance is most probably due to the difficulty in determining the true level of the continuous spectrum. In view of this difficulty, it would not be justifiable to discuss the discordance, which cannot be considered as having any physical significance.

REFERENCES

Abbott, C. G. 1908, *Smithsonian Ann.*, Vol. 2.
Aller, L. H. 1941, *Ap. J.*, **93**, 236.
———. 1951, *ibid.*, **113**, 125.
———. 1956, *Gaseous Nebulae* (New York: John Wiley & Sons, Inc.), p. 256.
Aller, L. H., Bowen, I. S., and Minkowski, R. 1955, *Ap. J.*, **122**, 62.
Barbier, D., and Chalonge, D. 1940, *Ann. d'ap.*, **3**, 2.
Berman, L. 1930, *Lick Obs. Bull.*, **15**, 86.
Breit, G., and Teller, E. 1940, *Ap. J.*, **91**, 215.
Code, A. 1956, private communication.
Fowle, F. E. 1933, *Smithsonian Misc. Coll.*, **88**, 611.
Kienle, H., Strassl, H., and Wempe, J. 1938, *Zs. f. Ap.*, **16**, 201.
MacRae, D., and Stock, J. 1954, *Nature*, **173**, 589.
Liller, W. 1955, *Ap. J.*, **122**, 235.
Liller, W., and Aller, L. H. 1954, *Ap. J.*, **120**, 48.
Page, T. L. 1936, *M.N.*, **96**, 627.
———. 1942, *Ap. J.*, **96**, 78.
Plaskett, H. H. 1931, *Pub. Dom. Ap. Obs. Victoria*, **4**, 187.
Popper, D. M. 1937, thesis, University of California.
Seaton, M. J. 1954, *Ann. d'ap.*, **17**, 296.
Spitzer, L., and Greenstein, J. L. 1951, *Ap. J.*, **114**, 407.
Stebbins, J., and Whitford, A. E. 1945, *Ap. J.*, **102**, 273.
White, M. L. 1952, *Ap. J.*, **115**, 71.
Williams, R. 1938, *Pub. Obs. Michigan*, **7**, 93.
———. 1939, *ibid.*, pp. 147 and 159.
Williams, R., and Hall, J. 1942, *Ap. J.*, **95**, 225.
Wilson, O. C., and Aller, L. H. 1954, *Ap. J.*, **119**, 243.
Wyse, A. B. 1942, *Ap. J.*, **95**, 359.

THE INTERPRETATION OF THE SPECTRUM OF NGC 7027

L. H. Aller and R. Minkowski
University of Michigan Observatory
and
Mount Wilson and Palomar Observatories
Carnegie Institution of Washington, California Institute of Technology
Received February 13, 1956

ABSTRACT

The spectrophotometric data for NGC 7027 are analyzed theoretically with a new value of the space absorption. Ionic concentrations derived from different forbidden-line multiplets of oxygen and sulphur substantiate this newer correction. Revised atomic abundances are obtained, but any substantial improvement in the analysis requires theoretical calculations of transition probabilities and target areas for forbidden-line excitation in the ions of elements such as iron.

I. REVISION OF THE ESTIMATE OF SPACE ABSORPTION

The first theoretical analysis of the newer spectrophotometric data of NGC 7027 (Bowen, Minkowski, and Aller 1955) was based on the assumption that the true Balmer decrement was given by Menzel's and Baker's "case B" (1938). This hypothesis was employed to evaluate the space absorption in accordance with the results suggested by an analysis of the Balmer decrements in some forty-odd planetaries (Aller 1951). A critical examination of the spectrophotometric data for NGC 7027 showed that this postulate of a case B Balmer decrement led to serious difficulties for two reasons.

a) Independently of any excitation mechanism, the ratio of the Paschen line intensities to the Balmer line intensities should be

$$\frac{I\,(Pa_n)}{I\,(Ba_n)} = \frac{A_{n3}\nu_{n3}}{A_{n2}\nu_{n2}}. \tag{1}$$

The Paschen line intensities corrected on the assumption of a case B Balmer decrement were very much too weak. The observational data are not completely decisive on this point, inasmuch as the underlying continuum could have been drawn too high.

b) The energy distribution in the nebular continuum appeared to be very abnormal.

Accordingly, we have attempted to make a new estimate of the space absorption by taking the Paschen line intensities at their face value. The lines utilized in this study are the transitions originating on the levels $n = 10$, 11, 12, 13, 15, and 16. The theoretical ratio $I(Pa)/I(Ba)$ is nearly 0.306 for all these lines. The observed values are exhibited in Table 1. The intensities of the weakest lines ($I < 1.0$) are very uncertain. The 9015 line falls in a region where the estimate of the background is very insecure. The effect of space absorption is to cut down the intensities of the lines by a factor of 3.76 over a base line $\lambda_1 = 3750$ to $\lambda_2 = 8750$. All the absorption corrections tabulated by Whitford (1948) must therefore be multiplied by a factor of 1.42 for this object.

II. DETERMINATION OF N_e AND T_e FROM THE [N II], [O III] LINES

We must now correct the observed intensities of the emission lines on the basis of our revised space absorption. The suggested corrections, $\Delta \log I$, are given in Table 2. The new estimates of N_e and T_e from the relative intensities of the auroral and nebular lines of [N II] and [O III] differ only slightly from those obtained previously (Aller 1954). The

auroral/nebular line-intensity ratios are 0.0129 and 0.046 for [O III] and [N II], respectively. Then, using equations (14) and (15) of the last-cited reference, we find $N_e = 6.3 \times 10^4$ and $T_e = 14000°$ K as compared with 7.7×10^4 and 14500° K, respectively.

III. THE REVISED BALMER DECREMENT IN NGC 7027

If the space-absorption correction of Table 2 is now employed in conjunction with the observed intensities (col. 2) of the Balmer lines, we obtain the corrected intensities listed in the third column of Table 3. These are compared with the theoretical intensities

TABLE 1

COMPARISON OF BALMER AND PASCHEN LINE INTENSITIES

n	$\lambda(Pa)$	I	$\lambda(Ba)$	I	$I(Pa)/I(Ba)$
10	9015	5.5	3798	3.5	1.57
11	8863	3.5	3770	3.3	1.06
12	8750	3.1	3750	2.7	1.15
13	8665	2.7	3734	2.3	1.18
15	8545	0.8:	3712	1.8	0.44
16	8502	0.6:	3704	1.7	0.35
Adopted ratio					1.15

TABLE 2

CORRECTIONS FOR SPACE ABSORPTION FOR LINE INTENSITIES IN NGC 7027

λ	$\Delta \log I$	λ	$\Delta \log I$	λ	$\Delta \log I$
3200	+0.260	4861	0.000	6500	−0.190
3600	+ .200	5000	− .020	7000	− .242
4000	+ .130	5500	− .076	7500	− .292
4500	+0.053	6000	−0.134	8000	−0.330

TABLE 3

COMPARISON OF OBSERVED AND THEORETICAL BALMER DECREMENTS FOR NGC 7027

λ (1)	I(Obs.) (2)	I(Corr.) (3)	$I(B)$ (4)	I(Coll.) (5)	$I(\mathfrak{H}=0.15)$ (6)
Hα 6563	650	410	255	532	405
Hβ 4861	100	100	100	100	100
Hγ 4340	33	40	50.5	32.2	40.7
Hδ 4101	16.3	21.3	30.5	15.0	22.1
H8 3889	8.8	12.6	13.7	5.4	9.1
H9 3835	4.6	6.6	9.9	3.6	6.5
H10 3797	3.5	5.2	7.4	2.5	4.8

for the thick nebula in radiative equilibrium (Menzel and Baker, case B), column 4, and with the intensity for pure collisional excitation for an assumed electron temperature of 14000° K (Chamberlain 1953), column 5. The observed intensity, corrected for space absorption, is seen to fall between these two extremes, thus suggesting that collisional excitation may play a role in the production of the Balmer line spectrum in this nebula.

Chamberlain (1953) showed that, if both collisions and radiative processes act to populate the levels, the factors b_n, introduced by Menzel (1937) to measure the deviation from thermodynamic equilibrium, may be written as

$$b_n = (1 - \mathfrak{H})\, b_n^B + \mathfrak{H}\, b_n^C , \tag{2}$$

where b_n^B and b_n^C are, respectively, the b_n factors computed for pure radiative excitation and for collisional processes in an optically thick nebula. They are given in Table 3 of Chamberlain's paper. The function $\mathfrak{H}$ is given by

$$\mathfrak{H} = \frac{a_\kappa(T_e)\, T_e^{3/2}}{G(T_e)\, K} \frac{N_1}{N_e} . \tag{3}$$

Here $a_\kappa(T_e)$ is the collision-ionization parameter,

$$a_\kappa(T_e) = \int_{v_0}^{\infty} Q_\kappa(v)\, v f(v)\, dv , \tag{4}$$

where Q_κ is the cross-section for ionizing collisions, $f(v)$ is the Maxwellian velocity distribution, and v_0 is the velocity corresponding to the ionization energy. $G(T_e)$ has been tabulated as a function of the electron temperature (Menzel, Baker, and Aller 1938), $K = 3.26 \times 10^{-6}$, and N_1 is the number of atoms in the ground level.

If both collisional and radiative processes are operative, we may write:

$$\frac{I_{n,2}}{I_{H\beta}} = \frac{(1 - \mathfrak{H})}{(1 - \mathfrak{H}) + (b_4^C / b_4^B)\, \mathfrak{H}} \left(\frac{I_{n,2}}{I_{H\beta}}\right)_B + \frac{\mathfrak{H}}{\mathfrak{H} + (b_4^B / b_4^C)\, (1 - \mathfrak{H})} \left(\frac{I_{n,2}}{I_{H\beta}}\right)_{coll} . \tag{5}$$

At $T = 14000°$ K, $b_4^C / b_4^B = 6.6$. With $\mathfrak{H} = 0.15$, we predict the Balmer decrement given in column 6 of Table 3. The agreement is satisfactory except for Hζ, which is blended with helium λ 3889; Hϵ has to be excluded because of blending with [Ne III]. Let us adopt $T_e = 14000°$ K and calculate the ratio N_1 / N_e from equation (3). We interpolate $a_\kappa(T_e) = 8.8 \times 10^{-14}$ from Chamberlain's data and take $G(T_e) = 0.165$ from the Harvard nebular series. With $\mathfrak{H} = 0.15$, we find $N_1 \sim \frac{1}{2} N_e$, which would imply that in the filaments where the hydrogen lines were produced the gas was only two-thirds ionized! An alternative possibility is that T_e is higher, so that a_κ is much larger and N_1 / N_e is correspondingly smaller. At any rate, NGC 7027 appears to be one nebula in which Miyamoto's (1938) suggestion of some collisional excitation appears to be fulfilled, although collisional excitation does not dominate, as it appears to do in certain radio-frequency sources (Minkowski and Aller 1954).

IV. IONIC CONCENTRATIONS OF OTHER ELEMENTS

We now employ the same methods as given previously (Aller 1954) to calculate the concentrations of the other ions. The line intensities to be employed are different because of the lessened influence of the space absorption, and, because of the new choice of N_e and T_e, the η-factors are slightly different. The largest change in the results is produced by the revision in the space-absorption correction. Table 4 lists for each ion the type of transition, the η-factor, the intensity I_n, and, finally, the ionic concentrations both for

the revised or "small" space absorption and for the initially assumed or "large" space absorption.

The nebular and auroral lines of [O II] give roughly similar ionic concentrations, and the nebular and transauroral [S II] lines likewise yield concordant results. It now appears that a temperature of 14000° K and $N_e = 6.5 \times 10^4$ explains the relative intensities of the principal forbidden lines in NGC 7027. It is possible that different filaments have different temperatures and densities, i.e., that no unique value of T_e and N_e can be assigned to the nebula as a whole. The [S II] radiation may be concentrated in slightly denser filaments, the [O II] radiation in less dense filaments. Quite possibly, the hydrogen radiation and the forbidden-line radiation are concentrated in different filaments.

The results for the heavier ions, for which the cross-sections have been estimated rather than calculated, are less encouraging. There are big discrepancies in the con-

TABLE 4

CONCENTRATIONS OF IONS IN NGC 7027

Ion	Type of Transition	η	I_n	Small Space Absorption (ions/cm³)	Large Space Absorption (ions/cm³)
N II	N	0.36	202	1.1	0.9
	A	.00184	9.3	1.0	0.9
O II	N	.860	21.2	1.1	1.9
	A	.0054	40.5	1.6	1.0
O III	N	.0537	1920	12.7	14.3
F IV	N	.0082	0.68	0.008	0.012
Ne III	N	.0026	95	2.0	2.8
Ne IV	N	.00115	4.1	1.3	2.0
Ne V	N	.00146	144	3.5	6.4
S II	N	.374	7.9	0.035	0.027
S II	TA	.00415	8.8	0.039	0.058
S III	A	.00045	10.6	0.80	0.57
Cl IV	N	.132	3.1	0.011	0.013
Cl IV	N	.0055	3.2	0.02	0.007
Cl IV	A	.000214	0.87	0.17	0.16
A III	N	.00259	40.6	0.28	0.18
A IV	A	.031	14.4	0.08	0.12
A IV	N	.000234	5.2	0.3	0.16
A V	N	0.00145	11.4	0.09	0.06
K IV	N	.....	2.2	0.022	0.015
K VI	N	.....	1.5	0.018	0.018
Ca V	N	.....	1.8	0.023	0.025

centrations of Cl IV and A IV ions, depending on whether they are computed from the nebular or the auroral transitions. The discordances clearly indicate the need for more accurate calculations of target areas for collisional excitation. The ions in particular need of attention are S III, Cl III, Cl IV, A III, A IV, and A V. Eventually, cross-sections for K IV, K VI, and Ca V and other metals also should be calculated. We return to this question in Section V.

An additional estimate of the density in the regions where the [O II] lines appear may be obtained from the circumstance that the $I(3726)/I(3729)$ ratio depends on the density (Ufford, Van Vleck, and Aller 1949; Seaton 1954). If we use the notation and cross-sections suggested by Seaton, we find:

$$r = \frac{I(^2D_{5/2} - {}^4S_{3/2})}{I(^2D_{3/2} - {}^4S_{3/2})} = 1.5 \left\{ \frac{1 + 3.26\,\chi}{1.02 + [10.4 + 4.0 \exp(-\chi_{23}/kT_e)]\,\chi} \right\}. \qquad (6)$$

Here $\chi = N_e/100\sqrt{T_e}$. Our formula differs from that of Seaton, in that we have included the influence of the ^2P term in setting up the equation of statistical equilibrium. With a ratio $r = 0.49$ for NGC 7027 and $T_e = 14000°$ K, N_e then turns out to be 1.7×10^4 electrons/cm^3, a value similar to that estimated from the surface brightness (Aller 1954; Liller and Aller 1954) but much smaller than the N_e obtained from the ratio of auroral to nebular line intensities. The effect of averaging over filaments of divers densities may affect the 3726/3729 intensity ratio differently than it affects the nebular/auroral line ratio. Errors in the observed intensity ratio, as well as in the cross-sections estimated by Seaton, may contribute further to the discrepancy.

V. THE COMPOSITION OF THE NEBULA

We must now examine what effects these revised ionic concentrations will have on the estimated composition of the nebula. The second and fifth columns of Table 5 give

TABLE 5

ABUNDANCES OF ELEMENTS

Atom	Small Absorption			Large Absorption	
	Obs. No.	Ionization Factor	Relative No.	Obs. No.	Relative No.
N	1.0	30:	5000:	0.9	4500:
O	14.0	3.8	10000	15.8	10000
F	0.008	3.2	5	0.012	6
Ne	6.8	1.2	1500	11.2	2500
S	0.83	8.2	1300	0.97	1300
Cl	0.18	3.5	120	0.16	86
A	0.69	1.8	240	0.37	110
K	0.040	2.5	18	0.032	13
Ca	0.023	3.6	16	0.025	15
H	.....	.....	1.17×10^7	.....	1.17×10^7
He	.....	.....	1×10^6	.....	1×10^6

the observed relative members of all the ions of each element for both space absorption assumptions. Thus, nitrogen is represented only by [N II], oxygen by [O II] and [O III], whereas neon is represented by [Ne III], [Ne IV], and [Ne V]. We must estimate the corrections necessary to reduce these observed abundances to the actual relative abundances of the elements involved. These ionization corrections appear to be about the same as those estimated earlier; the correction for the more highly ionized atoms seems very uncertain. The same ionization factor is applied to the second and fifth columns. For some elements the effect of the change in space absorption upon the abundance is pronounced.

It is obvious that the compositions of the planetary nebulae can never be estimated properly until the stage of ionization can be accurately determined. The element most suited to such a study (in NGC 7027) is iron. Were the transition probabilities and target areas for the collisional excitation of the lines of [Fe III], [Fe V], and [Fe VII] available, we could make a much better estimate of the distribution of atoms among various stages of ionization.

The correction factors are disagreeably large for sulphur and nitrogen, which are observed only in the lowest stages of ionization. Our factors may be too large for both these elements, which may be concentrated in filaments, so that their actual abundances may be smaller.

It is extremely difficult to find the concentration of neon. The proportion of Ne IV seems to be three or four times too small as compared with Ne III and Ne V. Putting it another way, the [Ne IV] lines are about three times as weak as they should be. Possibly the target areas for the ^{2}P terms in Ne IV are too high, or maybe there are two types of filaments—one a "high"-excitation and the other a "low"-excitation filament, in which Ne III and still lower-excitation stages prevail. Our estimate of the abundance of neon is therefore extremely shaky. The chlorine and argon concentrations are based on uncertain cross-sections. They do indicate values more nearly in harmony with those found for the stars. The metals are very poorly determined because of the uncertainty in the ionization correction. Further discussion does not appear warranted at this time.

REFERENCES

Aller, L. H. 1951, *Ap. J.*, **113**, 125.
———. 1954, *ibid.*, **120**, 401.
Bowen, I. S., Minkowski, R., and Aller, L. H. 1955, *Ap. J.*, **122**, 62.
Chamberlain, J. 1953, *Ap. J.*, **117**, 387.
Liller, W., and Aller, L. H. 1954, *Ap. J.*, **120**, 48.
Menzel, D. H. 1937, *Ap. J.*, **117**, 387.
Menzel, D. H., and Baker, J. G. 1938, *Ap. J.*, **88**, 52.
Menzel, D. H., Baker, J. G., and Aller, L. H. 1938, *Ap. J.*, **88**, 422.
Minkowski, R., and Aller, L. H. 1954, *Ap. J.*, **119**, 232. An error in the entry for a_3 (10000° K) requires a correction to the values of γ (O I) and γ(O III) in Table 2 as follows: γ(O I) = 62900, 2100, 330; and γ(O III) = 190000, 6400, and 1300; for T_e = 10000, 15000, and 18000, respectively.
Miyamoto, S. 1938, *Jap. Mem. Coll. Sci.*, **21**, 173.
Seaton, M. J. 1954, *Ann d'ap.*, **17**, 74.
Ufford, C. W., Van Vleck, J. H., and Aller, L. H. 1949, *Ap. J.*, **109**, 42.
Whitford, A. E. 1948, *Ap. J.*, **107**, 102.

THE CHEMICAL COMPOSITIONS OF FIVE STARS WHICH SHOW SOME OF THE CHARACTERISTICS OF POPULATION II

E. MARGARET BURBIDGE*
Kellogg Radiation Laboratory
California Institute of Technology
AND
G. R. BURBIDGE
Mount Wilson and Palomar Observatories
Carnegie Institution of Washington
California Institute of Technology
Received February 2, 1956; revised February 20, 1956

ABSTRACT

Abundances of all or some of the elements Mg, Al, Ca, Sc, Ti, Cr, Mn, Fe, Sr, Y, Zr, and Ba in the stars HD 84123, HD 106223, λ Boo, HD 161817, and 29 Cyg, relative to the standard population I star 95 Leo, have been obtained by curve-of-growth methods. These stars were all chosen because previous investigators had suggested that they had high-velocity characteristics or a general weakening of the spectral lines, which have been considered to be associated with stars of population II type, presently located in the solar neighborhood. It has been found that, while HD 84123 has a chemical composition practically indistinguishable from a normal population I star, λ Boo has a composition which is very similar to that of HD 19445 and HD 140283, studied by Chamberlain and Aller, which have only about 10 and 3 per cent, respectively, of the "normal" abundances of Fe and Ca. In the other stars the underabundance ratios for all the elements lie intermediate between these two extremes. In HD 106223 and λ Boo underabundance ratios of about 30 and ≥20 have been found for Ba, and these may be representative of the ratios for the very heavy elements. An attempt has been made to correlate the population II characteristics of these stars and of HD 19445 and HD 140283 in the following categories: (*a*) position on the HR diagram, (*b*) chemical composition, (*c*) kinematical properties, and (*d*) rotational properties. The theoretical implications of these results are discussed.

I. INTRODUCTION

Since Baade (1944) introduced the terms "population I" and "population II" to describe essentially stars which lie on the ordinary H-R diagram and stars with the H-R diagrams of globular clusters, the terms have been loosely used to describe stars which have other qualitative features that may be associated with the solar-neighborhood main sequence or with globular-cluster stars. It appears that a number of categories should be used, so that the stars may be classified according to (*a*) their position on the H-R diagram; (*b*) their chemical composition as determined by (i) high-dispersion spectrophotometric investigations to determine element abundances and (ii) qualitative spectral features which give a preliminary measure of chemical composition; (*c*) their kinematical properties (both their velocities and their spatial positions, which, together with their orbits, describe the situations from which they evolved, are included here); and (*d*) their rotational velocities, which also may have considerable bearing on their evolution. This classification scheme is somewhat similar to that suggested by von Weizsäcker (1951). In recent years a number of investigations have been made to try to elucidate the properties of stars which fall into one or more of these categories and to try to correlate them. The work of Schwarzschild and Schwarzschild (1950) and Schwarzschild, Spitzer, and Wildt (1951) showed that there was a probable correlation between properties in categories *b*, i, and *c*. Miss Roman (1954) has isolated a group of stars by using criteria in categories *a*, *b*, ii, and *c* and has suggested that these form "the

* Assisted by the joint program of the U.S. Office of Naval Research and Atomic Energy Commission.

purest Population II objects isolated as yet within 100 psc of the sun." She has also studied correlations between categories *b*, ii, and *c* for a number of high-velocity stars (Roman 1950, 1952). Chamberlain and Aller (1951) have made a detailed spectrophotometric investigation of HD 19445 and HD 140283 in comparison with a main-sequence A star and have found that there are underabundances of calcium and iron relative to this standard star. They have related this chemical-composition difference to the positions of the stars in the H-R diagram. Some discussion of this work will be given in the concluding section. In the investigation reported in this paper we have determined the chemical composition of a number of other stars which were originally chosen because, according to the categories given previously, they were thought to have at least one of the characteristics of population II. The stars which were chosen were HD 84123, HD 106223, λ Boo, HD 161817, 29 Cyg, and HD 151199. The last-named star has been found not to belong to population II according to any of these categories, and its chemical composition is discussed elsewhere (Burbidge and Burbidge 1956). Summaries of the previous descriptions of the other stars and hence the reasons why they were chosen are given below.

HD 84123.—This star was listed by Bidelman (1951*a*) as a star in which all the lines are abnormally weak. It was classified by him as F0p. There is no parallax of this star available.

HD 106223.—Bidelman (1951*b*) concluded that this star showed the (spectral) characteristics of the A-type subdwarfs.

λ *Boo.*—This star was originally described by Morgan, Keenan, and Kellman (1943) as a star with a general weakening of lines. It has a trigonometric parallax of $+0''.043$, giving $M = 2.4$.

HD 161817.—This star was chosen because of its extremely high velocity of -363 km/sec (Slettebak 1952*b* and other references given there; cf. Roman 1955) and because Slettebak considered that "its spectral characteristics place it somewhere between a main-sequence star and a subdwarf." No trigonometric parallax is available. The question of spectroscopic parallaxes will be discussed later.

29 Cyg.—This star was listed by Slettebak (1952*a*) as having general weakening of lines in its spectrum. He classified it as A2p (Slettebak 1954). From the Yale *Catalogue* (Jenkins 1952) its parallax is $+0''.033$, giving $M = 2.6$. If the star were really of type A2, it would be located about 1 mag. below the main sequence. Slettebak believed that, although it was not a true subdwarf, it was tending in this direction.

The standard star used was the main-sequence A star 95 Leonis which had already been used by Chamberlain and Aller (1951) in their investigation. Two spectra of each of these six stars were obtained with the coudé grating spectrograph of the McDonald Observatory during April and May, 1953. The dispersions used were $8\frac{1}{2}$ A/mm for 95 Leo, 29 Cyg, and λ Boo and 18 A/mm for HD 84123, HD 161817, and HD 106223. The calibration technique was similar to that described in previous papers (cf. Burbidge and Burbidge 1954). The spectra were traced with the Beals microphotometer at the Yerkes Observatory, and the reductions and analysis were carried out at the Mount Wilson and Palomar Observatories and the California Institute of Technology. In the sharp-line stars the lines were treated as triangles, but in 29 Cyg, HD 106223, and λ Boo the profiles were plotted and the areas determined. In Table 1 are given mean values of $-\log W/\lambda$ for each star.

II. ATMOSPHERIC PARAMETERS AND THE CURVES OF GROWTH

Comparison of our equivalent widths for 95 Leo and HD 161817 with those published by Chamberlain and Aller for 95 Leo and with an unpublished list for HD 161817, kindly loaned to us by Dr. J. L. Greenstein, shows that there is a systematic difference in the sense that the McDonald equivalent widths are larger than the Mount Wilson values. There appears to be a constant scale factor which is independent of line strength, and

TABLE 1

EQUIVALENT WIDTHS

λ	−log W/λ					
	HD 84123	95 Leo	HD 106223	λ Boo	HD 161817	29 Cyg
Mg I						
4167.27	4.55	4.90	.....	.....	.....	.....
4702.99	4.59	.....	.....	.....	.....	.....
Mg II						
4481.23	4.29	4.10	.....	4.65	4.21	4.33
Al I						
3944.01	4.30	4.61	4.34	.....	4.56	.....
Ca I						
4226.73	4.20	4.49	4.22	4.81	4.26	4.18
4302.53	.....	4.86	.....	.....	.....	.....
4454.78	4.77	.....	.....	.....	.....	4.56
Ca II						
3933.66	.....	3.46	3.35	3.98	3.29	3.40
Sc II						
4246.83	4.37	4.60	.....	.....	4.52	4.62
4374.46	.....	4.88	.....	.....	.....	.....
4415.56	.....	4.91	.....	.....	.....	.....
Ti II						
4290.22	.....	4.44	.....	.....	.....	4.67
4294.10	.....	4.53	.....	.....	.....	.....
4300.05	.....	4.47	.....	.....	.....	4.42
4301.93	.....	4.60	.....	.....	.....	.....
4386.86	.....	4.94	.....	.....	.....	.....
4395.03	.....	4.48	.....	.....	.....	4.48
4443.80	.....	4.51	.....	.....	.....	4.40
4450.49	.....	4.73	.....	.....	.....	.....
4468.49	.....	4.57	.....	.....	.....	4.57
4501.27	.....	4.56	.....	.....	.....	4.68
4563.76	.....	4.54	.....	.....	.....	4.68
4571.97	.....	4.55	.....	.....	.....	4.55
Cr I						
4254.35	4.46	4.73	4.69	.....	4.84	.....
4274.80	4.45	4.79	4.73	.....	4.96	.....
Cr II						
4252.62	5.25	5.05	.....	.....	.....	.....
4261.92	4.96	4.89	.....	.....	.....	.....
4555.02	.....	5.05	.....	.....	.....	.....
4588.22	.....	4.79	.....	.....	.....	.....
4592.09	.....	4.88	.....	.....	.....	.....
4616.64	.....	5.06	.....	.....	.....	.....
4618.83	.....	4.78	.....	.....	.....	.....
4634.11	.....	4.91	.....	.....	.....	.....
Mn I						
4030.76	4.28	4.76	.....	.....	.....	.....
4033.07	4.38	4.81	.....	.....	.....	.....
4034.49	4.59	5.04	.....	.....	.....	.....
4041.36	4.67	5.21	.....	.....	.....	.....

TABLE 1—*Continued*

λ	−log W/λ					
	HD 84123	95 Leo	HD 106223	λ Boo	HD 161817	29 Cyg
Fe I						
3930.30						4.34
3998.05		4.93				
4005.25	4.18	4.63	4.38	4.75	4.59	4.43
4009.72		5.26				
4017.15		5.37				
4021.87	4.66	5.22			4.97	
4044.61		5.40				
4045.82	4.10	4.32	4.23	4.64	4.39	4.35
4062.44		4.83				
4063.60	4.21	4.56	4.30	4.53	4.48	4.27
4067.98	4.72	5.27			4.96	
4071.74	4.29	4.60	4.24	4.74	4.49	4.43
4132.06	4.35	4.70	4.35		4.72	
4132.90	4.72				5.31	
4143.42		4.92			4.67	
4143.87		4.80			4.77	
4157.79	4.66	5.32				
4175.64	4.66	5.04	4.76		5.24	
4184.90		5.54				
4187.04		4.89			4.92	
4187.80		4.84			4.84	
4202.03						4.69
4210.35	4.62	5.18				
4216.19	4.83					
4219.36	4.72	4.94				
4222.22	4.71	5.19				
4227.43	4.45	4.73				
4233.61		5.12			4.95	
4235.94	4.39	4.72	4.54		4.78	
4247.43		4.99			5.15	
4248.23	5.18	5.27				
4250.12	4.58	4.84			4.99	
4250.79	4.43	4.76			4.77	
4260.48	4.30	4.63	4.56	4.84	4.69	4.66
4271.16		4.77				
4271.76		4.52				
4282.41		4.94	4.71		4.99	
4307.91						4.21
4375.93	4.65					
4383.55	4.22	4.54	4.18	4.65	4.41	4.33
4388.41		5.56				
4404.75	4.22	4.65	4.30	4.86	4.52	4.45
4415.12	4.30	4.70	4.38	4.93	4.61	4.69
4427.31	4.67	5.44	4.95			
4442.34	4.72	5.45			5.14	
4447.72	4.78	5.31			5.19	
4466.55	4.56	5.06				
4476.02	4.61	5.03				
4494.57	4.68	5.07			4.94	
Fe II						
3938.29	4.48				4.65	
4002.07		5.26				
4024.55		4.80			5.06	
4044.01		5.33				
4122.64		4.96			5.20	
4128.74		5.10			5.36	

TABLE 1—*Continued*

λ	−log W/λ					
	HD 84123	95 Leo	HD 106223	λ Boo	HD 161817	29 Cyg
4173.45	4.35	4.47	.....	.....	4.62	.....
4178.86	4.41	4.69	4.75	.....	4.69	.....
4233.17	4.22	4.44	4.32	4.89	4.40	4.51
4273.32	4.57	4.70	.....	.....	5.01	4.91
4296.57	4.60	4.66	.....	.....	4.94	.....
4303.17	4.36	4.54	.....	.....	4.72	.....
4351.76	.....	.....	4.43	.....	4.46	.....
4369.40	.....	5.07	.....	.....	.....	.....
4385.38	4.47	4.53	.....	.....	4.80	.....
4416.82	4.52	4.60	.....	.....	4.80	4.90
4472.92	4.95	5.03	.....	.....	5.29	.....
4489.18	.....	4.65	.....	.....	4.93	.....
4491.40	4.75	4.67	.....	.....	4.87	4.79
4508.28	4.53	4.59	.....	.....	4.70	.....
4515.34	4.59	4.59	.....	.....	4.87	.....
4520.23	4.70	4.82	.....	.....	4.91	4.84
4522.63	4.44	4.50	.....	.....	4.67	4.61
4541.52	4.81	4.78	.....	.....	4.98	.....
4549.4	4.13	.....	4.37	4.78	4.19	4.31
4555.89	4.54	4.61	.....	.....	4.66	.....
4576.33	4.81	4.91	.....	.....	5.04	.....
4582.84	4.81	4.94	.....	.....	5.05	.....
4583.83	4.34	4.46	.....	.....	4.50	.....
4620.51	.....	5.16	.....	.....	.....	.....
4629.34	4.50	4.71	.....	.....	4.75	4.65
4635.33	.....	5.19	.....	.....	.....	.....
4666.75	.....	5.13	.....	.....	.....	.....
Sr II						
4077.71	4.18	4.39	4.15	4.82	4.32	4.35
4215.52	4.28	4.47	4.31	.....	4.40	4.42
Y II						
4177.54	4.43	4.53	.....	.....	.....	.....
4374.94	.....	4.62	.....	.....	.....	.....
4398.02	4.84	5.09	.....	.....	.....	.....
Zr II						
4208.99	4.85	5.13	.....	.....	.....	.....
Ba II						
4554.03	4.37	4.53	4.68	.....	4.74	.....

hence it cannot be due to differences in the placing of the continuum. It might be due to an error in the slope of the calibration-curve (e.g., an intermittency effect) or to Eberhard effect in our plates, which were developed for $3\frac{3}{4}$ minutes in D19 at 68° F. If the latter is the case, we should not expect it to be present in the spectra of 29 Cyg, λ Boo, and HD 106223, in all of which the lines are broadened by rotation and are shallow.

By using the method of analysis described in the following paragraphs, it is probable that we have removed most of the effects on the abundances of this scale factor.

The abundances have been derived by the method of the curve of growth rather than by that of model atmospheres and computed equivalent widths. The limitations and uncertainties of this method are well known, and the effect for strong lines will be discussed

later. Values for the horizontal co-ordinate of the curve, log η_0, were taken from the work of Greenstein (1948) on τ UMa and of Buscombe (1951) on γ Gem. The apparent scale factor in the equivalent widths might, since it appears to be constant, appear as a bodily vertical shift of the curve, i.e., by using it, a spurious total effective velocity v would be obtained. To try to eliminate this, all the element abundances have been obtained relative to 95 Leo, through the following procedure. Curves of growth were first plotted for 95 Leo, using values of log η_0 determined from (*a*) γ Gem and (*b*) τ UMa, and abundances in 95 Leo were obtained relative to these three stars. This same procedure was carried out for each of the five other stars. The abundances, A, in these stars were then referred to those in 95 Leo by dividing them, for each separate element, by the ratio $A(95\ \text{Leo})/A(\gamma\ \text{Gem})$ and $A(95\ \text{Leo})/A(\tau\ \text{UMa})$, respectively. By this means it is hoped that systematic differences in equivalent-width measurement between us, Buscombe, and Greenstein have been eliminated. This will also eliminate spurious effects caused by the anomalously low apparent abundances of certain elements found by Greenstein for τ UMa, but it allows us to retain some idea of the random errors in fitting sets of points onto curves of growth.

The Theoretical Curve and the Damping Parameter

The theoretical curve of growth was chosen from the set computed by Wrubel (1949) for a Milne-Eddington model for various values of $B^{(0)}/B^{(1)}$, which is a function of temperature and pressure, and of the damping parameter, a. Preliminary values of T_{eff} and p_e obtained from inspection of the spectra suggested that $B^{(0)}/B^{(1)}$ was near to $\frac{1}{3}$ for 95 Leo and the other five stars (it is also $\frac{1}{3}$ for γ Gem). This value was confirmed when T_{eff} and p_e were derived from the subsequent analysis. In the usual notation (Aller 1953), $a = \delta'/\Delta\nu_0$. At the relatively low gas pressures of stars in this temperature range it is found by calculation that, for lines of Ca II, radiation damping predominates; this is probably true for other intermediate and heavy elements. In wave-length units the classical damping constant gives $\delta'_{\text{cl}}(\lambda) = \gamma_{\text{cl}}(\lambda)/4\pi = 0.000059$ A. For total effective velocities 3 and 4 km/sec, respectively, $\Delta\lambda_0 = 0.040$ and 0.053. Thus $a = 0.0015$ or 0.0011.

In Figure 1 the curve of growth for lines of Fe I, Fe II, Ti II, and Cr II in 95 Leo is shown, and in Figure 2 a composite curve for lines in those stars having appreciable underabundances is shown. Lines of Fe II have been given here for 29 Cyg and HD 161817, but for HD 106223 and λ Boo, where very few Fe II lines could be measured, we have shown the plot for Fe I lines.

The lines of Fe I and Fe II in 95 Leo, HD 84123, and HD 161817 fit quite well onto the curve of growth for $B^{(0)}/B^{(1)} = \frac{1}{3}$ and log $a = -2.6$. These stars are those with the greatest number of lines and hence those which best define the curve. Consequently, this curve was used for all the stars and for all the elements except magnesium. In his analysis of γ Gem, Buscombe mentions a computation for Mg II λ 4481 which leads to a value of the damping constant of three times the classical value. For a total effective velocity of 3 km/sec we find, then, that log $a = -2.4$ for this line, although Buscombe put log $a = -1.4$ to derive log η_0. In general, this line is quite strong, so that the derived abundance depends critically on log a. We have used log $a = -2.2$ in all the stars for this element. The abundance determination relative to τ UMa is further complicated by the high excitation potential of λ 4481, so that the curve-of-growth method is less likely to be valid. That the abundance determination of magnesium depends sensitively on the values of log a and the high-excitation effect can be shown as follows. If the published values of log η_0 for Mg II 4481 in τ UMa and γ Gem are used, together with the appropriate values of T_{exc} and κ_λ, we find that the abundance of magnesium in τ UMa is apparently forty times that in γ Gem; this is undoubtedly incorrect.

Although the relative abundances of magnesium in all the stars are ultimately referred to that in 95 Leo, so that some of the uncertainties are minimized, the results for this element should be given less weight than for the others.

The Velocity

The most determinate value of the total effective velocity v was obtained by using the Fe I and Fe II lines in 95 Leo. For this star, $v = 4$ km/sec, which is in agreement with the average value found by Buscombe for γ Gem and by Greenstein for τ UMa. This implies rather a large value for a main-sequence star, and this may be due in part to the scale factor mentioned earlier. The velocity v cannot be determined accurately for most of the other stars, because of the smaller number of lines available; therefore, v was set equal to 4 km/sec for all the stars. Thus, in deriving relative abundances by means of the equation (Buscombe 1951)

$$\Delta \log N_r = \Delta \log \eta_0 + \chi \Delta \theta_{\text{exc}} + \Delta \log \kappa_\lambda + \Delta \log v , \tag{1}$$

$\Delta \log v$ was put equal to zero. This procedure may introduce an error, which is believed to be small, into the abundance determinations.

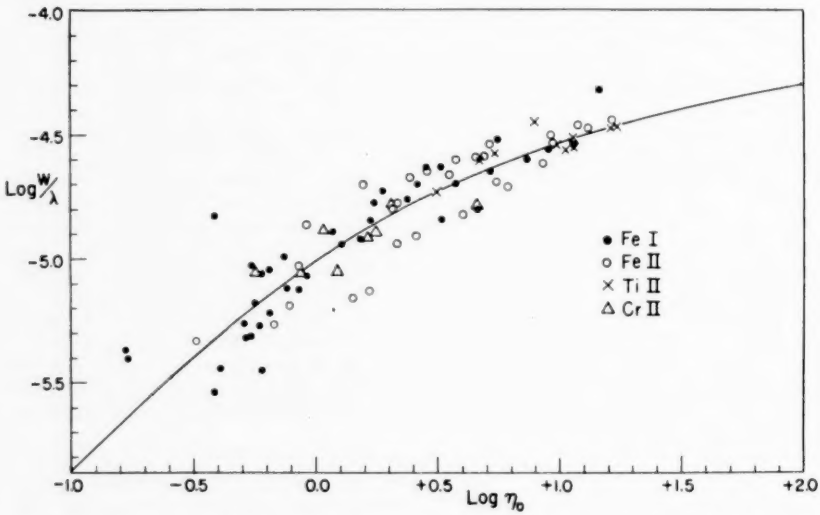

FIG. 1.—Curve of growth for Fe I, Fe II, Ti II, and Cr II in 95 Leo. The theoretical curve for $B^{(0)}/B^{(1)} = \frac{1}{3}$ and $\log a = -2.6$ is plotted.

Ionization and Excitation Temperatures, Electron Pressure

Since the opacity κ_λ depends sensitively on T_{ion} and p_e, these parameters must be derived as accurately as possible. A method of successive approximations was used as follows. Examination of the spectra suggested that T_{eff} for all the stars lay in the range 7400°–8500°. From the number of visible Balmer lines and the appearance of the wings of Hγ and Hδ preliminary estimates of p_e were made. The horizontal shifts to fit the Fe I and Fe II points onto the curves of growth then yielded estimates of the differences in ionization temperature, T_{ion}, between the different stars and γ Gem and τ UMa. For τ UMa the parameters given by Greenstein were used; for γ Gem we took $\theta_{\text{exc}} = 0.63$, $\theta_{\text{ion}} = 0.58$, and $\log p_e = 2.2$. This value for T_{ion} is lower than that used by Buscombe, slightly higher than that used by us in the analysis of α^2 CVn, and near to that used by Aller. Values of T_{exc} for the five stars were tried until consistent values of T_{ion} for both

τ UMa and γ Gem were found. With the temperatures determined in this way, p_e was calculated from the Stark profiles of the hydrogen lines from the formula (Unsöld 1938)

$$p_e = A\,(\Delta\lambda)\,(\Delta\lambda)^{5/2}\left\{1 + 4\,\frac{\kappa_\lambda}{\kappa}\,(1 - e^{-h\nu/kT})\left(\frac{h\nu}{kT}\right)^{-1}\right\}\frac{K_2 T}{640C},$$

where $C = 4.42 \times 10^{-17}(\mathrm{H}\gamma)$ and $3.09 \times 10^{-17}(\mathrm{H}\delta)$. Mean values of $A(\Delta\lambda)(\Delta\lambda)^{5/2}$ over regions of the profile where this quantity is reasonably constant were used. The adopted value of p_e was the mean of that obtained from Hγ and Hδ and that from the Inglis-Teller formula for the last resolvable Balmer line. Finally, T_{ion} was checked by using the Fe I and Fe II points and, where possible, the Cr I, Cr II, Ca I, Ca II, Mg I, and Mg II points also on the curve of growth. The value of κ_λ was derived from a plotted network of values which have been calculated by Greenstein (1948). The final parameters are given in Table 2.

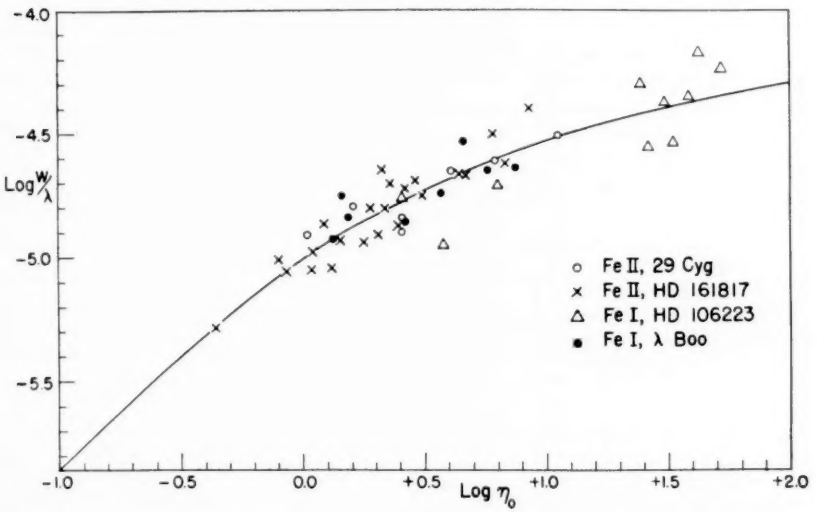

FIG. 2.—Composite curve of growth for Fe II in 29 Cyg and HD 161817 and for Fe I in HD 106223 and λ Boo. The theoretical curve for $B^{(0)}/B^{(1)} = \frac{1}{3}$ and $\log a = -2.6$ is plotted.

TABLE 2

ATMOSPHERIC PARAMETERS

	HD 84123	95 Leo	HD 106223	λ Boo	HD 161817	29 Cyg
θ_{exc}	0.81	0.68	0.81	0.73	0.73	0.70
θ_{ion}	0.74	0.62	0.75	0.67	0.66	0.67
log p_e	1.6	2.2	1.4	2.0	1.8	2.1
log κ_λ	−0.24	+0.34	−0.44	+0.12	+0.01	+0.20
T_{eff} ($1.1 \times T_{\mathrm{ion}}$)	7500°	9000°	7400°	8300°	8400°	8300°

III. RELATIVE ABUNDANCE RATIOS

Values of $\log N/N_{95}$ for iron (the ratio of the abundance of iron relative to that in 95 Leo), as derived via γ Gem and τ UMa and by means of the Fe I and Fe II lines separately, are listed in the last line of each part of Table 3. The headings "γ" and "τ" refer to quantities derived via γ Gem and τ UMa, respectively. They were obtained by means of equation (1), together with the Saha equation in the case of the Fe I lines (in all the stars iron is nearly all in the singly ionized state). They were converted from the abundances relative to γ Gem and τ UMa, also given in the table, as described in Section II.

The final mean abundance ratios for all elements, relative to 95 Leo, are listed in Table 4. The following points should be noted:

a) The abundance ratios for aluminum, calcium, strontium, and barium are based on resonance lines and do not depend on T_{exc}.

b) The abundance ratios which have been derived from lines of ionized elements do not depend critically on p_e and T_{ion}, since in all the stars analyzed here these elements

TABLE 3

ABUNDANCES OF IRON DERIVED VIA γ GEM AND τ UMA

	HD 84123		HD 106223		λ Boo		HD 161817		29 Cyg	
	γ	τ	γ	τ	γ	τ	γ	τ	γ	τ
	Fe I									
$\Delta \log \eta_0+\chi\Delta\theta$...	+1.24	−1.62	+1.14	−1.72	−0.10	−3.00	+0.30	−2.56	+0.64	−2.24
$\Delta \log \eta_0+\chi\Delta\theta+\Delta \log \kappa_\lambda$.....	+0.58	−0.24	+0.28	−0.54	−0.40	−1.26	− .11	−0.93	+ .42	−0.42
$\log N/N_{\gamma,\tau}$.....	−0.10	−0.53	−0.52	−0.96	−1.07	−1.55	− .52	−1.11	− .35	−0.81
$\log N/N_{95}$.....	−0.11	+0.03	−0.53	−0.40	−1.08	−0.99	−0.53	−0.55	−0.36	−0.25
	Fe II									
$\Delta \log \eta_0+\chi\Delta\theta$...	+0.74	−1.98	+0.40	−2.10	−0.81	−3.18	−0.06	−2.72	−0.02	−2.72
$\Delta \log \eta_0+\chi\Delta\theta+\Delta \log \kappa_\lambda$.....	+ .08	−0.60	− .46	−0.92	−1.11	−1.44	− .47	−1.09	− .24	−0.90
$\log N/N_{\gamma,\tau}$.....	+ .08	−0.60	− .46	−0.92	−1.11	−1.44	− .47	−1.09	− .24	−0.90
$\log N/N_{95}$.....	+0.07	−0.04	−0.47	−0.36	−1.12	−0.88	−0.48	−0.53	−0.25	−0.34

are almost completely in the singly ionized state (although considerable second ionization of strontium occurs in γ Gem).

c) The curve-of-growth method is likely to lead to errors in the case of strong lines such as those of Ca II and Sr II, where the abundance also depends critically on $\log a$. The tendency, seen in Table 4, for a correlation between derived abundance and excitation potential for magnesium, calcium, and strontium may be due to this. Problems in the determination of the abundance of magnesium by using λ 4481 have already been discussed.

d) The upper limit to the abundance of barium in λ Boo was obtained by setting the upper limit to the equivalent width of Ba II 4554 (which was not observed in this star) equal to the smallest measured Fe I equivalent width in λ Boo.

e) It may be asked how sensitive are the derived abundances to errors in the at-

mospheric parameters. Consider the extreme case of λ Boo. Suppose that there is zero turbulent velocity in this star ($v = v_{\text{thermal}}$), while v is still 4 km/sec in 95 Leo and γ Gem, and that κ_λ is as high as in γ Gem because both stars have the same T_{ion} and p_e. Then the abundance ratio for iron will be increased to 0.3 instead of 0.1. Alternatively, κ_λ might be as high as that in γ Gem if log p_e were still 2.0 or 2.1 but θ_{ion} were 0.9 or 0.8. Then T_{exc} could also be low, and the abundance ratio for iron could be as high as 0.8. So high a p_e and so low a T_{ion} would imply a very large p_g and an effective gravity log $g \cong 6$. Thus the star would have to be an "intermediate white dwarf" with a trigonometric parallax of at least 1″, or three times its measured value, which cannot be correct. Further, the color class (Slettebak 1954) would appear to rule out so low a temperature. We conclude that, in order to increase the abundance of iron to normal, the star should have T_{ion} and p_e corresponding to a slightly higher T_{eff} than indicated by the color class, a zero turbulent velocity, and an abnormally low T_{exc}. Such an unusual combination is very unlikely.

TABLE 4

ABUNDANCES RELATIVE TO 95 LEO

Element	HD 84123	29 Cyg	HD 161817	HD 106223	λ Boo	HD 19445	HD 140283
Mg	0.9	0.3	0.4	.....	0.01	.....	.....
Al	2.4	.....	0.5	1.0	.....	.....	.....
Ca	0.4	.8	2.1	0.9	.03	0.04	0.02
Sc	1.8	.6	0.4	.....	.....	.....	.....
Ti	.....	.6	.....	.....	.....	.....	.....
Cr	0.6	.....	0.2	0.1	.....	.....	.....
Mn	1.1	.....	.....	.....	.....	.....	.....
Fe	1.1	.5	0.3	0.4	.1	0.17	0.09
Sr	1.6	0.7	0.6	0.9	.03	.....	.....
Y	0.6	.....	.....	.....	.....	.....	.....
Zr	0.9	.....	.....	.....	.....	.....	.....
Ba	0.5	.....	0.09	0.03	≦0.05	.....	.....

IV. DISCUSSION

If we use the categories given at the beginning of this paper, we may consider that, from the point of view of category *a*, the purest members of population II among the homogeneous dwarf stars are stars which lie farthest below the population I main sequence. It is not yet clear whether the extreme subdwarfs do themselves define a second main sequence. From the point of view of category *b*, the most extreme cases are those of stars which have the largest underabundance ratios of the intermediate elements, the metals, and the heavy elements. From the point of view of category *c*, stars with the highest velocities and with orbits which pass through the galactic bulge are the most extreme examples of population II. From the point of view of category *d*, it may be tentatively suggested that stars having the smallest rotations are those nearest to population II in this category.

The relative abundances of all the elements are given in Table 4, and we have also included in this table the results of Chamberlain and Aller for HD 19445 and HD 140283. Their results for calcium, which have been obtained by using a model stellar atmosphere, may be more reliable than ours for this element. The stars have been arranged in order of their population II characteristic category *b*. It is reasonable to suppose that there is a roughly steady progression between HD 84123, which has more nearly the characteristics of 95 Leo as far as category *b* is concerned, and λ Boo, HD 19445, and HD 140283, which have underabundance ratios of about 30 for calcium and about 10 for iron. The results for HD 106223 and λ Boo suggest that the trend of the underabundance ratio

for barium is from about unity or slightly less in HD 84123 to values ≥ 20 for the most extreme cases studied here.

If we attempt to classify each star individually according to each of categories *a*–*d*, it is clear that HD 19445 and HD 140283 have more of the properties characteristic of population II than have the others. They have absolute magnitudes $M_{v_0} = +5.0$ and $+4.9$, respectively; these magnitudes have been derived by using the Mount Wilson spectroscopic parallaxes (Adams, Joy, Humason, and Brayton 1935). The magnitudes suggest that they lie intermediate between the main-sequence stars and the white dwarfs. However, it is worth remarking that the spectroscopic parallaxes may not be so well determined as has been thought. The use of the line strength of, for example, such a high-excitation line as Mg II 4481 in deriving the parallax of a star thought originally to be of type A4 but which later turned out to have a temperature corresponding to F6 is unreliable. In HD 19445 the trigonometric and spectroscopic parallaxes agree well, but in HD 140283 the trigonometric parallax, though it is small and consequently uncertain, is only one-third of the spectroscopic value. The total velocities of these stars are given by Miss Roman (1954) as 216 and 236 km/sec (assuming that $M = +5$) and the corresponding *z*-velocities are -73 and -19 km/sec. They both have narrow line profiles corresponding to small rotational velocities.

As far as its chemical composition (category *b*) is concerned, λ Boo can be grouped with these two stars, but it has $M = +2.4$, and its total space velocity is only 28 km/sec. Also it has a rotational velocity $v \sin i = 95$ km/sec (Slettebak 1954). HD 106223 also has considerable, but not extreme, underabundance ratios. Its absolute magnitude is not known, but if we assume that it has the same luminosity as λ Boo and 29 Cyg, its total space velocity is only 41 km/sec. From our plates the value of $v \sin i$ appears to be very similar to that of λ Boo, i.e., ~100 km/sec. As far as category *b* is concerned, HD 161817 is only of intermediate population II, its absolute magnitude is unknown, it has a very large space velocity (radial velocity $= -363$ km/sec; if the absolute magnitude were $+2.5$, the *z*-component would be -165 km/sec) and a small rotational velocity. Thus only in categories *c* and *d* can it be considered as a population II star. 29 Cyg has small underabundance ratios, its absolute magnitude is $+2.6$, its total space velocity is 22 km/sec, and $v \sin i = 85$ km/sec (Slettebak 1954). Thus only possibly in categories *a* and *b* can it be supposed to have even intermediate characteristics of population II. HD 84123 has practically normal chemical composition except for a possibly significant underabundance ratio for the heavy elements. The parallax is not known, the radial velocity is $+16.3$ km/sec, and the rotation is fairly small.

Thus it seems very clear that we must be extremely careful when we use the term "population II" to describe a star which has been found, so far, to have only one or two of the characteristics of this population listed in categories *a*–*d*, since it may not show the other characteristics to the same extent.

The occurrence of true *main-sequence* population II stars (having population II characteristics *b* and *c*), but with magnitudes as high as $+2.5$ and temperatures of about 8000°, in the solar neighborhood would be expected to be much rarer than that of later-type subdwarfs, if the globular-cluster, color-magnitude diagrams can be taken as a guide. In them the bulk of the main sequence comes to an end at $M = +3.5$; there is a small density of stars, whose evolutionary history is not understood, extending the main sequence to about $M = +2$ in M3 (Sandage 1953). In view of the high *z*-velocity of HD 161817, the possibility that it is similar to stars on the horizontal branch of globular-cluster diagrams cannot be entirely ruled out.

Having shown that there are intermediate types of stars between populations I and II, we shall consider as of some interest the evolutionary problems relating to some of the subclassifications. Some discussion of theoretical ideas underlying categories *a*, *b*, and *d* will be given.

Variations of chemical composition can be interpreted as arguments in support of

theories which suppose that all the elements have been synthesized in the interiors or the atmospheres of stars (Salpeter 1952; Hoyle 1954; Cameron 1955; Fowler, Burbidge, and Burbidge 1955*a*, *b*). The alternative hypothesis, that all the elements were synthesized in a short time in an ylem process, can explain gradations in chemical composition between the two extremes of populations only if it is supposed that, at the time of star formation, there was a powerful mechanism of element separation; the implications of this will not be discussed here. On the stellar-synthesis theory the stars with the most extreme abundance anomalies (λ Boo, HD 19445, HD 140283) were condensed out of material which had already gone through an earlier synthesis process in which some, but not many, of the metals, etc., were synthesized. (We have no information as to whether or not stars with even greater underabundance ratios are presently in existence.) This suggests that there was an epoch earlier than that in which the extreme stars of population II were formed, in which massive stars (perhaps 10–20 $M_\odot$) were formed. These could go through their whole evolutionary sequence in a total time scale of $\ll 10^9$ years; their contractional time scale is roughly proportional to M^{-3} and depends on the relative abundances of hydrogen and the other elements, while the time scale on the main sequence goes roughly as M^{-5}. Alternative possibilities for evolution in this very early epoch are that material ejected after synthesis in other galaxies or proto-galaxies contaminated the material out of which the extreme population II stars condensed or that the massive condensations of pure hydrogen formed in an epoch before the galaxies in a cluster began to separate. This latter possibility could be further investigated if the dynamical conditions in the turbulent gas at this epoch were specified.

The iron abundance is reduced in the extreme cases by a factor of about 10. This suggests that such stars condensed out of material processed in massive stars, only about 10 per cent of which went through the process suggested by Hoyle, in which the metal peak was synthesized in an equilibrium phase, as compared to the proportion of evolving stars which produced the elements out of which population I stars condensed. A similar argument suggests that only about 3 per cent of these stars, relative to those which produced population I abundances, have gone through the neutron-capture processes or the reactions involving α-particles suggested by Fowler *et al.* and by Hoyle, which produced calcium and the other intermediate elements.

The occurrence of stars with intermediate chemical abundances (29 Cyg, HD 161817, and HD 106223) suggests that element-synthesis processes have been going on continuously and that the relative numbers of stars which are particularly efficient in the synthesis processes are dependent on both the stellar masses and the ages.

From the scanty sample of stars studied here, it is difficult to determine the run of the underabundance ratios strontium/iron and barium/iron, but it may be that there is a tendency for the barium/iron ratio to decrease as we go to stars of lower metal abundances. On stellar-synthesis theories, strontium and barium are produced by neutron-source and neutron-capture processes which arise in a shell already containing the metals. At its maximum efficiency a process of this kind converts about 40 per cent of the metals to the very heavy elements, which can be built to about one thousand times the abundances in a normal population I main-sequence star. Thus, if the stars have only about 10 per cent of the normal metal abundances, the heavy elements will be built to only about one hundred times the population I abundances. Also, if the barium/iron ratio is lower for lower metal abundances, the relative number of massive stars in which neutron sources have arisen may be smaller than the corresponding numbers at the epochs and galactic locations in which the population I abundances have been synthesized.

It is well known that the position of a star on the H-R diagram is intimately connected with its chemical composition, and Reiz (1954) has shown that theoretical models in which $z = 0$ (star composed completely of hydrogen and helium) will tend to show subdwarfish characteristics. Although there are a number of uncertainties involved in

fitting the theoretical models with the observational data, it is possible that such models with $M \simeq 0.8\ M_\odot$–$1.3\ M_\odot$ lie in the region of the H-R diagram near to that occupied by subdwarfs with effective temperatures in the range ~6500°–7500°, i.e., about 1.5 mag. below the main sequence. Nothing is known observationally concerning the hydrogen/helium ratio in these stars. In principle, this ratio can be derived in two ways. The first is to use the contractional evolutionary stages, with an upper limit to the time scale ($< 5 \times 10^9$ years), in a way similar to that described for the sun by Henyey, Lelevier, and Levée (1955). For a given chemical composition and mass, these tracks are not unique (i.e., the star has no memory of its past history), but the end-points for gravitational contraction are fixed, and these are, of course, the beginning points for nuclear-energy sources. It may be that the method of Henyey *et al.* will be fairly simple to use to determine the hydrogen/helium ratio within quite narrow limits. The second method is just to consider the static structure of the star when it is burning on nuclear-energy sources in the subdwarf region of the H-R diagram. If the mass and metal content are accurately known, trial variations in the hydrogen/helium ratio should enable the true value to be determined.

As far as rotational properties (category *d*) are concerned, it has been suggested by Greenstein (Greenstein and Cuffey 1954; Greenstein 1956) that there is a correlation of population II characteristics *b* and *d*, in that stars with high velocities tend to have small rotations. If category *b* is also considered, then from our analysis we see that two stars (HD 106223 and λ Boo) with chemical compositions intermediate or of extreme population II character have values of $v \sin i \simeq 100$ km/sec. These values may be compared with the mean value $v \sin i = 136$ km/sec determined for main-sequence population I stars in the spectral range A3–A7 by Slettebak (1955). If a star has evolved from a homogeneous configuration with a smaller radius, we should expect its present rotation to be smaller than its initial value. Therefore it would seem reasonable to suppose that 29 Cyg, HD 106223, and λ Boo are "main-sequence" configuration stars. It would be interesting to know whether stars in the thinly populated extension of the main sequence in M3 (Sandage 1953) have appreciable rotations. The rotational properties of population II stars may assume great evolutionary significance if the exceptions to correlations between classifications *b*, *c*, and *d* can be conclusively established.

The observational material was obtained while the authors were working at the Yerkes and McDonald Observatories. The reductions and analysis were carried out at the Mount Wilson and Palomar Observatories and at the California Institute of Technology. We are indebted to both Dr. J. L. Greenstein and Dr. A. R. Sandage for helpful and interesting discussions and also to Dr. Greenstein for making available to us a copy of his paper on stars of low luminosity (Greenstein 1956).

REFERENCES

Adams, W. S., Joy, A. H., Humason, M. L., and Brayton, A. M. 1935, *Ap. J.*, **81**, 187.
Aller, L. H. 1953, *Astrophysics* (New York: Ronald Press), p. 252.
Baade, W. 1944, *Ap. J.*, **100**, 137.
Bidelman, W. P. 1951*a*, *Ap. J.*, **113**, 304.
———. 1951*b*, *A.J.*, **55**, 213.
Burbidge, G. R., and Burbidge, E. M. 1954, *Ap. J.*, **120**, 76.
———. 1956, *ibid.*, in press.
Buscombe, A. W. 1951, *Ap. J.*, **114**, 73.
Cameron, A. G. W. 1955, *Ap. J.*, **121**, 144.
Chamberlain, J. W., and Aller, L. H. 1951, *Ap. J.*, **114**, 52.
Fowler, W. A., Burbidge, G. R., and Burbidge, E. M. 1955*a*, *Ap. J.*, **122**, 271.
———. 1955*b*, *Ap. J. Suppl.*, **2**, 167.
Greenstein, J. L. 1948, *Ap. J.*, **107**, 151.
———. 1956, *Third Berkeley Symposium on Statistics* (Berkeley: University of California Press) (in press).
Greenstein, J. L., and Cuffey, J. 1954, *Pub. A.S.P.*, **66**, 187.

Henyey, L. G., Lelevier, R., and Levée, R. D. 1955, *Pub. A.S.P.*, **67**, 154.
Hoyle, F. 1954, *Ap. J. Suppl.*, **1**, 121.
Jenkins, L. 1952, *General Catalogue of Trigonometric Stellar Parallaxes* (New Haven: Yale University Observatory).
Morgan, W. W., Keenan, P. C., and Kellman, E. 1943, *Atlas of Stellar Spectra* (Chicago: University of Chicago Press).
Reiz, A. 1954, *Ap. J.*, **120**, 342.
Roman, N. G. 1950, *Ap. J.*, **112**, 554.
———. 1952, *ibid.*, **116**, 122.
———. 1954, *A.J.*, **59**, 307.
———. 1955, *Ap. J. Suppl.*, **2**, 195.
Salpeter, E. E. 1952, *Ap. J.*, **115**, 326.
Sandage, A. R. 1953, *A.J.*, **58**, 61.
Schwarzschild, M., and Schwarzschild, B. 1950, *Ap. J.*, **112**, 248.
Schwarzschild, M., Spitzer, L., and Wildt, R. 1951, *Ap. J.*, **114**, 398.
Slettebak, A. 1952*a*, *Ap. J.*, **115**, 575.
———. 1952*b*, *ibid.*, p. 576.
———. 1954, *ibid.*, **119**, 146.
———. 1955, *ibid.*, **121**, 653.
Unsöld, A. 1938, *Physik der Sternatmosphären* (Berlin: Springer), p. 241.
Weizsäcker, C. F. von. 1951, *Ap. J.*, **114**, 165.
Wrubel, M. H. 1949, *Ap. J.*, **109**, 66.

ANOMALOUS ABUNDANCES OF MANGANESE, STRONTIUM, AND EUROPIUM IN HD 151199

G. R. BURBIDGE
Mount Wilson and Palomar Observatories
Carnegie Institution of Washington
California Institute of Technology

AND

E. MARGARET BURBIDGE*
Kellogg Radiation Laboratory
California Institute of Technology

Received February 6, 1956

ABSTRACT

HD 151199 is a peculiar A-type star with the relatively large space velocity of 69 km/sec. Abundances of the elements Mg, Si, Ca, Cr, Mn, Fe, Sr, Ba, and Eu in this star have been determined relative to the standard main-sequence star 95 Leo. It is found that all the abundances are normal except for Mn, Sr, and Eu, which have overabundance ratios of 9, 65, and 130, respectively. It is pointed out that these anomalies are similar in some respects to those found in the magnetic stars α^2 CVn and HD 133029. It is suggested, therefore, that HD 151199 may also have a large surface magnetic field and that surface nuclear reactions may be responsible for the abundance anomalies.

I. INTRODUCTION AND RESULTS

HD 151199 was listed by Miczaika (1940) as a high-velocity star with a total velocity of 90 km/sec, and Miss Roman (1955) has also included it in her list of high-velocity stars with a total velocity of 69 km/sec. In the *Henry Draper Catalogue* the star is classified as A2p, the peculiarity being outstandingly strong lines of Sr II. Miczaika (1949) apparently used the strengths of the Sr II lines as well as the appearance of the hydrogen lines to derive his value of -0.4 for the absolute magnitude, which we believe now to be much too high. Miss Roman's $U - B$ and $B - V$ colors for the star correspond to those for a main-sequence star of type A2; the absolute magnitude which she used is consistent with this. Her spectral classification is A5p, and it will be seen later that the results of the present paper give an effective temperature corresponding to type A5. Clearly, the star belongs in the category of peculiar A-type stars. The characteristic tendency of peculiar A-type stars (including those with observed large magnetic fields) to have $U - B$ and $B - V$ colors which indicate a slightly earlier spectral type than that shown by the spectra (Provin 1953) is also present in this case. Although the velocity of HD 151199 is unusually high for a member of the solar-neighborhood population I, this star does not have any of the other properties which may be associated with population II.

Two calibrated spectra of the star were obtained with the coudé grating spectrograph at the McDonald Observatory in April, 1953. A dispersion of 18 A/mm was used. Microphotometer tracings were made at the Yerkes Observatory, and equivalent widths were determined in the usual way. In Table 1 we give mean values of $-\log W/\lambda$ for all the lines measured. Abundances of the elements were determined by the curve-of-growth method. For nearly all the elements this method was exactly similar to that described in a separate paper (Burbidge and Burbidge 1956), in which our measures of lines in the standard star 95 Leo were used in conjunction with published values for γ Gem given by Buscombe (1951) and values for τ UMa given by Greenstein (1948).

* Assisted by the joint program of the U.S. Office of Naval Research and Atomic Energy Commission.

The atmospheric parameters which we have determined for HD 151199 are: $\theta_{exc} = 0.68$, $\theta_{ion} = 0.64$, $\log p_e = 2.1$, $\log \kappa_\lambda = 0.25$, and $T_{eff} = 8700°$. The theoretical curve of growth was that computed for a Milne-Eddington model with $B^{(0)}/B^{(1)} = \frac{1}{3}$ and $\log a = -2.6$. Using the Fe I and Fe II lines, we found that the total effective velocity parameter $v = 4$ km/sec $= v(95\ \text{Leo})$.

The abundance of europium has been determined relative to that in α^2 CVn (Burbidge and Burbidge 1955*b*) and thence to that in the sun, by using the two lines Eu II λ 4129.73 and λ 4205.05. These lines are weak in HD 151199, but their identification is almost certainly correct. To compare the abundance ratio for europium with the other ratios,

TABLE 1

EQUIVALENT WIDTHS

λ	−log W/λ	λ	−log W/λ	λ	−log W/λ	λ	−log W/λ
Mg II		Mn II		Fe I *Cont.*		Fe II *Cont.*	
4481.23	4.04	4206.38	4.94	4442.34	4.84	4549.4	4.16
		4292.25	5.13	4447.72	4.72	4555.89	4.64
Si II				4476.02	4.82	4576.33	4.84
4130.88	4.56	Fe I		4494.57	4.81	4582.84	4.69
		4005.25	4.33			4583.83	4.54
Ca I		4021.87	4.81	Fe II		4629.34	4.68
4226.73	4.34	4045.82	4.29	3938.29	4.35		
		4063.60	4.36	4173.45	4.42	Sr II	
Ca II		4071.74	4.54	4178.86	4.38	4077.71	3.81
3933.66	3.13	4132.06	4.39	4233.17	4.35	4161.80	4.40
		4143.6	4.46	4273.32	4.92	4215.52	4.01
Cr I		4187.4	4.36	4296.57	4.54		
4254.35	4.63	4235.94	4.61	4385.38	4.40	Ba II	
4274.80	4.50	4250.5	4.48	4416.82	4.64	4554.03	4.56
		4260.48	4.53	4491.40	4.64		
Mn I		4271.5	4.37	4508.28	4.61		
4030.76	4.35	4282.41	4.63	4515.34	4.58	Eu II	
4033.07	4.40	4383.55	4.44	4520.23	4.91	4129.73	4.96
		4404.75	4.58	4522.63	4.50	4205.05	4.71

TABLE 2

ABUNDANCE RATIOS RELATIVE TO 95 LEO

Mg	Si	Ca	Cr	Mn	Fe	Sr	Ba	Eu
1.2	1.3	2.6	1.8	9	1.1	65	0.6	130

it has been assumed that the europium ratio $A(95\ \text{Leo})/A(\text{sun})$ is unity. All the ratios relative to 95 Leo are given in Table 2. The only values which depart significantly from unity are those for manganese, strontium, and europium. For manganese and strontium the following points should be noted.

Manganese.—Abundance ratios of 11.0 and 10.7, relative to 95 Leo, were found from the Mn I lines λ 4030.76 and λ 4033.07 by using γ Gem and τ UMa, respectively. Since these values are obtained from neutral lines, they are very sensitive to variations in the parameters p_e and T_{ion}. Therefore, the weak lines Mn II λ 4206.38 and λ 4292.25 were also used. The former is visible as a *very* weak line in 95 Leo and is present in the spectrum of τ UMa, while the latter is present in the spectrum of γ Gem. From these lines,

abundance ratios of 8 and 5 relative to 95 Leo were obtained via τ UMa and γ Gem, respectively. These values are not sensitive to variation in p_e and T_{ion}, but they are uncertain because of the intrinsic weakness of the lines. The tabulated ratio is the mean of all four values.

Strontium.—The lines Sr II λ 4077.71 and λ 4215.52 are so strong that the result depends critically on the value of the damping constant used. The weaker line λ 4161.80 was used as well, and, by putting successively $\log a = -1.8$, -2.2, and -2.6 and by making a direct comparison with 95 Leo, values of the ratio of 35, 62, and 78 were obtained. If the τ UMa measures are used and $\log a$ is put equal to -2.2, since this value gives the best fit of the three points to the curve, the ratio relative to 95 Leo is 85. Finally, the ratio can also be obtained by taking the measures in α^2 CVn (using tabulated values of $\log \eta_0$), and in this case the result is 66. The tabulated quantity is the mean of all five values.

II. CONCLUSIONS AND DISCUSSION

The abundance anomalies are similar in some respects to those previously found in the magnetic stars α^2 CVn and HD 133029 (Burbidge and Burbidge 1955*a*, *b*). However, HD 151199 does not have the anomalies in silicon and calcium which were found in these latter stars. Also, we have no results for yttrium and zirconium or for the rare earths, apart from europium. Since Eu II lines are the strongest of all the rare-earth group, we should expect that these lines would show up first. They are strongest in the magnetic stars which we have studied previously. In that work the overabundance ratio for europium was of the order of 10^3, and the other rare earths had ratios of the same magnitude. Thus our failure to detect lines of other rare-earth elements in the spectrum of HD 151199 does not mean that they may not also be overabundant by factors similar to that for europium. For example, if we suppose that the line Gd II λ 4251.73 is present with $W = 0.02$ equivalent angstroms, this would be below our limit of visibility, since the star has an appreciable rotation. The overabundance ratio for gadolinium relative to the sun, determined via the curve of growth for α^2 CVn, would then be about 60.

The remarks contained in the previous paragraph have been made in the light of an attempt to give a theoretical explanation of the abundance anomalies in magnetic stars (Burbidge and Burbidge 1955*b;* Fowler, Burbidge, and Burbidge 1955). This work has shown that anomalous element abundances can be built up in a thin skin of material on the surfaces of these stars (comprising only about 10^{-6} of the mass), if it is supposed that nuclear reactions take place on the surface after material in spot regions has been accelerated by changing magnetic fields. The nuclear processes which result, whether they take place through neutron or α-particle capture, give rise to anomalies which have a considerable spread in atomic weight. It is for this reason that we would not expect that strontium alone among the strontium, yttrium, and zirconium group or europium alone among the rare-earth group would have large overabundance ratios.

For reasons similar to those discussed for the magnetic stars (cf. Fowler *et al.* 1955, Sec. I), we do not believe that the anomalies can have been produced by nuclear processes in the stellar interior. Consequently, in the absence of any other explanation, there is a strong presumption that this star and other peculiar A-type stars showing similar anomalies have large surface magnetic fields.

It is of considerable interest to note that, as in α^2 CVn, the abundance of barium is normal in HD 151199 while europium is extremely overabundant. The detailed explanation for this remains unknown, although possible factors which may be important have been discussed elsewhere (Fowler *et al.* 1955, Sec. IV*a*).

The overabundance ratios for strontium and europium in HD 151199 are comparable, whereas in the magnetic stars previously studied their ratio is of the order of 1/20. If neutron-capture processes are responsible, this suggests that in each acceleration process a smaller proportion of neutrons per nucleus is made available to be captured than in

α^2 CVn and HD 133029. This is further borne out by the fact that the overabundance ratio of about 10^3 for elements in the rare-earth group, which is near or approaching the maximum, according to the unpublished neutron-curves of Cameron, has not been reached (cf. Fowler *et al.* 1955, Sec. IV). The overabundance ratio for manganese may be partially accounted for by a readjustment through reactions in the metal peak of the normal abundance-curve. The usual iron/manganese abundance ratio is about 70. To make this 7, about 15 per cent of the iron would have to be converted through a process in which $\Delta A = -1$, $\Delta Z = -1$. This, however, is a large fraction and would probably be converted only if resonant reactions occur.

This work is based on observations which were made at the Yerkes and McDonald Observatories. The reductions and analysis were carried out at the Mount Wilson and Palomar Observatories and at the California Institute of Technology.

REFERENCES

Burbidge, E. M., and Burbidge, G. R. 1955*a*, *Ap. J.*, **122**, 396.
———. 1956, *ibid.*, **124**, 116.
Burbidge, G. R., and Burbidge, E. M. 1955*b*, *Ap. J. Suppl.*, **1**, 431.
Buscombe, W. 1951, *Ap. J.*, **114**, 73.
Fowler, W. A., Burbidge, G. R., and Burbidge, E. M. 1955, *Ap. J. Suppl.*, **2**, 167.
Greenstein, J. L. 1948, *Ap. J.*, **107**, 151.
Miczaika, G. R. 1940, *A.N.*, **270**, 249.
———. 1949, *Zs. f. Ap.*, **26**, 11.
Provin, S. S. 1953, *Ap. J.*, **118**, 489.
Roman, N. G. 1955, *Ap. J. Suppl.*, **2**, 195.

A SPECTROPHOTOMETRIC ANALYSIS OF TWO METALLIC-LINE STARS

G. R. Miczaika, F. A. Franklin, A. J. Deutsch, and J. L. Greenstein
Harvard College Observatory
and
Mount Wilson and Palomar Observatories
Carnegie Institution of Washington, California Institute of Technology
Received February 8, 1956

ABSTRACT

Equivalent widths have been measured on Mount Wilson coudé spectra of the two metallic-line stars, 8 Comae and 15 Vulpeculae. Line profiles of some Balmer lines and the K line of Ca II have also been determined. The data are analyzed by curve-of-growth procedures, and the results indicate that the two stars resemble each other closely in their physical properties. They show high turbulent velocities of 4.8 and 3.8 km/sec, as does another metallic-line star, τ Ursae Majoris, implying that high atmospheric turbulence is definitely linked with metallicism. Opacity, ionization temperature, electron and gas pressure are also derived. The effective gravity determined spectroscopically is about ten times smaller than the gravitational value. Abundances of chemical elements do not differ from those of the sun by more than a factor of 3, except in the cases of Sc, Ca, Na, Sr, and Zn. Equivalent widths of lines in τ UMa, measured by Greenstein (1948), have been reanalyzed by use of the same line strengths (Bell 1950) as those used for 8 Com and 15 Vul. A comparison of 8 Com and 15 Vul with τ UMa shows that the first two exhibit similar, but less pronounced, abundance effects. Lack of a model prevents a reliable determination of the hydrogen abundance. Line strengths for more than five hundred lines are tabulated.

I. INTRODUCTION

Both 8 Comae (12^h14^m3; $23°35'$ [1900]; 6.15) and 15 Vulpeculae (19^h57^m0; $27°29'$ [1900]; 4.74) are members of that class of objects known as metallic-line stars. Their spectral types have been classified as A3 and A5, respectively, in the *Henry Draper Catalogue*.

Weaver (1952), using the hydrogen lines, classified the spectrum of 8 Com as A3 in the system of the Yerkes *Atlas*. The star is a member of the Coma cluster. Weaver has measured $P = 6.26$, $P - V = +0.06$; Bahner and Miczaika (1952) found $P = 6.24$, $P - V = +0.057$. Assuming a distance modulus, $m - M = +4.50$, which seems to be the most likely value, one obtains $M = +1.80$.

According to Slettebak (1949), the hydrogen lines of 15 Vul indicate a class of A8, while the K line corresponds to A6 and the metallic lines lead to F5 IV or F0 II–III. The trigonometric parallax of this star is listed in the 1952 edition of the *General Catalogue of Stellar Parallaxes* as $0''.025 \pm 0''.007$, resulting in an absolute magnitude of $+1.7 \pm 0.7$.

II. MEASUREMENTS

This paper presents a spectrophotometric investigation of the line spectrum of both stars. The spectrograms were taken by Armin J. Deutsch (8 Com) and Jesse L. Greenstein (15 Vul) with the grating spectrograph at the coudé focus of the 100-inch telescope. Table 1 lists the plates that have been used for measurement.

The spectrum of a star is flanked on either side by two sets of step-slit spectra for photometric calibration. The tracings of the spectrograms were made with the direct-intensity photometer of the Mount Wilson and Palomar Observatories. For most cases in Table 1, two adjacent plates were exposed simultaneously in the plateholder, in order to cover as long a strip of the spectrum as possible. Thus a small number of lines near the middle of the ranges quoted in Table 1 could not be measured because of their closeness to the edges of the two plates.

By making extensive use of Swensson's (1946) study of α CMi and of Greenstein's work (1948, 1949) on F stars, including the metallic-line star τ UMa, we simplified the

selection and identification of lines to be measured. We chose only lines which seemed unblended or very little affected by other contributors. In the case of 8 Com, we were somewhat less critical because of the smaller wave-length range available.

The process of measuring the equivalent widths consisted in guiding a polar planimeter around the profile of the line ten times. By applying the factors of the dispersion scale and the measured height of the continuum above the line of zero intensity, we transformed the readings into equivalent widths. Figure 1 plots the equivalent widths of 8 Com, measured on Ce 9193 against those of Ce 9186. Of all the plates measured, these two showed a minimum of scatter and correspond to a probable error of 1.2 per cent.

Table 2 contains the spectrophotometric measures of $-\log W/\lambda$ for the lines, and the

TABLE 1

SPECTROGRAMS OF 8 COM AND 15 VUL

Number Ce	Wave Length Range	Dispersion (A/mm)	Number Ce	Wave Length Range	Dispersion (A/mm)
5905.....	4823–5896	8.6	7112.....	5018–5896	4.2
6402.....	3799–4892	2.8	7116.....	3878–4892	2.8
6409.....	3799–4892	2.8	7233.....	5162–6162	5.6
6416.....	3815–4353	2.8	8136.....	5229–6588	5.6
6590.....	5890–6588	4.2	9186*.....	3848–4603	4.5
6901*.....	3838–4607	4.5	9193*.....	3895–4655	4.5

* Spectrograms of 8 Com.

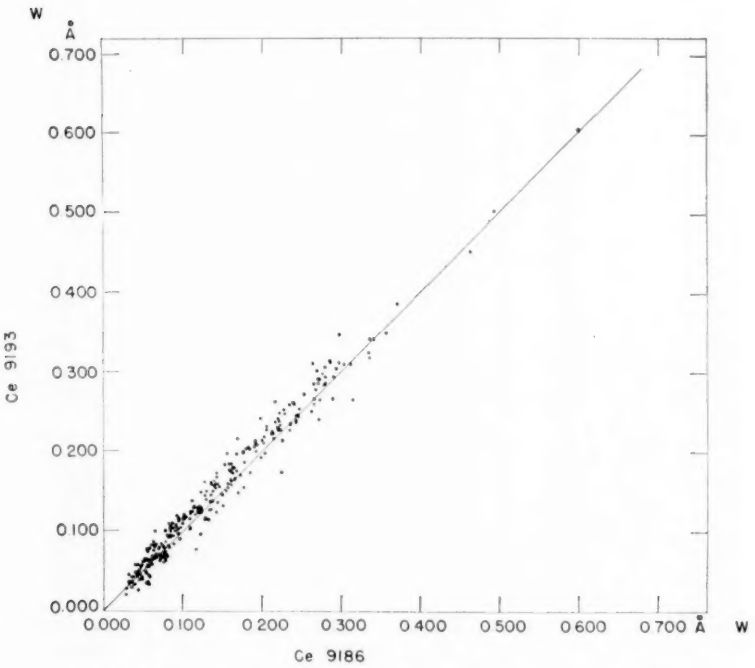

FIG. 1.—Comparison of equivalent widths of 8 Com measured on two plates

TABLE 2

EQUIVALENT WIDTHS AND STELLAR LINE STRENGTHS

λ	Element	−log W/λ		log η_0	
		8 Com	15 Vul	8 Com	15 Vul
3799.6	Fe I	.....	4.34	.....	+1.72
3805.3	Fe I	.....	4.43	.....	+1.40
3807.1	Ni I	.....	4.37	.....	+1.61
3807.5	Fe I	.....	4.59	.....	+0.90
3808.7	Fe I	.....	4.60	.....	+0.87
3810.8	Fe I	.....	4.56	.....	+0.98
3811.9	Fe I	.....	4.57	.....	+0.95
3813.0	Fe I	.....	4.16	.....	+2.44
3813.4	Ti II	.....	4.36	.....	+1.65
3814.1	Fe II	.....	4.48	.....	+1.23
3815.8	Fe I	.....	4.18	.....	+2.37
3818.3	V II	.....	4.48	.....	+1.23
3820.4	Fe I	.....	4.12	.....	+2.56
3821.2	Fe I	.....	4.39	.....	+1.54
3821.8	Fe I	.....	4.47	.....	+1.26
3824.4	Fe I	.....	4.11	.....	+2.60
3824.9	Fe II	.....	4.63	.....	+0.79
3825.9	Fe I	.....	4.21	.....	+2.26
3827.8	Fe I	.....	4.19	.....	+2.33
3829.4	Mg I	.....	4.22	.....	+2.22
3832.3	Mg I	.....	4.25	.....	+2.09
3839.3	Fe I	.....	4.59	.....	+0.90
3840.4	Fe I	.....	4.33	.....	+1.76
3841.1	Fe I	.....	4.28	.....	+1.97
3850.8	Fe I	4.20	4.32	+2.08	+1.80
3852.6	Fe I	4.40	4.58	+1.32	+0.92
3856.4	Fe I	4.14	4.16	+2.38	+2.50
3858.3	Ni I	4.23	4.23	+1.97	+2.18
3859.9	Fe I	4.13	4.13	+2.43	+2.53
3861.3	Fe I	4.65	4.79	+0.62	+0.42
3862.6	Si II	4.27	4.46	+1.13	+1.29
3865.6	Fe I	4.14	4.27	+2.38	+2.01
3867.2	Fe I	4.47	4.61	+1.10	+0.84
3871.8	Fe I	4.36	4.51	+0.97	+1.14
3872.5	Fe I	4.19	4.19	+2.13	+2.33
3873.8	Fe I	4.38	.....	+1.39	.....
3876.1	Fe I	4.70	.....	+0.50	.....
3878.1	Fe I	4.18	4.24	+2.18	+2.13
3884.3	Fe I	4.88	4.86	+0.17	+0.29
3885.5	Fe I	4.69*P*	.....	+0.52	.....
3886.3	Fe I	4.31*P*	4.33	+1.62	+1.76
3887.1	Fe I	4.51*P*	4.46	+0.97	+1.29
3897.5	Fe I	4.81	.....	+0.30	.....
3899.7	Fe I	4.22	4.35	+2.00	+1.68
3900.6	Ti II	4.08	4.17	+2.68	+2.40
3903.9	Fe I	4.41	4.63	+1.29	+0.79
3904.8	Ti I	4.91	.....	+0.12	.....
3906.5	Fe I	4.21	.....	+2.04	.....
3907.9	Fe I	4.57	4.75	+0.81	+0.51
3916.4	V II	4.30	4.59	+1.65	+0.90
3916.7	Fe I	4.52	4.68	+0.94	+0.67
3920.3	Fe I	4.25	4.28	+1.88	+1.97
3922.9	Fe I	4.18	4.25	+2.18	+2.09
3930.3	Fe I	4.20	4.18	+2.08	+2.37
3937.3	Fe I	4.93	5.09	+0.10	−0.07
3941.3	Fe I	4.73	4.89*p*	+0.15	+0.24
3942.4	Fe I	4.54	4.73*p*	+0.88	+0.55
3944.0	Al I	4.15	4.24	+2.33	+2.47
3947.0	Fe I	4.80	4.86	+0.31	+0.29

TABLE 2—*Continued*

λ	Element	−log W/λ		log η	
		8 Com	15 Vul	8 Com	15 Vul
3948.0	Fe I	4.56	4.66	+0.84	+0.72
3950.0	Fe I	4.58	4.73	+0.78	+0.55
3950.4	V II	4.41	4.44	+1.29	+1.36
3952.0	V II	4.34	4.63	+1.51	+0.79
3955.4	Fe I	4.70	4.84	+0.50	+0.33
3955.9	Fe I	4.82	.....	+0.28	.....
3961.5	Al I	4.19	4.30	+2.13	+1.89
3976.6	Fe I	4.50	4.67	+1.00	+0.70
3982.6	Y II	4.38	4.46	+1.39	+1.29
3986.2	Fe I	4.66	4.96	+0.60	+0.13
3986.8	Mg I	4.50	4.80	+1.00	+0.40
3987.6	Ti II	4.70	4.99	+0.50	+0.08
3988.5	La II	4.44	4.67	+0.57	+0.70
3989.1	Sc II	4.90	5.11	+0.13	−0.10
3996.0	Fe I	4.70	.....	+0.50	.....
3998.6	Ti I	4.70	.....	+0.50	.....
3999.0	.....	4.48	4.50	+1.06	+1.17
4001.7	Fe I	4.72	.....	+0.47	.....
4002.9	V II	4.58	4.80	+0.78	+0.40
4005.3	Fe I	4.16	.....	+2.28	.....
4005.7	V II	4.33	4.49	+1.55	+1.20
4006.3	Fe I	4.81	4.91	+0.30	+0.20
4008.2	V II	4.92	.....	+0.11	.....
4008.9	Ti I	4.90	.....	+0.13	.....
4009.7	Fe I	4.57	4.67	+0.81	+0.70
4023.4	V II	4.40	4.61	+1.32	+0.84
4028.4	Ti II	4.31	4.46	+1.62	+1.29
4030.8	Mn I	4.24	.....	+1.93	.....
4033.1	Mn I	4.30	4.38	+1.65	+1.58
4034.5	Mn I	4.49	4.59	+1.03	+0.90
4035.7	Mn I	4.31	4.52	+1.62	+1.04
4036.8	V II	4.79	5.09	+0.33	−0.07
4039.6	V II	5.03	.....	−0.07	.....
4040.7	Fe I	4.51*P*	4.74	+0.97	+0.53
4041.3	Mn I	4.55	4.61	+0.86	+0.84
4044.6	Fe I	4.73	4.87	+0.45	+0.28
4045.8	Fe I	3.96	4.02	+3.14	+2.86
4050.3	Zr II	4.89	4.98*p*	+0.01	+0.10
4055.5	Mn I	4.79	4.90	+0.33	+0.22
4056.2	Ti II	4.80	.....	+0.31	.....
4057.5	Mg I	4.33	4.54	+1.55	+1.04
4062.5	Fe I	4.53	4.69	+0.91	+0.65
4063.6	Fe I	4.08	4.10	+2.68	+2.63
4065.4	Fe I	5.04	5.08	−0.08	−0.06
4068.0	Fe I	4.51	4.66	+0.97	+0.72
4070.8	Fe I	4.55	4.72	+0.86	+0.57
4071.7	Fe I	4.16	4.27	+2.28	+2.01
4073.8	Fe I	4.60	4.77	+0.73	+0.47
4076.6	Fe I	4.43	.....	+1.21	.....
4077.7	Sr II	3.92	3.99	+3.35	+2.96
4079.9	Fe I	4.88	5.03	+0.17	+0.02
4080.2	Fe I	4.97	5.08	+0.03	−0.06
4082.1	Fe I	4.95	.....	+0.06	.....
4084.5	Fe I	4.67	4.77	+0.57	+0.47
4085.0	Fe I	4.62	.....	+0.70	.....
4086.7	La II	4.58	5.06	+0.78	−0.03
4087.1	Fe I	4.87	5.05	+0.18	−0.01
4096.0	Fe I	4.74	.....	+0.43	.....
4107.5	Fe I	4.72	4.73	+0.47	+0.55

TABLE 2—*Continued*

λ	Element	−log W/λ		log r_0	
		8 Com	15 Vul	8 Com	15 Vul
4109.1	Fe I	5.01	5.23	−0.03	−0.26
4111.8	V I	4.96	.....	+0.05	.....
4113.0	Fe I	4.80	5.00	+0.31	+0.06
4114.5	Fe I	4.84	5.01	+0.24	+0.04
4114.9	Fe I	5.11*P*	.....	−0.18	.....
4120.2	Fe I	4.96	5.04	+0.05	0.00
4121.3	Co I	4.88	4.93	+0.17	+0.18
4122.6	Fe II	4.41	4.57	+1.29	+0.95
4126.2	Fe I	4.83	5.05	+0.26	−0.02
4128.7	Fe II	4.59	4.76	+0.76	+0.49
4129.7	Eu II	4.68	4.80	+0.54	+0.40
4132.0	Fe I	4.21	4.28	+2.04	+1.97
4132.9	Fe I	4.62	4.80	+0.70	+0.40
4133.8	Fe I	4.60	4.80	+0.73	+0.40
4134.7	Fe I	4.46	4.58	+1.13	+0.92
4137.0	Fe I	4.59	4.78	+0.76	+0.45
4137.7	Ce II	4.72	4.93	+0.47	+0.18
4141.9	Fe I	4.84	.....	+0.24	.....
4143.4	Fe I	4.35	4.44	+1.48	+1.36
4143.9	Fe I	4.25	4.33	+1.88	+1.76
4145.8	Cr II	4.64	5.05	+0.65	−0.02
4147.7	Fe I	4.61	4.86	+0.72	+0.29
4150.3	Fe I	4.80	.....	+0.31	.....
4151.0	Zr II	4.65	4.91	+0.63	+0.20
4152.2	Fe I	4.28	4.64	+1.72	+0.76
4154.5	Fe I	4.43	.....	+1.21	.....
4154.8	Fe I	4.44	.....	+1.18	.....
4156.2	Zr II	4.40	4.57	+1.32	+0.95
4157.8	Fe I	4.56	4.70	+0.84	+0.62
4158.8	Fe I	4.63	4.96	+0.68	+0.13
4161.8	Sr II	4.43	.....	+1.21	.....
4167.3	Mg I	4.34	4.59	+1.51	+0.90
4167.9	Fe I	4.82	5.08	+0.28	−0.06
4174.9	Fe I	4.89	5.03	+0.15	+0.02
4175.6	Fe I	4.53	4.64	+0.91	+0.76
4176.6	Fe I	4.54	4.72	+0.88	+0.57
4177.5	Y II	4.11	4.17	+2.54	+2.40
4178.9	Fe II	4.24	4.29	+1.93	+1.93
4179.8	Zr II	5.00	5.10*p*	+1.03	−0.08
4181.8	Fe I	4.26	4.38	+1.83	+1.58
4182.4	Fe I	4.84	5.03	+0.24	+0.02
4183.4	V II	4.60	4.94	+0.73	+0.16
4187.0	Fe I	4.29	4.48	+1.35	+1.23
4187.8	Fe I	4.28	4.35	+1.73	+1.69
4191.4	Fe I	4.30	.....	+1.65	.....
4196.2	Fe I	4.58	4.93	+0.78	+0.18
4198.3	Fe I	4.16	4.27	+2.28	+2.01
4199.1	Fe I	4.31	4.40	+1.62	+1.50
4200.0	Fe I	5.22	5.48*p*	−0.32	−0.56
4200.9	Fe I	4.76	4.99	+0.39	+0.08
4202.0	Fe I	4.16	4.23	+2.28	+2.18
4204.0	Fe I	4.51	4.68	+0.97	+0.67
4206.7	Fe I	5.08*P*	.....	−0.14	.....
4207.1	Fe I	4.83	.....	+0.26	.....
4209.0	Zr II	4.56	4.66	+0.84	+0.72
4210.4	Fe I	4.43	4.65	+1.21	+0.74
4211.9	Zr II	4.62	4.69	+0.70	+0.65
4213.7	Fe I	4.77	4.97	+0.37	+0.12
4215.5	Sr II	4.06	4.12	+2.78	+2.56

TABLE 2—*Continued*

λ	Element	$-\log W/\lambda$		$\log \eta_0$	
		8 Com	15 Vul	8 Com	15 Vul
4216.2	Fe I	4.73	4.85	+0.45	+0.31
4219.4	Fe I	4.44	4.58	+1.18	+0.92
4220.3	Fe I	4.79	.....	+0.33	.....
4222.2	Fe I	4.50	4.62	+1.00	+0.81
4224.2	Fe I	4.50	4.67	+1.00	+0.70
4225.2	V II	4.42	4.60	+1.25	+0.87
4226.7	Ca I	4.14	4.16	+2.38	+2.44
4227.4	Fe I	4.24	4.34	+1.93	+1.72
4233.6	Fe I	4.41	4.51	+1.29	+1.14
4235.9	Fe I	4.24	4.31	+1.93	+1.85
4238.0	Fe I	4.77	4.91*p*	+0.37	+0.20
4238.4	La II	4.78	5.01	+0.35	+0.05
4238.8	Fe I	4.48	4.56	+1.06	+0.98
4242.4	Cr II	4.37	4.55	+1.42	+1.01
4244.8	Ni II	5.00	5.07	−0.02	−0.05
4245.3	Fe I	4.68	4.86	+0.54	+0.29
4246.1	Fe I	4.82	4.99	+0.28	+0.08
4246.8	Sc II	4.27	4.30	+1.78	+1.89
4247.4	Fe I	4.42	4.54	+1.25	+1.04
4248.2	Fe I	4.82	4.97	+0.28	+0.12
4250.1	Fe I	4.32	4.41	+1.59	+1.46
4250.8	Fe I	4.25	4.30	+1.88	+1.89
4251.7	Gd II	4.94	5.02	+0.08	+0.03
4252.6	Cr II	4.58	4.89	+0.77	+0.24
4254.4	Cr I	4.23	4.38	+0.78	+1.58
4260.5	Fe I	4.20	4.25	+2.08	+2.09
4261.9	Cr II	4.38	4.63	+1.39	+0.79
4267.0	Fe I	4.92	5.10*P*	+0.11	−0.08
4267.8	Fe I	4.80	4.94	+0.31	+0.16
4271.2	Fe I	4.33	4.41	+1.55	+1.46
4271.8	Fe I	4.20	4.25	+2.08	+2.09
4274.8	Cr I	4.29	4.49	+1.69	+1.20
4275.6	Cr II	4.44	4.73	+1.18	+0.55
4282.4	Fe I	4.40	4.44	+1.32	+1.36
4283.0	Ca I	4.61	4.72	+0.72	+0.57
4285.4	Fe I	4.80	4.90	+0.31	+0.22
4287.0	La II	4.78	5.04	+0.35	0.00
4289.7	Cr I	4.45	.....	+1.16	.....
4294.8	Sc II	5.05	5.17*p*	−0.09	−0.18
4296.6	Fe II	4.25	4.37	+1.85	+1.61
4300.1	Ti II	4.14	4.20	+2.38	+2.30
4300.8	Fe I	4.89	5.20*p*	+0.14	−0.22
4301.9	Ti II	4.25	4.36	+1.85	+1.65
4302.5	Ca I	4.43	4.57	+1.21	+0.95
4303.2	Fe II	4.27	4.36	+1.78	+1.65
4303.6	Nd II	4.76	5.01*p*	+0.39	+0.04
4309.6	Y II	4.39	4.39	+1.35	+1.54
4312.9	Ti II	4.30	4.34	+1.65	+1.72
4316.8	Ti II	4.71	4.84	+0.49	+0.33
4318.6	Ca I	4.63	4.91	+0.68	+0.20
4320.7	Sc II	4.31	4.34	+1.62	+1.72
4325.8	Fe I	4.20	4.21	+2.08	+2.26
4330.3	Ti II	4.80	4.88	+0.31	+0.26
4333.8	La II	4.72	4.92	+0.47	+0.19
4337.1	Fe I	4.83	4.88*P*	+0.26	+0.26
4337.9	Ti II	4.42	4.49	+1.25	+1.20
4351.0	Cr I	4.78	.....	+0.35	.....
4352.7	Fe I	4.70	4.65	+0.50	+0.74

TABLE 2—*Continued*

λ	Element	−log W_λ		log γ_0	
		8 Com	15 Vul	8 Com	15 Vul
4354.6	Sc II	.....	5.22*p*	.....	−0.24
4355.1	Ca I	5.14	5.05*p*	−0.23	−0.02
4367.6	Fe I	4.41	4.55*p*	+1.29	+1.01
4367.9	Fe I	4.80	.....	+0.31	.....
4369.4	Fe II	4.67	4.75*p*	+0.57	+0.51
4369.8	Fe I	4.65	4.79*p*	+0.63	+0.42
4374.5	Sc II	4.55	4.53*p*	+0.86	+1.07
4375.9	Fe I	4.64	4.66*p*	+0.64	+0.72
4379.2	V I	5.12	4.84*p*	−0.20	+0.33
4383.6	Fe I	4.19	4.21*p*	+2.13	+2.26
4385.3	Fe II	4.28	4.31*p*	+1.73	+1.85
4386.9	Ti II	4.52	4.61	+0.94	+0.84
4387.9	Fe I	4.88	5.14	+0.17	−0.14
4388.4	Fe I	4.71	4.88	+0.49	+0.26
4394.1	Ti II	4.42	4.46	+1.25	+1.29
4395.0	Ti II	4.18	4.20	+2.18	+2.30
4395.9	Ti II	4.52	4.61	+0.94	+0.84
4398.0	Y II	4.56	4.52	+0.84	+1.11
4404.8	Fe I	4.23	4.23	+1.96	+2.17
4413.6	Fe II	4.85	4.96	+0.22	+0.13
4415.1	Fe I	4.27	4.27	+1.78	+2.01
4415.6	Sc II	4.70	4.74	+0.50	+0.53
4416.8	Fe II	4.31	4.36	+1.62	+1.65
4417.7	Ti II	4.32	4.37	+1.59	+1.61
4421.9	Ti II	4.64	4.85	+0.65	+0.31
4425.4	Ca I	4.66	4.72	+0.60	+0.57
4427.3	Fe I	4.57	4.68	+0.81	+0.67
4430.6	Fe I	4.67	4.81	+0.57	+0.38
4433.2	Fe I	4.77	4.93	+0.37	+0.18
4433.8	Fe I	4.75	4.99	+0.41	+0.08
4435.0	Ca I	4.54	4.56	+0.88	+0.98
4435.7	Ca I	4.61	4.61	+0.72	+0.84
4442.3	Fe I	4.58	4.73	+0.78	+0.55
4443.2	Fe I	4.55	4.55	+0.86	+1.01
4443.8	Ti II	4.23	4.27	+1.96	+2.01
4446.8	Fe I	5.05	.....	−0.10	.....
4447.2	Fe I	5.31*P*	.....	−0.44	.....
4447.7	Fe I	4.57	4.69	+0.81	+0.65
4450.5	Ti II	4.29	4.39	+1.69	+1.54
4454.4	Fe I	4.70	.....	+0.50	.....
4455.9	Ca I	4.61	4.73	+0.72	+0.55
4461.7	Fe I	4.61	.....	+0.72	.....
4466.6	Fe I	4.48	4.55	+1.06	+1.01
4467.3	Sm II	5.08	5.20	−0.14	−0.22
4468.5	Ti II	4.21	4.27	+2.04	+2.01
4472.9	Fe II	4.53	4.69	+0.91	+0.65
4476.0	Fe I	4.44	4.54	+1.18	+1.04
4479.6	Fe I	4.90	5.27	+0.13	+2.01
4481.1	Mg II	3.89	4.02	+3.5	+2.86
4484.2	Fe I	4.78	5.01	+0.35	+0.05
4485.7	Fe I	4.91	5.27*p*	+0.12	−0.30
4486.9	Ce II	4.81	5.40*p*	+0.30	−0.46
4488.3	Ti II	4.49	4.60	+1.03	+0.87
4489.2	Fe II	4.37	4.43	+1.42	+1.40
4489.8	Fe I	5.11	.....	−0.19	.....
4490.8	Fe I	5.00	5.18	−0.02	−0.19
4491.4	Fe II	4.39	4.47	+1.36	+1.26
4494.6	Fe I	4.45	4.54	+1.16	+1.04

TABLE 2—*Continued*

λ	Element	−log W/λ		log η_0	
		8 Com	15 Vul	8 Com	15 Vul
4501.3	Ti II	4.22	4.28	+2.00	+1.97
4508.3	Fe II	4.29	4.36	+1.69	+1.65
4511.9	Cr I	5.01	5.27*p*	−0.04	−0.30
4515.3	Fe II	4.32	4.39	+1.59	+1.54
4520.2	Fe II	4.32	4.41*p*	+1.59	+1.46
4522.6	Fe II	4.18	4.24	+2.18	+2.13
4528.6	Fe I	4.29	4.42	+1.69	+1.43
4529.5	Ti II	4.47	4.56	+1.10	+0.98
4531.2	Fe I	4.68	4.84	+0.54	+0.33
4533.2	Ti I	4.75	.....	+0.41	.....
4534.0	Ti II	4.12	4.16	+2.49	+2.44
4534.8	Fe I	5.00	.....	−0.02	.....
4536.5	Fe I	.....	5.38*p*	.....	−0.43
4540.6	Cr I	5.06	.....	−0.11	.....
4540.8	Cr I	5.06	.....	−0.11	.....
4541.5	Fe II	4.38	4.45	+1.39	+1.32
4544.0	Ti II	4.88	4.95	+0.17	+0.15
4545.1	Ti II	4.81	4.72*p*	+0.30	+0.57
4546.0	Cr I	5.00	.....	−0.02	.....
4554.0	Ba II	4.20	4.23	+2.08	+2.18
4555.0	Cr II	4.47	4.61	+1.10	+0.84
4555.9	Fe II	4.27	.....	+1.78	.....
4558.7	Cr II	4.25	4.27*p*	+1.88	+2.01
4560.1	Fe I	4.96	.....	+0.05	.....
4562.4	Ce II	4.98	5.12	+0.01	−0.11
4563.8	Ti II	4.24	4.24	+1.93	+2.13
4572.0	Ti II	4.16	4.21	+2.28	+2.26
4576.3	Fe II	4.44	4.49	+1.18	+1.20
4578.6	Ca I	4.91	.....	+0.12	.....
4583.4	Ti II	4.83	.....	+0.26	.....
4583.8	Fe II	4.17	4.20	+2.23	+2.30
4585.9	Ca I	4.86	4.91	+0.20	+0.20
4588.2	Cr II	4.35	4.40	+1.48	+1.50
4591.5	Cr I	5.06	.....	−0.11	.....
4592.1	Cr II	4.47	.....	+1.10	.....
4602.9	Fe I	4.82	4.77	+0.28	+0.47
4605.0	Ni I	4.86	4.84	+0.20	+0.33
4606.2	Ni I	5.04	5.20	−0.08	−0.22
4611.3	Fe I	.....	4.64	.....	+0.76
4613.9	Zr II	5.09	.....	−0.16	.....
4616.1	Cr I	4.92	.....	+0.11	.....
4616.6	Cr II	4.50	4.69	+1.00	+0.64
4619.3	Fe I	5.03	.....	−0.07	.....
4620.5	Fe II	4.52	4.57	+0.94	+0.95
4625.1	Fe I	4.92	4.87*p*	+0.11	+0.28
4626.2	Cr I	5.06	5.04*p*	−0.11	0.00
4628.2	Ce II	.....	4.99*p*	.....	+0.08
4630.1	Fe I	5.28	5.15*p*	−0.40	+0.15
4634.1	Cr II	4.39	4.48	+1.36	+1.23
4635.3	Fe II	.....	4.81	.....	+0.38
4637.5	Fe I	5.06	5.12	−0.11	−0.11
4638.0	Fe I	4.87	4.96	+0.18	+0.13
4643.5	Fe I	5.02	5.22	−0.05	−0.24
4646.2	Cr I	4.79	5.08	+0.33	−0.06
4647.4	Fe I	4.76	4.82	+0.39	+0.36
4648.7	Ni I	4.66	4.74	+0.60	+0.53
4651.3	Cr I	5.25	.....	−0.36	.....
4652.2	Cr I	4.98	.....	+0.01	.....

TABLE 2—*Continued*

λ	Element	−log W/λ 15 Vul	log ν_0 15 Vul	λ	Element	−log W/λ 15 Vul	log ν_0 15 Vul
4666.8	Fe II	4.55	+1.01	5027.8	Fe I	5.25	−0.28
4668.1	Fe I	5.00	+0.06	5035.4	Ni I	4.72	+0.57
4673.2	Fe I	5.03	+0.01	5052.1	C I	4.60	+0.87
4678.8	Fe I	4.73	+0.55	5074.8	Fe I	4.71	+0.60
4685.3	Ca I	5.00	+0.06	5080.5	Ni I	4.61	+0.84
4686.2	Ni I	5.11	−0.10	5081.1	Ni I	4.72	+0.57
4703.0	Mg I	4.53	+1.07	5087.4	Y II	4.61	+0.84
4703.8	Ni I	4.97	+0.12	5097.0	Fe I	4.80	+0.40
4707.3	Fe I	4.84	+0.33	5099.9	Ni I	4.98	+0.10
4708.7	Ti II	4.90	+0.22	5115.4	Ni I	4.94	+0.16
4714.4	Ni I	4.56	+0.98	5121.6	Fe I	5.20	−0.22
4715.8	Ni I	4.91	+0.21	5123.7	Fe I	5.18	−0.19
4718.4	Cr I	5.35*p*	−0.40	5129.1	Ti II	4.51	+1.14
4722.2	Zn I	4.84	+0.33	5133.7	Fe I	4.62	+0.82
4727.4	Fe I	5.07	−0.05	5146.5	Ni I	4.75	+0.51
4731.4	Fe II	4.59	+0.90	5155.8	Ni I	5.00	+0.06
4735.9	Fe I	5.20	−0.22	5162.3	Fe I	4.56	+0.98
4736.8	Fe I	4.73	+0.55	5169.0	Fe II	4.11	+2.60
4754.0	Mn I	4.87	+0.28	5172.7	Mg I	4.22	+2.22
4756.5	Ni I	4.98	+0.10	5183.6	Mg I	4.18	+2.37
4775.9	C I	5.03	+0.01	5185.9	Ti II	4.67	+0.70
4780.0	Ti II	4.72	+0.57	5191.5	Fe I	4.39	+1.54
4789.6	Fe I	5.04	0.00	5192.3	Fe I	4.53	+1.08
4805.1	Ti II	4.48	+1.23	5197.6	Fe II	4.39	+1.54
4810.5	Zn I	4.73	+0.55	5200.4	Y II	4.68	+0.67
4812.3	Cr II	5.02	+0.03	5206.0	Cr I	4.34	+1.72
4823.5	Mn I	4.75	+0.51	5208.5	Cr I	4.43	+1.40
4829.0	Ni I	5.05	−0.02	5211.5	Ti II	4.99	+0.08
4848.2	Cr II	4.63	+0.79	5215.2	Fe I	4.79	+0.42
4876.4	Cr II	4.67	+0.70	5216.3	Fe I	4.85	+0.31
4883.7	Y II	4.53	+1.07	5217.4	Fe I	4.83	+0.35
4890.8	Fe I	4.64	+0.76	5229.9	Fe I	4.71	+0.60
4891.5	Fe I	4.43	+1.40	5232.9	Fe I	4.33	+1.76
4893.8	Fe II	5.26	−0.29	5234.6	Fe II	4.31	+1.85
4900.0	Y II	4.31	+1.85	5237.3	Cr II	4.62	+0.81
4904.4	Ni I	4.80	+0.40	5257.1	Cr I	4.82	+0.36
4919.0	Fe I	4.48	+1.23	5262.2	Ca I	4.71	+0.60
4920.5	Fe I	4.30	+1.89	5264.8	Fe II	4.62	+0.81
4923.9	Fe II	4.27	+2.01	5266.6	Fe I	4.57	+0.95
4934.0	Ba II	4.21	+2.26	5269.5	Fe I	4.25	+2.09
4942.5	Cr I	5.26	−0.29	5281.8	Fe I	4.78	+0.45
4946.4	Fe I	5.16	−0.17	5305.8	Cr II	4.85	+0.31
4966.1	Fe I	5.10	−0.08	5307.4	Fe I	4.96	+0.13
4973.1	Fe I	5.24	−0.27	5324.2	Fe I	4.50	+1.17
4980.2	Ni I	5.12	−0.11	5325.6	Fe II	4.65	+0.74
4989.0	Fe I	5.18	−0.19	5334.9	Cr II	4.77	+0.47
4993.4	Fe II	4.91	−0.20	5336.8	Ti II	4.55	+1.01
5001.9	Fe I	4.54	+1.04	5339.9	Fe I	4.70	+0.62
5014.9	Fe I	4.99	+0.08	5362.9	Fe II	4.38	+1.58
5017.6	Ni I	4.82	+0.36	5364.9	Fe I	4.66	+0.72
5018.4	Fe II	4.21	+2.26	5367.5	Fe I	4.65	+0.74
5027.2	Fe I	4.97	+0.12	5370.0	Fe I	4.56	+0.98

TABLE 2—*Continued*

λ	Element	$-\log W/\lambda$ 15 Vul	$\log \eta_0$ 15 Vul	λ	Element	$-\log W/\lambda$ 15 Vul	$\log \eta_0$ 15 Vul
5380.2.....	C I	4.81	+0.38	5948.6.....	Si I	5.03	+0.01
5381.0.....	Ti II	4.77	+0.47	5983.7.....	Fe I	5.18	−0.19
5383.4.....	Fe I	4.50	+1.17	5984.8.....	Fe I	4.93	+0.18
5389.5.....	Fe I	4.92	+0.19	5991.4.....	Fe II	4.89	+0.24
5393.2.....	Fe I	4.90	+0.22	6020.2.....	Fe I	4.95	+0.15
5397.1.....	Fe I	4.52	+1.11	6024.1.....	Fe I	4.77	+0.47
5400.5.....	Fe I	4.81	+0.38	6046.0.....	S I	5.10	−0.08
5404.1.....	Fe I	4.49	+1.20	6056.0.....	Fe I	5.15	−0.15
5405.8.....	Fe I	4.52	+1.11	6065.5.....	Fe I	4.96	+0.13
5409.1.....	Fe I	5.13	−0.13	6078.5.....	Fe I	5.20	−0.22
5409.8.....	Cr I	4.96	+0.13	6084.1.....	Fe II	5.11	−0.10
5410.9.....	Fe I	4.65	+0.74	6086.3.....	Ni I	5.37	−0.42
5414.1.....	Fe II	4.57	+0.95	6102.2.....	Fe I	5.08	−0.06
5418.8.....	Ti II	4.95	+0.15	6102.7.....	Ca I	4.89	+0.24
5424.1.....	Fe I	4.48	+1.23	6122.2.....	Ca I	4.67	+0.70
5425.3.....	Fe II	4.74	+0.53	6137.7.....	Fe I	4.80	+0.40
5429.7.....	Fe I	4.41	+1.46	6141.7.....	Ba II	4.35	+1.69
5434.5.....	Fe I	4.73	+0.55	6149.2.....	Fe II	4.80	+0.40
5445.0.....	Fe I	4.68	+0.67	6162.2.....	Ca I	4.56	+0.98
5446.9.....	Fe I	4.48	+1.23	6188.0.....	Fe I	5.29	−0.33
5487.7.....	Fe I	4.90	+0.22	6191.6.....	Fe I	4.90	+0.22
5497.5.....	Fe I	4.76	+0.49	6230.7.....	Fe I	4.83	+0.35
5506.8.....	Fe I	4.98	+0.10	6232.7.....	Fe I	5.14	−0.14
5510.7.....	Cr II	5.03	+0.02	6238.4.....	Fe II	4.73	+0.55
5526.8.....	Sc II	4.78	+0.45	6246.3.....	Fe I	4.87	+0.27
5528.4.....	Mg I	4.49	+1.20	6247.6.....	Fe II	4.48	+1.23
5534.9.....	Fe II	4.56	+0.98	6252.6.....	Fe I	5.06	−0.03
5554.9.....	Fe I	4.92	+0.19	6318.0.....	Fe I	4.82	+0.36
5565.7.....	Fe I	4.98	+0.10	6336.8.....	Fe I	5.20	−0.22
5569.6.....	Fe I	4.81	+0.38	6347.1.....	Si II	4.39	+1.54
5572.9.....	Fe I	4.64	+0.76	6371.4.....	Si II	4.56	+0.98
5576.1.....	Fe I	4.89	+0.24	6393.6.....	Fe I	4.99	+0.08
5582.0.....	Ca I	5.04	0.00	6400.1.....	Fe I	4.81	+0.38
5586.8.....	Fe I	4.54	+1.04	6408.0.....	Fe I	5.28	−0.31
5588.8.....	Ca I	4.56	+0.98	6411.7.....	Fe I	4.71	+0.60
5590.1.....	Ca I	5.04	0.00	6416.9.....	Fe II	4.74	+0.53
5592.3.....	Ni I	5.08	−0.06	6415.0.....	Fe I	5.09	−0.07
5601.3.....	Ca I	4.91	+0.21	6421.4.....	Fe I	5.08	−0.06
5615.6.....	Fe I	4.50	+1.17	6430.8.....	Fe I	4.93	+0.18
5669.0.....	Sc II	4.99	+0.08	6432.6.....	Fe II	4.77	+0.47
5682.6.....	Na I	4.93	+0.18	6439.1.....	Ca I	4.57	+0.95
5688.2.....	Na I	4.70	+0.62	6443.0.....	Fe II	5.24	−0.27
5708.4.....	Si I	5.24	−0.27	6456.4.....	Fe II	4.26	+2.05
5763.0.....	Fe I	4.81	+0.38	6462.6.....	Ca I	4.62	+0.81
5816.4.....	Fe I	5.30	−0.34	6491.3.....	Fe II	5.03	+0.01
5862.4.....	Fe I	5.00	+0.06	6493.8.....	Ca I	4.89	+0.24
5889.9.....	Na I	4.11	+2.60	6495.0.....	Fe I	4.78	+0.45
5895.9.....	Na I	4.15	+2.47	6496.9.....	Ba II	4.31	+1.85
5914.2.....	Fe I	4.76	+0.49	6516.1.....	Fe II	4.71	+0.60
5927.8.....	Fe I	5.36	−0.41	6587.7.....	C I	4.75	+0.51
5930.2.....	Fe I	4.88	+0.26				

laboratory values of their wave lengths. The symbols *p* and *P* indicate low and very low weight because of blending or distortion by plate grain, etc. Wright and Lee (1955) have measured equivalent widths of lines, in the wave-length region from λ 4000 to λ 4485, in the spectrum of 15 Vul on spectra taken at the Dominion Astrophysical Observatory. For 124 lines having W greater than 50 milliangstroms, the Mount Wilson values are only 2.5 per cent greater than those measured at Victoria.

The hydrogen lines and the K line cannot be satisfactorily measured on tracings of spectra with such high dispersion. Their equivalent widths, included in Table 3, are of rather low weight. The profiles of some hydrogen lines and of the K line have been derived and will be discussed later. The equivalent width of Hγ measured by Wright (1955) is about 8 per cent greater than the value given here. For 8 Com we obtained 960 measurements for 322 lines, about 3.0 measurements per line, and for 15 Vul we made a total of 1595 measurements of 502 lines, corresponding to 3.2 measurements per line.

TABLE 3

PROFILES OF Hγ, Hδ, H8, AND K (Ca II)

δλ (A)	8 Com				15 Vul			
	Hγ	Hδ	H8*	K	Hγ	Hδ	H8	K
0.0	97	95	85	91	87	87	84	91
0.5	87	85	78	87	70	71	72	83
1.0	75	78	70	80	62	63	65	67
2.0	65	70	62	46	53	54	56	31
3	59	64	56	31	47	47	49	16
4	54	58	49	20	41	42	44	8
5	50	53	42	10	36	37	39	4
6	46	51	38	5	33	34	34	2
8	40	44	27	1	25	26	26	.....
10	34	37	21	.....	21	22	18	.....
12	30	33	16	.....	16	17	15	.....
15	23	26	9	.....	11	11	9	.....
20	17	19	4	.....	5	5	4	.....
25	12	14	.....	.....	2	2	1	.....
35	6	7	.....	.....	.....	.....	.....	.....
W(A)	14.7	13.6	11.5*	4.53	11.0	11.0	10.2	3.81

* Available on one plate only.

III. THE CURVE OF GROWTH

The analysis of the line intensities follows conventional methods and uses the solar values of log X_0 derived by Bell (1951). These values have been reduced to the excitation temperatures of the two stars by a process of trial and error. Miss Bell gives values of log X_0'/p_c, where p_c denotes the continuous absorption coefficient, arbitrarily referred to λ = 5063 as unity. The values of p_c were taken from the theoretical tables of Chandrasekhar and Breen (1946) for wave lengths to the red of λ 4800 and from the empirical results of Münch (1945) for wave lengths to the violet of λ 4800. Although the absolute values of the continuous absorption coefficient vary considerably with temperature, the ratios of p_c are very insensitive to temperature, and since the excitation temperatures of both 8 Com and 15 Vul are fairly close to that of the sun, it has been assumed that

$$\log \frac{X}{p_c} = \log \frac{X_0'}{p_c} + 5040\left[\frac{1}{T(\odot)} - \frac{1}{T(*)}\right]. \qquad (1)$$

Excitation temperatures of 6480° ($\theta_{exc} = 0.78$) for 8 Com and 6075° ($\theta_{exc} = 0.83$) for 15 Vul are considered to be the best values to represent the observed line intensities. Miss Bell supplies the values of log X_0'/p_e for about 340 lines of Table 2. In order to insure greater accuracy in the values of solar line strengths, Miss Bell obtained these values by using three different curves of growth, for lines of high, intermediate, and low damping. She also considered the effects of the observed velocity gradient in the solar atmosphere. For these reasons her solar line strengths are very probably the best available. We obtained an empirical curve of growth for Fe I and partial curves for other atoms and ions, which we shifted horizontally to fit the Fe I curve (Figs. 2–7). No differences seemed to exist between the curves for atoms and those for ions. Consequently, for each star, a combined empirical curve of growth was then constructed from all lines for which solar values were available. The curves were finally fitted to one of Wrubel's (1949) theoretical ones.

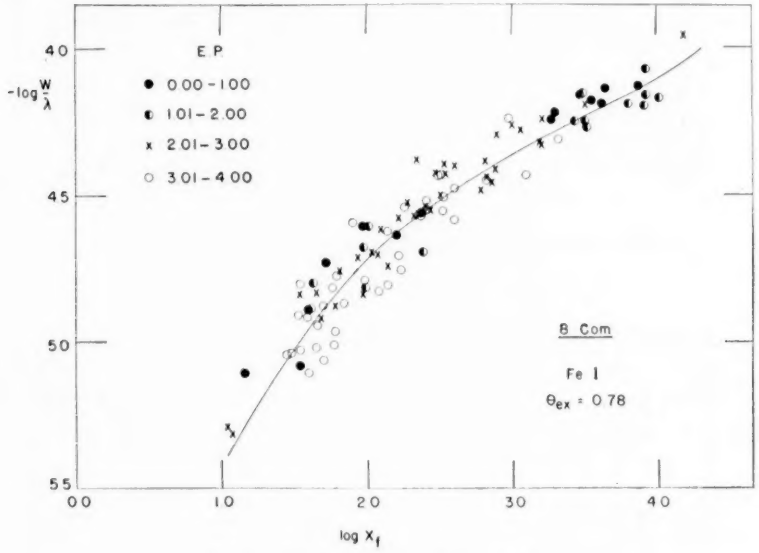

FIG. 2.—Curve of growth of 8 Com for Fe I

Wrubel's theoretical curves give log W/b as a function of log η_0, where b is the Doppler width in frequency units,

$$b = \frac{v}{c}\sqrt{\frac{2kT}{A\,m_0}}, \tag{2}$$

and

$$\eta_0 = \frac{\sigma_{\nu 0}}{\kappa_{\nu 0}} \tag{3}$$

is the ratio of the scattering coefficient to the continuous absorption coefficient, both evaluated at the center of the line. These curves have been computed for the formation of absorption lines according to the M-E model, for total flux, for various values of the damping constant, and for varying amounts of limb darkening. To simplify the reduc-

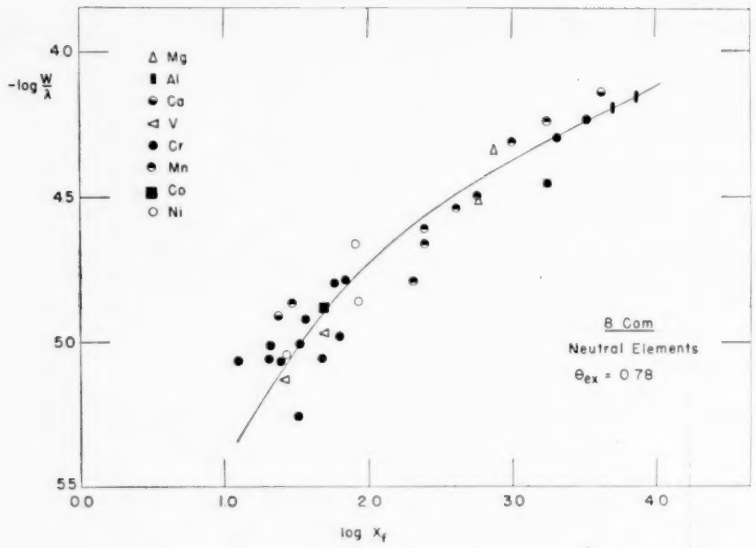

FIG. 3.—Curve of growth of 8 Com for neutral elements except Fe I

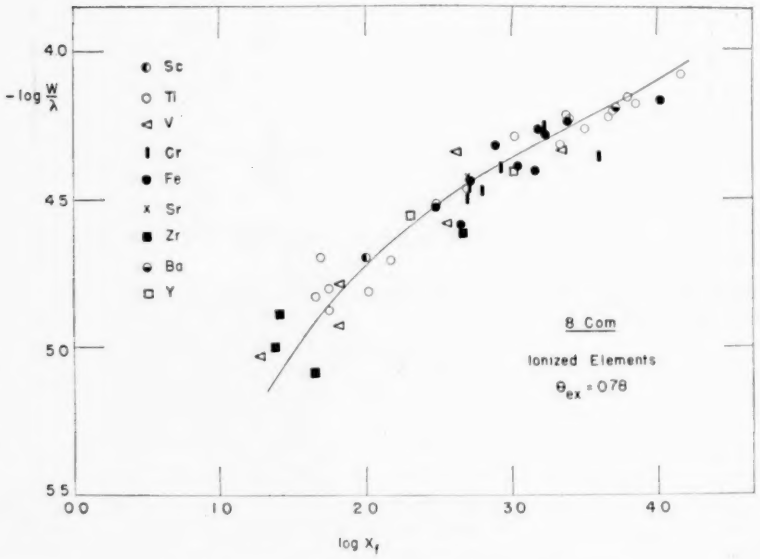

FIG. 4.—Curve of growth of 8 Com for ionized elements

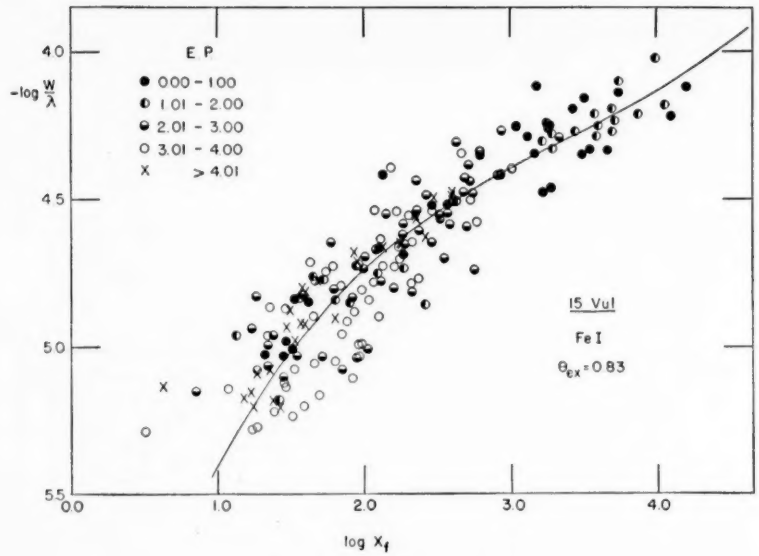

FIG. 5.—Curve of growth of 15 Vul for Fe I

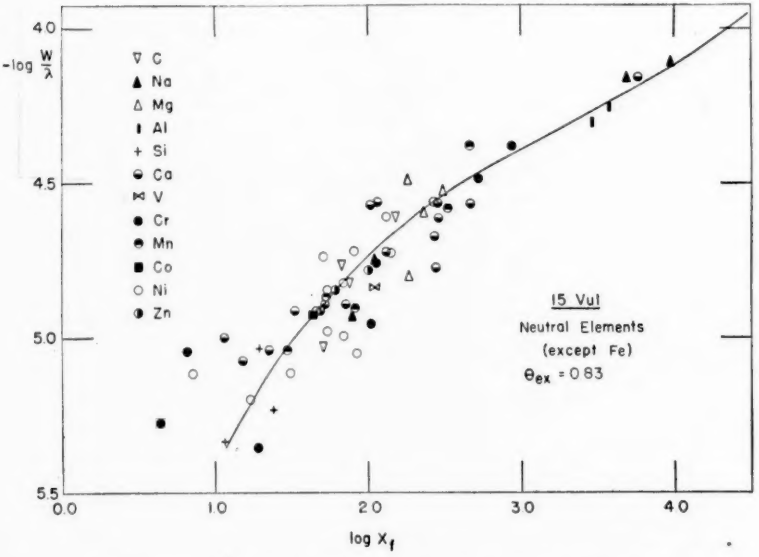

FIG. 6.—Curve of growth of 15 Vul for neutral elements except Fe I

tions for 15 Vul, a family of curves for $B^0/B^1 = \frac{1}{2}$ was derived by interpolation from Wrubel's data. Because of the narrower spectral range in the case of 8 Com, we reduced all η's to the case of $B^0/B^1 = \frac{1}{3}$.

The best fit of the empirical curve with a theoretical one gave a value of $\log a = -1.8$ for 15 Vul. Because of a lack of strong lines, we were unable to obtain an accurate value of $\log a$ in 8 Com, but -2.2 seems about right. By shifting the empirical curve horizontally and vertically and by employing the following equations:

$$\Delta \log \frac{W}{\lambda} = \log \frac{W}{\lambda} - \log \frac{W}{b}, \tag{4}$$

$$\Delta \log X = \log \frac{\sigma}{\kappa} - \log X, \tag{5}$$

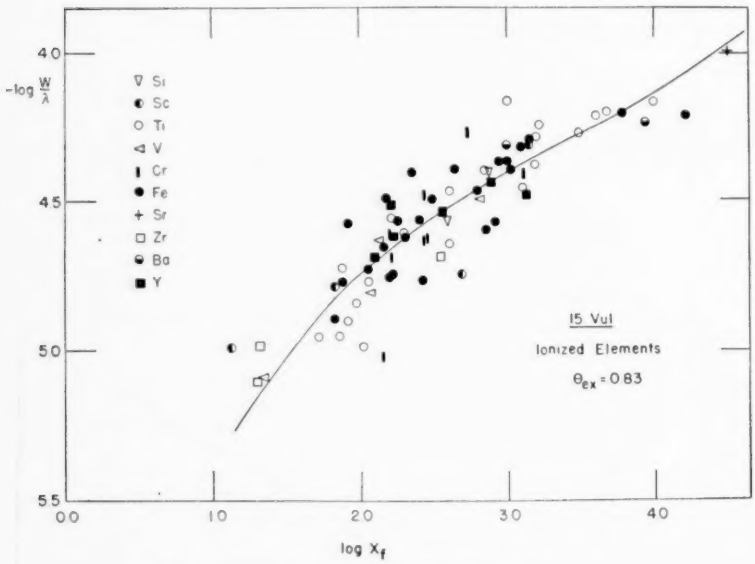

FIG. 7.—Curve of growth of 15 Vul for ionized elements

we derived atmospheric parameters (Table 4). These values for neutral iron are

$$\log \eta_0 = \log X - 1.55 \qquad (8 \text{ Com}), \tag{6}$$

$$\log \eta_0 = \log X - 1.46 \qquad (15 \text{ Vul}). \tag{7}$$

The velocity parameter is

$$\log V = \Delta \log \frac{W}{\lambda} + 10.48. \tag{8}$$

A comparison of some of these figures with the results of Greenstein for τ UMa and some normal F stars might be of interest here. He found $\log V = 5.60$ for τ UMa, and values of 5.44 and 5.46 for two normal F dwarfs. If we assume a kinetic temperature of 7000° K for

our two stars, turbulent velocities of 3.8 and 4.8 km/sec for 15 Vul and 8 Com result. Greenstein's value of V_t in τ UMa is 3.8 km/sec, again appreciably higher than for the more conventional F dwarfs. It thus seems beyond doubt that turbulence is linked with metallicism (cf. Deutsch 1956). A further study of turbulent motions in the atmospheres of 8 Com and 15 Vul is under way and will be published in a forthcoming paper.

Knowing the velocity parameter, V, and the ratio, a, of the effective natural line width to the Doppler width, we can now derive the ratio of the observed damping constant, Γ, to the classical one, γ_{cl}, and also of Γ/ν. From the equations

$$\Gamma = \frac{2\pi a V}{\lambda} \tag{9}$$

and

$$\gamma_{cl} = \frac{0.22}{\lambda^2}, \tag{10}$$

it follows that

$$\frac{\Gamma}{\gamma_{cl}} = 28.5\, a V \lambda. \tag{11}$$

TABLE 4

DATA DERIVED FROM THE CURVE OF GROWTH

	8 Com	15 Vul	τ UMa	
			Greenstein (1948)	Present Analysis
θ_{exc}	0.78	0.83	0.91	0.89
$\Delta \log W/\lambda$	4.78	4.87	4.58	4.85
$\Delta \log X_f$	−1.55	− 1.46	−1.28	−0.71
$\log a$	−2.2	− 1.8	−2.6	−2.4
$\log V$	5.70	5.61	5.60	5.63
V	4.8 km/sec	3.8 km/sec	3.8 km/sec	3.8 km/sec
Γ/γ_{cl}	7.6	15.6	3.0	5.4
Γ/ν	1.3×10^{-6}	2.6×10^{-6}	0.6×10^{-6}	0.9×10^{-6}

Note that the value of a in equations (9) and (11) is that defined by Unsöld and is twice as great as the a used by Wrubel for his theoretical curves. Hence in these two equations a must be replaced by $2a$ if Wrubel's curves are used.

The observed damping constants in 8 Com and 15 Vul are found to be, respectively, 7.6 and 15.6 times the classical value. For τ UMa, Γ/γ_{cl} is equal to 3.0.[1] The high value of Γ/γ_{cl} for 15 Vul is the result of the high value of $\log a$, whose value, however, is of fairly low weight. These values, together with data on the velocity parameters, are given in Table 4.

IV. ABUNDANCES, LEVEL OF IONIZATION, AND ELECTRON PRESSURE

We can put the defining equation for η_0:

$$\eta_0 = \sqrt{\pi}\, \frac{e^2 g f \lambda}{m c}\, \frac{e^{-\chi/kT}}{B(T)}\, \frac{N}{\kappa_\nu v}, \tag{12}$$

[1] The values in Table 7, *Ap. J.*, **107**, 171, must be multiplied by a factor of 2. In addition, the number −2.92 in eq. (20) in this reference should be corrected to read −2.62.

into the convenient form

$$\Delta \log \zeta_i \equiv \log \frac{N_i\,(*)\,/\,\kappa_\nu\,(*)}{N_i\,(\odot)\,/\,\kappa_\nu\,(\odot)} = \log \frac{\eta_{0i}\,(*)}{\eta_{0i}\,(\odot)} + \log \frac{V\,(*)}{V\,(\odot)} \qquad (13)$$

if we neglect the difference in the partition function, $B(T)$, between the star in question and the sun. The quantity $\log \eta_{0i}(*)/\eta_{0i}(\odot)$ can be readily determined for all lines whose equivalent widths have been measured and whose solar line strengths are known. All partition functions used in this analysis were taken from Aller's book (1953) or from the

TABLE 5

APPARENT (Δ LOG ζ_i) AND CORRECTED [LOG $z_i(*)/z_i(\odot)$] ABUNDANCES RELATIVE TO THE SUN

ELEMENT	Z	Δ LOG ζ_i		LOG $z_i(*)/z_i(\odot)$		
		8 Com	15 Vul	8 Com	15 Vul	τ UMa
C I	6	.....	−0.21 (4)	.....	−0.35	.....
Na I	11	.....	−0.37 (4)	.....	+ .49	+0.88 (3)
Mg I	12	−1.53 (2)	−1.64 (4)	−0.14	− .20	+0.2 (4)
Al I	13	−1.09 (2)	−1.23 (2)	− .06	− .12	+0.48 (2)
Si I	14	.....	−1.28 (2)	.....	+ .19	+0.88 (1)
Si II	14	.....	+0.13 (2)	.....	+ .18	.....
Si	14	.....	.....	.....	+ .18	.....
Ca I	20	−1.53 (6)	−1.28 (16)	− .54	− .27	−0.62 (6)
Sc II	21	−0.81 (2)	−0.44 (4)	− .90	− .53	−1.09 (2)
Ti I	.....	.....	.....	.....	.....	−0.14 (10)
Ti II	22	+0.03 (17)	+0.09 (20)	− .07	+ .01	−0.25 (17)
Ti	.....	.....	.....	.....	.....	−0.20
V I	23	−1.64 (2)	−1.19 (1)	− .34	+ .12	−0.45 (5)
V II	23	+0.14 (6)	−0.19 (4)	+ .04	− .27	−0.16 (1)
V	23	.....	.....	− .15	− .08	−0.40
Cr I	24	−1.06 (13)	−1.44 (7)	+ .17	− .13	+0.42 (9)
Cr II	24	+0.17 (6)	+0.05 (9)	+ .07	− .03	+0.25 (7)
Cr	24	.....	.....	+ .12	− .08	+0.34
Mn I	25	−1.28 (4)	−1.45 (5)	+ .13	.00	+0.31 (9)
Fe I	26	−1.46 (110)	−1.46 (184)	− .13	− .04	+0.10 (78)
Fe II	26	+0.05 (10)	+0.15 (25)	− .05	+ .07	+0.21 (15)
Fe	26	.....	.....	− .09	+ .02	+0.16
Co I	27	−1.70 (1)	−1.60 (1)	− .23	− .07	.....
Ni I	28	−1.13 (3)	−1.06 (15)	+ .38	+ .47	+0.98 (6)
Zn I	30	.....	−0.90 (2)	.....	+ .57	+0.74 (2)
Sr II	38	+0.46 (2)	+0.02 (1)	+ .51	+ .09	+0.01 (2)
Zr II	40	−0.17 (4)	−0.06 (3)	− .27	− .14	−0.99 (3)
Ba II	56	−0.31 (1)	+0.07 (2)	− .07	+ .33	+0.12 (2)
Y II	70	+0.29 (2)	+0.36 (6)	+0.22	+0.25	+0.11 (1)

work of Claas (1951). The apparent relative abundances, $\Delta \log \zeta_i$, of the observed elements are given in Table 5. They are not yet comparable with Greenstein's values for τ UMa and other normal F stars, as they still involve differences in ionization level and opacity of the atmospheres. To derive the level of ionization and electron pressure and to make results comparable with Greenstein's, we chose $\tau_0 = 0.25$ as a representative point in the atmosphere. Here $\theta_{\text{ion}} = 1.10\ \theta_{\text{exc}} = 0.92\ \theta_0$. For the corresponding point in the solar atmosphere, values of $\theta_{\text{ion}} = 0.95$ and $\log P_e = 0.80$ were computed by Greenstein. We determined the ionization level (Table 6) for these standard elements, Fe I,

Cr I, and V I, by using the data of Table 5 and the known level of ionization in the sun at $\tau_0 = 0.25$. Only a negligible fraction of the total number of atoms of these three standard elements is doubly ionized at the temperatures and electron pressures relevant to this analysis.

Greenstein's method (1948) was employed in the determination of log P_e and θ_{ion} from the observed stellar ionization. The procedure leads also to the determination of the opacity, by the relation

$$\log \frac{\kappa_\nu\,(*)}{\kappa_\nu\,(\odot)} = 0.02 - \langle \Delta \log\, \zeta_i\ (\text{ions}) \rangle_{\text{av}}\,. \tag{14}$$

Equation (14) follows directly from equation (13) if we note the following:

$$\log \frac{N_1(*)}{N_1(\odot)} = \log \frac{N(*)}{N(\odot)} - \log \frac{1 + N_0/N_1(*)}{1 + N_0/N_1(\odot)}\,. \tag{15}$$

TABLE 6

IONIZATION OF STANDARD ELEMENTS LOG $(1 - x)_i$

Element	Sun	8 Com	15 Vul
Fe I.....	−1.00	−2.58	−2.61
Cr I.....	−1.86	−3.07	−3.35
V I.....	−1.87	−3.61	−2.87

TABLE 7

DETERMINATION OF LOG P_e FROM IONIZATION

Star	$\theta_{\text{ion}} = 0.7$				$\theta_{\text{ion}} = 0.8$				$\theta_{\text{ion}} = 0.9$			
	Fe I	Cr I	V I	Mean*	Fe I	Cr I	V I	Mean*	Fe I	Cr I	V I	Mean*
8 Com..	1.46	1.61	1.07	1.44	0.53	0.79	0.27	0.57	−0.38	−0.02	−0.54	−0.29
15 Vul..	1.43	1.33	1.82	1.46	0.50	0.51	1.01	0.58	−0.41	−0.30	+0.20	−0.27

* The means have been computed with the following weights: Fe, 3; Cr, 2; V, 1.

For the standard elements we assume log $N(*)/N(\odot) = 0$. Thence it follows that

$$\left\langle \log \frac{N_1(*)}{N_1(\odot)} \right\rangle_{\text{av}} = -\left\langle \log \frac{1 + N_0/N_1(*)}{1 + N_0/N_1(\odot)} \right\rangle_{\text{av}} = 0.02\,. \tag{16}$$

Taking log $\kappa_\nu(\odot)$ as −0.54, we can then compute log $\kappa_\nu(*)$ from equation (14).

Table 7 presents the details of the derivation of log P_e and θ_{ion} by use of the three standard elements. The values of $\kappa_\nu(\text{H}^- + \text{H})$ as functions of P_e and θ have been taken from Greenstein's Table 10. We have, however, modified this table by adding the relatively minor contribution of electron scattering to the total opacity.

Using the hydrostatic equation,

$$\frac{dP}{d\tau} = \frac{g_e}{\bar{\kappa}(\tau)}\,, \tag{17}$$

and the assumption that P_e/P_g is roughly constant, Greenstein gives the equation for the effective gravity as follows:

$$g_e = \frac{P_g(\tau_0)\,\bar{\kappa}(\tau_0)}{2\,\tau_0}. \tag{18}$$

Log $\kappa_\nu/\bar{\kappa}$ equals approximately -0.3 and can be found in the tables given by Chandrasekhar and Münch (1946). In equation (18) the value $\tau_0 = 0.25$ is again assumed as the representative point.

The results for θ_{ion}, log P_e, log $\kappa(*)$, and g_e can be found in Table 8. This table also gives the gas pressure, P_g, as derived from Strömgren's (1944) tables for log $A = 3.8$.

The g_{gr} values of the surface gravity in Table 8 are estimated from luminosity and temperature. The effective gravity determined spectroscopically is about ten times

TABLE 8

OPACITY, IONIZATION TEMPERATURE, ELECTRON AND GAS PRESSURE, GRAVITY

	8 Com	15 Vul	τ UMa	
			Greenstein (1948)	Present Analysis
log κ_ν	−0.64	−0.62	−1.62	−1.19
θ_{ion}	+0.74	+0.74	+0.86	+0.86
log P_e	+1.12	+1.12	0.0	+0.12
log P_g	+3.0	+3.0	+2.7	+2.9
log g_{ef}	+3.0	+3.0	+1.6	+2.2
log g_{gr}	+3.8	+3.8	+4.0	+4.0

smaller than the gravitational value. This situation is even more pronounced in the other metallic-line star carefully investigated, τ UMa. All three stars resemble giants as far as the effective gravity is concerned. Yet in the giant stars the gravitational and effective gravities are either essentially the same or differ only slightly. The disagreement in the case of metallic-line stars certainly has a bearing on the mechanism that produces the high turbulence component of the velocity of these stellar atmospheres.

Now, with all the atmospheric parameters evaluated, we are in a position to convert the apparent abundance ratios into abundances relative to the sun. If the equation

$$z_i = \sum_r N_{i,r} \tag{19}$$

represents the number of atoms of element i in the state of ionization r per gram of material, the abundance ratio of the element in the stellar and solar atmospheres can be written thus:

$$\log \frac{z_{i,r}(*)}{z_{i,r}(\odot)} = \Delta \log \zeta_{i,r} - \log \frac{N_{i,r}(*)}{\sum_r N_{i,r}(*)} + \log \frac{N_{i,r}(\odot)}{\sum_r N_{i,r}(\odot)} + \log \frac{\kappa_\nu(*)}{\kappa_\nu(\odot)}. \tag{20}$$

In treating the rare earths as well as calcium, strontium, yttrium, and barium, we had to consider the fact that an appreciable fraction of the total number of atoms was doubly ionized.

The relative abundances thus derived are also listed in Table 5. Where an element appears in two stages of ionization, a straight mean value was taken as representing the abundance of the element, save in the case of vanadium, where the abundance deter-

mined from V I was felt to be of higher weight. A glance at these values shows immediately that the abundance differences are not so strongly pronounced as those found for τ UMa. In fact, there is no ratio exceeding a factor of 3, except for scandium, calcium, strontium, sodium, and zinc. In both stars, elements whose second ionization potentials lie near 12 volts may show abundance deficiencies (Fig. 8), an effect first found by Greenstein in his analysis of τ UMa. However, the accuracy of curve-of-growth methods is such that, with the possible exception of the foregoing five elements, no abundance difference relative to the sun can be considered significant. For the sake of uniformity, we have reanalyzed τ UMa, using Greenstein's equivalent widths and Miss Bell's solar line strengths. The reader is referred to Tables 4, 5, and 8 for a listing of the new and in some cases the earlier (Greenstein 1948) parameters. This reanalysis tends to raise the abun-

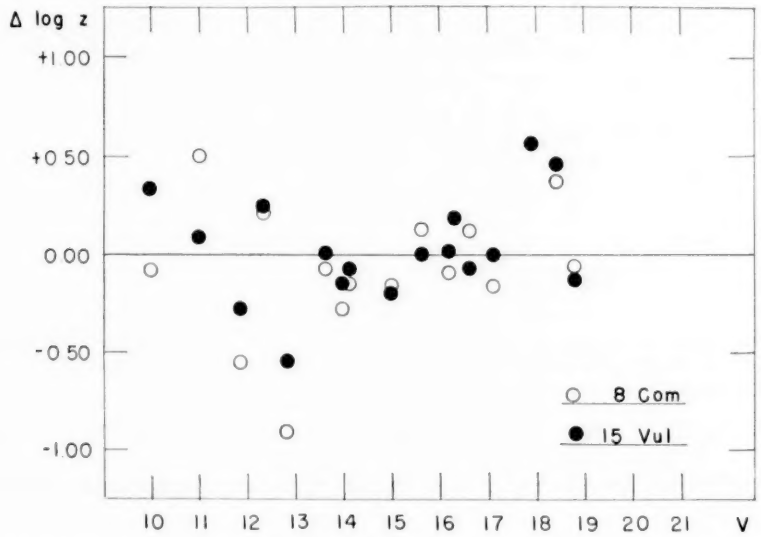

FIG. 8.—Abundances of elements in 8 Com and 15 Vul compared with the sun, plotted against the ionization potential V.

dances of the elements in τ UMa relative to the sun by factors of about 1.5–2. However, the abundance differences remain large and peculiar, especially the high values for zinc and nickel, which are common features of all our stars in which lines of these elements are accessible. It seems likely that a true abundance difference is in evidence here. As Miss Bell gives no solar line strengths for certain elements, most of which are rare earths, we include in Table 9 values of the abundances of these metals in 8 Com and 15 Vul compared with Greenstein's earlier (1948) τ UMa values.

V. LINE PROFILES

Profiles of the available hydrogen lines and the K line have been measured, together with their equivalent widths. The determination of equivalent widths is of low accuracy for lines with extended wings on high-dispersion spectra. The profiles obtained should be very little distorted by the apparatus function. Both stars under discussion have hydrogen profiles very similar to those of F stars in general, regardless of their luminosity, as Greenstein has already indicated. An interpretation of the profiles requires a model of the stellar atmosphere which is unavailable. The procedure outlined by Greenstein permits

the determination of the hydrogen abundance relative to the sun under the assumption that both stars follow the same model. However, even if this assumption holds, it leads to values which cannot be considered of high weight, because the method is highly sensitive to the adopted temperature.

Aller (1947) has also measured profiles of H and K lines in metallic-line stars and compared them to normal A stars. The results, including those from a curve-of-growth analysis, showed the lower temperature and opacity in the atmospheres of the "metallic" A stars as compared with normal A stars.

TABLE 9

APPARENT (Δ LOG ζ_i) AND CORRECTED [LOG $z_i(*)/z_i(\tau)$] ABUNDANCES BASED ON GREENSTEIN'S (1948) LOG η_0 FOR τ UMA

ELEMENT	Δ LOG ζ_i		LOG $z_i(*)/z_i(\tau)$	
	8 Com	15 Vul	8 Com	15 Vul
La II	−0.65 (6)	−1.12 (3)	+0.39	−0.06
Ce II	−0.61 (8)	−1.12 (3)	+ .37	− .12
Nd II	−0.63 (2)	−0.92 (1)	+ .41	+ .14
Sm II	−0.89 (2)	−0.88 (1)	+ .15	− .06
Eu II	−1.13 (2)	−1.41 (1)	− .09	− .35
Gd II	−0.77 (2)	−0.75 (1)	+0.27	+0.31

VI. LINE STRENGTHS

The equivalent widths of the two stars have been used to derive for each star log η_0, the stellar line strength for the lines in Table 2. This quantity can be applied to curve-of-growth analyses of other stars by using the relation

$$\log \eta_0(**) = \log \eta_0(*) + \Delta \log \zeta_i(**) - \Delta \log \zeta_i(*) - \log \frac{v(**)}{v(*)}, \qquad (21)$$

where (*) stands for either 8 Com or 15 Vul and (**) for the other star under consideration.

In conclusion, we should like to thank Mrs. May Kassim who measured some of the tracings.

REFERENCES

Aller, L. H. 1947, *Ap. J.*, **106**, 76.
———. 1953, *Astrophysics*, Vol. 1 (New York: Ronald Press Co.).
Bahner, K., and Miczaika, G. R. 1952, *Zs. f. Ap.*, **31**, 239.
Bell, B. 1951, Radcliffe thesis.
Chandrasekhar, S., and Breen, F. H. 1946, *Ap. J.*, **104**, 430.
Chandrasekhar, S., and Münch, G. 1946, *Ap. J.*, **104**, 446.
Claas, W. J. 1951, *Utrecht Obs. Res.*, **12**, 50.
Deutsch, A. J. 1956, *Principes fondamentaux de classification stellaire*, Publications du CNRS (Paris), p. 25.
Greenstein, J. L. 1948, *Ap. J.*, **107**, 151.
———. 1949, *ibid.*, **109**, 121.
Greenstein, J. L., and Hiltner, W. A. 1949, *Ap. J.*, **109**, 265.
Münch, G. 1945, *Ap. J.*, **102**, 385.
Slettebak, A. 1949, *Ap. J.*, **109**, 547.
Strömgren, B. 1944, *Pub. København Obs.*, No. 138.
Swensson, J. W. 1946, *Ap. J.*, **103**, 207.
Weaver, H. F. 1952, *Ap. J.*, **116**, 625.
Wright, K. O., and Lee, E. K. 1955, *Draft Reports I.A.U. Dublin Meeting*, p. 327.
Wrubel, M. H. 1949, *Ap. J.*, **109**, 66.

COMPARATIVE STUDY OF FIVE CARBON STARS IN THE VISUAL AND INFRARED SPECTRAL REGIONS*

YOSHIO FUJITA
Department of Astronomy, University of Tokyo
Received December 30, 1955; revised March 14, 1956

ABSTRACT

Medium-dispersion spectrograms of five carbon stars (WZ Cas, U Cyg, U Hya, V Aql, and RY Dra) have been investigated. A table of identified lines is given. It is confirmed that the C classification is consistent with the behavior of the lines.

The C classification of R-N type stars (Keenan and Morgan 1941) based upon low-dispersion spectra has played a considerable role in simplifying the complicated problem

TABLE 1

DATA ON PLATES

Star	Date	Exposure (minutes)	Emulsion
RY Dra	April 26, 1946	100	I-N*
V Aql	April 26, 1946	90	
V Aql	April 26, 1946	90	
RY Dra	April 26, 1946	20	103a-F
RY Dra	April 26, 1946	20	
U Hya	April 27, 1946	30	I-N*
U Hya	April 27, 1946	30	
U Hya	April 27, 1946	30	
RY Dra	April 27, 1946	100	I-N*
RY Dra	April 28, 1946	100	
U Cyg	May 20, 1946	50	I-N*
WZ Cas	May 20, 1946	60	
WZ Cas	May 20, 1946	60	
U Cyg	May 20, 1946	20	103a-F
WZ Cas	May 20, 1946	20	

* Sensitized.

of the spectral classification of late-type stars. Further, it should be pointed out that such a classification helps in the understanding of the ideas which should be developed in building up the physical characteristics of these stars. It seems to be of interest to investigate the C classification from the standpoint of spectroscopic analysis with medium dispersion. The materials investigated are coudé spectrograms, the details of which are given in Table 1. The spectral regions investigated are shown in Table 2.

* Preliminary reports have been given in *Les Particules solides dans les astres* (Liége 1955), p. 276; and *Proc. Jap. Acad.*, **31**, 76, 1955.

TABLE 2

THE SPECTRAL REGION INVESTIGATED

Star	Spectral Type (C Classification)	Spectral Region (in A)	Dispersion
WZ Cas	$C9_1$	5856–8400	.....
U Cyg	$C7_2$–$C9_2$	5961–7725	.....
U Hya	$C7_3$	6727–8712	49 A/mm
V Aql	$C6_4$	6451–8026	.....
RY Dra	$C4_4$	5717–8670	.....

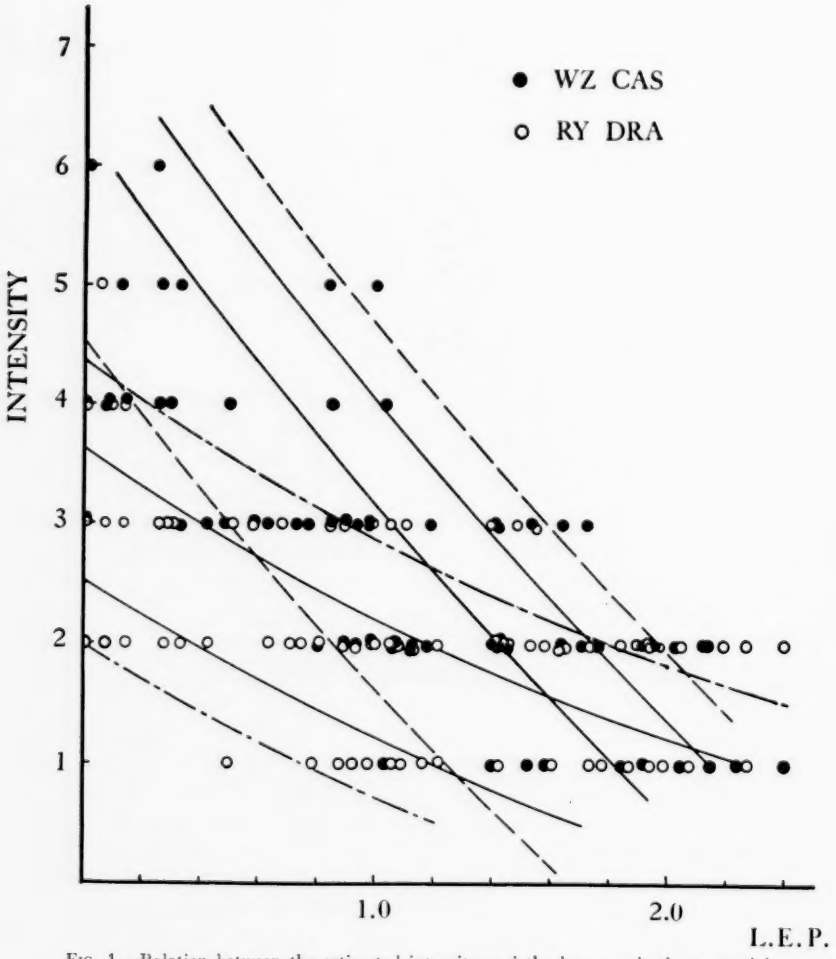

FIG. 1.—Relation between the estimated intensity and the lower excitation potential

TABLE 3
WAVE-LENGTHS AND INTENSITIES

Wave-length and Identification	WZ Cas		U Cyg		U Hya		V Aql		RY Dra	
	W.L.	Int.	W.L.	Int.	W.L.	Int.	W.L.	Int.	W.L.	Int.
5866.45 Ti72	5.7	2	---		---		---		5.5	1
5940.68 Ti2	9.3	4b							9.5	5
56.70 Fe14	7.1	5b	---						6.2	3
65.83 Ti154	5.2	1	5.3	2					5.6	1
74.13 74.54 C_2	3.2	1	4.3	2					3.0	1
78.54 Ti154	8.2	1	8.9	2					8.6	1
84.59 Ti2, 4.60 V49	5.8	4b	5.1	3					4.8	2
95.09 C_2	5.8	2	4.7	2d					6.0	2
6000.91 C2, 1.53 ScII20	1.0	2b	--						--	
08.65 V49, 9.45 Fe64	8.9	2b	8.6	2d					8.4	1
18.62 Ti70, 9.47 Ba7	9.7	2b	8.4	3					--	
23.41 Y3	4.4	4	4.8	2					3.8	4
26.14 C_2	7.6	1	6.3	2					6.5	2
31.68 Ti2, 2.12 C_2	2.8	3b	2.0	3					2.7	2
39.69 V34	0.4	2	0.9	2					1.0	2
48.64 V49	0.3	3	9.3	3					8.8	2
58.11 V34 C_2?	9.3	3	8.4	3b					8.8	2
62.88 Zr3, 2.89 Fe63, 3.12 Ba7	2.1	2b	3.3	3					3.6	1
67.13 LaII48	6.6	3	5.6	3					6.7	1
90.18 V34, 0.54 V33	1.3	2	0.6	2					1.0	1
6110.78 Ba7, 1.62 V34	0.9	2	1.5	2					0.9	2
20.86 Zr 24, 1.01 Ti153, 1.23 C_2	1.0	3	--						--	
22.22 Ca3	2.5	3	2.6	4b					2.6	3
38.44 Y3	9.0	3	8.7	3					8.5	3
43.23 Zr2	3.2	3	2.4	3					2.2	3

TABLE 3 (continued)

Wave-length and Identification	WZ Cas		U Cyg		U Hya		V Aql		RY Dra	
	W.L.	Int.	W.L.	Int.	W.L.	Int.	W.L.	Int.	W.L.	Int.
60.75 Na5, 2.17 Ca3, 3.56 Fe64	2.9	6	2.3	4					--	
70.34 V20	0.7	4	0.6	4					0.3	2
72.72 LaII4	2.5	4	2.7	3					2.9	4
_____ $C_2(C^{12}C^{13})$	3.2	6b	2.5	5b					2.9	5b
62_____ $CN(C^{12}N^{14}(2,0))$	1.3	3	0.5	2					1.3	3
13.06 Zr24, 3.87 V20	3.9	3	3.6	5					4.0	3
16.37 V19	6.8	4	6.5	3					6.3	3
21.66 Fe13	1.4	3	0.6	3					2.0	3
22.59 Y2	2.7	4	3.5	3					2.9	4
24.26 24.51 V20	4.5	6	5.3	5					5.2	3
30.74 V19, 0.97 Co37, 1.76 Sc3	1.6	4	1.3	5b					1.9	3
37.45 CN, 9.41 Sc2, 9.78 Sc3	--		8.1	2					9.0	2
40.14 V20	0.1	4	0.2	4					0.2	3
42.80 43.11 V19	2.6	4	3.2	5					3.7	2
44.51 Sc3, 5.21 V20, 5.63 ScII28	5.0	4	5.2	4					--	
49.92 La7	0.5	3	0.3	3					0.2	1
54.26 FeII1	4.6	2	4.4	2					4.9	2
58.60 V19, 8.96 Sc3, 9.89 $C^{13}N^{14}$	9.1	6	8.8	6					8.8	3
61.10 Ti104, 1.24 V20	1.6	5	1.7	4					1.3	3
64.83 Ti144, 5.14 Fe62, 6.32 V20	5.6	3b	5.7	4					6.1	3
68.50 Ti103, 8.84 V20	8.5	4	9.1	4					9.3	3
74.67 V19, 6.31 Sc2	6.0	4b	5.9	4					6.4	4
80.63 Fe13	0.4	4b	0.7	4					1.4	4
85.19 V19	5.2	5b	5.7	5					6.4	3
92.86 V19, 3.00 Ti103	2.8	3b	3.2	4	---		---		3.4	3

TABLE 3 (continued)

Wave-length and Identification	WZ Cas		UCyg		U Hya		V Aql		RY Dra	
	W.L.	Int.	W.L.	Int.	W.L.	Int.	W.L.	Int.	W.L.	Int.
6296.52 V19, 6.65 Ti1	6.5	3	6.2	4	---		---		--	
6300.70 ScII28	9.9	2	0.0	3					9.4	3
05.67 Sc2, 6.05 Sc3	6.1	5	6.2	6					5.9	4s
25.22 Ti1, 5.90 La2	5.6	4b	5.1	4					4.9	2
27.60 Ni44	7.5	4b	7.2	4					7.8	3
33.33 CN(5,1)	2.2	2	2.1	4					2.7	3
41.68 Ba6, 2.08 ScII28	--		1.6	2					--	
44.83 Sc1	4.7	4b	5.1	2					4.7	2
58.69 Fe13, 9.90 Ti1	8.9	3	8.4	5b					0.0	3
62.29 Sc1, 2.87 Cr6	3.0	3	2.9	3					3.2	1
78.82 Sc1	9.2	4b	8.9	4					9.2	2
81.42 Ti196	1.6	2b	2.0	3b					2.5	2
90.48 LaII33	9.1	3b	9.5	4					9.4	3
94.23 La7	4.1	3	3.7	4			---		4.4	2
6400.34 Fe13	1.0	3b	0.6	3			0.3	2	1.3	3
02.01 Y2	2.2	4	2.7	3			2.5	2	2.4	3
13.13 Ti1, 3.35 Sc1	3.7	4	3.4	5			3.0	2	3.5	4
19.15 Ti196	0.1	2	9.8	4			9.8	1	9.9	2
24.09 C_2?	5.8	3b	5.4	5			5.4	2	5.3	3
30.85 Fe62, 1.91 CN	1.3	3b	--				--		--	
35.02 Y2	5.3	3b	5.2	2			5.2	2	4.7	2
45.76 Zr57	4.5	5	4.3	5			4.8	3	4.3	3
49.81 Ca19? 0.23 Co37 etc	9.8	5b	0.6	7b			9.1	2	0.0	2
64.67 Fe13, 4.70 Ca19?	4.4	4	3.8	4			3.9	1	5.5	3
70.25 Zr65, 1.66 Ca18?	1.5	2b	0.6	3			0.6	2	0.7	2

TABLE 3 (continued)

Wave-length and Identification	WZ Cas		U Cyg		U Hya		V Aql		RY Lra	
	W.L.	Int.	W.L.	Int.	W.L.	Int.	W.L.	Int.	W.L.	Int.
75.63 Fe206	5.8	2	4.8	3			4.8	1	5.9	2
81.88 Fe109, CN(6,2)	1.7	2	1.6	2			1.6	2	1.9	2
93.78 Ca18?	4.7	3b	3.7	5			3.7	2	4.5	1
6501.21 Cr16	0.0	3	0.3	2			0.8	1	0.2	1
31.44 V48	0.6	1	0.3	1			0.0	1	0.9	1
32.89 Ni64	3.1	2	2.8	3			2.8	2	3.4	3
43.17 La7, 3.51 V48	3.0	3b	3.3	4b			--		3.0	2
47.58 Fe13	8.0	2	7.2	3b			7.2	3	7.5	2
54.23 Ti102	4.5	3	3.9	3			4.5	2	4.5	2
57.40 Y1, 8.02 V59	7.7	4	8.0	3			8.0	2	8.0	3
65.62 Ti, 5.88 V48	5.3	3b	6.3	3			6.3	2	5.4	2
70.96 La147	0.3	3	0.4	4			0.4	3	0.7	2
72.78 Ca1, 2.90 Cr16	3.8	2	3.3	3			--		--	
74.24 Fe13, 5.02 Fe206	5.0	3	5.7	3			6.2	3	5.6	2
84.89 Y1	4.5	4	4.0	4			4.2	3	3.8	3
95.33 Ba6	5.9	2	6.4	2			6.3	4	6.3	3
99.11 Ti49, 9.25 C_2	0.5	2	9.4	2			9.3	2	9.1	1
6609.68 Fe13	0.4	3s	0.4	2			0.9	2	0.5	2b
24.86 V48, 5.04 Fe13	5.2	3b	4.6	2			4.7	3	5.6	2
30.02 Cr16, 2.44 Co111?	1.1	3b	1.4	2			1.2	2	1.5	2
43.64 Ni43	4.3	2b	4.0	1			3.3	2	3.6	2
48.08 Fe13	9.0	2	9.1	1	---		9.1	1	8.7	2
50.80 La	1.6	3	1.8	2	1.6	2	1.3	2	2.1	2
63.45 Fe111	3.1	1	3.4	1	3.9	1	2.9	1	3.2	2
75.27 Ba6	5.1	2	5.5	2	4.9	2	4.9	2	5.2	2

TABLE 3 (continued)

Wave-length and Identification	WZ Cas		U Cyg		U Hya		V Aql		RY Lra	
	W.L.	Int.	W.L.	Int.	W.L.	Int.	W.L.	Int.	W.L.	Int.
6687.57 Y1	8.8	4	8.5	3	8.4	2	8.3	3	7.9	2
93.84 Ba6	4.4	2	4.1	1	3.8	1	3.8	1	4.6	1
6707.74 7.89 Li1	8.6	8	8.5	2	7.9	1	8.2	1	8.5	2
39.54 Fe34	0.1	1b	0.4	2d	0.1	2	0.4	1	0.5	2
43.12 Ti48	4.2	2	3.3	2d	2.6	2	2.8	4	3.8	2
48.43 Ti152	8.3	1	8.0	1	7.9	1	7.8	2	8.1	1
53.00 V31	3.5	2	3.3	1	3.4	1b	2.9	1	3.1	1
62.38 Zr1	2.2	4	2.9	3	3.3	2	3.2	4	3.2	2
71.04 Co54	0.4	1	0.4	1	0.7	1	0.9	1	0.9	1
74.28 LaII2	4.8	3	4.8	3d	3.8	2	4.5	2	4.7	2
91.02 Sr3	1.1	2	0.4	3b	0.8	2	0.5	1	0.7	1
93.71 Y1	4.0	3	4.7	3b	3.6	3b	3.3	5b	3.9	3b
6801.87 Fe34	0.5	1	2.1	2	0.9	1	1.5	3	1.6	1
08.88 LaIII	9.6	3	9.2	2b	9.2	2	9.4	3	9.7	2
12.40 V31	1.8	1	1.7	1	1.7	2	1.8	1	2.3	1
32.44 V31, 2.93 Zr1	3.2	4	3.8	3	2.9	2	2.5	2	3.1	4
37.91 LaII33	8.7	3	8.4	2b	8.5	1	8.8	2	8.6	2
41.89 V31	1.0	2	1.5	2	1.1	1	0.9	2	1.7	1
51.64 Fe34	2.1	1	1.8	3b	1.6	2	1.6	2	2.5	2
7001.57 Ni64	0.5	1d	0.8	3b	0.9	2	0.7	3	1.0	4
07.81 Ti100	7.1	1	7.6	2	7.5	2	7.2	1	6.8	1
37.04 Fe61, 7.53 Atm	8.0	3	7.9	6	7.7	1	7.0	5	7.4	3
45.96 La6	5.2	5	6.2	6	4.9	4	6.0	4	5.2	5
52.78 Atm, 2.87 Co54	2.8	4	3.8	6	3.3	3	3.1	5	3.1	3
59.94 Ba5, 0.45 Atm	0.1	5	0.6	6	0.0	5	0.6	5	0.5	5

TABLE 3 (continued)

Wave-length and Identification	WZ Cas		U Cyg		U Hya		V Aql		RY Dra	
	W.L.	Int.	W.L.	Int.	W.L.	Int.	W.L.	Int.	W.L.	Int.
68.37 LaI	8.0	5	8.1	6	7.7	4	8.5	3	8.5	2
84.25 Ti99, 4.97 Co54	4.0	2	4.9	3	3.8	2	4.0	3	4.1	2
____ CN(3,1)?	0.7	3	0.0	3	0.2	3	0.5	3	0.6	3
7102.95 Zr42	2.2	3d	2.7	3b	2.6	2	2.7	3	2.5	2
10.91 Ni64, 1.71 Zr23	0.9	1d	1.6	3b	1.6	3	0.8	4	1.0	3
24.47 Co53	3.8	1	4.6	1	4.0	2	4.2	2	4.5	2
30.34 Ti100	1.4	3b	1.6	4b	1.1	3	1.1	4	1.2	2
38.91 Ti99	8.8	2	9.1	3	9.4	3	9.0	4	9.5	2
48.15 Ca30	8.4	2b	8.5	5b	8.4	3	8.1	4	8.2	4b
54.69 Co89	5.6	2b	5.1	3	5.1	2	5.3	3	5.5	3
60.33 Ti98	9.9	2	0.7	3b	9.9	2	0.6	4	0.8	3
7334.17 La	3.8	3d	4.1	3b	3.5	2	4.3	2	3.6	2
54.58 Co53	4.7	4	5.1	4b	4.8	2	5.2	3	5.4	3b
63.74 Atm, 4.11 Ti97	3.2	4b	3.6	3b	2.3	2	2.7	2	2.6	2
7406.23 YII25	6.9	2	7.3	3	7.6	3	7.3	2	6.4	1
14.51 Ni62	5.1	2	5.8	3	6.3	4	5.3	3	5.2	3
37.16 Co53	7.2	2	7.7	2	7.6	3	7.5	3vb	7.4	3
39.89 Zr23, 0.60 Ti225	0.8	2d	0.9	3	0.9	4	1.1	3	0.5	2
50.32 YII25	0.2	2d	0.2	2	0.8	3	9.5	3	9.5	3
____ CN(6,3)	1.7	2	1.4	1	1.4	4	0.8	4vb	0.1	2
74.94 Ti142	5.1	3	5.3	3b	5.3	4	4.2	3	4.5	3
78.77 Co53, 9.61 Zr	9.2	2	9.3	2	9.5	3	9.7	3	9.0	2
83.48 LaIII	3.9	5b	4.7	4b	3.0	5	4.1	3	3.2	3
89.61 Ti225	0.1	1d	9.8	2	0.7	4	9.6	2	9.3	1
94.72 Fe33	4.8	3	4.6	3b	5.3	4b	4.6	3b	4.6	3

TABLE 3 (continued)

Wave-length and Identification	WZ Cas		U Cyg		U Hya		V Aql		RY Dra	
	W.L.	Int.	W.L.	Int.	W.L.	Int.	W.L.	Int.	W.L.	Int.
7554.73 Zr23	4.8	4	5.0	4	5.6	5	4.8	3	4.9	3
90.57 Co89	9.7	1	9.0	1	9.8	2	9.3	2	9.6	2
7664.91 K1, 5.95 Atm O_2	4.2	6	4.7	5	5.2	4	5.0	3	4.5	3
98.98 K1	7.9	6	8.7	4	8.2	3	8.5	2	7.8	2
7714.27 Ni62, 4.56 C_2(3,0)	4.0	4	4.0	3	4.7	3	5.4	2	5.7	2b
23.20 Fe108	3.7	2	4.1	2	4.4	3	3.7	2	4.2	2
32.12 C_2	2.1	2b	---		1.8	3	2.1	2	1.7	2
47.05 C_2	5.6	3			6.4	3	6.0	2	6.3	2
80.48 Ba5	1.3	2			1.7	2	--		--	
78 ___ CN(2, 0)	0.4	3			9.5	3	0.9	2	0.6	2
73.34 3.96 CN(2, 0)	3.4	3b			3.6	4	3.4	2	3.2	3
93.51 Atm, 4.15 CN(2, 0)	4.6	6			--		4.0	2	3.7	2
98.38 8.6 CN	7.9	5			7.6	5	6.9	5vb	6.9	4
7905.60 CN, 5.75 Ba10	4.7	3b			4.8	3	4.3	2	4.2	3
08.60 C_2?, 8.75 CN Atm	8.1	3			9.4	5	9.2	3	8.8	3
12.87 Fe12, 3.80 CN	3.4	3			3.6	3	3.5	2	2.6	2
17.71 C_2, 7.78 8.38 CN	7.1	5			7.3	5	7.8	2	6.8	5
33.12 3.48 CN	4.2	2			4.3	2	--		3.9	3
38.53 Ti151, 8.61 9.23 CN	8.6	2			9.3	3	8.5	2	8.8	3
44.38 CN, 4.65 Zr40	3.2	2			4.0	4	3.3	3b	2.7	3b
56.69 Zr41, 6.71 CN	6.7	2			7.6	2	7.1	2	6.3	2
62.61 3.13 CN, 4.97 CN Atm	3.4	2			4.3	2	3.7	2	2.9	2
87.36 Co89, 7.97 CN	6.8	5b			5.7	4	7.6	3	6.3	4
92.32 CN	2.7	3			3.3	2	--		2.1	2
95.63 CN, 6.80 Co79	5.3	3			6.3	3	5.4	2	5.5	2

TABLE 3 (continued)

Wave-length and Identification	WZ Cas		U Cyg		U Hya		V Aql		RY Dra	
	W.L.	Int.	W.L.	Int.	W.L.	Int.	W.L.	Int.	W.L.	Int.
99.88 0.30 CN	9.0	2			0.6	3	9.7	1	9.6	2
8002.40 CN	3.1	4b			3.1	5	4.0	3	3.1	3
10.09 CN	1.8	3b			2.8	4	1.5	3	1.2	3
17.04 CN	6.5	2			--		6.3	1	5.9	2
27.36 V30, 6.31 CN	6.6	6b			6.7	5	6.7	2	6.0	3
39.60 Atm, 0.28 CN	0.0	2			1.2	2	---		0.3	1
43.17 Atm, 3.87 4.40 CN	4.5	5			3.6	5			3.6	4
49.90 CN	1.0	4			1.6	4			0.5	4
60.25 CN	0.7	2s			1.0	3			0.0	1
67.26 CN(2, 1)	7.8	2			8.8	2			7.4	2
72.12 Zr40, 2.62 CN	2.1	2			1.9	3b			1.4	3b
81.52 2.54 CN	2.4	5			1.5	4			0.9	3
93.48 V30	3.2	4			3.3	4b			3.0	3b
8107.12 CN	6.0	2			5.7	4			7.3	3d
10.09 CN, 0.18 C_2	0.1	4			1.0	3			0.2	2
14.89 CN	5.2	3			4.3	3			4.8	3
18.91 CN	9.9	4			0.1	3			9.4	4
25.45 CN(3, 1) Atm, 6.23 CN	5.9	4			4.9	3			4.7	3
33.00 Zr40, 3.53 C2 stc	2.0	5b			2.8	3b			2.8	3b
49.69 Atm, 9.88 CN	9.2	3			0.2	3b			9.6	3
61.06 V30, 1.43 CN etc	1.2	4b			0.3	3			0.3	3
86.37 Atm, 6.73 V30	7.1	3b			7.2	3			6.8	3b
93.11 Atm, 4.79 4.82 Na4	3.8	3	---		4.9	2	---		3.8	2

Notes to TABLE 3.

b: broad.

d: diffuse.

s: sharp.

vb: very broad.

--- : out of the region which the investigated spectrograms show.

-- : unable to identify.

Microphotometer tracing of all these spectrograms has been carried out by the registering microphotometer of the Yerkes Observatory.

Wave lengths have been derived in the usual way and corrected for the radial velocity corresponding to each star. The identification of the lines was aided by the M.I.T. wave-length table, Rowland's preliminary table, Moore's *Revised Multiplet Table*, the *Solar Spectrum, λ 6600 to λ 13495*, by Babcock and Moore, our table of U Cyg (Fujita 1952), and the microphotometer tracings here described.

As no special consideration has been given to the spectrophotometry, only the visual estimation of each line has been determined. Table 3 gives the list of wave lengths, their identifications, and estimated intensities. In this table many faint lines (the identifications of which are uncertain), most of the A and B band lines of O_2 which seem to blot out the stellar features, and the region longward from 8200 A (as much of its structure may be blended with CN bands) have been excluded. After the identifications were made, atomic lines which are sensibly free from blends and are comparatively sharp were selected for the purpose of the following discussion.

The plotting of the estimated intensity against the lower excitation potential of each line clearly shows that the gradient of the mean curve becomes steeper as the spectral class proceeds from the early C type toward the late C (Fig. 1). Though the scatter is large, we can still recognize its systematic course and see that the C classification is quite consistent with the evidence from spectrograms of medium dispersion. The scatter seems to be reduced in some degree if we correct the estimated intensity of each line for the intensities of some telluric oxygen bands.

One of the remarkable features in the spectra of these five stars is the appearance of the K 7699 line. Because this line seems to be very sensitive to the spectral types concerned, as is shown in our photometric tracings, K 7699 can be considered a most effective indicator of the temperature which prevails in the atmosphere of these stars. As is shown in Table 3, WZ Cas has the highest and RY Dra the lowest value of this intensity.

Now, N_0, the number of neutral atoms per volume in the stellar atmosphere which is composed of n kinds of elements, can be written in the following equation (Fujita 1936):

$$N_0^{(i)} = \frac{\epsilon_i P}{g\bar{m}} - \frac{\epsilon_i}{g\bar{m}} K_i \ln \frac{P+K_i}{K_i} + \frac{\epsilon_i}{g\bar{m}} \frac{P^2}{P+K_i} \left[\sum \frac{\epsilon_i K_i}{P+K_i}\right]^{-1}$$

$$- \frac{\epsilon_i}{g\bar{m}} \int_0^P \frac{K_i P}{(P+K_i)^2} \left[\sum \frac{\epsilon_i K_i}{P+K_i}\right]^{-1} dP,$$

where

$$\bar{m} = \sum_{i=1}^{n} \epsilon_i m_i \ (i = 1, 2, \ldots, n) ;$$

ϵ_1, ϵ_2 are mean abundances of the elements; m_1 and m_2, atomic weights; K_1 and K_2, ionization functions; P, electron pressure; and g, surface gravity. Our calculation shows that the number of atoms of potassium between the temperature range of 1500°–5000° becomes a maximum around 1600° in case of giant stars and 2400° in the case of dwarf stars. Thus C9 corresponds to the lowest temperature: the latter increase with the decreasing suffix number of C.

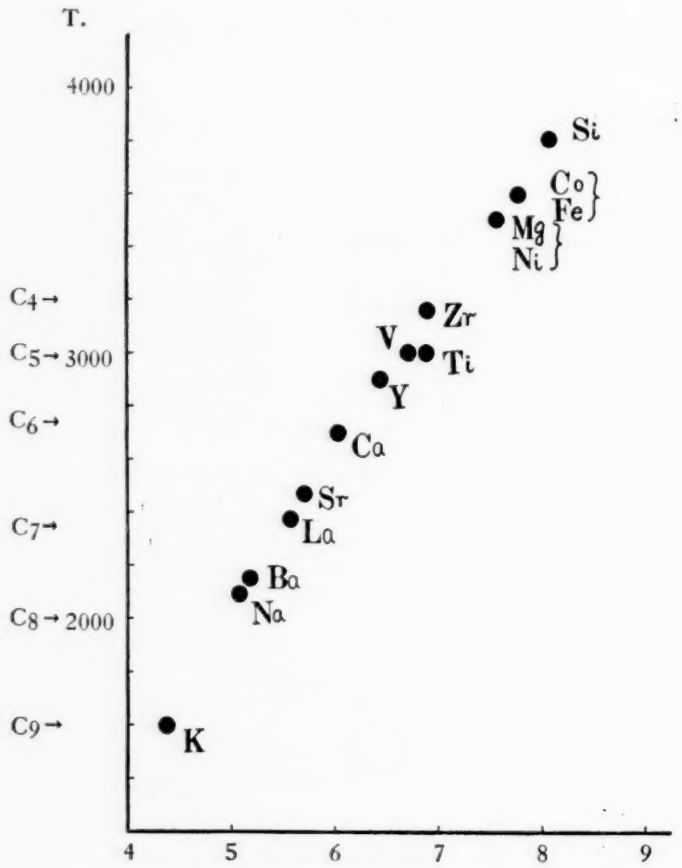

FIG. 2.—Ionization potential (*abscissa*) and the temperature, which shows the maximum number of atoms in giant stars.

For the other elements whose lines are observed on the spectrograms investigated, we can calculate the temperature at which the number of atoms becomes maximum. Comparing this with the observational data, we can derive the data of Figure 2, in which the estimated temperature is shown corresponding to each subclass of C.

However, as has been shown by several authors (McKellar and Stilwell 1944), the appearance of Li I 6708 is quite peculiar. It does not follow the usual formula, according to which its maximum should appear around C7 in giant stars. It shows very strong intensity in WZ Cas and is very faint in the other four stars. It is not certain whether this peculiarity is due to the unusual abundance of lithium or to another reason.

I should like to express my thanks to Professors W. W. Morgan and B. Strömgren for having put at my disposal the McDonald spectrograms and the Yerkes microphotometer.

REFERENCES

Fujita, Y. 1936, *Jap. J. Astr. Geophys.*, **13**, 141.
———. 1952, *Ap. J.*, **116**, 46.
Keenan, P. C., and Morgan, W. W. 1941, *Ap. J.*, **94**, 501.
McKellar, A., and Stilwell, W. H. 1944, *J.R.A.S. Canada*, **38**, 237.

THE RADIAL VELOCITY VARIATION OF THETA OPHIUCHI

A. Van Hoof, F. Bertiau, S.J., and R. Deurinck
Astronomical Institute of the University of Louvain
Received February 21, 1956

ABSTRACT

A rediscussion of Henroteau's 1920 and 1922 radial-velocity measurements and new observations with the 82-inch McDonald telescope in February, 1955, show that θ Ophiuchi very probably is a β Canis Majoris star with a period of 0.153846 day. The γ-velocity, as well as the amplitude of the radial-velocity variation, is variable. A beat period of about 68 days is suspected.

The variability of the radial velocity of θ Ophiuchi [R.A. = $17^h18.9^m$, Decl. = $-24°57'$ (1950)] was discovered by F. Henroteau (1922), who observed the star on one night in June, 1920, and on several nights in June and July, 1922. From his observations of 1922, Henroteau concluded that the star is of the β Canis Majoris type with a period of 0.28620 day. The observations of 1920 seemed to indicate that a large variation in the mean velocity was present, and, probably on account of the very large scatter of the individual points around his mean curve, Henroteau concluded that "perhaps other complications have to be expected."

Recent lists of β CMa stars do not include this object, the reasons for its exclusion being that (1) Henroteau's period is definitely too large for the spectral type (B2) and luminosity class (IV) to make the star fit into the period-luminosity and period-spectrum relations found to hold for β CMa stars (Blaauw and Savedoff 1953; McNamara 1953*a*, *b*) and (2) the form of Henroteau's radial-velocity curve resembles, with its sharp maximum and broad minimum, that of a spectroscopic binary with fairly large eccentricity rather than that of a β CMa star.

However, after an inspection of Henroteau's results for the different nights separately, there is reason to think that the period proposed by him is not correct. In fact, Henroteau's measurements, which are here reproduced graphically in Figure 1, reveal among other things that (1) on all the "even" Julian days the radial velocity goes through a maximum at about 0.7 day, while it goes through a minimum at this same time of the day on all the "odd" Julian days, and (2) the rise from minimum to maximum, as well as the fall from maximum to minimum, radial velocity lasts in most instances less than 0.1 day.

The first circumstance proves that the period must be very close to

$$P = \frac{1^d}{n + 0.5}, \qquad (1)$$

when n is an integer; the second circumstance reveals 5 to be the minimum value that should be tried for this integer and rules out the value 3, which actually is the one that corresponds to Henroteau's period of 0.28620 day.

In our opinion, which is strengthened by the results of our own measurements, Henroteau's investigation reveals further that the amplitude of the radial-velocity variation is variable; while it is large on JD 2422489, it is definitely smaller on JD 2423210 and 2423218 and increases again until the last night of the observations. This suggests that beats may be present, a phenomenon quite common among β CMa stars. This consideration, together with the expectation of a changing γ-velocity, has withheld us from constructing a mean curve with one of the periods derived from formula (1); instead, we drew curves with period $P = 0^d153846$ (corresponding to $n = 6$ in formula [1]) through

the points of the individual nights and adjusted their amplitudes and their mean velocities so as to get a reasonable scatter of the observations around them. We shall come back to these curves at the end of the present note.

In February, 1955, one of us (Bertiau) had the opportunity to take 29 spectrograms of θ Ophiuchi at the McDonald Observatory, as part of Dr. Blaauw's spectroscopic program of stars in the nearest associations. All plates were taken with the D camera at the coudé spectrograph and have a dispersion of about 35 A/mm.

Their measurement by the senior author gives the results collected in Table 1 and shown graphically in Figure 2. The lines measured were the hydrogen lines Hβ H15 and the He I lines between 4922 and 3819. In order to save labor, the computation of the mean errors has been limited to about half the total number of plates. The general average mean error per plate is seen to be of the order of 2 km/sec.

The only two nights on which several plates have been taken show the peculiarity to which we drew attention in considering Henroteau's results: at fraction 0.96 of the *even* Julian day, the radial velocity goes through a maximum, while it goes through a minimum at this same fraction of the *odd* Julian day.

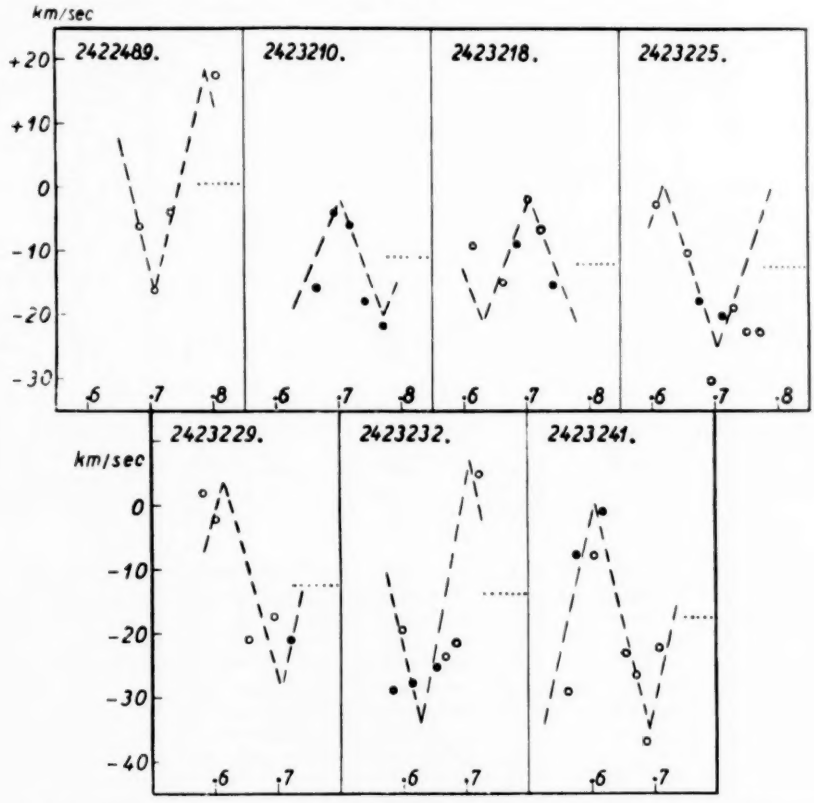

FIG. 1.—Henroteau's radial velocities for the Julian day marked on each plot. Abscissae are fractions of the Julian day. Dots represent observations qualified as "the best" by Henroteau.

From this we felt entitled to represent all the observations in one plot having the fraction of the Julian day corresponding to the time of the observation as abscissa. A mean curve was then drawn through the points of the *even* nights and another one through the points on the *odd* nights. As the nights of both sets are in regular alternation and are about equal in number, a variation in the amplitude or in the γ-velocity in the course of the 3 weeks covered by the observations must have affected the tracing of our two curves by practically the same amount, so that the period is very nearly equal to twice the distance between their points of intersection.

The result, 0.15 day, is closest to 1/6.5 day and, owing to the necessity to satisfy formula (1), the latter value or

$$P = 0^{d}.153846 = 3^{h}42^{m}$$

TABLE 1

RADIAL VELOCITIES OF θ OPHIUCHI OBSERVED IN FEBRUARY, 1955

Plate Cg	Night Feb., 1955	U.T.	JD 2430000	Radial Velocity (km/sec)	No. of Lines Used	Mean Error (km/sec)
1109	7–8	12:20	5146.014	− 5.3	24	±1.5
1110	7–8	12:43	.030	− 5.2	26	1.4
1132	8–9	11:36	.984	− 8.0	24	1.3
1162	9–10	11:50	7.993	−11.2	25	1.2
1163	9–10	12:01	8.001	−10.1	25	1.3
1204	11–12	11:42	9.988	− 6.1	20	1.4
1205	11–12	11:47	.991	− 7.3	24	.....
1282	14–15	12:03	53.002	−10.6	24	1.5
1283	14–15	12:09	.006	−10.5	25	.....
1364	16–17	11:54	4.996	− 8.0	24	1.2
1365	16–17	12:00	5.000	− 9.0	26	.....
1434	19–20	10:07	7.922	− 5.6	17	2.2
1436	19–20	10:58	.957	−11.8	24	.....
1439	19–20	11:44	.989	− 9.5	25	2.2
1443	19–20	12:50	8.035	− 6.7	20	.....
1444	19–20	13:00	.042	− 5.2	23	2.2
1546	24–25	9:30	62.896	−12.2	19	3.0
1547	24–25	9:47	.908	− 8.7	25	.....
1548	24–25	10:01	.918	− 7.4	23	.....
1549	24–25	10:16	.928	− 7.3	23	.....
1550	24–25	10:34	.941	− 7.2	18	2.3
1551	24–25	10:52	.953	− 4.2	20	.....
1552	24–25	11:08	.964	− 4.6	23	.....
1553	24–25	11:23	.975	− 2.9	20	.....
1554	24–25	11:38	.985	− 7.4	17	.....
1556	24–25	12:27	3.019	−10.1	24	2.4
1563	25–26	12:38	4.026	− 3.8	24	2.0
1580	27–28	12:37	6.026	− 5.3	19	±0.9

is a better approximation to the real period. We say "approximation," because there is not between the exact period and the duration of the solar day the nice commensurability illustrated by formula (1).

At the time of Henroteau's observations the radial velocities went through a maximum at fraction 0.70 of the even Julian day; in our observations there is a maximum observed at fraction 0.96 of the even Julian day, so that the preceding one must have occurred at 0.81. Hence the 1922 maximum is seen to be shifted $0^d11 + N$ periods forward in 1955, N being zero or a positive or negative integer. Because of the length of the interval between the two sets of observations, it is impossible to determine N and to improve P. The consideration, however, that the time of maximum radial velocity was practically the same in 1920 and in 1922 suggests that N is very small, 0 or +1 or −1 being the most probable values.

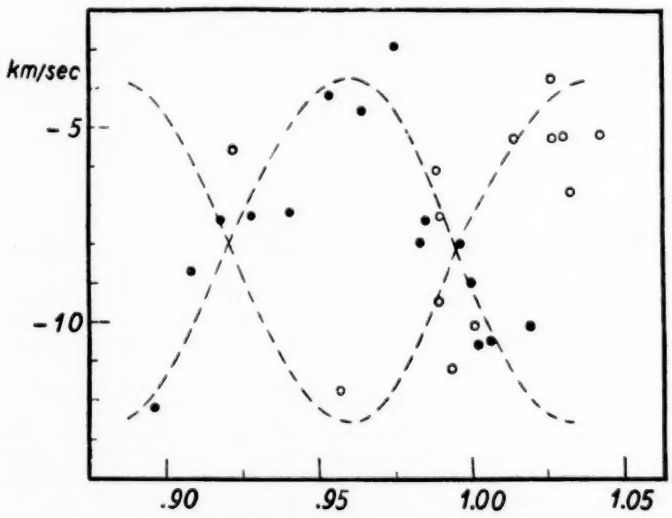

FIG. 2.—The new observations. Abscissae are fractions of the Julian day. Dots represent observations on the mornings of "odd" days in February, 1955 (= "even" Julian days); circles refer to observations on the mornings of "even" days in that same month (= "odd" Julian days).

The period proposed by us is therefore a very close approximation to the true period, and it places the star at the right spot in Struve's (1955) synoptic table of β CMa stars. With its spectral type B2 and luminosity class IV in Morgan's system, Θ Oph has indeed the expected absolute magnitude $M_v = -3.0$, as was determined recently by Bertiau from its membership of the Scorpio-Centaurus cluster.

The γ-velocity at the time of our observations was −8 km/sec, a value distinctly different from the 1920 and 1922 values, which were 0 and −15 km/sec, respectively. Henroteau's statement concerning the variability of the γ-velocity is therefore confirmed.

For the amplitude of the radial-velocity variation we find about 8 km/sec, which value is based mainly on the observations of February 19 and 24. This value is again definitely smaller than those that can be derived from Henroteau's observations. Beats may therefore well be present.

Taking into account the conclusions from the two foregoing paragraphs, we drew through Henroteau's points the curves shown as dashed lines in Figure 1. Some arbitrariness in their drawing was unavoidable, but, as they stand, they show a reasonable spread of the observations and seem to indicate (1) that the γ-velocity increased from about -12.5 km/sec at the beginning of the 1922 observations to about -17.5 km/sec near the end and (2) that the amplitude increased at the same time from about 20 km/sec to about 35 km/sec. The latter value has also been attained on the single night that the star has been under observation in 1920.

Assuming 35 km/sec to be the maximum amplitude (there is apparently no further increase between JD 2423232 and 2423241) and 8 km/sec to be the minimum amplitude (our observations, though inadequate for the purpose, seem to indicate a standstill in the amplitude variation), we have the following information for the determination of the hypothetical beat period:

$$1.\quad 2423239^{d} - 2422489^{d} = 750 \text{ days} = N' \times P' ,$$

$$2.\quad 2435162^{d} - 2423239^{d} = 11923 \text{ days} = (N'' + \tfrac{1}{2}) \times P'$$

where N' and N'' are integers and P' is the beat period; and

$$3.\quad \frac{P'}{2} > 30 \text{ days}.$$

All these requirements are fulfilled with $P' = 68.3$ days, which is believed to give at least the order of the minimum value that may be expected for the beat period. The result can, of course, not be said to rest on a very solid base, but it constitutes the only information that can be gained from the existing material, and it may therefore be useful to those who are planning further observations of this star. [The old Lick observations (Campbell and Moore 1928) are of little use as long as the variation of the γ-velocity remains unknown.]

Because of unsteady weather conditions, our material is rather heterogeneous and does not lend itself well to a study of possible changes in the line widths. Our impression is, however, that the lines are somewhat broader on the ascending branch of the radial-velocity-curve than they are on the descending branch. Should this really be the case, then it would indicate that $K_2 > K_1$ (in Struve's notations). The star would then in this respect be similar to β CMa.

REFERENCES

Blaauw, A., and Savedoff, M. P. 1953, *B.A.N.*, **13**, 69.
Campbell, W. W., and Moore, J. H. 1928, *Pub. Lick Obs.*, **16**, 253.
Henroteau, F. 1922, *Pub. Dominion Obs., Ottawa*, **8**, 1.
McNamara, D. H. 1953*a*, *Pub. A.S.P.*, **65**, 165.
———. 1953*b*, *ibid.*, p. 286.
Struve, O. 1955, *Pub. A.S.P.*, **67**, 150.

LINE BROADENING IN THE SPECTRA OF O- AND EARLY B-TYPE STARS*

ARNE SLETTEBAK
Perkins Observatory
Received February 8, 1956

ABSTRACT

Line profiles were measured from spectrograms of 10.2 A/mm dispersion for 43 stars of types O5–B2 and compared with theoretical line profiles computed under the assumption that axial rotation or large-scale atmospheric motions are responsible for the line broadening. Visual estimates of line broadening in the spectra of 110 additional O5–B5 stars were made for a statistical study of line broadening versus spectral type and luminosity class. Measures of the emission-line intensities in the O5–O8 stars suggest a correlation between the luminosity and the amount of emission for these stars. It was found that, with the observational material used, it was impossible to distinguish between axial rotation and large-scale atmospheric motions in a given star from a study of the line profiles. The statistical study of line broadening in the O5–B5 stars, however, yielded the following conclusions:

1. Large-scale atmospheric motions play an important role as broadening agents in the spectra of the O5–O8 stars of all luminosity classes and the high-luminosity stars of types O9–B1.

2. These large-scale atmospheric motions appear to increase with increasing temperature and increasing luminosity.

3. Axial rotation acts as an additional broadening mechanism for these stars but decreases with increasing luminosity at a given spectral type.

4. Among the O5–O8 stars both mechanisms probably act, but rapid axial rotation occurs more frequently in the stars of lower luminosity, while large-scale atmospheric motions dominate the line broadening in the stars of higher luminosity.

5. Among the O9–B1 stars the line broadening in the supergiant stars appears to be due almost entirely to large-scale atmospheric motions, while the line broadening in the main-sequence stars is due almost entirely to axial rotation. The O9–B1 stars of intermediate luminosity have lines broadened by both mechanisms. Large-scale atmospheric motions no longer dominate as line-broadening agents in the supergiant stars later than B1.

I. INTRODUCTION

A number of investigators (Elvey 1930; Westgate 1933; Slettebak 1949; Huang 1953) have included O- and early B-type stars in studies of line broadening. This class of stars was found to exhibit rather considerable line broadening, which was usually attributed to axial rotation. Recently, Struve (1952) gave several convincing arguments against a strict rotational interpretation of the broad lines which are often observed in the spectra of early-type supergiant stars. He pointed out that an entirely different effect, probably some kind of large-scale turbulence, must play a role in these stars.

The present investigation is an attempt to assess the relative importance of axial rotation as against large-scale atmospheric motions or any other agents which may be responsible for the broadened lines observed in the O- and early B-type stars. Two methods suggested themselves for this purpose. The first is a comparison of observed line profiles with theoretical profiles computed for various broadening agents. The second is a statistical study of line broadening as a function of spectral type and luminosity class.

The effect of large-scale atmospheric motions on line profiles has been considered by a number of investigators. In a study of η Aquilae, Schwarzschild, Schwarzschild, and Adams (1948) found a discrepancy between the turbulent velocities obtained from the curve of growth and those determined from line profiles, and they suggested large-scale photospheric motions as a possible explanation. The theory was advanced that these motions were caused by a convection with turbulent elements so large that their linear

* This investigation was carried out while the author was a guest investigator at the Mount Wilson and Palomar Observatories and was supported by a National Science Foundation grant.

dimensions exceeded the depth of the effective photospheric layers and hence had but little effect upon the equivalent widths and the curve of growth. In investigating a similar discrepancy for δ Canis Majoris, Unsöld and Struve (1949) also suggested large-scale turbulent motions as the most probable explanation. In the past few years Huang (1950*a*, *b*) and Huang and Struve (1952, 1953, 1954, 1955) have done considerable work on the problem of large-scale atmospheric motions. Of particular interest for the present investigation is their joint study (1953) of the B1 supergiant ρ Leonis, in which theoretical line profiles for axial rotation and for various kinds of mass motion were computed and compared with observed line profiles. Their results were essentially negative: the profiles of the weaker lines could be represented as due either to rotation or to vertical convection, with a step-function type of distribution in the velocities, while the stronger lines slightly favored convection.

A statistical study of line broadening as a function of position on the H-R diagram for the O- and early B-type stars may also help to differentiate between axial rotation and other broadening agents for these stars. Miss Underhill (1949*a*) has pointed out that stars of low surface gravity and high effective temperature are likely to have large-scale turbulent motions in their atmospheres due to radiation pressure effects. In the absence of axial rotation, a correlation between line broadening and position on the H-R diagram might then be expected to exist, with all stars showing some line broadening in the domain where the large-scale atmospheric motions exist. If axial rotation is the sole broadening agent, on the other hand, a sufficient number of observations should reveal some sharp-lined stars of all spectral types and luminosity classes, since some stars will be viewed pole-on. A statistical study of this kind has been made by Huang and Struve (1954), who considered B0–A2 stars of all luminosity classes and supergiant stars from O9 to F8. Their results suggest that the line broadening in the supergiant stars is due to mass motion in the atmosphere which has a spherical symmetry, such as convective motion, large-scale turbulent motion, etc.

II. OBSERVATIONAL MATERIAL

The spectrograms used for the determination of line profiles were all taken with the 32-inch camera of the coudé grating spectrograph of the Mount Wilson 100-inch telescope, which gives a dispersion of 10.2 A/mm. in the blue in the second order. A total of thirty-seven O- and early B-type stars was observed by the writer during the period January–March, 1955. The spectrograph slit for these exposures was set to correspond to 20 μ at the plate. All spectra were widened to 1 mm on the plate; this relatively large width was chosen in order to minimize plate-grain effects in the line-profile determinations. Eastman IIa-O plates were used throughout, developed in D-76 developer for 15 minutes at 66° F. A step-slit calibration was put on each plate with the standard equipment of the coudé spectrograph. In addition, spectrograms of eight stars, two of which were also observed by the writer, were kindly loaned to me by Dr. I. S. Bowen with the permission of Dr. J. B. Oke and Dr. L. Spitzer, Jr. These plates had been previously used by Dr. Oke (1954) in an investigation of the early O and Of stars and were extremely valuable as supplementary material in this study. The observational data for the latter set of plates are quite similar to those of the writer's plates and may be read in detail in Dr. Oke's paper. Microphotometer tracings of all the spectrograms were obtained with the Perkins microphotometer, using a magnification of 94. Calibration-curves for the reduction of the microphotometer tracings to an intensity scale were constructed at λ 4100 and λ 4500. Line profiles were determined for a total of forty-three stars, most of which were represented by more than one exposure. These stars are listed in Table 1.

In order to supplement the material described for statistical purposes, visual estimates of line broadening were made from spectrograms of 110 additional O- and early B-type stars. The large majority of the spectrograms examined in this way were taken by Dr. Guido Münch with the 100- and 200-inch telescopes, using dispersions of approximately

TABLE 1

MEASURES OF LINE BROADENING EXPRESSED AS TURBULENT OR ROTATIONAL VELOCITIES

No.	Designation	HD	MK	No. of Plates	$\overline{v^*}$ (km/sec)	$\overline{v \sin i}$ (km/sec)	p.e. of $\overline{v^*}$ (km/sec)
1*	AO Cas	1337 A	09 III	1	105:	135:	± 6
		1337 B			115:	145:	±16
2*	o Per	23180 A	B1 III	2	60:	75:	± 3
		23180 B			120:	150:	±10
3	ζ Per	24398	B1 Ib	2	40	55	± 3
4	ξ Per	24912	07	2	170	210	± 5
5	AE Aur	34078	09.5 V	1	< 20	< 20	
6		34656	07	3	70	90	± 3
7*		35921	09.5 III	1	160	195	±12
8	δ Ori	36486	09.5 II	2	110	140	± 5
9	λ Ori	36861	08	2	60	75	± 4
10*	θ^1 Ori C	37022	06 p	2	90:	115:	± 8
11*	θ^2 Ori	37041	09.5 V p	2	130:	165:	± 5
12	ι Ori	37043	09 III	2	110	140	± 5
13	ε Ori	37128	B0 Ia	2	65	85	± 2
14	ζ Ori	37742	09.5 Ib	2	90	120	± 2
15	κ Ori	38771	B0.5 Ia	2	60	80	± 2
16	139 Tau	40111	B1 Ib	2	100	130	± 3
17	χ^2 Ori	41117	B2 Ia	1	20:	30:	± 6
18		41161	09 n	1	250	300	±19
19		46150	06	3	110	140	± 6
20		46223	05	1	110	140	± 7
21*		47129 A	08	1	90:	110:	± 7
		47129 B			100:	130:	± 6
22		47432	09.5 II	1	80	105	± 3
23	S Mon	47839	07	2	70	90	± 7
24*		48099 A	06	1	70:	90:	±12
		48099 B			60:	75:	± 6
25		48434	B0 III	1	55	70	± 3
26*		54662	06	1	75:	95:	± 8
27	29 C Ma	57060	07 f	3	115	145	± 1
28	τ C Ma	57061	09 III	2	90	115	± 1
29*		57682	09 V	1	< 20	< 20	
30	ρ Leo	91316	B1 Ib	6	45	60	± 4
31	δ Sco	143275	B0 V	2	135	170	± 8
32	τ Sco	149438	B0 V	2	< 20	< 20	
33	ζ Oph	149757	09.5 V	6	290	350	± 8
34	9 Sgr	164794	05	1	110	140	± 7
35	15 Sgr	167264	B0 Ia	1	60	80	± 3
36	κ Aql	184915	B0.5 III	1	225	270	± 5
37	9 Sge	188001	08 f	2	85	110	± 3
38		190429 N	05 f	2	135	170	± 8
39		190864	06	2	75	100	± 6
40		192281	05 f	2	240	290	± 6
41		192639	08 f	2	95	120	± 6
42		193514	07 f	1	95	120	± 8
43*	10 Lac	214680	09 V	2	< 20	< 20	

Notes to Table 1

1. AO Cas. An eclipsing and spectroscopic binary with two spectra visible. The weaker spectrum appears to be similar in type to the stronger.

2. o Per. A spectroscopic binary with two spectra visible. The weaker spectrum appears to be similar in type to the stronger.

7. HD 35921. Spectroscopic binary, with a range of 86 km/sec. Some of the lines give the impression of being double on the plate, but this is very uncertain.

10. θ^1 Ori C. The absorption lines have a peculiar appearance: rather sharp cores with extended wings, which are shaded to the violet. This may be the result of a secondary spectrum, since the star is a known spectroscopic binary. The measured velocity contradicts the visual impression and should be regarded as an upper limit.

11. θ^2 Ori. The absorption lines are similar in shape to those of θ^1 Ori C, and the measured velocity should again be regarded as an upper limit.

21. HD 47129. A spectroscopic binary with two spectra visible. The measured velocities should be considered as uncertain, since the absorption lines of both components show changes in intensity and profile (Struve 1948).

24. HD 48099. The He II 4471 and 4026 lines appear double, with a separation of components of about 110 km/sec. The He II 4200, 4542, and 4686 lines appear single, but the latter is quite broad and asymmetrical.

26. HD 54662. The visual impression of absorption lines with rather sharp cores and extended wings contradicts the measured velocity, which should be regarded as an upper limit.

29. HD 57682. Standard sharp-lined star.

43. 10 Lac. Standard sharp-lined star.

The 09.5 V star, o Orionis, was also observed and was to have been included in this investigation, but the spectrum appeared to be composite and was therefore rejected for profile determination. The strong lines showed sharp cores with broad wings, while the weaker lines were relatively sharp. This is consistent with the observations of Miczaika (1950), who found a doubling of the H and He I lines.

TABLE 2

VISUAL ESTIMATES OF LINE BROADENING EXPRESSED AS TURBULENT VELOCITIES

No.	HD	MK	Dispersion (A/mm)	v^* (km/sec)
1*	108	O8fp	10	90
2*	1383	B1 II	10	70:
3	1743	BO III	10	50
4	2451	BO.5 IV	10	100:
5	2905	B1 Ia	28	40
6	5551	B1.5 Ib	10	$\leqslant$ 20
7	6182	B1 Ib p	10	40
8	6675	BO.5 III	5	50:
9	10125	O9.5 Ib	10	70:
10	13854	B1 Iab	5	50
11	13866	B2 Ib	10	30
12	14633	O8 V	5,10	100
13	15558	O6	10	100
14	15785	B1 Iab	10	90
15	17505	O7	10	100:
16	24432	B3 II	10	<20
17	30614	O9.5 Ia	5,28	70
18	31327	B2 Ib	10	$\leqslant$20
19	242908	O5	10	100:
20	242926	O6	10	70:
21	35633	BO.5 IV	10	100
22	39746	B1 II	10	200:
23	41398	B2 Ib	10	60
24	42088	O6	10	240
25	42379	B1 II	10	50
26	42400	B5 II	10	<20
27	43078	BO IV	10	100
28	43384	B3 Iab	10	$\leqslant$20
29	43753	BO.5 III	10	50
30	43818	BO II	10	70
31	46056	O8	10	120:
32	46149	O8	10	60
33	46966	O8	10	70:
34	47240	B1 Ib	10	100
35	48279	O8	10	100
36	+0°1576	O9 III:	10	150::
37	52266	O9 V	10	250:
38	55879	BO IV	10	40
39*	58978	BO IV? pe	10,28	200
40*	60848	O8 V: pe	10	300:
41	61347	O9 Ib	10	90:
42*	66811	O5f	5	150::
43	93521	O9 V p	10	250:
44	119608	B1 Ib	5	40:
45	149363	BO.5 III	10	70
46	157857	O7f	10	90:
47	158661	BO.5 Ib	10	70
48	161961	BO.5 III	10	40
49	162064	BO Ia	10	60
50	163800	O8	5	110

TABLE 2 (continued)

No.	HD	MK	Dispersion (A/mm)	v^* (km/sec)
51	164353	B5 Ib	28	≤20
52	165049	B2 III	10	<20
53	165319	BO Ia	10	60
54	166286	B1 II	10	100:
55	166287	B0.5 III	10	50:
56	166540	B0.5 IV	10	40
57	166546	09.5 III	10	50
58	166689	B1 Ib-II	10	50
59	167263	09 II	28	100:
60	167287	B1 Ib	10	200::
61	167659	08	10	100:
62	170716	B0.5 Ib	10	50
63	170938	B1 Ia	10	50
64	171589	07f	10	100
65	172275	06	10	100
66	173438	B0.5 Ia	10	60
67	173783	09 I	10	70:
68	173987	B0.5 Iab	10	60
69	-0°3584	08	10	80
70	177812	B1 Ib	10	50
71	186980	07.5	5	110
72	186994	BO III	10	100
73	187459	B0.5 Ib	5	100:
74	188209	09.5 III	10	60
75*	190603	B1.5 Ia+?	28	≤20
76	227634	BO Ib	10	90:
77	190967	B1 Ib-II	10	130:
78	227696	B0.5 IV:	10	200:
79	191139	B0.5 III	10	40
80	191201	BO III	5,10	110
81	191495	BO V	10	300::
82	191566	B0.5 IV	10	60::
83	191612	08	10	80:
84	228053	B1 II	10	60
85	191917	B1 III	10	30
86	191978	08	10	110
87	192422	B0.5 Ib	10	60:
88	194839	B0.5 Ia	10	60
89	195592	09.5 Ia	10	60
90	197460	B0.5 Ib	10	150
91	198478	B3 Ia	10	≤20
92	199216	B1 II	5,10	50
93	202124	09.5 Ib	10	90
94*	203064	08	28	230
95	203938	B0.5 IV	10	180
96*	206267	06	28	150:
97*	206773	BO V: pe	10	400::
98*	210809	09 Ib	10	90
99*	210839	06f	28	150:
100	214080	B1 Ib	5;10	80

TABLE 2 (continued)

No.	HD	MK	Dispersion (A/mm)	v^* (km/sec)
101	215733	B1 II	10	50:
102	215835	O6n	10	200:
103	216411	B1 Ia	10	70
104	216532	O8	10	200::
105	218915	O9 I	10	80
106	219188	B0.5 III	5	150::
107	223987	B1 Ib	10	70
108	224424	B1 Iab	10	60
109	225146	B0 Ib p	10	70:
110	225160	O8f	10	90

Notes to Table 2

1. HD 108. N III 4634, 4641, and He II 4686 emission.

2. HD 1383. He I 4026 and 4471 appear double with the components about equal in strength.

39. HD 58978. Double bright H β and Fe II emission.

40. HD 60848. Double bright Hβ.

42. HD 66811 = ζ Puppis. N III 4634, 4641, and He II 4686 emission.

75. HD 190603. Bright Hβ has P Cygni structure.

94. HD 203064 = 68 Cygni. N III 4634, 4641 emission.

96. HD 206267. Weak N III 4634, 4641 emission.

97. HD 206773. Double bright Hβ.

99. HD 210839. N III 4634, 4641, and He II 4686 emission.

5 and 10 A/mm. I am indebted to Dr. Münch for very kindly making his fine set of spectrograms available to me. The remaining spectrograms from which visual estimates of line broadening were made were obtained from the plate collection of the Mount Wilson and Palomar Observatories (10 A/mm) or were taken with the two-prism spectrograph of the 69-inch telescope of the Perkins Observatory (28 A/mm). The stars for which visual estimates were made are listed in Table 2.

The spectral types and luminosity classes of all stars included in this study are on the MK system and were obtained from the work of Morgan, Code, and Whitford (1955).

III. ANALYSIS OF THE LINE PROFILES

The choice of lines for line profile and subsequent line-broadening determinations in the O- and early B-type stars is a fairly straightforward, though not very satisfactory, process. The spectra of these stars are generally characterized by broad and shallow lines, of which only the strongest do not disappear entirely for cases of large broadening. Almost all the stronger lines are affected more or less by Stark effect, however, and some are blended with other lines in addition. The following seven lines were chosen and measured in all stars listed in Table 1 in which they appeared in sufficient strength: He I, II 4026; Si IV 4089; He II 4200; He I 4388; He I 4471; He II 4542; and He II 4686. The two most objectionable lines are probably the λ 4200 and λ 4542 lines of He II, which are strongly affected by Stark effect. The characteristic Stark wings of these lines were visible only in the main-sequence stars of type O9 and later listed in Table 1. The Stark effect should not play a large role for the B-type stars of high luminosity; nor should it affect the O-type stars in general, according to the work of Miss Underhill (1951). Since the He II 4686 line frequently appears in emission in the O5–O8 stars, it was measured only in stars later than O8. Of the seven lines chosen, five were judged sufficiently strong for accurate measurement per spectrogram, on the average.

Velocities were measured by comparing observed line profiles with theoretical line profiles computed for varying degrees of the broadening agent acting on unbroadened profiles. The two sharp-lined O9 V stars, 10 Lacertae and HD 57682, were chosen as sources of the unbroadened profiles, and the seven lines listed above were measured in both stars and an average profile for each line determined. Since the unbroadened lines will change in shape and intensity to a certain extent over the range of spectral types and luminosity classes covered, it would have been very desirable to use sharp-lined stars of different spectral types and luminosity classes as sources of the unbroadened profiles. Unfortunately, this was not possible, as may be seen from an inspection of Tables 1 and 2, where no sharp-lined stars are to be seen in the range O5–O8 or in the stars of higher luminosity in general. The unbroadened profiles determined at spectral type O9 probably represent the best compromise possible under the circumstances for the range of types considered. The Stark effect is again the greatest offender, particularly as it affects the He II lines. Both 10 Lacertae and HD 57682 showed strongly winged lines of He II 4200 and 4542. When these were used as "unbroadened" lines in the construction of theoretically broadened profiles which were then compared against observed profiles, they gave values of the broadening which were too small relative to the other lines. This is because the O5–O8 stars and the stars of higher luminosity in general do not show pronounced Stark wings, as has been mentioned. Broadening measures of λ 4200 and λ 4542 were finally handled by discarding the Stark-influenced profiles in the sharp-lined standard stars altogether and assuming that they could be represented by an average of the unbroadened profiles of λλ 4026, 4388, 4471, and 4686 when dealing with the O5–O8 and high-luminosity stars. This procedure gave measures of the broadening in excellent agreement with those from other lines. Of course, for large values of the broadening, the shapes of the unbroadened lines became relatively unimportant.

The mean velocity determined from the measurement of the observed lines in a given star was obtained by weighting each velocity by the equivalent width of the line used.

a) Axial Rotation

Line profiles broadened by axial rotation were computed from the unbroadened lines in the sharp-lined stars by the familiar method of Shajn and Struve (1929). The stellar disk was divided into twenty strips parallel to the axis of rotation, and a limb-darkening coefficient of 0.67 was employed. The rotationally broadened profiles were computed for either five or six values of the equatorial rotational velocity, from 25 to 400 km/sec. These profiles were then used to obtain the relation between the half-width of the line and the rotational velocity $v \sin i$ for each line considered. This is linear or nearly linear for all but the smallest velocities, as has been pointed out by Miss van Dien (1948) and by Oke and Greenstein (1954). The half-widths of the profiles observed in each star were measured and $v \sin i$'s determined from the respective half-width versus rotational velocity-curves. The mean value of $v \sin i$ for each star, weighted in the manner described previously, is listed in Table 1. The probable errors of these determinations will be about 20 per cent higher than the probable errors of the mean turbulent velocities, also listed in Table 1. Values of $v \sin i$ less than about 20 km/sec are highly uncertain, since the curves of the half-width versus $v \sin i$ flatten off at the lower limit. For this reason, it was decided not to attempt to distinguish between $v \sin i$'s less than 20 km/sec. The $v \sin i$'s listed for the individual components of the four two-line binaries in Table 1 are probably not too accurate, in view of the difficulty in separating the line contours in these systems. These stars are included in Table 1 for the sake of interest; they were not included in the statistical discussion in Section V.

b) Large-Scale Atmospheric Motions and Other Broadening Agents

Huang and Struve (1953) have derived broadening functions for various kinds of mass motion in stellar atmospheres. The broadened line profile is given by

$$A'(x) = \int_{-\infty}^{+\infty} B(x-y)\, A(y)\, dy ,$$

where $B(x)$ is the normalized broadening function and $A(x)$ is the unbroadened line profile. For the case of random motions of large eddies with a Maxwellian distribution of velocities, the broadening function is given by

$$B(x) = \frac{1}{\sqrt{\pi}} e^{-x^2},$$

where x is in units of the Gaussian width, defined as

$$(\Delta\lambda)_G = \frac{v^* \lambda}{c},$$

and v^* is the most probable velocity in the Maxwellian distribution. A simple method of determining $A'(x)$ for this case is to approximate $B(x)$ and $A(x)$ by Voigt functions, following the procedure of van de Hulst and Reesinck (1947). It was found that the unbroadened line profiles measured in the sharp-lined standard stars could be very closely approximated by properly chosen Voigt functions, while the broadening function for this Maxwellian case is an extreme case of the Voigt functions. Broadened line profiles were computed in this way for all lines considered for either five or six values of v^* ranging from 25 to 400 km/sec. As was done for the rotationally broadened profiles, curves of the half-width versus v^* were built up from the computed profiles, and values of v^* were obtained from the measured half-widths for all the stars in Table 1. The mean weighted values of v^* for the various stars are listed in Table 1, along with the probable error of the mean.

Another case considered by Huang and Struve which might be physically significant is

that of random motions of large eddies in the radial direction (such as vertical convection and prominences). If the velocities are distributed according to the Gaussian error law, the broadening function obtained by them for this case is

$$B(x) = \frac{6}{(3+2\beta)\sqrt{\pi}} \left\{ (1+\tfrac{1}{2}\beta)\, e^{-x^2} - \sqrt{\pi}\,|x|\,[1 - H(|x|)] - \tfrac{1}{2}\beta x^2 E_1(x^2) \right\},$$

where $H(x)$ is the probability integral, $E_1(x)$ is the exponential integral, and β is a constant of limb darkening. The unit of x is again the Gaussian width as defined previously. This broadening function may again be represented satisfactorily by a Voigt function, and the broadened line profiles are obtained from the standard unbroadened profiles in the manner described earlier. This was done for the Si IV 4089 line for five values of v^* ranging from 25 to 300 km/sec. The differences between these profiles and those computed under the assumption of random turbulence considered previously were found to

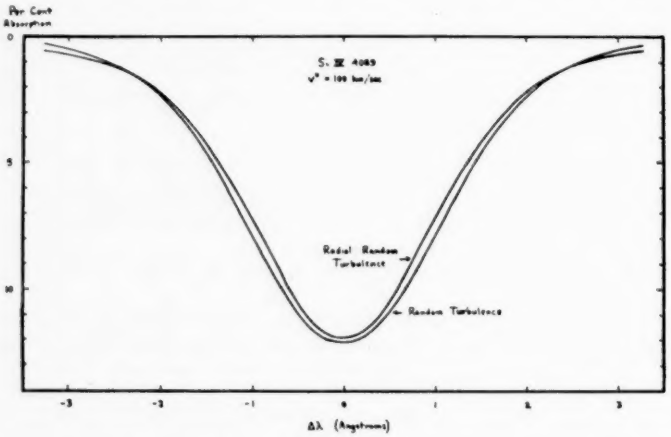

FIG. 1.—Line broadening by random motions of large eddies with a Maxwellian distribution of velocities compared with broadening by random motions of large eddies in the radial direction, as shown by the Si IV 4089 line with $v^* = 100$ km/sec.

be so small as to be indistinguishable with the present observational material. This is illustrated in Figure 1, in which the broadened line profiles of Si IV 4089 with $v^* = 100$ km/sec are compared for the two cases. It was therefore decided that the present observational material does not justify an attempt to distinguish between the various mechanisms of line broadening treated by Huang and Struve, and only the case of random motions of large eddies or large-scale turbulence was considered, under the assumption that this case is representative of large-scale atmospheric motions in general.

Another mechanism of line broadening which may play a role in the spectra of the O- and early B-type stars is electron scattering. Münch (1948) has shown that line profiles affected by electron scattering will have cores which are filled in quite appreciably by radiation of the neighboring continuum, while the removal of energy from the continuum will produce very extended and shallow wings. Münch (1953), from an inspection of spectra of early-type supergiants, states that electron scattering probably contributes to the broadening of lines but is not the main agent. His impression that electron scattering

is not the principal broadening mechanism is confirmed by the present observational material: the line profiles, in general, fail to show the characteristic form predicted by Münch.

c) Differentiation between Broadening Mechanisms from the Line Profiles

The results of this section are negative. With the present observational material, it was impossible to distinguish between axial rotation and large-scale atmospheric motions in a given star from a study of the line profiles. This may be most clearly seen from an inspection of Figure 2, in which the rotationally broadened profile corresponding to a $v \sin i$ of 100 km/sec is compared with the turbulence-broadened profile with a v^* of 75 km/sec for the Si IV 4089 line. The differences between the profiles are seen to be quite small—smaller, in fact, than the differences introduced by observational errors in individual

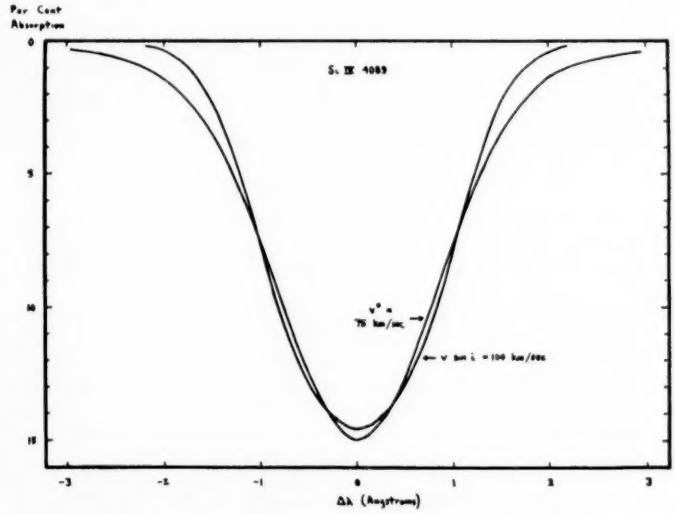

FIG. 2.—Comparison of the Si IV 4089 line broadened by rotation ($v \sin i = 100$ km/sec) and broadened by random motions of large eddies with a Maxwellian distribution of velocities ($v^* = 75$ km/sec).

profile determinations for the same line in a given star—and would be smaller still if both axial rotation and large-scale turbulence act as broadening agents. As might be expected, direct comparisons of observed with computed profiles were inconclusive; the observed profiles were found to fit both sets of computed profiles fairly well. Since the slopes of the rotationally broadened profiles are somewhat steeper than those of the turbulence-broadened profiles, a statistical approach was also attempted. Line widths at one-quarter and three-quarters of the central intensity were measured for all lines in all stars, and the ratios taken. The same ratio was measured for the computed profiles and plotted against velocity for each line. Two curves were obtained in this way for each of the seven lines considered; one for rotationally broadened profiles and one for turbulence-broadened profiles. The observed line-width ratios were then plotted in these diagrams, but the scatter was too large to draw any conclusions. Averaging of line profiles in the same star was also attempted, without additional success.

It is clear that the distinction between the broadening mechanisms as seen in the line

profiles is a subtle one and would require the highest observational accuracy in order to be detected. A concentrated effort on each star, using a large number of fine-grained spectrograms, would be necessary in order to make the differentiation attempted here.

Four stars with line profiles somewhat different in appearance should be mentioned. The O6 trapezium star θ^1 Orionis C and, to a lesser degree, the O9.5 Vp star θ^2 Orionis and the O6 star HD 54662 have lines with rather sharp cores and extended wings which fit neither the rotationally broadened nor the turbulence-broadened profiles. The visual impression from the spectrograms of these stars is that the lines are sharper than the velocities determined from the half-widths would indicate. Their profiles are similar to what one would expect if electron scattering were the broadening mechanism, but all three stars appear to lie close to the main sequence, and it is difficult to understand why they and not some other stars of higher luminosity show this effect. Both θ^1 Orionis C and θ^2 Orionis are spectroscopic binaries, and it is possible that a weak secondary spectrum may produce the effects noted here (see remarks to Table 1). Another possibility, since both stars are imbedded in nebulosity, is that the profiles have circumstellar cores. The fourth star is χ^2 Orionis (B2 Ia), the star of latest spectral type for which line profiles were determined. The profiles in this star do not fit the computed profiles very well, in the sense that the lines have rather steep sides and flat bottoms. The general appearance is perhaps more that of small-scale turbulence than large-scale atmospheric motions or rotation, but it should be pointed out that this impression is based on a single plate.

IV. LUMINOSITIES OF THE O5–O8 STARS

In order to study the variation of line broadening with position on the H-R diagram for the O-type stars, the absolute magnitudes of these stars must be known. In this section an attempt to find spectroscopic criteria for luminosity effects is made for the O5–O8 stars.

Spectroscopic criteria for luminosity effects in the O-type stars have been sought for some time, particularly by the Victoria workers. Petrie (1947), using absorption-line intensities in O-type stars with absolute magnitudes calculated from their interstellar K-line intensities, found no well-marked luminosity effects present. According to Miss Underhill (1949*b*), emission lines may be expected to occur in the early-type stars of higher luminosity. The absorption-line O-type stars are then the lower-luminosity stars, and one would not expect to find spectroscopic criteria of differing absolute magnitude among them. Miss Underhill (1951) further finds that the characteristic Stark wings in the early members of the Balmer series will disappear in the O-type stars, so that the well-marked negative absolute-magnitude effect which occurs at earlier spectral types should not be expected for the O-type stars.

Since the work of W. W. Morgan and others on aggregates of early-type stars, it has been possible to determine absolute magnitudes for those O-type stars which are aggregate members. Eleven of the O5–O8 stars listed in Table 1 are members of aggregates with known distances, and an attempt is made in the following sections to correlate various features in their spectra with their absolute magnitudes. The absolute magnitudes of these stars were calculated by means of the spectral types, apparent magnitudes, and C_1 colors listed by Morgan, Code, and Whitford (1955) and the aggregate distances given by Morgan, Whitford, and Code (1953). The normal colors for these stars and the ratio of reddening to total visual absorption used were taken from the work of Morgan, Harris, and Johnson (1953). The absolute magnitudes obtained in this way are listed in Table 3.

a) Emission Lines

The N III lines at λ 4634 and λ 4641 and the He II 4686 line occur frequently in emission in the O5–O8 stars and are the basis of the Of classification of these stars. These emissions are always broad and often rise only very slightly above the continuum, so that

TABLE 3

EMISSION LINE DATA FOR THE O5-O8 STARS

HD	MK	M_V	No. of Plates	Equivalent Widths (A)			Half-Widths (A)		
				N III 4634	N III 4641	He II 4686	N III 4634	N III 4641	He II 4686
24912	O7	-4.7	2	0.22	0.21	A	3.8	3.0	---
34656	O7	-5.0	3	0.22	0.45	A	3.0	4.6	---
36861	O8	----	2	(E)	(E)	A	---	---	---
37022	O6p	-4.9	2	A	A	E	---	---	---
46150	O6	-5.5	2	0.28	0.24	A	4.2	2.8	---
46223	O5	-5.4	1	0.22	0.63	A	3.6	3.9	---
47129	O8	-5.7	1	(E)	(E)	(E)	---	---	---
47839	O7	----	2	E	E	A	---	---	---
48099	O6	----	1	0.12	0.17	A	3.0	2.9	---
57060	O7f	----	3	0.38	0.50	1.01	3.9	3.6	3.0
164794	O5	-5.7	1	0.40	0.56	A	4.3	4.7	---
188001	O8f	----	2	0.29	0.59	0.29	2.7	3.4	2.2
190429 N	O5f	-6.7	2	0.40	0.87	3.69	3.8	4.2	9.0
190864	O6	-5.4	2	0.24	0.37	A	3.2	3.1	---
192281	O5f	----	2	(E)	(E)	A	---	---	---
192639	O8f	-5.8	2	0.32	0.60	E	2.9	2.9	---
193514	O7f	-6.0	1	0.42	0.50	E	3.0	2.2	---

The meaning of the symbols is as follows:

A: absorption lines.
E: moderate emission, but too weak for accurate measurement.
(E): very weak emission.

they are difficult to detect and to measure in all but the most pronounced cases. The widened spectrograms used in the present investigation are especially suitable for the detection of faint and broad features, with the result that emission lines, usually of N III, were found to be present in the spectra of all but one (HD 54662) of the O5–O8 stars listed in Table 1. These stars are listed in Table 3, together with the equivalent widths and half-widths of the emission lines when it was possible to measure them. These measures are necessarily inexact, in view of the nature of the lines and the relatively small number of plates measured.

Figure 3 shows a plot of the combined emission intensity of N III 4634 and 4641 for nine O5–O8 stars in Table 3 with known absolute magnitudes. Despite the small number

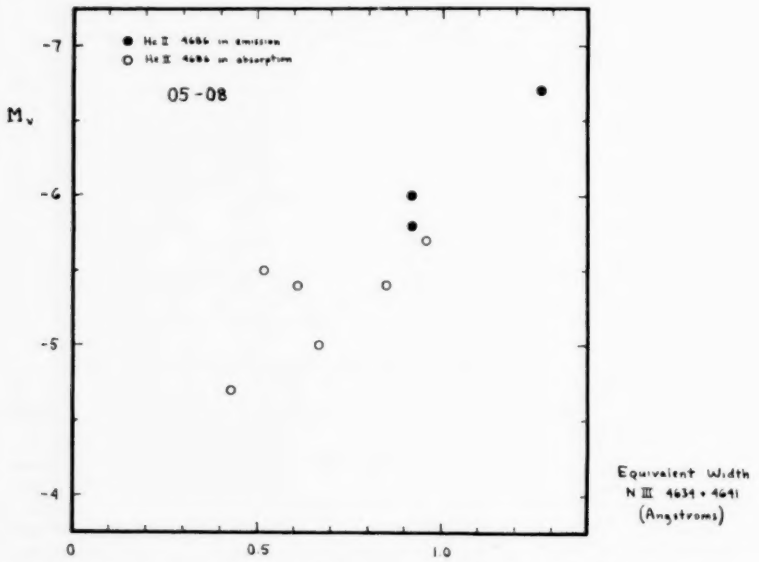

FIG. 3.—Combined equivalent widths of the emission lines *N* III 4634 and 4641 plotted against visual absolute magnitude for nine O5–O8 stars.

of stars, a definite correlation seems to exist, in the sense that the N III emission increases in strength with increasing luminosity. This correlation is strengthened by the fact that the O5–O8 stars in Tables 2 and 3 with weak or absent N III emission are relatively faint in those cases for which absolute magnitudes are available. The He II 4686 emission is apparently similarly correlated with absolute magnitude, but the sample is very small indeed (see Fig. 3 and Table 3). This confirms Miss Underhill's suggestion that the Of stars are the O-type stars of higher luminosity. It is also in agreement with the recent work of Wilson (1955) on emission lines in O-type stars.

One matter which should be studied further before a correlation of the type just discussed can be strictly applied is the variability of the emission lines in the Of stars reported by several investigators. This is a difficult observational problem and was not attempted with the present limited material. A spectroscopic investigation of the variability should stress greatly widened, fine-grain plates. Photoelectric studies, possibly with interference filters to isolate the λλ 4620–4700 region, would be extremely desirable.

b) Absorption-Line Equivalent Widths and Line Ratios

As a part of the reduction of the line profiles of stars listed in Table 1, equivalent widths were measured for all lines considered. In view of the fact that absolute magnitudes of O-type stars which are members of aggregates are now available, while other O-type stars can be sorted roughly according to absolute magnitude by their emission characteristics, a study of the type carried out by Petrie (1947) and by Miss Underhill (1953) was judged to be worth while.

Table 4 lists the measured equivalent widths of absorption lines in stars listed in Table 1. The number of plates measured is the same as in Table 1. No claim for high accuracy of these values is made, in view of the small number of plates employed. In a letter Miss Underhill (1955) writes about the O-type stars, and the writer is in full agreement: "I have found that 6 plates is a minimum requirement for each star. The lines are so bad that in order to be sure of what is in the spectrum you must measure quite a few plates."

A comparison of the present measured equivalent widths with those of Petrie (1947) for fourteen stars in common is shown in Figure 4. A comparison with the values of Miss Underhill (1953) shows a very similar diagram. There is thus a systematic difference of about 40 per cent between the present and the Victoria measures, in the sense that the latter run higher. A similar tendency was also noted by Merrill, Sanford, Wilson, and Burwell (1937) and by Oke (1954). A comparison with the equivalent widths of Williams (1936) for twelve stars in common showed somewhat less scatter, plus a systematic difference of about 20 per cent, in the sense that the latter values run higher.

The equivalent width of He I λ 4471, the mean equivalent width of He II λ 4200 and λ 4542, and the equivalent width of Si IV λ 4089, respectively, are plotted in Figures 5, 6, and 7 against spectral type. The O5–O8 stars are divided into the two luminosity groups $M_v \leq -5.0$ and $M_v > -5.0$, on the basis of the absolute magnitudes in Table 3 and the rough luminosity classification permitted by the emission-line–luminosity correlation discussed previously. Figures 5 and 6 show no evidence of an absolute-magnitude effect for He I or He II, but there is some evidence for a positive absolute magnitude for Si IV in the O6–O8 stars in Figure 7. Such an effect would not be surprising, since the Si IV λ 4089 line is a well-known absolute-magnitude indicator in the O9–B0 stars (Morgan, Keenan, and Kellman 1943). In any case the line would be of limited use for low-dispersion classification purposes, since it is already intrinsically quite weak in the spectra of the O5–O8 stars.

V. LINE BROADENING AND POSITION ON THE H-R DIAGRAM

With MK luminosity classes given for the stars of spectral type O9 and later and the possibility of arranging the O5–O8 stars according to luminosity, as discussed in Section IV, *a*, line broadening may now be shown on the spectrum–luminosity-class diagram. In Table 5, the line broadening in the spectrum of the star with the sharpest lines within each spectral-type-luminosity class group, expressed as a turbulent velocity, is listed; this is defined as the minimum line broadening. Table 6 lists the mean line broadening for all stars measured within a spectral-type-luminosity class group, again expressed as a turbulent velocity. Composite spectra have not been included in either diagram, so that both apply to single stars only.

An inspection of Table 5 shows, first, that the O5–O8 stars of all luminosity classes, the O9–B1 I*a*–II stars, and the O9–B0.5 III stars do not contain any sharp-lined representatives in the sample considered. If axial rotation were the sole broadening agent in these stars, however, some stars would be seen pole-on, and sharp-lined stars would be expected in all these regions of the spectrum–luminosity-class diagram for a sufficiently large sample of stars. It may be concluded, within the limits of the observational sample considered, that some broadening agent other than axial rotation plays an important role

TABLE 4

MEASURES OF EQUIVALENT WIDTHS OF ABSORPTION LINES

HD	He I, II 4026 (A)	Si IV 4089 (A)	He II 4200 (A)	He I 4388 (A)	He I 4471 (A)	He II 4542 (A)	He II 4686 (A)
1337 A	0.50:	0.29:	----	----	0.53:	----	0.23:
1337 B	0.23:	0.08:	----	----	0.23:	----	0.25:
23180 A	0.59:	0.13:	----	0.37:	0.67:	----	----
23180 B	0.23:	0.05:	----	0.16:	0.36:	----	----
24398	0.81	0.21	----	0.43	0.81	----	----
24912	0.63	0.30	0.39	----	0.68	0.38	0.35
34078	0.81:	0.32:	0.19:	0.51:	0.96:	0.39:	0.49:
34656	0.71	0.26	0.49	0.19:	0.70	0.57	0.34
35921	0.67:	0.28:	----	----	0.90:	----	0.37:
36486	0.75	0.54	----	0.31	0.84	0.23	0.29
36861	0.65	0.28	0.37	0.18	0.70	0.46	0.58
37022	0.66	0.19:	0.67:	----	0.63	0.54	E
37041	1.01	0.27	----	0.52	0.83	----	0.67
37043	0.80	0.35	0.23	0.33	0.67	0.36	0.40
37128	0.62	0.66	0.19	0.34	0.78	----	0.26
37742	0.63	0.55	0.23	0.27	0.83	----	0.29
38771	0.64	0.59	----	0.51	0.79	----	0.24
40111	0.76	0.36	----	0.50	0.82	----	0.22
41117	0.39:	0.11:	----	0.46:	0.71:	----	----
41161	0.57:	----	----	----	0.99:	----	----
46150	0.48	----	0.49	----	0.25	0.47	0.63
46223	0.42:	----	0.51:	----	----	0.36:	1.27:
47129 A	0.56:	----	0.22:	----	0.67:	0.67:	E
47129 B	0.21:	----	0.13:	----	0.18:	0.25:	E
47432	0.60:	0.47:	0.26:	----	0.88:	0.30:	0.24:
47839	0.55	0.17	0.49	----	0.59	0.44	0.68
48099 A	0.31:	----	----	----	0.19:	----	----
48099 B	0.22:	----	----	----	0.21:	----	----
48434	0.79:	0.57:	0.19:	0.53:	1.19:	----	0.44:
54662	0.94:	0.28:	----	0.20:	0.71:	0.75:	0.98:
57060	0.76	0.39	0.46	----	----	0.67	E
57061	0.56	0.35	0.27	0.23:	0.63	0.34:	0.32
57682	0.83:	0.27:	0.41:	0.43:	0.84:	0.37:	0.48:
91316	0.76	0.24	----	0.50	0.85	----	----
143275	0.85	0.32	----	0.49	0.92	----	0.43
149438	0.91	0.25	----	0.50	0.60	----	0.35
149757	0.86	----	----	----	0.72	----	0.67
164794	0.42:	----	0.80:	----	0.21:	0.80:	0.81:
167264	0.70:	0.53:	0.23:	0.39:	0.87:	0.15:	0.24:
184915	1.05:	0.59:	----	0.55:	1.23:	----	----
188001	0.66	0.46	0.35	----	0.71	0.51	E
190429 N	0.30	----	0.47	----	----	0.70	E
190864	0.60	0.32	0.34	----	0.36	0.44	0.37
192281	0.48	----	0.63	----	----	1.06	0.69
192639	0.64:	0.33:	0.80:	----	0.86:	0.49:	E
193514	0.47:	0.26:	0.51:	----	0.58:	0.62:	E
214680	0.81	0.35	0.38	0.38	0.63	0.37:	0.69:

All measures based on only one spectrogram or otherwise doubtful are followed by a colon.

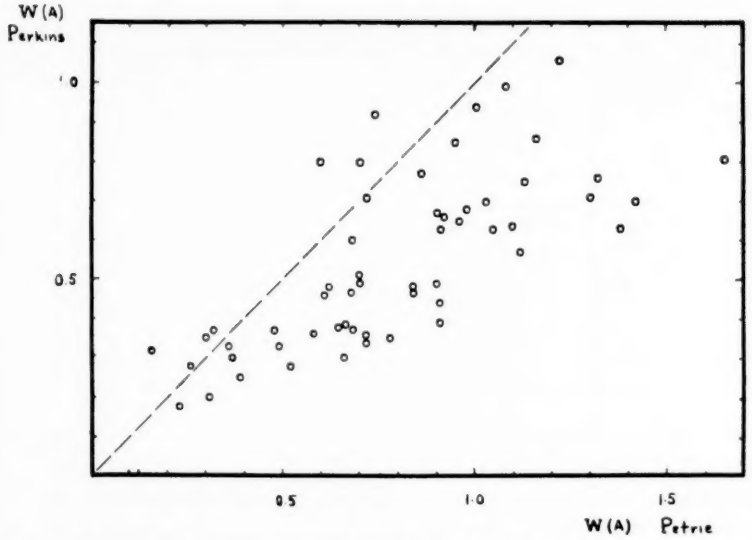

FIG. 4.—A comparison of the present measured equivalent widths with those of Petrie for fourteen stars in common.

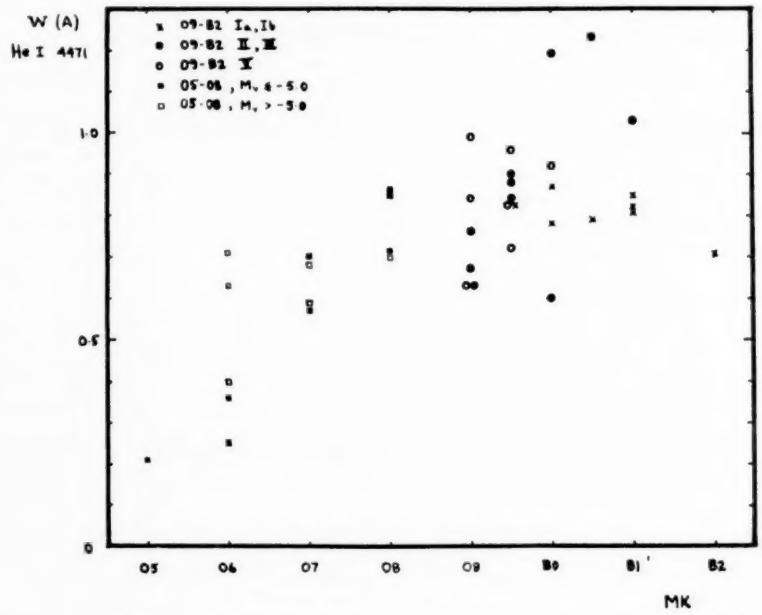

FIG. 5.—Equivalent widths of He I 4471 plotted for stars of different spectral types and luminosity classes.

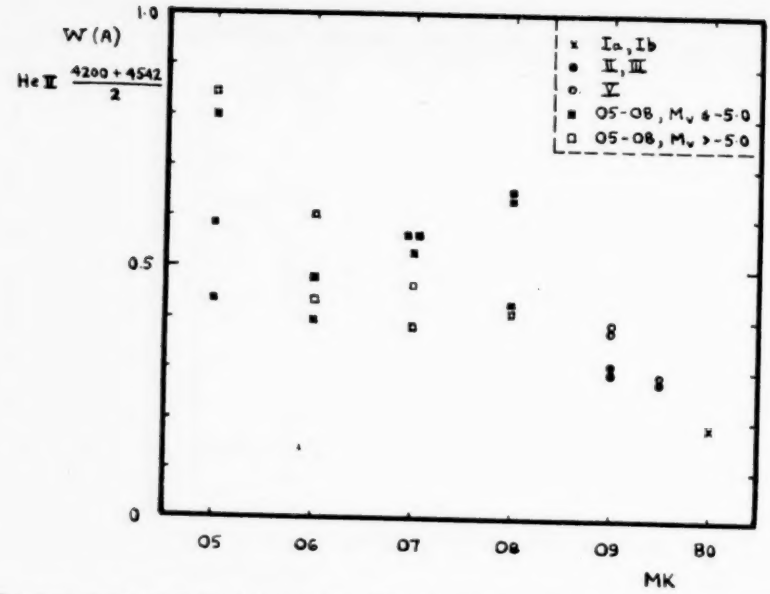

FIG. 6.—Average equivalent widths of He II 4200 and 4542 plotted for stars of different spectral types and luminosity classes.

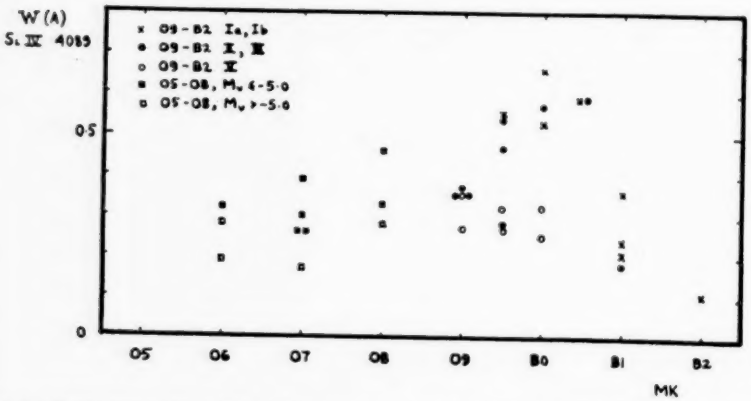

FIG. 7.—Equivalent widths of Si IV 4089 plotted for stars of different spectral types and luminosity classes.

for these stars. Huang and Struve (1954) found this effect earlier for twenty-five O9–A2 I*a*–I*b* stars.

With less certainty, two other effects may also be seen in Table 5. First, the minimum line broadening appears to increase with increasing temperature: it is largest in the O5–O8 stars and decreases within each luminosity class to very small values at B1.5. Second, a luminosity effect may be present, in the sense that the more luminous O5–O8 stars and the O9–B1 I*a*–II stars show larger values of the minimum line broadening than do the less luminous O5–O8 stars appear to and the O9–B1 III–V stars, respectively. These results are consistent with the interpretation of the minimum line broadening as due to large-scale atmospheric motions, since the latter would be expected to increase with increasing temperature and luminosity (Underhill 1949*a*). It should be pointed out that line broadening by electron scattering would also increase with increasing temperature and luminosity (Münch 1948). Although electron scattering may play a role in the broadening, it does not seem likely that it is the dominant effect, since the line profiles considered in this investigation do not resemble those broadened by electron scattering.

Another argument against axial rotation as the sole broadening agent in the O-type stars is due to Struve (1952). He pointed out that the high-luminosity O-type stars often show very broad emission lines—but, contrary to the tendency of the Be stars to exhibit double emission lines, these class O emission features are not double. This is confirmed by the present observations. Also unlike the Be stars, the widths of the class O emission features (see Table 3) are very similar to those of the strong absorption lines in these stars, suggesting that the emission and absorption arise at the same distance from the center of the star. This was also pointed out by Oke (1954).

An inspection of Table 6, which shows mean line broadening, expressed as turbulent velocity, in the spectrum–luminosity-class diagram, again brings out a correlation of line broadening with spectral type and with luminosity class. The average line broadening appears to decrease with increasing absolute magnitude at a given spectral type, contrary to the behavior of the minimum line broadening. If the latter is interpreted as due entirely to large-scale atmospheric motions, then another broadening agent, which decreases with increasing absolute magnitude, is indicated, and this is most probably axial rotation.

Several reasons may be given for believing axial rotation to be the additional broadening mechanism: (1) The line profiles considered in this investigation are consistent with computed line profiles broadened by axial rotation. (2) The rotational velocities of the B2–B5 stars show a luminosity dependence of the type indicated here (Slettebak and Howard 1955). (3) Very large values of the line broadening were found for some stars of lower luminosity in Tables 1 and 2—up to 300 km/sec, if the line broadening is expressed as a turbulent velocity. While such high values are consistent with rapid axial rotation, they are not consistent with our present picture of large-scale motions in stellar atmospheres (Unsöld 1955). (4) The star with the very large line broadening just quoted ($v^* = 300$ km/sec, or $v \sin i = 350$ km/sec) is classified O8 V:pe and shows Hβ double emission very similar to that shown by the Be stars. There seems to be no question that axial rotation is the dominant broadening mechanism for this star of lower luminosity.

Within the limits of the small number of stars considered, Table 6 also shows an increase in mean line broadening with increasing temperature for the O9–B1 stars of high luminosity.

It is interesting to note that the individual O9–B1 I*a*–I*ab* and O9–B0 I*b*–II stars which have gone into the averages in Table 6 have remarkably similar line broadening at a given spectral type and luminosity class. This may be seen in the small differences between the minimum line broadening listed in Table 5 and the mean line broadening listed in Table 6 for these stars. We conclude with Huang and Struve, who found this effect earlier (1954), that the line broadening is due to mass motion in the atmosphere

TABLE 5

MINIMUM LINE BROADENING, EXPRESSED AS TURBULENT VELOCITY, IN THE SPECTRUM-LUMINOSITY CLASS DIAGRAM

Luminosity	O5	O6	O7	O8	O9	O9.5	B0	B0.5	B1	B1.5	B2	B3	B5	Luminosity Class
						60 (2)	60 (4)'	60 (3)	40 (3)	≤20 (1)	20: (1)	≤20 (1)		Ia
$M_v \leq -5.0$	110 (4)	75 (6)	90: (5)	85 (6)	70: (2)			60 (1)	50 (3)			≤20 (1)	≤20 (1)	Iab or I
					90 (2)	70: (3)	70: (2)	50 (5)	40 (10)	≤20 (1)	≤20 (1)			Ib
									30: (2)					Ib-II
$M_v > -5.0$	240 (1)	75: (3)	70 (2)	60 (7)	100 (1)	80 (2)	70 (1)		50 (7)			<20 (1)	<20 (1)	II
					90 (3)	50 (3)	50 (4)	40 (8)	30 (1)		<20 (1)			III
							40 (3)	40 (6)						IV
All M_v	100: (6)	70: (11)	70 (8)	60 (18)	<20 (4)	<20 (3)	<20 (4)							V

The number of stars in each sample is in parentheses.

TABLE 6

MEAN LINE BROADENING, EXPRESSED AS TURBULENT VELOCITY, IN THE SPECTRUM-LUMINOSITY CLASS DIAGRAM

Luminosity	05	06	07	08	09	09.5	B0	B0.5	B1	Luminosity Class
$M_V \leq -5.0$	125 (4)	130 (6)	95 (5)	115 (6)		65 (2)	60 (4)	60 (3)	55 (3)	Ia
					75 (2)			60 (1)	65 (3)	Iab or I
					90 (2)	85 (3)	80 (2)	85 (5)	75 (10)	Ib
$M_V > -5.0$	240 (1)	140 (3)	120 (2)	130 (7)					40 (2)	Ib-II
					100 (1)	95 (2)	70 (1)		85 (7)	II
All M_V	160 (6)	125 (11)	100 (8)	115 (18)	115 (3)	90 (3)	80 (4)	85 (8)	30 (1)	III

The number of stars in each sample is in parentheses.

which has a spherical symmetry rather than an axial symmetry. In the range B0.5–B1 I*b*–II and O9–B1 III, the individual values which make up the averages in Table 6 begin to diverge from one another, and it is probable that axial rotation begins to play a role at this point for these stars. There is also considerable variation in line broadening among the O5–O8 stars in both high- and low-luminosity groups, indicating that axial rotation probably is of some importance as a broadening agent in the spectra of these stars. It would therefore seem that the degree of line broadening in a given O5–O8 star cannot, by itself, yield information about the absolute magnitude of the star.

Although only a handful of high-luminosity stars later than B1 were considered in this investigation, it is significant that these show relatively little line broadening, in contrast to the high-luminosity stars of earlier type. On the basis of the interpretation given here, it can be said that large-scale atmospheric motions no longer dominate as broadening agents in the spectra of these cooler stars. One star of later type which exhibits relatively large line broadening, however, is the B8 I*a* star β Orionis, for which a $v \sin i$ of 65 km/sec was found (Slettebak 1954). It would seem that the primary broadening mechanism in this star is axial rotation if the foregoing temperature dependence of the large-scale atmospheric motions is correct. The decrease of line broadening in the supergiant stars of spectral types later than B1 was found earlier by Huang and Struve (1954), but these investigators find appreciably larger line broadening in the spectra of these stars than is found in the present investigation.

The results of this section may be summarized as follows:

1. Large-scale atmospheric motions (such as large-scale turbulence, convection, etc.) play an important role as broadening agents in the spectra of the O5–O8 stars of all luminosity classes and the high-luminosity stars of types O9–B1.

2. These large-scale atmospheric motions appear to increase with increasing temperature and with increasing luminosity.

3. Axial rotation acts as an additional broadening mechanism for these stars but decreases with increasing luminosity at a given spectral type.

4. Among the O5–O8 stars, both mechanisms probably act, but rapid axial rotation occurs more frequently in the stars of lower luminosity, while large-scale atmospheric motions dominate the line broadening in the stars of higher luminosity.

5. Among the O9–B1 stars the line broadening in the supergiant stars appears to be due almost entirely to large-scale atmospheric motions, while the line broadening in the main-sequence stars is due almost entirely to axial rotation. The O9–B1 stars of intermediate luminosity have lines broadened by both mechanisms. Large-scale atmospheric motions no longer dominate as line broadening agents in the supergiant stars of spectral type later than B1.

It is a pleasure to record my indebtedness to Dr. O. Struve for calling my attention to this problem and for his continued interest. I also wish to thank Dr. I. S. Bowen for permitting me to visit the Mount Wilson and Palomar Observatories during the winter of 1955 as a guest investigator. The many courtesies shown me by Dr. Bowen and his colleagues were greatly appreciated. In particular, I am indebted to Drs. Guido Münch and Armin Deutsch for their co-operation and help at various stages of this investigation. Very helpful in preparing this paper were discussions with Dr. A. Unsöld, of Kiel University, and Dr. J. Stock, of the Hamburg Observatory, and the generous co-operation of Dr. O. Heckmann, director of the Hamburg Observatory. I also wish to thank Messrs. Jack Wright, Martin Helling, and Charles Pearson for computational assistance. This investigation was supported by a National Science Foundation grant.

REFERENCES

Dien, E. van. 1948, *J.R.A.S. Canada*, **42**, 249.
Elvey, C. T. 1930, *Ap. J.*, **71**, 221.
Huang, S. S. 1950*a*, *Ap. J.*, **112**, 399.

———. 1950*b*, *ibid.*, p. 418.
———. 1953, *ibid.*, **118**, 285.
Huang, S. S., and Struve, O. 1952, *Ap. J.*, **116**, 410.
———. 1953, *ibid.*, **118**, 463.
———. 1954, *Ann. d'ap.*, **17**, 85.
———. 1955, *Ap. J.*, **121**, 84.
Hulst, H. C. van de, and Reesinck, J. J. M. 1947, *Ap. J.*, **106**, 121.
Merrill, P. W., Sanford, R. F., Wilson, O. C., and Burwell, C. G. 1937, *Ap. J.*, **86**, 274.
Miczaika, G. R. 1950, *Ap. J.*, **111**, 443.
Morgan, W. W., Code, A. D., and Whitford, A. E. 1955, *Ap. J. Suppl.*, **2**, 41.
Morgan, W. W., Harris, D. L., and Johnson, H. L. 1953, *Ap. J.*, **118**, 92.
Morgan, W. W., Keenan, P. C., and Kellman, E. 1943, *An Atlas of Stellar Spectra* (Chicago: University of Chicago Press).
Morgan, W. W., Whitford, A. E., and Code, A. D. 1953, *Ap. J.*, **118**, 318.
Münch, G. 1948, *Ap. J.*, **108**, 116.
———. 1953, private correspondence.
Oke, J. B. 1954, *Ap. J.*, **120**, 22.
Oke, J. B., and Greenstein, J. L. 1954, *Ap. J.*, **120**, 384.
Petrie, R. M. 1947, *Pub. Dom. Ap. Obs. Victoria*, **7**, 321.
Schwarzschild, M., Schwarzschild, B., and Adams, W. S. 1948, *Ap. J.*, **108**, 207.
Shajn, G., and Struve, O. 1929, *M.N.*, **89**, 222.
Slettebak, A. 1949, *Ap. J.*, **110**, 498.
———. 1954, *ibid.*, **119**, 146.
Slettebak, A., and Howard, R. F. 1955, *Ap. J.*, **121**, 102.
Struve, O. 1948, *Ap. J.*, **107**, 327.
———. 1952, *Pub. A.S.P.*, **64**, 118.
Underhill, A. B. 1949*a*, *M.N.*, **109**, 562.
———. 1949*b*, *Ap. J.*, **110**, 340.
———. 1951, *Pub. Dom. Ap. Obs. Victoria*, **8**, 385.
———. 1953, *Mém. Soc. R. Sci. Liége*, **14**, 374.
———. 1955, private correspondence.
Unsöld, A. 1955, *Physik der Sternatmosphären* (2d ed.; Berlin: Springer-Verlag), p. 456.
Unsöld, A., and Struve, O. 1949, *Ap. J.*, **110**, 455.
Westgate, C. 1933, *Ap. J.*, **77**, 141.
Williams, E. G. 1936, *Ap. J.*, **83**, 279.
Wilson, R. 1955, *Observatory*, **75**, 222.

REDISCUSSION OF ECLIPSING BINARIES. I. Z HERCULIS*

DANIEL M. POPPER
Department of Astronomy, University of California, Los Angeles
Received February 18, 1956

ABSTRACT

Z Herculis is removed from the group of stars showing major discrepancies between published photometric and spectrographic analyses by means of new photoelectric and spectrographic data. The importance is emphasized of carrying out photoelectric observations in at least two colors simultaneously on a color system, preferably the U, B, V system, which is well calibrated against spectral type. The use of spectrograms in the visual region of the spectrum has proved advantageous.

The principal properties of the two components of the system are given in the accompanying table.

$B-V$	+0.47	+0.91	Luminosity (solar units)	4.7	2.8
Radius (solar units)	1.6	2.6	M_v	+2.9	+3.8
Mass (solar units)	1.22	1.10	Spectral type	F4 IV–V	K0 IV

The properties of each star lie within the range of those of other stars of similar type. At least one component of the system shows slow intrinsic variations.

INTRODUCTION

Z Her[1] is an eclipsing variable of the seventh magnitude, with an F-type spectrum, partial eclipses, and period very close to 4 days. The existing spectrographic orbit dates from 1919 (Adams and Joy 1919). Baglow (1952) has published a two-color photoelectric study of the light-curve. Analysis of the system has remained in an unsatisfactory state principally because of uncertainty concerning the nature of the fainter, cooler component. According to published descriptions of the spectrum, it is an F-type star, whereas from the depths of minima, according to Baglow, it is of type K or M. This kind of discrepancy is of fairly common occurrence (e.g., Wyse 1934). It has seemed worthwhile to obtain new data in an attempt to clarify the matter.

The present study of Z Her is based on new spectrograms obtained at the McDonald, Lick, and Mount Wilson Observatories and on a two-color photoelectric light-curve obtained at Lick, supplemented by a few observations at McDonald. My light-curves are similar to those of Baglow, but the treatment differs in several respects.

SPECTROGRAPHIC DATA

Figure 1 shows the photographic region of the spectrum of Z Her near one node, when the brighter component is receding (McDonald spectrogram, original dispersion 26 A/mm at Hγ). A spectrogram of α CMi, spectrum F5 IV–V, is shown for comparison. Although there is evidence of a second component in the spectrum of Z Her, e.g., at Hδ, λ 4226, λ 4271, Hγ, none of its lines appear free of serious blending with lines of the brighter component. Careful examination of Mount Wilson coudé plates of this region of the spectrum only accentuates the difficulty. It is clear that a reliable spectral type of the fainter component cannot be obtained from such plates and that radial velocities of this component must be treated with caution.

At the time of mid-primary eclipse the fainter component of Z Her contributes 60

* This investigation was made possible in part by a co-operative arrangement with the Mount Wilson and Palomar Observatories.

[1] HD 163930, var.; F5p; α_{1900} 17^{h}53^m.6; δ_{1900} + 15°9′.

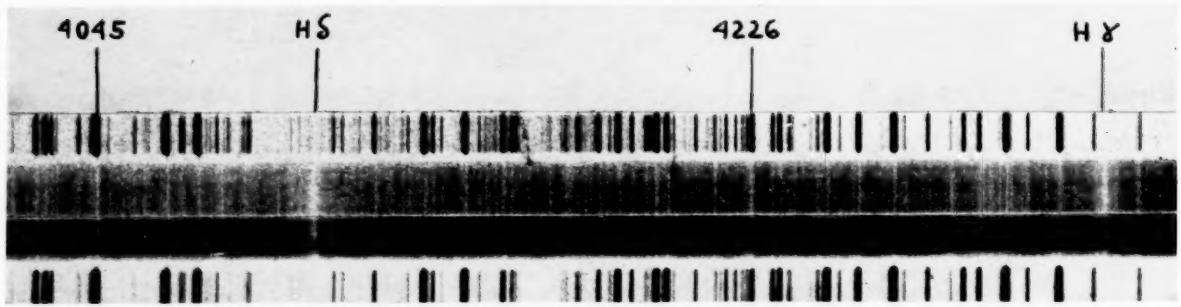

FIG. 1.—*Above:* α CMi; *below:* Z Herculis, 0.80 phase. McDonald Observatory spectrograms

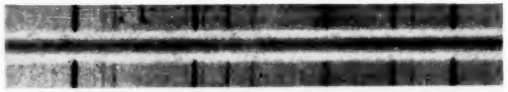

FIG. 2.—D lines in Z Herculis, 0.09 phase. Mount Wilson coudé spectrogram

per cent of the light of the system in the photographic region. A weak spectrogram obtained for me at Mount Hamilton near the time of mid-primary eclipse in the summer of 1951 by William Wehlau shows λ 4226 and the G band definitely strengthened, indicating a combined spectral type in the vicinity of G5. Figure 2 shows the region of the D lines on a coudé spectrogram. Although the cooler star (longward displacement) is nearly 1 mag. fainter than the hotter star in this region of the spectrum, the D lines are of approximately equal intensity, those of the cooler star being broader. This is confirming evidence that the cooler star is considerably later in type, since the D lines strengthen greatly and broaden from type F to type K.

Thus the evidence is that the secondary component is considerably cooler than the primary, but no reliable evaluation of its spectral type can be obtained from the spectrograms. It will be seen in the discussion of the photometric data that the color, surface brightness, and luminosity of this component place it at spectral type K0 IV. My estimate of the spectral type of the primary component on McDonald spectrograms is F4. Miss Roman (1956) gives F6 V for the composite spectrum at maximum light.

TABLE 1

COUDÉ VELOCITIES OF Z HERCULIS

PLATE CE	U.T.	PHASE	VELOCITIES (km/sec)			RESIDUALS (O−C) (km/sec)		
			V_1	V_2(Abs.)	V_2(Em.)	V_1	V_2(Abs.)	V_2(Em.)
	1954							
9168	Apr. 10.44	0!954	− 21.6	.....	− 76	+0.7	.....	−3
9272	June 13.38	.968	− 27.3	.....	− 70	+2.1	.....	−5
9276	June 14.33	.207	−127.1	+ 38	+ 51	−0.6	− 6	+7
9388	Sept. 16.18	.711	+ 35.9	−126	−136	+1.1	+10	0
	1955							
9796	May 3.34	.106	− 96.4	+ 6	.....	+1.2	− 5	.....
9845	June 11.29	.860	+ 14.9	−127	.....	−3.2	− 9	.....
9849	June 12.22	.094	− 92.2	+ 3	.....	+0.4	− 3	.....
9853	June 13.23	.347	−116.0	+ 31	+ 38	−1.5	+ 1	+8
10022	Sept. 3.17	0.867	+ 15.8	−119	−114	0	− 4	+1

The only lines in the photographic region of the spectrum belonging to the cooler component that are definitely unblended are the emission lines of H and K discovered by Hiltner (1947). To put the radial-velocity determinations of this component on a firm basis, recourse was had to the visual region of the spectrum where the cooler component is relatively brighter and where few strong lines are present to cause blending difficulties (see Fig. 2). A new spectrographic orbit has been determined from coudé spectrograms alone by using principally the photographic region of the spectrum for the brighter component and the visual region plus H and K emission for the fainter. The emission lines, being diffuse, are relatively difficult to measure.

Table 1 lists the coudé observations. The phases are obtained from the light-elements discussed later. From these velocities the circular elements of Table 2 have been computed. Since the differences between absorption and emission velocities are probably not significant, the adopted value of K_2 is a weighted mean. Figure 3 shows the coudé velocities and the curves given by the adopted elements, from which the residuals of Table 1 have been computed.

From the elements in Table 2 we obtain

$$a \sin i = 14.0 \text{ solar radii}, \qquad \mathfrak{M}_1 \sin^3 i = 1.20, \qquad \mathfrak{M}_2 \sin^3 i = 1.08 ,$$

where a is the radius of the relative orbit, i is the orbital inclination, and the masses, $\mathfrak{M}$, are in solar units. The more massive star is brighter and is eclipsed at zero phase; that is, it is the hotter star.

The evidence from Z Her lends support to Eggen's (1955) conjecture that the H and K emission lines in subgiant components of eclipsing binaries show the same velocity amplitude as the corresponding absorption lines. Revisions of the spectral types of the cooler component of Z Her and of the components of AW Her (Popper 1956), plus new material on VV Mon, strengthen the tentative conclusion that strong emission lines at H and K appear in the spectra of subgiant components of eclipsing binaries only near type K0.

TABLE 2

ELEMENTS OF THE VELOCITY-CURVES

	Absorption	Emission	Adopted	Adams and Joy
K_1 (km/sec)	83.4±0.6 (p.e.)	.....	+83.4	+ 88.2
K_2 (km/sec)	91.0±2.1	97.7±1.6 (p.e.)	+93.0	+101.8
γ (km/sec)	−46.1±0.4	−44.4±1.2	−46.1	− 46.5
P (assumed)	3.993 days			

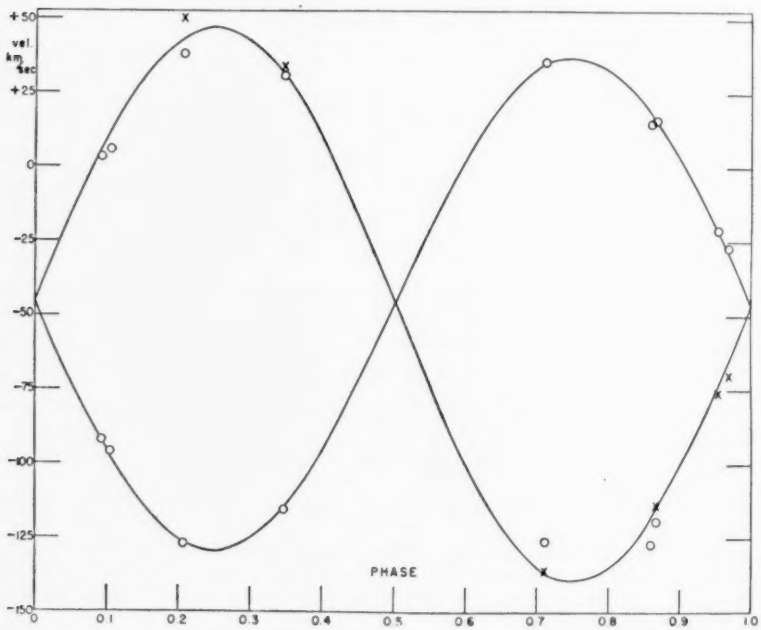

FIG. 3.—Coudé velocities of Z Herculis. *Circles:* absorption lines; *crosses:* emission lines. The hotter, brighter star has velocities of approach after zero phase.

If the periods of axial rotation and orbital revolution of the larger star are equal, the range of equatorial velocities computed from the period and radius of the star is 64 km/sec. The measured widths of the emission lines correspond to a velocity spread of about 50 km/sec. Sanford (1951) found a similar ratio of observed to predicted emission-line widths for the components of AR Lac.

PHOTOMETRIC DATA

Photometric observations of Z Her in two colors, very nearly on the B, V system, were obtained on 25 nights from July 10 through September 3, 1951, with a photoelectric photometer on the 12-inch refractor at the Lick Observatory. This instrument, which employed a 1P21 photomultiplier, linear amplifier, and recording potentiometer, is described by Weaver (1952). A few additional observations were obtained in August, 1953, with a similar photometer on the 13-inch reflector at the McDonald Observatory. The observing technique has been mentioned previously (Popper 1955). The comparison star was HD 164043.[2] Its magnitude and color are $V = 7.18$ and $B - V = +0.53$. This comparison star was also used by Baglow (1952) in his two-color study of Z Her in May and early June of the same year, so that the two sets of observations are quite similar and can be discussed together conveniently. Corrections for differential extinction rarely amounted to as much as 0.003 mag.

Because the period of Z Her equals very nearly 4 days, only four sections of the light-curve can be observed from a single station in one observing season. In the 1951 season in the western United States those sections included parts of the eclipses. Figures 4, 5, and 6 show the photometric observations. The unit of light in all cases is the light of the comparison star.

Times of Minima

Primary eclipse was observed on 5 nights, secondary eclipse on 6 nights. On 3 of the 5 nights, primary minimum was observed well past mid-eclipse (*crosses* in Fig. 5), a phase not quite reached by Baglow. My date of primary minimum is JD_{helioc} 2433852.9058 ± 0.0002 (estimated), 0.0140 day later than predicted by the elements in the *General Catalogue of Variable Stars* and 0.0035 day earlier than Baglow had estimated. The period of Z Her has been suspected of variability. All phases used in this paper are expressed in fractions of a period after primary minimum, the dates of which have been computed from the light-elements,

$$JD_{helioc} = 2433852.9058 + 3.99280E .$$

Although secondary minimum was observed beyond predicted mid-eclipse on 5 nights, the rise in brightness (*crosses* in Fig. 6) is insufficient to determine whether a slight displacement of secondary minimum is present.

Light-Curve between Minima

Analysis of the light-curve between minima is hampered by a lack of sufficient points, essentially four being obtained in a season. The observations, shown in Figure 4, are summarized in Table 3. Baglow's observations are given for comparison, as are some observations made at McDonald in 1953. It is clear that the light-curve undergoes slow changes, as indicated by the observations near phases 0.25 and 0.75. The effect is best shown by the magnitude differences (mean of two colors), phase 0.75 ***minus*** phase 0.25: Baglow, May, 1951, −0.005 mag.; Lick, July–August, 1951, −0.020 mag.; McDonald, August, 1953, +0.024 mag. Examination of the data in Table 3 leads to the conclusion that the differences are due to *increases* in brightness near 0.75 phase (Lick 1951) or 0.25 phase (McDonald 1953) rather than to decreases at the opposite phases. As may be seen

[2] HD164043, 7.1; F8; α_{1900} 17^h54^m2; δ_{1900} + 14°52′.

in Figure 4, during the Lick and McDonald observations the differences repeat so well from revolution to revolution that there can be no doubt as to their reality. One is reminded of the variations in the case of AR Lac (Wood 1946; Kron 1947), which is a system somewhat resembling Z Her. The observations are inadequate to determine which component of the system of Z Her is responsible for the variations.

Because of the small number of points between minima and because of the variations in the light-curve, rectification constants may not be evaluated in the usual way. On the

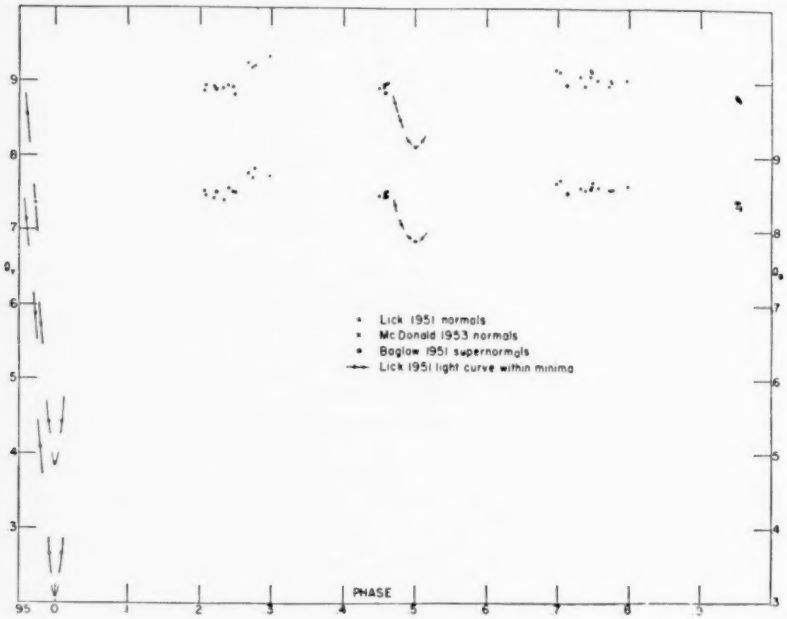

FIG. 4.—Photoelectric observations of Z Herculis. *Above:* yellow; *below:* blue. The unit of ordinates is the light of the comparison star.

TABLE 3*

LIGHT OF Z HERCULIS OUTSIDE ECLIPSE

PHASE	LICK, JULY–AUG., 1951		McDONALD, AUG., 1953		BAGLOW, MAY, 1951	
	Yellow	Blue	Yellow	Blue	Yellow	Blue
Near 0P.25	0.890	0.848	0.924	0.876	0.889	0.851
Near .46	.895	.848	.....	.....	.887	.847
Near .75	.911	.862	0.901	0.857	.897	.852
Near 0.95	0.878	0.836	.....	.....	0.881	0.840

* Unit is the light of HD 164043 in each color.

other hand, indications from the light-curves and predictions from theory agree that reflection and ellipticity effects in this system should be small, so that the uncertainties introduced into the results by a particular rectification procedure will be small. To carry out rectification of the Lick observations, I have adopted the constants in Table 4. The

TABLE 4

RECTIFICATION COEFFICIENTS

	Yellow	Blue		Yellow	Blue		Yellow	Blue
A_0	+0.890	+0.845	A_2	−0.004	−0.003	C_2	+0.003	+0.003
A_1	−0.0065	−0.004	C_0	+0.0085	+0.008	Nz	+0.029	+0.027

notation and precepts are those of Russell and Merrill (1952). The light outside eclipse is given by

$$l = A_0 + A_1 \cos\theta + A_2 \cos 2\theta ,$$

the reflected light by

$$C_0 - A_1 \cos\theta + C_2 \cos 2\theta .$$

The assumption was made that the cause of increased light near 0.75 phase does not affect the rest of the light-curve. The adopted reflection coefficients, A_1, C_0, and C_2, were obtained from theory; A_0 and A_2 from the observations, the light at 0.75 phase being neglected.

The photometric eccentricity of the system, Nz, is obtained from A_0, A_2, C_0, and C_2. The dynamical eccentricities, z, of the individual components, predicted from the properties of the system derived later, are 0.004 for the brighter, smaller, and hotter star, and 0.020 for the fainter. The weighted ratio, N, of photometric to dynamical eccentricity is 3.3.

TABLE 5

LIGHT AT MINIMA

MINIMUM	OBSERVED (UNIT = COMPARISON STAR)		RECTIFIED (UNIT = LIGHT OUTSIDE ECLIPSE)	
	Yellow	Blue	Yellow	Blue
Primary	0.388	0.310	0.452	0.381
Secondary	0.810	0.786	0.908	0.930

It is to be emphasized that all the adopted quantities in Table 4 except N_z have uncertainties of a few units in the third decimal and that these uncertainties do not seriously affect the results of the analysis in the next sections; N_z is uncertain in the second decimal.

Depths of Minima

The observed and rectified brightnesses at mid-primary and -secondary eclipses, as obtained from the Lick observations, are given in Table 5 (see Figs. 5 and 6). Most of the change from observed to rectified light comes from the change in units of light, a minor amount (<0.02) from reflection and ellipticity effects. From the rectified light-

values in Table 5 one may evaluate (*a*) the colors of the individual components; (*b*) the surface-brightness ratio; and (*c*) the ratio of the radii.

a) The color of the light lost at any phase of either eclipse is simply the color of the eclipsed star. In Table 6 the colors of the components are obtained from the depths of the minima in the two colors. The corresponding spectral types are taken from Johnson and Morgan (1953). Corrections for differential limb darkening in the two colors and for reflected light, which are considered later, cannot change the colors of the stars by more than 0.02 mag.

b) The ratio of the surface brightnesses of the two stars is 6.0 in yellow light and 8.8 in blue light. The correction for reflected light is small. Adopting the temperature

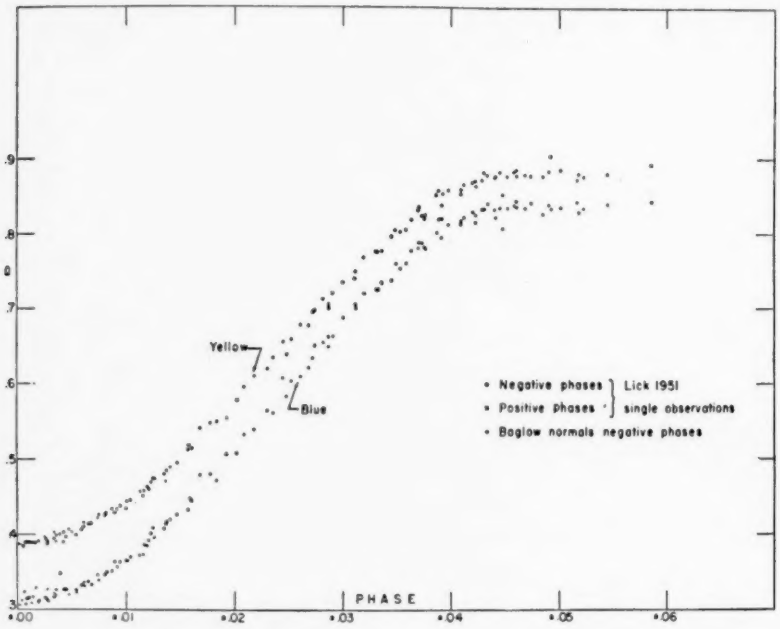

FIG. 5.—Primary minimum of Z Herculis

scale of Morgan and Keenan (1951) and Kuiper's (1938) bolometric corrections, we find the corresponding spectral-type difference to be F4–K3 V or F4–G5 III. Thus we see that the evidence from the colors of the stars and that from their surface brightnesses are in good agreement and do not contradict the evidence from the spectrograms. The most reliable indicator of spectral type in such a system, where the spectra always appear blended, is probably the color of the star. This statement is true, however, only if the observations are carried out in a *carefully standardized* color system, a practice not generally followed by observers of eclipsing variables. Three colors observed at the same time would be preferable to two, and, because of the calibration in terms of spectral type, the *U*, *B*, *V* system should be approximated. The colors of *both* components cannot, of course, be obtained so simply as in the case of Z Her unless both minima are sufficiently deep that the color of the eclipsed light can be determined with adequate precision.

c) If one assumes that the effective sizes of the components of an eclipsing system are the same in two colors and at both minima, the ratio of the radii may, in favorable cases, be obtained solely from the depths of the two minima in both colors. For the case of uniformly illuminated disks the relation is

$$k_U^2 = \frac{|\Delta l_0^{tr}|}{|\Delta l_0^{uc}|},$$

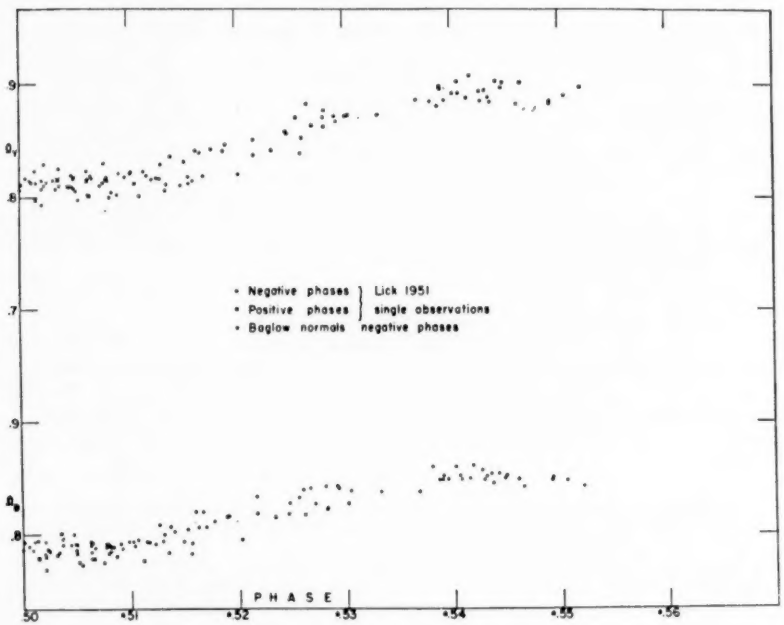

FIG. 6.—Secondary minimum of Z Herculis. *Above:* yellow; *below:* blue

TABLE 6

COLORS OF Z HERCULIS ($B - V$ SYSTEM)

Color difference, Z Her (outside eclipse) − HD 164043	+0.056 ± 0.001 mag.	
Color of HD 164043	+ .53 ± .01	
Color of Z Her outside eclipse	+0.59 ± 0.01	
	Hotter Star	Cooler Star
Color difference, eclipsed light − light outside eclipse	−0.13 mag.	+0.30 mag.
Color, $B-V$	+0.46	+0.89
Corresponding spectral type	F5–F6	K2 V G8–K0 IV G5 III

where k_U is the ratio of the radii ($k_U \leqq 1$) in the uniform hypothesis, Δ signifies the difference between the two colors, l_0^{tr} is the light at mid-eclipse when the smaller star is in front (transit), and l_0^{oc} the light at mid-eclipse when the larger star is in front (occultation). The unit of light in each color must be the uneclipsed light of the system. From the larger color difference at primary minimum in the case of Z Her (see Table 5), we conclude immediately that the deeper eclipse must be an occultation, and we obtain $k_U^2 = 0.022/0.071$, or $k_U = 0.56$. I have found that this simple method of deciding in favorable cases whether the primary minimum is a transit or an occultation and of evaluating k_U was also proposed by Danjon (1928). It does not appear to have been used.

This method of determining k may be extended to darkened disks if one assumes the degree of limb darkening for each color and for each star to be known. From the depths of the two minima in a single color, one determines, with the aid of appropriate tables for the adopted degrees of limb darkening, a relation between k and p_0, where p_0 is the geometrical depth of eclipse. A second relation is obtained for the other color, and the intersection of the two relations yields values of k and p_0. The relevant tables in *Princeton Contribution* No. 23 (Merrill 1950) are tables of ${}^{x_g, x_s}k(q_0, \alpha_0^{oc})$ and of ${}^{x_s}p(k, \alpha)$. The quantities x_g and x_s are the limb-darkening coefficients for the larger and the smaller star, respectively; α is the fractional loss of light; q_0 is a quantity obtained from the depths of the minima. In applying the method to Z Her, I have assumed the degrees of darkening and obtained the results shown in Table 7.

TABLE 7

SOLUTION FROM DEPTHS OF MINIMA

	Yellow	Blue		Yellow	Blue
x_g (adopted)	0.6	0.8	α_0^{oc}	0.80	0.81
x_s (adopted)	0.4	0.6	L_s (light of smaller star)	.69	.77
k	0.61		L_g (light of larger star)	0.31	0.23
p_0	−0.55				

There is some evidence that light on the disks of subgiant stars near spectral type K0, which the cooler component of Z Her turns out to be, is more strongly concentrated toward the center than the cosine law of limb darkening predicts (e.g., AR Lac, RT Lac). To test the effect of such a distribution of light, I have predicted the depths of secondary minima in Z Her, using the values of k, p_0, and light of the components from Table 7, and the law of limb darkening given by the Gaposchkins (1945) for thick atmospheres. With the least extreme form of darkening given by them (their $n = 3$), the predicted depths do not differ by more than 0.001 mag. from those observed in either color, so that the results in Table 7 would not require modification on this account. It should not be concluded, however, that such a darkening law will not, in general, affect the depth of a transit eclipse—see, for example, the case of V356 Sgr (Popper 1955). The geometry of eclipse of Z Her is such that at mid-secondary eclipse the smaller star reaches from about the center of the larger star to somewhat beyond its limb, so that the average surface brightness of that part of the larger star covered at mid-eclipse approximates the average for the star as a whole. Such would not be the case for a central transit.

The method used in this section of obtaining k, p_0, α_0, and L from the depths of the minima in two colors will, in a favorable case, lead to a solution that is more determinate than that obtained in the usual manner from the shape and depths of minima in a single color. The observed quantities, Δl_0^{tr} and Δl_0^{oc}, being color differences, are determined with considerable precision in two-color photoelectric observations and are little affected by

ellipticity, reflection, intrinsic variability, etc. The method will not yield determinate results if the two stars are nearly the same color or if the eclipses are shallow, i.e., in the same cases in which the usual method is indeterminate.

From the results in Table 7 we see that the magnitude difference between the components of Z Her in blue light is 1.3 mag. Petrie (1950) found 0.4 mag. from photometry of the spectrum. Severe blending and the large differences in the equivalent widths of lines in the spectra of stars with such different spectral types make the spectrographic determination very uncertain.

Shape of Primary Minimum

Solution of the light-curve in the usual way from the shape of primary minimum (Fig. 5) and the depths of minima in a single color shows that k lies between 0.55 and 0.65, and α_0 between 0.85 and 0.77. This result is in good agreement with that from the depths of the minima in two colors. The solution from the depths alone appears the more determinate and will be adopted. Baglow (1952) concluded that k lies between 0.55 and 0.75. The yellow light-curves of both observers are difficult to fit near phase 0^p.01, the curvature being less than theory predicts.

The sizes of the stars and orbital inclination are well determined from the light-curve. Using $k = 0.60$ and the rectified primary minimum at depths of 0.6 and 0.9 of the maximum depth, we obtain $r_g = 0.180$, $r_s = 0.109$, $i = 85°.1$, where r_g and r_s are, respectively, the radii of the larger and of the smaller star in units of the radius of the relative orbit. Using $k = 0.61$, $p_0 = -0.55$, and the rectified phase of the beginning of eclipse, we obtain $r_g = 0.189$, $r_s = 0.115$, $i = 82°.6$. We adopt $r_g = 0.185$, $r_s = 0.113$, $i = 84°$, and the photometric solution is complete except for corrections to the values of L in Table 7 for reflected light. These amount to less than 0.01 and are neglected. The close agreement of the results of this discussion with those of the completely independent investigation by Baglow should inspire confidence in their essential correctness.

DISCUSSION

The masses, luminosities, and radii of the components of Z Her can be computed from the data presented, except that, in addition, effective temperatures must be adopted to compute the luminosities. The effective temperatures should be consistent with the observed spectral types, particularly as derived from the colors, $B - V$. They must also satisfy the surface-brightness criterion,

$$\log\left(\frac{L_s}{L_g}\right) - 2\log k = 4\log\left(\frac{T_{es}}{T_{eg}}\right) + 0.4\,(BC_s - BC_g)\,,$$

where L_s and L_g are the brightnesses of the stars in yellow light (Table 7) and T_e and BC are the effective temperatures and bolometric corrections. The temperatures and bolometric corrections adopted are 6700° and −0.03 mag. for the hotter star, corresponding to spectral type F4 (Keenan and Morgan 1951), and 4600° and −0.35 mag. for the cooler star, corresponding to spectral type K0 IV. The color difference between the components is a bit less than that predicted by the surface-brightness ratio, but the discrepancy is not greater than the effects of uncertainties in the temperature scale and in the observations.

It is my opinion that the computed luminosities of most eclipsing binaries can be put on a sound basis only if effective temperatures are adopted primarily from properly standardized color observations. Estimated spectral types of blended spectra are not, in general, sufficiently trustworthy for this purpose. They should be used as checks on the colors, rather than vice versa. The fourth-power dependence of luminosity upon surface temperature should also be borne in mind.

Table 8 gives the principal results of the photometric analysis. Table 9 shows the properties of the two stars. With the exception of $B - V$, M_V, and spectral type, all quantities in Table 9 are in solar units. The uncertainties shown are meant to convey an idea as to the reliability of the results, which depend on a variety of data of widely differing precision. The luminosity classes given are those corresponding to the computed values of M_V. They have not been evaluated from the spectra. The F star is 0.7 mag. and the K star 2.2 mag. more luminous than a main-sequence star of the same color (Johnson and Morgan 1953).

Each component of Z Her has a mass and luminosity lying within the limits of the mass-luminosity plot for visual double stars as shown by Strand and Hall (1954), although the F star lies nearly 1 mag. above the mean relation for stars of its mass. It may be recalled that stars having probable errors in their luminosities up to ± 1.2 mag. are included in this plot.

TABLE 8

PHOTOMETRIC RESULTS

	Hotter Star	Cooler Star		Hotter Star	Cooler Star
L (yellow)	0.69 ±0.04	0.31 ±0.04	T_e	6700° ± 300°	4600° ± 250°
L (blue)	.77 ± .04	.23 ± .04	V	7.72 mag.	8.59 mag.
r	.113± .007	.185± .015			
$B-V$	+0.47 ±0.02	+0.91 ±0.03	i	84° ± 1°	

TABLE 9

PROPERTIES OF THE STARS

	Hotter Star	Cooler Star		Hotter Star	Cooler Star
$B-V$	+0.47±0.02	+0.91±0.03	M_V	+2.9±0.2	+3.8±0.3
Mass	1.22± .06	1.10± .04	Spectral type	F4 IV–V	K0 IV
Radius	1.6 ± .1	2.6 ± .2			
Luminosity	4.7 ±0.8	2.8 ±0.7	Density	0.30	0.06

The essential result of this investigation is that improved spectrographic and photometric observations give a consistent picture of the components of the system, the values shown in Table 9 being among the better determinations in so far as eclipsing binaries are concerned. The importance of carrying out the photometric observations in a well-standardized color system is again emphasized. The principal remaining uncertainties in the properties of Z Her are due to intrinsic variations in the light of at least one component. These variations are worthy of further observation.

The photometric observations at Mount Hamilton in 1951 were supported by a contract with the Office of Naval Research. I am indebted to the directors of the Mount Wilson, Lick, and McDonald Observatories for the opportunities of using equipment at those institutions.

REFERENCES

Adams, W. S., and Joy, A. H. 1919, *Ap. J.*, **49**, 179.
Baglow, R. L. 1952, *Pub. David Dunlap Obs.*, **2**, 1.
Danjon, A. 1928, *Ann. Obs. Strasbourg*, **2**, Part 1, p. 138.

Eggen, O. J. 1955, *Pub. A.S.P.*, **67**, 315.
Hiltner, W. A. 1947, *Ap. J.*, **106**, 481.
Johnson, H. L., and Morgan, W. W. 1953, *Ap. J.*, **117**, 313.
Keenan, P. C., and Morgan, W. W. 1951, *Astrophysics*, ed. J. A. Hynek (New York: McGraw-Hill Book Co.), p. 20.
Kron, G. E. 1947, *Pub. A.S.P.*, **59**, 261.
Kuiper, G. P. 1938, *Ap. J.*, **88**, 429.
Merrill, J. E. 1950, *Princeton Contr.*, No. 23.
Payne-Gaposchkin, C., and Gaposchkin, S. 1945, *Ap. J.*, **101**, 56.
Petrie, R. M. 1950, *Pub. Dom. Ap. Obs. Victoria*, **8**, 319.
Popper, D. M. 1955, *Ap. J.*, **121**, 56.
———. 1956, *Pub. A.S.P.* (in press).
Roman, N. G. 1956, *Ap. J.*, **123**, 246.
Russell, H. N., and Merrill, J. E. 1952, *Princeton Contr.*, No. 26, chap. 4.
Sanford, R. F. 1951, *Ap. J.*, **113**, 299.
Strand, K. Aa., and Hall, R. G. 1954, *Ap. J.*, **120**, 322.
Weaver, H. F. 1952, *Ap. J.*, **116**, 612.
Wood, F. B. 1946, *Princeton Contr.*, No. 21.
Wyse, A. B. 1934, *Lick Obs. Bull.*, **17**, 37.

REDISCUSSION OF ECLIPSING BINARIES. II. S ANTLIAE*

DANIEL M. POPPER
Department of Astronomy, University of California, Los Angeles
Received March 19, 1956

ABSTRACT

On the basis of a new series of spectrograms of S Antliae it is concluded that the spectrum lines of the fainter component cannot be measured. Consequently, the masses and radii of the components cannot be determined. Correlation of the velocity-curve with a new light-curve shows that the hotter star is also the brighter and thus removes an ambiguity present in earlier discussions of the system.

INTRODUCTION

In 1949 Mr. A. R. Hogg, of the Commonwealth Observatory, Canberra, suggested that it would be desirable to obtain some new spectrographic observations of the 16-hour eclipsing binary, S Antliae,[1] to supplement those of Joy (1926). The observations were needed, in particular, to determine whether the brighter or fainter component is eclipsed at primary minimum. Such a long interval had elapsed between the dates of Joy's spectrograms, obtained in 1917–1921, and Hogg and Bowe's photoelectric light-curve (Hogg and Bowe 1950), obtained in 1949, that the correlation of spectrographic and photoelectric phases was uncertain by half a revolution. I did not obtain a series of spectrograms of S Antliae until 1954, five years after Hogg and Bowe's light-curve was observed. Upon examining the references to photometric observations of this star, it seemed that there was still some uncertainty in the phase correlations. Consequently, on a visit to the Lowell Observatory in the winter of 1955 a photoelectric light-curve of S Antliae was obtained. The present discussion is based on the more recent spectrographic and photometric observations.

SPECTROGRAPHIC DATA

Twenty-six prismatic spectrograms of S Antliae, having a dispersion of 34 A/mm at Hγ, were obtained principally with the Cassegrain spectrograph of the 100-inch telescope in 1954. The exposure times were 30 minutes (0.03 of the period). Because of improvements in spectrographs and photographic emulsions in the last thirty-five years, these spectrograms are stronger, wider, finer-grained, and extend to considerably shorter wave lengths than those obtained by Joy in 1917–1921 (Joy 1926).

The spectrograms are listed in Table 1. Phases are in fractions of the period after the middle of the deeper minimum. Spectrograms obtained near each of the nodes are reproduced in Figure 1. The lines of the brighter component have been placed together in the reproduction, the difference in radial velocity of about 160 km/sec between the two plates being shown by the relative positions of the two comparison spectra. Since the brighter component has negative velocities after the deeper minimum, it is seen immediately that the brighter star is the hotter, in agreement with Joy's conclusion.

The spectrograms have been examined and compared carefully to find the lines of the second component, use having been made of a spectrum comparator constructed particularly for this purpose. The only consistent evidence I am able to see that the fainter component is present is in the H lines; Hδ and Hγ show wings displaced in the opposite direction from the strong lines. In addition, it can be readily seen (Fig. 1) that the strong

* This investigation was made possible in part by a co-operative arrangement with the Mount Wilson and Palomar Observatories.

[1] HD 82610, var.; F0; α_{1900} $9^h27^m.9$; δ_{1900} $-28°11'$.

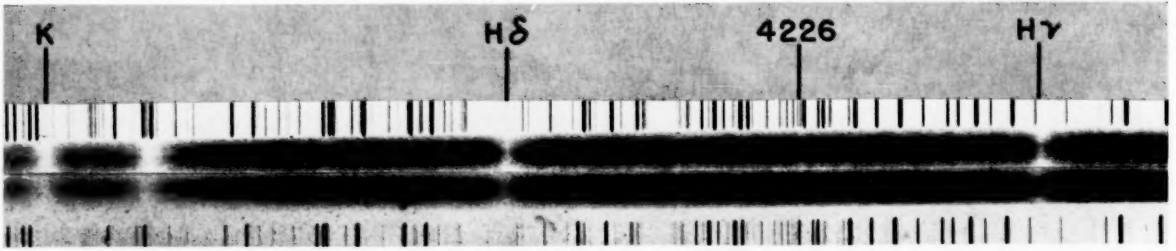

FIG. 1.—Spectrograms of S Antliae. *Above:* plate E2778, 0.324 phase; *below:* plate E2802*a*, 0.834 phase. The spectrograms have been displaced relative to each other by the amount of their velocity difference, 160 km/sec, so that the stellar lines of the brighter component coincide.

components of Hγ do not show so large a radial-velocity variation as do the remaining lines. The same effect can be seen in Hδ. These effects of blending are confirmed by the radial-velocity measures of the H lines and, to a lesser extent, of other strong lines.

Thus it is evident that lines of the fainter component influence the appearance and positions of the stronger lines in the spectrum of S Antliae, so that the brightness ratio cannot be so large as the value 8:1 derived by Hogg and Bowe for the case of the brighter star being eclipsed at primary minimum. On the other hand, the lines of the fainter component do not appear as separate lines in the spectrum, so that the variation in the radial velocity of the fainter component cannot be determined with any degree of confidence.

TABLE 1

SPECTROGRAMS OF S ANTLIAE

Plate	U.T.	$JD_{helioc.}$ 2430000+	Phase	No. of Lines	Velocity (km/sec)	O−C (km/sec)
	1952					
γ 32446*a*	Apr. 5.211	4107.714	0.923	16	+ 53	+11
b	5.233	.736	.957	13	+ 15	− 8
	1954					
E2776	Feb. 11.285	4784.789	.236	22	−101	− 8
2777	11.314	.818	.281	22	− 85	+ 7
2778	11.342	.846	.324	22	− 86	− 2
2779	11.369	.873	.366	21	− 65	+ 5
2780	11.394	.898	.404	22	− 53	0
2781	11.421	.925	.446	22	− 26	+ 6
2794	Apr. 9.132	4841.635	.915	21	+ 47	+ 1
2795*a*	9.159	.662	.956	19	+ 8	−16
b	9.188	.691	.001	22	+ 2	+ 4
2796*a*	9.215	.718	.043	20	− 30	− 4
b	9.241	.744	.083	19	− 60	−13
2797	9.269	.772	.126	21	− 77	−10
2802*a*	May 12.147	4874.648	.834	22	+ 76	− 3
b	12.170	.671	.869	21	+ 70	+ 4
2861*a*	14.144	4876.645	.914	21	+ 50	+ 4
b	14.167	.668	.949	22	+ 33	+ 5
2885	Dec. 12.437	5088.938	.352	20	− 72	+ 3
2886*a*	12.465	.966	.395	21	− 52	+ 6
b	12.490	.991	.434	22	− 26	+12
c	12.516	5089.017	.474	22	− 8	+ 8
d	12.541	.042	.513	20	− 3	− 9
	1956					
2931*a*	Jan. 2.417	5474.920	.686	12	+ 83	0
b	2.458	.961	.750	20	+ 91	0
c	2.490	.993	0.799	21	+ 85	− 2

Consequently, the radii and masses of the components of S Antliae must remain unknown. Examination of Joy's older plates, which, for reasons stated, are less suited to the purpose than the new ones, does not alter this conclusion. I wish to express appreciation to Dr. Joy for advice in this matter.

The spectral type of the brighter component appears a bit earlier than F0, in agreement with Joy's estimate of A8. The spectral type of the fainter component cannot be estimated from the spectrograms. From the apparent strength of its hydrogen lines, discussed in the second preceding paragraph, I should not expect it to be later than about F5. The color of the combined light, obtained from the photometric observations, corresponds to type F0. The surface-brightness ratio, 1.7, obtained by Hogg and Bowe, corresponds to a spectral-type difference A8–F3.

Radial-velocity measurements in the spectrum of a system such as S Antliae are beset with two difficulties. First, because of the width (axial rotation) and number of the lines, blending effects within the spectrum of a single component are serious, so that the normal wave length to be adopted for a given line is uncertain. Second, blending between lines of the two components will affect the positions of the lines. To analyze these problems, a separate velocity curve was drawn for each of the twenty-two lines chosen for measurement. Provisional values of K and γ were obtained by a graphical method for each line in the relation,

$$V = \gamma - K \sin \theta ,$$

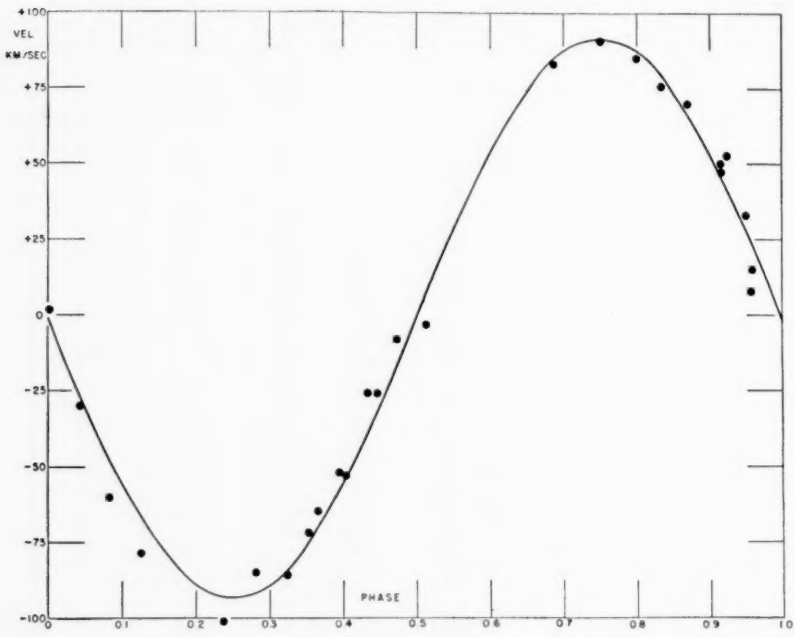

FIG. 2.—Radial velocities of S Antliae. The velocities are relative to an arbitrary zero. The curve is obtained from the adopted elements. Phases are in fractions of the period measured from the deeper eclipse.

where V is the measured velocity based upon an assumed wave length and θ is the phase angle measured from primary minimum. For seventeen of the twenty-two lines the values of K so obtained are scattered between 87 and 105 km/sec, the mean being 94.5. The values of K for the five strongest lines measured, K, Hδ, 4226, Hγ, and 4481, are, on the other hand, 70, 66, 77, 48.5, and 80 km/sec, respectively. Consequently, these five lines were omitted from the radial-velocity reductions. The systematic difference, which is assumed to be due to blending with lines of the fainter component, is readily seen for Hγ in Figure 1. In order to obtain a consistent system of wave lengths for the remaining seventeen lines, the velocities measured for each line were corrected by subtracting the value of γ obtained for that line. The resulting mean velocities are listed in Table 1 and

plotted in Figure 2. The value of K obtained from these velocities and upon which the curve of Figure 2 and residuals of Table 1 are based, is

$$K = 92.3 \pm 1.5 \text{ km/sec} .$$

The difference between this value of K and the value 94.5 obtained from the individual lines is caused by different effective weighting of the lines in the two methods, as is the difference of γ from zero, its value being -1.2 ± 1.0. The smaller value of K, 81 km/sec, obtained by Joy almost certainly results from his having included the stronger lines, which give systematically smaller velocity variations. A unique solution for the center

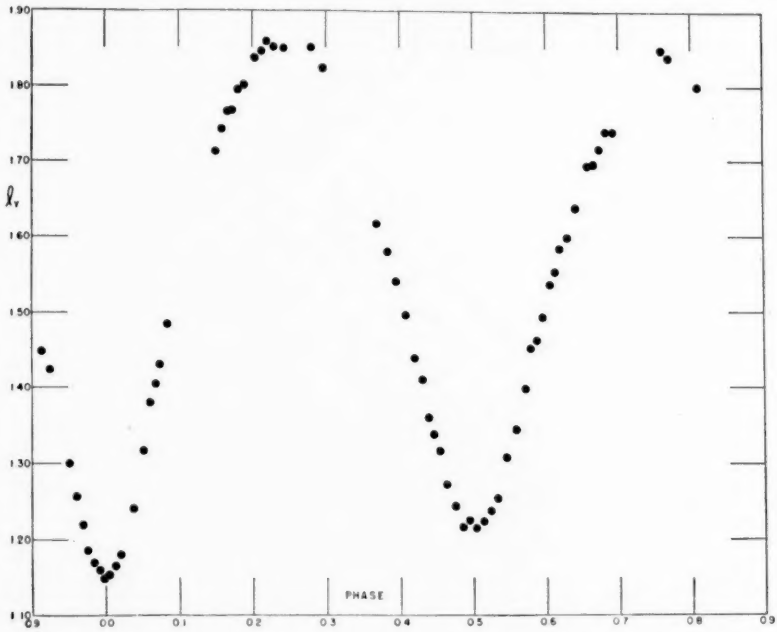

FIG. 3.—Light-curve of S Antliae in yellow light. Phases as in Fig. 2. The unit of the ordinates is the yellow light of the comparison star multiplied by 3.98. Each point is the mean of from three to five comparisons.

of mass velocity, γ, is not given by the procedure adopted. A value in the vicinity of $+15$ km/sec is indicated. From the value of K and the period we derive the following results:

$$a_1 \sin i = 1.2 \text{ solar radii} , \qquad f(m) = 0.05 \text{ solar masses} .$$

PHOTOMETRIC DATA

S Antliae was observed on 10 nights between January 24 and February 8, 1955, with a photoelectric photometer attached to the 21-inch Cassegrain reflector at the Lowell Observatory. This instrument employs a 1P21 photomultiplier, A.C. linear amplifier, and Brown recorder. The color filters are those of the U, B, V system (Johnson and

Morgan 1953). Most of the observations were through the yellow filter. The comparison star employed was HD 82575.[2] The comparison star used by Hogg and Bowe (1950), ξ^2 Antliae, differs too much in zenith distance from S Antliae, as seen from Flagstaff, to be useful. The observing was carried out within 2 hours of the meridian because of the relatively large zenith distance of the stars. The correction for differential extinction between the two stars at an hour angle of 2 hours is 0.007 mag. in yellow light. Figure 3 shows the yellow light-curve.

Times of Minima and Period

The observed time of primary minimum is JD_{helioc} 2435139.929 ± 0.001 (est.). Combining this result with Hogg and Bowe's observed date of primary minimum leads to a period of 0.648345 day, while combining Hogg and Bowe's and my minima with the older set of observations compiled by Luizet (1904) gives a period of 0.648342. The minima of the older set appear to require a period of 0.648340, so there is evidence of a slight lengthening of the period. The period 0.648345 has been used in conjunction with my observed time of primary minimum to compute the phases used in this paper.

The epoch of zero phase published by Luizet and used by Joy (1926) in his analysis of the system refers to the *deeper* eclipse. This conclusion is contrary to that reached by Hogg and Bowe. As confirmed by a letter from Mr. Hogg, the paper by Hogg and Bowe unfortunately contains an error in the date of primary minimum. The epoch JD 2432920.7715 is incorrect, so that conclusions drawn with its use are invalid. The time of primary minimum observed by Hogg and Bowe is JD 2432962.139. It was this mistake that caused the difficulty in phase correlation mentioned in the introduction of this paper.

Discussion of the Light-Curve

The observations in yellow light outside eclipse (0.15 or more of the period from both minima) are fitted by the relation

$$l_Y = l_0 (1 + 0.029 \cos \theta - 0.147 \cos 2\theta),$$

θ being the phase measured from primary minimum. This relation is in good agreement with that of Hogg and Bowe for unfiltered light:

$$l - l_0 (1 + 0.024 \cos \theta - 0.145 \cos 2\theta).$$

In particular, the sign of the coefficient of cos θ is confirmed to be the opposite of that given by the usual reflection effect. (Their published value of the coefficient of cos 2θ, -0.016, is a misprint.)

Rectification of the light-curve in the usual way leads to fractional losses of light of 0.194 at primary minimum and 0.094 at secondary. These values are to be compared with 0.194 and 0.112, obtained by Hogg and Bowe. The spectrographic results show unambiguously that the brighter star is eclipsed at the deeper minimum and hence is the hotter. This result is in agreement with that adopted by Joy but is contrary to that favored by Hogg and Bowe.

I have not considered it worthwhile to carry the analysis of the light-curve of S Antliae any further. Rectification procedures are, for a system with components as greatly distorted as those of S Antliae, at best uncertain. When, as in this case, the stars are nearly in contact, the mass ratio is unknown, and the eclipses are partial, it is doubtful that meaningful results can be obtained. In the solution by Hogg and Bowe, as well as that by Joy, it was assumed that the two stars are ellipsoids of the same shape, the geometrical ellipticities being the same as the photometric ellipticities. These assumptions are

[2] HD 82575; 8.1 F0; α_{1900} 9^h27^m7; δ_{1900} $-28°36'$.

poorly based, as are conclusions determined from them. The result of Hogg and Bowe, for example, that, if the brighter star is eclipsed at the deeper minimum, the brightness ratio of the components is 8/1, is not compatible with the spectrographic observations. Since, in any case, the masses and radii of the components of S Antliae cannot be obtained because the radial velocities of the fainter component are not observable, inability to solve the light-curve does not deprive us of information concerning the basic properties of the stars of this system.

The principal purpose of the 1955 photoelectric observations of S Antliae was to determine the epoch of the deeper eclipse. Because of the limited observing time available and the large zenith distance of the star, it was considered advisable to concentrate on the light-curve in a single color. As a result, color variations of S Antliae are not very well determined. The $B - V$ color shows no systematic variations with phase larger than 0.01 mag. The color of the system is

$$B - V = +0.33 \pm 0.01 , \qquad U - B = -0.01 \pm 0.01 .$$

These colors are those of a main-sequenced star of spectral type F0 (Johnson and Morgan 1953). At maximum light the magnitude of the system is $V = 6.28$.

DISCUSSION

The most important conclusion to be drawn from this investigation is that S Antliae should be removed from lists of stars of which the masses and radii of the components are presumed to be determined observationally.

It has been a privilege to use the facilities of the Mount Wilson and Lowell Observatories, as well as to discuss the problem of S Antliae with Dr. Joy. I am indebted to Mr. Hogg for emphasizing the desirability of obtaining a new series of spectrograms.

REFERENCES

Hogg, A. R., and Bowe, P. W. A. 1950, *M.N.*, **110**, 373.
Johnson, H. L., and Morgan, W. W. 1953, *Ap. J.*, **117**, 313.
Joy, A. H. 1926, *Ap. J.*, **64**, 351.
Luizet, M. 1904, *A.N.*, **165**, 291.

DIFFUSION AND SEVERING OF MAGNETIC LINES OF FORCE

E. N. PARKER
Enrico Fermi Institute, University of Chicago

AND

M. KROOK
Harvard College Observatory

Received January 6, 1956; revised March 20, 1956

ABSTRACT

The general asymptotic form for the magnetic field in a diffusing flux tube is developed and applied to the problem of severing magnetic lines of force in a medium with finite electrical conductivity. Calculations of the details of the severing and reconnection of lines of force are given for the formation of an idealized free meridional magnetic ring in a hydromagnetic dynamo, for the merging of idealized neighboring rings, and for the straightening of the lines in a twisted tube, in order to illustrate the general qualitative features of these processes as they would presumably occur in the core of the earth. The problem of two nearly intersecting slender flux tubes is considered in order to demonstrate how the lines of force of the lesser tube are diverted into the denser tube.

I. INTRODUCTION

It is well known that the lines of force of a magnetic field contained within a volume of fluid of infinite electrical conductivity are carried along by the fluid, just as are vortex lines in an inviscid fluid. The lines of force retain their identity, and any two elements of fluid threaded by the same line of force will always be so threaded; conversely, two elements of fluid which are not initially threaded by the same line can never be threaded. Hence, lines of force cannot cut across one another or sever in any way. Knots tied in the field are preserved, just as they are in an ordinary piece of string.

In a fluid of *finite* electrical conductivity (the effective conductivity may be greatly reduced by turbulent diffusion), the preservation of lines of force is no longer the case. Lines of force continually break and reconnect, as is illustrated by the fact that an infinitely long twisted flux tube in a motionless fluid will lose its twist if the conductivity σ is not infinite. For this reason it is not sufficient as an analogy to hydromagnetic processes to picture in one's mind how the fluid motions may deform a bundle of material strings. With the deformation, one must intersperse periods of diffusion, allowing severing and reconnection of the individual strings.

In this paper we shall first develop the solution of the hydromagnetic diffusion equation for an untwisted and for a twisted flux tube. Since the diffusion equation is linear, we may then superpose solutions and investigate how separate tubes will merge into each other. We shall not attempt the general case of more broadly distributed fields, except to remark that they may be constituted by a suitable superposition of flux tubes.

We are particularly interested in illustrating in a qualitative way the severing and reconnecting of lines of force as the phenomenon occurs in a hydromagnetic dynamo (Parker 1955). In such a dynamo a rope of flux of the toroidal field extending through a rising rotating (cyclonic) region of conducting fluid is carried along by the fluid and is bent into a loop, as shown in Figure 1, *a*. As a result of diffusion, the loop ultimately severs from the rope of flux from which it was formed, yielding a free ring and leaving the initial more or less straight rope unchanged (Fig. 1, *b*). The free ring at the same time merges with neighboring rings (Fig. 1, *c*, *d*) and amplifies the poloidal field. That the process can occur has been demonstrated by formal methods, but an illustration of the rearranging and reconnecting of the individual lines of force has not been given.

II. GENERAL THEORY

The diffusion of a magnetic field in a motionless fluid of conductivity σ is given by

$$\frac{\partial \boldsymbol{B}}{\partial t} = \frac{1}{\mu\sigma} \nabla^2 \boldsymbol{B} \tag{1}$$

in m.k.s. units. A rigorous analytical solution of equation (1) for a general curved, lumpy

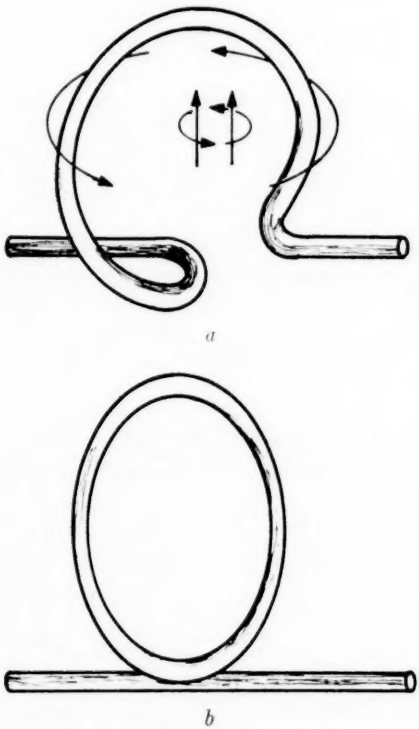

a

b

FIG. 1*a* and *b*.—*a*, Twisted loop formed in a rope of flux in the toroidal magnetic field in the earth's core by cyclonic fluid motions. *b*, The free magnetic ring resulting from the twisted loop by diffusion and severing of the lines of force.

flux tube is out of the question, but if we restrict ourselves to *slender* flux tubes, the solution reduces to a straightforward procedure.

a) Untwisted Flux Tube

Consider a long, straight, untwisted flux tube lying along the z-axis. The field density is assumed to depend only on the distance ρ from the z-axis and the azimuthal angle ϕ measured around the z-axis. The initial field $B_z(\rho, \phi, 0)$ is given. That we refer to the magnetic field as forming a flux tube implies that, beyond some distance $\rho = L$, $B_z(\rho, \phi, 0)$ is negligible.

We shall now show formally the intuitively obvious fact that, for sufficiently large values of t, $B_z(\rho, \phi, t)$ becomes a Gaussian function of ρ and independent of ϕ. For a magnetic field in the z-direction of density $B_z(\rho, \phi, t)$, equation (1) reduces to

$$\mu\sigma \frac{\partial B_z}{\partial t} = \frac{1}{\rho} \frac{\partial}{\partial \rho} \left(\rho \frac{\partial B_z}{\partial \rho} \right) + \frac{1}{\rho^2} \frac{\partial^2 B_z}{\partial \phi^2}. \tag{2}$$

By separating the variables, it is readily shown that the general solution in an unbounded space is of the form

$$B_z(\rho, \phi, t) = \sum_{n=0}^{\infty} \exp(\pm in\phi) \int_0^{\infty} dk\, k \psi_n(k) J_n(k\rho) \exp\left(-\frac{k^2 u^2}{4} \right), \tag{3}$$

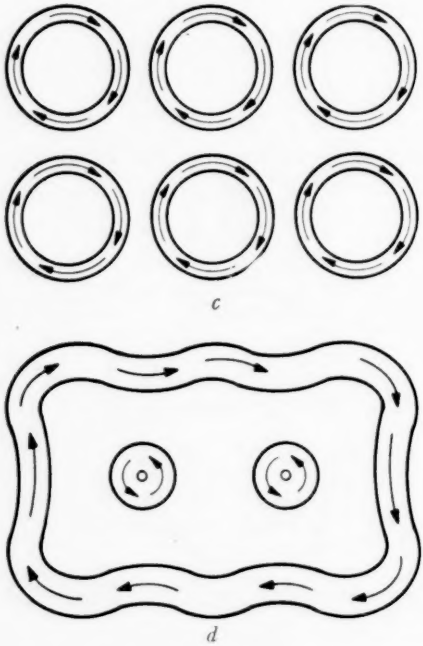

FIG. 1*c* and *d*.—*c*, A number of free magnetic rings in a given meridional plane. *d*, The diffusive coalescence of the meridional rings which forms a single large loop in the meridional plane and contributes to the dipole component of the geomagnetic field.

where

$$u^2 = \frac{4t}{\mu\sigma} \tag{4}$$

and $\psi_n(k)$ is a function to be determined from the initial field $B_z(\rho, \phi, 0)$.

To compute $\psi_n(k)$, we put $t = 0$ in equation (3) and invert, multiplying by $\exp(\mp im\phi) J_m(k\rho)$ and integrating over ρ and ϕ. We obtain (Sneddon 1951)

$$\psi_n(k) = \frac{1}{2\pi} \int_0^{2\pi} d\phi \int_0^{\infty} d\rho\, \rho \exp(\mp in\phi) J_n(k\rho) B_z(\rho, \phi, 0) .$$

Substituting this result in equation (3), we have

$$B_z(\rho, \phi, t) = \frac{1}{2\pi}\sum_{n=0}^{\infty} \exp(\pm in\phi) \int_0^{2\pi} d\alpha \int_0^{\infty} ds\, s \exp(\mp in\alpha) B_z(s, \alpha, 0)$$
$$\times \int_0^{\infty} dk\, k J_n(k\rho) J_n(ks) \exp\left(-\frac{k^2u^2}{4}\right).$$

Carrying out the integration over k (Watson 1944), we obtain

$$B_z(\rho, \phi, t) = \frac{1}{\pi u^2} \exp\left(-\frac{\rho^2}{u^2}\right) \sum_{n=0}^{\infty} \exp(\pm in\phi) \tag{5}$$
$$\times \int_0^{2\pi} d\alpha \int_0^{\infty} ds\, s \exp(\mp in\alpha) B_z(s, \alpha, 0) \exp\left(-\frac{s^2}{u^2}\right) I_n\left(\frac{2\rho s}{u^2}\right),$$

where I_n represents a modified Bessel function of order n.

To obtain the asymptotic form of $B_z(\rho, \phi, t)$ for large values of t, we note that the integration over s need be only between the limits zero and L as a consequence of the assumed vanishing of $B_z(\rho, \phi, 0)$ for $\rho > L$. Then, when t is sufficiently large that $u \gg L$, we expand the exponential function and the modified Bessel function in the integrand in a series of ascending powers of s/u. Since

$$I_n(x) = \frac{(x/2)^n}{n!} + \frac{(x/2)^{n+2}}{2!(n+2)!} + \cdots,$$

we obtain the asymptotic form,

$$B_z(\rho, \phi, t) \sim \frac{1}{\pi u^2} \exp\left(-\frac{\rho^2}{u^2}\right) \int_0^{2\pi} d\alpha \int_0^{L} ds\, s B_z(s, \alpha, 0)$$
$$\times \left\{1 + \frac{\rho s}{u} \exp\left[\pm i(\phi - \alpha)\right] + O^2\left(\frac{s}{u}\right)\right\}.$$

The term which is $O(s/u)$ is the integral I,

$$I \equiv \int_0^{2\pi} d\alpha \int_0^{L} ds\, s B_z(s, \alpha, 0) \frac{s}{u} \exp(\mp i\alpha),$$

which may be written

$$I = \frac{1}{2\pi u} \int_0^{L} dx \int_0^{L} dy\, (x \mp iy) B_z(s, \alpha, 0),$$

where x and y are the Cartesian co-ordinates,

$$x = s\cos\alpha, \qquad y = s\sin\alpha.$$

It follows that the real and imaginary parts of I form the moment of $B_z(s, \alpha, 0)$ about the y- and x-axes, respectively. Thus, by locating the origin at the "center of gravity" of the magnetic field, we make I vanish, and $B_z(\rho, \phi, t)$ reduces to

$$B_z(\rho, \phi, t) \sim \frac{\Phi_z}{\pi u^2} \exp\left(-\frac{\rho^2}{u^2}\right)\left[1 + O^2\left(\frac{L}{u}\right)\right], \tag{6}$$

where Φ_z is the total flux in the tube. Thus the flux density in a diffusing magnetic flux tube rapidly assumes a rotationally symmetric Gaussian distribution. It follows that the

general characteristics of a diffusing tube will be satisfactorily reproduced if we assume that the field density is *initially* a Gaussian function; for, no matter what the initial distribution may have been, it will be nearly Gaussian by the time the flux tube has diffused significantly, viz., when $t > 4\mu\sigma L^2$.

For our calculations, then, we shall let

$$B_z(\rho, 0) = \frac{\Phi_z}{\pi a^2} \exp\left(-\frac{\rho^2}{a^2}\right) \tag{7}$$

when $t = 0$. It may be shown from equation (5), by expanding in a power series or else by substituting direct'y in equation (2), that

$$B_z(\rho, \phi, t) = \frac{\Phi_z}{\pi w^2} \exp\left(-\frac{\rho^2}{w^2}\right) \tag{8}$$

when $t > 0$. We have put

$$w^2 = a^2 + u^2 = a^2 + \frac{4t}{\mu\sigma}. \tag{9}$$

Having so far confined ourselves to a formal discussion of straight flux tubes, we remark now that equation (8) obviously applies in good approximation to a flux tube that is neither exactly straight nor of uniform cross-section, so long as the radius of curvature, R, and the characteristic length of variation, S, of the cross-section are both large compared to the tube radius, w.

To demonstrate that equation (8) satisfies equation (1) so long as $w/R \ll 1$, consider a flux tube in the form of a ring of radius R circling the z-axis and lying in the xy-plane. Then the axis of the tube is the circle $\rho' = R$ and $z' = 0$ in the cylindrical co-ordinate system (ρ', μ', z'). The distance ρ from the axis of the tube becomes

$$\rho = [(\rho' - R)^2 + z'^2]^{1/2}.$$

Substituting in equation (1), we find that equation (8) neglects terms $O(w/R)$.

Using a straight flux tube of variable radius w, it is readily shown that equation (8) neglects terms $O^2(w/S)$.

b) Twisted Flux Tube

Consider a long, straight tube containing flux which is twisted about the axis of the tube like the strands of a rope. If the axis of the tube is taken to lie along the z-axis, then the magnetic field of the tube may be decomposed into a field in the z-direction and a field in the ϕ-direction. The diffusion of the former was discussed previously, and the latter we shall discuss now.

From the hydromagnetic equation

$$\frac{\partial \boldsymbol{B}}{\partial t} = \nabla \times (\boldsymbol{v} \times \boldsymbol{B}) \tag{10}$$

it is readily shown that twisting a flux tube, with the fluid velocity

$$\boldsymbol{v} = \boldsymbol{e}_\phi v(\rho, z), \tag{11}$$

leaves the z-component of $\boldsymbol{B}$ unchanged and produces only a ϕ-component, given by

$$B_\phi = B_z \int dt \frac{\partial v}{\partial z}; \tag{12}$$

$\boldsymbol{e}_\phi$ represents a unit vector in the ϕ-direction. Thus B_ϕ is independent of ϕ and a function only of ρ, z, and t. The diffusion equation (1) reduces to

$$\mu\sigma \frac{\partial B_\phi}{\partial t} = \frac{1}{\rho}\frac{\partial}{\partial \rho}\left(\rho \frac{\partial B_\phi}{\partial \rho}\right) - \frac{B_\phi}{\rho^2} + \frac{\partial^2 B_\phi}{\partial z^2} \tag{13}$$

for the ϕ-component. Following the same procedure as in the previous section, we shall develop the asymptotic form of B_ϕ for large values of t.

By separating the variables in equation (13), we find that the general solution in an unbounded space is

$$B_\phi(\rho, z, t) = \int_0^\infty d k_1 k_1 J_1(k_1\rho) \exp\left(-\frac{k_1^2 u^2}{4}\right) \times \int_0^\infty d k_2 \exp(i k_2 z) \exp\left(-\frac{k_2^2 u^2}{4}\right) \theta(k_1, k_2) , \tag{14}$$

in which $\theta(k_1, k_2)$ is a function to be determined from the initial conditions, $B_\phi(\rho, z, 0)$, and u^2 is given in equation (4).

To determine $\theta(k_1, k_2)$, we set $t = 0$ in equation (14), multiply by $\rho J_1(k_1 \rho) \exp(-ik_2 z)$, and integrate over ρ from 0 to $+\infty$ and over z from $-\infty$ to $+\infty$. We obtain (Sneddon 1951)

$$\theta(k_1, k_2) = \frac{1}{2\pi}\int_0^\infty d\rho \rho J_1(k_1\rho) \int_0^\infty d z \exp(-ik_2 z) B_\phi(\rho, z, 0) . \tag{15}$$

We now substitute equation (15) in equation (14). The integral over k_1 may be found in Watson (1944). The integration over k_2 involves the integral

$$\int_{-\infty}^{+\infty} d x \exp(-\alpha x^2 - \beta x) = \left(\frac{\pi}{\alpha}\right)^{1/2} \exp\left(\frac{\beta^2}{4\alpha}\right). \tag{16}$$

We obtain, ultimately,

$$B_\phi(\rho, z, t) = \frac{2}{u^3\sqrt{\pi}} \exp\left(-\frac{\rho^2}{u^2}\right) \int_0^\infty d s\, s \exp\left(-\frac{s^2}{u^2}\right) I_1\left(\frac{2\rho s}{u^2}\right) \times \int_{-\infty}^{+\infty} d\zeta \exp\left[-\left(\frac{z-\zeta}{u}\right)^2\right] B_\phi(s, \zeta, 0) . \tag{17}$$

Again, we remark that, in a flux tube of finite diameter, $B_\phi(\rho, z, 0)$ must be negligible for ρ greater than some value L. Expanding the exponential and Bessel functions in the integrand in ascending powers of s/u, we obtain

$$B_\phi(\rho, z, t) \sim \frac{2\rho}{u^4} \exp\left(-\frac{\rho^2}{u^2}\right) \int_0^\infty d s\, s^2 Q(s) \tag{18}$$

for large t. Here $Q(s)$ is the integral

$$Q(\rho) = \frac{1}{u\sqrt{\pi}} \int_{-\infty}^{+\infty} d\zeta \exp\left[-\frac{(z-\zeta)^2}{u^2}\right] B_\phi(\rho, \zeta, 0) \tag{19}$$

and represents an average over ζ of $B_\phi(\rho, \zeta, 0)$ for a distance of the order of u on each side of $\zeta = z$. Formula (18) now becomes

$$B_\phi(\rho, z, t) \sim \frac{2\rho}{u^4} \exp\left(-\frac{\rho^2}{u^2}\right) \int_0^\infty ds\, s^2 \langle B_\phi \rangle (s, 0) \left[1 + O^2\left(\frac{L}{u}\right)\right] \tag{20}$$

as the asymptotic form of B_ϕ.

Since we are interested primarily in flux tubes that have undergone significant diffusion, we shall use the asymptotic Gaussian forms given by equations (6) and (20) for all values of t. Thus we assume that initially the ϕ-component of the magnetic field has the form

$$B_\phi(\rho, 0) = B_0 \frac{\rho}{a} \exp\left(-\frac{\rho^2}{a^2}\right) \tag{21}$$

in conjunction with the z-component, given in equation (7). For $t > 0$,

$$B_\phi(\rho, t) = B_0 \frac{a^3 \rho}{w^4} \exp\left(-\frac{\rho^2}{w^2}\right) \tag{22}$$

rigorously, as in equation (8); w is given in equation (9).

The angle ϑ between a line of force and the direction of the axis of the twisted flux tube is given by

$$\tan \vartheta = \frac{B_\phi}{B_z}. \tag{23}$$

Using equations (8) and (22), we obtain

$$\tan \vartheta = \frac{\pi B_0 a^2 \rho}{\Phi_z w^2}. \tag{24}$$

The distance Λ along the z-axis required for one turn of a line of force around the tube is

$$\Lambda = 2\pi\rho \cot \vartheta = \frac{2\Phi_z w^2}{B_0 a^2}. \tag{25}$$

We see that Λ is independent of ρ and increases with time as w^2.

The total flux circulating about the z-axis per unit length of tube is

$$\begin{aligned} \Phi_\phi(t) &= \int_0^\infty d\rho B_\phi(\rho, t) \\ &= \frac{B_0 a^3}{2w^2} \\ &= \Phi_\phi(0) \frac{a^2}{w^2}. \end{aligned} \tag{26}$$

The magnetic energy of $B_\phi(\rho, t)$ per unit length is

$$\begin{aligned} \epsilon_\phi(t) &= 2\pi \int_0^\infty d\rho\, \rho \frac{B_\phi^2(\rho, t)}{2\mu} \\ &= \frac{\pi B_0^2 a^6}{8\mu w^4} \\ &= \frac{\pi \Phi_\phi^2(0)\, a^4}{2\mu w^4}. \end{aligned} \tag{27}$$

From equation (8) it is readily shown that the magnetic energy of $B_z(\rho, t)$ per unit length is

$$\epsilon_z(t) = \frac{\Phi_z^2}{4\pi\mu w^2}. \tag{28}$$

Hence

$$\frac{\epsilon_\phi(t)}{\epsilon_z(t)} = \frac{\epsilon_\phi(0)}{\epsilon_z(0)}\left(\frac{a}{w}\right)^2. \tag{29}$$

If we suppose, after Lundquist (1951), that a flux tube is unstable when $\epsilon_\phi > \epsilon_z$, then

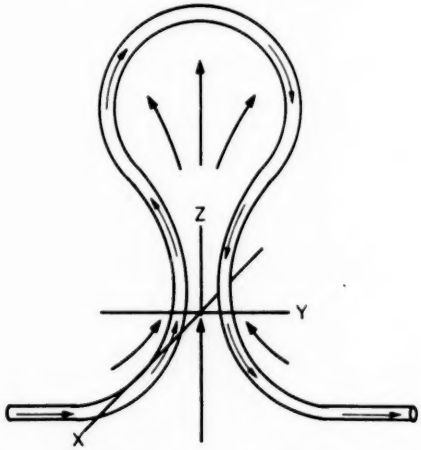

FIG. 2*a*.—Ω-shaped loop: the idealized form of a loop, in order that the severing to form a free ring may be treated quantitatively.

we expect that in nature we shall find only those tubes in which ϵ_ϕ is initially less than ϵ_z. Accordingly, equation (29) gives an upper limit on the twisting, $\epsilon_\phi(t)/\epsilon_z(t)$,

$$\frac{\epsilon_\phi(t)}{\epsilon_z(t)} < \left(\frac{a}{w}\right)^2. \tag{30}$$

In the next section we shall show in a typical case of the severing of a loop to form a free ring that $w \cong 40a$ by the time that 90 per cent of the lines of force are severed and reconnected. Equation (30) implies that, by then, $\epsilon_\phi(t) < 0.0006\epsilon_z(t)$.

III. MERGING AND SEVERING OF FLUX TUBES

a) Ω-shaped Loop

Consider the idealized loop shown in Figure 2*a* formed by a rising clump of fluid displacing the initially straight, slender tube of flux upward into a billowing loop shaped like a capital omega. In order to treat quantitatively the severing by diffusion, we suppose that the lower portions of the legs of the loop lie in the yz-plane, are close together, and are located symmetrically about the zx-plane. For convenience, we put the position of closest approach of the legs at $z = 0$; and in the region about $z = 0$ where the legs are close together, we represent their axes by

$$y_0 = \pm f(z), \tag{31}$$

where $f(z)$ is an even function of z and a minimum at $z = 0$. We see that the merging of two neighboring coplanar magnetic rings, as shown in Figure 2*b*, admits of the same formulation.

The angle, $\theta(z)$, between the z-axis and the axis of either leg at some value of z is equal to

$$\theta(z) \cong \frac{df}{dz} \tag{32}$$

for small values of df/dz. The distance l of a point $(0, y_1, z_1)$ from the axis $y_0 = f(z)$ is related to the difference in y-co-ordinates of the point and the axis at $z = z_1$ by

$$l \cong [y_1 - f(z_1)] \cos \theta(z_1), \tag{33}$$

provided that l is much less than the radius of curvature R of the leg. Near $z = 0$, dy/df is $O(z/R)$. Thus

$$l = [y_1 - f(z_1)] \left[1 + O^2\left(\frac{z}{R}\right)\right]. \tag{34}$$

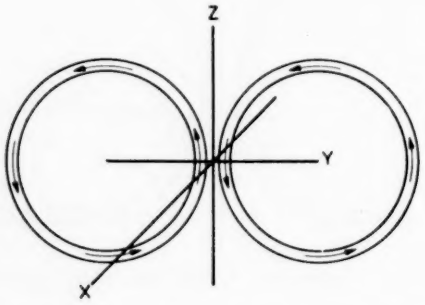

FIG. 2*b*.—The idealized form of two meridional rings, in order that their coalescence may be treated as the same problem as the severing in the Ω-shaped loop.

The field of either leg is assumed to be of the form (8). If $(\boldsymbol{e}_x, \boldsymbol{e}_y, \boldsymbol{e}_z)$ represents a set of vectors, each of unit length, along the x-, y-, and z-axes, respectively, then the field in either leg may be written

$$\boldsymbol{B}_{1,2}(x, y, z, t) = \frac{\Phi_z}{\pi w^2} \exp\left\{-\frac{x^2 + [y \pm f(z)]^2}{w^2}\right\}\left[\pm \boldsymbol{e}_z - \boldsymbol{e}_y \frac{df}{dz} + O^2\left(\frac{z}{R}\right)\right]. \tag{35}$$

We have chosen the flux in the original straight tube to be directed in the positive y-direction. Thus the $\pm$ sign refers to the left- $(y < 0)$ and right- $(y > 0)$ hand legs, respectively, in Figures 2*a* and 2*b*. The net field is the sum of the fields of the two individual legs, or

$$\boldsymbol{B}(x, y, z, t) = -\frac{2\Phi_z}{\pi w^2} \exp\left[-\frac{x^2 + y^2 + f^2(z)}{w^2}\right] \times \left[\boldsymbol{e}_y \frac{df}{dz} \cosh \frac{2y f(z)}{w^2} + \boldsymbol{e}_z \sinh \frac{2y f(z)}{w^2}\right] + O^2\left(\frac{z}{R}\right). \tag{36}$$

The lines of force are everywhere parallel to the yz-plane and satisfy the differential equation,

$$\frac{dy}{dz} = \frac{B_y}{B_z} = \frac{df}{dz} \coth \frac{2yf(z)}{w^2} + O^2\left(\frac{z}{R}\right). \tag{37}$$

Using $f(z)$ in place of z as the independent variable, we write

$$\frac{dF}{dY} = \tanh 2YF, \tag{38}$$

where

$$Y = \frac{y}{w}, \qquad F(z, t) = \frac{f(z)}{w}. \tag{39}$$

In order to integrate equation (38), we introduce the new variables α and β, defined as follows:

$$\alpha = F + Y, \qquad \beta = F - Y. \tag{40}$$

Then, substituting in equation (38) and solving for $d\alpha/d\beta$, we obtain the equation

$$\frac{d\alpha}{d\beta} = -\exp(\alpha^2 - \beta^2), \tag{41}$$

in which the variables are separable. Integrating and transforming back to F and Y, we have

$$\operatorname{erf}(F + Y) + \operatorname{erf}(F - Y) = C, \tag{42}$$

where C is the constant of integration. We recognize $Y + F$ and $Y - F$ as the distance in units of the tube diameter w from the axes $Y = \pm F(z, t)$ of the original flux tubes.

Erf (x) is an odd function of x, and, for large positive values of x,

$$\operatorname{erf}(x) \sim 1 - \frac{\exp(-x^2)}{x\sqrt{\pi}}\left[1 + O\left(\frac{1}{x^2}\right)\right]. \tag{43}$$

Now the lines of force are distinguished by the associated value of C, and the lines all begin and end at infinity. Using expression (43) in equation (42), it is readily seen that, far out on the positive y-axis, we have $C = 0$. Swinging around toward the positive z-axis and remaining at large distances from the origin, we see that C increases to $+1$ as we reach the tube axis $Y = F(z, t)$, because $F(z, t) \gg 1$ for large z; $C = 2$ on the positive z-axis and thereafter decreases, having the value of unity on the tube axis $Y = -F(z, t)$ and reaching zero far out on the negative y-axis. Since $F(z, t)$ is an even function of z, it follows that C has the same values at $-z$ as at $+z$.

Consider a point at large z near $Y = F(z, t)$ so that $|F(z, t) - Y|$ is of the order of unity, but $[F(z, t) + Y] \gg 1$. Then, using equation (43), equation (42) reduces to

$$\operatorname{erf}(F - Y) \sim C - 1, \tag{44}$$

which tells us that $F - Y$ is independent of z. Hence the lines of force are parallel to the axis of the tube, and the field of the tube $Y = F(z, t)$ is undisturbed by the presence of the other tube, $Y = -F(z, t)$, as we would expect. In the tube $Y = F(z, t)$, the field

density varies with y as $\exp[-(F-Y)^2]$. Thus the number of lines of force N between Y and the tube axis is proportional to

$$N \propto \int_F^Y dY \exp[-(F-Y)^2], \tag{45}$$

$$\propto \operatorname{erf}(F-Y). \tag{46}$$

Comparing formulae (46) and (44), we see that $C-1$ is directly proportional to the number of lines of force between the axis of either tube and the line of force determined by the given value of C.

Returning to the vicinity of the origin, consider the lines of force which have reconnected across the z-axis by diffusing into the other tube. On the z-axis, equation (42) reduces to

$$2 \operatorname{erf} F(z, t) = C, \tag{47}$$

which allows us to compute the value of C for the line of force crossing the z-axis at any given z. Here $F(z, t)$ is a monotonically increasing function of z; the minimum value is $F(0, t)$. Hence all those lines of force for which C lies in the range

$$2 \operatorname{erf} F(0, t) < C \leq 2 \tag{48}$$

cross the z-axis and therefore have been reconnected between, rather than remaining connected along, the tubes. Because of increasing w, $F(z, t)$ is a monotonically decreasing function of time, going to zero in the limit as t becomes large. We see, then, that, in the limit, expression (48) becomes $0 < C < 2$ and all the lines of force have reconnected; the original two tubes have been completely severed across $z = 0$, and the severed ends are joined across $y = 0$. Thus the loop shown in Figure 2*a* is free of the original tube of flux, and the two rings in Figure 2*b* are merged into one.

The total flux, Φ_1, which has been severed at $z = 0$ and reconnected across the z-axis by diffusion is

$$\Phi_1 = \left| \int_{-\infty}^{+\infty} dx \int_0^{\infty} dz B_y \big|_{y=0} \right| \tag{49}$$

above the y-axis; the same number of lines of force have been reconnected below the y-axis. Using equation (40), it is readily shown that

$$\Phi_1 = \Phi_z [1 - \operatorname{erf} F(0, t)]. \tag{50}$$

The flux Φ_2 still connected along each original flux tube is

$$\Phi_2 = \Phi_z - \Phi_1 = \Phi_z \operatorname{erf} F(0, t). \tag{51}$$

The tension across $z = 0$ in each tube is

$$\begin{aligned} S_z &= \int_{-\infty}^{+\infty} dx \int_0^{+\infty} dy \left(\frac{B_z^2}{2\mu} \right)_{z=0} \\ &= \frac{\Phi_z^2}{4\pi\mu w^2} \{ 1 - \exp[-2F(0, t)] \}. \end{aligned} \tag{52}$$

Far from the origin the tension in each tube is

$$S = \frac{\Phi_z^2}{4\pi\mu w^2}. \tag{53}$$

Thus, in each quadrant, the net force pulling the fluid away from the origin toward $|z| \gg 1$ is

$$S - S_a = \frac{\Phi_z^2}{4\pi\mu w^2} \exp\left[-2F^2(0, t)\right] + O^2\left(\frac{w}{R}\right). \tag{54}$$

Figures 3*a* and 3*b* show the lines of force for the special case that $f(z)$ is the parabola,

$$f(z) = b + \frac{z^2}{2R}, \tag{55}$$

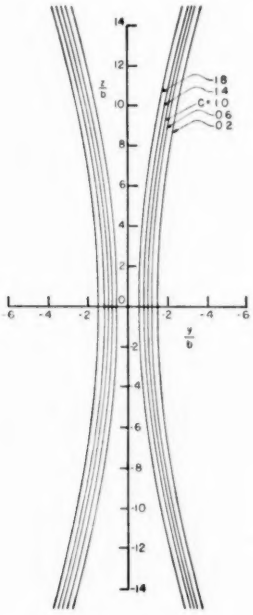

FIG. 3*a*.—The initial configuration of the lines of force in the neighborhood of the origin in Figs. 2*a* and 2*b* for $w = b/2$.

with radius of curvature R in the vicinity of $z = 0$. In the figures we have put $b/R = 0.02$. Initially, we let $b = 2w$, so that the tubes are clearly separate. In Figure 3*b*, w has increased to $2b$; about half the lines, those for which $C > 1.04$, are reconnected. By the time that $w = 18b$, about 90 per cent of the flux is severed.

Now, while Figure 3 illustrates how the lines of force in an Ω-shaped loop will reconnect to form a free ring, it must be remembered that the problem has been idealized by considering a slender flux tube bent so as to form a broad loop which is very narrow across the base; because the sides of the resulting ring are far apart, interdiffusion and cancellation of lines of force are negligible, and the total flux circulating around the final ring is

just equal to the initial flux in the rope forming the loop. In an actual hydromagnetic dynamo the flux forming an Ω-shaped loop will not form a slender rope, and the loop will not be particularly narrow across the base; hence the two sides of the loop or ring will interdiffuse and the flux circulating around the final ring will be rather less than the initial flux in the rope forming the loop. Our calculations, then, serve to illustrate the manner in which the lines of force reconnect during the formation of a ring, without representing a quantitative description of actual dynamo fields.

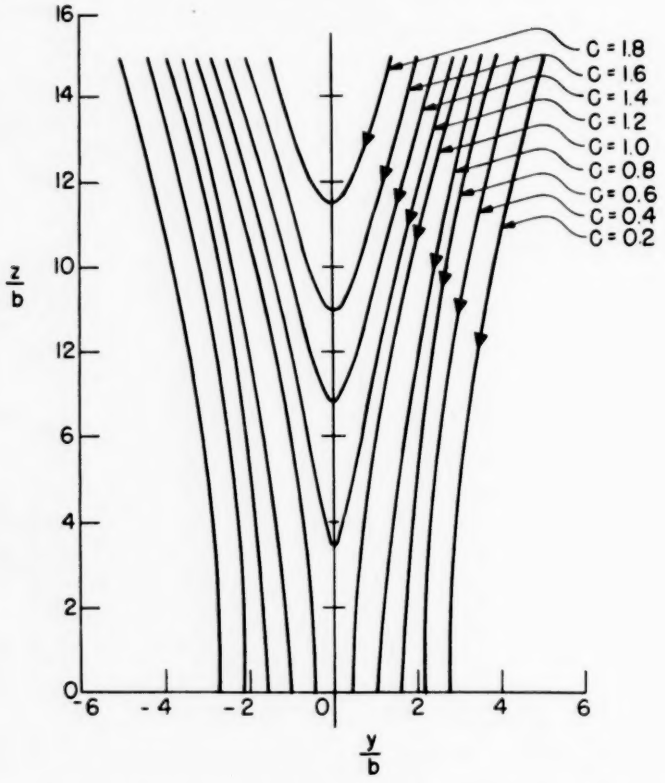

FIG. 3*b*.—The lines of force in the neighborhood of the origin after diffusion when the tube width w has increased to $w = 2b$.

b) Simple Loop

In this section we shall develop as briefly as possible the diffusion of a simple loop, as shown in Figure 4. Symmetry makes it possible to treat only half the region of intersection. With the co-ordinate axes oriented as shown in Figure 4, we confine our attention to the region for which $z > 0$. The tube axis lies along $x = y = 0$ and along $x = 2b$, $y = f(z)$ in the vicinity of the origin, and it is the interdiffusion of these two segments of

the initial looped tube that we shall consider. Adopting equation (8) as the form of the field in each tube, it is readily seen that the fields are

$$\boldsymbol{B}_1(x, y, z, t) = -\boldsymbol{e}_z \frac{\Phi\mu\sigma}{\pi w^2} \exp\left(-\frac{x^2+y^2}{w^2}\right), \tag{56}$$

$$\boldsymbol{B}_2(x, y, z, t) = -\frac{\Phi\mu\sigma}{\pi w^2} \exp\left[-\frac{(x-2b)^2+(y-f(z))^2}{w^2}\right] \times\left(\boldsymbol{e}_y \frac{df}{dz}+\boldsymbol{e}_z\right). \tag{57}$$

The total field $\boldsymbol{B}$ is the sum of $\boldsymbol{B}_1$ and $\boldsymbol{B}_2$.

The lines of force lie in planes parallel to the yz-plane and satisfy

$$\frac{dz}{dy} = \frac{B_z}{B_y} = \frac{dz}{df}\left[1+\exp\left(\frac{4b^2-4bx+f^2-2fy}{w^2}\right)\right]. \tag{58}$$

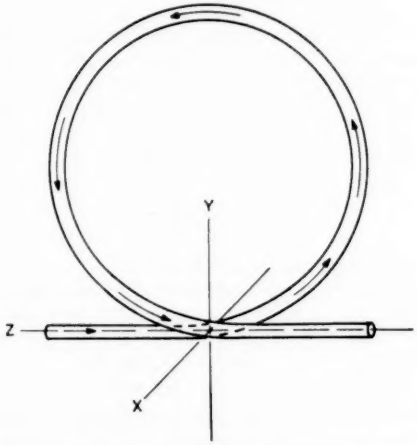

FIG. 4.—Another simple form of loop in a flux tube before diffusion

Then

$$\frac{dF}{dY} = 1+\phi(x)\exp(F^2-2FY), \tag{59}$$

where

$$\phi(x) = \exp\left(\frac{4b^2-4bx}{w^2}\right). \tag{60}$$

To integrate equation (59), we let

$$u = F - Y.$$

Then

$$\frac{du}{dY} = \phi \exp(+u^2)\exp(-Y^2), \tag{61}$$

and

$$\phi(x)\,\mathrm{erf}\;Y-\mathrm{erf}\,(F-Y)=C\,. \tag{62}$$

To simplify the discussion of the lines of force, we consider sufficiently large values of t that $b/w \ll 1$. Then

$$\phi(x)=1+O\left(\frac{b^2}{w^2}\right),$$

and equation (62) reduces to

$$\mathrm{erf}\;Y-\mathrm{erf}\,(F-Y)=C+O\left(\frac{b^2}{w^2}\right). \tag{63}$$

For large positive values of z, equation (63) reduces to

$$\mathrm{erf}\,(F-Y)\sim 1-C \tag{64}$$

near $Y=F$, and

$$\mathrm{erf}\;Y\sim 1+C \tag{65}$$

near $Y=0$. Thus, as in the previous section, the tubes are not distorted or reconnected where they are far apart; $1\pm C$ is a direct measure of the number of lines of force between the given line of force and the axes of the tubes. C ranges from $+2$ far out on the positive y-axis to $+1$ at $Y=F$, to -1 at $Y=0$, and to -2 far out on the negative y-axis.

Figure 5 shows the lines of force when $w \gg b$ and

$$f(z)=\frac{z^2}{2R}.$$

We have put $w/R=0.02$, as in the previous section.

We see from Figure 5 that the loop has severed from the original straight rope of flux and has become a free ring. No lines of force connect the ring and the straight rope. The line of force $C=0$ lies along $Y=\frac{1}{2}F(z,t)$ and divides the ring from the straight rope.

c) Intersecting Flux Tubes

Consider two slender flux tubes whose axes are separated by a distance $2b$ at the point of closest approach. We represent the flux carried by each tube by Φ_1 and Φ_2 and their initial diameters by $2a_1$ and $2a_2$, respectively. We let s_1 and s_2 represent the distance from their axes to some point (x, y, z). From equation (9) we find that their diameters at time t are $2w_{1,2}$, where

$$(w_{1,2})^2=\frac{4t}{\mu\sigma}\left[1+\frac{(a_{1,2})^2\mu\sigma}{4t}\right]. \tag{66}$$

Thus, for sufficiently large values of t, w_1 and w_2 are both equal to u, defined in equation (4), to within terms of the order of $(a_{1,2})^2\mu\sigma/t$. From equation (6) or (8) it follows that the field density in either tube may be written

$$B_{1,2}=\frac{\Phi_{1,2}}{\pi u^2}\exp\left[-\left(\frac{s_{1,2}}{u}\right)^2\right]. \tag{67}$$

Now, by the time t is sufficiently large that the tube radius u is large compared to b, it is obvious that to a sufficient degree of approximation we may regard the two axes of the tubes as intersecting at a point P, instead of passing only within the relatively small

distance b. We are considering flux tubes which curve only over distances which are large compared to $a_{1,2}$, b, and u; hence in the vicinity of P the axes of the two tubes lie very nearly in a plane S. Suppose, then, that we construct a rectangular co-ordinate system (x, y, z), as shown in Figure 6, with origin at P, with the x-axis perpendicular to S, and with the z-axis bisecting the angle 2ϑ between the two tube axes.

The tube axes may be approximated as the straight lines

$$y = z \tan \vartheta \tag{68}$$

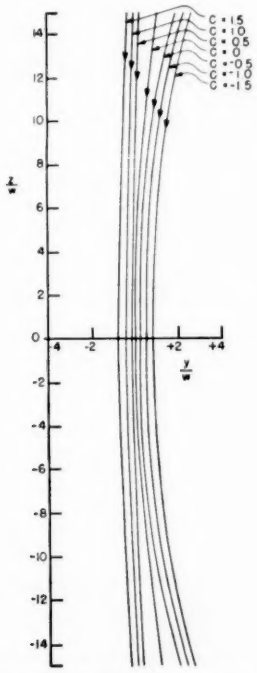

FIG. 5.—The lines of force in the vicinity of the origin in Fig. 4 after diffusion

in the vicinity of P. It is readily shown that

$$(s_{1,2})^2 = x^2 + (y \cos \vartheta \pm z \sin \vartheta)^2 . \tag{69}$$

We may substitute equation (69) in equation (67) and formally integrate the equations for the lines of force. It is interesting to note, however, that the formal calculation can be replaced by the following arguments: The x-component of the magnetic field is zero, and the ratio of the y- and z-components is independent of x; hence the lines of force are confined planes parallel to the yz-plane, and the configuration of the lines is independent of x; therefore, the flux between, say, the zx-plane and a line of force is independent of position on the line of force. It follows that on any line of force in the yz-plane we must have

$$\int d s_1 B(s_1) + \int d s_2 B(s_2) = \text{function of } t , \tag{70}$$

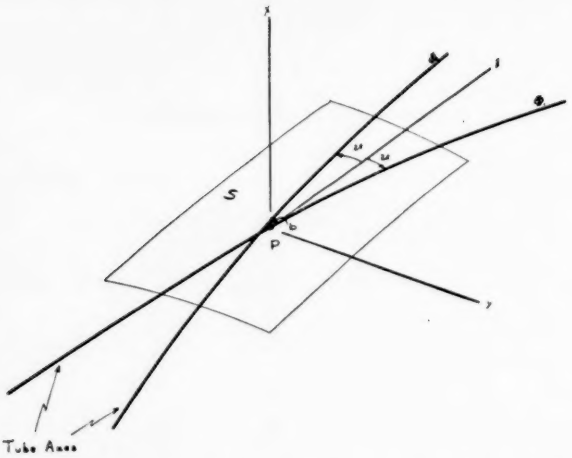

FIG. 6.—The local rectangular co-ordinate system (x, y, z) for treating the interdiffusion of two nearly intersecting flux tubes, with axes shown by the heavy lines.

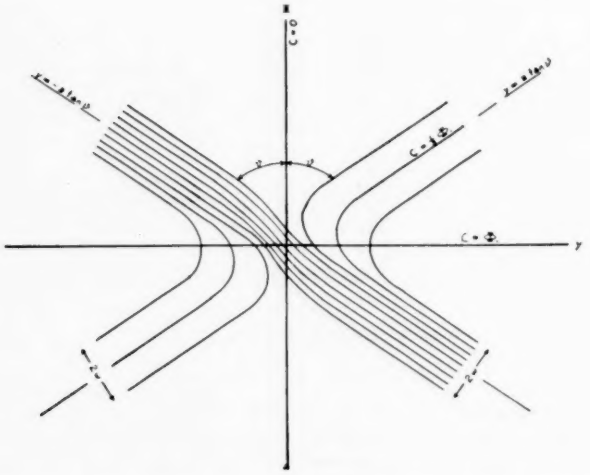

FIG. 7.—Schematic drawing of the final pattern of the lines of force of the two flux tubes with axes shown in Fig. 6, showing how the flux of the weaker tube has been completely severed and reconnected into the stronger tube.

where the integration is from the zx-plane out to any point (y, z) on the line of force. Using equation (67) and properly choosing the constant of integration, equation (70) reduces to

$$2C = \Phi_1\left[\operatorname{erf}\left(\frac{y\cos\vartheta - z\sin\vartheta}{w}\right) + 1\right] + \Phi_2\left[\operatorname{erf}\left(\frac{y\cos\vartheta + z\cos\vartheta}{w}\right) - 1\right], \quad (71)$$

where C is the total flux between the plane $y = 0$ and the cylinder parallel to the z-axis generated by the line of force.

The lines of force are shown schematically in Figure 7 for the special case that $\Phi_2 > \Phi_1$. One should note that the lines of force of the tube with the lesser flux are diverted into the tube with greater flux. If $\Phi_1 = \Phi_2$, then, obviously, there would be no lines of force crossing the xz-plane ($y = 0$), and the tubes would be completely reconnected.

REFERENCES

Lundquist, S. 1951, *Phys. Rev.*, **83**, 307.
Parker, E. N. 1955, *Ap. J.*, **122**, 293.
Sneddon, I. N. 1951, *Fourier Transforms* (2d ed.; New York: McGraw-Hill Book Co.).
Watson, G. N. 1944, *Bessel Functions* (Cambridge: At the University Press), p. 395.

AXISYMMETRIC MAGNETIC FIELDS AND FLUID MOTIONS*

S. CHANDRASEKHAR
Enrico Fermi Institute, University of Chicago
Received March 27, 1956

ABSTRACT

The equations of hydromagnetics appropriate for an incompressible inviscid fluid of finite electrical conductivity are considered in case the magnetic fields and the fluid motions have symmetry about an axis. By using a known theorem that a solenoidal vector field can be expressed as a superposition of a poloidal and a toroidal field, the equations are reduced to four equations for four governing scalars. In the limiting case of infinite electrical conductivity, a general relation is derived which includes, as special cases, the known theorems on force-free fields, isorotation, and conditions for hydrostatic equilibrium. Some integral relations which follow from the four equations are also derived.

1. INTRODUCTION

The equations of hydromagnetics governing the velocity ($\boldsymbol{v}$) and the magnetic ($\boldsymbol{H}$) fields in a fluid conductor present problems of considerable mathematical complexity. The complexity arises, in part, from the nonlinearity of the equations. The nonlinear terms are of three kinds: the terms $(\boldsymbol{v}\cdot\text{grad})\boldsymbol{v}$ and $\boldsymbol{H}\times\text{curl}\,\boldsymbol{H}$, representing the inertia and the electromagnetic forces in the equation for $\boldsymbol{v}$, and the term curl $(\boldsymbol{v}\times\boldsymbol{H})$, representing electromagnetic induction in the equation for $\boldsymbol{H}$. It is on this account that most of the hydromagnetic problems which have been solved are those which allow a linearization of the equations. The large class of stability problems which have been successfully investigated in recent years is in this category. In these problems one supposes that an external magnetic field is present, and one examines the behavior of the system in the neighborhood of a well-defined stationary solution of the equations; this leads one to characteristic value problems in linear equations (albeit of high orders). Similarly, in current investigations of the dynamo problem (cf. Bullard and Gellman 1954; Elsasser 1955, 1956) by ignoring the equation for $\boldsymbol{v}$ and assuming $\boldsymbol{v}$ to be given, one reduces the problem to a linear one for characterizing the magnetic field. While the class of such linear problems which one might usefully investigate is by no means exhausted (cf. Chandrasekhar 1956*c*), it would appear that hydromagnetics has now reached a stage of development at which further understanding depends on considering the complete set of equations. In this connection the possibility should not be overlooked that, by not considering all the equations of a problem, we may miss discovering certain essential novelties which result as a consequence of imposing on a system conformity with two different sets of laws: such as conformity with the laws of electrodynamics and hydrodynamics. Thus there is some danger in being too exclusively guided by analogy with the behavior of the system when it obeys only one or the other set of laws. An example of this has recently been found (Chandrasekhar 1956*b*).

It is the object of this paper to make a systematic beginning in the study of the complete set of equations of hydromagnetics. However, the treatment will be restricted to the case in which the fluid motions and the magnetic fields have symmetry about an axis. It should be realized that this restriction to axisymmetry may have far-reaching consequences, such as Cowling's theorem (Cowling 1934; Backus and Chandrasekhar 1956) on the impossibility of a self-excited homogeneous dynamo.

In addition to axisymmetry, it will be supposed that the fluid is incompressible and

* The research reported in this paper has been supported in part by the Geophysics Research Directorate of the Air Force Cambridge Research Center, Air Research and Development Command, under Contract AF 19(604)-299 with the University of Chicago.

inviscid. The neglect of viscosity is justifiable in most cases (cf. Bullard 1956); but the restriction to incompressibility (except in the context of the earth's core) is not. Nevertheless, the latter assumption is essential if we are not to complicate a problem already beset with considerable mathematical difficulties.

It will be shown that the equations derived under the restrictions stated enable a unified treatment of the diverse "laws" (such as the law of isorotation) which have been discussed in the literature. Also certain general integral relations will be derived which exhibit the net effects of the interaction between the fluid motions and the magnetic field.

2. THE EQUATIONS OF THE PROBLEM

The equations of hydromagnetics appropriate for an incompressible, inviscid fluid of finite electrical conductivity (σ) are well known. They are (cf. Bullard 1956)

$$-\frac{\partial \boldsymbol{H}}{\partial t} = \operatorname{curl}\left(\frac{1}{4\pi\sigma}\operatorname{curl}\boldsymbol{H} - \boldsymbol{v}\times\boldsymbol{H}\right) \tag{1}$$

and

$$\frac{\partial \boldsymbol{v}}{\partial t} + (\boldsymbol{v}\cdot\operatorname{grad})\,\boldsymbol{v} - \frac{1}{4\pi\rho}\operatorname{curl}\boldsymbol{H}\times\boldsymbol{H} = -\operatorname{grad}\left(\frac{p}{\rho}+\mathfrak{V}\right), \tag{2}$$

where $\mathfrak{V}$ denotes the gravitational potential, ρ the density, and p the pressure. Further,

$$\operatorname{div}\boldsymbol{H} = 0 \qquad \text{and} \qquad \operatorname{div}\boldsymbol{v} = 0\,. \tag{3}$$

Using the identity

$$(\boldsymbol{v}\cdot\operatorname{grad})\,\boldsymbol{v} = \operatorname{curl}\boldsymbol{v}\times\boldsymbol{v} + \operatorname{grad}(\tfrac{1}{2}\,|\,\boldsymbol{v}\,|^2)\,, \tag{4}$$

we can rewrite equation (2) in the form

$$\frac{\partial \boldsymbol{v}}{\partial t} = \frac{1}{4\pi\rho}\operatorname{curl}\boldsymbol{H}\times\boldsymbol{H} - \operatorname{curl}\boldsymbol{v}\times\boldsymbol{v} - \operatorname{grad}\left(\frac{p}{\rho}+\tfrac{1}{2}\,|\,\boldsymbol{v}\,|^2+\mathfrak{V}\right). \tag{5}$$

Instead of $\boldsymbol{H}$, it is convenient to introduce the variable

$$\boldsymbol{h} = \frac{\boldsymbol{H}}{\sqrt{(4\pi\rho)}}\,, \tag{6}$$

which is of the dimensions of a velocity. It is also convenient to make the equations non-dimensional by measuring length in a certain unit R (appropriate for the problem on hand),

$$t \text{ in the unit } 4\pi\sigma R^2$$

and

$$\boldsymbol{h} \text{ and } \boldsymbol{v} \text{ in the unit } (4\pi\sigma R)^{-1}\,. \tag{7}$$

If we are dealing with the earth's core, these units have the values (cf. Bullard 1954)

$$R = 3.47\times10^{8}\text{ cm}\,,$$

$$4\pi\sigma R^2 = 1.44\times10^{5}\text{ years}\,, \tag{8}$$

and

$$(4\pi\sigma R)^{-1} = 7.65\times10^{-5}\text{ cm/sec}\,.$$

In the units stated, the equations for $\boldsymbol{h}$ and $\boldsymbol{v}$ can be expressed in the forms

$$\frac{\partial \boldsymbol{h}}{\partial t} = -\operatorname{curl}\boldsymbol{E} \tag{9}$$

and

$$\frac{\partial \boldsymbol{v}}{\partial t} = \mathfrak{L} - \text{grad}\, \varpi\,, \tag{10}$$

where

$$\boldsymbol{E} = \text{curl}\, \boldsymbol{h} - \boldsymbol{v} \times \boldsymbol{h}\,, \tag{11}$$

$$\mathfrak{L} = \text{curl}\, \boldsymbol{h} \times \boldsymbol{h} - \text{curl}\, \boldsymbol{v} \times \boldsymbol{v} \tag{12}$$

and

$$\varpi = \frac{p}{\rho} + \tfrac{1}{2} |\, \boldsymbol{v}\, |^2 + \mathfrak{V}\,. \tag{13}$$

We can eliminate ϖ from equation (10) by taking its curl; thus

$$\frac{\partial}{\partial t} \text{curl}\, \boldsymbol{v} = \text{curl}\, \mathfrak{L}\,. \tag{14}$$

3. THE EQUATIONS IN THE AXISYMMETRIC CASE

As Lüst and Schlüter (1954; see also Chandrasekhar 1956*a*) have recently pointed out, any axisymmetric solenoidal vector field can be expressed as a superposition of a *poloidal* and a *toroidal* field in terms of two scalars. Thus

$$\boldsymbol{h} = -\varpi \frac{\partial P}{\partial z}\, \mathbf{1}_\varpi + \varpi T \mathbf{1}_\varphi + \frac{1}{\varpi} \frac{\partial}{\partial \varpi} (\varpi^2 P)\, \mathbf{1}_z\,, \tag{15}$$

and

$$\boldsymbol{v} = -\varpi \frac{\partial U}{\partial z}\, \mathbf{1}_\varpi + \varpi V \mathbf{1}_\varphi + \frac{1}{\varpi} \frac{\partial}{\partial \varpi} (\varpi^2 U)\, \mathbf{1}_z\,, \tag{16}$$

where ϖ, φ, and z define a system of cylindrical polar co-ordinates (with the axis of symmetry in the z-direction), $\mathbf{1}_\varpi$, $\mathbf{1}_\varphi$, and $\mathbf{1}_z$ are unit vectors along the three principal directions, and P, T, U, and V are four scalars which are azimuth-independent.

As is evident from equations (15) and (16), the field derived from a poloidal scalar has nonvanishing components only in the meridional planes, while the field derived from a toroidal scalar has nonvanishing components only in the transverse φ-direction. Thus U defines currents which are entirely meridional, while V defines motions which are entirely rotational.

When we consider the vorticity of an axisymmetric solenoidal vector field, we find a certain reciprocity: the poloidal field gives rise to a toroidal vorticity, and, conversely, a toroidal field gives rise to a poloidal vorticity. Thus the current (which is proportional to curl $\boldsymbol{H}$) derived from a poloidal magnetic field is toroidal and conversely. Specifically, we have

$$\text{curl}\, \boldsymbol{h} = -\varpi \frac{\partial T}{\partial z}\, \mathbf{1}_\varpi - \varpi \Delta_5 P \mathbf{1}_\varphi + \frac{1}{\varpi} \frac{\partial}{\partial \varpi} (\varpi^2 T)\, \mathbf{1}_z \tag{17}$$

and

$$\text{curl}\, \boldsymbol{v} = -\varpi \frac{\partial V}{\partial z}\, \mathbf{1}_\varpi - \varpi \Delta_5 U \mathbf{1}_\varphi + \frac{1}{\varpi} \frac{\partial}{\partial \varpi} (\varpi^2 V)\, \mathbf{1}_z\,, \tag{18}$$

where

$$\Delta_5 = \frac{\partial^2}{\partial \varpi^2} + \frac{3}{\varpi}\frac{\partial}{\partial \varpi} + \frac{\partial^2}{\partial z^2} \tag{19}$$

is the Laplacian operator for axisymmetric functions in five-dimensional Euclidean space.

We now return to equations (9) and (14), which govern $\boldsymbol{h}$ and $\boldsymbol{v}$. First, we find from equations (15), (16), and (17) that

$$\begin{aligned}
\boldsymbol{E} &= \operatorname{curl} \boldsymbol{h} - \boldsymbol{v} \times \boldsymbol{h} \\
&= \left\{ -\varpi \frac{\partial T}{\partial z} - V \frac{\partial}{\partial \varpi}(\varpi^2 P) + T \frac{\partial}{\partial \varpi}(\varpi^2 U) \right\} \mathbf{1}_\varpi \\
&+ \left\{ -\varpi \Delta_5 P + \frac{\partial P}{\partial z}\frac{\partial}{\partial \varpi}(\varpi^2 U) - \frac{\partial U}{\partial z}\frac{\partial}{\partial \varpi}(\varpi^2 P) \right\} \mathbf{1}_\varphi \\
&+ \left\{ \frac{1}{\varpi}\frac{\partial}{\partial \varpi}(\varpi^2 T) + \varpi^2 T \frac{\partial U}{\partial z} - \varpi^2 V \frac{\partial P}{\partial z} \right\} \mathbf{1}_z \\
&= E_\varpi \mathbf{1}_\varpi + E_\varphi \mathbf{1}_\varphi + E_z \mathbf{1}_z \qquad \text{(say)};
\end{aligned} \tag{20}$$

and, in terms of the components of $\boldsymbol{E}$,

$$\operatorname{curl} \boldsymbol{E} = -\frac{\partial E_\varphi}{\partial z}\mathbf{1}_\varpi + \left(\frac{\partial E_\varpi}{\partial z} - \frac{\partial E_z}{\partial \varpi} \right) \mathbf{1}_\varphi + \frac{1}{\varpi}\frac{\partial}{\partial \varpi}(\varpi E_\varphi)\, \mathbf{1}_z . \tag{21}$$

Equation (9) now gives

$$\begin{aligned}
\frac{\partial}{\partial t} \left\{ -\varpi \frac{\partial P}{\partial z}\mathbf{1}_\varpi + \varpi T \mathbf{1}_\varphi + \frac{1}{\varpi}\frac{\partial}{\partial \varpi}(\varpi^2 P)\, \mathbf{1}_z \right\} \\
= \frac{\partial E_\varphi}{\partial z}\mathbf{1}_\varpi - \left(\frac{\partial E_\varpi}{\partial z} - \frac{\partial E_z}{\partial \varpi} \right) \mathbf{1}_\varphi - \frac{1}{\varpi}\frac{\partial}{\partial \varpi}(\varpi E_\varphi)\, \mathbf{1}_z .
\end{aligned} \tag{22}$$

For the defining scalars P and T this equation implies

$$\frac{\partial P}{\partial t} = -\frac{E_\varphi}{\varpi} \tag{23}$$

and

$$\frac{\partial T}{\partial t} = -\frac{1}{\varpi}\left(\frac{\partial E_\varpi}{\partial z} - \frac{\partial E_z}{\partial \varpi} \right). \tag{24}$$

Now, substituting for the components of $\boldsymbol{E}$ in accordance with equation (20), we find, after some reductions, that

$$\frac{\partial P}{\partial t} = \Delta_5 P - \frac{1}{\varpi^3}\frac{\partial(\varpi^2 P, \varpi^2 U)}{\partial(z, \varpi)} \tag{25}$$

and

$$\frac{\partial T}{\partial t} = \Delta_5 T + \frac{1}{\varpi}\left\{ \frac{\partial(V, \varpi^2 P)}{\partial(z, \varpi)} - \frac{\partial(T, \varpi^2 U)}{\partial(z, \varpi)} \right\}. \tag{26}$$

Next, considering equation (14), we find that

$$\begin{aligned}\mathfrak{L} &= \operatorname{curl} \boldsymbol{h}\times\boldsymbol{h} - \operatorname{curl} \boldsymbol{v}\times\boldsymbol{v}\\ &= \Big\{ -\Delta_5 P\,\frac{\partial}{\partial\varpi}(\varpi^2 P) - T\,\frac{\partial}{\partial\varpi}(\varpi^2 T) + \Delta_5 U\,\frac{\partial}{\partial\varpi}(\varpi^2 U) + V\,\frac{\partial}{\partial\varpi}(\varpi^2 V)\Big\}\mathbf{1}_\varpi\\ &+ \Big\{ -\frac{\partial P}{\partial z}\,\frac{\partial}{\partial\varpi}(\varpi^2 T) + \frac{\partial T}{\partial z}\,\frac{\partial}{\partial\varpi}(\varpi^2 P) + \frac{\partial U}{\partial z}\,\frac{\partial}{\partial\varpi}(\varpi^2 V) - \frac{\partial V}{\partial z}\,\frac{\partial}{\partial\varpi}(\varpi^2 U)\Big\}\mathbf{1}_\varphi \qquad (27)\\ &+ \Big\{ -\varpi^2 T\,\frac{\partial T}{\partial z} - \varpi^2\,\frac{\partial P}{\partial z}\,\Delta_5 P + \varpi^2 V\,\frac{\partial V}{\partial z} + \varpi^2\,\frac{\partial U}{\partial z}\,\Delta_5 U\Big\}\mathbf{1}_z\\ &= \mathfrak{L}_\varpi\mathbf{1}_\varpi + \mathfrak{L}_\varphi\mathbf{1}_\varphi + \mathfrak{L}_z\mathbf{1}_z \qquad \text{(say)}.\end{aligned}$$

In terms of the components of $\mathfrak{L}$, equation (14) gives (cf. eqs. [18] and [21])

$$\frac{\partial}{\partial t}\Big\{ -\varpi\,\frac{\partial V}{\partial z}\,\mathbf{1}_\varpi - \varpi\Delta_5 U\,\mathbf{1}_\varphi + \frac{1}{\varpi}\,\frac{\partial}{\partial\varpi}(\varpi^2 V)\,\mathbf{1}_z\Big\} \qquad (28)$$

$$= -\frac{\partial\mathfrak{L}_\varphi}{\partial z}\,\mathbf{1}_\varpi + \Big(\frac{\partial\mathfrak{L}_\varpi}{\partial z} - \frac{\partial\mathfrak{L}_z}{\partial\varpi}\Big)\mathbf{1}_\varphi + \frac{1}{\varpi}\,\frac{\partial}{\partial\varpi}(\varpi\mathfrak{L}_\varphi)\,\mathbf{1}_z.$$

From this equation we conclude that

$$\frac{\partial V}{\partial t} = \frac{\mathfrak{L}_\varphi}{\varpi} \qquad (29)$$

and

$$-\Delta_5\,\frac{\partial U}{\partial t} = \frac{1}{\varpi}\Big(\frac{\partial\mathfrak{L}_\varpi}{\partial z} - \frac{\partial\mathfrak{L}_z}{\partial\varpi}\Big). \qquad (30)$$

Now, substituting for the components of $\mathfrak{L}$ in accordance with equation (27), we find, after some reductions, that

$$\varpi^3\,\frac{\partial V}{\partial t} = \frac{\partial(\varpi^2 T, \varpi^2 P)}{\partial(z,\varpi)} - \frac{\partial(\varpi^2 V, \varpi^2 U)}{\partial(z,\varpi)} \qquad (31)$$

and

$$\varpi\Delta_5\,\frac{\partial U}{\partial t} = \frac{\partial(\Delta_5 P, \varpi^2 P)}{\partial(z,\varpi)} - \frac{\partial(\Delta_5 U, \varpi^2 U)}{\partial(z,\varpi)} + \varpi\,\frac{\partial T^2}{\partial z} - \varpi\,\frac{\partial V^2}{\partial z}. \qquad (32)$$

Equations (25), (26), (31), and (32) are the basic equations of the present theory. We shall rewrite them in the following forms:

$$\varpi^3\Delta_5 P - \varpi^3\,\frac{\partial P}{\partial t} = \frac{\partial(\varpi^2 P, \varpi^2 U)}{\partial(z,\varpi)}, \qquad (33)$$

$$\varpi\Delta_5 T - \varpi\,\frac{\partial T}{\partial t} = \frac{\partial(T, \varpi^2 U)}{\partial(z,\varpi)} - \frac{\partial(V, \varpi^2 P)}{\partial(z,\varpi)}, \qquad (34)$$

$$\varpi^3\,\frac{\partial V}{\partial t} = \frac{\partial(\varpi^2 T, \varpi^2 P)}{\partial(z,\varpi)} - \frac{\partial(\varpi^2 V, \varpi^2 U)}{\partial(z,\varpi)}, \qquad (35)$$

and

$$\varpi\Delta_5\,\frac{\partial U}{\partial t} - \frac{\partial(\Delta_5 P, \varpi^2 P)}{\partial(z,\varpi)} + \frac{\partial(\Delta_5 U, \varpi^2 U)}{\partial(z,\varpi)} = \varpi\,\frac{\partial T^2}{\partial z} - \varpi\,\frac{\partial V^2}{\partial z}. \qquad (36)$$

4. SOME GENERAL RELATIONS AND CONSEQUENCES

Some general consequences which follow from equations (33)–(36) will now be discussed. Consider, first, equations (33) and (34), which govern the magnetic field. It is apparent from these equations that the poloidal field is unaffected by the presence of either toroidal magnetic fields or rotational motions. There is thus, in Elsasser's terminology, no "feedback" from the toroidal to the poloidal field. However, there is a feedback from the poloidal to the toroidal field through a coupling with the rotational motions. It should be particularly noted in this connection that this coupling between the poloidal magnetic field and the toroidal motions exists only in case of nonuniform rotation; for, if V is constant, the Jacobian involving V in equation (34) will vanish and there will be no coupling.

Thus equations (33) and (34) explicitly reveal what Elsasser (1955) has described as the "remarkable topological asymmetry" in the feedback mechanism between the poloidal and the toroidal fields.

Solutions of equations (33) and (34) in certain special cases are obtained in the paper following this one (Chandrasekhar 1956*c*); they disclose the extent to which internal motions can influence the free decay of a magnetic field in a fluid conductor. These latter considerations are relevant to the problem of the origin of the earth's magnetic field.

a) The Limiting Case of Infinite Electrical Conductivity

We shall now consider the form of the equations in case the electrical conductivity tends to infinity. In this limiting case the particular units (given in eq. [7]) which have been used in writing the equations governing $\boldsymbol{h}$ and $\boldsymbol{v}$ in nondimensional variables lose their meanings. Nevertheless, it is clear that, by introducing the variable $\boldsymbol{h}$ as defined in equation (6) and continuing to measure the various quantities in their conventional units, we can still reduce the equations to the forms (33)–(36), with the one difference that the terms in $\Delta_5 P$ and $\Delta_5 T$ in equations (33) and (34) will be absent. Thus the equations for P and T in this limiting case are

$$-\varpi^3 \frac{\partial P}{\partial t} = \frac{\partial (\varpi^2 P, \varpi^2 U)}{\partial (z, \varpi)} \tag{37}$$

and

$$-\varpi \frac{\partial T}{\partial t} = \frac{\partial (T, \varpi^2 U)}{\partial (z, \varpi)} - \frac{\partial (V, \varpi^2 P)}{\partial (z, \varpi)} . \tag{38}$$

Equations (35) and (36) will continue to be valid.

If, in the limiting case considered, the conditions are further stationary, the relevant equations are

$$\frac{\partial (\varpi^2 P, \varpi^2 U)}{\partial (z, \varpi)} = 0 , \tag{39}$$

$$\frac{\partial (T, \varpi^2 U)}{\partial (z, \varpi)} - \frac{\partial (V, \varpi^2 P)}{\partial (z, \varpi)} = 0 , \tag{40}$$

$$\frac{\partial (\varpi^2 T, \varpi^2 P)}{\partial (z, \varpi)} - \frac{\partial (\varpi^2 V, \varpi^2 U)}{\partial (z, \varpi)} = 0 , \tag{41}$$

and

$$-\frac{\partial (\Delta_5 P, \varpi^2 P)}{\partial (z, \varpi)} + \frac{\partial (\Delta_5 U, \varpi^2 U)}{\partial (z, \varpi)} = \varpi \frac{\partial T^2}{\partial z} - \varpi \frac{\partial V^2}{\partial z} . \tag{42}$$

One integral of these equations is obvious: equation (39) implies that

$$\varpi^2 P = \text{Function}\,(\varpi^2 U)\,. \tag{43}$$

b) The Law of Isorotation and Its Generalization

An interesting special case of equations (39)–(42) arises when

$$U = 0\,, \tag{44}$$

i.e., when there are no meridional currents. In this case equation (39) is clearly satisfied, and equations (40) and (41) would require that

$$V = \text{Function}\,(\varpi^2 P) \tag{45}$$

and

$$\varpi^2 T = \text{Function}\,(\varpi^2 P)\,. \tag{46}$$

Relation (45) is an expression of the law of isorotation of Ferraro (1937) and Alfvén (1943). Relation (46) was derived earlier by Chandrasekhar and Prendergast (1956) as one of the conditions for hydrostatic equilibrium of a magnetic star; but we now see that the relation is more general and requires for its validity only the absence of meridional motions.

It should be noted here that the law of isorotation would follow from equation (40) equally if, instead of setting $U = 0$, we set $T = 0$. However, in this latter case, equation (41) will require

$$\varpi^2 V = \text{Function}\,(\varpi^2 U) \qquad (T = 0)\,; \tag{47}$$

and the elimination of $\varpi^2 U$ between equations (43) and (47) will make $\varpi^2 V$ a function of $\varpi^2 P$, contradicting the law of isorotation. Consequently, *in the framework of equations (39)–(42) we cannot suppose that $T = 0$ unless $U = 0$.*

Returning to the case $U = 0$, we have yet to consider equation (42). When $U = 0$, this equation is

$$\frac{\partial\,(\Delta_5 P,\, \varpi^2 P)}{\partial\,(z,\, \varpi)} + \varpi\,\frac{\partial T^2}{\partial z} - \varpi\,\frac{\partial V^2}{\partial z} = 0\,. \tag{48}$$

The general solution of this equation can be found as follows:

In view of equations (45) and (46), we can define two functions $G(\varpi^2 P)$ and $g(\varpi^2 P)$ such that

$$2G\,(\varpi^2 P) = \frac{d}{d\,(\varpi^2 P)}\,\varpi^4 T^2 \tag{49}$$

and

$$2\,g\,(\varpi^2 P) = \frac{d}{d\,(\varpi^2 P)}\,V^2\,. \tag{50}$$

With these definitions, it can be readily verified that

$$\frac{\partial\,(G/\varpi^2,\, \varpi^2 P)}{\partial\,(z,\, \varpi)} = +\varpi\,\frac{\partial T^2}{\partial z} \tag{51}$$

and

$$\frac{\partial\,(\varpi^2 g,\, \varpi^2 P)}{\partial\,(z,\, \varpi)} = -\varpi\,\frac{\partial V^2}{\partial z}\,. \tag{52}$$

We can now combine equations (48), (51), and (52) to give

$$\frac{\partial\,(\Delta_5 P + G/\varpi^2 + \varpi^2 g,\ \varpi^2 P)}{\partial\,(z,\ \varpi)} = 0\,. \tag{53}$$

Hence

$$\Delta_5 P + \frac{1}{\varpi^2}\,G\,(\varpi^2 P) + \varpi^2 g\,(\varpi^2 P) = \Phi\,(\varpi^2 P)\,, \tag{54}$$

where Φ is an arbitrary function of the argument. Using equations (49) and (50), we can rewrite equation (54) in the form

$$\Delta_5 P = -T\,\frac{d}{d\,(\varpi^2 P)}\,(\varpi^2 T) - \varpi^2 V\,\frac{d\,V}{d\,(\varpi^2 P)} + \Phi\,(\varpi^2 P)\,, \tag{55}$$

which makes the dependence of P on T and V explicit.

It may be recalled here that in deriving equation (55) from equations (39)–(42) we have made only one assumption, namely, that $U = 0$. Equation (55) therefore represents the general integral of the equations in case $U = 0$.

Equation (55) includes as special cases the theorems on force-free fields (Lüst and Schlüter 1954; Chandrasekhar 1956*a*); Ferraro's (1954) condition for hydrostatic equilibrium in case $T = V = U = 0$; the law of isorotation; and, finally, the theorems of Chandrasekhar and Prendergast (1956). It therefore represents the complete generalization of these different theorems.

c) A Stationary Solution of Equations (35)–(38)

It is apparent from equations (39)–(42) that

$$P = U \text{ and } T = V \tag{56}$$

is a solution. It corresponds to a stationary solution of equations (35)–(38).

Equation (56) represents, under conditions of axisymmetry, the special solution

$$\boldsymbol{v} = \frac{\boldsymbol{H}}{\sqrt{(4\pi\rho)}} \text{ and } \frac{p}{\rho} + \tfrac{1}{2}\,|\,\boldsymbol{v}\,|^2 + \mathfrak{V} = \text{Constant} \tag{57}$$

of the general equations

$$\frac{\partial \boldsymbol{H}}{\partial t} = \operatorname{curl}\,(\boldsymbol{v} \times \boldsymbol{H}) \tag{58}$$

and

$$\frac{\partial \boldsymbol{v}}{\partial t} = \frac{1}{4\pi\rho}\operatorname{curl}\,\boldsymbol{H} \times \boldsymbol{H} - \operatorname{curl}\,\boldsymbol{v} \times \boldsymbol{v} - \operatorname{grad}\left(\frac{p}{\rho} + \tfrac{1}{2}\,|\,\boldsymbol{v}\,|^2 + \mathfrak{V}\right). \tag{59}$$

It has been shown (Chandrasekhar 1956*b*) that equation (57) represents a *stable* solution of equations (58) and (59). In case the fields and motions are axisymmetric, the periods of oscillation about the stationary solution (56) can be discussed by linearizing equations (35)–(38) in the neighborhood of this solution. The analysis reveals some novel aspects of hydromagnetic oscillations; they will be considered in a separate paper.

5. THE BOUNDARY CONDITIONS

For the sake of definiteness we shall suppose that the fluid is confined in a sphere of radius R. Let this radius R be the unit of length chosen in § 2. Boundary conditions are then required on the sphere $|\boldsymbol{r}| = 1$.

In spherical polar co-ordinates the expressions for $\boldsymbol{h}$ and $\boldsymbol{v}$ are

$$\boldsymbol{h} = -\frac{\partial}{\partial \mu}[(1-\mu^2)P]\,\mathbf{1}_r - \frac{(1-\mu^2)^{1/2}}{r}\frac{\partial}{\partial r}(r^2P)\,\mathbf{1}_\vartheta + r(1-\mu^2)^{1/2}T\mathbf{1}_\varphi \tag{60}$$

and

$$\boldsymbol{v} = -\frac{\partial}{\partial \mu}[(1-\mu^2)U]\,\mathbf{1}_r - \frac{(1-\mu^2)^{1/2}}{r}\frac{\partial}{\partial r}(r^2U)\,\mathbf{1}_\vartheta + r(1-\mu^2)^{1/2}V\mathbf{1}_\varphi, \tag{61}$$

where $\mathbf{1}_r$, $\mathbf{1}_\vartheta$, and $\mathbf{1}_\varphi$ are unit vectors along the arcs dr, $rd\vartheta$, and $r\sin\vartheta d\varphi$ in the three principal directions. The corresponding expression for the current $\boldsymbol{j}$ is

$$\begin{aligned} 4\pi\boldsymbol{j} &= \operatorname{curl}\boldsymbol{h} \\ &= -\frac{\partial}{\partial \mu}[(1-\mu^2)T]\,\mathbf{1}_r - \frac{(1-\mu^2)^{1/2}}{r}\frac{\partial}{\partial r}(r^2T)\,\mathbf{1}_\vartheta - r(1-\mu^2)^{1/2}\Delta_5 P\mathbf{1}_\varphi, \end{aligned} \tag{62}$$

where now

$$\Delta_5 = \frac{\partial^2}{\partial r^2} + \frac{4}{r}\frac{\partial}{\partial r} + \frac{1-\mu^2}{r^2}\frac{\partial^2}{\partial \mu^2} - \frac{4\mu}{r^2}\frac{\partial}{\partial \mu}. \tag{63}$$

The boundary conditions on the magnetic field are

$$\boldsymbol{h} \text{ and } \boldsymbol{j}\cdot\mathbf{1}_r \text{ are continuous on } r = 1\,. \tag{64}$$

If no current flows in the volume exterior to $r = 1$, the continuity of the normal component of $\boldsymbol{j}$ requires

$$\boldsymbol{j}\cdot\mathbf{1}_r = 0 \text{ for } r = 1 \qquad (\boldsymbol{j} \equiv 0 \text{ for } r > 1)\,. \tag{65}$$

According to equation (62), this latter condition implies that

$$T = 0 \text{ on } r = 1. \tag{66}$$

On the other hand, the continuity of $\boldsymbol{h}$ on $r = 1$ requires

$$P \text{ and } \frac{\partial P}{\partial r} \text{ to be continuous on } r = 1\,. \tag{67}$$

To apply the boundary conditions (67), we must know the equation governing P outside $r = 1$. On the same assumption as before regarding $\boldsymbol{j}$ (namely, $\boldsymbol{j} \equiv 0$ outside $r = 1$), the equation is

$$\Delta_5 P = 0\,. \tag{68}$$

The resulting conditions on P are explicitly derived in the paper following this one (Chandrasekhar 1956*c*, § 4).

It should be pointed out here that, in many astrophysical connections, the assumption that no current flows in the external regions is not justifiable on physical grounds. In these latter connections it appears more reasonable to suppose that the field outside is force-free (cf. Lüst and Schlüter 1954); if this assumption is made, it can be shown that (cf. Chandrasekhar 1956*a*)

$$P = T = 0 \text{ on } r = 1 \qquad \text{(force-free case)}\,. \tag{69}$$

As for the boundary conditions on $\boldsymbol{v}$, it is clear that we must in all cases require that its normal component vanish on the boundary. According to equation (61), this requires that

$$U = 0 \text{ on } r = 1 . \tag{70}$$

In the absence of viscosity there are no other conditions on $\boldsymbol{v}$.

6. INTEGRAL RELATIONS

Letting

$$[\phi, \psi] = \frac{\partial(\phi, \psi)}{\partial(z, \varpi)} = \frac{\partial\phi}{\partial z}\frac{\partial\psi}{\partial\varpi} - \frac{\partial\phi}{\partial\varpi}\frac{\partial\psi}{\partial z}, \tag{71}$$

we can rewrite equations (33)–(36) more compactly in the forms

$$\varpi^3\Delta_5 P - \varpi^3\frac{\partial P}{\partial t} = [\varpi^2 P, \varpi^2 U] , \tag{72}$$

$$\varpi\Delta_5 T - \varpi\frac{\partial T}{\partial t} = [T, \varpi^2 U] - [V, \varpi^2 P] , \tag{73}$$

$$\varpi^3\frac{\partial V}{\partial t} = [\varpi^2 T, \varpi^2 P] - [\varpi^2 V, \varpi^2 U] , \tag{74}$$

and

$$\varpi\Delta_5\frac{\partial U}{\partial t} = [\Delta_5 P, \varpi^2 P] - [\Delta_5 U, \varpi^2 U] + \varpi\frac{\partial T^2}{\partial z} - \varpi\frac{\partial V^2}{\partial z}. \tag{75}$$

Quite generally, we may supplement these equations by the boundary conditions (cf. eqs. [66], [67], and [70])

$$T = U = 0 \text{ on } r = 1 . \tag{76}$$

The following integral relations will now be derived from equations (72)–(76):

$$\iint\varpi^3\{(\Delta_5 P)^2 - T\Delta_5 T\}\, d\varpi\, dz = -\frac{1}{2}\frac{d}{dt}\iint\varpi^3(T^2 + V^2)\, d\varpi\, dz + \iint\varpi^3\left(U\Delta_5\frac{\partial U}{\partial t} + \frac{\partial P}{\partial t}\Delta_5 P\right) d\varpi\, dz , \tag{77}$$

$$\iint\varpi^3(U\Delta_5 T + V\Delta_5 P)\, d\varpi\, dz = \iint\varpi^3\left(U\frac{\partial T}{\partial t} + V\frac{\partial P}{\partial t}\right) d\varpi\, dz , \tag{78}$$

$$\iint\varpi^5 P\Delta_5 P\, d\varpi\, dz = \frac{1}{2}\frac{d}{dt}\iint\varpi^5 P^2\, d\varpi\, dz , \tag{79}$$

$$\iint\varpi^5 U\Delta_5 P\, d\varpi\, dz = \iint\varpi^5 U\frac{\partial P}{\partial t}\, d\varpi\, dz , \tag{80}$$

and

$$\iint\varpi^5 T\Delta_5 P\, d\varpi\, dz = \iint\varpi^5\left(T\frac{\partial P}{\partial t} + U\frac{\partial V}{\partial t}\right) d\varpi\, dz , \tag{81}$$

where the integrations are over the whole volume.

First, we state the following elementary lemma:

$$\int\int f\,[\phi,\psi]\,d\varpi dz = -\int\int \phi\,[f,\psi]\,d\varpi dz\,, \tag{82}$$

provided, at least, that one of the two functions, f or ϕ, vanishes on the boundary. This lemma is needed in the proofs of relations (77)–(81) given below.

Multiplying equation (73) by $\varpi^2 T$, integrating over the range of the variables, and successively transforming the integrals by making use of the lemma (eq. [82]) and using one or another of the remaining equations, we find

$$\begin{aligned}
&\int\int \varpi^3 T\Delta_5 T\,d\varpi dz - \frac{1}{2}\frac{d}{dt}\int\int \varpi^3 T^2 d\varpi dz \\
&= \int\int \varpi^2 T\,[T,\varpi^2 U]\,d\varpi dz - \int\int \varpi^2 T\,[V,\varpi^2 P]\,d\varpi dz \\
&= -\int\int \varpi^2 U\,[T,\varpi^2 T]\,d\varpi dz + \int\int V\,[\varpi^2 T,\varpi^2 P]\,d\varpi dz \\
&= -\int\int \varpi^3 U\frac{\partial T^2}{\partial z}\,d\varpi dz + \int\int V\left\{\varpi^3\frac{\partial V}{\partial t} + [\varpi^2 V,\varpi^2 U]\right\} d\varpi dz \\
&= -\int\int \varpi^3 U\frac{\partial T^2}{\partial z}\,d\varpi dz + \frac{1}{2}\frac{d}{dt}\int\int \varpi^3 V^2 d\varpi dz - \int\int \varpi^2 U\,[\varpi^2 V,\ V]\,d\varpi dz \\
&= -\int\int \varpi^3 U\left(\frac{\partial T^2}{\partial z} - \frac{\partial V^2}{\partial z}\right) d\varpi dz + \frac{1}{2}\frac{d}{dt}\int\int \varpi^3 V^2 d\varpi dz \\
&= -\int\int \varpi^2 U\left\{\varpi\Delta_5\frac{\partial U}{\partial t} - [\Delta_5 P,\varpi^2 P] + [\Delta_5 U,\varpi^2 U]\right\} d\varpi dz + \frac{1}{2}\frac{d}{dt}\int\int \varpi^3 V^2 d\varpi dz \\
&= -\int\int \varpi^3 U\Delta_5\frac{\partial U}{\partial t}\,d\varpi dz - \int\int \Delta_5 P\,[\varpi^2 U,\varpi^2 P]\,d\varpi dz + \frac{1}{2}\frac{d}{dt}\int\int \varpi^3 V^2 d\varpi dz \\
&= -\int\int \varpi^3 U\Delta_5\frac{\partial U}{\partial t}\,d\varpi dz + \int\int \varpi^3\Delta_5 P\left(\Delta_5 P - \frac{\partial P}{\partial t}\right) d\varpi dz + \frac{1}{2}\frac{d}{dt}\int\int \varpi^3 V^2 d\varpi dz\,.
\end{aligned} \tag{83}$$

Rearranging, we have equation (77).

Similarly, multiplying equation (73) by $\varpi^2 U$ and integrating, we obtain

$$\begin{aligned}
\int\int \varpi^3 U\Delta_5 T\,d\varpi dz - \int\int \varpi^3 U\frac{\partial T}{\partial t}\,d\varpi dz &= \int\int \varpi^2 U\{[T,\varpi^2 U] - [V,\varpi^2 P]\}\,d\varpi dz \\
&= \int\int V\,[\varpi^2 U,\varpi^2 P]\,d\varpi dz = -\int\int \varpi^3 V\left(\Delta_5 P - \frac{\partial P}{\partial t}\right) d\varpi dz\,.
\end{aligned} \tag{84}$$

This proves equation (78).

Next, multiplying equation (72) by $\varpi^2 P$ and integrating, we obtain

$$\int\int \varpi^5 P\Delta_5 P\,d\varpi dz - \frac{1}{2}\frac{d}{dt}\int\int \varpi^5 P^2 d\varpi dz = \int\int \varpi^2 P\,[\varpi^2 P,\varpi^2 U]\,d\varpi dz = 0\,, \tag{85}$$

which is equation (79). Equation (80) similarly follows from equation (72) after multi-

plication by $\varpi^2 U$ and integration. Finally, multiplying equation (72) by $\varpi^2 T$ and integrating, we obtain the last of the required relations; thus

$$\int\int \varpi^5 T \Delta_5 P \, d\varpi \, dz - \int\int \varpi^5 T \frac{\partial P}{\partial t} \, d\varpi \, dz$$

$$= \int\int \varpi^2 T \, [\varpi^2 P, \varpi^2 U] \, d\varpi \, dz = -\int\int \varpi^2 U \, [\varpi^2 P, \varpi^2 T] \, d\varpi \, dz \tag{86}$$

$$= \int\int \varpi^2 U \left\{ \varpi^3 \frac{\partial V}{\partial t} + [\varpi^2 V, \varpi^2 U] \right\} d\varpi \, dz = \int\int \varpi^5 U \frac{\partial V}{\partial t} \, d\varpi \, dz .$$

Applications of the integral relations derived in this section will be given in a later paper.

REFERENCES

Alfvén, H. 1943, *Ark., f. Mat. Astr. o. Fys.*, Vol. **29A**, No. 19.
Backus, G., and Chandrasekhar, S. 1956, *Proc. Nat. Acad. Sci.*, **42**, 105.
Bullard, E. C. 1955, *Proc. R. Soc. London, A*, **233**, 289.
Bullard, E. C., and Gellman, H. 1954, *Phil. Trans. R. Soc. London, A*, **247**, 213.
Chandrasekhar, S. 1956*a*, *Proc. Nat. Acad. Sci.*, **42**, 1.
———. 1956*b*, *ibid.*, **42**, 273.
———. 1956*c*, *Ap. J.*, **124**, 244.
Chandrasekhar, S., and Prendergast, K. 1956, *Proc. Nat. Acad. Sci.*, **42**, 5.
Cowling, T. G. 1934, *M.N.*, **94**, 39.
Elsasser, W. M. 1955, *Am. J. Phys.*, **23**, 590.
———. 1956, *ibid.*, **24**, 85.
Ferraro, V. C. A. 1937, *M.N.*, **97**, 458.
———. 1954, *Ap. J.*, **119**, 407.
Lüst, R., and Schlüter, A. 1954, *Zs. f. Ap.*, **34**, 263.

EFFECT OF INTERNAL MOTIONS ON THE DECAY OF A MAGNETIC FIELD IN A FLUID CONDUCTOR*

S. CHANDRASEKHAR
Enrico Fermi Institute, University of Chicago
Received March 27, 1956

ABSTRACT

The decay of a magnetic field in a fluid conductor with internal motions is considered in case the magnetic and velocity fields have symmetry about an axis. The underlying characteristic value problems are solved for certain simple velocity fields. The method of solution is based on a new classification of the basic axisymmetric modes of the magnetic field in terms of Gegenbauer polynomials. The principal conclusion of the paper is that velocity fields of reasonable patterns and magnitudes can alter the time of decay that will obtain in the absence of motions by quite large factors. The bearing of this result on the problem of the origin of the earth's magnetic field is briefly discussed. Certain other related questions are also considered.

1. INTRODUCTION

Current interest in the interaction between fluid motions and magnetic fields is in large measure due to the many astrophysical and geophysical phenomena which appear to be manifestations of this interaction. Indeed, the possibilities one might envisage by requiring a fluid to conform simultaneously to the laws of hydrodynamics and electrodynamics are so many that it might be profitable, in the first instance, to begin at the two ends. We might, for example, start from a well-understood hydrodynamic situation and see how the phenomenon is altered progressively as a magnetic field of increasing strength is impressed on the fluid. In recent years several such problems have been studied (cf. Chandrasekhar 1953); and in some cases the theoretical predictions have been confirmed by experiments (Lehnert 1952, 1955; Nakagawa 1955). Or we might start from a well-understood electrodynamic situation and see how the phenomenon is progressively altered as fluid motions of increasing strength are allowed to be present. It is somewhat surprising that no such problem has hitherto been analyzed. It is the object of this paper to consider one such problem. The problem we shall consider is the free decay of a magnetic field in a fluid conductor. If there are no internal motions, the equation governing the decay is

$$\nabla^2 \boldsymbol{H} = \frac{1}{4\pi\sigma} \frac{\partial \boldsymbol{H}}{\partial t}, \tag{1}$$

where σ denotes the electrical conductivity. The solution of this problem is well known: it is, in fact, one of the standard problems in electrodynamics (cf. Stratton 1941). We now ask: How is this decay affected if the fluid is in a state of internal motions? Apart from its theoretical interest, the problem appears to be relevant for discussions relating particularly to the origin of the earth's magnetic field. This context in which the problem first suggested itself is described in the next section.

2. THE PHYSICAL CONTEXT OF THE PROBLEM

The problem of the decay of a magnetic field in a fluid conductor is the first one to which one's attention is directed when one considers the origin of the earth's magnetic field. The reason is the following:

* The research reported in this paper has been supported in part by the Geophysics Research Directorate of the Air Force Cambridge Research Center, Air Research and Development Command, under Contract AF 19(604)-299 with the University of Chicago.

According to the solution of equation (1), the mode which decays most slowly is characterized by a mean life (cf. eq. [31]):

$$\tau = \frac{4\sigma R^2}{\pi}. \tag{2}$$

It has been estimated by Bullard and Gellman (1954) that the electrical conductivity of the earth's core is 3×10^{-6} e.m.u.; this value of σ, together with the known radius ($=3.5 \times 10^8$ cm) of the core, leads to a mean life

$$\tau \text{ (earth's core)} = 14000 \text{ years}. \tag{3}$$

On the other hand, paleomagnetic studies have established that, apart from secular variations, the earth has retained its magnetic field at approximately its present strength throughout most of its history (except, possibly, for brief periods during reversals; cf. Runcorn 1955*a*, *b*, in this connection). Consequently, there must be some mechanism which maintains the field and prevents its decay.

It was first suggested by Larmor (1919) as a possible explanation that the earth's magnetic field might be maintained by fluid motions in the core in the manner of a self-exciting dynamo. This suggestion received a serious setback when Cowling (1934; see also Backus and Chandrasekhar 1956) proved that steady dynamo action is impossible if the magnetic field and the fluid motions have axial symmetry. The possibility, nevertheless, of dynamo action has been explored, intensively, in recent years by Bullard and Gellman (1954), by Parker (1955), and by Elsasser (1955, 1956).

Bullard avoids a direct conflict with Cowling's theorem by considering velocity and magnetic fields which are azimuth-dependent. More particularly, Bullard and Gellman (1954) have sought to solve the electromagnetic equations numerically by using a particular velocity distribution and adjusting its magnitude to give a steady field. The method of solution is based on expansion in orthogonal functions; and, as Bullard (1955) has himself expressed, "it is difficult to establish the existence of solutions by numerical methods."

In contrast to Bullard, Parker and Elsasser have sought to avoid a conflict with Cowling's theorem by giving up, also, the idea of a strictly steady dynamo. They devise a sequence of interactions—nonuniform rotation generating a toroidal magnetic field from an initial poloidal field; a succession of rising "cyclones" creating, out of the toroidal field, loops of flux in the meridional planes, these loops coalescing and generating a poloidal field—and try to establish by semiquantitative arguments the inherent plausibility of the scheme by examining each element of the sequence separately.

The foregoing brief account of the current investigations on the dynamo problem discloses one surprising lacuna. The lacuna becomes apparent when we restate the underlying arguments as follows: One knows that in the absence of internal motions the earth's magnetic field will decay with a mean life of the order of 14000 years; "therefore," one seeks to devise fluid motions of a pattern and intensity which will prevent the decay altogether and maintain a steady state. In so arguing, one has not sought to clarify to one's self the extent to which given internal motions can retard (or accelerate) the free decay of a magnetic field in a fluid conductor. For example, one can ask: Can the time of decay of 14000 years, in the absence of internal motions, be prolonged to 500000 years (say) by velocity fields of reasonable magnitudes and patterns? If this were possible, the problem of the origin of the earth's magnetic field would take on a different complexion. For, the earth's magnetic field appears to reverse itself at intervals of the order of a quarter- to a half-million years by passing through an intermediate transitory phase of nearly zero random field (cf. Hospers 1954; Runcorn 1955*b*). One can therefore ask whether any particular meaning can be attached to constructing—if one can!—dynamos which will maintain themselves for periods longer than between reversals. In

all cases it is clear that the extent to which the decay of a magnetic field in a fluid conductor can be retarded or accelerated by internal motions of assigned patterns is an important theoretical question. It is to answering this question that this paper is principally devoted.

In concluding this section it may be simply stated that the problem considered in this paper is relevant in other astronomical connections, as, for example, the growth and decay of the magnetic fields of sunspots (cf. Cowling 1946); but in these other connections the physical problems are not as direct.

3. THE EQUATIONS OF THE PROBLEM

In considering the problem of the decay of a magnetic field in a fluid conductor with internal motions, we shall restrict ourselves to the case when the fluid is incompressible, the conductivity is constant, and the velocity and the magnetic fields have symmetry about an axis. The equations valid under these conditions have been derived in the preceding paper (Chandrasekhar 1956*b*; this paper will be referred to hereafter as "Paper I") They are (Paper I, eqs. [33] and [34]):

$$\Delta_5 P - \frac{\partial P}{\partial t} = \frac{1}{\varpi^3} \frac{\partial (\varpi^2 P, \varpi^2 U)}{\partial (z, \varpi)} \tag{4}$$

and

$$\Delta_5 T - \frac{\partial T}{\partial t} = \frac{1}{\varpi} \frac{\partial (T, \varpi^2 U)}{\partial (z, \varpi)} - \frac{1}{\varpi} \frac{\partial (V, \varpi^2 P)}{\partial (z, \varpi)}, \tag{5}$$

where it may be recalled that length, time, and velocity are measured in the units (Paper I, eq. [7]),

$$R\,(=3.47\times 10^{8}\ \text{cm}), \quad 4\pi\sigma R^2\,(=1.44\times 10^{5}\ \text{years}), \quad \text{and} \quad (4\pi\sigma R)^{-1}\,(=7.65\times 10^{-5}\ \text{cm/sec}), \tag{6}$$

respectively. (The values given in parentheses are those which are appropriate for the earth's core.) In equations (4) and (5) P and T are the scalars defining the poloidal and toroidal parts of the magnetic field, and U and V are the scalars defining the meridional and rotational motions. Thus (Paper I, eqs. [15] and [16])

$$\boldsymbol{h} = -\varpi \frac{\partial P}{\partial z} \mathbf{1}_\varpi + \varpi T \mathbf{1}_\varphi + \frac{1}{\varpi} \frac{\partial}{\partial \varpi} (\varpi^2 P)\, \mathbf{1}_z \tag{7}$$

and

$$\boldsymbol{v} = -\varpi \frac{\partial U}{\partial z} \mathbf{1}_\varpi + \varpi V \mathbf{1}_\varphi + \frac{1}{\varpi} \frac{\partial}{\partial \varpi} (\varpi^2 U)\, \mathbf{1}_z, \tag{8}$$

where $\boldsymbol{h} = \boldsymbol{H}/(4\pi\rho)^{1/2}$ is a quantity of the dimensions of a velocity.

In considering equations (4) and (5), we shall regard the velocity scalars U and V as given and seek solutions for the scalars P and T characterizing the magnetic field.

It will be observed that there is a fundamental difference in the equations governing the poloidal and toroidal fields: The decay of the poloidal field is unaffected by the presence of toroidal fields or rotational motions; it is affected only by the presence of meridional motions. On the other hand, the decay of the toroidal field is affected by the presence of a poloidal field, provided there is nonuniform rotation.

Considering, first, the equation satisfied by P, we can separate the time dependence by writing

$$P(z, \varpi)\, e^{-\lambda^2 t} \quad \text{in place of} \quad P(z, \varpi, t) \tag{9}$$

and obtain

$$\Delta_5 P + \lambda^2 P = \frac{1}{\varpi^3} \frac{\partial (\varpi^2 P, \varpi^2 U)}{\partial (z, \varpi)} . \tag{10}$$

This equation is valid only for $r \leq 1$. For $r > 1$, the equation governing P is

$$\Delta_5 P = 0 . \tag{11}$$

For a specified velocity field, U, we must seek solutions of equations (10) and (11) which have no singularity at the origin, vanish at infinity, and are such that

$$P \text{ and } \frac{\partial P}{\partial r} \quad \text{are continuous on} \quad r = 1 . \tag{12}$$

These boundary conditions clearly define a characteristic value problem for λ^2; and in the context of the physical problem discussed in § 2, greatest interest is attached to the dependence of the lowest characteristic value for λ^2 on the sign and amplitude of the specified velocity field.

Considering, next, the equation for T, we can express the general solution as a superposition of a solution of the homogeneous equation

$$\Delta_5 T - \frac{\partial T}{\partial t} = \frac{1}{\varpi} \frac{\partial (T, \varpi^2 U)}{\partial (z, \varpi)} , \tag{13}$$

together with a particular solution of the nonhomogeneous equation (5). Equation (13), like equation (10), can be solved by considering exponentially decaying solutions. Thus, writing

$$T (z, \varpi)\ e^{-\lambda^2 t} \quad \text{in place of} \quad T (z, \varpi, t) , \tag{14}$$

we obtain

$$\Delta_5 T + \lambda^2 T = \frac{1}{\varpi} \frac{\partial (T, \varpi^2 U)}{\partial (z, \varpi)} . \tag{15}$$

The boundary conditions with respect to which this equation must be solved are

$$T = 0 \quad \text{on} \quad r = 1 \quad \text{and nonsingular at} \quad r = 0 . \tag{16}$$

This is again a characteristic value problem for λ^2; and its solution will determine the "free decay" of a toroidal field in the absence of nonuniform rotation or poloidal fields. If a poloidal field should be present and the rotation is nonuniform, then there will be an additional "induced" term (proportional to P) in the time variation of T. In particular, if the poloidal field which is present is one of the fundamental modes determined by the characteristic value problem for P, we can find a particular solution for T which will decay exponentially with the same mean life as the inducing field. Thus the decay of a toroidal field will, in general, consist of two terms: a free decay and an induced decay. In this paper we shall not consider this latter term: we shall, in effect, suppose that V is constant.

4. THE SOLUTION OF THE DECAY PROBLEM IN THE ABSENCE OF MOTIONS

The fundamental modes of decay of a magnetic field in a spherical conductor have been the subject of extensive investigations and go back to Horace Lamb (1881). Their classification in terms of the solutions of the vector-wave equation are well known through Elsasser's (1946*a*, *b*, and 1947) systematization. Nevertheless, the particular classification of the axisymmetric modes which we shall need appears to be novel in this connection. We shall therefore begin with a description of this classification.

a) The Poloidal Modes

In the absence of motions the equations governing the poloidal scalar, P, are (cf. eqs. [10] and [11])

$$\Delta_5 P = -\alpha^2 P \qquad (r \leqslant 1) \quad (17)$$

and

$$\Delta_5 P = 0 \qquad (r > 1)\,, \quad (18)$$

where, for later convenience, we have used α^2 in place of λ^2.

In spherical polar co-ordinates the axisymmetric five-dimensional Laplacian, Δ_5, is

$$\Delta_5 = \frac{\partial^2}{\partial r^2} + \frac{4}{r}\frac{\partial}{\partial r} + \frac{1-\mu^2}{r^2}\frac{\partial^2}{\partial \mu^2} - \frac{4\mu}{r^2}\frac{\partial}{\partial \mu}. \quad (19)$$

The fundamental solutions of equation (17) which are free of singularity at the origin are (cf. Chandrasekhar 1956*a*, eq. [17])

$$P_n = \frac{J_{n+3/2}(\alpha r)}{r^{3/2}} C_n^{3/2}(\mu) \qquad (r \leqslant 1)\,, \quad (20)$$

where $C_n^{3/2}(\mu)$ is the Gegenbauer polynomial[1] and $J_{n+3/2}$ is the Bessel function of order $(n+\frac{3}{2})$. The corresponding solution of equation (18) is

$$P_n = \frac{A}{r^{n+3}} C_n^{3/2}(\mu) \qquad (r > 1)\,, \quad (21)$$

where A is a constant to be determined.

The boundary conditions at $r = 1$ (eq. [12]) require

$$J_{n+3/2}(\alpha) = A \qquad \text{(continuity of } P \text{ at } r = 1) \quad (22)$$

and

$$\left\{\frac{d}{dr}\left[r^{1/2} J_{n+3/2}(\alpha r)\right]\right\}_{r=1} = \left[\frac{d}{dr}\left(\frac{A}{r^{n+1}}\right)\right]_{r=1} \quad (23)$$

$$\left(\text{continuity of } \frac{d}{dr}(r^2 P) \text{ at } r = 1\right).$$

On simplifying equation (23) and eliminating A by means of equation (22), we find

$$\tfrac{1}{2} J_{n+3/2}(\alpha) + \alpha J'_{n+3/2}(\alpha) = -(n+1) A = -(n+1) J_{n+3/2}(\alpha) \quad (24)$$

or

$$\alpha J'_{n+3/2}(\alpha) + (n+\tfrac{3}{2}) J_{n+3/2}(\alpha) = 0\,. \quad (25)$$

But the quantity on the left-hand side of this last equation is $J_{n+1/2}(\alpha)$. Hence the equation for determining α is

$$J_{n+1/2}(\alpha) = 0\,. \quad (26)$$

The characteristic values of α are, therefore, the roots of $J_{n+1/2}(x)$.

To distinguish the different zeros of the Bessel functions of different orders, we shall let

$$\alpha_{j,\,m} \text{ denote the } j\text{th zero of } J_{m+3/2}(x)\,. \quad (27)$$

This notation will be used consistently in this paper.

[1] The notation is that of Watson (1944).

The fundamental solutions representing the various poloidal modes are, therefore,

$$P_{n,j} = \frac{J_{n+3/2}(\alpha_{j,n-1}r)}{r^{3/2}} C_n^{3/2}(\mu) . \tag{28}$$

We shall call this the (n, j) *poloidal mode*. In particular, the solution describing the zero-order modes is

$$P_{0,j} = \frac{J_{3/2}(\alpha_{j,-1}r)}{r^{3/2}}, \tag{29}$$

where $\alpha_{j,-1}$, being the jth zero of $J_{1/2}(x)$ (which is proportional to $\sin x/\sqrt{x}$), is given by

$$\alpha_{j,-1} = j\pi \qquad (j = 1, 2, \ldots) . \tag{30}$$

The corresponding decay times are (cf. eqs. [6] and [9])

$$\tau_j = \frac{4\pi\sigma R^2}{\alpha_{j,-1}^2} = \frac{4\sigma R^2}{j^2\pi} \qquad (j = 1, 2, \ldots) . \tag{31}$$

The functions $P_{n,j}$ provide a complete set of orthogonal functions in the unit sphere in five dimensions. The orthogonality relations are

$$\int_{-1}^{+1} C_n^{3/2}(\mu) C_m^{3/2}(\mu) (1-\mu^2)\, d\mu = \frac{2(n+1)(n+2)}{2n+3} \delta_{mn} \tag{32}$$

and

$$\int_0^1 r J_{n+3/2}(\alpha_{j,n-1}r) J_{n+3/2}(\alpha_{k,n-1}r)\, dr = \tfrac{1}{2} [J_{n+3/2}(\alpha_{j,n-1})]^2 \delta_{jk} . \tag{33}$$

b) The Toroidal Modes

In the absence of motions, the toroidal modes of decay are given by the solutions of the equation

$$\Delta_5 T = -\alpha^2 T , \tag{34}$$

which are finite at the origin and which satisfy the boundary condition

$$T = 0 \qquad \text{on} \qquad r = 1 . \tag{35}$$

Accordingly, the fundamental solutions describing the various toroidal modes are

$$T_{n,j} = \frac{J_{n+3/2}(\alpha_{j,n}r)}{r^{3/2}} C_n^{3/2}(\mu) . \tag{36}$$

We shall call this the (n, j) *toroidal mode*. In particular, the solution describing the zero-order modes is

$$T_{0,j} = \frac{J_{3/2}(\alpha_{j,0}r)}{r^{3/2}}, \tag{37}$$

where $\alpha_{j,0}$ is the jth zero of $J_{3/2}(x)$. For later reference we may note here that

$$\alpha_{1,0}^2 = 20.19 . \tag{38}$$

The lowest toroidal mode, therefore, decays with a mean life which is about half that of the lowest poloidal mode.

The functions $T_{n,j}$, like the functions $P_{n,j}$, form a complete set of orthogonal functions in the unit sphere in five dimensions. The orthogonality relation (33) is now replaced by

$$\int_0^1 r J_{n+3/2}(a_{j,n} r)\, J_{n+3/2}(a_{k,n} r)\, dr = \tfrac{1}{2}\,[J'_{n+3/2}(a_{j,n})]^2 \delta_{jk}\,. \tag{39}$$

c) Some Useful Formulae

We have seen that the fundamental solutions for the poloidal and toroidal modes are expressed in terms of the Gegenbauer polynomials. We shall find, when working with them, the need for the various recurrence relations which these polynomials satisfy. Accordingly, we shall list here, for later reference, the most important of these relations:

$$\mu C_n^{3/2} = \frac{1}{2n+3}\,[(n+1)\,C_{n+1}^{3/2} + (n+2)\,C_{n-1}^{3/2}]\,, \tag{40}$$

$$(1-\mu^2)\,\frac{dC_n^{3/2}}{d\mu} = \frac{1}{2n+3}\,[-n(n+1)\,C_{n+1}^{3/2} + (n+2)(n+3)\,C_{n-1}^{3/2}]\,, \tag{41}$$

$$\begin{aligned}\mu^2 C_n^{3/2} &= \frac{(n+1)(n+2)}{(2n+3)(2n+5)}\,C_{n+2}^{3/2} \\ &+\left[\frac{(n+1)(n+3)}{(2n+3)(2n+5)} + \frac{n(n+2)}{(2n+3)(2n+1)}\right] C_n^{3/2} + \frac{(n+1)(n+2)}{(2n+3)(2n+1)}\,C_{n-2}^{3/2}\,,\end{aligned} \tag{42}$$

$$\begin{aligned}\mu(1-\mu^2)\,\frac{dC_n^{3/2}}{d\mu} &= -\frac{n(n+1)(n+2)}{(2n+3)(2n+5)}\,C_{n+2}^{3/2} + \frac{3n(n+3)}{(2n+5)(2n+1)}\,C_n^{3/2} \\ &+ \frac{(n+1)(n+2)(n+3)}{(2n+3)(2n+1)}\,C_{n-2}^{3/2}\,,\end{aligned} \tag{43}$$

$$\begin{aligned}\mu\,\frac{d}{d\mu}(1-\mu^2)\,C_n^{3/2} &= -\frac{(n+2)^2(n+1)}{(2n+3)(2n+5)}\,C_{n+2}^{3/2} - \frac{(n+2)(n+1)}{(2n+5)(2n+1)}\,C_n^{3/2} \\ &+ \frac{(n+1)^2(n+2)}{(2n+3)(2n+1)}\,C_{n-2}^{3/2}\,.\end{aligned} \tag{44}$$

5. THE INFLUENCE OF FLUID MOTIONS ON THE DIFFERENT MODES OF THE MAGNETIC FIELD

To make the characteristic value problems formulated in § 3 definite, we must specify the velocity field. For this reason it is important that we have some initial idea as to the patterns of fluid motion to which the various modes of the magnetic field are most sensitive. In this section we shall try to obtain this preliminary information by considering the rate of change of an integral property of the field (such as its energy) in the presence of prescribed motions.

a) The Toroidal Modes

In the absence of nonuniform rotation, the equation satisfied by the toroidal scalar is (eq. [5])

$$\Delta_5 T - \frac{\partial T}{\partial t} = \frac{1}{\varpi}\,[T, \varpi^2 U]\,, \tag{45}$$

where, for the sake of brevity, we have introduced the notation (cf. Paper I, eq. [71])

$$[\phi, \psi] = \frac{\partial(\phi, \psi)}{\partial(z, \varpi)}. \tag{46}$$

Multiplying equation (45) by $\varpi^3 T$ and integrating over the range of the variables, we have

$$\int\int \varpi^3 T \Delta_5 T \, d\varpi \, dz - \frac{1}{2}\frac{d}{dt}\int\int \varpi^3 T^2 \, d\varpi \, dz = \int\int \varpi^2 T \, [T, \varpi^2 U] \, d\varpi \, dz. \tag{47}$$

Transforming the integral on the right-hand side of this equation by first using the lemma of Paper I, § 6 (eq. [82]), and then integrating by parts, we obtain

$$\begin{aligned} \int\int \varpi^2 T \, [T, \varpi^2 U] \, d\varpi \, dz &= -\int\int \varpi^2 U \, [T, \varpi^2 T] \, d\varpi \, dz \\ &= -\int\int \varpi^3 U \frac{\partial T^2}{\partial z} \, d\varpi \, dz \\ &= +\int\int \varpi^3 T^2 \frac{\partial U}{\partial z} \, d\varpi \, dz. \end{aligned} \tag{48}$$

Using this last result in equation (47), we have

$$-\frac{d\mathfrak{T}}{dt} = \int\int \varpi^3 \left(-T\Delta_5 T + T^2 \frac{\partial U}{\partial z} \right) d\varpi \, dz, \tag{49}$$

where

$$\mathfrak{T} = \tfrac{1}{2}\int\int \varpi^3 T^2 \, d\varpi \, dz, \tag{50}$$

is a measure of the energy in the field.

Since U must vanish on the boundary (cf. Paper I, eq. [70]), it is clear that the normal modes of the meridional motions are described by the same functions as the toroidal modes of the magnetic field.

We shall suppose, then, that

$$U = \beta T_{m,k}, \tag{51}$$

where β is a constant, and, further, that

$$T = T_{n,j} \quad \text{at} \quad t = 0. \tag{52}$$

For T and U thus prescribed, equation (49) gives

$$-\frac{d}{dt}\mathfrak{T}(n, j; m, k) = \int\int \varpi^3 T_{n,j}^2 \left(\alpha_{j,n}^2 + \beta \frac{\partial T_{m,k}}{\partial z} \right) d\varpi \, dz, \tag{53}$$

since

$$\Delta_5 T_{n,j} = -\alpha_{j,n}^2 T_{n,j}. \tag{54}$$

By using the orthogonality relations (32) and (39) we can rewrite equation (53) in the form

$$-\frac{d}{dt}\mathfrak{T}(n, j; m, k) = \frac{(n+1)(n+2)}{2n+3}[J'_{n+3/2}(\alpha_{j,n})]^2 \alpha_{j,n}^2 + \beta I(n, j; m, k; T), \tag{55}$$

where

$$I(n, j; m, k; T) = \int\int \varpi^3 T_{n,j}^2 \frac{\partial T_{m,k}}{\partial z} \, d\varpi \, dz \tag{56}$$

is the matrix element which characterizes the interaction between the (n, j) toroidal mode and the (m, k) velocity mode.

In spherical polar co-ordinates, equation (56) takes the form

$$I(n, j; m, k; T) = \int_0^1 \int_{-1}^{+1} r^4 (1-\mu^2) T_{n,j}^2 \left(\mu \frac{\partial}{\partial r} + \frac{1-\mu^2}{r} \frac{\partial}{\partial \mu}\right) T_{m,k} \, dr \, d\mu . \quad (57)$$

Substituting for $T_{m,k}$ in accordance with equation (36) and making use of the recurrence relations (40) and (41), we find

$$I(n, j; m, k; T) = \frac{1}{2m+3} \int_0^1 \int_{-1}^{+1} dr \, d\mu \, r^4 (1-\mu^2) T_{n,j}^2$$
$$\times \left\{ \frac{d}{dr} \left[\frac{J_{m+3/2}(\alpha_{k,m} r)}{r^{3/2}} \right] [(m+1) C_{m+1}^{3/2} + (m+2) C_{m-1}^{3/2}] \right. \quad (58)$$
$$\left. + \frac{J_{m+3/2}(\alpha_{k,m} r)}{r^{5/2}} [-m(m+1) C_{m+1}^{3/2} + (m+2)(m+3) C_{m-1}^{3/2}] \right\} .$$

From equation (58) certain selection rules can be derived from which one can infer the different velocity modes which will interact with a given toroidal mode of the magnetic field and give rise to a nonvanishing matrix element, $I(n, j; m, k; T)$. In this paper we shall, however, restrict ourselves to the case

$$n = 0 \qquad \text{when} \qquad T = T_{0,j} = \frac{J_{3/2}(\alpha_{j,0} r)}{r^{3/2}} . \quad (59)$$

The general case has, meantime, been treated by Siciy Pao (1956).

Since $T_{0,j}^2$ is angle-independent, it is apparent from equation (58) that only the velocity modes $(1, k)$ can arrest (or accelerate) the initial decay of the magnetic energy in the $(0, j)$ toroidal mode. Thus

$$I(0, j; m, k; T) = 0 \qquad \text{for } m \neq 1 , \quad (60)$$

and, when $m = 1$,

$$I(0, j; 1, k; T)$$
$$= \frac{4}{5} \int_0^1 r^4 \left[\frac{J_{3/2}(\alpha_{j,0} r)}{r^{3/2}} \right]^2 \left\{ \frac{d}{dr} \left[\frac{J_{5/2}(\alpha_{k,1} r)}{r^{3/2}} \right] + 4 \frac{J_{5/2}(\alpha_{k,1} r)}{r^{3/2}} \right\} dr . \quad (61)$$

By making use of the recurrence relations satisfied by the Bessel functions, we can reduce the integral on the right-hand side to give

$$I(0, j; 1, k; T) = \tfrac{4}{5} \alpha_{k,1} \int_0^1 [J_{3/2}(\alpha_{j,0} r)]^2 J_{3/2}(\alpha_{k,1} r) \frac{dr}{\sqrt{r}} . \quad (62)$$

With $I(0, j; 1, k; T)$ given by equation (62), we have (cf. eq. [55])

$$-\frac{d}{dt} \mathfrak{T}(0, j; 1, k) = \tfrac{2}{3} [J'_{3/2}(\alpha_{j,0})]^2 \alpha_{j,0}^2 + \beta I(0, j; 1, k; T) . \quad (63)$$

We shall return to this equation in § 5, *c*, after we have derived a similar formula for the poloidal modes.

b) The Poloidal Modes

The equation satisfied by the poloidal scalar is (eq. [4])

$$\Delta_5 P - \frac{\partial P}{\partial t} = \frac{1}{\varpi^3}[\varpi^2 P, \varpi^2 U] \ . \tag{64}$$

Multiplying this equation by $\varpi^3 P$ and integrating over the range of the variables, we obtain, as in § 5, *a* (cf. eq. [49]),

$$-\frac{d\mathfrak{P}}{dt} = \int\int \varpi^3 \left(-P\Delta_5 P - P^2 \frac{\partial U}{\partial z} \right) d\varpi dz \ , \tag{65}$$

where

$$\mathfrak{P} = \tfrac{1}{2}\int\int \varpi^3 P^2 d\varpi dz \ . \tag{66}$$

We shall suppose that

$$P = P_{n,j} \qquad \text{at } t = 0 \tag{67}$$

and that the velocity field is the same as that considered in § 5, *a*, equation (51). Then equation (65) gives

$$-\frac{d}{dt}\mathfrak{P}(n,\ j;\ m,\ k) = \int\int \varpi^3 P_{n,j}^2 \left(\alpha_{j,n-1}^2 - \beta \frac{\partial T_{m,k}}{\partial z} \right) d\varpi dz \ ; \tag{68}$$

and, by using the orthogonality relation (33), we obtain

$$-\frac{d}{dt}\mathfrak{P}(n,\ j;\ m,\ k) = \frac{(n+1)\ (n+2)}{2n+3}\left[J_{n+3/2}(\alpha_{j,n-1}) \right]^2 \alpha_{j,n-1}^2 - \beta I\ (n,\ j;\ m,\ k;\ P) \ , \tag{69}$$

where

$$I\ (n,\ j;\ m,\ k;\ P) = \int\int \varpi^3 P_{n,j}^2 \frac{\partial T_{m,k}}{\partial z}\, d\varpi dz \ . \tag{70}$$

For the case $n = 0$, we find, as in § 5, *a*, that the matrix element

$$I\ (0,\ j;\ m,\ k;\ P) = 0 \qquad \text{if } m \neq 1 \tag{71}$$

and that, when $m = 1$ (cf. eq. [62]),

$$I\ (0,\ j;\ 1,\ k;\ P) = \tfrac{4}{5}\alpha_{k,1}\int_0^1 \left[J_{3/2}(\alpha_{j,-1}r) \right]^2 J_{3/2}(\alpha_{k,1}r)\frac{dr}{\sqrt{r}} \ . \tag{72}$$

With $I(0, j;\ 1,\ k;\ P)$ given by equation (72), we have (cf. eq. [69])

$$-\frac{d}{dt}\mathfrak{P}(0,\ j;\ 1,\ k) = \tfrac{2}{3}\left[J_{3/2}(\alpha_{j,-1}) \right]^2 \alpha_{j,-1}^2 - \beta I\ (0,\ j;\ 1,\ k;\ P) \ , \tag{73}$$

which is the present analogue of equation (63).

c) Numerical Results

The matrix elements $I(0, j;\ 1,\ k;\ T)$ and $I(0, j;\ 1,\ k;\ P)$ have been evaluated numerically for the cases $j = 1$ and $k = 1$, 2, and 3. The resulting numerical forms of equations (63) and (73) are

$$-\frac{d}{dt}\mathfrak{T}\ (0,\ 1;\ 1,\ k) = \begin{cases} 1.817 + 0.29660\beta & (k=1) \ , \\ 1.817 + 0.05413\beta & (k=2) \ , \\ 1.817 - 0.00746\beta & (k=3) \ , \end{cases} \tag{74}$$

and

$$-\frac{d}{dt}\mathfrak{P}(0,1;1,k)=\begin{cases}\frac{4}{3}-0.14112\beta & (k=1),\\ \frac{4}{3}+0.03446\beta & (k=2),\\ \frac{4}{3}-0.01982\beta & (k=3).\end{cases} \tag{75}$$

Remembering that the unit of velocity appropriate for the earth's core is 7.6×10^{-5} cm/sec and that velocities of the order of 10^{-2} cm/sec are believed to exist, we can conclude from equations (74) and (75) that the prevalence of motions of the order contemplated will profoundly alter the rate of decay of the earth's magnetic field such as will obtain in the total absence of motions.

Two further points which are worth noting are, first, that we can retard or accelerate the initial rate of decay by simply changing the sign of β (i.e., the sense of the meridional circulation) and, second, that the lowest velocity mode (1, 1), which interacts with both the (0, 1) poloidal and the (0, 1) toroidal modes, affects them in *opposite* ways—a fact which should be kept in mind if we should wish to select a velocity field which will retard the decay of both the poloidal and the toroidal fields.

6. THE EFFECT OF THE VELOCITY MODE $(1, i)$ ON THE DECAY OF TOROIDAL MAGNETIC FIELDS

We now return to the principal problem of the paper, namely, that of determining the effect of internal motions on the decay of a magnetic field.

In this section we shall consider the effect of meridional currents on the decay of toroidal magnetic fields. As we have seen in § 3, this leads us directly to the following characteristic value problem: To determine λ^2 so that the equation

$$\Delta_5 T+\lambda^2 T=\frac{1}{\varpi}\frac{\partial(T,\varpi^2U)}{\partial(z,\varpi)} \tag{76}$$

allows solutions which are free of singularity at the origin and which vanish on the unit sphere.

In spherical polar co-ordinates, equation (76) has the form

$$\Delta_5 T+\lambda^2 T=-\frac{\partial T}{\partial r}\left[\frac{\partial}{\partial\mu}(1-\mu^2)\,U\right]+\frac{1}{r^2}\frac{\partial}{\partial r}(r^2U)\left[(1-\mu^2)\frac{\partial T}{\partial\mu}\right], \tag{77}$$

where Δ_5 is now given by equation (19).

Now, to make the characteristic value problem definite, we must specify a velocity field. Since the preliminary discussion in § 5 has shown that the lowest toroidal mode, (0, 1), is sensitive mostly to the presence of the velocity modes $(1, i)$, we shall suppose that this is the pattern of the velocity field which is present. In other words, we shall assume that

$$U=\beta\frac{J_{5/2}(\alpha_{i,1}r)}{r^{3/2}}\mu=\beta U_1(r)\,\mu \qquad \text{(say)}, \tag{78}$$

where β is a constant. For this chosen form of U, equation (77) becomes

$$\Delta_5 T+\lambda^2 T=\beta\left[(3\mu^2-1)\,U_1\frac{\partial T}{\partial r}+\mu(1-\mu^2)\frac{\partial T}{\partial\mu}\frac{1}{r^2}\frac{d}{dr}(r^2U_1)\right]; \tag{79}$$

and in the solution of this equation we shall mostly be interested in the dependence of the lowest characteristic value of λ^2 on β.

The method of solution we shall adopt consists in expanding T in terms of the basic

toroidal functions $T_{n,j}$. It is, however, convenient to carry out this expansion in two steps: First, we expand T in the Gegenbauer polynomials $C_n^{3/2}(\mu)$ in the manner

$$T = \sum_{n=0}^{\infty} T_n(r)\, C_n^{3/2}(\mu)\,, \tag{80}$$

and then expand the radial functions, $T_n(r)$, in terms of $J_{n+3/2}(\alpha_{j,n} r)$.

For T given by equation (80),

$$\Delta_5 T = \sum_{n=0}^{\infty} \mathfrak{D}_n T_n C_n^{3/2}(\mu)\,, \tag{81}$$

where

$$\mathfrak{D}_n = \frac{d^2}{dr^2} + \frac{4}{r}\frac{d}{dr} - \frac{n(n+3)}{r^2}\,. \tag{82}$$

Substituting the expansions (80) and (81) in equation (79), we get

$$\begin{aligned}\sum_{n=0}^{\infty} \mathfrak{D}_n T_n C_n^{3/2} + \lambda^2 \sum_{n=0}^{\infty} T_n C_n^{2/2} \\ = \beta\Big[U_1 \sum_{n=0}^{\infty} \frac{dT_n}{dr}(3\mu^2 - 1) C_n^{3/2} + \frac{1}{r^2}\frac{d}{dr}(r^2 U_1) \sum_{n=0}^{\infty} T_n \mu (1-\mu^2) \frac{dC_n^{3/2}}{d\mu}\Big]\,.\end{aligned} \tag{83}$$

Using the recurrence relations (42) and (43) and equating the terms in the different orders of the Gegenbauer polynomials (which we can, in view of their orthogonality), we find

$$\begin{aligned}\mathfrak{D}_n T_n + \lambda^2 T_n \\ = \beta\Big\{ &\frac{n(n-1)}{(2n-1)(2n+1)}\Big[3U_1 \frac{dT_{n-2}}{dr} - (n-2) T_{n-2} \frac{1}{r^2}\frac{d}{dr}(r^2 U_1)\Big] \\ &+ \frac{(n+3)(n+4)}{(2n+3)(2n+7)}\Big[3U_1 \frac{dT_{n+2}}{dr} + (n+5) T_{n+2} \frac{1}{r^2}\frac{d}{dr}(r^2 U_1)\Big] \\ &+ \Big[\frac{3(n+1)(n+3)}{(2n+3)(2n+5)} + \frac{3n(n+2)}{(2n+3)(2n+1)} - 1\Big] U_1 \frac{dT_n}{dr} \\ &+ \frac{3n(n+3)}{(2n+1)(2n+5)} T_n \frac{1}{r^2}\frac{d}{dr}(r^2 U_1)\Big\}\,.\end{aligned} \tag{84}$$

We now expand $T_n(r)$ in terms of $J_{n+3/2}(\alpha_{j,n} r)$ in the manner

$$T_n(r) = \sum_{j=1}^{\infty} A_{n,j} \frac{J_{n+3/2}(\alpha_{j,n} r)}{r^{3/2}}\,, \tag{85}$$

where $A_{n,j}$ are constants. For T_n given by equation (85),

$$\mathfrak{D}_n T_n = -\sum_{j=1}^{\infty} \alpha_{j,n}^2 A_{n,j} \frac{J_{n+3/2}(\alpha_{j,n} r)}{r^{3/2}} \tag{86}$$

and

$$r^{3/2}\frac{dT_n}{dr}=\frac{1}{2n+3}\sum_{j=1}^{\infty}A_{n,j}\alpha_{j,n}\left[nJ_{n+1/2}(\alpha_{j,n}r)-(n+3)J_{n+5/2}(\alpha_{j,n}r)\right] \tag{87}$$

$$=\frac{1}{2n+3}\sum_{j=1}^{\infty}A_{n,j}\alpha_{j,n}\Phi_{n,j} \qquad \text{(say)}.$$

Also it can be verified that

$$\frac{d}{dr}(r^2U_1)=\tfrac{1}{5}\alpha_{i,1}\left[3J_{3/2}(\alpha_{i,1}r)-2J_{7/2}(\alpha_{i,1}r)\right]\sqrt{r}=\mathfrak{U}(r)\sqrt{r}\quad\text{(say)}. \tag{88}$$

Inserting equations (86)–(88) in equation (84), we have

$$\begin{aligned}
&\sum_{j=1}^{\infty}(-\alpha_{j,n}^2+\lambda^2)A_{n,j}J_{n+3/2}(\alpha_{j,n}r)\\
&=\frac{\beta}{r^{3/2}}\Bigg[\frac{n(n-1)}{(2n-1)(2n+1)}\Bigg\{-(n-2)\mathfrak{U}(r)\sum_{k=1}^{\infty}A_{n-2,k}J_{n-1/2}(\alpha_{k,n-2}r)\\
&\qquad+\frac{3J_{5/2}(\alpha_{i,1}r)}{2n-1}\sum_{k=1}^{\infty}A_{n-2,k}\alpha_{k,n-2}\Phi_{n-2,k}\Bigg\}\\
&\qquad+\frac{(n+3)(n+4)}{(2n+5)(2n+7)}\Bigg\{(n+5)\mathfrak{U}(r)\sum_{k=1}^{\infty}A_{n+2,k}J_{n+7/2}(\alpha_{k,n+2}r)\\
&\qquad+\frac{3J_{5/2}(\alpha_{i,1}r)}{2n+7}\sum_{k=1}^{\infty}A_{n+2,k}\alpha_{k,n+2}\Phi_{n+2,k}\Bigg\}\\
&\qquad+\frac{3n(n+3)}{(2n+1)(2n+5)}\mathfrak{U}(r)\sum_{k=1}^{\infty}A_{n,k}J_{n+3/2}(\alpha_{k,n}r)\\
&+\Bigg\{\frac{3(n+1)(n+3)}{(2n+3)(2n+5)}+\frac{3n(n+2)}{(2n+3)(2n+1)}-1\Bigg\}\frac{J_{5/2}(\alpha_{i,1}r)}{2n+3}\sum_{k=1}^{\infty}A_{n,k}\alpha_{k,n}\Phi_{n,k}\Bigg].
\end{aligned} \tag{89}$$

Multiplying equation (89) by $rJ_{n+3/2}(\alpha_{j,n}r)$ and integrating from 0 to 1, we get

$$\begin{aligned}
&\tfrac{1}{2}(-\alpha_{j,n}^2+\lambda^2)\left[J'_{n+3/2}(\alpha_{j,n})\right]^2A_{n,j}\\
&=\beta\Bigg[\frac{n(n-1)}{(2n-1)(2n+1)}\sum_{k=1}^{\infty}A_{n-2,k}P(n-2,k;n,j)+\sum_{k=1}^{\infty}A_{n,k}P(n,k;n,k)\\
&\qquad+\frac{(n+3)(n+4)}{(2n+5)(2n+7)}\sum_{k=1}^{\infty}A_{n+2,k}P(n+2,k;n,j)\Bigg],
\end{aligned} \tag{90}$$

where the expressions for the various matrix elements on the right-hand side can be written down by comparison with equation (89).

Equation (90) clearly provides an infinite determinant for λ^2. It is apparent that the matrix is reducible if we include terms only in $n=0$ and 1. For this reason, it would

appear that we can get a good approximation to the lowest characteristic root by considering only the submatrix $(0, k; 0, j)$. In this approximation the characteristic determinant simplifies considerably and is given by (cf. eqs. [89] and [90])

$$\tfrac{1}{2}\left(-\alpha_{j,0}^2+\lambda^2\right)\left[J'_{3/2}(\alpha_{j,0})\right]^2 A_{0,j}=\beta\sum_{k=1}^{\infty}A_{0,k}P(0,\,k;\,0,\,j)\,, \tag{91}$$

where

$$P(0,\,k;\,0,\,j)=\tfrac{2}{5}\alpha_{k,0}\int_0^1 J_{5/2}(\alpha_{i,1}r)\,J_{5/2}(\alpha_{k,0}r)\,J_{3/2}(\alpha_{j\,0}r)\frac{dr}{\sqrt{r}}\,. \tag{92}$$

The characteristic determinant provided by equation (91) has been solved numerically for the cases $i = 1$ and 2. The results are summarized in Tables 1 and 2, where

TABLE 1

THE EFFECT OF THE VELOCITY MODE (1, 1) ON THE DECAY OF TOROIDAL MAGNETIC FIELDS

THE LOWEST CHARACTERISTIC ROOT λ^2 FOR VARIOUS VALUES OF THE AMPLITUDE, β, OF THE VELOCITY MODE

β	λ^2			β	λ^2		
	2d Approx.	3d Approx.	4th Approx.		2d Approx.	3d Approx.	4th Approx.
0*	20.19	20.19	20.19	0*	20.19	20.19	20.19
− 2	18.03	18.04	18.04	+ 5	25.92	25.90	25.90
− 4	15.96	15.98	15.98	+ 10	32.1	31.9	31.9
− 6	13.98	14.03	14.03	+ 15	38.6	38.0	38.0
− 8	12.11	12.22	12.22	+ 20	45.6	44.0	44.0
−10	10.35	10.54	10.50	+ 30	60.8	55.6	56.0
−12	8.73	9.02	8.95	+ 40	78.3	66.6	67.6
−14	7.28	7.67	7.53	+ 50	103	77.1	79.2
−16	6.06	6.50	6.24	+ 60	.....	87.3	90.8
−18	5.13	5.52	5.10	+ 70	.....	97.2	102
−20	4.70	4.72	4.07	+100	.....	126	138
−22	.....	4.09	3.15				
−24	.....	3.58	2.32				
−26	.....	3.14	1.55				
−28	.....	2.69	0.84				
−30	.....	2.14	0.17				

* The value for $\beta = 0$ is exact.

the different "approximations" refer to the number of rows and columns in the characteristic matrix which were included in the evaluation of the characteristic root. The convergence of the characteristic roots toward a limiting value as we go to higher approximations appears satisfactory, particularly in the case $i = 1$. In any case, it would appear that the general nature of the dependence of λ^2 on β (illustrated in Figs. 1 and 2) has been established. We shall return to a discussion of this dependence in § 8.

7. THE EFFECT OF THE VELOCITY MODE $(1, i)$ ON THE DECAY OF POLOIDAL MAGNETIC FIELDS

In this case the equation to be solved is

$$\Delta_5 P+\lambda^2 P=\frac{1}{\varpi^3}\frac{\partial(\varpi^2 P,\,\varpi^2 U)}{\partial(z,\,\varpi)}\,; \tag{93}$$

TABLE 2

THE EFFECT OF THE VELOCITY MODE (1, 2) ON THE DECAY OF TOROIDAL MAGNETIC FIELDS

THE LOWEST CHARACTERISTIC ROOT λ^2 FOR VARIOUS VALUES OF THE AMPLITUDE, β, OF THE VELOCITY MODE

β	λ^2			β	λ^2		
	2d Approx.	3d Approx.	4th Approx.		2d Approx.	3d Approx.	4th Approx.
0*	20.19	20.19	20.19	0*	20.19	20.19	20.19
− 1	19.94	19.95	19.95	+ 5	20.34	20.49	20.48
− 2	19.60	19.63	19.64	+10	19.46	19.86	19.88
− 3	19.13	19.21	19.23	+15	18.1	18.7	18.9
− 4	18.53	18.67	18.73	+20	16.4	17.3	17.7
− 5	17.78	18.00	18.12	+25	14.6	15.6	16.4
− 6	16.9	17.2	17.4	+30	12.7	13.8	15.1
− 7	15.8	16.2	16.6	+35	10.8	11.8	13.7
− 8	14.5	14.9	15.8	+40	8.8	9.8	12.4
− 9	13.1	13.5	14.8	+45	6.7	7.7	11.2
−10	11.5	11.8	13.9	+50	4.7	5.6	9.9
−11	9.7	9.9	13.0	+55	2.6	3.4	8.7
−12	7.8	7.8	12.1	+60	0.5	1.2	7.6
−13	5.7	5.4	11.4				
−14	3.6	2.8	11.0				
−15	1.3	0.1	10.9				
−16	.....	.....	11.4				

* The value for $\beta = 0$ is exact.

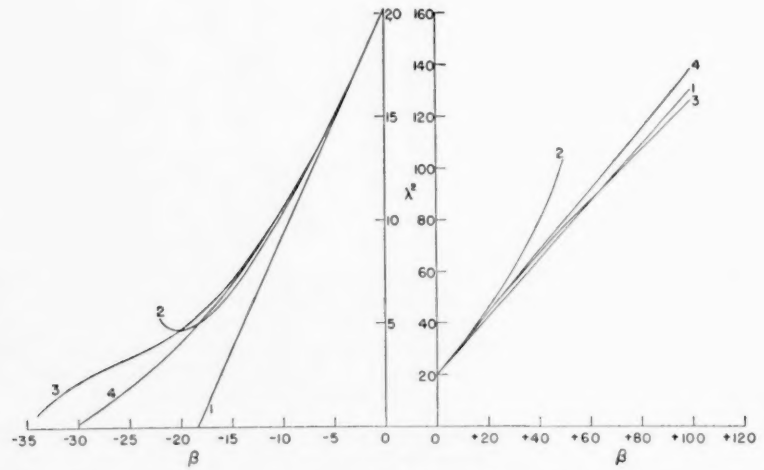

FIG. 1.—The effect of the velocity mode (1, 1) on the decay of toroidal magnetic fields. The lowest characteristic root λ^2 for various values of the amplitude, β, of the velocity mode. The curves are labeled by the order of the approximation on which they are derived.

and the boundary conditions are that the solution of this equation, which is finite at the origin, and its normal derivative both join continuously (on the unit sphere) a solution of the equation

$$\Delta_5 P = 0 \ , \tag{94}$$

which vanishes at infinity. In spherical polar co-ordinates, the equation is

$$\Delta_5 P + \lambda^2 P = -\frac{1}{r^2}\frac{\partial}{\partial r}(r^2 P)\left[\frac{\partial}{\partial \mu}(1-\mu^2)\,U\right] + \frac{1}{r^2}\frac{\partial}{\partial r}(r^2 U)\left[\frac{\partial}{\partial \mu}(1-\mu^2)\,P\right] ; \tag{95}$$

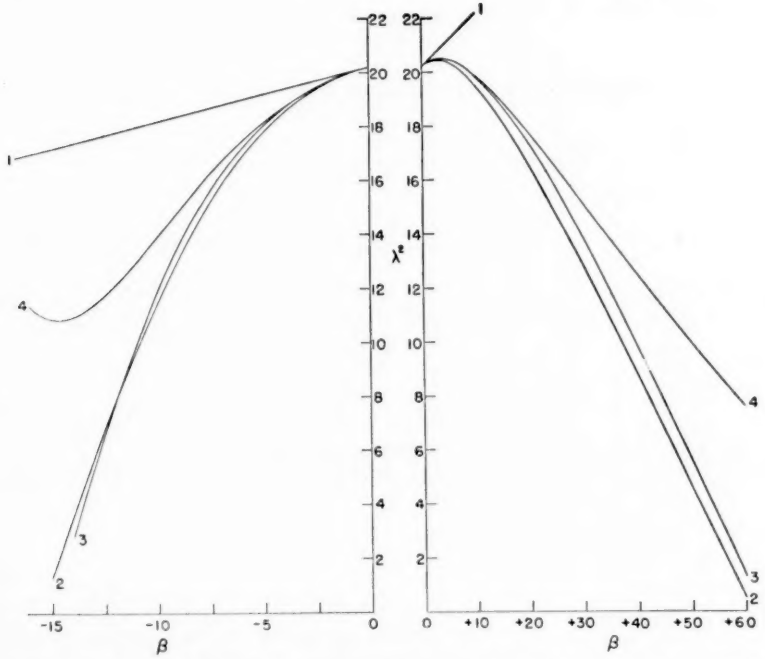

FIG. 2.—The effect of the velocity mode (1, 2) on the decay of toroidal magnetic fields. The lowest characteristic root λ^2 for various values of the amplitude, β, of the velocity mode. The curves are labeled by the order of the approximation on which they are derived.

and with the same assumption regarding the velocity field as in § 6 (eq. [78]) we have

$$\Delta_5 P + \lambda^2 P = \beta\left\{(3\mu^2-1)\,U_1\left[\frac{1}{r^2}\frac{\partial}{\partial r}(r^2 P)\right] + \left[\frac{1}{r^2}\frac{d}{dr}(r^2 U_1)\right]\mu\frac{\partial}{\partial \mu}(1-\mu^2)\,P\right\} . \tag{96}$$

In solving equation (96), we shall expand P in terms of the basic poloidal functions $P_{n,j}$. Thus, letting

$$P = \sum_{n=0}^{\infty}\sum_{j=1}^{\infty} A_{n,j}\,\frac{J_{n+3/2}(\alpha_{j,n-1}r)}{r^{3/2}}\,C_n^{3/2}(\mu) \ , \tag{97}$$

where the $A_{n,j}$'s are constants, we find, as in § 6, that we are led to the following infinite system of equations:

$$\begin{aligned}
&\sum_{j=1}^{\infty} (-\alpha_{j,n-1}^2 + \lambda^2)\, A_{n,j} J_{n+3/2}(\alpha_{j,n-1} r) \\
&= \frac{\beta}{r^{3/2}} \Bigg[\Bigg\{ \frac{n(n-1)}{(2n-1)(2n+1)} \Bigg\} - n\,\mathfrak{U}(r) \sum_{k=1}^{\infty} A_{n-2,k} J_{n-1/2}(\alpha_{k,n-3} r) \\
&\qquad + \frac{3 J_{5/2}(\alpha_{i,1} r)}{2n-1} \sum_{k=1}^{\infty} A_{n-2,k} \alpha_{k,n-3} \Psi_{n-2,k} \Bigg\} \\
&\quad + \frac{(n+3)(n+4)}{(2n+5)(2n+7)} \Bigg\{ (n+3)\,\mathfrak{U}(r) \sum_{k=1}^{\infty} A_{n+2,k} J_{n+7/2}(\alpha_{k,n+1} r) \\
&\qquad + \frac{3 J_{5/2}(\alpha_{i,1} r)}{2n+7} \sum_{k=1}^{\infty} A_{n+2,k} \alpha_{k,n+1} \Psi_{n+2,k} \Bigg\} \\
&\qquad - \frac{(n+1)(n+2)}{(2n+1)(2n+5)} \mathfrak{U}(r) \sum_{k=1}^{\infty} A_{n,k} J_{n+3/2}(\alpha_{k,n-1} r) \\
&\quad + \Bigg\{ \frac{3(n+1)(n+3)}{(2n+3)(2n+5)} + \frac{3n(n+2)}{(2n+3)(2n+1)} - 1 \Bigg\} \frac{J_{5/2}(\alpha_{i,1} r)}{2n+3} \sum_{k=1}^{\infty} A_{n,k} \alpha_{k,n-1} \Psi_{n,k} \Bigg]
\end{aligned} \tag{98}$$

where

$$\Psi_{n,k} = [\,(n+2)\, J_{n+1/2}(\alpha_{k,n-1} r) - (n+1)\, J_{n+5/2}(\alpha_{k,n-1} r)\,] \tag{98'}$$

and $\mathfrak{U}(r)$ has the same meaning as in equation (88).

Multiplying equation (98) by $r J_{n+3/2}(\alpha_{j,n-1} r)$ and integrating from 0 to 1, we get

$$\begin{aligned}
&\tfrac{1}{2}(-\alpha_{j,n-1}^2 + \lambda^2)\, [J_{n+3/2}(\alpha_{j,n-1})]^2 A_{n,j} \\
&= \beta \Bigg[\frac{n(n-1)}{(2n-1)(2n+1)} \sum_{k=1}^{\infty} A_{n-2,k} Q(n-2,\, k;\, n,\, j) + \sum_{k=1}^{\infty} A_{n,k} Q(n,\, k;\, n,\, j) \\
&\qquad + \frac{(n+3)(n+4)}{(2n+5)(2n+7)} \sum_{k=1}^{\infty} A_{n+2,k} Q(n+2,\, k;\, n,\, j) \Bigg],
\end{aligned} \tag{99}$$

where the expressions for the various matrix elements on the right-hand side can be written down by comparison with equation (98). Equation (99) provides the required characteristic determinant for λ^2.

Again, in view of the structure of the characteristic matrix given by equation(99), it appears that we can (as in § 6) obtain a satisfactory approximation to the lowest characteristic root by considering only the submatrix $(0, k; 0, j)$. In this approximation the characteristic determinant is given by

$$\tfrac{1}{2}(-\alpha_{j,-1}^2 + \lambda^2)\, [J_{3/2}(\alpha_{j,-1})]^2 A_{0,j} = \beta \sum_{k=1}^{\infty} A_{0,k} Q(0,\, k;\, 0,\, j)\,, \tag{100}$$

where (cf. eqs. [98] and [99])

$$Q(0, k; 0, j) =$$
$$-\frac{2a_{k,-1}}{15}\int_0^1 J_{5/2}(a_{i,1}r)\,[2J_{1/2}(a_{k,-1}r) - J_{5/2}(a_{k,-1}r)]\,J_{3/2}(a_{j,-1}r)\frac{dr}{\sqrt{r}} \quad (101)$$
$$-\frac{2a_{i,1}}{25}\int_0^1 [3J_{3/2}(a_{i,1}r) - 2J_{7/2}(a_{i,1}r)]\,J_{3/2}(a_{k,-1}r)\,J_{3/2}(a_{j,-1}r)\frac{dr}{\sqrt{r}}.$$

The characteristic determinant provided by equation (100) has been solved numerically for the cases $i = 1$ and 2. The results are summarized in Tables 3 and 4 (and

TABLE 3

THE EFFECT OF THE VELOCITY MODE (1, 1) ON THE DECAY OF POLOIDAL MAGNETIC FIELDS

THE LOWEST CHARACTERISTIC ROOT λ^2 FOR VARIOUS VALUES OF THE AMPLITUDE, β, OF THE VELOCITY MODE

β	λ^2		β	λ^2	
	2d Approx.	3d Approx.		2d Approx.	3d Approx.
0*	9.870	9.870	0*	9.870	9.870
− 2	10.549	10.552	+ 2	9.153	9.154
− 4	11.198	11.212	+ 4	8.391	8.387
− 6	11.82	11.86	+ 6	7.571	7.548
−10	13.01	13.15	+ 8	6.68	6.61
−15	14.4	14.8	+10	5.70	5.56
−20	15.8	16.5	+12	4.60	4.38
−30	18.4	20.0	+14	3.37	3.05
			+15	2.70	2.34
			+16	1.98	1.59
			+17	1.22	0.82
			+18	0.41	0.02

* The value for $\beta = 0$ is exact.

illustrated in Figs. 3 and 4), where the different "approximations" again refer to the number of rows and columns in the characteristic matrix which were included in the evaluation of the characteristic root.

8. SOME CONCLUSIONS AND SOME QUESTIONS

In considering the results summarized in Tables 1–4 and Figures 1–4, we should, of course, remember that they have been derived for particular velocity fields. The velocity modes assumed are the (1, 1) and the (1, 2) modes. These modes, in the usual treatments of thermal convection (Chandrasekhar 1952; Backus 1955), will be described as belonging to $l = 2$. And it is known that the first mode to be excited by thermal instability in a fluid sphere is $l = 1$ and $j = 1$; however, the Rayleigh numbers required to excite the modes $l = 2$ are not very much larger: thus, for a sphere with a rigid boundary, the Rayleigh numbers for the onset of instability are 8.04×10^3 for $l = 1$ and 1.04×10^4 and 1.33×10^4 for the two modes (1, 1) and (1, 2) belonging to $l = 2$. Therefore, the velocity modes assumed in §§ 6 and 7 can very well prevail.

The principal conclusion to be drawn from the results of §§ 6 and 7 is, then, that, with suitable amplitudes and signs, likely patterns of meridional currents can alter the times of decay of a magnetic field by quite large factors. It would, indeed, appear that factors of the order of 20 or more can be achieved by $|\beta| \sim 30$. Values of β of this order correspond to velocities which are very moderate. Thus in the earth's core (where the unit of velocity adopted has the value 7.7×10^{-5} cm/sec) $|\beta| \sim 30$ corresponds to velocities of the order of 2×10^{-4} cm/sec; and this is five or six times as small as the velocities which are believed to be present.

The conclusion, as it pertains to the earth, can be stated somewhat differently as follows: Velocities that are believed to prevail in the earth's core correspond to $|\beta| \sim 200$. From the results derived in §§ 6 and 7, it would certainly appear that velocities of

TABLE 4

THE EFFECT OF THE VELOCITY MODE (1, 2) ON THE DECAY OF POLOIDAL MAGNETIC FIELDS

THE LOWEST CHARACTERISTIC ROOT λ^2 FOR VARIOUS VALUES OF THE AMPLITUDE, β, OF THE VELOCITY MODE

β	λ^2		β	λ^2	
	2d Approx.	3d Approx.		2d Approx.	3d Approx.
0*	9.870	9.870	0*	9.870	9.870
− 3	9.584	9.577	+ 1	9.950	9.949
− 5	9.37	9.36	+ 2	10.02	10.01
−10	8.77	8.76	+ 3	10.08	10.06
−15	8.12	8.14	+ 4	10.13	10.08
−20	7.45	7.51	+ 5	10.16	10.06
−25	6.75	6.90	+ 6	10.17	9.98
−30	6.04	6.29	+ 7	10.15	9.83
−35	5.32	5.69	+ 8	10.1	9.5
−40	4.53	5.10	+ 9	10.0	9.0
−45	3.87	4.52	+10	9.9	8.2
−50	3.14	3.95	+11	9.6	7.0
−55	2.40	3.40	+12	9.3	5.3
−60	1.66	2.85	+13	8.9	.....
−65	0.92	2.30	+14	8.4	.....
−70	0.18	1.77	+15	7.7	.....
−75	.....	1.24	+18	4.7	.....

* The value for $\beta = 0$ is exact.

this magnitude (if of proper pattern and sign) can prolong the times of decay by factors of the order of 50 or more. To the question raised in § 2: "Can the time of decay of 14000 years, in the absence of internal motions, be prolonged to 500000 years (say) by velocities of reasonable magnitudes and patterns?" the answer would seem to be "Yes"; and if the answer is "Yes," the subsequent remarks in § 2 relative to the origin of the earth's magnetic field should have substance.

While the foregoing represents the principal conclusion of this paper, the analysis has disclosed aspects of the decay of a magnetic field in the presence of fluid motions which are unexpected and which raise a number of further questions. We may comment on some of these.

First, we may notice that, in agreement with what was indicated in § 5, the velocity mode (1, 1) has opposite effects on the poloidal and the toroidal fields: thus meridional circulation of a sense which retards the decay of poloidal fields accelerates the decay of

toroidal fields, and conversely. At first sight, this might appear an unfortunate fact, as one might have hoped that the principal velocity pattern which retards the decay of the poloidal field will also retard the decay of the toroidal field; but this does not appear to be the case. However, it should be remembered in this connection that, if the fluid is in a state of nonuniform rotation (as the earth's core most likely is), then, as has been pointed out in § 3, there will be in the decay of the toroidal field a term induced by the poloidal field and proportional to it. If the free decay is a strongly damped term in the prevailing meridional circulation, then it is the induced term which will be decisive.

A second fact which emerges from the results of §§ 6 and 7 is that it is not *always* true that a reversal of the sense of the meridional circulation is accompanied by a reversal of

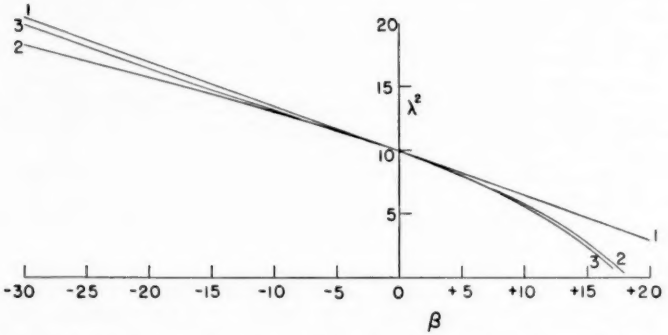

FIG. 3.—The effect of the velocity mode (1, 1) on the decay of poloidal magnetic fields. The lowest characteristic root λ^2 for various values of the amplitude, β, of the velocity mode. The curves are labeled by the order of the approximation on which they are derived.

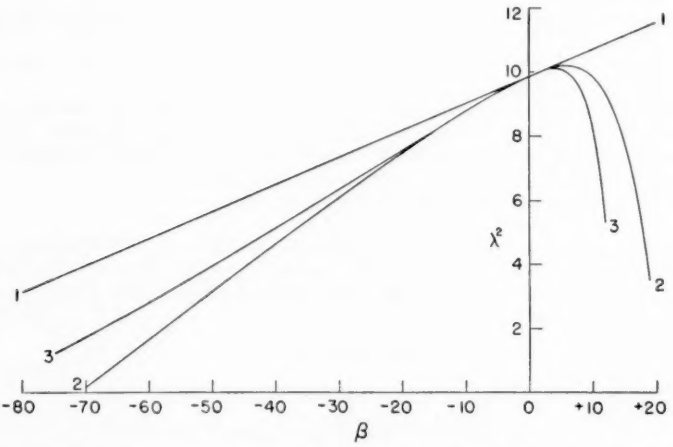

FIG. 4.—The effect of the velocity mode (1, 2) on the decay of poloidal magnetic fields. The lowest characteristic root λ^2 for various values of the amplitude, β, of the velocity mode. The curves are labeled by the order of the approximation on which they are derived.

its effect on the decay of a magnetic field. The (1, 1) velocity mode does act in this way with respect to both the poloidal and the toroidal fields (see Figs. 1 and 3). But the (1, 2) mode acts differently. Thus a negative β results in a slowing-down of the decay of both toroidal and poloidal fields; although a slightly positive β does result in a slightly accelerated decay, the trend is soon reversed; and for increasing β the decay is retarded (as when β is negative) (see Figs. 2 and 4).

The analysis of §§ 6 and 7 discloses, therefore, aspects of the decay problem which require much detailed investigation. And several related questions also suggest themselves. Some of these are the following.

1. Equations (10) and (15) are not self-adjoint. Can one still assume that the solutions belonging to the different characteristic values provide a complete basis for the expansion of an arbitrary function which satisfies the boundary conditions of the problem? If not, how is one to express the decay of an arbitrary field?

2. Are the characteristic values of equations (10) and (15) necessarily positive? In particular, are complex roots excluded?

3. Why is it that sometimes the reversal of the sense of the meridional circulation is accompanied by a reversal of its effects on the magnetic field and sometimes not?

4. What is the asymptotic behavior of λ^2 as $\beta \to +\infty$ and as $\beta \to -\infty$?

5. What is the general nature of the induced term in the decay of a toroidal field?

Answers to the foregoing questions may be expected to throw some light on the interpretation of a number of astrophysical and geophysical phenomena in which magnetic fields play a role. One example may be given.

Cowling (1946) has pointed out that, for a typical sunspot ($R = 10^9$ cm; $\sigma = 10^{-8}$ e.m.u.), the time of decay may be estimated at 300 years. Nevertheless, the magnetic field of a sunspot grows to its full strength in a matter of days; similarly, the time it takes for the field to disappear, once it has started to decline, is also a matter of days. As Cowling has emphasized, these facts raise a number of very difficult questions. But there is one circumstance which would appear to be relevant to this problem and which does not seem to have been considered. It is this: The unit of velocity appropriate to the problem on hand is $(\sigma R)^{-1} = 0.1$ cm/sec; and it is known that systematic velocities of the order of 1 km/sec are present in sunspots. Consequently, $\beta \sim 10^6$, and one can ask: What does β of this magnitude imply for the decay and growth of magnetic fields? And can it be that a suitable pattern of velocity with $\beta \sim 10^6$ can alter the decay (and growing) time of magnetic fields by a factor of the order of 10^4–10^5? Answers to questions 3 and 4 are clearly very relevant to this problem.

It is possible that, to answer with some degree of completeness the various questions that have been raised (and others that will naturally occur), one may have to look for a simplified model to which exact analytical methods can be applied to a greater extent than appears possible with the ones considered in this paper.

The subject is being pursued along several directions.

In concluding this paper, it is again a pleasure to record my indebtedness to Miss Donna Elbert, who carried out the extensive numerical work which underlies the calculations included in this paper. My thanks are also due to Miss Siciy Pao for carefully checking the manuscript.

REFERENCES

Backus, G. E. 1955, *Phil. Mag.*, **46**, 1310.
Backus, G. E., and Chandrasekhar, S. 1956, *Proc. Nat. Acad. Sci.*, **42**, 105.
Bullard, E. C. 1955, *Proc. R. Soc. London, A*, **233**, 289.
Bullard, E. C., and Gellman, H. 1954, *Phil. Trans. R. Soc. London, A*, **247**, 213.
Chandrasekhar, S. 1952, *Phil. Mag.*, **43**, 1317.
———. 1953, *M.N.*, **113**, 667.
———. 1956*a*. *Proc. Nat. Acad. Sci.*, **42**, 1.
———. 1956*b*. *Ap. J.*, **124**, 232.

Chandrasekhar, S., and Prendergast, K. 1956, *Proc. Nat. Acad. Sci.*, **42**, 5.
Cowling, T. G. 1934, *M.N.*, **94**, 39.
———. 1946, *ibid.*, **106**, 218.
Elsasser, W. M. 1946*a*, *Phys. Rev.*, **69**, 106.
———. 1946*b*. *ibid.*, **70**, 202.
———. 1947, *ibid.*, **72**, 821.
———. 1955, *Am. J. Phys.*, **23**, 590.
———. 1956, *ibid.*, **24**, 85.
Hospers, J. 1954, *Proc. Konink. Nederl. Akad. Wetensch.*, Ser. B, **57**, 112.
Lamb, H. 1881, *Proc. London Math. Soc.*, **13**, 51.
Larmor, J. 1919, *Brit. Assoc. Reports*, p. 159; see also *Mathematical and Physical Papers*, **2**, 611 (Cambridge: At the University Press, 1929).
Lehnert, B. 1952, *Ark. f. Fys.*, **5**, 69.
———. 1955, *Proc. R. Soc. London*, *A*, **233**, 299.
Nakagawa, Y. 1955, *Nature*, **175**, 417.
Pao, S. 1956, *Ap. J.*, **124**, 266.
Parker, E. 1955, *Ap. J.*, **122**, 129.
Runcorn, S. K. 1955*a*, *Trans. Am. Geophys. Union*, **36**, 191.
———. 1955*b*, *Endeavour*, **14**, 153.
Stratton, J. A. 1941, *Electromagnetic Theory* (New York: McGraw-Hill Book Co.), chap. 7.
Watson, G. N. 1944, *A Treatise on the Theory of Bessel Functions* (2d ed.; Cambridge: At the University Press), p. 137.

ON THE EFFECT OF FLUID MOTION ON THE INITIAL DECAY OF A MAGNETIC FIELD IN A SPHERE

SICIY C. PAO*
Physics Department, University of Chicago
Received March 30, 1956

ABSTRACT

Selection rules are derived which govern the interaction between the various axisymmetric modes of velocity and magnetic fields in a fluid conductor. These selection rules determine the initial rate of decay of a magnetic field.

1. INTRODUCTION

In studying the influence of axially symmetric fluid motion on the natural decay of axially symmetric magnetic fields in a sphere at initial time, one encounters the problem of evaluating the integral of the product of three Gegenbauer polynomials:

$$\int_{-1}^{+1} C_l^{3/2}(\mu)\, C_m^{3/2}(\mu)\, C_n^{3/2}(\mu)\, (1-\mu^2)\, d\mu\,. \tag{1}$$

The value of such an integral enables one to obtain the selection rule for the interaction between possible modes of velocity and magnetic fields at time $t = 0$. It is the object of this paper to present a method of evaluating the integral and to show what one can understand with the aid of its result about the effect of fluid motion on a magnetic field at $t = 0$.

2. THE EQUATIONS FOR THE RATE OF ENERGY DECAY IN A MAGNETIC FIELD

Chandrasekhar (1956) has shown in the previous paper that for both velocity and magnetic fields having axial symmetry, one has the following general equations which determine the rate of decay of energy in the toroidal component (T) and in the poloidal component (P):

$$-\frac{1}{2}\frac{d}{dt}\int\int \varpi^2 T^2\, d\varpi\, dz = \int\int \varpi^3 \left(-T\Delta_5 T + T^2\frac{\partial}{\partial z}\frac{U}{\varpi}\right) d\varpi\, dz \tag{2}$$

and

$$-\frac{1}{2}\frac{d}{dt}\int\int \varpi^2 P^2\, d\varpi\, dz = \int\int \varpi^3 \left(-P\Delta_5 P - P^2\frac{\partial}{\partial z}\frac{U}{\varpi}\right) d\varpi\, dz\,. \tag{3}$$

In equations (2) and (3) U is the poloidal scalar of velocity field, and ϖ and z are the radial and the vertical components in cylindrical polar co-ordinates. As shown in the previous paper, at $t = 0$ the fundamental toroidal and poloidal modes of the magnetic field in the absence of fluid motions are given by

$$T_{n,\,i} = \frac{J_{n+3/2}(a_{j,\,n} r)}{r^{3/2}}\, C_n^{3/2}(\mu) \tag{4}$$

* [Miss Siciy Catherine Pao died unexpectedly on April 17. A career rich in promise thus ended at the moment of its flowering.—S. CHANDRASEKHAR.]

and

$$P_{n,\,j} = \frac{J_{n+3/2}(\alpha_{j,\,n-1}r)}{r^{3/2}} C_n^{3/2}(\mu)\,, \tag{5}$$

where $\mu = \cos\vartheta$ and $\alpha_{j,\,m}$ is the zero of $J_{m+3/2}(x)$.

Let $U = \beta T_{m,\,k}$, where β is a parameter determining the magnitude of the velocity. Substituting equations (4), (5), and (6) in equations (2) and (3), one has

$$-\frac{d\mathfrak{T}}{dt} = \frac{(n+1)(n+3)}{2n+3}\,\alpha_{j,\,n}^2\,[J'_{n+3/2}(\alpha_{j,\,n})]^2 + \beta I(n,\,j;\,m,\,k;\,T) \tag{6}$$

and

$$-\frac{d\mathfrak{P}}{dt} = \frac{(n+1)(n+3)}{2n+3}\,\alpha_{j,\,n-1}^2\,[J_{n+3/2}(\alpha_{j,\,n-1})]^2 - \beta I(n,\,j;\,m,\,k;\,P) \tag{7}$$

where

$$\mathfrak{T} = \tfrac{1}{2}\int\int\int \varpi^3 T^2\,d\varpi\,dz; \qquad \mathfrak{P} = \tfrac{1}{2}\int\int\int \varpi^3 P^2\,d\varpi\,dz\,, \tag{8}$$

$$\begin{aligned} I(n,\,j;\,m,\,k;\,T) &= \frac{m+1}{2m+3}\int_{-1}^{+1}[C_n^{3/2}(\mu)]^2 C_{m+1}^{3/2}(\mu)(1-\mu^2)\,d\mu \\ &\quad\times\int_0^1 J_{n+3/2}^2(\alpha_{j,\,n}r)\left[r\,\frac{d}{dr}\,\frac{J_{m+3/2}(\alpha_{k,\,m}r)}{r^{3/2}} - m\,\frac{J_{m+3/2}(\alpha_{k,\,m}r)}{r^{3/2}}\right]dr\,, \\ &+\frac{m+2}{2m+3}\int_{-1}^{+1}[C_n^{3/2}(\mu)]^2 C_{m-1}^{3/2}(\mu)(1-\mu^2)\,d\mu \\ &\quad\times\int_0^1 J_{n+3/2}^2(\alpha_{j,\,n}r)\left[r\,\frac{d}{dr}\,\frac{J_{m+3/2}(\alpha_{k,\,m}r)}{r^{3/2}} + (m+3)\,\frac{J_{m+3/2}(\alpha_{k,\,m}r)}{r^{3/2}}\right]dr\,, \end{aligned} \tag{9}$$

and

$$\begin{aligned} I(n,\,j;\,m,\,k;\,P) &= \frac{m+1}{2m+3}\int_{-1}^{+1}[C_n^{3/2}(\mu)]^2 C_{m+1}^{3/2}(\mu)(1-\mu^2)\,d\mu \\ &\quad\times\int_0^1 J_{n+3/2}^2(\alpha_{j,\,n-1}r)\left[r\,\frac{d}{dr}\,\frac{J_{m+3/2}(\alpha_{k,\,m}r)}{r^{3/2}} - m\,\frac{J_{m+3/2}(\alpha_{k,\,m}r)}{r^{3/2}}\right]dr \\ &+\frac{m+2}{2m+3}\int_{-1}^{+1}[C_n^{3/2}(\mu)]^2 C_{m-1}^{3/2}(\mu)(1-\mu^2)\,d\mu \\ &\quad\times\int_0^1 J_{n+3/2}^2(\alpha_{j,\,n-1}r)\left[r\,\frac{d}{dr}\,\frac{J_{m+3/2}(\alpha_{k,\,m}r)}{r^{3/2}} + (m+3)\,\frac{J_{m+3/2}(\alpha_{k,\,m}r)}{r^{3/2}}\right]dr\,. \end{aligned} \tag{10}$$

In equations (7) and (8), $I(n, j; m, k; T)$ and $I(n, j; m, k; P)$ represent the interaction between the different modes of velocity and magnetic fields. Although at present the values of the integrals involving the Bessel functions in equations (9) and (10) are not known, one can determine the modes of velocity field which have no effect on the decay

on the basis of the integrals involving Gegenbauer polynomials only and can thus obtain the selection rule.

3. EVALUATION OF $\int_{-1}^{+1} C_l^{3/2}(\mu)\, C_m^{3/2}(\mu)\, C_n^{3/2}(\mu)\,(1-\mu^2)\, d\mu$

The method used here of evaluating the above integral is essentially one which Adams, in 1878, used to evaluate the integral of the product of three Legendre polynomials. Its essential step is to express the product of two polynomials in terms of a linear combination of single polynomials.

For the Gegenbauer polynomials, one has the recurrence formula

$$\mu C_n^{3/2} = \frac{n+1}{2n+3} C_{n+1}^{3/2} + \frac{n+2}{2n+3} C_{n-1}^{3/2}, \tag{11}$$

and $C_1^{3/2} = 3\mu$, $C_0^{3/2} = 1$. Using equation (11), one obtains

$$C_1^{3/2} C_n^{3/2} = 3\,\frac{n+1}{2n+3} C_{n+1}^{3/2} + 3\,\frac{n+2}{2n+3} C_{n-1}^{3/2}. \tag{12}$$

Using equations (11) and (12), one has

$$C_2^{3/2} C_n^{3/2} = \frac{3\cdot 5\,(n+1)(n+2)}{1\cdot 2\,(2n+3)(2n+5)} C_{n+2}^{3/2} + \frac{3\cdot 3}{1}\,\frac{n(n+3)}{(2n+1)(2n+5)} C_n^{3/2} + \frac{3\cdot 5\,(n+1)(n+2)}{1\cdot 2\,(2n+1)(2n+3)} C_{n-2}^{3/2}. \tag{13}$$

Similarly,

$$C_3^{3/2} C_n^{3/2} = \frac{3\cdot 5\cdot 7\,(n+1)(n+2)(n+3)}{1\cdot 2\cdot 3\,(2n+3)(2n+5)(2n+7)} C_{n+3}^{3/2} + \frac{3\cdot 3\cdot 5n\,(n+1)(n+4)}{1\cdot 2\,(2n+1)(2n+3)(2n+7)} C_{n+1}^{3/2} + \frac{3\cdot 3\cdot 5\,(n-1)(n+2)(n+3)}{1\cdot 2\,(2n-1)(2n+3)(2n+5)} C_{n-1}^{3/2} + \frac{3\cdot 5\cdot 7n\,(n+1)(n+2)}{1\cdot 2\cdot 3\,(2n-1)(2n+1)(2n+3)} C_{n-3}^{3/2}, \tag{14}$$

$$\begin{aligned} C_4^{3/2} C_n^{3/2} = {} & \frac{3\cdot 5\cdot 7\cdot 9\,(n+1)(n+2)(n+3)(n+4)}{1\cdot 2\cdot 3\cdot 4\,(2n+3)(2n+5)(2n+7)(2n+9)} C_{n+4}^{3/2} \\ & + \frac{3\cdot 3\cdot 5\cdot 7n\,(n+1)(n+2)(n+5)}{1\cdot 2\cdot 3\,(2n+1)(2n+3)(2n+5)(2n+9)} C_{n+2}^{3/2} \\ & + \frac{3\cdot 3\cdot 5\cdot 5\,(n-1)\,n\,(n+3)(n+4)}{1\cdot 2\cdot 2\,(2n-1)(2n+1)(2n+5)(2n+7)} C_n^{3/2} \\ & + \frac{3\cdot 3\cdot 5\cdot 7\,(n-2)(n+1)(n+2)(n+3)}{1\cdot 2\cdot 3\,(2n-3)(2n+1)(2n+3)(2n+5)} C_{n-2}^{3/2} \\ & + \frac{3\cdot 5\cdot 7\cdot 9\,(n-1)\,n\,(n+1)(n+2)}{1\cdot 2\cdot 3\cdot 4\,(2n-3)(2n-1)(2n+1)(2n+3)} C_{n-4}^{3/2}, \end{aligned} \tag{15}$$

and

$$
\begin{aligned}
C_5^{3/2}C_n^{3/2} = {} & \frac{3\cdot5\cdot7\cdot9\cdot11\,(n+1)(n+2)(n+3)(n+4)(n+5)}{1\cdot2\cdot3\cdot4\cdot5\,(2n+3)(2n+5)(2n+7)(2n+9)(2n+11)}\,C_{n+5}^{3/2} \\
& + \frac{3\cdot3\cdot5\cdot7\cdot9n\,(n+1)(n+2)(n+3)(n+6)}{1\cdot2\cdot3\cdot4\,(2n+1)(2n+3)(2n+5)(2n+7)(2n+11)}\,C_{n+3}^{3/2} \\
& + \frac{3\cdot3\cdot5\cdot5\cdot7\,(n-1)\,n\,(n+1)(n+4)(n+5)}{1\cdot2\cdot2\cdot3\,(2n-1)(2n+1)(2n+3)(2n+7)(2n+9)}\,C_{n+1}^{3/2} \\
& + \frac{3\cdot3\cdot5\cdot5\cdot7\,(n-2)(n-1)(n+2)(n+3)(n+4)}{1\cdot2\cdot2\cdot3\,(2n-3)(2n-1)(2n+3)(2n+5)(2n+7)}\,C_{n-1}^{3/2} \\
& + \frac{3\cdot3\cdot5\cdot7\cdot9\,(n-3)\,n\,(n+1)(n+2)(n+3)}{1\cdot2\cdot3\cdot4\,(2n-5)(2n-1)(2n+1)(2n+3)(2n+5)}\,C_{n-3}^{3/2} \\
& + \frac{3\cdot5\cdot7\cdot9\cdot11\,(n-2)(n-1)\,n\,(n+1)(n+2)}{1\cdot2\cdot3\cdot4\cdot5\,(2n-5)(2n-3)(2n-1)(2n+1)(2n+3)}\,C_{n-5}^{3/2}.
\end{aligned}
\tag{16}
$$

By induction, for $m \leq n$, we have

$$
\begin{aligned}
C_m^{3/2}C_n^{3/2} = {} & \sum_{r=0}^{m} \frac{(2r+1)!!\,(2m+1-2r)!!\,(2n+1-2r)!!\,(n+m+2-r)!}{r!\,(m-r)!\,(n-r)!\,(2n+2m+3-2r)!!} \\
& \times \frac{(2n+2m+3-4r)}{(n+m+2-2r)(n+m+1-2r)}\,C_{n+m-2r}^{3/2} \\
= {} & \sum_{r=0}^{m} \frac{2\Gamma(2r+2)\Gamma(2m+2-2r)\Gamma(2n+2-2r)\Gamma(n+m+3-r)\Gamma(n+m+2-r)}{\Gamma^2(r+1)\Gamma^2(m-r+1)\Gamma^2(n+1-r)\Gamma(2n+2m+4-2r)} \\
& \times \frac{(2n+2m+3-4r)}{(n+m+2-2r)(n+m+1-2r)}\,C_{n+m-2r}^{3/2}.
\end{aligned}
\tag{17}
$$

Also,

$$
\int_{-1}^{+1} C_m^{3/2}C_n^{3/2}\,(1-\mu^2)\,d\mu = \frac{2(m+1)(m+2)}{2m+3}\,\delta_{m,n}. \tag{18}
$$

Therefore, the required integral is

$$
\begin{aligned}
& \int_{-1}^{+1} C_l^{3/2}C_m^{3/2}C_n^{3/2}\,(1-\mu^2)\,d\mu \\
& = \frac{2^2\Gamma(2r+2)\Gamma(2m+2-2r)\Gamma(2n+2-2r)\Gamma(n+m+3-r)\Gamma(n+m+2-r)}{\Gamma^2(r+1)\Gamma^2(m+1-r)\Gamma^2(n+1-r)\Gamma^2(2n+2m+4-2r)} \\
& \qquad \times \delta_{l,\,n+m-2r},
\end{aligned}
\tag{19}
$$

where $r = 0, 1, 2, \ldots, m$, for $m \leq n$. It is clear from equation (19) that the triangle rule which Adams obtained for the Legendre polynomials, namely, that the integral is nonvanishing only when $n - m \leq l \leq n + m$, is true also for the Gegenbauer polynomials. Another restriction is that $n + m + l$ should be even if the integral is to be nonvanishing.

4. THE SELECTION RULE

The integrals involving Gegenbauer polynomials in equations (9) and (10) are

$$\int_{-1}^{+1} [C_n^{3/2}]^2 C_{m+1}^{3/2} (1-\mu^2)\, d\mu \qquad \text{and} \qquad \int_{-1}^{+1} [C_n^{3/2}]^2 C_{m-1}^{3/2} (1-\mu^2)\, d\mu\,;$$

these differ from zero simultaneously only if, according to equation (19), $m = 2n - 2r + 1$, $r = 0, 1, \ldots, n$. Therefore, $I(n, j; m, k; T)$ and $I(n, j; m, k; P)$ are different from zero only when $m = 2n - 2r + 1$, where $r = 0, 1, \ldots, n$. The natural decay of magnetic fields of definite mode n is affected initially only by those velocity fields of mode m such that $m = 2n - 2r + 1$, $r = 0, 1, \ldots, n$.

I wish to express my gratitude to Professor S. Chandrasekhar for suggesting the problem involved in this paper and for his tireless encouragement and instruction.

APPENDIX

The integral

$$\int_{-1}^{+1} C_l^\lambda C_m^\lambda C_n^\lambda (1-\mu^2)^{\lambda-1/2} d\mu$$

for arbitrary λ will be evaluated here. The procedure is the same as that for $\lambda = \frac{3}{2}$.

The recurrence formula for arbitrary λ is

$$\mu C_n^\lambda = \frac{n+1}{2n+2\lambda} C_{n+1}^\lambda + \frac{n+2\lambda-1}{2n+2\lambda} C_{n-1}^\lambda, \qquad C_0^\lambda = (2\lambda-2)!!\ \text{and}\ C_1^\lambda = (2\lambda)!!\,\mu.$$

Therefore,

$$C_1^\lambda C_n^\lambda = (2\lambda)!! \frac{n+1}{2n+2\lambda} C_{n+1}^\lambda + (2\lambda)!! \frac{n+2\lambda-1}{2n+2\lambda} C_{n-1}^\lambda,$$

$$C_2^\lambda C_n^\lambda = \frac{(2\lambda+2)!!}{1\cdot 2} \frac{(n+1)(n+2)}{(2n+2\lambda)(2n+2\lambda+2)} C_{n+2}^\lambda + (2\lambda)!!2\lambda \frac{n(n+2\lambda)}{(2n+2\lambda-2)(2n+2\lambda+2)} C_n^\lambda + \frac{(2\lambda+2)!!}{1\cdot 2} \frac{(n+2\lambda-2)(n+2\lambda-1)}{(2n+2\lambda-2)(2n+2\lambda)} C_{n-2}^\lambda,$$

$$C_3^\lambda C_n^\lambda = \frac{(2\lambda+4)!!}{1\cdot 2\cdot 3} \frac{(n+1)(n+2)(n+3)}{(2n+2\lambda)(2n+2\lambda+2)(2n+2\lambda+4)} C_{n+3}^\lambda + \frac{(2\lambda+2)!!2\lambda}{1\cdot 2} \frac{n(n+1)(n+2\lambda+1)}{(2n+2\lambda-2)(2n+2\lambda)(2n+2\lambda+4)} C_{n+1}^\lambda + \frac{(2\lambda+2)!!2\lambda}{1\cdot 2} \frac{(n-1)(n+2\lambda-1)(n+2\lambda)}{(2n+2\lambda-4)(2n+2\lambda)(2n+2\lambda+2)} C_{n-1}^\lambda + \frac{(2\lambda+4)!!}{1\cdot 2\cdot 3} \frac{(n+2\lambda-3)(n+2\lambda-2)(n+2\lambda-1)}{(2n+2\lambda-4)(2n+2\lambda-2)(2n+2\lambda)} C_{n-3}^\lambda,$$

and

$$C_4^\lambda C_n^\lambda = \frac{(2\lambda+6)\,!!}{1\cdot 2\cdot 3\cdot 4}\,\frac{(n+1)(n+2)(n+3)(n+4)}{(2n+2\lambda)(2n+2\lambda+2)(2n+2\lambda+4)(2n+2\lambda+6)}\,C_{n+4}^\lambda$$

$$+\frac{(2\lambda+4)\,!!\,(2\lambda)}{1\cdot 2\cdot 3}\,\frac{n(n+1)(n+2)(n+2\lambda+2)}{(2n+2\lambda-2)(2n+2\lambda)(2n+2\lambda+2)(2n+2\lambda+6)}\,C_{n+2}^\lambda$$

$$+\frac{(2\lambda+2)\,!!\,(2\lambda)(2\lambda+2)}{1\cdot 2\cdot 2}\,\frac{(n-1)n(n+2\lambda)(n+2\lambda+1)}{(2n+2\lambda-4)(2n+2\lambda-2)(2n+2\lambda+2)(2n+2\lambda+4)}\,C_n^\lambda$$

$$+\frac{(2\lambda+4)\,!!\,(2\lambda)}{1\cdot 2\cdot 3}\,\frac{(n-2)(n+2\lambda-2)(n+2\lambda-1)(n+2\lambda)}{(2n+2\lambda-6)(2n+2\lambda)(2n+2\lambda-2)(2n+2\lambda+2)}\,C_{n-2}^\lambda$$

$$+\frac{(2\lambda+6)\,!!}{1\cdot 2\cdot 3\cdot 4}\,\frac{(n+2\lambda-4)(n+2\lambda-3)(n+2\lambda-2)(n+2\lambda-1)}{(2n+2\lambda-6)(2n+2\lambda-4)(2n+2\lambda-2)(2n+2\lambda)}\,C_{n-4}^\lambda .$$

By induction, for $m \leq n$, we have

$$C_m^\lambda C_n^\lambda = \sum_{r=0}^{m} \frac{(2\lambda+2m-2r-2)\,!!\,(2\lambda+2r-2)\,!!\,(n+m-2r)\,!\,(2n+2\lambda-2-2r)\,!!}{(m-r)\,!\,r\,!\,(2\lambda-2)\,!!\,(n-r)\,!\,(2n+2\lambda+2m-2r)\,!!}$$

$$\times\frac{(n+2\lambda+m-r-1)\,!}{(n+2\lambda+m-2r-1)\,!}\,(2n+2\lambda+2m-4r)\,C_{m+n-2r}^\lambda$$

$$=\sum_{r=0}^{m}\frac{\Gamma(m+n-2r+1)\,\Gamma(m+n+2\lambda-r)\,(2\lambda+2r-2)\,!!\,(2m+2\lambda-2r-2)\,!!}{\Gamma(r+1)\,\Gamma(n-r+1)\,\Gamma(m-r+1)\,\Gamma(m+n+2\lambda-2r)\,(2\lambda-2)\,!!}$$

$$\times\frac{(2n+2\lambda-2r-2)\,!!}{(2n+2m+2\lambda-2r)\,!!}\,(2n+2\lambda+2m-4r)\,C_{m+n-2r}^\lambda .$$

Also,

$$\int_0^1 C_m^\lambda C_n^\lambda\,(1-\mu^2)^{\lambda-1/2}d\mu = \frac{2\Gamma(n+2\lambda)}{(2n+2\lambda)\,\Gamma(n+1)}\,\delta_{m,n} .$$

Therefore,

$$\int_{-1}^{+1} C_l^\lambda C_m^\lambda C_n^\lambda\,(1-\mu^2)^{\lambda-1/2}d\mu$$

$$=\frac{2\Gamma(m+n+2\lambda-r)\,(2\lambda+2r-2)\,!!\,(2m+2\lambda-2r-2)\,!!\,(2n+2\lambda-2r-2)\,!!}{\Gamma(r+1)\,\Gamma(n-r+1)\,\Gamma(m-r+1)\,(2\lambda-2)\,!!\,(2n+2m+2\lambda-2r)\,!!}$$

$$\times\,\delta_{l,\,m+n-2r} ,$$

where $r = 0, 1, 2, \ldots, m$ $(m \leq n)$.

REFERENCES

Adams, J. C. 1878, *Proc. R. Soc. London*, *A*, **27**, 63.
Chandrasekhar, S. 1956, *Ap. J.*, **124**, 244.

RADIATIVE EQUILIBRIUM OF A LINE-ABSORBING ATMOSPHERE. II

JEAN I. F. KING
Geophysics Research Directorate, Air Force Cambridge Research Center
Cambridge 39, Massachusetts
Received February 16, 1956

ABSTRACT

The transfer theory of nongray atmospheres of finite thickness is developed. This planetary thermal problem is treated by using both an invariance attack and the method of discrete ordinates. The emergent intensity, corresponding vertical thermal structure, and constants of the problem are expressed in exact form in terms of nongray X- and Y-functions and their moments. The alternative method of discrete ordinates is used in parallel fashion, the elimination of constants is achieved, and equivalent expressions are obtained for the X- and Y-functions and their moments in quotient polynomial form.

INTRODUCTION

In his treatise on radiative transfer, Chandrasekhar (1950)[1] has the implicit aim of expressing the solutions of a wide variety of scattering and absorption problems in terms of X- and Y-functions and their moments. In the radiative-equilibrium context he develops an invariance method which relates the law of darkening and vertical thermal structure of a stellar atmosphere to an H-function, which is itself a solution of a nonlinear integral equation. His technique is immediately applicable to the planetary problem, but the stellar model of a gray, semi-infinite homogeneous atmosphere is not.

The most striking characteristic of the absorption coefficient of an infrared-active atmospheric constituent is its line structure, which causes the coefficient to vary by as much as 10^4 from one line to the next. Equally apparent is the finite thickness of a planetary atmosphere compared with the semi-infinite, optically opaque stellar case. The third important difference is the pressure broadening of the spectral lines, which enhances the wings of the lines with increasing depth. In the formalism to follow, we extend the invariance method and its approximate, finite-stream counterpart to treat a nongray, finite, homogeneous atmosphere. Thus the first two planetary characteristics are accounted for; the third, pressure broadening, is not.

Before specifying our problem we note that in the far infrared ($\lambda > 5\ \mu$) the planetary atmosphere is almost exclusively heated from below. Although the sun is the prime source of energy, less than 1 per cent of its radiation lies in the far infrared. Our heat source is the lower boundary, which absorbs the unreflected solar beam in the visible and re-emits this energy as black-body thermal radiation characteristic of its temperature.

This, then, is the *planetary thermal problem: to determine the radiative-equilibrium law of darkening and vertical thermal structure for a nongray, finite, plane-parallel atmosphere heated solely from below by uniform, isotropic radiation.*

TRANSFER EQUATIONS

The monochromatic equation of transfer for a homogeneous plane-parallel atmosphere can be written (King 1955*b*) as

$$\mu\lambda \frac{dI(\tau, \mu, \nu)}{d\tau} = I(\tau, \mu, \nu) - B(T\tau, \nu) , \tag{1}$$

[1] Because of the frequency of citation, this book will hereafter be designated in the text as "*R.T.*," followed by the pertinent chapter and equation number.

where $\theta = \cos^{-1}\mu$ is the zenith angle, $1/\lambda = \kappa_\nu/\bar{\kappa}$ is the ratio of the monochromatic to the mean absorption coefficient, and $\tau = \bar{\kappa}u$ is the optical thickness averaged over a band width $\Delta\nu$. The specific intensity, I, is a function of depth, direction, and frequency, while the isotropic source function, B, is given by the Planck formula as

$$B(T, \nu) = \frac{2h\nu^3/c^2}{e^{h\nu/kT} - 1}. \tag{2}$$

Since the temperature is a single-valued function of the depth, we can regard the source function in the transfer equation as an implicit function of the optical depth τ.

The integral form of the differential equation (1) for the top of the atmosphere ($\tau = 0$) yields, as the intensity emerging in a direction $\cos^{-1}\mu$ at frequency ν,

$$I(0, \mu, \nu) = \int_0^\infty B(\tau, \nu)\, e^{-\tau/\mu\lambda} \frac{d\tau}{\mu\lambda}. \tag{3}$$

Over a narrow band, B can be taken as sensibly constant compared to the wide fluctuations of the absorption coefficient over the lines of the band. Thus we can write

$$I(0, \mu\lambda) = \frac{\mathfrak{B}(1/\mu\lambda)}{\mu\lambda}, \tag{4}$$

where

$$\mathfrak{B}(p) = \int_0^\infty B(\tau)\, e^{-p\tau} d\tau$$

is the Laplace transform of $B(\tau)$. This equation justifies the importance placed upon the limb darkening, for a complete knowledge of the emergent intensity suffices to determine uniquely the vertical thermal structure of the atmosphere.

We add the radiative equilibrium constraint by requiring that the source function balance the average intensity. Thus

$$B(\tau) = \frac{1}{2}\int_{-1}^{1}\int_0^1 I(\tau, \mu\lambda) \frac{d(\nu/\Delta\nu)}{\lambda}\, d\mu. \tag{5}$$

The substitution of this constraint in equation (1) yields, as the integrodifferential equation of equilibrium radiant transfer to be solved,

$$\mu\lambda \frac{dI(\tau, \mu\lambda)}{d\tau} = I(\tau, \mu\lambda) - \frac{1}{2}\int_{-1}^{1}\int_0^1 I(\tau, \mu\lambda) \frac{d(\nu/\Delta\nu)}{\lambda}\, d\mu. \tag{6}$$

THE EXACT SOLUTION BY THE INVARIANCE METHOD

Nongray X- and Y-Functions

Chandrasekhar (*R.T.*, IV), making use of an invariance principle formulated by Ambarzumian (1942), has shown that the intensity emerging from a *gray, semi-infinite* atmosphere can be expressed in terms of an H-function, where $H(\mu)$ is the solution of a simple nonlinear integral equation. For *finite* atmospheres an analogous role is played by certain X- and Y-functions, themselves solutions of a pair of nonlinear integral equations. In the context of a *nongray, semi-infinite* atmosphere, the author (King 1955*b*) has shown that the line structure can be accounted for by suitably generalizing H to be a two-variable function of μ and the frequency ν. This proves possible because of the mathematical similarity in which the μ and ν configuration spaces enter into the structure of the transfer equation, already evident from equation (1). We anticipate, therefore, that the solution of the *nongray, finite* atmosphere problem can be expressed in terms of two variable X- and Y-functions.

The nongray X- and Y-functions are found to be the solutions of the equations

$$X(\mu\lambda) = 1 + \frac{\mu\lambda}{2}\int_0^1\int_0^1 \frac{[X(\mu\lambda)\,X(\mu'\lambda') - Y(\mu\lambda)\,Y(\mu'\lambda')]}{\mu\lambda+\mu'\lambda'}\,d\mu'\,\frac{d(\nu'/\Delta\nu)}{\lambda'}, \tag{7}$$

$$Y(\mu\lambda) = e^{-\tau_1/\mu\lambda} + \frac{\mu\lambda}{2}\int_0^1\int_0^1 \frac{[Y(\mu\lambda)\,X(\mu'\lambda') - X(\mu\lambda)\,Y(\mu'\lambda')]}{\mu\lambda-\mu'\lambda'}\,d\mu'\,\frac{d(\nu'/\Delta\nu)}{\lambda'}. \tag{8}$$

We omit the proof here, sufficing to note that $X(\mu\lambda)$ and $Y(\mu\lambda)$ can be derived by analogous extension from Chandrasekhar's $X(\mu)$- and $Y(\mu)$-functions and the author's $H(\mu\lambda)$-function.

Certain relations and theorems, again obvious extensions from the gray case, are tabulated here for later use. The moments of X and Y, now functions of band structure as well, are defined as

$$\alpha_n = \int_0^1\int_0^1 X(\mu\lambda)\,(\mu\lambda)^n\,d\mu\,\frac{d(\nu/\Delta\nu)}{\lambda}, \tag{9}$$

$$\beta_n = \int_0^1\int_0^1 Y(\mu\lambda)\,(\mu\lambda)^n\,d\mu\,\frac{d(\nu/\Delta\nu)}{\lambda}. \tag{10}$$

The substitutions

$$\frac{\mu\lambda}{\mu\lambda+\mu'\lambda'} = 1 - \frac{\mu'\lambda'}{\mu\lambda+\mu'\lambda'}, \qquad \frac{\mu\lambda}{\mu\lambda-\mu'\lambda'} = 1 + \frac{\mu'\lambda'}{\mu\lambda-\mu'\lambda'}, \tag{11}$$

coupled with the moments α_n and β_n yield useful forms of equation (7) and (8). Thus

$$\frac{1}{2}\int_0^1\int_0^1 \frac{\mu'\lambda'}{\mu\lambda+\mu'\lambda'}[X(\mu\lambda)\,X(\mu'\lambda') - Y(\mu\lambda)\,Y(\mu'\lambda')]\,d\mu'\,\frac{d(\nu'/\Delta\nu)}{\lambda'} = 1 - \left(1 - \frac{\alpha_0}{2}\right)X(\mu\lambda) - \frac{\beta_0}{2}\,Y(\mu\lambda), \tag{12}$$

$$\frac{1}{2}\int_0^1\int_0^1 \frac{\mu'\lambda'}{\mu\lambda-\mu'\lambda'}[Y(\mu\lambda)\,X(\mu'\lambda') - X(\mu\lambda)\,Y(\mu'\lambda')]\,d\mu'\,\frac{d(\nu'/\Delta\nu)}{\lambda'} = -e^{-\tau_1/\mu\lambda} + \frac{\beta_0}{2}\,X(\mu\lambda) + \left(1 - \frac{\alpha_0}{2}\right)Y(\mu\lambda). \tag{13}$$

Theorem 3 (*R.T.*, VIII, eq. [35]) for the nongray case becomes

$$\left(1 - \frac{\alpha_0}{2}\right)\alpha_2 + \frac{\beta_0}{2}\,\beta_2 + \tfrac{1}{4}(\alpha_1^2 - \beta_1^2) = \frac{\bar{\lambda}}{3}, \tag{14}$$

where

$$\bar{\lambda} = \int_{\Delta\nu}\lambda\,\frac{d\nu}{\Delta\nu} = \int_{\Delta\nu}\kappa_\nu\,\frac{d\nu}{\Delta\nu}\int_{\Delta\nu}\frac{1}{\kappa_\nu}\,\frac{d\nu}{\Delta\nu} \tag{15}$$

is the product of the arithmetic and the harmonic means of the absorption coefficient.

The Invariance Method

This approach to the planetary thermal problem divides the emergent intensity into two parts: the attenuated beam which passes through unscattered and the portion of

the incident intensity diffusely transmitted through the atmosphere which suffers one or more scattering processes. Thus (*R.T.*, X, eq. [192])

$$I(0, \mu\lambda) = I_0 e^{-\tau_1/\mu\lambda} + \frac{1}{2\mu\lambda}\int_0^1\int_0^1 I_0 T(\mu\lambda, \mu'\lambda')\, d\mu' \frac{d(\nu'/\Delta\nu)}{\lambda'}, \tag{16}$$

where the nongray transmission function is given by

$$T(\mu\lambda, \mu'\lambda') = \frac{\mu\lambda\mu'\lambda'}{\mu\lambda - \mu'\lambda'}\left[Y(\mu\lambda)\, X(\mu'\lambda') - X(\mu\lambda)\, Y(\mu'\lambda')\right]. \tag{17}$$

The intensity diffusely reflected is similarly found to be

$$I(\tau_1, -\mu\lambda) = \frac{1}{2\mu\lambda}\int_0^1\int_0^1 I_0 S(\mu\lambda, \mu'\lambda')\, d\mu' \frac{d(\nu'/\Delta\nu)}{\lambda'}, \tag{18}$$

with the scattering function given as

$$S(\mu\lambda, \mu'\lambda') = \frac{\mu\lambda\mu'\lambda'}{\mu\lambda + \mu'\lambda'}\left[X(\mu\lambda)\, X(\mu'\lambda') - Y(\mu\lambda)\, Y(\mu'\lambda')\right]. \tag{19}$$

Two integrals involving S and T, of immediate use, can be obtained by substitution from equations (13) and (12),

$$t(\mu\lambda) = \frac{1}{2}\int_0^1\int_0^1 T(\mu\lambda, \mu'\lambda')\, d\mu' \frac{d(\nu'/\Delta\nu)}{\lambda'} = \mu\lambda\left[\frac{\beta_0}{2} X(\mu\lambda) + \left(1 - \frac{\alpha_0}{2}\right) Y(\mu\lambda) - e^{-\tau_1/\mu\lambda}\right], \tag{20}$$

$$s(\mu\lambda) = \frac{1}{2}\int_0^1\int_0^1 S(\mu\lambda, \mu'\lambda')\, d\mu' \frac{d(\nu'/\Delta\nu)}{\lambda'} = \mu\lambda\left[1 - \left(1 - \frac{\alpha_0}{2}\right) X(\mu\lambda) - \frac{\beta_0}{2} Y(\mu\lambda)\right]. \tag{21}$$

In view of the isotropic, uniform nature of the incident intensity I_0, we can substitute these expressions for s and t in equations (16) and (18). Thus

$$I(0, \mu\lambda) = I_0\left[\frac{t(\mu\lambda)}{\mu\lambda} + e^{-\tau_1/\mu\lambda}\right] = I_0\left[\frac{\beta_0}{2} X(\mu\lambda) + \left(1 - \frac{\alpha_0}{2}\right) Y(\mu\lambda)\right], \tag{22}$$

$$I(\tau_1, -\mu\lambda) = I_0 \frac{s(\mu\lambda)}{\mu\lambda} = I_0\left[1 - \left(1 - \frac{\alpha_0}{2}\right) X(\mu\lambda) - \frac{\beta_0}{2} Y(\mu\lambda)\right]. \tag{23}$$

We can uncover various relations among the constants by calculating the flux and K-integrals which the problem satisfies. The requirement of constant flux demands, at the top and bottom,

$$F = 2\int_0^1\int_0^1 I(0, \mu\lambda)\, \mu d\mu d\frac{\nu}{\Delta\nu} = I_0\left[\beta_0\alpha_1 + (2 - \alpha_0)\,\beta_1\right] \tag{24}$$

and

$$F = I_0 - 2\int_0^1\int_0^1 I(\tau_1, -\mu\lambda)\, \mu d\mu d\frac{\nu}{\Delta\nu} = I_0\left[(2 - \alpha_0)\,\alpha_1 + \beta_0\beta_1\right]. \tag{25}$$

These are equal if and only if

$$\alpha_0 + \beta_0 = 2 \, . \tag{26}$$

From the equivalent expressions (24) and (25) we have the important relation connecting the incident intensity to the flux,

$$\frac{I_\varrho}{F} = \frac{1}{\beta_0 (\alpha_1 + \beta_1)} \, . \tag{27}$$

The intensities, emerging from top and bottom, can now be written

$$I(0, \mu\lambda) = I_\varrho \frac{\beta_0}{2} [X(\mu\lambda) + Y(\mu\lambda)] \, , \tag{28}$$

$$I(\tau_1, -\mu\lambda) = I_\varrho \left\{ 1 - \frac{\beta_0}{2} [X(\mu\lambda) + Y(\mu\lambda)] \right\} . \tag{29}$$

Adding equations (28) and (29), we discover that

$$I(0, \mu\lambda) + I(\tau_1, -\mu\lambda) = I_\varrho \, , \tag{30}$$

which indicates here the presence of a law of detailed balancing.

To obtain the nongray, finite Hopf-Bronstein relation, we note the fact, obvious from equation (4), that the source function at the top of the atmosphere is equal to the grazing emergent intensity. Thus

$$B(0) = I(0, 0) \, . \tag{31}$$

Now from equation (28), since $X(0) = 1$ and $Y(0) = 0$, we have

$$I(0, 0) = \frac{\beta_0}{2} I_\varrho \, . \tag{32}$$

Combining equations (27), (31), and (32) yields the desired relation,

$$\frac{B(0)}{F} = \frac{1}{2 (\alpha_1 + \beta_1)} \, . \tag{33}$$

An evaluation of the K-integral at top and bottom gives

$$K(0) = \frac{1}{2} \int_0^1 \int_0^1 I(0, \mu\lambda) \, \mu^2 d\mu\lambda d \frac{\nu}{\Delta\nu} = I_\varrho \frac{\beta_0}{4} (\alpha_2 + \beta_2) = \frac{F}{4} Q \tag{34}$$

and

$$\begin{aligned} K(\tau_1) &= \frac{1}{2} \int_0^1 \int_0^1 I_\varrho \mu^2 d\mu\lambda d \frac{\nu}{\Delta\nu} + \frac{1}{2} \int_0^1 \int_0^1 I(\tau_1, -\mu\lambda) \, \mu^2 d\mu\lambda d \frac{\nu}{\Delta\nu} \\ &= I_\varrho \left[\frac{\bar{\lambda}}{3} - \frac{\beta_0}{4} (\alpha_2 + \beta_2) \right] = \frac{F}{4} (\tau_1 + Q) \, . \end{aligned} \tag{35}$$

From equations (34) and (27) we find

$$Q = \frac{\alpha_2 + \beta_2}{\alpha_1 + \beta_1} \, . \tag{36}$$

Thus the Q-constant of the K-integral is the ratio of the second to the first moment of the X- and Y-functions.

Adding $K(0)$ and $K(\tau_1)$, we uncover the interesting relation which links all four constants of the problem,

$$\frac{I_v}{F} = \frac{3}{\bar{\lambda}} \frac{\tau_1 + 2Q}{4} . \tag{37}$$

Still another can be obtained from equation (37) and Theorem 3 (eq. [14]),

$$\tau_1 = \frac{4\bar{\lambda}/3}{\beta_0 (\alpha_1 + \beta_1)} - 2 \frac{\alpha_2 + \beta_2}{\alpha_1 + \beta_1} = \frac{\alpha_1 - \beta_1}{\beta_0} . \tag{38}$$

THE APPROXIMATE SOLUTION BY THE METHOD OF DISCRETE ORDINATES

The General Solution in Terms of Undetermined Constants

Using the invariance method, we have obtained the emergent intensity (eq. [28]) as a function of a pair of integral equations which can be solved by iterative methods. This, in principle, solves our problem, since from equation (4) the source function can be expressed in terms of the inverse Laplace transform of the emergent intensity. In practice, however, this evaluation becomes extremely tedious, since the function $X(\mu\lambda) + Y(\mu\lambda)$ has a branch cut along the negative real axis. Although obscured by formalism, the method of discrete ordinates, first devised by Wick (1943), avoids this difficulty by replacing this branch cut with appropriate simple poles. As the order of approximation increases without limit, the poles become infinitely dense, and the exact solution is approached.

This method is displayed in detail in *R.T.*, III, for the case of a gray, semi-infinite atmosphere. We shall attempt no complete, parallel development here, emphasizing rather the alterations in the formalism necessary to treat the finite, nongray model. In any event the gray, semi-infinite results can be reclaimed at every step by letting the optical thickness τ_1 approach infinity and placing λ equal to unity.

The essence of the discrete ordinate method consists in the replacement of the integro-differential equation of equilibrium radiant transfer (eq. [6]) by its approximate equivalent, the system of $2mn$ linear differential equations,

$$\mu_i \lambda_j \frac{dI_{ij}}{d\tau} = I_{ij} - \frac{1}{2} \sum_{k,\, l} a_k b_l I_{kl} . \tag{39}$$[2]

These equations have, as their *characteristic equation*,

$$\frac{1}{2} \sum_{i,\, j} \frac{a_i b_j}{1 + \mu_i \lambda_j k} = 1 . \tag{40}$$

Our task, therefore, is to express the emergent intensity and source function as explicit functions involving only the roots k_α and the constants $\mu_i \lambda_j$ of the characteristic equation.

The set of equations (39) has the general solution

$$I_{ij} = b \Big[\sum_{\alpha} \Big(\frac{L_\alpha e^{-k_\alpha \tau}}{1 + \mu_i \lambda_j k_\alpha} + \frac{L_{-\alpha} e^{k_\alpha \tau}}{1 - \mu_i \lambda_j k_\alpha} \Big) + \mu_i \lambda_j + \tau + Q \Big] , \tag{41}$$

where the $2mn$ integration constants b, Q, and $L_{\pm\alpha}$ are to be determined from the boundary constraints and expressed as functions of the roots of the characteristic equation.

[2] Unless otherwise specified, i and k will run through *all* the integers, $i, k = \pm 1, \ldots, \pm n$; j and l through the positive integers, $j, l = 1, \ldots, n$, while α and β will run through the integers, $\alpha, \beta = \pm 1, \ldots, (mn - 1)$, with zero excluded for all indices.

From the equilibrium constraint, equation (5), the source function in this approximation becomes

$$B(\tau) = \frac{1}{2}\int_{-1}^{1}\int_{0}^{1} I(\tau, \mu\lambda)\,\frac{d(\nu/\Delta\nu)}{\lambda}\,d\mu = \frac{1}{2}\sum_{i,j} a_i b_j I_{ij}. \tag{42}$$

The general solution for I_{ij} substituted in this equation yields, after some algebraic manipulation involving the characteristic equation,

$$B(\tau) = b\Big[\sum_{\alpha}\,(L_\alpha e^{-k_\alpha\tau} + L_{-\alpha}e^{k_\alpha\tau}) + \tau + Q\Big]. \tag{43}$$

The constant b is simply related to the constant flux filtering upward through the atmosphere. Thus we find, by generalizing *R.T.*, III, equation (37),

$$F = 2\int_{-1}^{1}\int_{0}^{1} I\,d\,\frac{\nu}{\Delta\nu}\,\mu d\mu = 2\sum_{i,j} a_i\mu_i b_j\lambda_j I_{ij}. \tag{44}$$

Upon substituting for the intensity in this equation, all terms, save one, vanish, to leave

$$F = 2b\sum_{i} a_i\mu_i^2\sum_{j} b_j\lambda_j^2. \tag{45}$$

Now, since

$$\sum_i a_i\mu_i^2 = \int_{-1}^{1}\mu^2 d\mu, \qquad \sum_j b_j\lambda_j^2 = \int_0^1 \lambda d\,\frac{\nu}{\Delta\nu}, \tag{46}$$

we have

$$b = \frac{3}{\lambda}\frac{F}{4}. \tag{47}$$

We note further that our model atmosphere has no radiation incident on the top but is bathed at the bottom by the isotropic, uniform intensity I_g. This requires from our general solution that

$$I_{-ij}(0) = \frac{3}{\lambda}\frac{F}{4}\Big[\sum_{\alpha}\Big(\frac{L_\alpha}{1-\mu_i\lambda_j k_\alpha} + \frac{L_{-\alpha}}{1+\mu_i\lambda_j k_\alpha}\Big) - \mu_i\lambda_j + Q\Big] = \frac{3}{\lambda}\frac{F}{4}\,S(\mu_i\lambda_j) = 0 \tag{48}$$

and

$$I_{ij}(\tau_1) = \frac{3}{\lambda}\frac{F}{4}\Big[\sum_{\alpha}\Big(\frac{L_\alpha e^{-k_\alpha\tau_1}}{1+\mu_i\lambda_j k_\alpha} + \frac{L_{-\alpha}e^{k_\alpha\tau_1}}{1-\mu_i\lambda_j k_\alpha}\Big) + \mu_i\lambda_j + \tau_1 + Q\Big] = I_g + \frac{3}{\lambda}\frac{F}{4}\,T(\mu_i\lambda_j) = I_g. \tag{49}$$

By defining S and T in this fashion, we can state our boundary conditions succinctly as requiring that

$$S(\mu_i\lambda_j) = T(\mu_i\lambda_j) = 0 . \tag{50}$$

The finite-stream analogue to the law of detailed balancing, equation (30), requires the intensities emerging from top and bottom to balance the incident intensity I_ϱ. Thus

$$\begin{aligned} I_{ij}(0) + I_{-ij}(\tau_1) &= I_\varrho \\ &= I_\varrho + \frac{3}{\lambda}\frac{F}{4}[S(-\mu_i\lambda_j) + T(-\mu_i\lambda_j)] . \end{aligned} \tag{51}$$

Explicitly, this demands, in turn, that

$$S(-\mu_i\lambda_j) + T(-\mu_i\lambda_j) = \frac{3}{\lambda}\frac{F}{4}\left[\sum_a (L_{-a} + L_a e^{-k_a\tau_1})\left(\frac{1}{1-\mu_i\lambda_j k_a} + \frac{e^{k_a\tau_1}}{1+\mu_i\lambda_j k_a}\right) + \tau_1 + 2Q\right] - I_\varrho = 0 . \tag{52}$$

Manifestly, this equation considered as a polynomial in $\mu_i\lambda_j$ is identically zero if and only if

$$L_{-a} = -L_a e^{-k_a\tau_1} , \tag{53}$$

$$\frac{I_\varrho}{F} = \frac{3}{\lambda}\frac{\tau_1 + 2Q}{4} . \tag{54}$$

From a comparison of equations (54) and (37) we conclude that the Q, a constant of the general solution, equation (41), for the finite-stream method is equivalent to the Q-constant of the K-integral defined as the ratio of moments of the X- and Y-functions. We note further that the identity, equation (52), holds for S and T as continuous functions of $\mu\lambda$ if relations (53) and (54) are valid. Hence we conclude that the relationship here exhibited is exact and that, quite generally,

$$T(\mu\lambda) = -S(\mu\lambda) . \tag{55}$$

We are now in a position to express the emergent intensity as a continuous function of μ and λ. Using equation (4) and the lower boundary condition of our problem, we have

$$\begin{aligned} I(0, \mu\lambda) &= \int_0^\infty B(l)\, e^{-l/\mu\lambda}\frac{dl}{\mu\lambda} \\ &= \int_0^{\tau_1} B(l)\, e^{-l/\mu\lambda}\frac{dl}{\mu\lambda} + I_\varrho e^{-\tau_1/\mu\lambda} . \end{aligned} \tag{56}$$

By substituting for the source function from equation (43), we find, after some manipulation, that

$$I(0, \mu\lambda) = \frac{3}{\lambda}\frac{F}{4}[S(-\mu\lambda) + e^{-\tau_1/\mu\lambda}S(\mu\lambda)] , \tag{57}$$

where $S(\mu\lambda)$, now a continuous function of $\mu\lambda$, is, as before,

$$S(\mu\lambda) = \sum_a\left(\frac{L_a}{1-\mu\lambda k_a} + \frac{L_{-a}}{1+\mu\lambda k_a}\right) - \mu\lambda + Q . \tag{58}$$

Before solving the problem by obtaining explicit expressions for the L_α's and Q, we define the following functions, convenient in the ensuing development:

$$P(x) = \prod_{i,\,j} x - \mu_i\lambda_j\,, \tag{59}$$

$$R(x) = \prod_{\alpha} 1 - k_\alpha x\,, \qquad R_\alpha(x) = \prod_{\beta\neq\alpha} 1 - k_\beta x\,, \tag{60}$$

$$W(x) = R(-x)\,R(x) = \prod_{\alpha} 1 - k_\alpha^2 x^2\,, \tag{61}$$

$$W_\alpha(x) = R(-x)\,R_\alpha(x)\,. \tag{62}$$

By multiplying $S(\mu\lambda)$ by $W(\mu\lambda)$, we clear $S(\mu\lambda)$ of fractions and obtain a polynomial expression in $\mu\lambda$ of degree $2mn - 1$. This ploynomial from condition (50) must have mn roots at $\mu\lambda = \mu_i\lambda_j$. Hence we can write, using relation (59),

$$S(\mu\lambda)\,W(\mu\lambda) = P(\mu\lambda)\;s(\mu\lambda)\,, \tag{63}$$

where $s(\mu\lambda)$ is a polynomial of degree $mn - 1$ yet to be determined.

Upon substituting for S from this equation, equation (57) can be written

$$I(0,\,\mu\lambda) = \frac{3}{\lambda}\frac{F}{4}\frac{P(-\mu\lambda)}{(R-\mu\lambda)}\,\frac{\{\,s(-\mu\lambda) + e^{-\tau_1/\mu\lambda}\,[P(\mu\lambda)\,/P(-\mu\lambda)\,]\;s(\mu\lambda)\,\}}{R(\mu\lambda)}\,. \tag{64}$$

We now make use of an implicit constraint on the emergent intensity which just suffices to solve our problem. This is the requirement that *the emergent intensity must be bounded throughout the range of* μ *and* λ. This condition is reminiscent of the semi-infinite problem requirement that none of the intensities could increase faster than e^τ as $\tau \longrightarrow \infty$. This required all $L_{-\alpha}$'s to vanish. Returning to equation (64), we note from relation (60) that

$$R\left(\frac{1}{k_\alpha}\right) = 0\,. \tag{65}$$

Hence the requirement of the boundedness of $I(0,\,\mu\lambda)$ *demands that*

$$s\left(\frac{-1}{k_\alpha}\right) = -\,e^{-k_\alpha\tau_1}\,\frac{P(1/k_\alpha)}{P(-1/k_\alpha)}\;s\left(\frac{1}{k_\alpha}\right). \tag{66}$$

Chandrasekhar (1947) has shown that this functional equation suffices to determine uniquely, except for the factor of proportionality k, the polynomial $G(\mu\lambda)$ of degree $mn - 1$, where

$$s(\mu\lambda) = kG(\mu\lambda) \tag{67}$$

and

$$G(\mu\lambda) = \sum_{\substack{mn-1\\ 2\text{ terms}}} \epsilon_l^{(0)} \prod_{i=1}^{l} \prod_{j=1}^{mn-1-l} \frac{k_{ri}+k_{sj}}{k_{ri}-k_{sj}} \prod_{i=1}^{l} 1 + k_{ri}\mu\lambda \prod_{j=1}^{mn-1-l} (1 - k_{sj}\mu\lambda)\;\rho\left(\frac{1}{k_{sj}}\right), \tag{68}$$

$$F(\mu\lambda) = \sum_{\substack{mn-1\\ 2\text{ terms}}} \epsilon_l^{(e)} \prod_{i=1}^{l} \prod_{j=1}^{mn-1-l} \frac{k_{ri}+k_{sj}}{k_{ri}-k_{sj}} \prod_{i=1}^{l} 1 + k_{ri}\mu\lambda \prod_{j=1}^{mn-1-l} (1 - k_{sj}\mu\lambda)\;\rho\left(\frac{1}{k_{sj}}\right). \tag{69}$$

The $r_1, \ldots, r_l$ and $s_1, \ldots, s_{mn-1-l}$ are selections of l, $mn-1-l$ distinct integers from the set $1, 2, \ldots, mn-1$. The sequences $\epsilon_l^{(0)}$ and $\epsilon_l^{(e)}$ are given by

$$\epsilon_l^{(0)} = +1, \quad (-1)^{mn-1}, \quad -1, \quad (-1)^{mn}, \quad +1, \quad \ldots, \tag{70}$$

$$\epsilon_l^{(e)} = +1, \quad (-1)^{mn}, \quad -1, \quad (-1)^{mn-1}, \quad +1, \quad \ldots, \tag{71}$$

and ρ is defined as

$$\rho\left(\frac{1}{k_a}\right) = e^{-k_a \tau_1} \frac{P(1/k_a)}{P(-1/k_a)}. \tag{72}$$

To obtain the proportionality constant k, we equate the coefficients of the highest power of $\mu\lambda$ in equation (67). Substituting for $s(\mu\lambda)$ from equation (63), we find

$$(-1)^{mn} \prod_a k_a^2 = k\, g^{(mn-1)}, \tag{73}$$

where $g^{(mn-1)}$, the coefficient of the $(\mu\lambda)^{mn-1}$ term of $G(\mu\lambda)$, is determined from equation (68) as

$$g^{(mn-1)} = \prod_a k_a \sum_{\substack{mn-1 \\ 2 \text{ terms}}} \epsilon_l^{(e)} \prod_{i=1}^{l} \prod_{j=1}^{mn-1-l} \frac{k_{ri} + k_{sj}}{k_{ri} - k_{sj}} \rho\left(\frac{1}{k_{sj}}\right), \tag{74}$$

which, from the expression (69) defining $F(\mu\lambda)$, is equivalent to

$$g^{(mn-1)} = \prod_a k_a F(0). \tag{75}$$

This determination of k has solved the problem, for we can now write $S(\mu\lambda)$ as a quotient polynomial involving only the roots and constants of the characteristic equation. Thus, substituting equation (67) for s and equations (73) and (75) for k, S becomes

$$S(\mu\lambda) = (-1)^{mn} \prod_a k_a \frac{P(\mu\lambda)}{W(\mu\lambda)} \frac{G(\mu\lambda)}{F(0)}. \tag{76}$$

The first constant we evaluate, directly related to the Hopf-Bronstein relation, is $S(0)$. From the defining relations (59) and (61) for P and W,

$$P(0) = (-1)^{mn} \prod_{i,j} \mu_i \lambda_j, \qquad W(0) = 1, \tag{77}$$

so that, from equation (76),

$$S(0) = \prod_{i,j} \mu_i \lambda_j \prod_a k_a \frac{G(0)}{F(0)}. \tag{78}$$

We digress for a moment to determine the product terms. The characteristic equation (40) can be rewritten slightly, since

$$\mu_{-i} = -\mu_i \quad \text{and} \quad \sum_{i,j} a_i b_j = 2, \tag{79}$$

in the form

$$\sum_{i,\,j} \frac{a_i b_j \mu_i^2 \lambda_j^2 k^2}{1 - \mu_i^2 \lambda_j^2 k^2} = 0 \qquad (i = 1, \ldots, n) \,. \tag{80}$$

We can express this summation as a quotient polynomial whose numerator involves the roots of the equation

$$\sum_{i,\,j} \frac{a_i b_j \mu_i^2 \lambda_j^2 k^2}{1 - \mu_i^2 \lambda_j^2 k^2} = \frac{c k^2 \prod_{\alpha} k^2 - k_\alpha^2}{\prod_{i,\,j} 1 - \mu_i^2 \lambda_j^2 k^2} \qquad (i = 1, \ldots, n) \,, \tag{81}$$

where the constant of proportionality, c, can be determined by taking $k \longrightarrow \infty$ as

$$c = (-1)^{mn-1} \prod_{i,\,j} \mu_i^2 \lambda_j^2 \qquad (i = 1, \ldots, n) \,. \tag{82}$$

With this substitution for c and taking the limit as $k \longrightarrow 0$, equation (81) yields

$$\begin{aligned} \sum_{i,\,j} a_i b_j \mu_i^2 \lambda_j^2 &= \Big(\prod_{i,\,j} \mu_i \lambda_j \prod_{\alpha} k_\alpha \Big)^2 \\ &= \frac{\lambda}{3} \qquad (i = 1, \ldots, n) \end{aligned} \tag{83}$$

from equation (46). Relation (83) then gives

$$S(0) = \sqrt{\frac{\lambda}{3} \frac{G(0)}{F(0)}} \,. \tag{84}$$

Besides the physical content, this relation excites mathematical interest by linking in such simple fashion the zeros of three functions.

The Elimination of the Constants

From the defining relation (58) for $S(\mu\lambda)$ we can express the integration constants L_α as

$$L_\alpha = \lim_{\mu\lambda \to 1/k_\alpha} (1 - \mu\lambda k_\alpha)\, S(\mu\lambda) \,. \tag{85}$$

Using the polynomial expression (76) of $S(\mu\lambda)$ and relation (62), we find

$$L_\alpha = (-1)^{mn} \prod_{\alpha} k_\alpha \frac{P(1/k_\alpha)}{R_\alpha(1/k_\alpha)} \frac{G(1/k_\alpha)}{R(-1/k_\alpha) F(0)} \,, \tag{86}$$

where, from equation (68),

$$G\Big(\frac{1}{k_\alpha}\Big) = \prod_{\beta} \Big(1 + \frac{k_\beta}{k_\alpha}\Big) \sum_{\substack{mn-2 \\ 2 \text{ terms} \\ r_i,\, s_j \neq \alpha}} \epsilon_l^{(0)} \prod_{i=1}^{l} \prod_{j=1}^{mn-1-l} \frac{k_{r_i} + k_{s_j}}{k_{r_i} - k_{s_j}} \rho\Big(\frac{1}{k_{s_j}}\Big) \,. \tag{87}$$

This can be written, using relation (60) and by defining G_a as the function G with all terms in which r_i, $s_j = a$ are excluded, as

$$G\left(\frac{1}{k_a}\right) = R\left(\frac{-1}{k_a}\right) G_a(0) \ . \tag{88}$$

Using this result in relation (86), we have

$$L_a = (-1)^{mn} \prod_a k_a \frac{P(1/k_a)}{R_a(1/k_a)} \frac{G_a(0)}{F(0)} . \tag{89}$$

Now the nongray analogue for Chandrasekhar's expression for L_a in a semi-infinite atmosphere can be written (*R.T.*, III, eq. [66])

$$L_a(\infty) = (-1)^{mn} \prod_a k_a \frac{P(1/k_a)}{R_a(1/k_a)} , \tag{90}$$

so that L_a for a finite atmosphere can be expressed as merely a factor times the corresponding infinite case. Thus

$$L_a(\tau_1) = L_a(\infty) \frac{G_a(0)}{F(0)} . \tag{91}$$

Our notation threatens to be overly concise. Let us introduce a whiff of reality by writing explicitly the finite-atmosphere factor for $L_1(\tau_1)$ in the $n \times m = 2 \times 2$ approximation. Thus

$$\begin{aligned} G_1(0) &= 1 - \rho_2\rho_3 + \left(\frac{k_2+k_3}{k_2-k_3}\right)(\rho_2 - \rho_3) \ , \\ F(0) &= 1 - \rho_1\rho_2\rho_3 + \left(\frac{k_2+k_3}{k_2-k_3}\right)\left(\frac{k_3+k_1}{k_3-k_1}\right)(\rho_1\rho_2 - \rho_3) \\ &\quad + \left(\frac{k_3+k_1}{k_3-k_1}\right)\left(\frac{k_1+k_2}{k_1-k_2}\right)(\rho_2\rho_3 - \rho_1) \\ &\quad + \left(\frac{k_1+k_2}{k_1-k_2}\right)\left(\frac{k_2+k_3}{k_2-k_3}\right)(\rho_3\rho_1 - \rho_2) \ , \end{aligned} \tag{92}$$

where, for brevity, we have written

$$\rho_a = \rho\left(\frac{1}{k_a}\right). \tag{93}$$

The integration constant Q can be expressed as the limit of a function of $S(\mu\lambda)$ in a fashion similar to equation (85) for L_a. With the substitution $k = -1/\mu\lambda$, it can be easily verified, from relation (58), that

$$Q = \lim_{k\to 0}\left[\frac{d}{dk}\, kS\left(\frac{-1}{k}\right)\right] = \lim_{k\to 0} \frac{d}{dk} \ln\left[kS\left(\frac{-1}{k}\right)\right] . \tag{94}$$

By performing the indicated operations on the polynomial expression (76) of S, we obtain the unmanageable, but explicit, result

$$Q = \sum_{i,\,j} \mu_i \lambda_j$$

$$\frac{\sum\limits_{\substack{mn-1 \\ 2 \text{ terms}}} \epsilon_{l-1}^{(0)} \prod\limits_{i=1}^{l} \prod\limits_{j=1}^{mn-1-l} \frac{k_{ri}+k_{sj}}{k_{ri}-k_{sj}} \left[\sum\limits_{i=1}^{l} \sum\limits_{j=1}^{mn-1-l} \frac{1}{k_{ri}} - \frac{\rho\,(1/k_{sj})}{k_{sj}} \right] \rho\,(1/k_{sj})}{\sum\limits_{\substack{mn-1 \\ 2 \text{ terms}}} \epsilon_{l-1}^{(0)} \prod\limits_{i=1}^{l} \prod\limits_{j=1}^{mn-1-l} \frac{k_{ri}+k_{sj}}{k_{ri}-k_{sj}} \rho\,(1/k_{sj})} \tag{95}$$

A less arduous method for determining Q can be found by noting from equation (58) that

$$S\,(0) = \sum_{a} L_a\,(1 - e^{-k_a \tau_1}) + Q. \tag{96}$$

Substituting for $S(0)$ from equation (84) and L_a from equation (91), we have

$$Q = \sqrt{\frac{\bar{\lambda}}{3}} \frac{G\,(0)}{F\,(0)} - \sum_{a} L_a\,(\infty) \frac{G_a\,(0)}{F\,(0)} (1 - e^{-k_a \tau_1}) . \tag{97}$$

The explicit expression for the emergent intensity is obtained by substituting the polynomial expression (76) for S in equation (57), yielding

$$I\,(0,\,\mu\lambda) = \frac{3}{\bar{\lambda}} \frac{F}{4} \frac{(-1)^{mn} \prod\limits_{a} k_a}{W\,(\mu\lambda)\,F\,(0)} \left[P\,(-\mu\lambda)\,G\,(-\mu\lambda) + e^{-\tau_1/\mu\lambda} P\,(\mu\lambda)\,G\,(\mu\lambda) \right] . \tag{98}$$

Remembering definition (72) for $\mathfrak{S}$ and relation (83), we can write more conveniently

$$I\,(0,\,\mu\lambda) = \sqrt{\frac{3}{\bar{\lambda}}} \frac{F}{4} \frac{(-1)^{mn} P\,(-\mu\lambda)}{\prod\limits_{i,\,j} \mu_i \lambda_j R\,(-\mu\lambda)} \left[\frac{G\,(-\mu\lambda) + \rho\,(\mu\lambda)\,G\,(\mu\lambda)}{R\,(\mu\lambda)\,F\,(0)} \right] . \tag{99}$$

But here we recognize at once that the common factor is merely the nongray analogue of Chandrasekhar's H-function (*R.T.*, III, eq. [60]),

$$H\,(\mu\lambda) = \frac{(-1)^{mn} P\,(-\mu\lambda)}{\prod\limits_{i,\,j} \mu_i \lambda_j R\,(-\mu\lambda)} , \tag{100}$$

so that

$$I\,(0,\,\mu\lambda) = \sqrt{\frac{3}{\bar{\lambda}}} \frac{F}{4} H\,(\mu\lambda) \left[\frac{G\,(-\mu\lambda) + \rho\,(\mu\lambda)\,G\,(\mu\lambda)}{R\,(\mu\lambda)\,F\,(0)} \right] . \tag{101}$$

Since the nongray, semi-infinite emergent intensity is given by (cf. *R.T.*, III, eq. [61])

$$I\,(0,\,\mu\lambda)_{\tau_1 \to \infty} = \sqrt{\frac{3}{\bar{\lambda}}} \frac{F}{4} H\,(\mu\lambda) , \tag{102}$$

we see once again that *the finite atmosphere differs from the corresponding semi-infinite case merely by the "finite factor"*

$$\frac{I(0, \mu\lambda)}{I(0, \mu\lambda)_{\tau_1 \to \infty}} = \frac{G(-\mu\lambda) + \rho(\mu\lambda) G(\mu\lambda)}{R(\mu\lambda) F(0)} \tag{103}$$

The source function, equation (43), can be written

$$B(\tau) = \frac{3}{\bar{\lambda}} \frac{F}{4} \left\{ \sum_a L_a [e^{-k_a \tau} - e^{-k_a(\tau_1 - \tau)}] + \tau + Q \right\} \tag{104}$$

Upon substituting from equations (91) and (97) for L_a and Q, we obtain

$$B(\tau) = \frac{3}{\bar{\lambda}} \frac{F}{4} \left\{ \tau + \sqrt{\frac{\bar{\lambda}}{3}} \frac{G(0)}{F(0)} - \sum_a L_a(\infty) \frac{G_a(0)}{F(0)} [(1 - e^{-k_a \tau}) - e^{-k_a \tau_1}(1 + e^{k_a \tau})] \right\}. \tag{105}$$

This completes the formal solution of the problem.

RELATIONS ESTABLISHED BETWEEN THE TWO METHODS

In recapitulation, it is instructive to display side by side the equivalent expressions for the various parameters of the problem. Thus from equations (27), (32), (57), and (84) we obtain equivalent relations between the grazing emergent intensity and the flux

$$I(0, 0) = \frac{F}{2(\alpha_1 + \beta_1)} = \sqrt{\frac{3}{\bar{\lambda}}} \frac{F}{4} \frac{G(0)}{F(0)}. \tag{106}$$

Since the source function at the top of the atmosphere is equal to the grazing emergent intensity, the Hopf-Bronstein constant for the invariance and the finite-stream methods is

$$\frac{B(0)}{F} = \frac{1/2}{\alpha_1 + \beta_1} = \sqrt{\frac{3}{\bar{\lambda}}} \frac{G(0)}{4F(0)}. \tag{107}$$

The limb darkening can be expressed alternatively in the two schemes from equations (28), (32), and (101) as

$$\frac{I(0, \mu\lambda)}{I(0, 0)} = X(\mu\lambda) + Y(\mu\lambda) = H(\mu\lambda) \left[\frac{G(-\mu\lambda) + \rho(\mu\lambda) G(\mu\lambda)}{R(\mu\lambda) G(0)} \right] \tag{108}$$

Since, from *R.T.*, VIII, equation (4),

$$X(\mu\lambda) \to H(\mu), \qquad Y(\mu\lambda) \to 0,$$

and

$$G(-\mu\lambda) \to R(\mu\lambda), \qquad \text{as} \qquad \tau_1 \to \infty \tag{109}$$

from equation (68), we must associate the term involving $G(-\mu\lambda)$ with the X-functions. Thus the finite-stream approximations to the nongray X- and Y-functions are

$$X(\mu\lambda) = H(\mu\lambda) \frac{G(-\mu\lambda)}{R(\mu\lambda) G(0)} \tag{110}$$

and

$$Y(\mu\lambda) = H(\mu\lambda) \frac{\rho(\mu\lambda) G(\mu\lambda)}{R(\mu\lambda) G(0)}. \tag{111}$$

Except for one hiatus, we have developed complete, parallel solutions to the planetary thermal problem. That gap is this: no exact solution for the source function has been obtained analogous to the approximate expression (105). Recently Yamamoto (1955), by extending the method of Mark (1947), has obtained the following exact solution for a *gray, finite* atmosphere:

$$B(\tau) = \frac{3F}{4}\left\{\tau + Q - \frac{L}{2\sqrt{3}}\left[\int_0^1 \frac{e^{-\tau/\mu} - e^{-(\tau_1-\tau)/\mu}}{H(\mu)Z(\mu)}\,d\mu\right]\right\}, \tag{112}$$

where

$$Q = \frac{\alpha_2(\infty) + \{[(1/3) + E_4(\tau_1)]I_1(\tau_1) - [(1/2) - E_3(\tau_1)]I_2(\tau_1)\}\alpha_1(\infty)/f(\tau_1)}{\alpha_1(\infty) + \{[(1/2) + E_3(\tau_1)]I_1(\tau_1) - [1 - E_2(\tau_1)]I_2(\tau_1)\}\alpha_1(\infty)/f(\tau_1)} \tag{113}$$

and

$$L = \frac{\alpha_1(\infty)}{\alpha_1(\infty) + \{[(1/2) + E_3(\tau_1)]I_1(\tau_1) - [1 - E_2(\tau_1)]I_2(\tau_1)\}\alpha_1(\infty)/f(\tau_1)}. \tag{114}$$

We have rewritten Yamamoto's expressions slightly, using the fact that

$$q(\infty) = \frac{\alpha_2(\infty)}{\alpha_1(\infty)}. \tag{115}$$

In equations (113) and (114), $I_1(\tau_1)$ and $I_2(\tau_1)$ are complicated integrals which have been evaluated numerically by Yamamoto. We now show how this lengthy procedure can be avoided and the constants Q and L be simply expressed as moments of the X- and Y-functions. Equation (36) already tells us that

$$Q = \frac{\alpha_2 + \beta_2}{\alpha_1 + \beta_1}, \tag{116}$$

while a comparison of the denominators of equations (113) and (114) leads to the conclusion that

$$L = \frac{2/\sqrt{3}}{\alpha_1 + \beta_1}, \tag{117}$$

where we have used the fact (*R.T.*, V, eq. [26]) that

$$\alpha_1(\infty) = \frac{2}{\sqrt{3}}. \tag{118}$$

The values of the constants have been evaluated from Chandrasekhar's (1948) tables for the X- and Y- functions, corrected to agree with his machine tabulation (Chandrasekhar and Elbert 1952) and are listed in Table 1. The exact values, $Q(0) = \frac{2}{3}$ and $L(0) = 2/\sqrt{3}$, cast doubt upon the accuracy of Yamamoto's final four figures in his corresponding tabulation.

By using Hopf's q-function, we can write the source function in an exact expression of surpassing elegance and simplicity. This q-function, defined for a *gray, semi-infinite* atmosphere, is given as

$$B(\tau) = \tfrac{3}{4}F[\tau + q(\tau)]. \tag{119}$$

By permitting $\tau_1 \to \infty$, from equation (112) we can write

$$q(\tau) = \frac{\alpha_2(\infty)}{\alpha_1(\infty)} - \frac{1}{3\alpha_1(\infty)}\int_0^1 \frac{e^{-\tau/\mu}\,d\mu}{H(\mu)Z(\mu)}. \tag{120}$$

TABLE 1

Q- and L-Constants for a Gray, Finite Atmosphere

τ_1	Q	L
0	0.66666667	1.15470054
0.005	0.66747	1.14378
0.01	0.66821	1.13662
0.02	0.66962	1.12571
0.03	0.67089	1.11719
0.04	0.67210	1.11012
0.05	0.67323	1.10397
0.06	0.67429	1.09861
0.07	0.67529	1.09381
0.08	0.67625	1.08948
0.09	0.67716	1.08554
0.10	0.67804	1.08193
0.11	0.67887	1.07859
0.12	0.67967	1.07549
0.13	0.68045	1.07261
0.14	0.68118	1.06992
0.15	0.68189	1.06740
0.16	0.68257	1.06504
0.17	0.68323	1.06280
0.18	0.68386	1.06069
0.19	0.68448	1.05871
0.20	0.68507	1.05682
0.25	0.68776	1.04864
0.30	0.6901	1.0421
0.35	0.6921	1.0368
0.40	0.6938	1.0325
0.45	0.6954	1.0287
0.5	0.6968	1.0256
0.6	0.6992	1.0201
0.7	0.7010	1.0159
0.8	0.7025	1.0126
0.9	0.7039	1.0101
1.0	0.7049	1.0079
	0.71044609	1.00000000

This q-function has been studied extensively and evaluated to a high degree of accuracy by Kourganoff (1952), using a variational method. By substituting expression (120) for $q(\tau)$ in equation (112), we obtain

$$B(\tau) = \tfrac{3}{4}F\{\tau + Q(\tau_1) - L(\tau_1)\,[q(\tau_1 - \tau) - q(\tau)]\}. \tag{121}$$

DEDUCTIONS AND CONCLUSIONS

Choice of Band-Absorption Model

The formalism framed thus far has been noncommittal as to the choice of the band-absorption model. However, the calculation of the quadrature constants (the b_j's and λ_j's of eq. [39]) is greatly facilitated if a model of some simplicity is chosen.

An appropriate array, which reproduces the main features of a far-infrared absorption band, is the Elsasser (1938) model of equally spaced, equally intense, Lorentz-broadened lines. The absorption coefficient is

$$\kappa_\nu = \frac{S}{d}\,\frac{\sinh \beta}{\cosh \beta - \cos 2\pi\nu/d}, \tag{122}$$

with

$$\lambda = \frac{\bar{\kappa}}{\kappa_\nu} = \frac{\cosh \beta - \cos 2\pi\nu/d}{\sinh \beta}, \qquad \lambda = \coth \beta, \tag{123}$$

where S and d are the line intensity and spacing and the line-overlap parameter, $\beta = 2\pi a/d$ is the ratio of line half-width to spacing. In addition to its analytical simplicity, the Elsasser model incorporates in a single parameter the gamut from complete line separation to complete overlapping. For $\beta \ll 1$ the lines partake of a narrow, intense, δ-function representation, while for $\beta \gg 1$ the overlapping becomes complete and approaches the gray model atmosphere ($\lambda \to 1$) of constant absorption coefficient.

The quadrature constants of the Elsasser band have been calculated, using a two-point Gaussian formula for various values of the line-overlap parameter β (King 1955*a*).

Hopf-Bronstein Constant

Figure 1 illustrates the effect of nongrayness and varying atmospheric thickness on the Hopf-Bronstein constant. The quantity actually plotted is the constant L, which from equations (33) and (117) is the Hopf-Bronstein constant normalized by division with the gray, semi-infinite value. Thus

$$L = \frac{[B(0)]_{\tau_1,\,\beta}}{[B(0)]_{\infty,\,\infty}} = \frac{2/\sqrt{3}}{\alpha_1 + \beta_1}. \tag{124}$$

For the nongray cases L is calculated from the equivalent approximate expression, which from equations (84), (96), and (107), is

$$L = \sqrt{3}\,\tanh \beta\left[Q + \sum_a L_a\,(1 - e^{-k_a\tau_1})\right]. \tag{125}$$

The constants Q and L_a have been computed for representative pairs of τ_1 and β and are tabulated elsewhere. Figure 1 and Table 2 show that the effects of "finiteness" and nongrayness act in opposite directions. A finite atmosphere enhances, while a deviation from grayness diminishes, the grazing intensity and upper boundary source function over the gray, semi-infinite case.

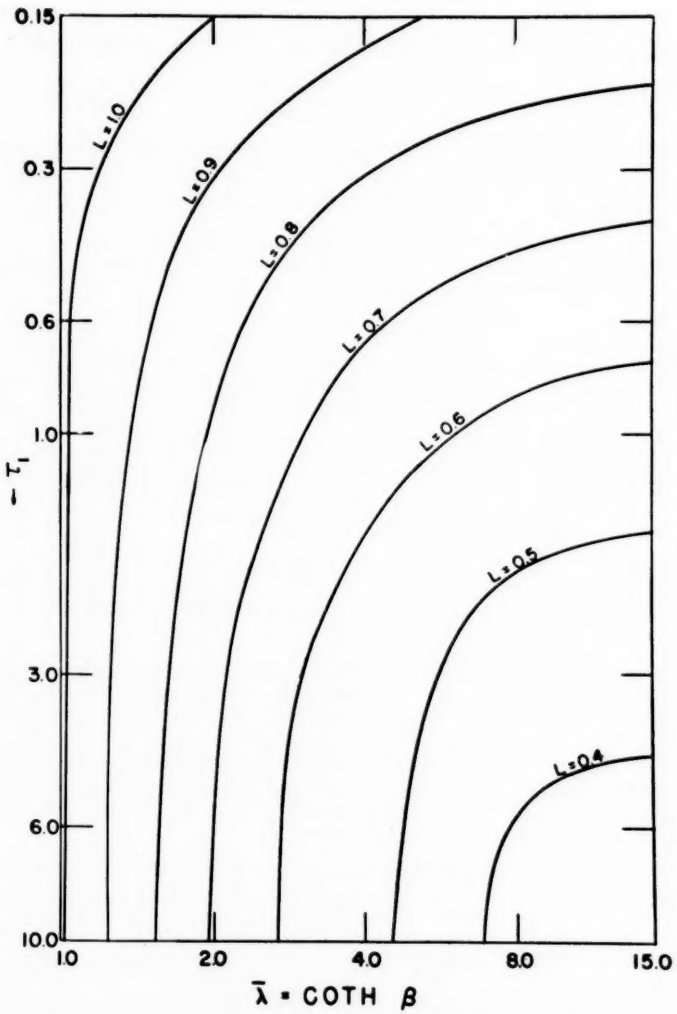

FIG. 1.—Map of Hopf-Bronstein relation as function of line structure and thickness of the atmosphere.

Effect of Band Structure

The monochromatic law of darkening for a nongray, semi-infinite atmosphere in radiative equilibrium is given by equation (102),

$$I(0, \mu\lambda) = \sqrt{\frac{3}{\lambda}}\frac{F}{4}H(\mu\lambda) , \tag{126}$$

with the nongray H-function a solution of the integral equation (King 1955*b*)

$$H(\mu\lambda) = 1 + \frac{\mu\lambda}{2}H(\mu\lambda)\int_0^1\int_0^1 \frac{H(\mu'\lambda')}{\mu\lambda + \mu'\lambda'}\,d\mu'\,\frac{d(\nu'/\Delta\nu)}{\lambda'} . \tag{127}$$

This H-function has been computed by IBM 650 equipment for the Elsasser band model, using four values of the line-overlap parameter β (see Table 3).

TABLE 2

L-CONSTANTS FOR A GRAY, FINITE ATMOSPHERE

τ_1	β					
	0.1	0.3	0.6	1.0	2.0	∞
0.2	0.8131*	0.8921*	0.9695*	1.0244*	1.0649*	1.0549†
1.0	.4901*	.6591*	.8175*	0.9208*	1.0016*	1.0107†
3.0	.4522‡	.5667*	.7487*	0.8792*	0.9808*	
∞	0.3160§	0.5400§	0.7330§	0.8730§	0.9820§	1.0000§

* $n \times m = 2 \times 2$ approximation.
† Exact (Chandrasekhar 1948; Chandrasekhar and Elbert 1952).
‡ $n \times m = 2 \times 3$ approximation. § Exact (King 1955*b*).

The emergent intensity for a nongray band is simply

$$I_\beta(0, \mu) = \sqrt{\frac{3}{\lambda}}\frac{F}{4}\int_0^1 H(\mu\lambda)\,d\frac{\nu}{\Delta\nu} = \sqrt{\frac{3}{\lambda}}\frac{F}{4}H_\beta(\mu) . \tag{128}$$

These Elsasser band H-functions are plotted in Figure 2. The tendency of line structure to sharpen the contrast between the center and limb of the planetary disk is noteworthy. By extrapolation we can conclude that, as the spectral lines become increasingly narrow, the limb intensity approaches zero and becomes thermally invisible.

The source function for an Elsasser band model semi-infinite atmosphere, drawn in Figure 3, shows a similar behavior. Line structure invariably tends to lower the equilibrium temperature over the corresponding gray case, the cooling effect increasing monotonically with the deviation from grayness.

Effect of Finite Atmospheric Thickness

The law of darkening for a gray ($\lambda = 1$), finite atmosphere is, from equation (108),

$$\frac{I(0, \mu)}{I(0, 0)} = X(\mu) + Y(\mu) , \tag{129}$$

where X and Y are, of course, functions of τ_1 as well as μ. Table 4, compiled from the tabulations of Chandrasekhar, Elbert, and Franklin (1952), lists these functions, and in Figure 4 curves are drawn for several optical thicknesses. The lower black-body boundary of the finite atmosphere betrays its presence by a characteristic leveling-off or "shouldering" tendency of the curve. This shoulder effect becomes more pronounced with

TABLE 3

Non-Gray H-Functions for Elsasser Band Models

μ		$\upsilon/\frac{1}{2}d=0.0$	$\upsilon/\frac{1}{2}d=0.1$	$\upsilon/\frac{1}{2}d=0.2$	$\upsilon/\frac{1}{2}d=0.3$	$\upsilon/\frac{1}{2}d=0.4$
0.1	$\beta = 0.1$	1.11131	1.55678	2.08943	2.56789	3.00463
	$\beta = 0.3$	1.11929	1.19300	1.36195	1.56651	1.77707
	$\beta = 0.6$	1.12249	1.14643	1.21101	1.30183	1.40566
	$\beta = 1.0$	1.14628	1.15674	1.18640	1.23088	1.28460
0.2	$\beta = 0.1$	1.18694	1.80874	2.52109	3.18857	3.81519
	$\beta = 0.3$	1.18797	1.31007	1.57896	1.89615	2.22119
	$\beta = 0.6$	1.20861	1.25009	1.36079	1.51505	1.69077
	$\beta = 1.0$	1.25638	1.27512	1.32814	1.40751	1.50336
0.3	$\beta = 0.1$	1.24901	1.99172	2.84827	3.66999	4.46199
	$\beta = 0.3$	1.24779	1.40921	1.75793	2.16673	2.58930
	$\beta = 0.6$	1.28556	1.34227	1.49305	1.70285	1.94245
	$\beta = 1.0$	1.35745	1.38374	1.45813	1.56961	1.70458
0.4	$\beta = 0.1$	1.30253	2.14169	3.12329	4.08497	5.03347
	$\beta = 0.3$	1.30188	2.49741	1.91536	2.40616	2.91958
	$\beta = 0.6$	1.35670	1.42731	1.61486	1.87614	2.17581
	$\beta = 1.0$	1.45300	1.48645	1.58118	1.72338	1.89600
0.5	$\beta = 0.1$	1.34998	2.27177	3.36678	4.46040	5.56127
	$\beta = 0.3$	1.35179	1.57795	2.05855	2.62608	3.22708
	$\beta = 0.6$	1.42369	1.50732	1.72948	2.03978	2.39748
	$\beta = 1.0$	1.54474	1.58509	1.69952	1.87164	2.08110
0.6	$\beta = 0.1$	1.39281	2.38826	3.58867	4.80954	6.06042
	$\beta = 0.3$	1.39848	1.65271	2.19155	2.83258	3.51933
	$\beta = 0.6$	1.48749	1.58351	1.83881	2.19655	2.61100
	$\beta = 1.0$	1.63361	1.68073	1.81444	2.01593	2.26173
0.7	$\beta = 0.1$	1.43197	2.49476	3.79478	5.13980	6.53958
	$\beta = 0.3$	1.44256	1.72294	2.31685	3.02927	3.80069
	$\beta = 0.6$	1.54875	1.65669	1.94403	2.34811	2.81853
	$\beta = 1.0$	1.72030	1.77403	1.92671	2.15722	2.43905
0.8	$\beta = 0.1$	1.46814	2.59350	3.98883	5.45613	7.00378
	$\beta = 0.3$	1.48448	1.79948	2.43611	3.21849	4.07390
	$\beta = 0.6$	1.60794	1.72741	2.04597	2.49560	3.02147
	$\beta = 1.0$	1.80518	1.86547	2.03691	2.29616	2.61380
0.9	$\beta = 0.1$	1.50183	2.68604	4.17327	5.76136	7.45657
	$\beta = 0.3$	1.52455	1.85293	2.55053	3.40177	4.34084
	$\beta = 0.6$	1.66536	1.79607	2.14523	2.63985	3.22077
	$\beta = 1.0$	1.88861	1.95538	2.14539	2.43324	2.78652
1.0	$\beta = 0.1$	1.53341	2.77343	4.35000	6.05785	7.90014
	$\beta = 0.3$	1.56304	1.91380	2.66095	3.58038	4.60267
	$\beta = 0.6$	1.72127	1.86300	2.24225	2.78141	3.41717
	$\beta = 1.0$	1.97083	2.04401	2.25249	2.56875	2.95762

TABLE 3—continued

μ		$v/\frac{1}{2}d=0.5$	$v/\frac{1}{2}d=0.6$	$v/\frac{1}{2}d=0.7$	$v/\frac{1}{2}d=0.8$	$v/\frac{1}{2}d=0.9$	$v/\frac{1}{2}d=1.0$
0.1	$\beta = 0.1$	3.39622	3.73532	4.01276	4.21915	4.34669	4.38982
	$\beta = 0.3$	1.97744	2.15661	2.30593	2.41818	2.48790	2.51155
	$\beta = 0.6$	1.51177	1.61130	1.69690	1.76256	1.80382	1.81788
	$\beta = 1.0$	1.34186	1.39720	1.44586	1.48373	1.50775	1.51597
0.2	$\beta = 0.1$	4.39416	4.91002	5.34217	5.66942	5.87389	5.94354
	$\beta = 0.3$	2.53328	2.81647	3.05586	3.23807	3.35216	3.39098
	$\beta = 0.6$	1.87056	2.03994	2.18634	2.29919	2.37037	2.39469
	$\beta = 1.0$	1.60568	1.70490	1.79232	1.86057	1.90393	1.91878
0.3	$\beta = 0.1$	5.21254	5.89518	6.47605	6.92065	7.20046	7.29581
	$\beta = 0.3$	3.00104	3.38006	3.70432	3.95327	4.10998	4.16354
	$\beta = 0.6$	2.18888	2.42251	2.62564	2.78296	2.88251	2.91656
	$\beta = 1.0$	1.84908	1.98965	2.11394	2.21117	2.27304	2.29426
0.4	$\beta = 0.1$	5.95061	6.79740	7.52559	8.08669	8.44131	8.56274
	$\beta = 0.3$	3.42677	3.89917	4.30691	4.62182	4.82090	4.88890
	$\beta = 0.6$	2.48592	2.78168	3.04011	3.24102	3.36848	3.41215
	$\beta = 1.0$	2.08140	2.26232	2.42263	2.54832	2.62843	2.65594
0.5	$\beta = 0.1$	6.64275	7.65287	8.52806	9.20598	9.63537	9.78282
	$\beta = 0.3$	3.82790	4.39271	4.88353	5.26427	5.50555	5.58831
	$\beta = 0.6$	2.76978	3.12666	3.43979	3.68406	3.83921	3.89241
	$\beta = 1.0$	2.30670	2.52742	2.72342	2.87737	2.97554	3.00928
0.6	$\beta = 0.1$	7.30540	8.47853	9.50074	10.29601	10.80030	10.97333
	$\beta = 0.3$	4.21288	4.86973	5.44351	5.89015	6.17398	6.27117
	$\beta = 0.6$	3.04465	3.46218	3.82980	4.11726	4.30015	4.36291
	$\beta = 1.0$	2.52714	2.78734	3.01887	3.20093	3.31719	3.35711
0.7	$\beta = 0.1$	7.94786	9.28376	10.45369	11.36557	11.94600	12.14477
	$\beta = 0.3$	4.58652	5.33547	5.99233	6.50491	6.83107	6.94300
	$\beta = 0.6$	3.31301	3.79104	4.21310	4.54360	4.75432	4.82660
	$\beta = 1.0$	2.74401	3.04358	3.31055	3.52069	3.65497	3.70110
0.8	$\beta = 0.1$	8.57486	10.07404	11.39147	12.42159	13.07702	13.30229
	$\beta = 0.3$	4.95184	5.79274	6.53275	7.11162	7.48027	7.60688
	$\beta = 0.6$	3.57654	4.11489	4.59137	4.96512	5.20346	5.28541
	$\beta = 1.0$	2.95814	3.29701	3.59939	3.83759	3.98987	4.04220
0.9	$\beta = 0.1$	9.19075	10.85364	12.31906	13.46711	14.19849	14.44982
	$\beta = 0.3$	5.31082	6.24376	7.06714	7.71218	8.12348	8.26480
	$\beta = 0.6$	3.83627	4.43488	4.96586	5.38286	5.64892	5.74053
	$\beta = 1.0$	3.17017	3.54830	3.88599	4.15231	4.32264	4.38116
1.0	$\beta = 0.1$	9.79768	11.62453	13.23802	14.50326	15.31159	15.58646
	$\beta = 0.3$	5.66460	6.68986	7.59676	8.30841	8.76232	8.91822
	$\beta = 0.6$	4.09308	4.75195	5.33732	5.79761	6.09162	6.19272
	$\beta = 1.0$	3.38055	3.79788	4.17092	4.46531	4.65365	4.71854

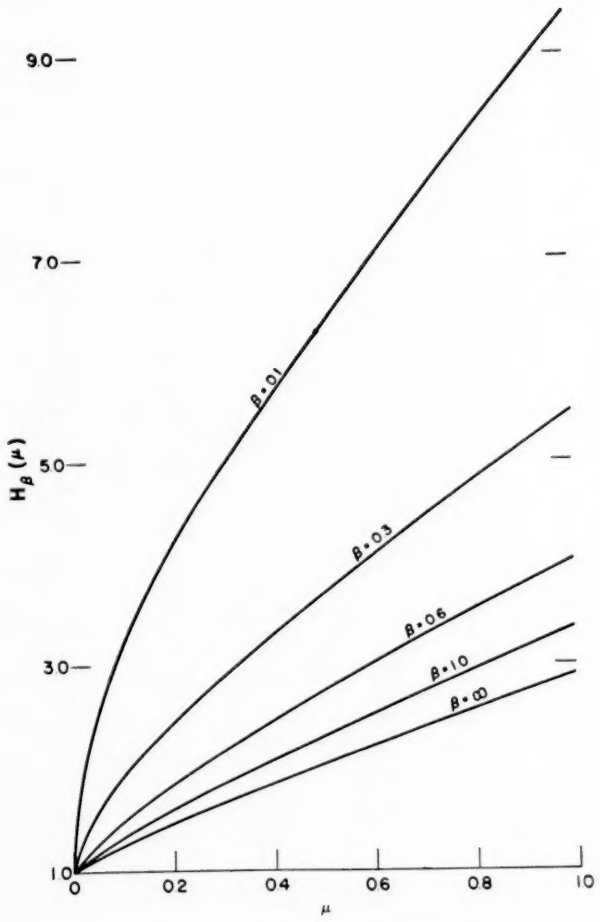

FIG. 2.—Elsasser band-model H-functions

increasing transparency of the atmosphere, the intensity-curve approaching a step function as $\tau_1 \to 0$.

The equation of the envelope to the family of intensity-curves follows readily from a theorem of Chandrasekhar on X- and Y-functions (*R.T.*, VIII, eqs. [13] and [14]), which states that

$$\frac{\partial X(\mu, \tau_1)}{\partial \tau_1} = \frac{\beta_{-1}(\tau_1)}{2} Y(\mu, \tau_1) \tag{130}$$

and

$$\frac{\partial Y(\mu, \tau_1)}{\partial \tau_1} = \frac{\beta_{-1}(\tau_1)}{2} X(\mu, \tau_1) - \frac{Y(\mu, \tau_1)}{\mu}. \tag{131}$$

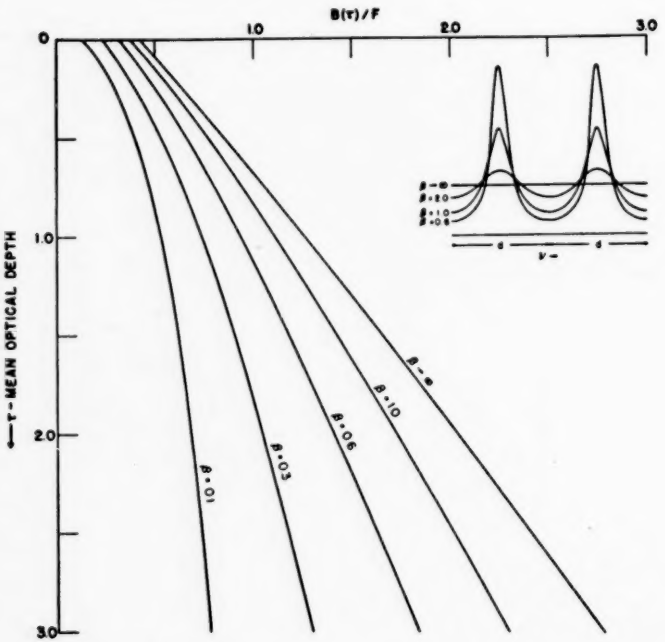

FIG. 3.—Source functions for Elsasser band-model semi-infinite atmospheres

Clearly, the envelope-curve must satisfy the condition

$$\frac{\partial}{\partial \tau_1}[X(\mu, \tau_1) + Y(\mu, \tau_1)] = 0. \tag{132}$$

This leads immediately to the transcendental equation for the envelope-curve,

$$X(\mu, \tau_1) + Y(\mu, \tau_1) = \frac{2}{\mu} \frac{Y(\mu, \tau_1)}{\beta_{-1}(\tau_1)}. \tag{133}$$

TABLE 4

X- and Y-Functions for a Gray Atmosphere

μ	$\tau_1 = 0.05$	$\tau_1 = 0.10$	$\tau_1 = 0.15$	$\tau_1 = 0.20$	$\tau_1 = 0.25$	$\tau_1 = 0.5$	$\tau_1 = 1.0$
0	1.00000	1.00000	1.00000	1.00000	1.00000	1.0000	1.0000
0.02	1.15353	1.07683	1.06836	1.06647	1.06569	1.0638	1.0630
0.04	1.39605	1.20623	1.14774	1.12887	1.12233	1.1157	1.1135
0.06	1.56446	1.35162	1.25351	1.20805	1.18665	1.1646	1.1608
0.08	1.67743	1.47659	1.36227	1.29767	1.26112	1.2133	1.2060
0.10	1.75690	1.57795	1.46163	1.38723	1.33982	1.2634	1.2496
0.12	1.81547	1.65982	1.54869	1.47115	1.41752	1.3156	1.2926
0.14	1.86029	1.72661	1.62392	1.54747	1.49127	1.3696	1.3353
0.16	1.89563	1.78181	1.68889	1.61597	1.55975	1.4244	1.3778
0.18	1.92420	1.82807	1.74517	1.67720	1.62267	1.4793	1.4204
0.20	1.94775	1.86731	1.79421	1.73190	1.68016	1.5334	1.4632
0.22	1.96752	1.90098	1.83724	1.78087	1.73262	1.5861	1.5062
0.24	1.98430	1.93017	1.87521	1.82481	1.78047	1.6373	1.5494
0.26	1.99876	1.95568	1.90892	1.86442	1.82415	1.6866	1.5926
0.28	2.01133	1.97818	1.93904	1.90025	1.86414	1.7339	1.6357
0.30	2.02235	1.99816	1.96609	1.93275	1.90078	1.7791	1.6786
0.32	2.03211	2.01602	1.99050	1.96236	1.93450	1.8222	1.7210
0.34	2.04080	2.03208	2.01264	1.98946	1.96555	1.8633	1.7632
0.36	2.04858	2.04658	2.03278	2.01431	1.99424	1.9024	1.8046
0.38	2.05561	2.05975	2.05123	2.03716	2.02083	1.9396	1.8454
0.40	2.06198	2.07176	2.06814	2.05826	2.04549	1.9751	1.8855
0.42	2.06777	2.08277	2.08368	2.07781	2.06845	2.0088	1.9248
0.44	2.07306	2.09289	2.09805	2.09594	2.08985	2.0409	1.9634
0.46	2.07792	2.10219	2.11138	2.11281	2.10985	2.0716	2.0012
0.48	2.08239	2.11081	2.12375	2.12854	2.12858	2.1008	2.0380
0.50	2.08653	2.11880	2.13527	2.14326	2.14615	2.1285	2.0741
0.52	2.09036	2.12625	2.14603	2.15702	2.16266	2.1551	2.1092
0.54	2.09392	2.13318	2.15609	2.16995	2.17821	2.1804	2.1437
0.56	2.09723	2.13965	2.16552	2.18211	2.19287	2.2046	2.1772
0.58	2.10033	2.14573	2.17439	2.19357	2.20671	2.2277	2.2099
0.60	2.10322	2.15142	2.18272	2.20437	2.21981	2.2499	2.2416
0.62	2.10595	2.15678	2.19059	2.21456	2.23223	2.2711	2.2727
0.64	2.10850	2.16182	2.19801	2.22423	2.24399	2.2914	2.3030
0.66	2.11091	2.16659	2.20503	2.23340	2.25517	2.3109	2.332
0.68	2.11318	2.17110	2.21169	2.24210	2.26582	2.3296	2.362
0.70	2.11532	2.17536	2.21798	2.25035	2.27593	2.3476	2.391
0.72	2.11735	2.17940	2.22398	2.25822	2.28558	2.3648	2.416
0.74	2.11928	2.18325	2.22969	2.26573	2.29479	2.3814	2.443
0.76	2.12110	2.18688	2.23511	2.27288	2.30359	2.3975	2.469
0.78	2.12284	2.19036	2.24029	2.27969	2.31200	2.4128	2.494
0.80	2.12448	2.19367	2.24522	2.28623	2.32005	2.4276	2.518
0.82	2.12606	2.19683	2.24994	2.29247	2.32777	2.4420	2.543
0.84	2.12756	2.19984	2.25445	2.29845	2.33515	2.4557	2.566
0.86	2.12899	2.20273	2.25878	2.30419	2.34225	2.4690	2.588
0.88	2.13036	2.20549	2.26292	2.30969	2.34906	2.4819	2.611
0.90	2.13167	2.20813	2.26688	2.31496	2.35563	2.4943	2.632
0.92	2.13292	2.21067	2.27070	2.32003	2.36193	2.5062	2.653
0.94	2.13413	2.21310	2.27436	2.32490	2.36799	2.5179	2.673
0.96	2.13528	2.21544	2.27788	2.32960	2.37384	2.5291	2.693
0.98	2.13639	2.21768	2.28126	2.33411	2.37947	2.5400	2.713
1.00	2.13745	2.21985	2.28453	2.33846	2.38491	2.5506	2.732

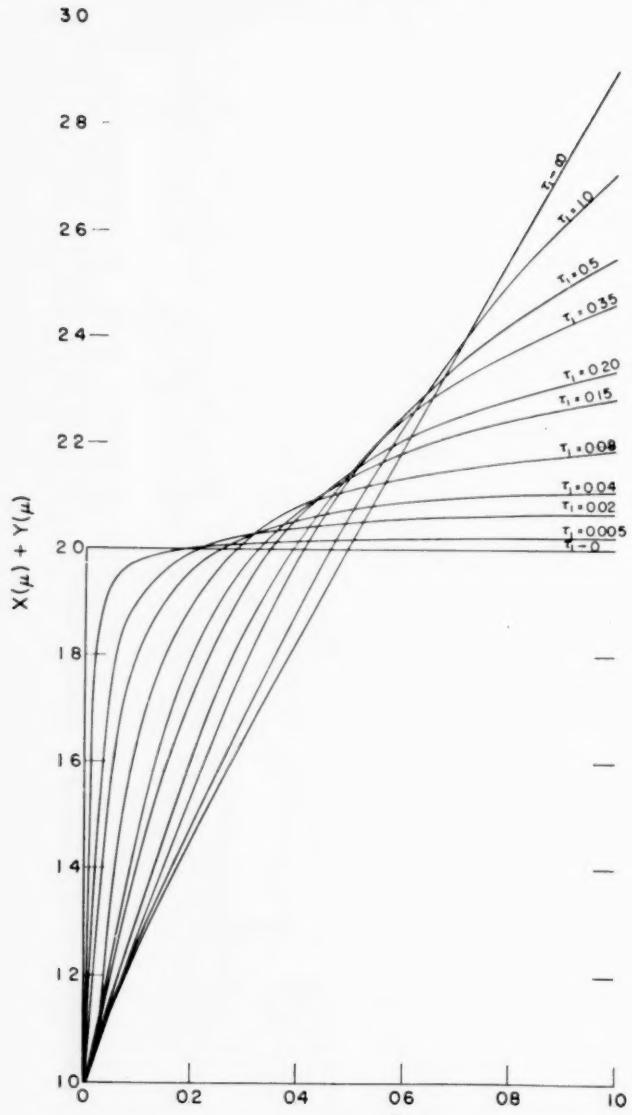

FIG. 4.—Law of darkening for gray atmospheres of varying thicknesses

The measure of the author's debt to Professor S. Chandrasekhar may be gained from the number of times his treatise on *Radiative Transfer* is cited in the article. The author wishes to acknowledge, as well, the computational help of John J. Hanrahan.

REFERENCES

Ambarzumian, V. A. 1942, *Russ. Astr. J.*, **19**, 1.
Chandrasekhar, S. 1947, *Ap. J.*, **106**, 152.
———. 1948, *ibid.*, **108**, 92.
———. 1950, *Radiative Transfer* (Oxford: Clarendon Press).
Chandrasekhar, S., and Elbert, D. 1952, *Ap. J.*, **115**, 269.
Chandrasekhar, S., Elbert, D., and Franklin, A. 1952, *Ap. J.*, **115**, 244.
Elsasser, W. M. 1938, *Phys. Rev.*, **54**, 126.
King, J. I. F. 1955*a*, *Ap. J.*, **121**, 425.
———. 1955*b*, *ibid.*, p. 711.
Kourganoff, V. 1952, *Basic Methods in Transfer Problems* (Oxford: Clarendon Press).
Mark, C. 1947, *Phys. Rev.*, **72**, 558.
Wick, G. C. 1943, *Zs. f. Phys.*, **121**, 702.
Yamamoto, G. 1955, *Sci. Repts. Tohoku University*, Series 5, Geophysics, **7**, 1.

THE EXTINCTION OF THE LIGHT OF THE NIGHT SKY. I*

G. COSTANTINE
Ministry of Education
AND
A. HAMMAD
Faculty of Science, Cairo University
Received September 21, 1954; revised February 21, 1956

ABSTRACT

The mathematical theory of the plane-parallel model of the scattering atmosphere with an emitting layer above it is being refined by making use of Chandrasekhar's recent work on radiative transfer. Thus *exact* expressions are derived for the intensity of the diffused light received at the ground for three forms of the emission from the layer. These exact expressions are less elaborate to evaluate than are the approximate expressions adopted by the previous investigators. Numerical comparison is then made between the exact and approximate solutions, and questions of interest in connection with the nightglow are discussed in the light of the numerical results.

INTRODUCTION

Methods of observation of the night-sky spectrum and its interpretation have advanced to an extent that necessitates a more adequate theory for the determination of the heights of emission than is yet available. The problem seems to have been first dealt with by van Rhijn (1921), who considered the emitting layer to be thin and neglected the attenuation of radiation in its passage through the earth's atmosphere. Attempts to allow for the attenuation of radiation by scattering were made, notably by Dufay (1938), Piotrowski (1947), and Barbier (1944, 1949, 1952). In these investigations expressions were obtained for the transmitted part of the light in the case of plane and curved atmospheres. For the diffused part, however, the curvature of the earth's surface was neglected, and only approximate expressions were obtained.

In this paper *exact* expressions are derived for the diffused part of the light received at the ground, on the basis of Chandrasekhar's exact solution of the problem of radiative transfer in a plane-stratified atmosphere. The effect of the curvature of the earth's surface on the values of the intensity of the diffused light will be discussed in Part II.

The equation of radiative transfer in a plane-stratified atmosphere in which absorption is negligible and scattering is isotropic is (Chandrasekhar 1950)

$$\mu \frac{\partial I}{\partial \tau} = -I + \tfrac{1}{2}\int_{-1}^{+1} I(\tau, \mu')\, d\mu' .$$

The following boundary conditions will be adopted:

$$\text{(i)} \qquad I_+(0, \mu) = 0 ,$$

which means that no light is returned from the ground, and

$$\text{(ii)} \qquad I_-(\tau_1, \mu) = I_0(\mu) ,$$

where τ_1 is the normal optical thickness of the atmosphere below the emitting layer; $I_0(\mu)$ defines the state of emission from the layer.

* Published with the aid of a grant from the American Astronomical Society.

The solution of this equation under these boundary conditions is, for the downgoing light,

$$I_-(\tau, \mu)\ e^{-\tau/\mu} = I_0(\mu)\ e^{-\tau_1/\mu} + \mu^{-1}\int_\tau^{\tau_1} J(\tau')\ e^{-\tau'/\mu} d\tau',$$

where

$$J(\tau) = \tfrac{1}{2}\int_{-1}^{+1} I(\tau, \mu)\, d\mu;$$

the first term corresponds to the transmitted part of the light, and the second gives the diffused part.

For the light received at the ground, we have

$$I_-(0, \mu) = I_0(\mu)\ e^{-\tau_1/\mu} + \mu^{-1}\int^{\tau_1} J(\tau')\ e^{-\tau'/\mu} d\tau'$$

$$= I_0(\mu)\ e^{-\tau_1/\mu} + D(\mu), \text{ say}.$$

According to Chandrasekhar (1950), we have

$$D(\mu) = (\tfrac{1}{2}\mu)\int_0^1 I_0(\mu')\, T(\tau_1, \mu, \mu')\, d\mu', \tag{1}$$

where

$$T(\tau_1, \mu, \mu') = \left(\frac{\mu\mu'}{\mu - \mu'}\right)[Y(\mu)\, X(\mu') - X(\mu)\, Y(\mu')],$$

$$X(\mu) = 1 + \frac{\mu}{2}\int_0^1 (\mu + \mu')^{-1}[X(\mu)\, X(\mu') - Y(\mu)\, Y(\mu')]\, d\mu',$$

and

$$Y(\mu) = e^{-\tau_1/\mu} + \frac{\mu}{2}\int_0^1 (\mu - \mu')\ [Y(\mu)\, X(\mu') - X(\mu)\, Y(\mu')]\, d\mu'. \tag{2}$$

THE EXACT EVALUATION OF THE DIFFUSED LIGHT

We now proceed to determine $D(\mu)$ for various forms of emission from the layer.

(i) Isotropic emission: in this case $I_0(\mu) = \text{Const.} = I_0$, say. Thus we get from equations (1) and (2)

$$D(\mu) = \tfrac{1}{2} I_0 [\beta_1 X(\mu) - \beta_2 Y(\mu)] + I_0 [Y(\mu) - e^{-\tau_1/\mu}],$$

where

$$\beta_1 = \int_0^1 Y(\mu')\, d\mu' \qquad \text{and} \qquad \beta_2 = \int_0^1 X(\mu')\, d\mu'.$$

It can be shown that $\beta_1 + \beta_2 = 2$, so that $D(\mu)$ takes the simple form

$$D(\mu) = \tfrac{1}{2} I_0 \beta_1 [X(\mu) + Y(\mu)] - I_0 e^{-\tau_1/\mu}. \tag{3}$$

Tables for the functions $X(\mu)$ and $Y(\mu)$ are now available (Chandrasekhar, Elbert, and Franklin 1952), so that β_1 can now be evaluated. Table 1 gives the values of β_1 for some values of τ_1.

(ii) We next consider a law of emission of the form $I_0(\mu) = I_0/\mu$, which means that

the emission from the layer in any direction is proportional to the thickness of the layer in that direction. In this case equations (1) and (2) give

$$D(\mu) = I_0 \mu^{-1} [Y(\mu) - e^{-\tau_1/\mu}] . \tag{4}$$

It may be interesting to note that the exact expressions for $D(\mu)$ given in equations (3) and (4) are less elaborate to evaluate than the approximate ones derived by Piotrowski (1947) and Barbier (1949, 1952).

(iii) Finally, we consider the case of an emission from the layer, following van Rhijn's law (1921), namely,

$$I_0(\mu) = \frac{I_0}{\sqrt{\{1 - [a \sin \theta / (a + h)]^2\}}} ,$$

where $\mu = \cos\theta$, a is the radius of the earth, and h is the height of the emitting layer above the ground. It is thought that, in this way, the plane case can be made to correspond to the actual curved case. It is interesting to note that this law of emission includes i and

TABLE 1

VALUES OF β_1

τ_1	0.05	0.10	0.15	0.20	0.25	0.50	1.00
β_1	0.9129	0.8579	0.8141	0.7771	0.7448	0.6253	0.4841

ii as limiting cases; it reduces to ii when $h/a \to 0$ and to i when $h/a \to \infty$. Law i would therefore correspond to an incident flux at the upper boundary of the scattering layer that is independent of direction, i.e., radiation from infinity ($h/a = \infty$).

For law of emission iii, the integral giving $D(\mu)$ has been evaluated by quadrature for a number of values of μ, h/a, and τ_1.

NUMERICAL RESULTS AND CONCLUSIONS

We compare in Table 2 the values of the diffused light received at the ground, obtained from the exact expressions given in the previous section, for the three laws of emission under consideration, with those obtained from the approximate expressions adopted by the previous investigators. Barbier (1949) adopts the first and second approximations of Chandrasekhar (1948, 1950), denoted in Table 2 by D_1 and D_2, respectively; the values that would be obtained from Piotrowski's approximation (1947) are denoted by D_p. It may be mentioned that Cabannes, Dufay, and Gauzit (1938) took the following values for the diffused light received at the ground for all values of h and τ_1:

$$\theta = 0^\circ \quad \text{and} \quad 80^\circ ,$$

$$D = 0.030 \quad \text{and} \quad 0.165 .$$

A glance at Table 2 will show that this is really a very rough approximation.

Table 2 indicates how the intensity of the diffused light received at the ground depends upon the direction of reception and the height of the emitting layer. It is clear that the most intense light is received from the horizontal and neighboring directions and that the intensity decreases gradually toward the zenith. Further, the intensity decreases as h increases.

Another question of interest which can be discussed in the light of the numerical results given in Table 2 is the ratio of the intensities of the diffused light received from two given directions. It may be interesting to note that this ratio is not sensitive to the variation of h but depends only on the optical thickness of the atmosphere. For instance, $D(0.2)/D(1)$ is approximately equal to 4.5 for $\tau_1 = 0.05$ and reduces to 2 for $\tau_1 = 0.50$, for all values of h.

Table 2 also indicates the degree of accuracy of the approximations adopted by Barbier (1949) and Piotrowski (1947). These approximations are quite satisfactory for large values of h/a and τ_1. For small values of h/a, however, the error becomes large, especially

TABLE 2

EXACT AND APPROXIMATE VALUES OF $D(\mu)$

$\{I_0(\mu) = I_0/\sqrt{1 - [a \sin\theta/(a+h)]^2},\ I_0 = 1\}$

h/a	Law of Emission	$\tau_1 = 0.05$ μ			$\tau_1 = 0.50$ μ		
		1.0	0.5	0.2	1.0	0.5	0.2
0.....	ii	$D_1 = 0.042$	0.081	0.191	0.333	0.520	0.703
		$D_2 = .061$	.119	.276	.411	.670	.843
		$D = .093$	.185	.415	.447	.682	.861
0.01....	iii	$D_1 = .041$	.080	.187	.326	.510	.690
		$D_2 = .053$	.104	.240	.390	.606	.800
		$D = .059$	.114	.266	.376	.582	.751
		$D_p = .043$	.083	.194	.337	.530	.722
0.10...	iii	$D_1 = .036$	.070	.164	.287	.448	.606
		$D_2 = .040$	.078	.181	.300	.468	.620
		$D = .039$	.076	.178	.286	.445	.586
		$D_p = .034$	.067	.156	.271	.426	.581
∞.....	i	$D_1 = .024$	.047	.110	.192	.300	.406
		$D_2 = .024$	.048	.110	.192	.302	.398
		$D = 0.024$	0.048	0.110	0.192	0.298	0.397

for small values of τ_1, amounting to 30 per cent for $h/a = 0$, $\tau_1 = 0.05$ in the case of D_2. For $h/a = 0.01$, $\tau_1 = 0.50$, the error is about 10 per cent in the case of D_2 and 27 per cent in the case of D_p.

REFERENCES

Barbier, D. 1944, *Ann. de géophys.*, **1**, 144.
———. 1949, *ibid.*, **5**, 83.
———. 1952, *Ann. d'ap.*, **15**, 247.
Cabannes, J., Dufay, J., and Gauzit, J. 1938, *Ap. J.*, **88**, 164.
Chandrasekhar, S. 1947, *Ap. J.*, **106**, 152.
———. 1950, *Radiative Transfer* (Oxford: Clarendon Press).
Chandrasekhar, S., Elbert, D., and Franklin, A. 1952, *Ap. J.*, **115**, 244.
Piotrowski, S. L. 1947, *Ap. J.*, **106**, 466.
Rhijn, D. J. van. 1921, *Pub. Astr. Lab. Groningen*, No. 21.

THE EXTINCTION OF THE LIGHT OF THE NIGHT SKY. II*

G. COSTANTINE
Ministry of Education
AND
A. HAMMAD
Faculty of Science, Cairo University
Received October 19, 1954; revised February 21, 1956

ABSTRACT

The paper is a preliminary investigation on the effect of curvature on the values of the intensity of light received at the ground from an emitting layer that lies at a height h above the ground. The intervening atmosphere is one of small optical thickness, in which absorption is negligible and scattering is isotropic. It is found by numerical calculation that curvature effects are negligible for moderate and high altitudes of observation. For low altitudes of observation, however, curvature leads to about a 7 per cent rise in the values of the total intensity and thus cannot be neglected.

INTRODUCTION

In Part I the problem of the scattering of light in a plane-stratified atmosphere, with the emitting layer above it, was considered, and exact expressions were derived for the intensity of the diffused light received at the ground, on the assumption that absorption is negligible and scattering is isotropic.

In the present paper we consider the case of an isotropically scattering, spherically symmetric atmosphere of small optical thickness, which rests on a spherical ground of radius a, with the emitting layer at a height h above the ground. In such a case the radiation field at a point P is symmetric about OP, where O is the center of the ground. On this account, the intensity at P will be a function of two parameters only, viz., the distance r of P from O and the angle λ which PO makes with the ray of light.

Consider a parallel beam traveling in the downward direction s. Its intensity I_- at a point P, distance s from the luminescent layer, satisfies the equation

$$-\frac{\partial I_-}{\partial s} = \sigma\rho\,[I_-(r, \lambda) - \tfrac{1}{2}\int_{-1}^{+1} I(r, \lambda')\,d\eta']\,, \tag{1}$$

where σ is the mass scattering coefficient, ρ is the density of the atmosphere at P, and $\eta' = \cos\lambda'$. If we write

$$t = \int_0^s \sigma\rho\,ds\,, \qquad J = \tfrac{1}{2}\int_{-1}^{+1} I(r, \lambda')\,d\eta'\,,$$

then

$$dt = \sigma\rho\,ds = -\sigma\rho\sec\lambda\,dr\,, \tag{2}$$

and equation (1) takes the form

$$-\frac{\partial I_-}{\partial t} = I_- - J\,. \tag{3}$$

* Published with the aid of a grant from the American Astronomical Society.

Similarly, for the upgoing light, we have

$$\frac{\partial I_+}{\partial t} = I_+ - J \,. \tag{4}$$

On integration, we have

$$I_- (r, \lambda) = I_0 (\psi)\, e^{-t} + e^{-t} \int_0^t e^{t'} J (t')\, dt' \,, \tag{5}$$

$$I_+ (r, \lambda) = e^t \int_t^{t_1} e^{-t'} J (t')\, dt' \,, \tag{6}$$

on the assumption that no light is returned from the ground where $t = t_1$; $I_0(\psi)$ is the intensity of emission from the layer in the direction of the ray, and ψ is the value of λ at the layer.

ATMOSPHERES OF SMALL OPTICAL THICKNESS

We consider atmospheres of small optical thickness. Starting with the case of *zero optical thickness*, equation (1) reduces to

$$-\frac{\partial I_-}{\partial s} = 0 \,,$$

which gives, on integration,

$$I_- (r, \lambda) = \text{Const.} = I_0 (\psi) \,. \tag{7}$$

Similarly, for the upgoing light, we get

$$I_+ (r, \lambda) = 0 \,. \tag{7'}$$

We shall confine our consideration to the important case, in which the emission from the layer in any direction is proportional to the thickness of the layer in that direction. This gives, in the case of a thin layer,

$$I_0 (\psi) = I_0 \sec \psi \,.$$

Thus equation (7) takes the form

$$I_- (r, \lambda) = I_0 \sec \psi = \frac{I_0}{\sqrt{\{1 - [r \sin \lambda / (a + h)]^2\}}} \,. \tag{8}$$

At the ground, equation (8) reduces to

$$I_- (a, \theta) = \frac{I_0}{\sqrt{\{1 - [a \sin \theta / (a + h)]^2\}}} \,,$$

which gives van Rhijn's formula (1921).

From equations (7′) and (8) we get

$$J (r) = \tfrac{1}{2} \int_{-1}^{+1} I (r, \lambda)\, d\eta = \frac{a + h}{4r}\, I_0 \log \frac{a + h + r}{a + h - r} \,. \tag{9}$$

If the optical thickness of the atmosphere is small but not negligible, which is the case with the spectral lines in the visible part of the nightglow, we can substitute for J in

equation (5) from equation (9) and thus get for the diffused light, given by the second term in the right-hand side of equation (5), the expression

$$D(\lambda) = e^{-t}\int_0^t e^{t'} J(t')\, dt' .$$

At the ground, this is

$$D(\theta) = e^{-t_1}\int_0^{t_1} e^{t'} J(t')\, dt' = \frac{a+h}{4} I_0 e^{-t_1}\int_0^{t_1} e^{t'} r^{-1} \log\left(\frac{a+h+r}{a+h-r}\right) dt' . \tag{10}$$

Writing $r = a + y$, we get

$$D(\theta) = G_1 + G_2 + G_3 ,$$

where

$$G_1 = \tfrac{1}{4} I_0 (a+h)\ e^{-t_1}\int_0^{t_1} e^{t'} (a+y)^{-1} \log\left(\frac{2a+h}{h}\right) dt' ,$$

$$G_2 = \tfrac{1}{4} I_0 (a+h)\ e^{-t_1}\int_0^{t_1} e^{t'} (a+y)^{-1} \log\left(1+\frac{y}{2a+h}\right) dt' ,$$

$$G_3 = -\tfrac{1}{4} I_0 (a+h)\ e^{-t_1}\int_0^{t_1} e^{t'} (a+y)^{-1} \log\left(1-\frac{y}{h}\right) dt'$$

$$= -\tfrac{1}{4} I_0 (a+h)\ e^{-t_1}\int_0^{h} \sigma\rho \sec\lambda\, e^{t'} (a+y)^{-1} \log\left(1-\frac{y}{h}\right) dy ,$$

by means of equation (2).

It is possible to see from general considerations that G_2 and G_3 are negligible compared to G_1. A glance at the integrands in G_1 and G_2 suffices to show that $G_1 \gg G_2$. For instance, if $h = 100$ km, then

$$\frac{\log[1 + y/(2a+h)]}{\log[(2a+h)/h]} < 0.2 \text{ per cent} ,$$

so that, in this case, $G_2/G_1 < 0.2$ per cent.

As regards G_3, it is sufficient to remember that above 50 km from the ground the density ρ is vanishingly small, so that the large values of $\log(1 - y/h)$ near the upper limit of integration of G_3 are counterbalanced by the vanishingly small values of ρ, so that the contribution to G_3 of that part of the interval near $y = h$ will be negligible. To support such a conclusion numerically, we have considered a special density distribution which resembles quite closely the actual distribution, namely, the distribution

$$\rho = \rho_0 e^{-y/H} ,$$

where H is the height of the homogeneous atmosphere. For such a distribution, it is clear that G_1 lies between the limits

$$\tfrac{1}{4} I_0 t_1 \log\frac{2a+h}{h}\left\{\begin{matrix}\dfrac{a+h}{a}\\ 1\end{matrix}\right\}.$$

Also, G_3 lies between the limits

$$\tfrac{1}{4} I_0 \tau_1 R \left\{ \begin{matrix} \dfrac{a+h}{a} \sec\theta \\ \sec\psi \end{matrix} \right\},$$

where

$$R = H^{-1} \int_0^h e^{-y/H} \log\left(1 - \frac{y}{h}\right) dy$$

$$= e^{-h/H} \left[\log\left(\frac{h}{H}\right) + \gamma - E_i\left(\frac{h}{H}\right) \right],$$

in which E_i is the well-known Glaisher's integral and γ is Euler's constant. The relation between the optical thickness t_1 and the normal optical thickness τ_1 is $t_1 = f(\theta)\tau_1$, where $f(\theta)$ is a function that differs very little from $\sec\theta$ for small and moderate values of θ. Values

TABLE 1

INTENSITIES OF LIGHT RECEIVED AT THE GROUND FOR PLANE AND CURVED ATMOSPHERES ($\tau_1 = 0.05$)

h/a		μ^{-1}			
		1	2	4	11.47
0.02	transmitted	*0.951*	*1.713*	*2.603*	*2.624*
		0.951	1.713	2.610	2.761
	diffused	*0.053*	*0.103*	*0.197*	*0.473*
		0.059	0.117	0.227	0.624
0.10	transmitted	*0.951*	*1.468*	*1.725*	*1.329*
		0.951	1.468	1.730	1.398
	diffused	*0.039*	*0.076*	*0.146*	*0.350*
		0.040	0.080	0.155	0.397

for this function are supplied by the *Smithsonian Meteorological Tables* (1951). In this way a numerical comparison has been made between G_1 and G_3 for a number of values of h/a and θ, for the case $\tau_1 = 0.05$. It is found that G_3/G_1 never exceeds 2 per cent. Thus, within such a limit of accuracy, we can assume the diffused light to be represented by G_1 or, more simply, by the arithmetic mean of its upper and lower bounds, i.e.,

$$D(\theta) = \tfrac{1}{4} I_0 (1 - e^{-t_1}) \left(1 + \frac{h}{2a}\right) \log\left(1 + \frac{2a}{h}\right). \tag{11}$$

The error in this approximation to G_1 is less than $h/2a$ per cent, which is only 5 per cent for an extreme case of $h = 600$ km.

NUMERICAL RESULTS AND CONCLUSIONS

We shall now compare the values of the transmitted and diffused parts of the light received at the ground in the case of plane atmospheres with those in the case of curved atmospheres. This is done in Table 1 for $\tau_1 = 0.05$, the values corresponding to the plane case being given in italics.

It can be seen from this table that the diffused part is much smaller than the transmitted one, especially for high altitudes of observation. For low altitudes of observation, however, the diffused light becomes appreciable but does not exceed 20 per cent of the total light. Remembering that the error in our estimation of the diffused light does not exceed $h/2a$ per cent of its value, it can be seen that the error in our estimation of the total light will not exceed $h/10a$ per cent. This amounts to about 1 per cent for an extreme case of $h = 600$ km. Within such a limit of accuracy, the table serves to indicate the effect of curvature on the values of the intensity of light received at the ground. It can be seen that curvature increases the values of the intensity, the increase being most noticeable for low altitudes of observation; for instance, for sec $\theta = 11.47$, $h/a = 0.10$, $\tau_1 = 0.05$, the increase is about 7 per cent. Thus, for low altitudes of observation, curvature must be taken into account. For moderate and high altitudes of observation, the table shows that the plane case corresponds closely to the curved one, the difference between the values of the intensity in the two cases being less than 1 per cent. Thus for such altitudes of observation the curved case can be replaced by the simpler case of plane atmospheres.

REFERENCES

Barbier, D. 1944, *Ann. de géophys.*, **1**, 144.
Rhijn, P. J., Van. 1921, *Pub. Astr. Lab. Groningen*, No. 21.
Smithsonian Meteorological Tables, 1951, p. 422.

CHEMICAL HEATING FOR METEORITES

HAROLD C. UREY AND BERTRAM DONN
Enrico Fermi Institute for Nuclear Studies, University of Chicago
Received February 24, 1956

ABSTRACT

Recent dating methods for meteorites indicate that the separation of the iron-silicate phase and the last removal of argon took place within a short interval of time. Within this interval the iron-nickel alloys, kamacite and taenite, must have been formed at great depths and incorporated into the chondrites. All this does not seem possible with radioactive heating. We suggest that the initial accumulation of the parent body contained a large proportion of unstable compounds which produced the required heating through subsequent reaction. This may have taken place in several stages. A very low-temperature sun would have been necessary for such material to condense.

It has been evident to students of meteorites that some melting process was involved in their formation. The existence of silicate minerals resulting from solidification of a melt and of massive iron bodies is the most direct evidence for this. The achondrites are simpler than the chondrites. The latter appear to be brecciated mixtures of silicate minerals and metallic nickel-iron, all compacted to rather strong objects. It is generally supposed that the rounded chondrules got their shape by solidifying to a glass while falling freely.

Three methods of dating place the ages of the meteorites at about 4.5×10^9 years. The Pb^{206}/Pb^{207} age (Patterson 1955) is the last time since the leads of the iron meteorites, Canyon Diablo and Henbury, were associated with uranium, and this fixes the time since metallic iron was separated from the silicates of the stone meteorites, presumably by the separation of the liquid phases in a gravitational field. The Rb^{87}–Sr^{87} age (Schumacher 1956) is the time since the strontium of the Pasamonte achondrite was separated to a large degree from the rubidium of the chondrites, presumably by crystallization in a silicate melt. The K^{40}–A^{40} age (Gerling and Pavlova 1951; Wasserberg and Hayden 1955) is the time since argon was last removed from the meteorites. It is always a minimum age, because some argon may have been lost by mild heating since some early high-temperature epoch. Hence the smaller ages secured by Gerling and his coworkers may not be the time since the objects were formed. All the ages, within the limits of error, are the same, indicating that all processes took place in a short period of time. However, heating subsequent to the formation process would not affect the Pb^{206}/Pb^{207} or the Rb^{87}–Sr^{87} ages if no chemical separations or mixing occurred. The Brenham Township pallasite consists of both metallic phase with Widmanstätten figures and silicate phase, mostly olivine. It has been dated by the K^{40}–A^{40} method by Thomson and Mayne (1955), who found 3.5×10^9 years. Their value for the potassium content is 0.019 per cent. However, Edwards (1956) gives evidence that the potassium content is lower, namely, 0.009 per cent, and hence that the age again is in the neighborhood of 4.5×10^9 years. Thus the kamacite and taenite of this meteorite were already formed at that time, since heating the meteorite to several hundreds of degrees so that the iron-nickel alloys could separate by diffusion would surely cause a loss of argon.

Beck, Stevenson, and LaPaz (1951) found kamacite and taenite in the LaLande chondrite, which has not been dated. Recent work has shown that the Beardsley and Holbrook chondrites also contain these two iron-nickel phases,[1] and these meteorites have been dated by the K^{40}–A^{40} method as about 4.5×10^9 years.

[1] We are indebted to Mrs. Betty Nielson, of the Institute of Metals, for microscopic identification of these phases and to Miss A. Pletenger and Professor W. Zachariasen for the X-ray identification of these phases in the metal of these meteorites.

Uhlig (1954) concludes that the kamacite and taenite could not have been formed except by cooling to low temperatures (to 300°–400° C or lower), high pressure (10^5 atm.), and during long periods of time, although not necessarily measured in billions of years. It is not possible to fit these requirements into the schedule of dates discussed above. Uhlig (1956) has indicated that somewhat higher temperatures for shorter periods of time would be a permissible solution of the diffusion problem for the formation of kamacite and taenite. The high pressures required according to Uhlig still necessitate the formation of the kamacite and taenite rather deep in a large planetary object. (The pressure at the center of the moon is 5×10^4 atm.) The presence of diamond in the Canyon Diablo iron, as observed by Ksanda and Henderson (1939), also requires the existence of high pressures during its formation.

The problem of melting iron within large bodies, e.g., of lunar size or greater, and cooling them to some 500° C in order to form kamacite and taenite, all within a time span which lies within the limits of error of the dating methods, is a difficult one. Radioactive heating by potassium, uranium, and thorium would require a long time. After melting, these elements must have been completely removed from the interior, for otherwise the object would not cool at all, and, besides, some billions of years are required to cool the object to the required temperature, as shown by calculations on the moon (Urey 1951).[2] Even if short-lived radioelements were present, such as Al^{26}, the cooling time could not be fitted in between the Pb^{206}/Pb^{207} dates or the Rb^{87}–Sr^{87} date and the K^{40}–A^{40} dates of the chondrites. Radioactive heating of any kind seems to be definitely excluded.

One of us (Urey 1951, 1952, 1954) has suggested that solar heating by a high-temperature primitive sun would provide a mechanism for the melting observed in meteorites, the removal of part of the silicate in order to account for the variation in density and composition of the planets, and yet retain the nonvolatile elements in solar proportions. This proposed source of heat does not provide the high pressures required for producing the kamacite, taenite, and the diamonds of meteorites. The source of heating proposed below does not provide a suitable mechanism for some of these conditions, as will be explained later.

In a recent paper Donn and Urey (1956) proposed that chemical explosions cause the outbursts of comet halos. It was suggested that free radicals are condensed in the comet heads, as Whipple previously proposed, and that these react to form stable molecules when triggered by solar corpuscular radiation. The energy available from such reactions can be estimated from approximate data available.[3] Table 1 gives the heats of reaction for some typical reactions at 298° K. When necessary, heats of vaporization are estimated as 10000 cal/mole.

Rice and Freamo (1951) have prepared NH, condensed it to a solid, and showed that it is not destroyed by atomic hydrogen, at least not more than superficially. The presence of CH in interstellar space is proved by its absorption spectrum. Whipple's (1950) icy-conglomerate model for comets assumes the existence of condensed molecules of this kind. Swings (1952) and others have discussed such possibilities. The energies available enable us to understand how cometary flares can occur as Donn and Urey (1956) have suggested.

It seems entirely reasonable to expect that similar condensations of free radicals occurred during the origin of the solar system. There is no compelling reason for the usual assumption that only stable molecules were present. In fact, the marked deviations from thermodynamic equilibrium that are the characteristic feature of nonstellar astronomical

[2] These are being repeated with more recent data. The conclusions are much the same as those arrived at previously.

[3] See *Selected Values of Chemical Thermodynamic Properties* (Circ. No. 500, National Bureau of Standards).

problems, coupled with the low temperatures present, strongly suggest that terrestrially unstable compounds may have played a dominant role (see Donn 1955). In this case chemical heating could have been available. It would take place quickly, perhaps even explosively, though not necessarily so. The exact effects would depend on concentrations of high-energy molecules relative to stable molecules such as CH_4, NH_3, H_2O, and C; carbon compounds similar to organic substances, FeO, FeS, silicates, etc. Accumulation and reaction may have alternated.

A specific course of events may be given as an illustration. Accumulation of silicates and iron sulphide with free radicals and other condensible gases occurred until a substantial body, many kilometers in magnitude, was formed. Reaction was started in some way. Reduction of iron to some extent and melting of silicates and iron occurred. Some cooling of the mass followed, at least until the surface was cooled. Then another layer was accumulated, and again reaction occurred, followed by cooling. This may have been repeated many times until an object of planetary size accumulated. The resulting object may have been at some 500° C throughout, with pressures suitable for the formation

TABLE 1

HEATS OF REACTION

Reaction	cal/gm (298° K)	ΔH per mole* (kcal at 298° K)
$2\ OH(s) = H_2O_2$	1300	− 45
$4\ OH(s) = 2\ H_2O(g) + O_2(g)$	1700	−116
$2\ CH(s) = C_2H_2(g)$	8000	−210
$2\ CH(s) = 2\ C(s) + H_2(g)$	10000	−264
$4\ NH(s) = NH_4N_3$	3000	−176
$2\ NH(s) = N_2 + H_2$	3300	− 98
$2\ CH(s) + 10\ OH(s) = 2\ CO_2 + 6\ H_2O$	4000	−800
$C_2H_2(s) + 5\ H_2O_2(l) = 2\ CO_2 + 6\ H_2O$	1800	−360
$C + O_2(g) = CO_2(g)$	1900	− 94
$C + \frac{1}{2}\ O_2(g) = CO(g)$	940	− 26.4

* ΔH is the change in heat content for the numbers of gram molecules indicated in the equation.

of kamacite, taenite, and diamonds. The time required depends on the rate of accumulation, and, since we have no physically valid theory for this process, no definite estimates for the duration of the process can be made. Undoubtedly, many other possible sequences of events may be postulated as reasonably as the one given, which is designed to account for these special high-pressure mineral species. Following the formation of such a planetary object, it was then necessary to break this lunar-size object into very small pieces of less than millimeter sizes and incorporate them into the chondrites. Or, if the object was not completely broken up, it was necessary to remove material from deep within the body where pressures were high, in order to secure the kamacite and taenite. Or the kamacite and taenite of the chondrites are low-pressure varieties of these phases and then the chondrites may have been formed as superficial conglomerates as Urey and Craig (1953) assumed.

This method of heating does not supply a method for producing a variation in density of the planets. Also, the condition that the more volatile elements, such as mercury, arsenic, zinc, and cadmium (Urey 1954), were not lost during the escape of gaseous materials from high-temperature objects is not easily met, though it is probable that meeting this condition is not impossible.

Only the imine radical, NH, has been condensed to a solid at liquid nitrogen tem-

peratures, and it reacts to ammonium azide at $\sim 150°$ K. Lower temperatures may be required for the condensation of other radicals, and there is no experimental proof that they will not be destroyed by atomic hydrogen. Thus the temperature must be lower than that of objects now in the asteroidal belt; hence we conclude that the sun had a low temperature when these objects accumulated, provided that the heating process discussed here actually occurred and that the accumulation took place at some 3 A.U. from the sun and not at greater distances, as is possible in the case of the comets. This means that the temperatures must be lower than those assumed by ter Haar (1948) when he discussed condensation in the solar nebula and even lower than those which have been assumed by Kuiper (1953).

It seems most likely that chemical heating processes as described contributed to the series of events leading to the formation of the meteorites and solar system generally but that this does not exclude contributions of heat from other sources.

REFERENCES

Beck, C. W., Stevenson, R. G., and LaPaz, L. 1951, *Cont. Meteoritical Soc.*, **5**, 11; *Pop. Astr.*, **59**, No. 2, 93.
Delsemme, A. H., and Swings, P. 1952, *Ann. d'ap.*, **15**, 1. See also Haser, L. 1955, *C.R.*, **241**, 742.
Donn, B. 1955, *Extrait Mém. in 8° Soc. Roy. Sci. Liége*, 4th Series, **15**, Part 1, 571.
Donn, B., and Urey, H. C. 1956, *Ap. J.*, **123**, 339.
Edwards, G. 1955, *Geochim. et Cosmochim. Acta*, **8**, 285.
Gerling, E. K., and Pavlova, T. G. 1951, *Doklady Akad. Nauk, U.S.S.R.*, **77**, 85.
Haar, D. ter. 1948, *Kgl. Dansk. Vidensk. Selsk., Math.-fys. Midd.*, Vol. **25**, No. 3.
Ksanda, C. J., and Henderson, E. P. 1939, *Am. Mineralogist*, **24**, 677.
Kuiper, G. P. 1953, *Proc. Nat. Acad. Sci.*, **39**, 1159.
Patterson, C. C. 1955, *Geochim. et Cosmochim. Acta*, **7**, 151, and references given in this paper.
Rice, F. O., and Freamo, M. 1951, *J. Am. Chem. Soc.*, **73**, 5529.
Schumacher, E. 1956, *Zs. f. Naturforsch.*, in press.
Thomson, S. J., and Mayne, K. I. 1955, *Geochim. et Cosmochim. Acta*, **7**, 169.
Uhlig, H. H. 1954, *Geochim. et Cosmochim. Acta*, **6**, 282.
———. 1956, private communication.
Urey, H. C. 1951, *Geochim. et Cosmochim. Acta*, **1**, 207.
———. 1952, *The Planets* (New Haven: Yale University Press).
———. 1954, *Ap. J. Suppl.*, Vol. **1**, No. 6.
Urey, H. C., and Craig, H. 1953, *Geochim. et Cosmochim. Acta*, **4**, 72.
Wasserberg, G. J., and Hayden, R. J. 1955, *Phys. Rev.*, **97**, 86.
Whipple, F. L. 1950, *Ap. J.*, **111**, 375.

METEOR IONIZATION AND ITS DEPENDENCE ON VELOCITY*

GERALD S. HAWKINS
Harvard College Observatory
Received January 30, 1956

ABSTRACT

The ionizing efficiency of evaporated meteor atoms is found to be strongly dependent on the velocity of the meteor.

The relation between the brightness of a meteor and the ion density in the trail has been investigated by Greenhow and Hawkins (1952), Whipple (1955), and Evans and Hall (1955). There is disagreement on how the ionizing efficiency varies with meteor velocity, and it is of interest to assess the published results so that a scale of radio magnitudes can be established.

For a meteoroid of mass m, moving with velocity v, the visible energy produced per second, I, is given by the equation

$$I = -\frac{1}{2}\frac{dm}{dt}v^2\tau\,, \tag{1}$$

where τ is the luminous efficiency.

The number of electrons per meter, q, along the trail is given by the equation

$$q = -\frac{dm}{dt}\frac{1}{v}\frac{\beta}{\mu}, \tag{2}$$

where μ is the mass and β is the probability of ionization of an evaporated meteor atom.

Öpik (1937) has estimated that the absolute visual magnitude, M, of a meteor radiating I watts at a range of 100 km is given by the expression

$$M = 7.1 - 2.5\log_{10} I\,. \tag{3}$$

Hence, eliminating dm/dt between equations (1) and (2) and substituting for I in equation (3), we find

$$M = 7.1 - 2.5\log_{10}\frac{\mu}{2} - 2.5\log_{10}\left(\frac{\tau}{\beta}v^3 q\right). \tag{4}$$

If we assume the mean mass of a meteor atom to be 10^{-25} kg, equation (4) becomes

$$M = 70.35 - 2.5\left(\log\frac{\tau}{\beta} + 3\log v + \log q\right). \tag{5}$$

Correlations between meteor brightness and electron density in the trail have been made for the perseid and geminid meteor streams. Thus the constants of equation (5) have been evaluated for two meteor velocities.

* This research was supported by the Massachusetts Institute of Technology, Lincoln Laboratory, contract No. AF19(122)-458, subcontract No. 57. Reproduction in whole or in part permitted for any purpose of the U.S. government.

From the observations of perseid meteors by Millman (1950) and the measurements of diffusion coefficient by Greenhow and Neufeld (1955), we may deduce that[1]

$$M = 40.75 - 2.5 \log_{10} q \qquad \text{for} \qquad v = 6.0 \times 10^4 \text{ m/sec}. \tag{6}$$

Similarly, from the observations of geminid meteors by Prentice (Kaiser 1955) and the heights deduced by Millman (1950), we find that

$$M = 39.89 - 2.5 \log_{10} q \qquad \text{for} \qquad v = 3.6 \times 10^4 \text{ m/sec}. \tag{7}$$

Evans and Hall (1955) concluded from equations (6) and (7) that τ/β varied as v^{-3}. Actually, $\tau/\beta = 3.194 \times 10^{-3}$ for perseid meteors and 3.295×10^{-2} for geminids, which leads to the expression

$$\frac{\tau}{\beta} = 2 \times 10^{19} v^{-4.56}, \tag{8}$$

where v is in meters per second.

TABLE 1

δM, THE VELOCITY INDEX

	v (km/sec)				
	20	30	40	50	60
δM in units of visual magnitude.....	1.9	1.2	0.7	0.3	0.0

Thus we must conclude that the ratio of luminous efficiency to ionizing probability is strongly dependent on velocity. The exponent in equation (8) is in fair agreement with the value of 3.88 deduced by Whipple (1955) from the occurrence rate of meteors observed photographically and by radio-echo methods. The luminous efficiency τ is approximately proportional to velocity for photographic meteors, so that we may assume provisionally that β, the ionizing probability, varies as $v^{5.6}$.

An indirect determination of the variation of ionizing probability with velocity has been made by Evans and Hall (1955) from the gradient of the curve of height versus velocity of meteor trails. They found the ionizing probability to be proportional to $v^{0.5}$; that is to say, β was almost independent of velocity. This work has been criticized by Whipple (1955), who considers that diffusion of the trail and recombination of ions may seriously affect the observations. A further criticism is that the zenith angle χ of the trail (Herlofson 1948) has not been taken into account. For example, if we assume $\chi = 70°$ for low-velocity meteors and $\chi = 10°$ for high-velocity meteors, this is sufficient to change the computed index of β from $v^{0.5}$ to $v^{3.5}$. Thus the method requires further study before it can be considered reliable.

[1] A re-evaluation of the radio-visual correlation by Millman (1956) shows that the gradient in eq. (6) is -2.6 and not -2.5. The conclusions concerning the dependence of ionizing efficiency on velocity are unaffected by this change.

We may therefore take equation (8) as correct and substitute in equation (5) to establish a provisional scale of magnitudes for radio meteors. The absolute visual magnitude, M, of a meteor producing a trail with q electrons/m is then given by the relation

$$M = 40.75 - 2.5 \log_{10} q - \delta M , \tag{9}$$

where δM is a small term dependent on the velocity v of the meteor. This term is tabulated in Table 1.

REFERENCES

Evans, S., and Hall, J. E. 1955, *Meteors*, ed. T. R. Kaiser (London, England: Pergamon Press), pp. 18–22.
Greenhow, J. S., and Hawkins, G. S. 1952, *Nature*, **170**, 355.
Greenhow, J. S., and Neufeld, E. L. 1955, *J. Atm. Terr. Phys.*, **6**, 100.
Herlofson, N. 1948, *Phys. Soc. Rept. Prog. Phys.*, **11**, 444.
Kaiser, T. R. 1955, *Meteors*, ed. T. R. Kaiser (London, England: Pergamon Press), pp. 63, 64.
Millman, P. M. 1950, *J.R.A.S. Canada*, **44**, 209.
———. 1956, *Canadian J. Phys.*, **34**, 50.
Öpik, E. 1937, *Pub. Obs. Astr. U. Tartu*, Vol. **24**, No. 5.
Whipple, F. L. 1955, *Ap. J.*, **121**, 241.

ANNOUNCEMENT

PAPERS PUBLISHED IN THE *ASTROPHYSICAL JOURNAL* WITH THE AID OF GRANTS FROM THE AMERICAN ASTRONOMICAL SOCIETY

Readers will have noticed that the *Astrophysical Journal* publishes fairly frequently papers sent from countries outside the United States, Canada, and Mexico. It is perhaps not widely known that the publication of these papers has been made possible only by the financial assistance which the *Astrophysical Journal* has received from the American Astronomical Society. In the case of papers from abroad, the customary page charges (see the Announcement in *Ap. J.*, **121**, 290, 1955) have not generally been applied against the sponsoring institutions; the American Astronomical Society has paid them instead. Without this generous support, the *Astrophysical Journal* could not have fulfilled its obligations to astronomers of all countries. The extent of this support can be seen from the following twenty-three papers which have been published in Volumes **116**–**123** (inclusive) of the *Astrophysical Journal* with the aid of grants from the American Astronomical Society.

G. R. Miczaika, Badische Landessternwarte, Heidelberg-Königstuhl, Germany. "The Light-Variability of 16 Lacertae," **116**, 99–105.

Kenneth R. W. Brewer, University of London Observatory, London, England. "HD 50169, a Spectrum Variable with Emission at $H\alpha$," **118**, 265–280.

E. Fermi, Institute for Nuclear Studies, University of Chicago. "Galactic Magnetic Fields and the Origin of Cosmic Radiation" (Henry Norris Russell Lecture), **119**, 1–6.

Alladi Ramakrishnan and P. M. Mathews, Department of Physics, University of Madras, Madras, India. "On the Solution of an Integral Equation of Chandrasekhar and Münch," **119**, 81–90.

Yoshio Fujita, Department of Astronomy, University of Tokyo, Tokyo, Japan. "On the Spectrum of Chi Cygni near the Time of Light-Maximum," **119**, 141–145.

Alladi Ramakrishnan, Department of Physics, University of Madras, Madras, India. "A Stochastic Model of a Fluctuating Density Field," **119**, 443–455.

Evry Schatzman, Institut d'Astrophysique de Paris, Paris, France. "On the Effect of Electron Screening on Thermonuclear Energy Generation," **119**, 464–465.

Alladi Ramakrishnan, Department of Physics, University of Madras, Madras, India. "A Stochastic Model of a Fluctuating Density Field. II," **119**, 682–685.

Lyman Spitzer, Jr., Princeton University Observatory, Princeton, New Jersey. "Behavior of Matter in Space" (Henry Norris Russell Lecture), **120**, 1–17.

P. Whittle, University Institute of Statistics, Uppsala, Sweden. "A Statistical Investigation of Sunspot Observations, with Special Reference to H. Alfvén's Sunspot Model," **120**, 251–260.

Ingrid Torgard, Lund Observatory, Lund, Sweden. "The Location of Cepheids with Respect to the Spiral Arms in the Anticenter Region of the Milky Way," **120**, 370–372.

J. L. Pawsey, Division of Radiophysics, University Grounds, Sydney, New South Wales, Australia. "A Catalogue of Reliably Known Discrete Sources of Cosmic Radio Waves," **121**, 1–5.

C. Plumpton and V. C. A. Ferraro, Queen Mary College, University of London, London, England. "On Toroidal Magnetic Fields in the Sun and Stars," **121**, 168–174.

Ali M. Naqvi and S. P. Talwar, University of Delhi, Delhi, India. "An Identification of the Coronal Line λ 5694," **121**, 287–289.

B. Lehnert, Royal Institute of Technology, Stockholm, Sweden. "Magnetohydrodynamic Waves under the Action of the Coriolis Force. II," **121**, 481–490.

T. Y. Teng Fan, "The Character of the Instability of an Incompressible Fluid of Constant Kinematic Viscosity and Exponentially Varying Density," **121**, 508–520.

J. Grandjean and R. M. Goody, Imperial College, London, England. "The Concentration of Carbon Dioxide in the Atmosphere of Mars," **121**, 548–552.

K. D. ABHYANKAR and A. S. RAMANATHAN, Kodaikanal Observatory, India. "Equivalent Widths of Atomic Lines in Sunspot Spectra, **121,** 739–749.

ALLADI RAMAKRISHNAN, Department of Physics, University of Madras, Madras, India. "On Stellar Statistics," **122,** 24–31.

I. W. BUSBRIDGE, St. Hugh's College, Oxford, England. "On the X- and Y-Functions of S. Chandrasekhar," **122,** 327–348.

MOGENS RUDKJØBING, University Observatory, Copenhagen, Denmark. "On the Determination of the Mass of a Spherically Symmetric Cluster," **122,** 357–358.

M. K. ALY, Helwan Observatory, Egypt. "Preliminary Note on Measures of Coronal Emission Lines Observed at the Total Solar Eclipse, February 25, 1952, by B. Lyot and M. K. Aly," **122,** 438–444.

ALLADI RAMAKRISHNAN and S. K. SRINIVASAN, Department of Physics, University of Madras, Madras, India. "Correlation Problems in the Study of the Brightness of the Milky Way," **123,** 479–485.

S. CHANDRASEKHAR
Managing Editor

THE ASTROPHYSICAL JOURNAL SUPPLEMENT SERIES

These *Supplements* are intended to provide a medium for the publication of extensive investigations, such as wave-length lists of stars of special interest, photometric data, results of numerical integrations pertaining to stellar interiors, model stellar atmosphere calculations, and original memoirs.

Supplement No. 21

"Stellar Spectra in Milky Way Regions"
V. A Region in Monoceros
VI. A Region in Camelopardalis

S. W. McCuskey

Spectral class data, photographic magnitudes, and blue-red color indices for 3219 stars in two areas of the Milky Way are presented in tabular form with identification charts. The limiting magnitude is about 12.3 and the areas cover 32.6 square degrees. (Published March 1956. Price $1.25)

Subscriptions

$8.00 per volume
Canada, $8.75. Foreign, $9.50.

To members of the American Astronomical Society, $6.00 per volume. Orders now accepted.

THE UNIVERSITY OF CHICAGO PRESS
5750 ELLIS AVENUE CHICAGO 37, ILLINOIS

THE OBSERVATORY

FOUNDED 1877

* * *

A Magazine presenting current developments in Astronomy by means of Articles, Correspondence, Notes on discoveries and Reviews of important astronomical books. The papers read at the Meetings (Astronomical & Geophysical) of the Royal Astronomical Society and the discussions which follow are also fully reported.

* * *

Annual subscription for 6 issues, post free, £1 (U.S.A. and Canada, $3.00) should be sent to

The Editors, ROYAL GREENWICH OBSERVATORY
Herstmonceux Castle, Hailsham, Sussex, England

The Second Volume in a Distinguished Series

THE EARTH AS A PLANET

The Solar System—Volume II

Edited by GERARD P. KUIPER

This is the second of four volumes designed to collect and systematize our knowledge of the solar system. Like its predecessor, *The Sun*, it is conceived as both a reference book for the specialist and a source of general information for the general reader with some knowledge of the physical sciences.

Consisting of authoritative articles written by internationally eminent specialists, *The Earth as a Planet* is a complete and fully documented handbook, covering the entire range of physics, geochemistry, oceanography, and biochemistry as they apply to the earth in its planetary aspect. Among the many topics treated are the rotation of the earth; the nature of the earth's interior; the growth of continents; current systems of oceans and atmospheres; the life-cycles of methane, carbon dioxide, oxygen, and nitrogen; the absorption spectrum of the atmosphere; the physics and chemistry of the upper atmosphere; and the appearance of the earth from interplanetary space.

Contributions by

SIR HAROLD SPENCER JONES
FRED L. WHIPPLE
J. TUZO WILSON
D. R. BATES
HORACE R. BYERS
LEO GOLDBERG
SIR EDWARD BULLARD
A. B. MEINEL
BRIAN MASON
CLYDE T. HOLLIDAY
ANDRÉ DANJON
SIR HAROLD JEFFREYS
J. W. CHAMBERLAIN
H. U. SVERDRUP
M. NICOLET
G. E. HUTCHINSON

752 pages *$12.50*

The remaining two volumes in the series will consist of *Planets and Comets, Part 1, Planets and Satellites* and *Planets and Comets, Part 2, Minor Planets, Meteorites, Comets, Origin of the Solar System.*

from your bookseller or from

THE UNIVERSITY OF CHICAGO PRESS
5750 ELLIS AVENUE CHICAGO 37, ILLINOIS